Birla Central Library
PILANI (Rajasthan)
Class No. 621.38413 B12
Book No. B81T
Accession No. 26128

Theory and Application of
RADIO-FREQUENCY HEATING

GEORGE H. BROWN, Ph.D.
Research Engineer
RCA Laboratories, Princeton, N. J.

CYRIL N. HOYLER, M.S.
Research Engineer
RCA Laboratories, Princeton, N. J.

AND

RUDOLPH A. BIERWIRTH, M.S.
Chief Engineer, Sound Incorporated, Chicago, Ill.;
Formerly Research Engineer, RCA Laboratories, Princeton, N. J.

Second Printing

D. VAN NOSTRAND COMPANY, Inc.
TORONTO NEW YORK LONDON

NEW YORK
D. Van Nostrand Company, Inc., 250 Fourth Avenue, New York 3

TORONTO
D. Van Nostrand Company (Canada), Ltd., 228 Bloor Street, Toronto

LONDON
Macmillan & Company, Ltd., St. Martin's Street, London, W.C. 2

COPYRIGHT, 1947
BY
D. VAN NOSTRAND COMPANY, INC.

All Rights Reserved
This book, or any parts thereof, may not be reproduced in any form without written permission from the authors and the publishers.

First Published April 1947
Reprinted September 1948

PRINTED IN THE UNITED STATES OF AMERICA

PREFACE

The preparation of this volume has been prompted by the many sincere questions propounded by engineers skilled in their profession but unfamiliar with radio-frequency phenomena, and by the consciousness that the technical literature concerning the basic principles of radio-frequency heating is extremely meager.

It is the authors' hope that this work will prove helpful to industrial engineers who may have occasion to use radio-frequency generators in solving their heating problems and that it will be of benefit to those radio engineers who must inevitably become the exponents of a new industrial tool.

Since the art of radio-frequency heating is rapidly becoming a science, any attempt at completeness in displaying the underlying principles must make use of the powerful methods of mathematical analysis. Where mathematical derivations are made throughout the text, graphical displays have been used to convey the conclusions which were reached by analytical means. The principles have been illustrated by experimental data and often by a description of a complete laboratory experiment. Some of these experiments, conducted by the authors in the RCA Laboratories, have resulted in the design and installation of industrial equipment. Many others have been carried out so recently that they await future exploitation, while a number of the experiments had for their sole purpose the establishment of certain principles and the accumulation of knowledge which would be of assistance in solving problems at present unpropounded.

Radio and electrical engineers have long understood the physical phenomenon by which metallic conductors as well as semi-conductors become heated when electric currents are forced through the materials in question; and the experience of finding heated insulators in regions of strong alternating electrical fields has been a familiar one. In fact, in the design of efficient systems for the transfer of electrical power, familiarity with governing principles has been of paramount importance so that overheating would not occur in conductors carrying heavy currents or in insulators under the stress of high alternating voltages. Except for a few notable pioneers, most radio engineers have struggled valiantly to prevent heating by means of radio-frequency power. Only within the past few years have serious efforts been made to discover and apply radio-frequency heating techniques to the problems of industry in an extensive manner.

When an alternating electric current is passed through a mass of material, the manner in which the current flows and consequently the manner in which heat is generated is greatly dependent on the conductivity of the material and on the frequency of the alternations. If the conductivity is high and the frequency is high, the current tends to crowd to the outside of the mass, and surface or near-surface heating results. On the other hand, if the conductivity is low, then the current distribution tends to be uniform and heat is generated throughout the mass. It is thus possible to heat the material internally without the difficulty of conducting the heat through the outer layers.

These two characteristics of high-frequency heating — namely, the uniform heating of poor conductors and the surface heating of good conductors — are of primary importance and have provided a solution to many a knotty heating problem. Although the surface heating of poor conductors or the uniform heating of good conductors may often be desirable, in many cases radio-frequency heating can be of little assistance.

Since the generation of radio-frequency power is a comparatively costly process, the decision to utilize this type of heating hinges upon three considerations.

1. If the use of radio-frequency heating accomplishes the chosen task faster or cheaper than the simpler heating techniques, the decision may be in favor of radio-frequency heating. Ease of control of a process may also be a factor.
2. When a sufficiently better product results from the use of radio-frequency energy, the choice is obvious.
3. If the designated problem cannot be solved by any other known method, radio-frequency power will be used without further ado.

There has been some tendency, particularly in trade journals, to refer to "induction heating" and "electrostatic heating." The former term is generally applied to the heating of metals where currents are induced by transformer action. The term is descriptive, and generally accurate. However, metal heating is often accomplished by conduction currents without the transformer action. The latter term, "electrostatic heating," has been applied to high-frequency heating of poor conductors. It is difficult to understand how such a misnomer came to be applied to a situation where the electric field alternates at a rate of millions of cycles per second, and often hundreds of millions of cycles per second. This same type of heating has sometimes been called "dielectric" heating. The authors have felt more satisfied to include under the heading of "radio-frequency" heating the broad applications in which materials of any kind are heated by means of radio-frequency currents. It should be stated that there is no definite boundary which divides radio frequencies from low frequencies. Indeed, the fundamental principles apply to all frequencies, and the effects which are sometimes attributed to radio frequencies differ from the effects at low frequencies only as to degree.

Except in certain illustrative examples where the exception is evident, the rationalized practical system of electrical units is used throughout the book. In this system, magnetic intensity H is expressed in ampere-turns per centimeter. Magnetic flux density B is expressed in webers per square centimeter ($= 10^8$ maxwells per square centimeter). Permeability $\mu = B/H = \mu_r \cdot \mu_0$ where $\mu_0 = 4\pi \times 10^{-9}$ is the permeability of free space and μ_r is the relative permeability of a material. Electric intensity E is expressed in volts per centimeter. Electric displacement D is expressed in coulombs per square centimeter. Permittivity $p = D/E = p_0\epsilon$ where p_0 is the permittivity of free space and is equal to 8.85×10^{-14}. The dielectric constant of the material ϵ may be regarded as the relative permittivity of the material. It is of interest to note that, in this system of units, $(\mu_0/p_0)^{\frac{1}{2}} = 120\pi$ and $(\mu_0 p_0)^{-\frac{1}{2}} = 3 \times 10^{10}$.

The authors wish to express their appreciation to Miss Veronica Moran, of the RCA Laboratories secretarial staff, for her work in typing the manuscript; to Mrs. F. M. Lundahl, Patent Department, Radio Corporation of America, who prepared the drawings; and to Mr. N. W. Newell, staff photographer of the RCA Laboratories, who produced all the photographs used in this volume.

RCA Laboratories,
Princeton, N. J.
February 1947.

G. H. B.
C. N. H.
R. A. B.

Authors are partial to their wit, 'tis true,
But are not critics to their judgment too?

Alexander Pope, *Essay on Criticism*, 1711

CONTENTS

PAGE

Preface iii

List of Tables xiii

CHAPTER 1

Axial Current Flow in a Cylindrical Conductor 1

Current flow through a conducting cylinder — distribution affected by physical properties of material and frequency of applied voltage — general formula for field distribution — specific reference to cylinder which is: a perfect insulator, a dielectric with very lower power factor, a dielectric with high power factor, a good conductor.

CHAPTER 2

Induced Currents in Cylindrical Conductors 27

Mathematical treatment of idealized case of induction heating — circular current paths are concentric with axis of load — magnetic intensity lines parallel to axis — equations display power absorption per unit length — critical frequency for efficient coupling.

CHAPTER 3

Induction Heating Applied to Conductors of Small Diameter. 33

Results of Chap. 2 applied to conductors 5 mils to 40 mils in diameter — detailed experimental study — correlation of field intensity to wire size, heating time, and frequency — experimental application to hardening knitting-machine needles and surgical needles.

CHAPTER 4

Current Flow in Flat Metal Sheets of Great Thickness 45

Distribution of electric intensity and current density in a flat metal sheet when current flows parallel to boundary — distribution related to cylinder of large radius — importance of current crowding to surface when surface-hardening steel — tabulation of actual magnitudes of pertinent electric values.

PAGE

CHAPTER 5

Current Flow in Flat Metal Sheets of Limited Thickness 55

Extension of Chap. 4 to thin sheets — alteration of current distribution by limiting thickness — critical frequency for induction-heating thin strip related to conductivity, permeability, and thickness of material.

CHAPTER 6

Strip Heating 63

Experimental application of Chap. 5 — examination of complete power requirements for heating specific steel strip.

CHAPTER 7

Current Flow in Laminar Sheets 68

Modification of current distribution in metal sheets when surface layer has different electrical properties from the core of metal — examined for: steel heated above Curie point in a thin surface layer, copper-plated steel.

CHAPTER 8

Conductors Carrying Current Parallel to Metal Sheets 72

Induced current crowds under exciting conductor — current distribution affected by radius of conductor and spacing — coupling efficiency related to electric properties and geometry involved — distribution of induced current in a large cylinder surrounded by multi-turn coil.

CHAPTER 9

Efficiency of Induction Heating Coils 91

Equivalent circuit of induction heating — effect of frequency on efficiency of coupling — voltage on and current in coil as frequency is changed — correlation of experimental data with theoretical implications — characteristics of and measurements on current transformer for induction heating.

CHAPTER 10

Effect of Temperature on the Electrical Properties of Metals 102

Determination of electrical properties of metal at elevated temperatures — use of a copper standard — examination of peculiarities of iron and steel in vicinity of Curie point.

PAGE

CHAPTER 11

Annealing Brass and Bronze by Radio-Frequency Heating 115
Cartridge brass rod, cartridge cups — experimental procedure — comparison of radio-frequency heating and oven annealing — evaluation of results — radio-frequency wattmeter measurements — theoretical consideration — illustrative example — annealing phosphor bronze — conclusions.

CHAPTER 12

Laboratory Experiments with Typical Induction-Heating Problems . . 136
Paint baking, continuous process for metal radio tubes — setscrew hardening, semi-automatic method for hardening screwdriver slot — soldering, multiple soldering operation — brazing, solution of critical brazing operation — welding, chain links, under pressure.

CHAPTER 13

The Differential Equation of Heat Flow in One Dimension. 143
Differential equation of heat flow for energy generated within the medium.

CHAPTER 14

Solutions of the Heat-Flow Differential Equation 146
Generalized integral equation is solution of heat-flow equation of Chap. 13 — analogy between heat flow and electrical transmission line of series inductances, series generators and shunt conductances — specific application to currents induced in: plate of infinite thickness, plate of finite thickness — general design curves for heating metals by induced currents — temperature distribution related to time, thickness, electrical characteristics of metals, and frequency of induced currents.

CHAPTER 15

Elementary Applications of the Heat-Flow Equations 166
Application of descriptive curves of Chap. 14 to: sealing collapsible metal tubes, detonating explosive rivets.

CHAPTER 16

Case Hardening of Steel 173
Relative permeability with high magnetic intensities — skin thickness of steel — thermal constants of iron and steel — temperature distribution in very thick plates as a function of frequency and power

PAGE

concentration — surface hardening of steel by self quenching — heating effect in thin metallic layers — self quenching by scanning — a mathematical formulation of the scanning problem — surface temperature as a function of scanning speed and power — surface temperature as a function of conductor height — a nomograph for determining surface temperature — control of depth of hardening — effect of frequency on scanning efficiency.

CHAPTER 17

Radio-Frequency Heating of Poor Electrical Conductors. 206

Conduction of currents in metals — dielectric losses in solids — measurements of dielectric properties of solids by means of a Q-meter — measurements of dielectric properties of liquids with a Q-meter — the concentric transmission-line method of determining dielectric properties— Debye's relation and the equivalent circuit of polar liquids.

CHAPTER 18

Heat-Flow Problems in Wood-Gluing Presses. 234

Two hot plates — temperature distribution in the wood as a function of time and thickness — energy absorbed by the wood. One hot plate and one cold plate — temperature distribution in the wood as a function of time and thickness — energy absorbed by the wood. Radio-frequency heating with cold plates — assumptions established — mathematical solution for temperature at any point (transmission-line analogy) — temperature distribution in the wood as a function of time and thickness — some specific examples of radio-frequency heating applications. Hot plates and radio-frequency heating — temperature distribution in the wood — methods of supplying heat energy to plates at radio-frequency potential.

CHAPTER 19

Some Specific Press Problems 264

Relationship of power concentration, voltage gradient, and dielectric properties in radio-frequency gluing — methods of coupling to a press — elimination of standing waves on long presses.

CHAPTER 20

A Radio-Frequency Sewing Machine 280

Comparison of hot-plate and radio-frequency heating — an experimental sewing machine — power requirements — bar sealing — special sewing machine attachments — categories of use for this sewing machine.

PAGE

CHAPTER 21

Electrodes of Special Shapes 298
Equipotential surfaces — electrodes for cylindrical loads — power absorbed by cylinder — effect of air space — electrodes for irregular loads — coupling to thin sheets.

CHAPTER 22

Radio-Frequency Dehydration 307
Radio-frequency drying in a reduced atmosphere — power requirements for drying — rayon drying — penicillin dehydration — penicillin activity or potency — initial experiments with radio-frequency heating — a radio-frequency bulk reducer for penicillin — drying in the final container — electrical conductivity of penicillin — application of radio-frequency heating to other pharmaceuticals — the spinning-cup principle applied to a continuous bulk concentrator.

CHAPTER 23

Pasteurization and Sterilization. 328
Radio-frequency treatment of infested products — pasteurization of milk — pasteurization of beer — the effect of the electric field on micro-organisms.

CHAPTER 24

The Treatment of Food by Radio-Frequency Power. 343
Cooking — destroying mold spores in bread — roasting coffee — thawing frozen vegetables — electrical characteristics of a box of frozen spinach — blanching vegetables — heating pork roll for destruction of trichina organisms.

APPENDIX A

A Means for Finding the Complete Solution to the Differential Equation (14.07) 353

APPENDIX B

The Operational Solution of Equation (18.21) 355

APPENDIX C

The Solution of the Integral Appearing in the Scanning Equation. . . 359

Index 365

LIST OF TABLES

TABLE PAGE

1 Tabulation of the Functions ber(x), bei(x), ber$'(x)$ and bei$'(x)$ . . 18

2 Resistance and Reactance per Centimeter of Length of a Copper Cylinder 1 Centimeter in Diameter 23

3 Field Relations at the Surface of a Metal Conductor 54

4 Single Turn Coil around a Steel Bar 86

5 Data Pertaining to Microphotographs of Brass 120

6 The Results of Annealing Brass Cups 124

7 The Effect of Power and Temperature on the Annealing of Brass . 128

8 Test Results on Bronze Samples 134

9 Thermal Constants of Representative Materials 150

10 Specific values of the Function $f(\theta,x)$ 159

11 Relation between the Measured Ratio $\mathcal{R}$ and the Parameter m . . 225

12 Correction Factor for Finding the Half-Wave Length in the Dielectric 225

13 Voltage Distribution Calculated from the Equivalent Circuit Compared with the Measured Distribution. 233

14 Heating Time of Wood in a Hot-Plate Press 239

15 Energy Absorbed by Wood Placed in a Press with Two Hot Plates. 244

16 The Temperature of a Glue-Line at $x = b/14$ as a Percentage of the Temperature at the Center for Several Heating Times . . . 253

17 The Ratio of Temperature Increments at the Center, with and without Plate Losses; the Ratio of Power Requirements to Attain a Specified Center Temperature with and without Plate Losses, in Terms of Various Heating Times and Thicknesses. These Curves Apply to Wood Heated by Radio Frequency in a Press with Plates Remaining at Room Temperature 255

TABLE PAGE

18 Comparison of Radio-Frequency Heating with Hot-Plate Heating. For Radio-Frequency Heating the Press Plates Remained at 80° F. For Hot Plate Heating the Plates were Maintained at 400° F 258

19 Physical Properties of Typical Thermoplastic Materials 282

20 Test Results on Milk Supply *X* 335

21 Test Results on Milk Supply *Y*. 336

22 Plate Counts of Unfiltered Beer 339

23 Electrical Properties of Box of Frozen Spinach versus Frequency, When the Temperature is −32° C 346

24 Electrical Properties of Box of Frozen Spinach versus Frequency, When the Temperature is −7° C 346

25 Electrical Properties of Box of Frozen Spinach versus Temperature, When the Frequency is 40 Megacycles 347

26 Electrical Properties of Box of Spinach versus Frequency, When the Temperature is +20° C 347

27 Coupling Efficiency in the Induction Heating of Pork Roll . . . 350

28 Temperature Distribution in Induction-Heated Pork Roll. 350

Chapter 1

AXIAL CURRENT FLOW IN CYLINDRICAL CONDUCTORS

It is the purpose of this chapter to examine a simple problem of current flow through a conducting cylinder, and to show the ways in which this current distribution is affected by a number of factors; principally the physical properties of the material, but also the frequency of oscillation of the applied voltage.

Before proceeding with a detailed discussion of the current distribution, it seems desirable to say a few words concerning the electrical constants of materials. Let us examine a cube of material which is 1 centimeter on a side. If two opposite faces of the cube are coated with a good metallic conductor, and the admittance (reciprocal of impedance) is measured between these two plates, it will be found that, in general, the admittance consists of a conductive term and a susceptive term. Thus, the equivalent circuit corresponds to that shown in Fig. 1, a resistance shunted by a capacitance.

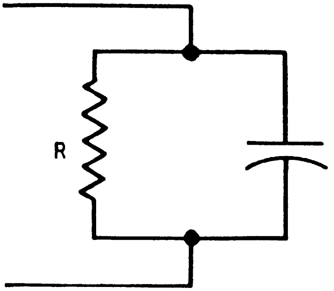

FIG. 1. Equivalent circuit for a cube of material.

For this cube the admittance may be written as*

$$\mathbf{Y} = \frac{1}{R} + j\omega C, \tag{1.01}$$

where R is in ohms, C is in farads and $\omega = 2\pi f$, with f, the frequency, given

---

[*] Throughout the text, the authors have used complex-number symbolism when treating sinusoidally-varying functions. Bold-face italics indicate a phasor quantity, thus $\boldsymbol{H}$; while the absolute values of phasor quantities are indicated by simple italics, H. The absolute magnitudes of voltage and current phasors are to be considered as r.m.s. values.

in cycles per second. Here the resistance R is that of a 1-centimeter cube so that $\frac{1}{R}$ actually represents the conductivity σ, in mho-centimeters, of the material between the conducting plates.

In measuring the capacity C it is assumed that there are no edge effects and that all the flux between the plates passes through the cube of material under examination. This condition can be fulfilled by choosing the cube at the center of a capacitor composed of very large conducting plates separated by a 1-centimeter thickness of the material in question. In free space the capacity of an imaginary centimeter-cube is 8.85×10^{-14} farad which is the permittivity, p_0, of free space. When a material of dielectric constant ϵ is included between the plates the capacity of the unit-cube becomes

$$C = p_0\epsilon = p \text{ farads}, \tag{1.02}$$

where p is the permittivity of the material between the plates. We can then express the admittance of the cube as

$$Y = \sigma + j\omega p. \tag{1.03}$$

The actual values of σ and p that apply to a set of experimental conditions depend to some extent upon the frequency at which measurement is made.

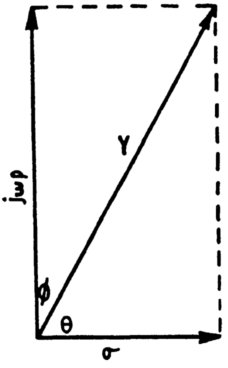

FIG. 2. Admittance diagram of a complex capacitor.

If an alternating voltage V is applied across the network of Fig. 1 the current I that will flow is given by

$$\begin{aligned} I &= VY \\ &= V(\sigma + j\omega p) \end{aligned} \tag{1.04}$$

The admittance of the capacitor is complex and can be represented pictorially as shown in Fig. 2. Changes in the conductivity of the material between the plates will be reflected in this diagram by a change in angle θ. Also, the power absorbed by the network in Fig. 1 is dependent on the conductivity of the shunting resistor. Hence, the ratio of σ to the total admittance Y is actually a measure of the "power factor" of the circuit. From Fig. 2 this ratio is seen to be $\sigma/Y = \cos\theta$ so that we may write

$$\text{Power factor} = \frac{\sigma}{\sqrt{\sigma^2 + (\omega p)^2}}. \tag{1.05}$$

Dividing numerator and denominator by ωp yields

$$\text{Power factor} = \frac{\dfrac{\sigma}{\omega p}}{\sqrt{\left(\dfrac{\sigma}{\omega p}\right)^2 + 1}}. \tag{1.06}$$

In a capacitor with a good dielectric there is little leakage current. This is equivalent to saying that σ is very small — particularly with reference to ωp. Thus the denominator in (1.06) approaches unity, and to a close approximation,

$$\text{Power factor} = \frac{\sigma}{\omega p}. \tag{1.07}$$

Fig. 2 defines this relationship as the cotangent θ or the tangent ϕ, where ϕ is commonly designated the "loss angle" of a capacitor. In a capacitor with a perfect dielectric, σ is zero, so that its power factor, from (1.06) or (1.07) is zero. Under this condition the current leads the voltage by exactly 90° and the loss angle ϕ is zero. Evidently, then, the loss angle ϕ represents the angular departure of a capacitor from perfection.

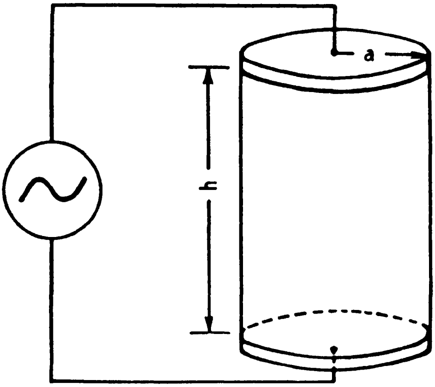

Fig. 3. The cylindrical section has a voltage impressed between opposite ends.

As the conductivity of the material between the plates of the capacitor increases, the term $(\sigma/\omega p)^2$ in (1.06) becomes very large and the power factor approaches unity for its value. For a generalized study of the behavior of a material in an electric field, choose a right circular cylindrical section of the material having a length h and a radius a as shown in Fig. 3. The ends are covered with highly conducting metallic plates and a voltage V is impressed across these plates at the ends of the cylinder. If we assume that no fringing occurs at the edges of the conducting plates then currents will flow axially through the cylinder. The current density, as well as the electric and magnetic field intensities, will have axial symmetry, and thus we need to consider only the variation of these quantities as a function of distance from the center of the cylinder.

If we now slice a disc from the cylinder and look down on the disc from above, we have the situation shown in Fig. 4, where the electric intensity vectors point out of the paper. The total current flowing out of the paper through the area covered by the ring which has an infinitesimal width dr is

$$\boldsymbol{E}(\sigma + j\omega p)2\pi r \cdot dr, \tag{1.08}$$

where $\boldsymbol{E}$ is the mean value of electric intensity across the ring. Actually, the electric intensity $\boldsymbol{E}$ is a function of the radius as will later be shown but it will be of equal magnitude at all points of equal radius around the ring.

The current flowing through the ring of Fig. 4 is the difference between the total current enclosed by the outer circumference and that enclosed by the inner circumference. These currents may be found by taking the line integral of the magnetic intensities $\boldsymbol{H}$ and $\boldsymbol{H} + (d\boldsymbol{H}/dr)dr$, respectively, along the inner and outer boundaries of the ring, and hence, the current in the ring is given by

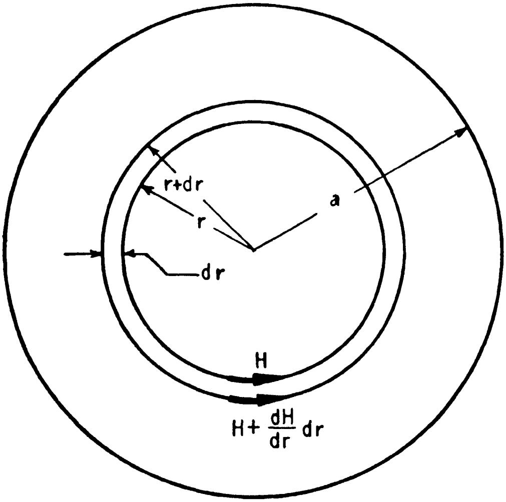

FIG. 4. A slice is taken across the cylinder. The electric field intensity points out of the paper.

$$2\pi(r + dr)\left(\boldsymbol{H} + \frac{d\boldsymbol{H}}{dr}dr\right) - 2\pi r\boldsymbol{H} = \boldsymbol{E}(\sigma + j\omega p)2\pi r \cdot dr. \tag{1.09}$$

By dropping second order differentials, this equation becomes

$$\frac{d\boldsymbol{H}}{dr} + \frac{\boldsymbol{H}}{r} = \boldsymbol{E}(\sigma + j\omega p). \tag{1.10}$$

In Fig. 5 a vertical plane is passed through the axis of the cylinder and a small patch of width dr and height dz is examined. Setting the line integral of electric intensity around this patch equal to the negative time rate of change of the magnetic flux through the patch we write:

$$\left(\mathbf{E} + \frac{d\mathbf{E}}{dr}\,dr\right)dz - \mathbf{E}\cdot dz = j\omega\mu\mathbf{H}\cdot dr\cdot dz, \qquad (1.11)$$

or

$$\frac{d\mathbf{E}}{dr} = j\omega\mu\mathbf{H}. \qquad (1.12)$$

When (1.12) is solved for $\mathbf{H}$ and substituted in (1.10), a differential equation in terms of the electric intensity $\mathbf{E}$ alone is obtained.

$$\frac{d^2\mathbf{E}}{dr^2} + \frac{1}{r}\frac{d\mathbf{E}}{dr} - \mathbf{E}[j\omega\mu(\sigma + j\omega p)] = 0. \qquad (1.13)$$

This is a Bessel differential equation, having the general solution

$$\mathbf{E} = AJ_0(\mathbf{m}r) + BK_0(\mathbf{m}r). \qquad (1.14)$$

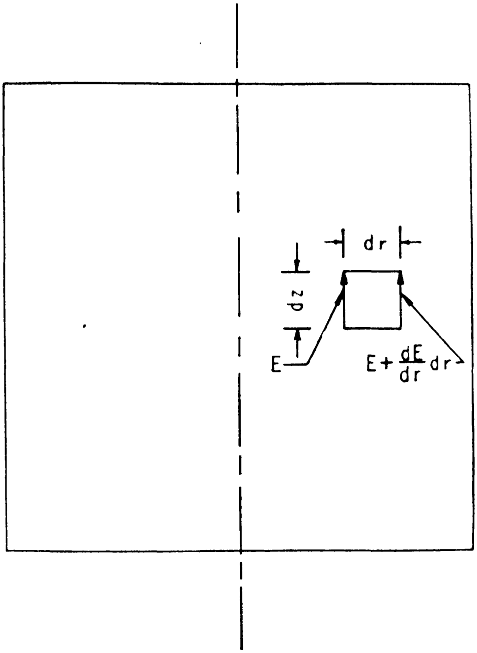

FIG. 5. A slice taken in a vertical plane through the cylinder is used to set up the equation (1.11). The magnetic intensity through the patch points into the page.

Here A and B are arbitrary constants; $J_0(\mathbf{m}r)$ is a Bessel function of the first kind and zeroth order; $K_0(\mathbf{m}r)$ is a Bessel function of the second kind and zeroth order, and

$$\mathbf{m}^2 = -j\omega\mu(\sigma + j\omega p). \qquad (1.15)$$

Since $K_0(\mathbf{m}r)$ becomes infinite as r approaches zero,* we may drop this function from the solution. Then (1.14) reduces to the simple form

$$\mathbf{E} = AJ_0(\mathbf{m}r). \qquad (1.16)$$

---

* E. Jahnke and F. Emde, *Tables of Functions with Formulae and Curves*, 3d revised Ed. (B. G. Teubner, 1938), G. E. Stechert and Company, New York, p. 131.

The Bessel function $J_0(mr)$ has the form of an infinite series, and is tabulated in many places,*

$$J_0(mr) = 1 - \frac{(mr)^2}{2^2} + \frac{(mr)^4}{2^2 \cdot 4^2} - \frac{(mr)^6}{2^2 \cdot 4^2 \cdot 6^2} + \frac{(mr)^8}{2^2 \cdot 4^2 \cdot 6^2 \cdot 8^2} - \cdots. \quad (1.17)$$

It may be readily seen that $J_0(mr)$ is equal to unity when r is zero. If the electric intensity on the axis ($r = 0$) is called E_0, the electric intensity at any point a distance r from the axis is

$$E = E_0 J_0(mr). \quad (1.18)$$

We may now obtain the magnetic intensity at any point in the material by substituting (1.18) in (1.12). However, an examination of the derivative of the Bessel function $J_0(mr)$ is a necessary preliminary step.

Differentiating (1.17) yields

$$\frac{d}{dr} J_0(mr) = -m\left[\frac{(mr)}{2} - \frac{(mr)^3}{2^2 \cdot 4} + \frac{(mr)^5}{2^2 \cdot 4^2 \cdot 6} - \frac{(mr)^7}{2^2 \cdot 4^2 \cdot 6^2 \cdot 8} + \cdots\right]. \quad (1.19)$$

In (1.19) the series expression within the bracket is known as the Bessel function of the first kind and first order; and is written as $J_1(mr)$. Thus (1.19) may be written as $\frac{d}{dr} J_0(mr) = -mJ_1(mr)$.

Now, we are prepared to rewrite (1.12) in terms of (1.18) and find the magnetic intensity to be

$$H = \frac{-mE_0 J_1(mr)}{j\omega\mu} \quad (1.20)$$

The total current flowing in the cylinder of radius a is

$$I_T = 2\pi a H_{r=a} = \frac{-2\pi m a E_0 J_1(ma)}{j\omega\mu}. \quad (1.21)$$

The electric intensity at the surface of the cylinder, that is, the voltage per unit length along the surface of the cylinder, is readily obtained from (1.18).

$$E_{r=a} = E_0 J_0(ma). \quad (1.22)$$

By dividing (1.21) into (1.22), we obtain the impedance for a unit length of cylinder.

$$Z(\text{ohms per unit length}) = \frac{-j\omega\mu J_0(ma)}{2\pi m a J_1(ma)}. \quad (1.23)$$

---

* E. Jahnke and F. Emde, *loc. cit.*, p. 128.

The total impedance may be computed by multiplying the impedance per unit length by the total length of the cylinder.

Up to this point, the equations have been derived with great generality. The analysis has been carried through in such a way that it may be applied to any material, a good conductor, a poor conductor, or a perfect insulator. At this stage the investigation may conveniently be separated into four categories by examining the behavior of:

1. A perfect insulator.
2. A dielectric material with very low power factor.
3. A dielectric material with high power factor.
4. A good conductor.

In this way the whole range of characteristics associated with radio-frequency heating may be displayed.

1. A Perfect Insulator. A perfect insulator would not be heated by the passage of current, but an examination of the distribution of electric field yields results which help in evaluating the problems of heating dielectric materials with very low power factors.

If the cylinder is composed of a material which is a perfect insulator, the conductivity term in (1.15) becomes zero. Also, for materials which may be classified as poor conductors, it is safe to state that magnetic properties will not be exhibited, and the permeability will be that of free space (μ_0). Then (1.15) becomes

$$m = \omega\sqrt{\mu_0 p} = \frac{2\pi f}{3 \cdot 10^{10}}\sqrt{\epsilon}. \tag{1.24}$$

Since the velocity of radio waves in free space is $3 \cdot 10^{10}$ centimeters per second, the wavelength in free space, λ_0, is

$$\lambda_0 = \frac{3 \cdot 10^{10}}{f}, \tag{1.25}$$

where the wavelength is measured in centimeters, and the frequency is expressed in cycles.* Thus

$$m = \frac{2\pi}{\lambda_0}\sqrt{\epsilon}. \tag{1.26}$$

From (1.18), the electric intensity through the cylinder is

$$E = E_0 J_0\left(\frac{2\pi r}{\lambda_0}\sqrt{\epsilon}\right). \tag{1.27}$$

---

* Although it is strictly correct to speak of the frequency in terms of "cycles per second," long usage and standardization have led to the use of other units. One *kilocycle* is equal to one thousand cycles per second, and one *megacycle* is equal to one million cycles per second. This terminology will be followed unless otherwise specified.

Fig. 6 shows the distribution of electric intensity as a function of the quantity $\frac{r}{\lambda_0}\sqrt{\epsilon}$. It is interesting to note that the electric intensity may go to zero at certain places in the dielectric and may even reverse completely in phase, so that at any given instant, current may be flowing upward in one annular ring while it is flowing downward through another.

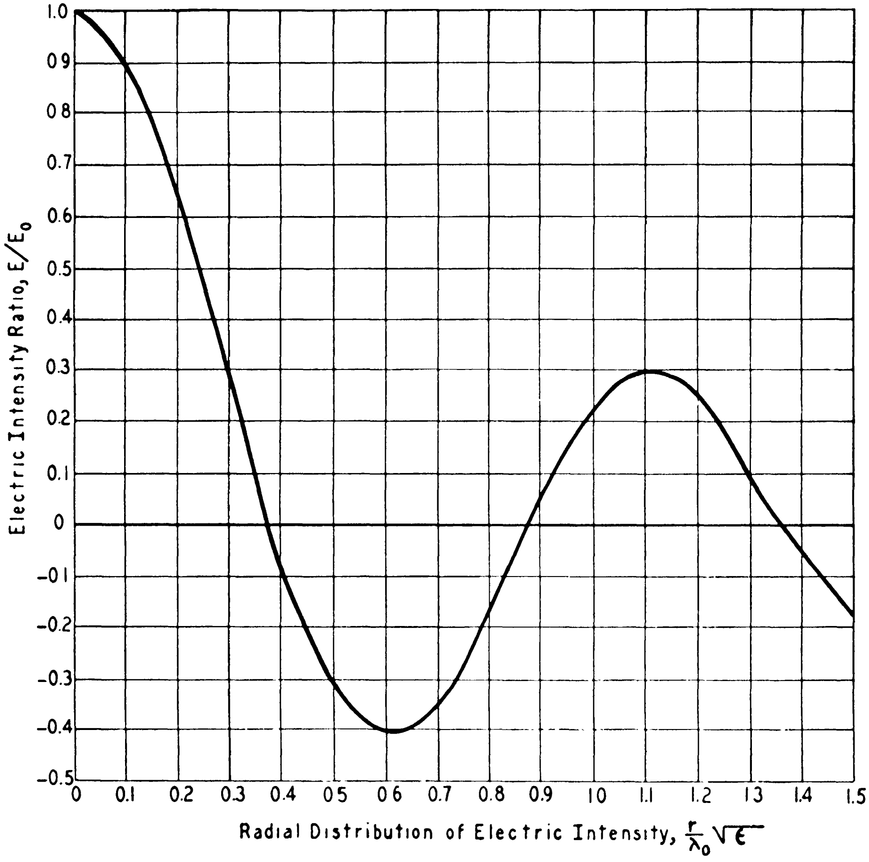

FIG. 6. Electric intensity distribution in dielectric cylinders.

The diagram of Fig. 6 may be used as a master from which distribution for specific cases can be constructed. Fig. 7 shows the distribution of electric intensity as a function of distance from the center of a cylinder, where the cylinder has a radius of 50 centimeters and the material has a dielectric constant of 2. The curves have been plotted for a number of frequencies. It may be seen that the distribution is essentially uniform when the frequency is 10 megacycles or less. For higher frequencies, the intensity drops off near the outer part of the cylinder. At 200 megacycles the electric field near the surface of the cylinder is directly out of phase with the electric field in the center of the cylinder.

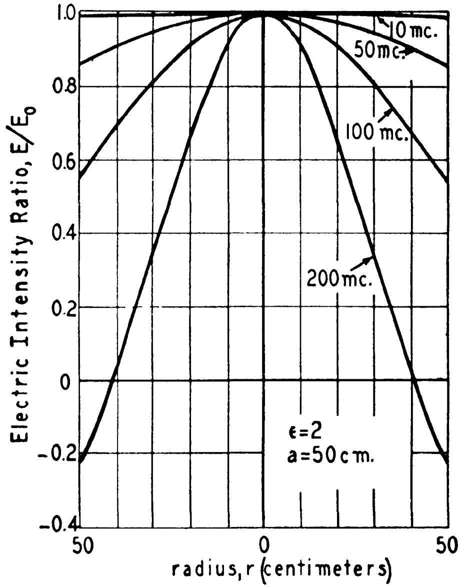

FIG. 7. Electric intensity distribution through a dielectric cylinder for a number of frequencies. The dielectric constant is 2.

Fig. 8 shows similar distributions where the cylinder with a radius of 50 centimeters now has a dielectric constant of 81. It may be seen that for this example, the frequency must be 1 megacycle or less for uniform field distribution.

The impedance per unit length of perfect insulator may be found by substituting (1.24) into (1.23) and remembering that

$$\sqrt{\frac{\mu_0}{p_0}} = 120\pi. \tag{1.28}$$

Then, with the help of (1.26), (1.23) becomes

$$\boldsymbol{Z}(\text{ohms per centimeter}) = \frac{-j60}{a\sqrt{\epsilon}}\,\frac{J_0\left(\dfrac{2\pi a}{\lambda_0}\sqrt{\epsilon}\right)}{J_1\left(\dfrac{2\pi a}{\lambda_0}\sqrt{\epsilon}\right)}. \tag{1.29}$$

Fig. 9 shows the reactance of a slab of dielectric material of thickness 1 centimeter and radius 50 centimeters. The dielectric constant is 2. At very low frequencies, the reactance is capacitive but the change to an inductive reactance soon takes place. The reactance variation is similar to that found at the input terminals of a transmission line which is open-circuited at the far end.

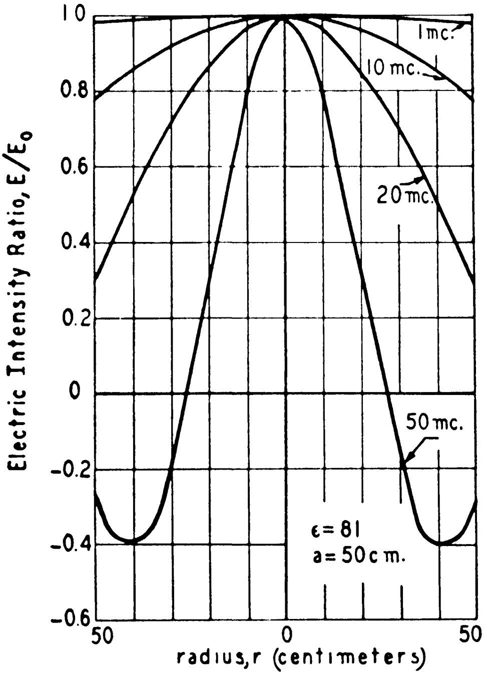

FIG. 8. The dielectric constant is now 81, so that uneven distributions occur at lower frequencies.

When the radius a is very small or when the frequency of the applied voltage is low, the Bessel function $J_0\left(\frac{2\pi a}{\lambda_0}\sqrt{\epsilon}\right)$ approaches unity, and $J_1\left(\frac{2\pi a}{\lambda_0}\sqrt{\epsilon}\right)$ is approximated by $\frac{\pi a}{\lambda_0}\sqrt{\epsilon}$. Then (1.29) becomes

$$Z = -j\frac{60\lambda_0}{\pi a^2 \epsilon}, \tag{1.30}$$

but

$$60\lambda_0 = \frac{2\pi \cdot 3 \cdot 10^{10} \cdot 60}{2\pi f} = \frac{1}{\omega p_0},$$

so that (1.30) may be written

$$Z = \frac{-j}{\omega \pi a^2 p_0 \epsilon}, \tag{1.31}$$

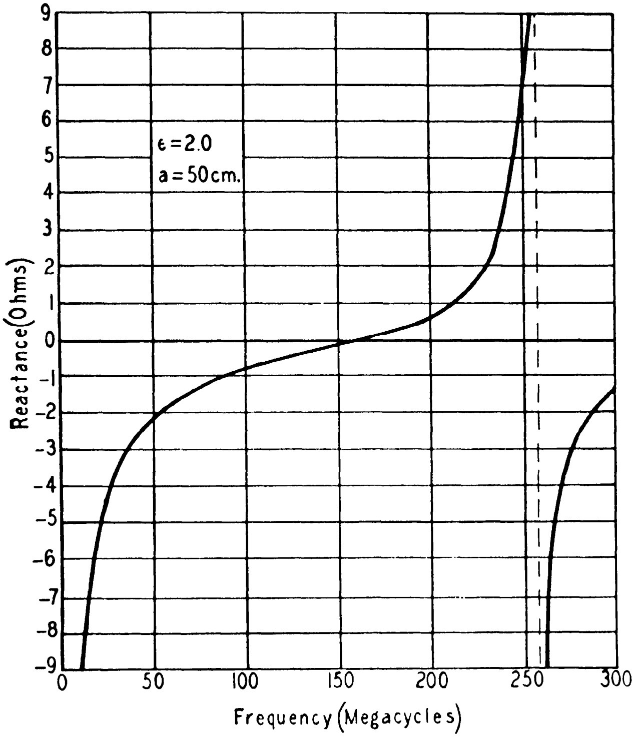

FIG. 9. The reactance of a slab of dielectric material of thickness 1 centimeter and radius 50 centimeters.

or the reciprocal of the impedance (the admittance) is given by

$$Y = j\omega \pi a^2 p_0 \epsilon. \tag{1.32}$$

By reference to (1.02) the term $\pi a^2 p_0 \epsilon$ in (1.31) and (1.32) is identified as the low-frequency or electrostatic capacity between two plates of radius a separated by a dielectric medium 1 centimeter thick having a dielectric constant ϵ. We have here shown that the more detailed analysis which was concluded in (1.29) and which takes into account high-frequency effects, degenerates to the well-known relations of (1.31) and (1.32) when the frequency is low. The solid curve of Fig. 10 shows the true admittance calculated from (1.29), while the broken curve shows the approximation expressed by (1.32).

2. A Dielectric Material with Very Low Power Factor. If the material which constitutes the cylinder has a very low power factor, ($\sigma \ll \omega p$), (1.15) may be written (assuming $\mu = \mu_0$),

$$m^2 = \omega^2 \mu_0 p_0 \epsilon \left(1 - j\frac{\sigma}{\omega p_0 \epsilon}\right) = \left(\frac{2\pi}{\lambda_0}\sqrt{\epsilon}\right)^2 (1 - j\Delta), \tag{1.33}$$

where Δ is the power factor, a number small compared to unity. [c.f. (1.07).] When (1.33) is substituted into (1.17) and all terms which contain the square or higher powers of Δ are dropped, the electric intensity distribution given by (1.18) is

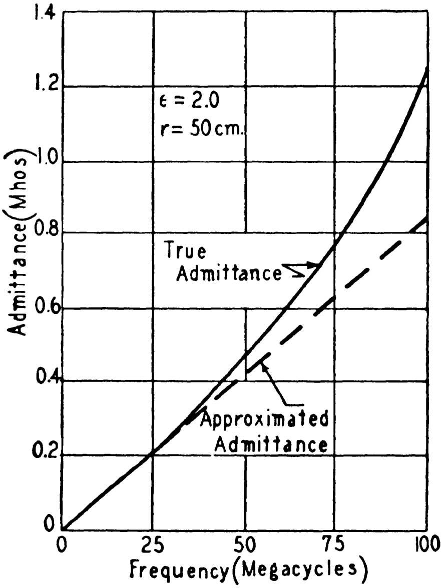

FIG. 10. The admittance of a slab of dielectric material of thickness 1 centimeter and radius 50 centimeters. The solid curve is the true admittance, while the broken curve is the approximation of (1.32).

$$E = E_0 \left[J_0\left(\frac{2\pi r}{\lambda_0}\sqrt{\epsilon}\right) + j\Delta \left(\frac{\pi r}{\lambda_0}\sqrt{\epsilon}\right) J_1 \left(\frac{2\pi r}{\lambda_0}\sqrt{\epsilon}\right)\right]. \tag{1.34}$$

If it is remembered that Δ is small, the observation may be made that (1.34) is, for all practical purposes, the same as (1.27), the distribution of electric intensity in a perfect dielectric. The electric intensity distribution will be very similar to the distribution shown in Fig. 6, except that the last term in (1.34) prevents the field from going to zero at the points shown in Fig. 6.

This observation permits the use of a device familiar to the circuit engineer. That is, in low-loss systems, the power dissipated may be computed with a high degree of accuracy by first calculating the voltages (or currents) throughout the system on the assumption of zero loss, and then finding the power dissipated if the same distribution of voltages prevailed when the materials become slightly conducting.

On this basis, the power per unit volume generated in the material at any point a distance r from the center is

$$P(\text{watts per cubic centimeter}) = \sigma E^2 = \sigma E_0{}^2 J_0{}^2\left(\frac{2\pi r}{\lambda_0}\sqrt{\epsilon}\right). \qquad (1.35)$$

The total power P_T generated in a cylinder 1 centimeter long and of radius a centimeters is

$$P_T = \int_{r=0}^{r=a} 2\pi r\sigma E^2 dr = \frac{2\pi\sigma E_0{}^2}{(2\pi\sqrt{\epsilon}/\lambda_0)^2}\int_{x=0}^{x=\frac{2\pi a}{\lambda_0}\sqrt{\epsilon}} xJ_0{}^2(x)dx, \qquad (1.36)$$

or

$$P_T = \pi a^2\sigma E_0{}^2\left[J_0{}^2\left(\frac{2\pi a}{\lambda_0}\sqrt{\epsilon}\right) + J_1{}^2\left(\frac{2\pi a}{\lambda_0}\sqrt{\epsilon}\right)\right]. \qquad (1.37)$$

Since the volume of this cylinder 1 centimeter in length is πa^2, the average power per cubic centimeter is

$$P_{av} = \sigma E_0{}^2\left[J_0{}^2\left(\frac{2\pi a}{\lambda_0}\sqrt{\epsilon}\right) + J_1{}^2\left(\frac{2\pi a}{\lambda_0}\sqrt{\epsilon}\right)\right]. \qquad (1.38)$$

Then the actual power distribution in terms of the average power density is obtained by dividing (1.35) by (1.38).

$$\frac{P}{P_{av}} = \frac{J_0{}^2\left(\frac{2\pi r}{\lambda_0}\sqrt{\epsilon}\right)}{J_0{}^2\left(\frac{2\pi a}{\lambda_0}\sqrt{\epsilon}\right) + J_1{}^2\left(\frac{2\pi a}{\lambda_0}\sqrt{\epsilon}\right)}. \qquad (1.39)$$

To visually present the effect of this relation, the curves of Fig. 11 have been constructed by the use of (1.39). Here the cylinder is considered to have a radius of 50 centimeters, while the material has a dielectric constant of 2. It is readily seen that a frequency of 10 megacycles yields a substantially uniform generation of energy, while at 50 and 100 megacycles, the energy generated at the center is considerably in excess of the energy generated at some distance from the center.

In many plastic-heating problems, it is desirable to heat uniformly. Therefore, the generation of heat must be substantially the same throughout the mass. If we set, as an arbitrary objective, the condition that the power generated per cubic centimeter at the center is not to exceed the power density near the surface by more than five per cent, an upper limit on the frequency to be used is given by the relation

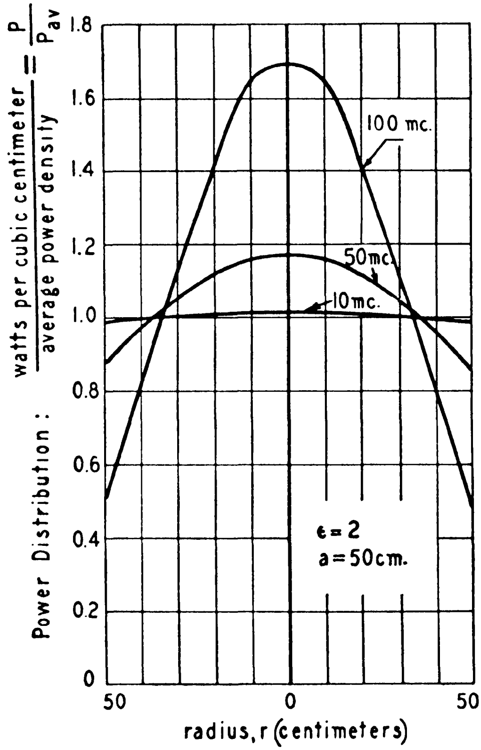

FIG. 11. Power distribution through a dielectric cylinder.

$$f_{megacycles} = \frac{1482}{a_{cm}\sqrt{\epsilon}} = \frac{584}{a_{inches}\sqrt{\epsilon}}. \qquad (1.40)$$

3. A Dielectric Material with High Power Factor. The problem of obtaining numerical results for a material which has a rather high power factor is more difficult because of the absence of tables of functions which describe the action. To gain an insight into the picture, we shall examine the field distribution in a material which has a power factor angle of 45 degrees, that is, $\sigma = \omega p$ in (1.15). Then (assuming $\mu = \mu_0$),

$$m^2 = \omega^2 \mu_0 p_0 \epsilon (1 - j) = \left(\frac{2\pi}{\lambda_0}\sqrt{\epsilon}\right)^2 (1 - j). \tag{1.41}$$

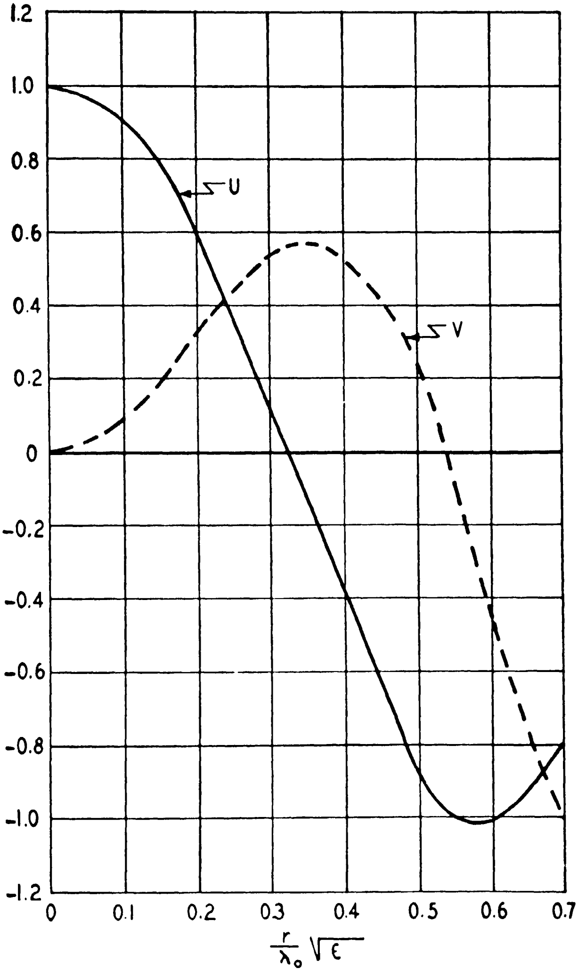

FIG. 12. A plot of the functions U and V used in (1.42).

When this value of m^2 is substituted into (1.18), with the aid of (1.17), the electric field intensity distribution is of the form:

$$\boldsymbol{E} = E_0(U + jV), \tag{1.42}$$

where

$$U = 1 - \frac{\left(\frac{2\pi r}{\lambda_0}\sqrt{\epsilon}\right)^2}{2^2} + \frac{2\left(\frac{2\pi r}{\lambda_0}\sqrt{\epsilon}\right)^6}{2^2 \cdot 4^2 \cdot 6^2} - \frac{4\left(\frac{2\pi r}{\lambda_0}\sqrt{\epsilon}\right)^8}{2^2 \cdot 4^2 \cdot 6^2 \cdot 8^2} + \frac{4\left(\frac{2\pi r}{\lambda_0}\sqrt{\epsilon}\right)^{10}}{2^2 \cdot 4^2 \cdot 6^2 \cdot 8^2 \cdot 10^2} - \cdots, \tag{1.43}$$

and

$$V = \frac{\left(\frac{2\pi r}{\lambda_0}\sqrt{\epsilon}\right)^2}{2^2} - \frac{2\left(\frac{2\pi r}{\lambda_0}\sqrt{\epsilon}\right)^4}{2^2 \cdot 4^2} + \frac{2\left(\frac{2\pi r}{\lambda_0}\sqrt{\epsilon}\right)^6}{2^2 \cdot 4^2 \cdot 6^2} - \frac{4\left(\frac{2\pi r}{\lambda_0}\sqrt{\epsilon}\right)^{10}}{2^2 \cdot 4^2 \cdot 6^2 \cdot 8^2 \cdot 10^2} + \frac{8\left(\frac{2\pi r}{\lambda_0}\sqrt{\epsilon}\right)^{12}}{2^2 \cdot 4^2 \cdot 6^2 \cdot 8^2 \cdot 10^2 \cdot 12^2} - \cdots. \tag{1.44}$$

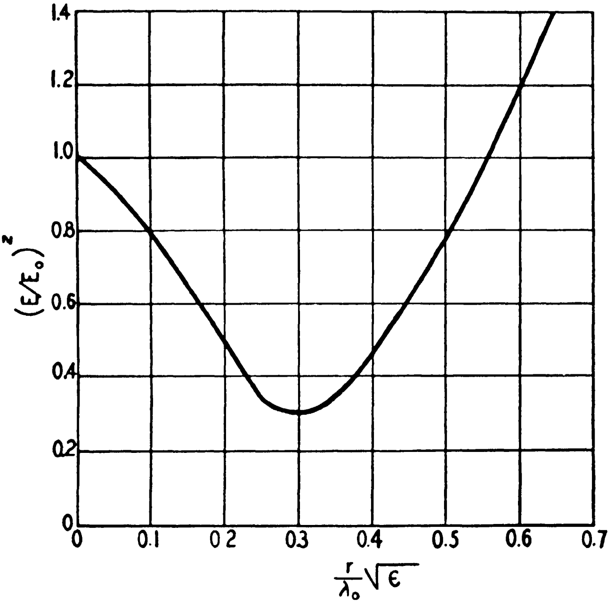

FIG. 13. $(E/E_0)^2 = U^2 + V^2$.

Fig. 12 shows U and V as functions of $\frac{r}{\lambda_0}\sqrt{\epsilon}$. An examination of this diagram reveals that (1.42) yields results somewhat similar to (1.34) with Δ set equal to unity. The correspondence is, however, far from exact. Since the power generated per cubic centimeter is proportional to the square of the electric intensity, the plot of $U^2 + V^2$ shown in Fig. 13 may be regarded as showing the distribution of energy generation. If the quantity $\frac{r}{\lambda_0}\sqrt{\epsilon}$ is less than 0.2, the distribution is essentially the same as it was for the case of a material with very low power factor, and the limiting relation of (1.40) applies.

4. A Good Conductor. In the case of a very good conductor, the conductance current is extremely large in comparison to the capacitive current. This is the equivalent of stating that in (1.15) we may drop the term ωp. However, it cannot be assumed that the relative permeability of all good conductors will be identically equal to unity, so that μ must be retained.

Then (1.15) becomes:

$$m^2 = -j\omega\mu\sigma = -j2\pi f\mu\sigma. \tag{1.45}$$

At this point, it is advantageous to introduce a new symbol, s, which may be called the *skin thickness*, where

$$s = \frac{1}{\sqrt{\pi\mu\sigma f}} = \frac{1}{2\pi\sqrt{10^{-9}\mu_r\sigma f}}. \tag{1.46}$$

Since the conductivity is measured in mhos per centimeter cube and the frequency is expressed in cycles, the skin thickness will be given in centimeters.

From (1.45) and (1.46)

$$m = \sqrt{-j}\cdot\frac{\sqrt{2}}{s} \tag{1.47}$$

and (1.18) yields

$$E = E_0J_0\left(\sqrt{-j}\cdot\frac{\sqrt{2}\,r}{s}\right). \tag{1.48}$$

We shall digress to examine the special type of Bessel function which occurs as a result of the complex argument. From the definition of the Bessel function of the first kind and zeroth order, as in (1.09), the complex argument yields:

$$J_0(\sqrt{-j}\,x) = 1 + j\frac{x^2}{2^2} - \frac{x^4}{2^2\cdot 4^2} - j\frac{x^6}{2^2\cdot 4^2\cdot 6^2} + \frac{x^8}{2^2\cdot 4^2\cdot 6^2\cdot 8^2}$$
$$+ j\frac{x^{10}}{2^2\cdot 4^2\cdot 6^2\cdot 8^2\cdot 10^2} - \cdots. \tag{1.49}$$

When the real and imaginary terms are separated, two separate series are obtained. The real terms form a series which Kelvin named $\operatorname{ber}(x)$, the real part of the Bessel function, while the other series was called $\operatorname{bei}(x)$, the imaginary part of the Bessel function, where

$$\operatorname{ber}(x) = 1 - \frac{x^4}{2^2 \cdot 4^2} + \frac{x^8}{2^2 \cdot 4^2 \cdot 6^2 \cdot 8^2} - \frac{x^{12}}{2^2 \cdot 4^2 \cdot 6^2 \cdot 8^2 \cdot 10^2 \cdot 12^2} + \cdots \tag{1.50}$$

and

$$\operatorname{bei}(x) = \frac{x^2}{2^2} - \frac{x^6}{2^2 \cdot 4^2 \cdot 6^2} + \frac{x^{10}}{2^2 \cdot 4^2 \cdot 6^2 \cdot 8^2 \cdot 10^2} - \cdots. \tag{1.51}$$

The derivative of (1.50) is

$$\operatorname{ber}'(x) = -\frac{x^3}{2^2 \cdot 4} + \frac{x^7}{2^2 \cdot 4^2 \cdot 6^2 \cdot 8} - \frac{x^{11}}{2^2 \cdot 4^2 \cdot 6^2 \cdot 8^2 \cdot 10^2 \cdot 12} + \cdots, \tag{1.52}$$

while the derivative of (1.51) is

$$\operatorname{bei}'(x) = \frac{x}{2} - \frac{x^5}{2^2 \cdot 4^2 \cdot 6} + \frac{x^9}{2^2 \cdot 4^2 \cdot 6^2 \cdot 8^2 \cdot 10} - \cdots. \tag{1.53}$$

These four functions are tabulated by Jahnke and Emde,[*] Savidge,[†] and Dwight.[‡]

TABLE 1. TABULATION OF THE FUNCTIONS $\operatorname{ber}(x)$, $\operatorname{bei}(x)$, $\operatorname{ber}'(x)$ AND $\operatorname{bei}'(x)$.

x	$\operatorname{ber}(x)$	$\operatorname{bei}(x)$	$\operatorname{ber}'(x)$	$\operatorname{bei}'(x)$
0.0	1.000	0.00	0.00	0.00
0.5	0.999	0.0625	−0.0078	0.2499
1.0	0.9844	0.2496	−0.0624	0.4999
1.5	0.9211	0.5576	−0.2100	0.7302
2.0	0.7517	0.9723	−0.4931	0.9170
2.5	0.3999	1.4571	−0.9436	0.9983
3.0	−0.2214	1.9376	−1.5698	0.8805
3.5	−1.1936	2.2833	−2.3361	0.4353
4.0	−2.5634	2.2927	−3.1347	−0.4911
4.5	−4.2991	1.6859	−3.7537	−2.0526
5.0	−6.2301	0.1160	−3.8442	−4.3538
10.0	138.8405	56.3704	51.373	135.23
20.0	47583.7	11500.8	24325.1	41491.5
∞	∞	∞	∞	∞

---

[*] E. Jahnke and F. Emde, *loc. cit.*, p. 246.

[†] H. G. Savidge, "Tables of the Ber and Bei and Ker and Kei Functions with Further Formulae for Their Computation," *Philosophical Magazine*, Vol. 19, January 1910, pp. 49–58.

[‡] H. B. Dwight, "A Precise Method of Calculation of Skin Effect in Isolated Tubes," *Journal of the American Institute of Electrical Engineers*, Vol. 42, No. 8, August 1923, p. 830.

Returning now to (1.18), the electric intensity throughout the cylinder is

$$\boldsymbol{E} = E_0\left[\operatorname{ber}\left(\frac{\sqrt{2}\,r}{s}\right) + j\operatorname{bei}\left(\frac{\sqrt{2}\,r}{s}\right)\right], \tag{1.54}$$

having an absolute value of

$$E = E_0\sqrt{\left[\operatorname{ber}\left(\frac{\sqrt{2}\,r}{s}\right)\right]^2 + \left[\operatorname{bei}\left(\frac{\sqrt{2}\,r}{s}\right)\right]^2}. \tag{1.55}$$

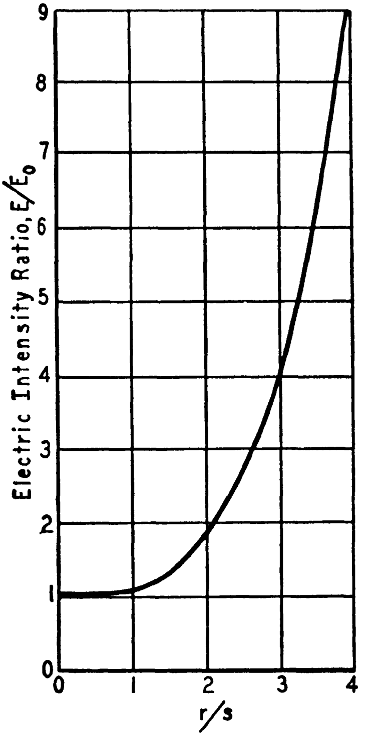

FIG. 14. The electric intensity distribution in a cylinder of high conductivity.

The electric intensity as a function of position from the center of the cylinder is shown by Fig. 14. It may be noted that this is a perfectly general curve, since the position, r, is expressed in terms of the skin thickness, s. Since the current density at any point, measured in amperes per square centimeter, is obtained by simply multiplying the electric intensity by the conductivity, ($E\sigma$), Fig. 14 may be regarded as also showing the current density distribution. The electric intensity (and current density) increases greatly as the point which is being examined moves away from the axis of the cylinder.

The power generated per cubic centimeter is the product of the conductivity and the square of the electric intensity, ($E^2\sigma$), so that it is evident that the power generated in the outer regions of a cylinder of good conductivity greatly exceeds the power generated near the center.

The impedance of this cylinder may be obtained from (1.23) by observing that

$$maJ_1(ma) = -\frac{\sqrt{2}\,a}{s}\left[\operatorname{ber}'\left(\frac{\sqrt{2}\,a}{s}\right) + j\operatorname{bei}'\left(\frac{\sqrt{2}\,a}{s}\right)\right]. \tag{1.56}$$

Then

$$\boldsymbol{Z} = j\frac{\omega\mu s}{2\pi a\sqrt{2}}\,\frac{\operatorname{ber}\left(\frac{\sqrt{2}\,a}{s}\right) + j\operatorname{bei}\left(\frac{\sqrt{2}\,a}{s}\right)}{\operatorname{ber}'\left(\frac{\sqrt{2}\,a}{s}\right) + j\operatorname{bei}'\left(\frac{\sqrt{2}\,a}{s}\right)}. \tag{1.57}$$

This impedance per unit length may be separated into a resistance and a reactance term.

$$\boldsymbol{Z}(\text{ohms per centimeter}) = R_{ac} + jX_{ac} \tag{1.58}$$

where the resistance per unit length is

$$R_{ac} = \frac{\omega\mu s}{2\pi a\sqrt{2}}\,\frac{\operatorname{ber}\left(\frac{\sqrt{2}\,a}{s}\right)\operatorname{bei}'\left(\frac{\sqrt{2}\,a}{s}\right) - \operatorname{bei}\left(\frac{\sqrt{2}\,a}{s}\right)\operatorname{ber}'\left(\frac{\sqrt{2}\,a}{s}\right)}{\left[\operatorname{ber}'\left(\frac{\sqrt{2}\,a}{s}\right)\right]^2 + \left[\operatorname{bei}'\left(\frac{\sqrt{2}\,a}{s}\right)\right]^2} \tag{1.59}$$

and the reactance per unit length is

$$X_{ac} = \frac{\omega\mu s}{2\pi a\sqrt{2}}\,\frac{\operatorname{ber}\left(\frac{\sqrt{2}\,a}{s}\right)\operatorname{ber}'\left(\frac{\sqrt{2}\,a}{s}\right) + \operatorname{bei}\left(\frac{\sqrt{2}\,a}{s}\right)\operatorname{bei}'\left(\frac{\sqrt{2}\,a}{s}\right)}{\left[\operatorname{ber}'\left(\frac{\sqrt{2}\,a}{s}\right)\right]^2 + \left[\operatorname{bei}'\left(\frac{\sqrt{2}\,a}{s}\right)\right]^2} \tag{1.60}$$

The resistance per unit length to direct current is

$$R_{dc} = \frac{1}{\sigma\pi a^2} \tag{1.61}$$

Then dividing (1.59) by (1.61)

$$\frac{R_{ac}}{R_{dc}} = \frac{1}{2}\left(\frac{\sqrt{2}\,a}{s}\right) \frac{\operatorname{ber}\left(\frac{\sqrt{2}\,a}{s}\right) \operatorname{bei}'\left(\frac{\sqrt{2}\,a}{s}\right) - \operatorname{bei}\left(\frac{\sqrt{2}\,a}{s}\right) \operatorname{ber}'\left(\frac{\sqrt{2}\,a}{s}\right)}{\left[\operatorname{ber}'\left(\frac{\sqrt{2}\,a}{s}\right)\right]^2 + \left[\operatorname{bei}'\left(\frac{\sqrt{2}\,a}{s}\right)\right]^2}. \tag{1.62}$$

Dividing (1.60) by (1.61) yields

$$\frac{X_{ac}}{R_{dc}} = \frac{1}{2}\left(\frac{\sqrt{2}\,a}{s}\right) \frac{\operatorname{ber}\left(\frac{\sqrt{2}\,a}{s}\right) \operatorname{ber}'\left(\frac{\sqrt{2}\,a}{s}\right) + \operatorname{bei}\left(\frac{\sqrt{2}\,a}{s}\right) \operatorname{bei}'\left(\frac{\sqrt{2}\,a}{s}\right)}{\left[\operatorname{ber}'\left(\frac{\sqrt{2}\,a}{s}\right)\right]^2 + \left[\operatorname{bei}'\left(\frac{\sqrt{2}\,a}{s}\right)\right]^2}. \tag{1.63}$$

Equations (1.62) and (1.63) are plotted in Fig. 15 as functions of a/s, the radius measured in terms of the skin thickness. It may be seen that the

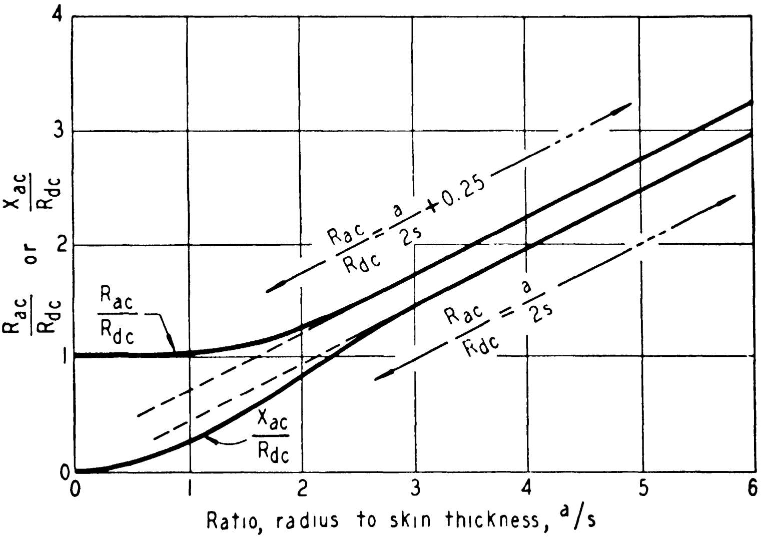

FIG. 15. High-frequency resistance and reactance of cylindrical conductors.

alternating-current resistance increases rapidly as a/s increases. For a fixed cylinder diameter, the increase in the ratio of alternating-current resistance to direct-current resistance is entirely due to a decrease in skin thickness. Inspection of (1.46) shows that increases in frequency, conductivity, and permeability all decrease the skin thickness.

Examination of Fig. 15 reveals the following approximations which are of great value.

$$\text{When } a/s > 2, \qquad \frac{R_{ac}}{R_{dc}} = \frac{a}{2s} + 0.25. \tag{1.64}$$

$$\text{When } a/s > 2.5, \qquad \frac{X_{ac}}{R_{dc}} = \frac{a}{2s}. \tag{1.65}$$

The value of Fig. 15 will be illustrated by a sample problem, that of determining the resistance and reactance for a cylinder 1 centimeter in length and 1 centimeter in diameter ($a = 0.5$ centimeter), at frequencies of 100 cycles and 1,000,000 cycles (1 megacycle). The cylinder is composed of copper. Then the conductivity at ordinary temperatures is $\sigma = 5.8 \times 10^5$ mhos for a centimeter cube. The relative permeability of copper is unity.

From (1.61), the resistance to direct current is

$$R_{dc} = \frac{1}{5.8 \times 10^5 \pi (0.5)^2} = 2.2 \times 10^{-6} \text{ ohm per centimeter.}$$

From (1.46), the skin thickness at 100 cycles is

$$s = \frac{1}{2\pi \sqrt{10^{-9} \times 5.8 \times 10^5 \times 100}} = 0.662 \text{ centimeter.}$$

Then

$$a/s = \frac{0.5}{0.662} = 0.755.$$

Using this value of a/s in Fig. 15, R_{ac}/R_{dc} is found to be 1.03, so $R_{ac} = 1.03 \times 2.2 \times 10^{-6} = 2.266 \times 10^{-6}$ ohm per centimeter at 100 cycles. From the same figure, we find that X_{ac}/R_{dc} is 0.14, so the intrinsic reactance is $0.14 \times 2.2 \times 10^{-6} = 0.308 \times 10^{-6}$ ohm per centimeter at 100 cycles.

At a frequency of 1,000,000 cycles, the skin thickness is 0.00662 centimeter. Then $a/s = 75.5$, a value not included on Fig. 15. However, from (1.64)

$$R_{ac}/R_{dc} = \frac{75.5}{2} + 0.25 = 38.0,$$

and $R_{ac} = 38 \times 2.2 \times 10^{-6} = 83.6 \times 10^{-6}$ ohm per centimeter at 1 megacycle. From (1.65), $X_{ac}/R_{dc} = 37.75$, and $X_{ac} = 83.05 \times 10^{-6}$ ohm per centimeter at 1 megacycle.

Similar calculations yielded the results set forth in Table 2.

TABLE 2. RESISTANCE AND REACTANCE PER CENTIMETER OF LENGTH OF A COPPER CYLINDER 1 CENTIMETER IN DIAMETER.

Frequency (cycles)	Skin Thickness (centimeters)	a/s	R (microhms per centimeter)	X (microhms per centimeter)
0	∞	0	2.2	0
10	2.08	0.24	2.2	0.055
10^2	0.662	0.755	2.265	0.308
10^3	0.208	2.4	3.19	2.5
10^4	0.0662	7.55	8.84	8.31
10^5	0.0208	24.0	26.95	26.4
10^6	0.00662	75.5	83.6	83.05
10^7	0.00208	240.0	264.5	264.0
10^8	0.000662	755.0	831.0	830.5

To demonstrate the significance of the skin thickness as well as the relation shown by (1.64), let us examine the two current-carrying conditions shown in Fig. 16. The figure on the left depicts a conducting shell of outer radius, a, and of thickness, s. The mean radius of the shell is $\left(a - \frac{s}{2}\right)$, so the cross-sectional area is $2\pi s\left(a - \frac{s}{2}\right)\cdot$ We now imagine that the current is flowing uniformly through the cross-hatched area shown in Fig. 16a. The resistance to this current flow is then the direct-current resistance.

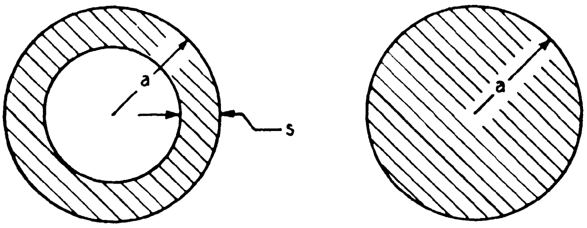

(a) (b)

FIG. 16. High frequency currents crowd to the surface of the conductor, while direct currents distribute uniformly throughout the cross section.

$$R_1 = \frac{1}{\sigma \cdot 2\pi s\left(a - \frac{s}{2}\right)}.$$

The direct-current resistance of the solid cylinder of Fig. 16b is

$$R_2 = \frac{1}{\sigma \cdot \pi a^2}.$$

Then

$$\frac{R_1}{R_2} = \frac{a^2}{2s\left(a - \frac{s}{2}\right)} = \frac{a}{2s} \cdot \frac{1}{\left(1 - \frac{s}{2a}\right)}.$$

When $\frac{s}{2a} \ll 1$,

$$\frac{1}{1 - \frac{s}{2a}} \doteq 1 + \frac{s}{2a}$$

and

$$\frac{R_1}{R_2} = \frac{a}{2s}\left(1 + \frac{s}{2a}\right) = \frac{a}{2s} + 0.25.$$

This resistance ratio is exactly the same as (1.64).

The power generated in the material at any point a distance r from the center is

$$\begin{aligned} P(\text{watts per cubic centimeter}) &= E^2\sigma \\ &= \sigma E_0^2 \left\{\left[\operatorname{ber}\left(\frac{\sqrt{2}\,r}{s}\right)\right]^2 + \left[\operatorname{bei}\left(\frac{\sqrt{2}\,r}{s}\right)\right]^2\right\}. \qquad (1.66) \end{aligned}$$

The total power generated in a cylinder 1 centimeter long and of radius a centimeters is

$$P_T = E^2_{r=a} \frac{R_{ac}}{R_{ac}^2 + X_{ac}^2}. \qquad (1.67)$$

The average power per cubic centimeter is then

$$P_{av} = \frac{P_T}{\pi a^2} = \frac{E^2_{r=a}}{\pi a^2} \frac{R_{ac}}{R_{ac}^2 + X_{ac}^2} \qquad (1.68)$$

and

$$\frac{P}{P_{av}} = \frac{\sigma \pi a^2 E_0^2}{E^2_{r=a} R_{ac}} \left\{\left[\operatorname{ber}\left(\frac{\sqrt{2}\,r}{s}\right)\right]^2 + \left[\operatorname{bei}\left(\frac{\sqrt{2}\,r}{s}\right)\right]^2\right\}(R_{ac}^2 + X_{ac}^2). \qquad (1.69)$$

If we note that $\sigma \pi a^2 = \frac{1}{R_{dc}}$, and also substitute

$$E^2_{r=a} = E_0^2 \left\{\left[\operatorname{ber}\left(\frac{\sqrt{2}\,a}{s}\right)\right]^2 + \left[\operatorname{bei}\left(\frac{\sqrt{2}\,a}{s}\right)\right]^2\right\}$$

in (1.69), we find that

$$\frac{P}{P_{av}} = \frac{R_{ac}}{R_{dc}}\left[1+\left(\frac{X_{ac}/R_{dc}}{R_{ac}/R_{dc}}\right)^2\right]\frac{\left[\operatorname{ber}\left(\frac{\sqrt{2}\,r}{s}\right)\right]^2+\left[\operatorname{bei}\left(\frac{\sqrt{2}\,r}{s}\right)\right]^2}{\left[\operatorname{ber}\left(\frac{\sqrt{2}\,a}{s}\right)\right]^2+\left[\operatorname{bei}\left(\frac{\sqrt{2}\,a}{s}\right)\right]^2}\cdot \tag{1.70}$$

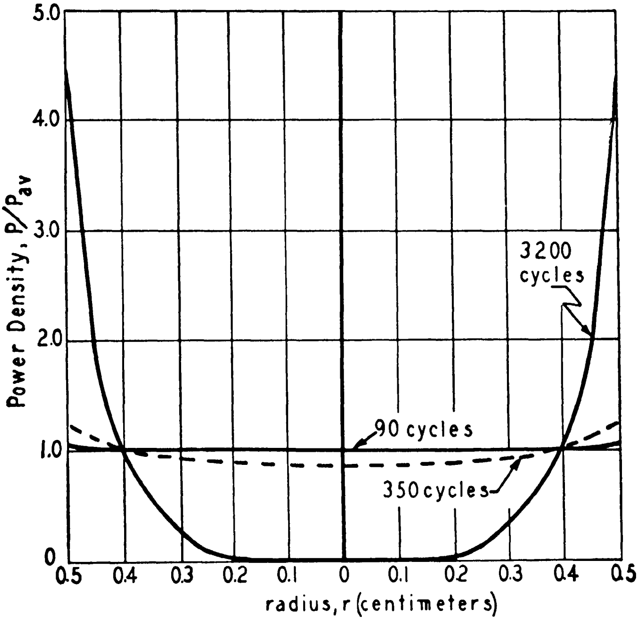

FIG. 17. Power density in a copper cylinder.

If we make use of the approximations of (1.64) and (1.65), then (1.70) becomes

$$\frac{P}{P_{av}} = \frac{\left[\frac{1}{2}\left(\frac{a}{s}\right)^2+\frac{1}{4}\frac{a}{s}+\frac{1}{16}\right]}{\frac{1}{2}\frac{a}{s}+\frac{1}{4}}\left\{\frac{\left[\operatorname{ber}\left(\frac{\sqrt{2}\,r}{s}\right)\right]^2+\left[\operatorname{bei}\left(\frac{\sqrt{2}\,r}{s}\right)\right]^2}{\left[\operatorname{ber}\left(\frac{\sqrt{2}\,a}{s}\right)\right]^2+\left[\operatorname{bei}\left(\frac{\sqrt{2}\,a}{s}\right)\right]^2}\right\}\cdot \tag{1.71}$$

Fig. 17 shows this ratio of power densities for a copper cylinder of radius 0.5 centimeter, at several operating frequencies. It may be seen that the density of power is practically constant throughout the cylinder when the frequency is 90 cycles. At 350 cycles, a slight increase is noticeable near the surface of the cylinder, while at 3200 cycles, the power concentration near the surface is very marked. The skin thicknesses corresponding to these frequencies are

Frequency (cycles)	Skin thickness (centimeters)
90	0.699
350	0.354
3200	0.116

In this chapter, a general formula for electric field distribution throughout a cylinder in which axial currents are flowing has been developed. The distribution, as well as the impedance of the cylinder, has been shown to depend upon the frequency, conductivity, and dielectric constant of the material. Where the material was a good dielectric with low power factor, the power was generated uniformly throughout the material. When the frequency was increased, or the diameter of the cylinder became large, the power concentration became less near the outer surface of the cylinder. Quite the reverse effect was found when the cylinder was a good conductor. Here, at high frequencies, the power concentration was greatly increased at the surface.

Chapter 2

INDUCED CURRENTS IN CYLINDRICAL CONDUCTORS

In the preceding chapter, axial current flow in cylindrical conductors was examined. The lines of magnetic intensity formed circles concentric with the axis. The purpose of this chapter is to examine a related case, where the lines of electric intensity and the current paths form circles concentric with the axis, while the magnetic intensity lines are parallel to the axis. This is the condition that exists when a conducting cylinder is surrounded by a solenoid as shown in Fig. 18. The magnetic intensity is parallel to the axis as long as we do not approach the ends of the solenoid. To examine the conditions in a conducting cylinder we may represent the magnetic intensity of the solenoid by a uniform field with a strength of $\boldsymbol{H}_0$ ampere turns per centimeter.

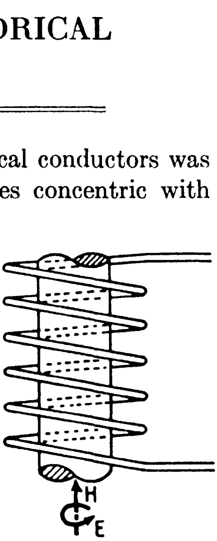

FIG 18. A conducting cylinder surrounded by a solenoid.

The conducting cylinder of radius a is now placed in the solenoid. If we examine slices of the cylinder as we did in Figs. 4 and 5, we arrive at a set of differential equations having the following solutions which are appropriate to the specified conditions.

The magnetic field intensity within the cylinder is

$$\boldsymbol{H} = \boldsymbol{A}\left[\operatorname{ber}\left(\frac{\sqrt{2}\,r}{s}\right) + j \operatorname{bei}\left(\frac{\sqrt{2}\,r}{s}\right)\right], \tag{2.01}$$

where s is the skin thickness defined by equation (1.46). The conductivity of the cylinder is σ mhos per centimeter cube, μ_r is the relative permeability of the cylinder, while the current in the solenoid has a frequency of f cycles per second.

The quantity r in equation (2.01) is the radial distance from the axis to the point where the intensity is reckoned.

The electric intensity at the same point is

$$\boldsymbol{E} = \frac{-\sqrt{2}A}{\sigma s}\left[\operatorname{ber}'\left(\frac{\sqrt{2}\,r}{s}\right) + j\operatorname{bei}'\left(\frac{\sqrt{2}\,r}{s}\right)\right]. \tag{2.02}$$

The reader may be interested to observe that in this treatment of the inductively-coupled cylinder we have interchanged the role of the electric and magnetic intensities as used in the first chapter, where axial current flow was considered. In the case of axial flow, the electric intensity pointed in the direction of the axis of the cylinder, while the magnetic intensity was circumferential. In the case treated here, the magnetic intensity is parallel to the axis, while the electric intensity is circumferential. Thus we may note that the magnetic intensity given by (2.01) has exactly the same form as the electric intensity given by (1.54).

The constant A appearing in equation (2.01) is evaluated by turning to the boundary conditions at the surface of the cylinder. Here the magnetic intensity just inside the cylinder must be equal to the magnetic intensity just outside. The magnetic intensity outside the cylinder is made up of the impressed intensity $\boldsymbol{H}_0$ and the added intensity set up by currents flowing within the cylinder. An extended analysis reveals that where the radius of the cylinder remains very small compared to the wave length, the added intensity just outside the cylinder is very nearly equal to the impressed intensity, so that the total magnetic intensity just outside the surface of the cylinder is $2\boldsymbol{H}_0$. Then by equating this field to that given by (2.01) at the boundary, it is seen that

$$2\boldsymbol{H}_0 = A\left[\operatorname{ber}\left(\frac{\sqrt{2}\,a}{s}\right) + j\operatorname{bei}\left(\frac{\sqrt{2}\,a}{s}\right)\right] \tag{2.03}$$

and (2.01) becomes

$$\boldsymbol{H} = 2\boldsymbol{H}_0\frac{\left[\operatorname{ber}\left(\frac{\sqrt{2}\,r}{s}\right) + j\operatorname{bei}\left(\frac{\sqrt{2}\,r}{s}\right)\right]}{\left[\operatorname{ber}\left(\frac{\sqrt{2}\,a}{s}\right) + j\operatorname{bei}\left(\frac{\sqrt{2}\,a}{s}\right)\right]}, \tag{2.04}$$

whereas the electric intensity is

$$\boldsymbol{E} = \frac{-\sqrt{2}\cdot 2\boldsymbol{H}_0}{\sigma s}\,\frac{\left[\operatorname{ber}'\left(\frac{\sqrt{2}\,r}{s}\right) + j\operatorname{bei}'\left(\frac{\sqrt{2}\,r}{s}\right)\right]}{\left[\operatorname{ber}\left(\frac{\sqrt{2}\,a}{s}\right) + j\operatorname{bei}\left(\frac{\sqrt{2}\,a}{s}\right)\right]}. \tag{2.05}$$

These last two equations show the variation of magnetic intensity and electric intensity throughout the cylinder. However, our purpose in this chapter is to learn something of the ability of the cylinder to absorb power from the impressed field, in terms of cylinder diameter, electrical constants, and the frequency of the applied field. Therefore, no detailed examination of the field distribution will be attempted here.

The absolute value of the electric intensity is

$$E = \frac{\sqrt{2}\cdot 2H_0}{\sigma s}\sqrt{\frac{\left[\operatorname{ber}'\left(\frac{\sqrt{2}\,r}{s}\right)\right]^2 + \left[\operatorname{bei}'\left(\frac{\sqrt{2}\,r}{s}\right)\right]^2}{\left[\operatorname{ber}\left(\frac{\sqrt{2}\,a}{s}\right)\right]^2 + \left[\operatorname{bei}\left(\frac{\sqrt{2}\,a}{s}\right)\right]^2}}. \tag{2.06}$$

The total power absorbed in a unit length of the cylinder is

$$P \text{ (watts per unit length)} = \int_{r=0}^{r=a} 2\pi r E^2 \sigma \, dr. \tag{2.07}$$

On substituting (2.06) in (2.07), we find that

$$P = \frac{8\pi H_0{}^2}{\sigma}\cdot\left(\frac{\sqrt{2}\,a}{s}\right)\frac{\operatorname{ber}\left(\frac{\sqrt{2}\,a}{s}\right)\operatorname{ber}'\left(\frac{\sqrt{2}\,a}{s}\right) + \operatorname{bei}\left(\frac{\sqrt{2}\,a}{s}\right)\operatorname{bei}'\left(\frac{\sqrt{2}\,a}{s}\right)}{\left[\operatorname{ber}\left(\frac{\sqrt{2}\,a}{s}\right)\right]^2 + \left[\operatorname{bei}\left(\frac{\sqrt{2}\,a}{s}\right)\right]^2}. \tag{2.08}$$

In (2.08) let

$$F = \sqrt{2}\cdot\frac{\operatorname{ber}\left(\frac{\sqrt{2}\,a}{s}\right)\operatorname{ber}'\left(\frac{\sqrt{2}\,a}{s}\right) + \operatorname{bei}\left(\frac{\sqrt{2}\,a}{s}\right)\operatorname{bei}'\left(\frac{\sqrt{2}\,a}{s}\right)}{\left[\operatorname{ber}\left(\frac{\sqrt{2}\,a}{s}\right)\right]^2 + \left[\operatorname{bei}\left(\frac{\sqrt{2}\,a}{s}\right)\right]^2}. \tag{2.09}$$

Then

$$P = \frac{8\pi H_0{}^2}{\sigma}\cdot\frac{a}{s}\cdot F. \tag{2.10}$$

Fig. 19 shows the quantity $\frac{a}{s}\cdot F$ as a function of a/s, the radius measured in terms of the skin thickness. It is seen that when a/s is less than unity, $\frac{a}{s}\cdot F$ is approximated quite well by the expression $\frac{1}{4}\left(\frac{a}{s}\right)^4$. Under this condition, the power per unit length is

$$P \doteq \frac{2\pi H_0^2}{\sigma}\left(\frac{a}{s}\right)^4. \tag{2.11}$$

When a/s is greater than 5 the quantity $\frac{a}{s}\cdot F$ becomes approximately a/s, so that the power per unit length is

$$P \doteq \frac{8\pi H_0^2}{\sigma}\cdot\frac{a}{s}. \tag{2.12}$$

The curve drawn in Fig. 19 may be used with (2.10) to estimate the power absorbed per unit length of cylinder when the impressed field H_0 is known. Fig. 19 indicates the importance of using high frequencies to effectively couple energy into a cylindrical conductor. However, a plot of the function F, as

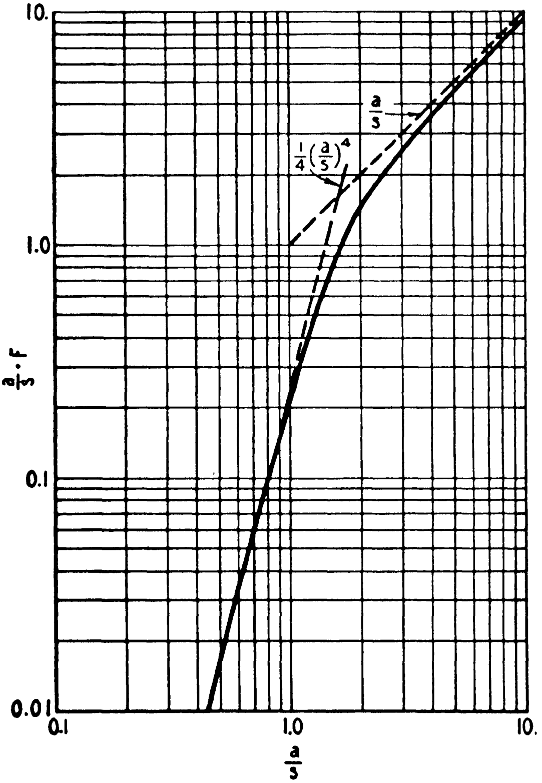

FIG. 19. The quantity $\frac{a}{s}F$ as used in (2.10).

seen in Fig. 20, helps to establish an upper limit on the frequency necessary for efficient coupling.

Since H_0 has been regarded as a constant in (2.08), the implication is that the current in the exciting solenoid has been held constant. Therefore, the power lost in the solenoid is proportional to the radio-frequency resistance of the solenoid. For the copper conductor used in the solenoid, the ratio of radius to skin thickness is usually large so that the resistance varies as the square root of the frequency. Thus, when we plot F alone, we have effectively divided out the square root of frequency in $(1/s)$ from (2.10). We may now regard the curve of Fig. 20 as being *proportional* to the ratio of the power absorbed in the cylinder to the power lost in the exciting solenoid. It is seen from Fig. 20 that, when a/s is greater than 2.25, the knee of the curve has been passed and no great benefit is derived by increasing the frequency further. We may then define a critical frequency for effective coupling to a

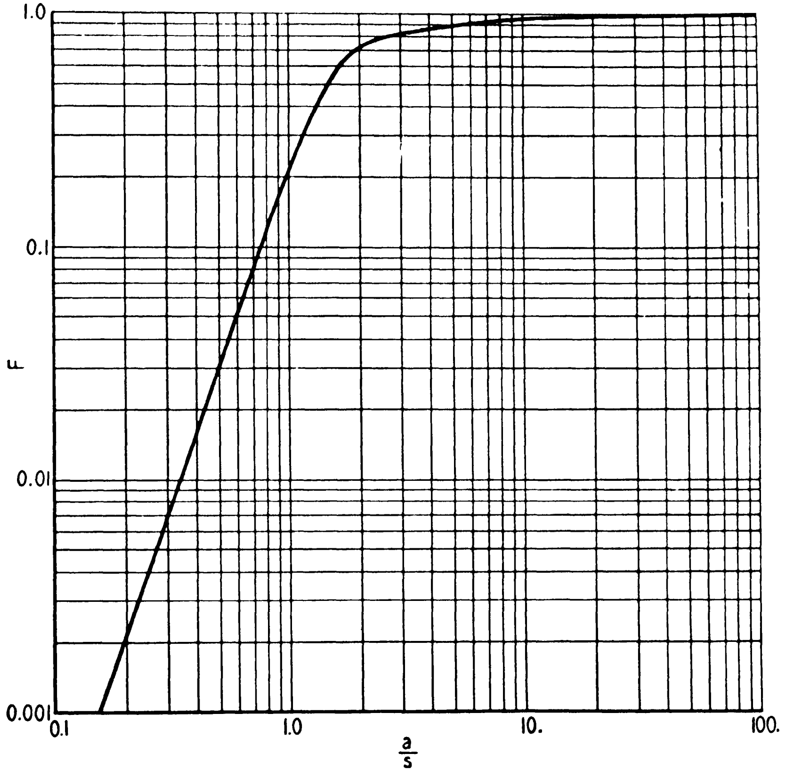

FIG. 20. The function F of (2.09) is plotted as a function of a/s.

cylinder. When a/s equals 2.25, the corresponding frequency is

$$f_c = \frac{128.5 \times 10^6}{\sigma \mu_r a^2}, \tag{2.13}$$

where

f_c = critical frequency in cycles;
σ = conductivity of cylinder in mhos per centimeter cube;
μ_r = relative permeability of the cylinder;
a = radius of cylinder in centimeters.

The application of this theory to the heating of small parts will be treated in Chapter 3, together with a discussion of many attentuating factors that are not readily handled mathematically.

Chapter 3

INDUCTION HEATING APPLIED TO CONDUCTORS OF SMALL DIAMETER

Induction heating is ordinarily associated with comparatively low frequencies, of the order of 500 kilocycles and less. However, when the induction heating of metal parts of small diameter is attempted at such frequencies, the results are usually very disappointing.

In Chapter 2, theoretical consideration was given to the power absorbed by a conducting cylinder placed in a solenoid carrying radio-frequency current, and an expression (2.13) was obtained for the critical frequency for efficient coupling. Fig. 21 shows the critical frequency plotted against diameter for various materials at several temperatures. It will be noted that the critical frequency rises with temperature because of the decrease in conductivity. In the case of steel, a marked change occurs at the Curie point where the permeability drops from a value of several hundred to unity, so that the critical frequency for a temperature slightly above the Curie point is several hundred times greater than that for a temperature at or slightly below that point.

The hardening of steel requires a temperature of about 815° C which is well above the Curie point. Accordingly, the critical frequency for heating steel needles and similar objects of small diameter to the hardening temperature is high. For instance, for a diameter of 0.015 inch, the critical frequency is 40 megacycles. Although it is desirable to operate at or above the critical frequency, a lower frequency may be used at a sacrifice in efficiency. If the loss in the coupling coil is large compared to the loss in the load, as is generally the case when the load is of small diameter, then the factor F of equation (2.09) may be considered a measure of the efficiency. Fig. 22 shows how the efficiency is then affected by a deviation from the critical frequency.

When the part to be heated has sections of different diameters, the problem of securing uniform temperature rise becomes rather complex and diffiult to solve mathematically. It is not sufficient merely to choose a frequency t or above the critical frequency for the smallest diameter section, but the eat losses and the thermal capacity of the various sections must also be onsidered. From (2.12), it is evident that if the frequency is high enough,

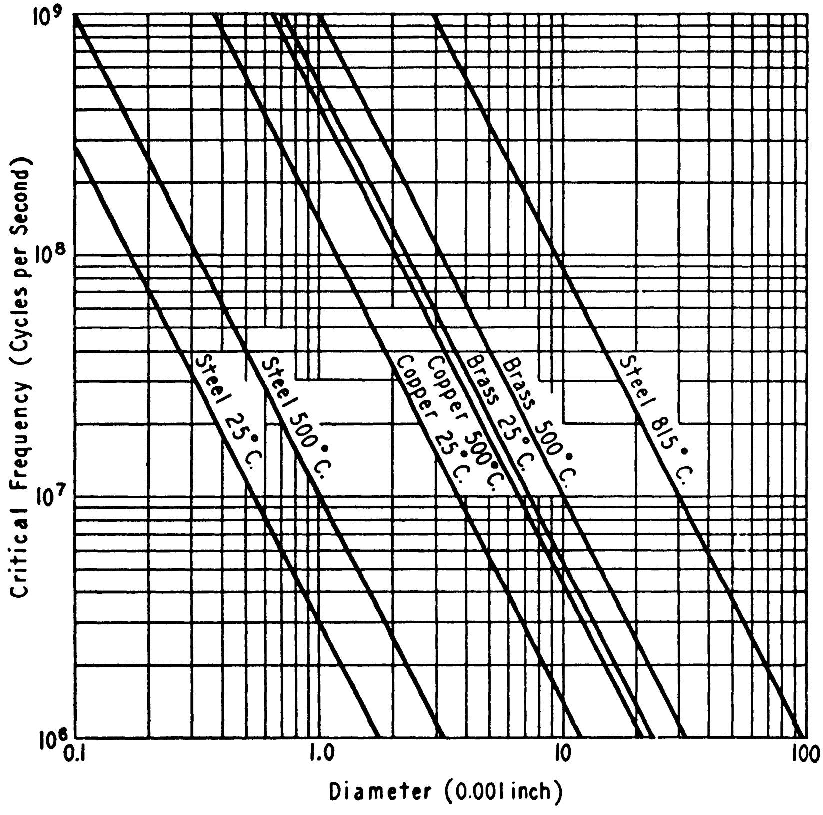

FIG. 21. Critical frequency as a function of wire size.

then the power transfer per unit of surface area $(P/2\pi a)$ is the same for all sections. However, uniform temperature rise will result only if the heating period is sufficiently long for the temperature to reach the steady state condition and if the heat losses are proportional to the surface area. If the heating period is very short, the temperature rise of the larger diameter section will be lower than that for the smaller diameter section because of the relatively greater amount of energy required to heat the larger section. For instance, a section 0.030 inch in diameter receives only three times as much power as a section 0.010 inch in diameter but the mass to be heated is nine times as great.

The heat losses are mainly those due to radiation and to conduction through the surrounding atmosphere. The radiation loss is proportional to the surface area and for oxidized steel can be calculated from the following expression:

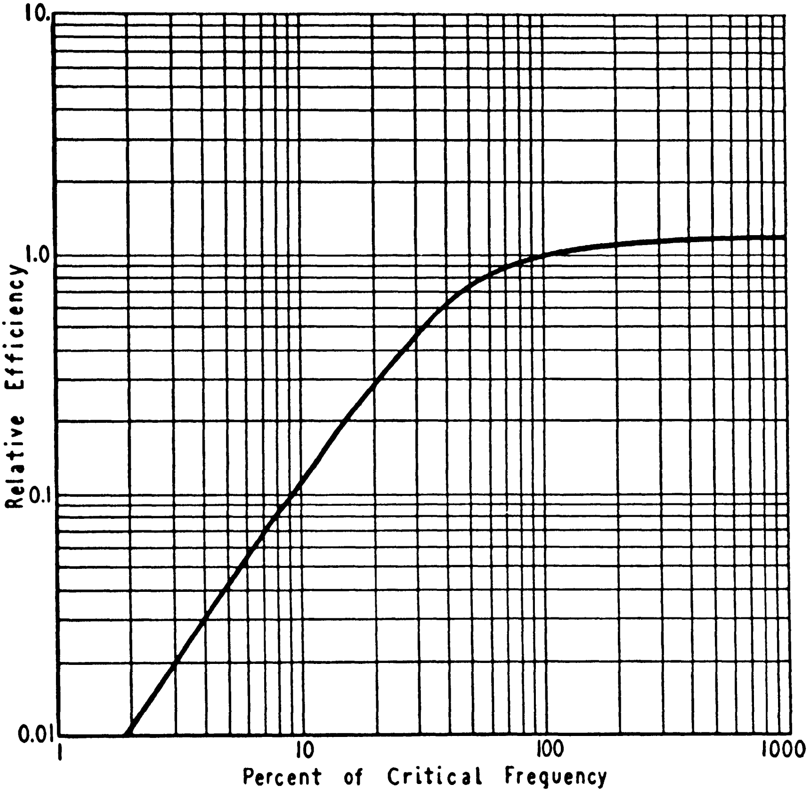

FIG. 22. Relative efficiency is affected by deviations from the critical frequency.

Radiation loss in watts per square centimeter $= 5.135 \times 10^{-12}(u^4 - u_0^4)$, (3.01)

where

u = temperature of heated body, in degrees Kelvin;
u_0 = temperature of surroundings, in degrees Kelvin.

Since the radiation loss is proportional to the surface area, the uniform heating of sections of different diameter can be realized if the following conditions are fulfilled:

1. The frequency is at or above the critical frequency.
2. The heating period is long enough for all parts to reach the steady state condition.
3. The space surrounding the load is highly evacuated so that conduction loss is eliminated.

It should be remembered, however, that the thermal conductivity of air and other gases does not change as the pressure is changed until the pressure becomes so low that the free path of the molecules approaches the conduction path in magnitude. Because of the high degree of vacuum required, it would not ordinarily be practical to utilize a vacuum in this manner to secure uniform heating.

The power lost by conduction between concentric cylinders, in watts per square centimeter of inner conductor surface is given by the expression:

$$\frac{8.374k(u_1 - u_2)}{d_1 \log_e \dfrac{d_2}{d_1}}, \tag{3.02}$$

where k = the thermal conductivity of the medium between the cylinders.
= 0.000136 calorie/second/square centimeter per degree Centigrade/centimeter, for air at 815° C.
= 0.000096 calorie/second/square centimeter per degree Centigrade/centimeter, for air at 260° C.
u_1, u_2 = temperatures of the inner and outer cylinders, respectively, in degrees Centigrade.
d_1 = diameter of inner cylinder, in centimeters.
d_2 = inner diameter of outer cylinder, in centimeters.

From this expression it is evident that the conduction loss per unit of surface area will increase as the diameter of cylinder being heated decreases. Fig. 23 shows the radiation and conduction losses for oxidized steel at 260° C and at 815° C. The inner diameter of the solenoid was assumed to be $\frac{3}{16}$ inch.

The effect of the conduction loss is to give a lower temperature rise for a small section than for a larger section even though the power transfer per unit of surface area is the same. Since a short heating period results in the reverse temperature distribution, it is possible to choose a heating period of such duration as to result in a uniform temperature rise in two sections of different diameter even though conduction loss occurs. This heating period can best be determined experimentally.

Experimental Data. A group of tests was made to determine how the magnetic field intensities required to heat music wire to the hardening temperature of about 815° C varied with wire diameter and heating time for frequencies of 27 megacycles and 140 megacycles.

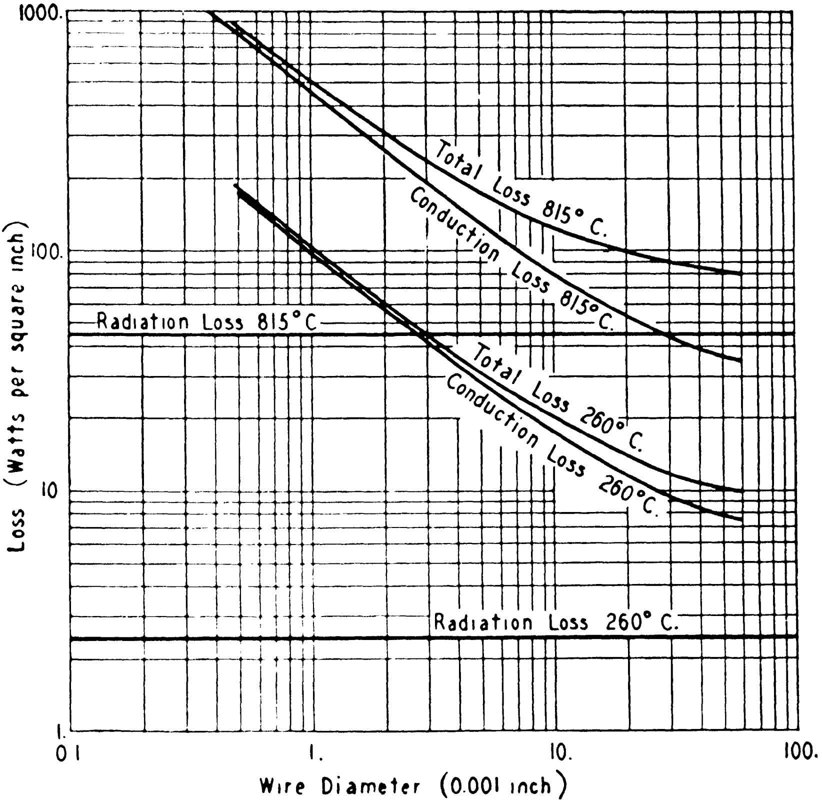

FIG. 23. Radiation and conduction losses for oxidized steel.

The 27-megacycle measurements were made with a 2-kilowatt push-pull oscillator as shown in Fig. 24. The coupling coil consisted of 8 turns of $\frac{1}{8}$-inch diameter copper tubing wound with an inside diameter of $\frac{1}{4}$ inch and a length of $1\frac{1}{2}$ inches. Compressed air was blown through the coil for cooling. The coil was tuned with a 300-micromicrofarad variable air capacitor. The tuning capacitor and coupling to the oscillator were adjusted so that the current through the coil was not affected appreciably by the placing of the wire load in the coil. This condition was possible to realize quite readily because of the large power capability of the oscillator compared to the power taken by the load. The current was controlled by varying the plate voltage of the oscillator, the relationship being practically linear. An adjustable electric timer was used for controlling the heating period. The wire samples were water quenched immediately following the heating period. The wire was in an annealed condition initially and the current through the coil was increased to the point where hardening just occurred. Figs. 25 and 26 show

FIG. 24. The 2-kilowatt oscillator used in the 27-megacycle measurements.

the results of these tests. From Fig. 21 it will be found that 27 megacycles is the critical frequency for a steel wire of 0.018 inch diameter at 815° C. Fig. 25 shows that this is the diameter below which the field intensity rises steeply.

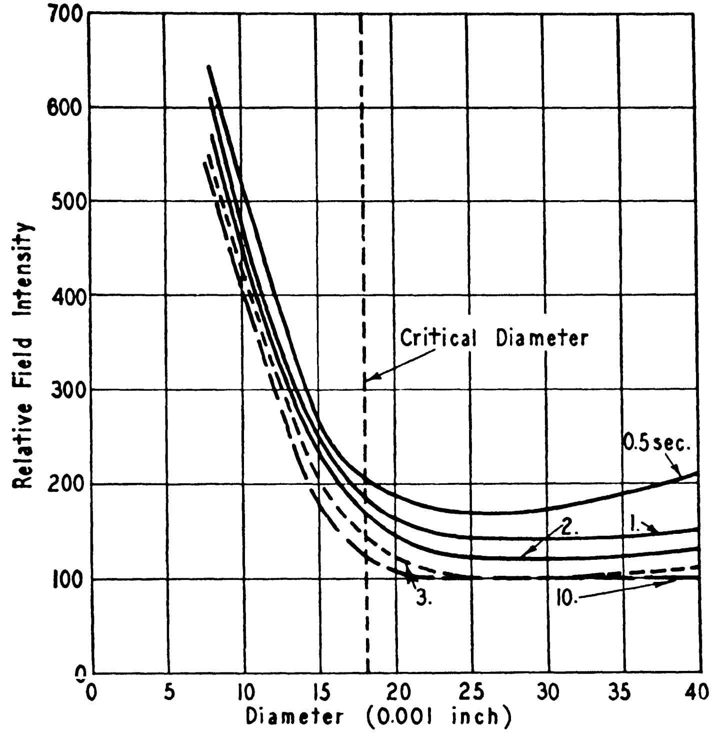

FIG. 25. Relative field intensity as a function of wire diameter for several heating times. (Frequency is 27 megacycles.)

The 140-megacycle measurements were made in a similar manner using a 750-watt oscillator. The wire diameters used at this frequency were smaller so that air quenching was used instead of water quenching. Figs. 27 and 28 show the results of the 140-megacycle tests. Fig. 27 shows quite markedly how the length of the heating cycle affects the relative temperature of sections of different diameters. For instance, with a $\frac{1}{2}$-second heating period, an 0.008-inch diameter section requires about 70 per cent of the field intensity needed to produce the same temperature rise in a 0.020-inch diameter section. For the same field intensity, therefore, the 0.008-inch diameter section would be heated much more than the 0.020-inch diameter section. With a 6-second heating period, the reverse is true, whereas with a

3-second heating period, the temperature rise is about the same for both diameters.

Heat Treatment of Knitting Needles. A commonly-used size of knitting-machine needle of the spring-beard type has a somewhat flattened body with a mean diameter of 0.020 inch and a spring beard with a diameter of 0.007 inch. This needle must be heat treated to harden and temper it so that it is springy but not brittle. It is apparent from Fig. 25 that a frequency of 27 megacycles is much too low to secure uniform heating of such a needle to the hardening temperature. Experiments made at that frequency failed to produce hardening of the small diameter beard even with a very short heating period and with a field intensity high enough to overheat the body of the needle.

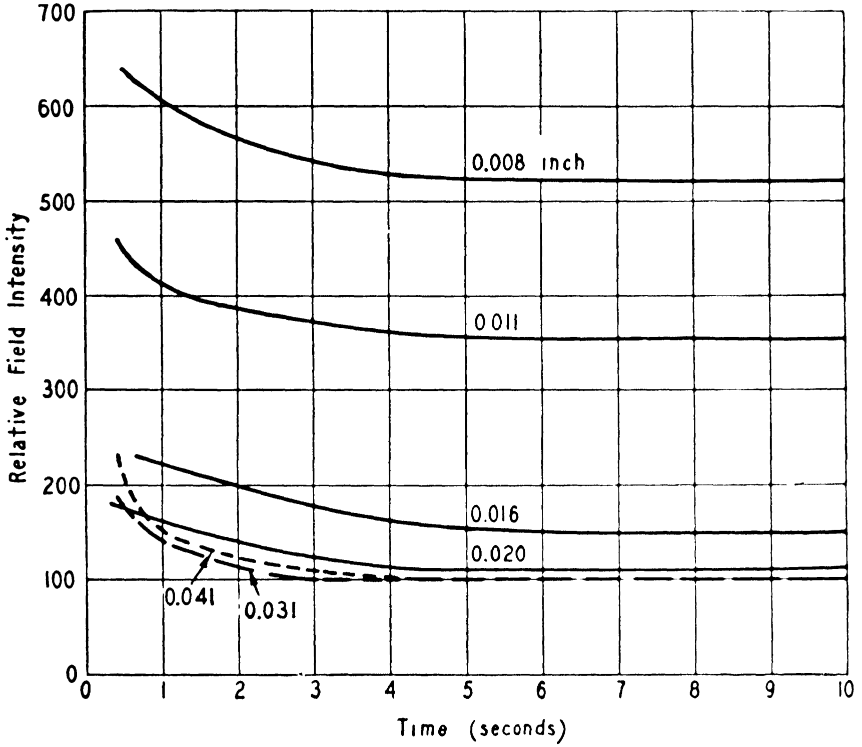

FIG. 26. Relative field intensity as a function of heating time, for several wire diameters. (Frequency is 27 megacycles.)

From Fig. 27, a frequency of 140 megacycles appears suitable for this application, with a heating period of about 3 seconds. Experimental results

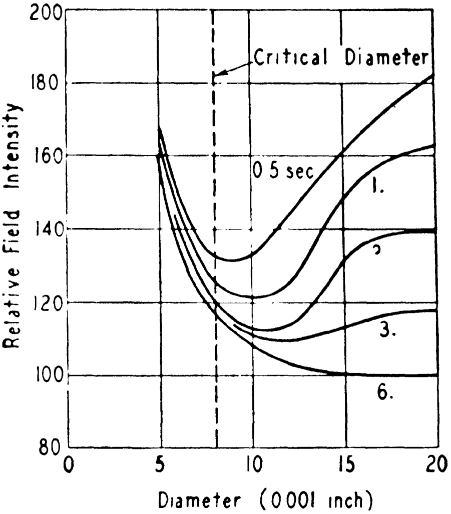

FIG. 27. Relative field intensity as a function of wire diameter for several heating times. (Frequency is 140 megacycles).

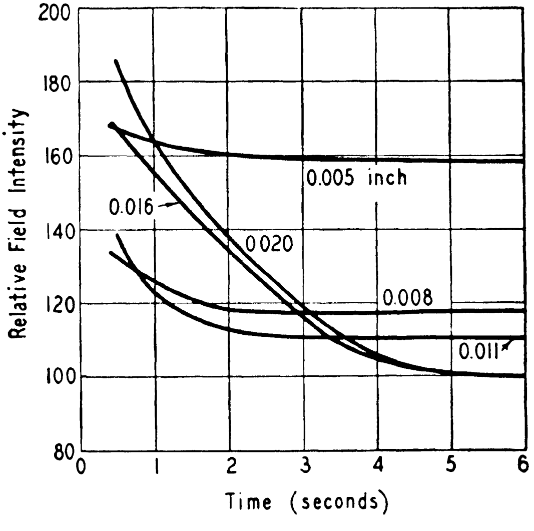

FIG. 28. Relative field intensity as a function of heating time, for several wire diameters. (Frequency is 140 megacycles).

verified this conclusion. Uniform heating was obtained at this frequency with a heating period of 2½ seconds. Fig. 29 shows the experimental set-up used in these tests. The needle was placed in a glass tube inside the coupling coil, and nitrogen gas was passed through the tube to prevent oxidation and scaling of the needle. The flow of the gas was interrupted during the heating period to prevent the stream of gas from cooling the needle. At the finish of the heating period the flow of gas helped to quench the needle. As mentioned before, with diameters as small as those involved here the loss of heat is so rapid through radiation and conduction to the surrounding atmosphere that no other quenching medium such as water or oil is required.

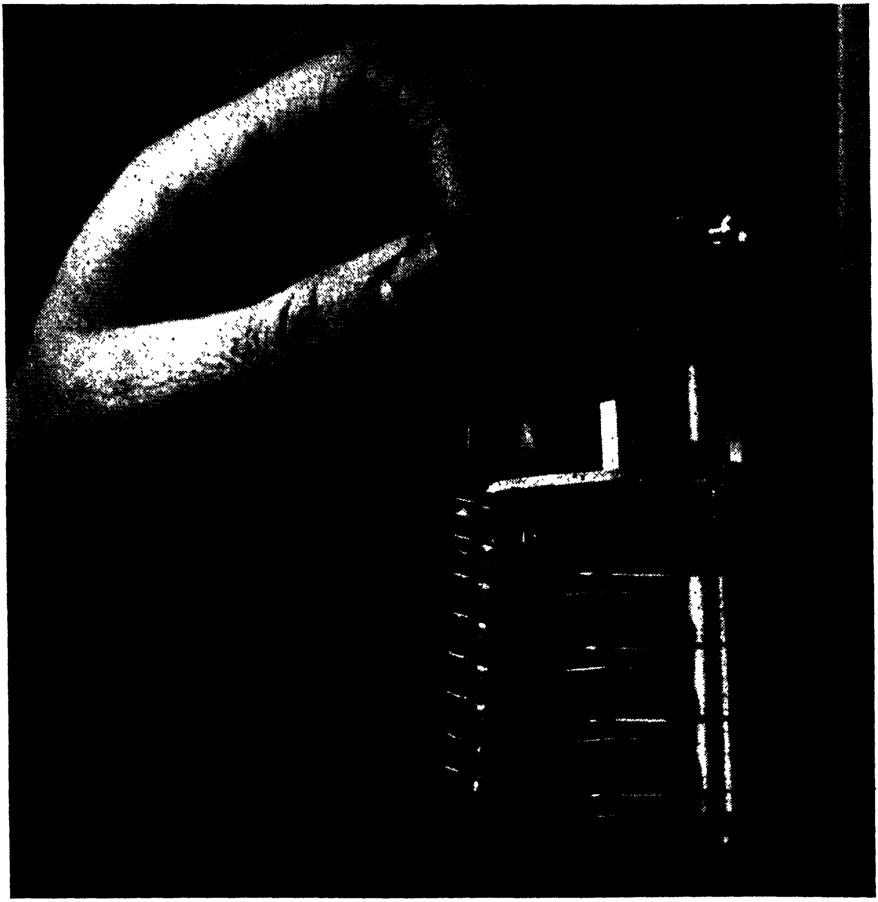

FIG. 29. Experimental arrangement for treating knitting-machine needles.

Heat Treatment of Surgical Needles. Eyeless surgical needles made of stainless steel have a curved body which must be hardened and a grooved end which must be soft to permit clamping to the suture. The ordinary procedure is to harden the entire needle in a hydrogen atmosphere and then anneal only the grooved portion. This annealing process requires localized heating which is difficult to achieve when the object must be maintained in a non-oxidizing atmosphere.

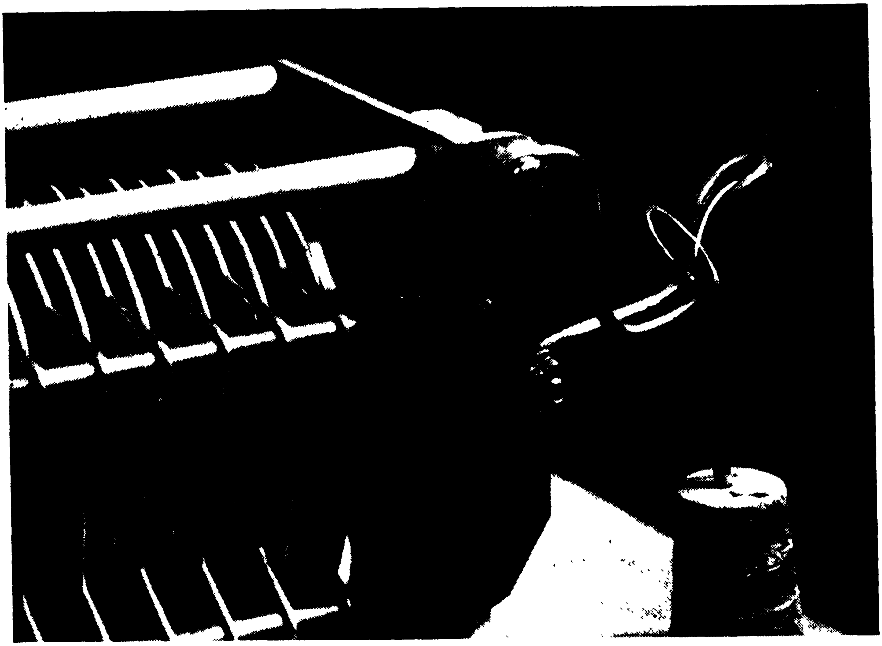

FIG. 30. Experimental arrangement for treating surgical needles.

A consideration of (2.13) showed that a frequency in the neighborhood of 30 megacycles was necessary for good coupling efficiency. The experimental arrangement shown in Fig. 30 made use of a U-shaped inductor. Equation (2.13) was established on the assumption of solenoidal coils. However, it serves to establish the order of magnitude in this case. It may be seen in Fig. 30 that only the curved portion of the needle was heated. The shank of the needle was inserted in a copper sleeve. The sleeve served as a support for the needle and at the same time shielded the shank of the needle, thus preventing undue heating of the shank. An atmosphere of forming gas* was used to prevent scaling. The needles were heated to hardening temperature in 1 second. No quenching medium other than the atmosphere was found necessary because of the rapid cooling of the needle. The needles were tempered by heating them again at reduced power to the drawing temperature. The frequency of 30 megacycles was found to be quite satisfactory for this operation.

---

*Non-oxidizing-mixture usually consisting of 90 percent nitrogen and 10 percent hydrogen.

Chapter 4

CURRENT FLOW IN FLAT METAL SHEETS OF GREAT THICKNESS

As a first approach to the study of current flow in metal sheets, we shall examine the case of current flow parallel to the boundary of a metal sheet which is infinite in extent. The electric and magnetic intensities in the metal are oriented as shown in Fig. 31. The dimension, x, measures the distance from the boundary to the point under examination.

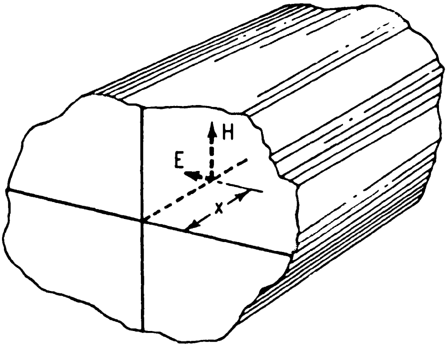

FIG. 31. The electric and magnetic intensities in a metal sheet.

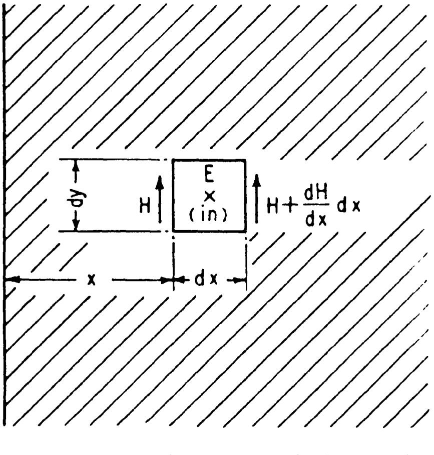

FIG. 32. A small patch used in determining the circuitation of the magnetic intensity.

The current density at any point is in phase with the electric intensity vector and is given by σE amperes per square centimeter, where σ is the conductivity of the metal.

Then if we examine the small patch shown in Fig. 32 and remember that the line integral of the magnetic intensity around the patch is equal to the current through the patch, with the right-hand rule applying, we find

$$\boldsymbol{H} \cdot dy - \left(\boldsymbol{H} + \frac{d\boldsymbol{H}}{dx} dx\right) dy = \sigma \boldsymbol{E} \cdot dx \cdot dy, \tag{4.01}$$

or

$$\frac{d\boldsymbol{H}}{dx} = -\sigma \boldsymbol{E}. \tag{4.02}$$

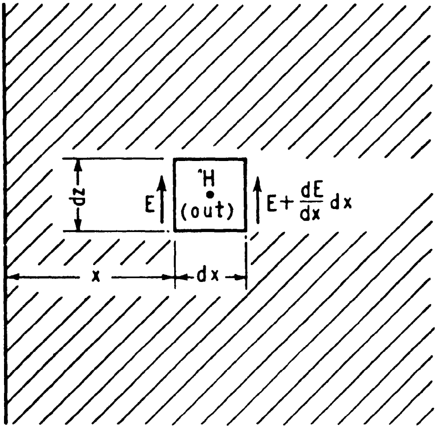

FIG. 33. The small patch used to establish (4.03).

Another little patch shown in Fig. 33 may then be examined. Here the magnetic intensity points out of the page. Using the relation that the line integral of the electric intensity around the patch is equal to the negative time rate of change of magnetic flux density through the patch, we find

$$\left(\boldsymbol{E} + \frac{d\boldsymbol{E}}{dx} dx\right) dz - \boldsymbol{E} \cdot dz = -j\omega\mu \boldsymbol{H} \cdot dx \cdot dz \tag{4.03}$$

or

$$\frac{d\boldsymbol{E}}{dx} = -j\omega\mu \boldsymbol{H}. \tag{4.04}$$

Differentiating (4.02) with respect to x and substituting (4.04) in the result yields

$$\frac{d^2\boldsymbol{H}}{dx^2} = +j\mu\sigma\omega \boldsymbol{H}. \tag{4.05}$$

The solution to this differential equation is

$$H = A\epsilon^{-\sqrt{j\mu\sigma\omega}\,x} + B\epsilon^{+\sqrt{j\mu\sigma\omega}\,x}, \tag{4.06}$$

where A and B are arbitrary constants not yet evaluated.

Using (1.46), we find that

$$\sqrt{j\mu\sigma\omega} = \frac{\sqrt{2j}}{s} = \frac{1}{s}(1+j)$$

so that (4.06) becomes

$$\begin{aligned} H &= A\epsilon^{-\frac{x}{s}} \cdot \epsilon^{-j\frac{x}{s}} + B\epsilon^{+\frac{x}{s}} \cdot \epsilon^{+j\frac{x}{s}} \\ &= A\epsilon^{-\frac{x}{s}}\left(\cos\frac{x}{s} - j\sin\frac{x}{s}\right) + B\epsilon^{+\frac{x}{s}}\left(\cos\frac{x}{s} + j\sin\frac{x}{s}\right). \end{aligned} \tag{4.07}$$

From (4.07) and (4.02), we find the electric intensity to be

$$E = \frac{1+j}{s\sigma}\left(A\epsilon^{-\frac{x}{s}} \cdot \epsilon^{-j\frac{x}{s}} - B\epsilon^{+\frac{x}{s}} \cdot \epsilon^{+j\frac{x}{s}}\right) \tag{4.08}$$

It may be seen that the second term in (4.07) and (4.08) becomes infinite as the distance x becomes very large. Since we are dealing for the moment with conditions near the surface of a sheet which is infinitely thick, it seems expedient to set B equal to zero, thus dropping the last term in (4.07) and (4.08). Then, in the very thick sheet, the magnetic intensity is simply

$$H = A\epsilon^{-\frac{x}{s}} \cdot \epsilon^{-j\frac{x}{s}} = A\epsilon^{-\frac{x}{s}}\left(\cos\frac{x}{s} - j\sin\frac{x}{s}\right) \tag{4.09}$$

and the electric intensity is

$$E = \frac{1+j}{s\sigma} A\epsilon^{-\frac{x}{s}} \cdot \epsilon^{-j\frac{x}{s}} = \frac{1+j}{s\sigma} A\epsilon^{-\frac{x}{s}}\left(\cos\frac{x}{s} - j\sin\frac{x}{s}\right). \tag{4.10}$$

These two relations show that the magnetic and electric intensities drop off exponentially as we leave the surface, and lag in phase at the same time. A study of these two equations also reveals that the electric intensity leads the magnetic intensity at the same point by a phase angle of 45°. A detailed examination of the mode of variation will be made later.

The coefficient A may be evaluated by a study of Fig. 34, where a plane electromagnetic wave is impinging normally on the surface of the conductor.

The magnetic and electric intensities which comprise this wave are $\bar{H}_1$ and $\bar{E}_1$, where*

$$\bar{H}_1 = H_1\epsilon^{+j\frac{2\pi y}{\lambda_0}} \tag{4.11}$$

and

$$\bar{E}_1 = 120\pi H_1\epsilon^{+j\frac{2\pi y}{\lambda_0}}. \tag{4.12}$$

The wave length of the exciting field, in free space, is λ_0. The reference distance, y, is measured outward from the metal surface.

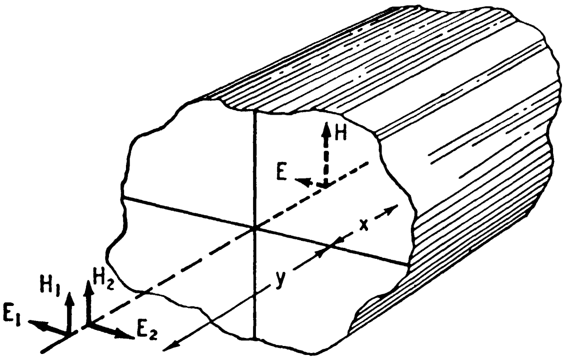

Fig. 34. The electric and magnetic intensity relations when a plane electromagnetic wave impinges on a metal half-space.

Part of this impinging wave is reflected from the surface, while a small part passes into the metal. The reflected wave is

$$\bar{H}_2 = H_2\epsilon^{-j\frac{2\pi y}{\lambda_0}} \tag{4.13}$$

and

$$\bar{E}_2 = 120\pi H_2\epsilon^{-j\frac{2\pi y}{\lambda_0}} \tag{4.14}$$

The magnetic and electric intensities in the metal are given by (4.09) and (4.10). At the boundary, $x = 0$, $y = 0$, the magnetic fields are continuous, that is, the component of magnetic intensity parallel to the surface in free space at the surface is just equal to the magnetic intensity in the metal at the surface. Under this condition, (4.09), (4.11), and (4.13) yield

$$H_1 + H_2 = A. \tag{4.15}$$

The electric fields at the same surface are also continuous, so that (4.10),

---

* George W. Pierce, *Electric Oscillations and Electric Waves*, 1st ed., 3d Impression, 1920, McGraw-Hill Book Company, Inc., New York, p. 392.

(4.12), and (4.14) give

$$120\pi H_1 - 120\pi H_2 = \frac{1+j}{s\sigma} A. \qquad (4.16)$$

We assume that the value H_1 for the impinging wave is known. Then solving (4.15) and (4.16) for H_2 in terms of H_1,

$$H_1 \left(1 - \frac{1+j}{120\pi s\sigma}\right) = H_2 \left(1 + \frac{1+j}{120\pi s\sigma}\right) \qquad (4.17)$$

and

$$A \left(1 + \frac{1+j}{120\pi s\sigma}\right) = 2H_1. \qquad (4.18)$$

In Chapter 1, we showed that copper, with a conductivity σ equal to 5.8×10^5 mhos for a centimeter cube, had a skin thickness of 0.00662 centimeter at a frequency of 1,000,000 cycles. For this condition,

$$120\pi s\sigma = 1{,}448{,}000,$$

so that, for all practical purposes, (4.17) becomes

$$H_2 = H_1 \qquad (4.19)$$

and

$$A = 2H_1. \qquad (4.20)$$

The relation shown in (4.20) is that postulated in Chapter 2, where the conducting cylinder was treated.

The magnetic intensity in the metal then becomes

$$H = 2H_1 \epsilon^{-\frac{x}{s}} \cdot \epsilon^{-j\frac{x}{s}} = 2H_1 \epsilon^{-\frac{x}{s}} \left(\cos\frac{x}{s} - j \sin\frac{x}{s}\right), \qquad (4.21)$$

and the electric intensity is

$$E = \frac{1+j}{s\sigma} 2H_1 \epsilon^{-\frac{x}{s}} \cdot \epsilon^{-j\frac{x}{s}} = \frac{1+j}{s\sigma} 2H_1 \epsilon^{-\frac{x}{s}} \left(\cos\frac{x}{s} - j \sin\frac{x}{s}\right). \qquad (4.22)$$

Before proceeding with a further discussion of the flat-sheet problem, it seems interesting to re-examine the equations for the cylinder of Chapter 2 when the radius of the cylinder is very large, and the point of examination is near the surface of the cylinder. To assist in this procedure, we make use of the approximations of Dwight* for the Bessel functions of large argument.

---

* H. B. Dwight "A Precise Method of Calculation of Skin Effect in Isolated Tubes," *Journal of the American Institute of Electrical Engineers*, Vol. 42, No. 8, August 1923, p. 829, Equations (16) and (17).

For z very large,

$$\operatorname{ber} z = \frac{\epsilon^{\frac{z}{\sqrt{2}}}}{\sqrt{2\pi z}} \cos\left(\frac{z}{\sqrt{2}} - \frac{\pi}{8}\right);$$

$$\operatorname{bei} z = \frac{\epsilon^{\frac{z}{\sqrt{2}}}}{\sqrt{2\pi z}} \sin\left(\frac{z}{\sqrt{2}} - \frac{\pi}{8}\right);$$

$$\operatorname{ber}' z = \frac{\epsilon^{\frac{z}{\sqrt{2}}}}{\sqrt{2\pi z}} \cos\left(\frac{z}{\sqrt{2}} + \frac{\pi}{8}\right);$$

$$\operatorname{bei}' z = \frac{\epsilon^{\frac{z}{\sqrt{2}}}}{\sqrt{2\pi z}} \sin\left(\frac{z}{\sqrt{2}} + \frac{\pi}{8}\right).$$

When these approximations are introduced in (2.04) and (2.05), the following expressions result:

$$\boldsymbol{H} = 2H_0 \sqrt{\frac{a}{r}} \cdot \epsilon^{\frac{r-a}{s}} \cdot \epsilon^{+j\frac{r-a}{s}} \tag{4.23}$$

and

$$\boldsymbol{E} = \frac{-\sqrt{2} \cdot 2H_0}{\sigma s} \sqrt{\frac{a}{r}} \cdot \epsilon^{\frac{r-a}{s}} \cdot \epsilon^{+j\frac{r-a}{s}} \cdot \epsilon^{+j\frac{\pi}{4}}. \tag{4.24}$$

Fig. 35 shows the conditions on a cylinder of large radius. The distance in from the surface is

$$x = a - r$$

When x is very small compared to a and r, the ratio a/r is very close to unity. Then (4.23) and (4.24) become

$$\boldsymbol{H} = 2H_0\epsilon^{-\frac{x}{s}} \cdot \epsilon^{-j\frac{x}{s}} \tag{4.25}$$

and

$$\boldsymbol{E} = -\frac{1+j}{s\sigma} 2H_0\epsilon^{-\frac{x}{s}} \cdot \epsilon^{-j\frac{x}{s}}. \tag{4.26}$$

These approximate relations for the large cylinder are seen to be identical with equations (4.21) and (4.22) for the flat sheet, except for the negative sign in equation (4.26). This is occasioned because the electric intensity direction for the cylinder shown in Fig. 35 is exactly reversed from the condition of Fig. 34.

Let us now examine the state of affairs in the metal as shown in Fig. 36. We shall confine ourselves to a long column of metal with a cross section of 1 square centimeter. The current density flowing across the area, *b*, from (4.22), is

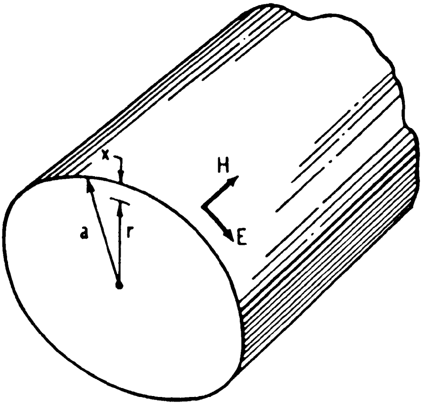

Fig. 35. The electric and magnetic intensity relations in a cylinder heated by induction.

$$\boldsymbol{J}(\text{amperes per square centimeter}) =$$

$$\sigma \boldsymbol{E} = \frac{1+j}{s}\,(2\boldsymbol{H}_1)\epsilon^{-\frac{x}{s}} \cdot \epsilon^{-j\frac{x}{s}}. \quad (4.27)$$

The total current flowing through the side of the column under the patch *a*, which is 1 centimeter on a side, is

$$\boldsymbol{I}_t = \int_{x=0}^{x=\infty} \boldsymbol{J} \cdot dx. \quad (4.28)$$

When (4.27) is substituted in (4.28) and the integration carried out, it is found that,

$$\boldsymbol{I}_t = 2\boldsymbol{H}_1. \quad (4.29)$$

Thus the total integrated current is in phase with the magnetic intensity at the surface, and is equal to twice the primary magnetic intensity.

The power dissipated as heat in the

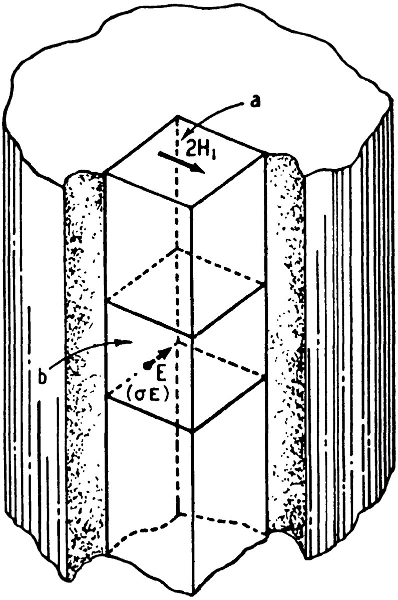

Fig. 36. Electric intensity and current flow relations in a submerged cube.

little cube of which the area b comprises one face is σE^2, where the absolute value of E is used. Then the power density is

$$P(\text{watts per cubic centimeter}) = \frac{2(2H_1)^2}{s^2\sigma}\cdot\epsilon^{-\frac{2x}{s}}. \tag{4.30}$$

When this expression is integrated throughout the length of the column, the total power in the column beneath the patch, a, which has unit area, is found to be

$$P_t(\text{watts per square centimeter of surface}) = \int_{x=0}^{x=\infty} P\,dx = \frac{(2H_1)^2}{s\sigma}. \tag{4.31}$$

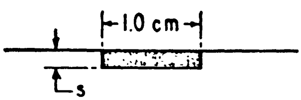

FIG. 37. A small patch on the surface of the metal. The thickness of the patch is equal to the skin thickness.

On substituting (4.29) in (4.31),

$$P_t = \frac{I_t^2}{s\sigma}. \tag{4.32}$$

This last expression reveals the true significance of the skin thickness, s, which was defined in Chapter 1. Let us turn for the moment to the small patch in Fig. 37. This patch has a width of 1 centimeter and a height of s centimeters. The total current I_t is assumed to flow into the paper through this patch, which has an area of s square centimeters.

The resistance of the volume of metal which has an area of s square centimeters and extends into the paper 1 centimeter is $\frac{1}{s\sigma}$.

Then the total power dissipated in this volume is the resistance multiplied by the square of the current, or

$$P_t = \frac{I_t^2}{s\sigma}.$$

This expression is identical with (4.32). Thus, if the total current flows uniformly in a layer whose depth is the skin thickness, the power dissipated will be exactly the same as if the current were distributed by the true exponential law.

Returning now to the power density expression, we substitute (4.31) in (4.30) and find

$$P(\text{watts per cubic centimeter}) = \frac{2}{s}P_t\epsilon^{-\frac{2x}{s}}. \tag{4.33}$$

The current density for a number of distances below the surface is shown in Fig. 38. Again we see that the current density lags in phase as we go deeper into the material, and the current density decreases rapidly. It is interesting to note that the current density at a depth of three skin thicknesses is approximately out of phase with the surface current density. This current, although small is thus actually flowing in the opposite direction to the surface current.

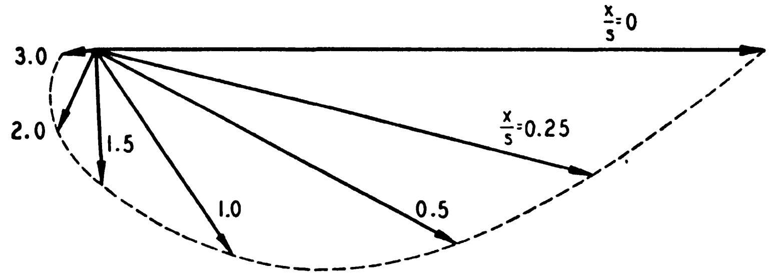

Fig. 38. Vector current density relations in the metal.

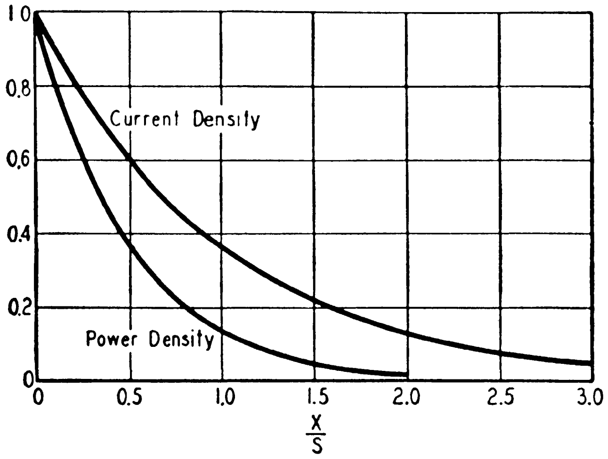

Fig. 39. Relative current density and power density in the metal.

Fig. 39 shows the relative current density as a function of the distance from the surface. At a depth equal to the skin thickness, the current density is 36.8 per cent of the density at the surface. On this same diagram, the relative power density is 13.5 per cent of the density at the surface. It is also interesting to note that over 86 per cent of the total power is lost in a layer equal to the skin thickness.

Actual magnitudes of the quantities appearing in this discussion may be illuminating. Table 3 has been constructed for this purpose.

In this chapter, we have examined the mechanics of high-frequency current-flow on flat, thick conductors. The crowding of the current to the surface of the conductor, with the attendant generation of heat near the surface is of great value in surface-hardening of steels. In this connection, equation (4.33) will be especially useful in later chapters where the case-hardening of steel will be considered quantitatively.

TABLE 3. FIELD RELATIONS AT THE SURFACE OF A METAL CONDUCTOR.

Material	Copper
Conductivity	5.8 × 10^5 mhos for a centimeter cube
Frequency	1,000,000 cycles
Skin thickness	0.00662 centimeter
Power applied	1.0 watt per square centimeter of surface
Magnetic intensity impinging on surface	31.0 ampere-turns per centimeter
Magnetic intensity reflected	31.0 ampere-turns per centimeter
Magnetic intensity in the metal at the surface	62.0 ampere-turns per centimeter
Total current under 1 square centimeter patch	62.0 amperes
Current density just under surface	13,220 amperes per square centimeter
Electric intensity impinging on surface	11,680 volts per centimeter
Electric intensity reflected (approximate)	11,680 volts per centimeter
Electric intensity in metal at the surface	0.0228 volt per centimeter
Power density at the surface	302.0 watts per cubic centimeter

Chapter 5

CURRENT FLOW IN FLAT METAL SHEETS OF LIMITED THICKNESS

In the preceding chapter, the penetration of current in metals was examined for the case of very thick sheets. However, it is sometimes necessary to heat metal sheets where the thickness of the sheet is of the same order as the skin thickness of the metal. It is the purpose of this chapter to investigate the manner in which the current distribution through the sheet is altered by limiting the thickness. We have already seen that a plane wave impinging normally on a metal plane undergoes almost perfect reflection, but that large currents are induced in the metal. Equation (4.08) showed that the electric intensity in the metal, and hence the current density, consisted of two terms. The first term represents a wave which is being propagated into the metal, dropping off exponentially while suffering a uniform phase lag. The second term represents a wave reflected from the far boundary of the metal sheet. This wave decreases exponentially as it moves from the far boundary toward the initial bounding surface. Equation (4.10) was obtained by assuming that the sheet was of infinite thickness so that this last wave could be neglected.

When the sheet is limited in thickness, the last term in (4.08) cannot be neglected. However, the reflection at the far surface is not total so that an additional wave propagates away into space beyond the sheet. In general, this latter wave is extremely weak. The condition of these waves is shown in Fig. 40, for a sheet of thickness *a*.

The main wave incident on the surface is

$$\bar{\boldsymbol{H}}_1 = \boldsymbol{H}_1\epsilon^{+j\frac{2\pi y}{\lambda_0}} \tag{5.01}$$

and

$$\bar{\boldsymbol{E}}_1 = 120\pi\boldsymbol{H}_1\epsilon^{+j\frac{2\pi y}{\lambda_0}}; \tag{5.02}$$

whereas the reflected wave is

$$\bar{\boldsymbol{H}}_2 = \boldsymbol{H}_2\epsilon^{-j\frac{2\pi y}{\lambda_0}} \tag{5.03}$$

and

$$\bar{E}_2 = 120\pi H_2 \epsilon^{-j\frac{2\pi y}{\lambda_0}}. \qquad (5.04)$$

From (4.07) and (4.08), the magnetic intensity in the metal is

$$H = A\epsilon^{-\frac{x}{s}} \cdot \epsilon^{-j\frac{x}{s}} + B\epsilon^{+\frac{x}{s}} \cdot \epsilon^{+j\frac{x}{s}}, \qquad (5.05)$$

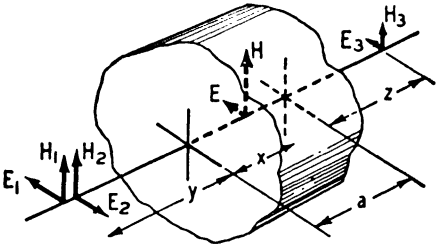

FIG. 40. The electric and magnetic field relations when a plane electromagnetic wave impinges on a thin metal sheet.

whereas the electric intensity in the metal is

$$E = \frac{1+j}{s\sigma}\left(A\epsilon^{-\frac{x}{s}} \cdot \epsilon^{-j\frac{x}{s}} - B\epsilon^{+\frac{x}{s}} \cdot \epsilon^{+j\frac{x}{s}}\right). \qquad (5.06)$$

The wave that continues on into the space beyond the sheet is

$$\bar{H}_3 = H_3\epsilon^{-j\frac{2\pi z}{\lambda_0}} \qquad (5.07)$$

and

$$\bar{E}_3 = 120\pi H_3 \epsilon^{-j\frac{2\pi z}{\lambda_0}}. \qquad (5.08)$$

At the boundary, $x = 0$, $y = 0$, the magnetic intensities are continuous so (5.01), (5.03) and (5.05) yield

$$H_1 + H_2 = A + B. \qquad (5.09)$$

Since the electric intensities are also continuous at the same boundary, from (5.02), (5.04), and (5.06) we find that

$$120\pi(H_1 - H_2) = \frac{1+j}{s\sigma}(A - B). \qquad (5.10)$$

On the far boundary, $x = a$, $z = 0$, the magnetic intensities are also equal.

Making use of (5.05) and (5.07),

$$H_3 = A\epsilon^{-\frac{a}{s}} \cdot \epsilon^{-j\frac{a}{s}} + B\epsilon^{+\frac{a}{s}} \cdot \epsilon^{+j\frac{a}{s}}. \tag{5.11}$$

The condition of continuity of the electric intensity at the same boundary makes necessary the relation,

$$120\pi H_3 = \frac{1+j}{s\sigma}\left(A\epsilon^{-\frac{a}{s}} \cdot \epsilon^{-j\frac{a}{s}} - B\epsilon^{+\frac{a}{s}} \cdot \epsilon^{+j\frac{a}{s}}\right). \tag{5.12}$$

If we now solve this set of simultaneous equations for A and B in terms of H_1 and substitute in (5.06), we find

$$E = \frac{(2H_1)}{s\sigma}(1+j)$$

$$\left\{\frac{\epsilon^{-\frac{x}{s}}\cos\frac{x}{s} + \epsilon^{-\frac{2a-x}{s}}\cos\left(\frac{2a-x}{s}\right) - j\left[\epsilon^{-\frac{x}{s}}\sin\frac{x}{s} + \epsilon^{-\frac{2a-x}{s}}\sin\left(\frac{2a-x}{s}\right)\right]}{1 - \epsilon^{-\frac{2a}{s}}\cos\frac{2a}{s} + j\epsilon^{-\frac{2a}{s}}\sin\frac{2a}{s}}\right\}. \tag{5.13}$$

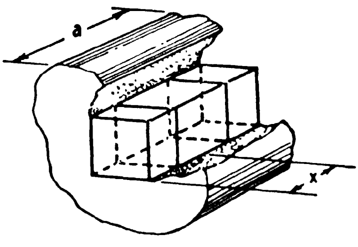

Fig. 41. The submerged cube to which (5.14) applies.

In arriving at (5.13), the same approximation used in establishing (4.19) and (4.20) was invoked. That is, $120\pi s\sigma$ is very large compared to unity. This places a limitation on (5.13) and the equations that follow in this chapter, in that the formulas hold for small values of a, but in some cases degenerate as a actually approaches zero.

The power density, in watts per centimeter cube, is then obtained by multiplying the square of the absolute value of (5.13) by the conductivity of the metal. This expression is the power density in the little cube shown in Fig. 41. An integration of this latter expression yields the total power lost in the box which has ends of area 1 square centimeter and length a. When the power density relation is divided by the equation for total power lost in the box, we obtain,

P(watts per cubic centimeter) =

$$\frac{2}{s}P_t\left\{\frac{\epsilon^{-\frac{2x}{s}} + \epsilon^{-\frac{2(2a-x)}{s}} + 2\epsilon^{-\frac{2a}{s}}\cos\left[\frac{2(a-x)}{s}\right]}{1 - \epsilon^{-\frac{4a}{s}} + 2\epsilon^{-\frac{2a}{s}}\sin\frac{2a}{s}}\right\}. \tag{5.14}$$

It is interesting to note that when the thickness *a* is made infinite, (5.14) degenerates to exact correspondence with (4.33).

Fig. 42 shows the expression included within the braces of (5.14) as a function of the distance into the material for a number of sheet thicknesses. When the sheet is extremely thin, the power dissipation becomes uniform throughout the sheet. It may be seen that when the sheet has a thickness which is more than twice the skin thickness, *s*, the power density distribution is essentially the same as for the infinitely thick sheet. For this condition, the power density distribution given by (4.33) may be used. This is an important point where heat flow is considered in later chapters because of the extreme simplicity of this expression. The use of (5.14) would be unwieldy in the extreme without adding to the generality of treatment.

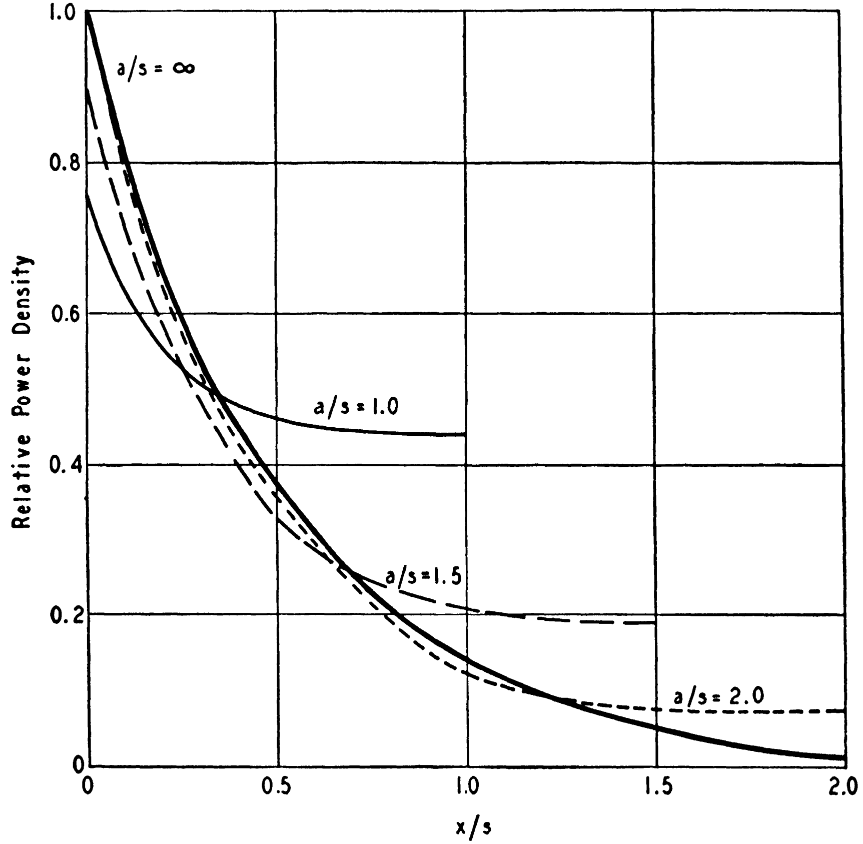

FIG. 42. Relative power density in strips of various thicknesses. These curves are calculated from the portion of (5.14) included in braces.

Induction Heating of Thin Strip. Equations (5.13) and (5.14) apply to the heating of a thin strip of metal where the exciting field is applied from one side only. This would be the case where the current-carrying conductor was placed parallel to a thin sheet. Also, if a tube which had a radius large compared to the wall thickness were to be heated by placing the tube in a solenoid, the above equations would apply. Here all of the applied magnetic intensity is on one side of the sheet. However, if we were to induction-heat a wide thin strip by running it through a current-carrying coil as shown in Fig. 43, the applied magnetic intensity would be on both sides of the sheet.

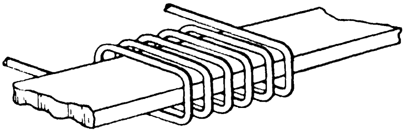

Fig. 43. A thin strip runs through a current-carrying coil.

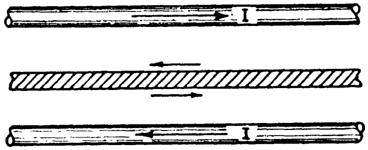

Fig. 44. A small section of the sheet is shown between two elements of the coil.

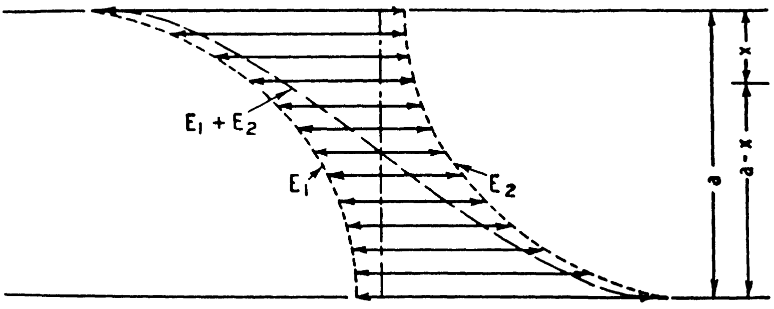

Fig. 45. The arrows pointing to the left show the current flow in the sheet due to the top conductor, while the arrows pointing to the right show the current flow due to the bottom conductor.

Fig. 44 shows a small section of the sheet between two conductors of the coil. The upper conductor with current flowing to the right would induce currents in the top of the sheet which would flow toward the left. The lower conductor carries current which flows to the left, and will induce current flow on the bottom of the sheet. This induced current will flow toward the right. Since both of these currents penetrate into the sheet, they will oppose each other and from symmetry conditions the current density at the exact center of the sheet will be zero. In Fig. 45, the set of arrows pointing to the left depicts the electric intensity (or current density) due to the upper conductor, while those pointing to the right represent the electric intensity due to the bottom conductor.

The electric intensity, $\boldsymbol{E}_1$, may be reckoned directly from (5.13) while the electric intensity, $\boldsymbol{E}_2$, is found by substituting $a - x$ for x in (5.13). The total electric intensity is then found by subtracting $\boldsymbol{E}_2$ from $\boldsymbol{E}_1$. It should be remembered that the current density is always given by multiplying the electric intensity by the conductivity. The resulting total electric intensity is

$$\begin{aligned} \boldsymbol{E} = \boldsymbol{E}_1 - \boldsymbol{E}_2 = \frac{(2\boldsymbol{H}_1)(1+j)}{s\sigma} & \Bigg\{ \epsilon^{-\frac{x}{s}} \cos\frac{x}{s} + \epsilon^{-\frac{2a-x}{s}} \cos\left(\frac{2a-x}{s}\right) \\ & - \epsilon^{-\frac{a-x}{s}} \cos\left(\frac{a-x}{s}\right) - \epsilon^{-\frac{a+x}{s}} \cos\left(\frac{a+x}{s}\right) \\ & - j\left[\epsilon^{-\frac{x}{s}} \sin\frac{x}{s} + \epsilon^{-\frac{2a-x}{s}} \sin\left(\frac{2a-x}{s}\right) \right. \\ & \left. - \epsilon^{-\frac{a-x}{s}} \sin\left(\frac{a-x}{s}\right) - \epsilon^{-\frac{a+x}{s}} \sin\left(\frac{a+x}{s}\right)\right]\Bigg\} \\ & \div \left(1 - \epsilon^{-\frac{2a}{s}} \cos\frac{2a}{s} + j\epsilon^{-\frac{2a}{s}} \sin\frac{2a}{s}\right). \end{aligned} \tag{5.15}$$

Equation (5.15) has been used to construct the curves of Fig. 46, which show the relative current density distribution through the strip. As the strip increases in thickness, the distribution of current is exponential from the surface, with the action at either surface virtually independent of the distance to the other surface.

The total power lost throughout the strip, under a little patch of surface which has an area of 1 square centimeter, is obtained by squaring the absolute magnitude of (5.15), multiplying by the conductivity, and integrating through the strip. This procedure yields

$$P_t(\text{watts per square centimeter of surface}) = \frac{8H_1^2}{s\sigma} \cdot G, \tag{5.16}$$

where G is the following function of $\frac{a}{s}$:

$$\begin{aligned} G = \Bigg[1 - \epsilon^{-\frac{4a}{s}} - 2\epsilon^{-\frac{a}{s}}\left(\sin\frac{a}{s} + \cos\frac{a}{s}\right) + \epsilon^{-\frac{2a}{s}}\left(\sin\frac{2a}{s} + \sin\frac{a}{s}\right) \\ + 2\epsilon^{-\frac{3a}{s}}\left(\cos\frac{a}{s} - \sin\frac{a}{s}\right)\Bigg] \div \left(1 + \epsilon^{-\frac{4a}{s}} - 2\epsilon^{-\frac{2a}{s}} \cos\frac{2a}{s}\right). \end{aligned} \tag{5.17}$$

A plot of the factor G is given in Fig. 47. It may be seen that G has very small values when the thickness of the strip is small, but the function rises quickly to unity when the strip thickness is two or three times greater than the skin thickness.

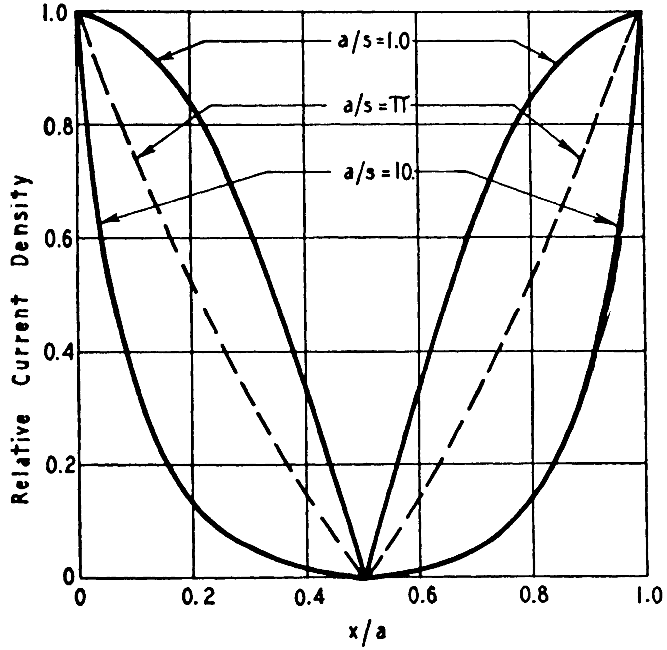

FIG. 46. Relative current density distribution through the metal sheet when the sheet is excited from both sides.

When G is unity, (5.16) has a value exactly twice that shown by (4.31). Physically, this is correct, since we are now absorbing power on both surfaces of the strip. Thus, in stating that (5.16) above is the expression for the watts absorbed per square centimeter of surface we must remember that we really mean the power absorbed in a box which has a square top and bottom of area 1 square centimeter each, and a height equal to a, the thickness of the strip.

When a/s is 2.25, we are at the knee of the curve and the power absorption is not materially increased by going to greater values of a/s. Thus we may arrive at an expression for a critical frequency for effective coupling to a thin strip. When a/s equals 2.25, the corresponding frequency is

$$f_c = \frac{128.5 \times 10^6}{\sigma \mu_r a^2}, \tag{5.18}$$

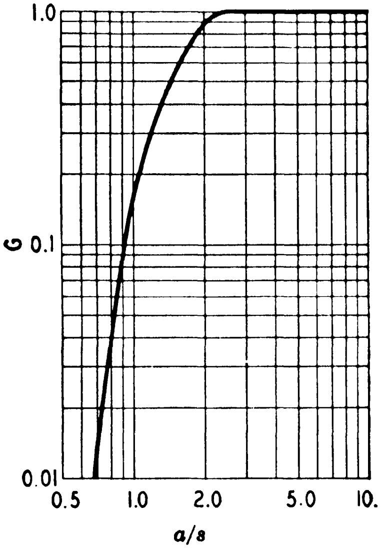

FIG. 47. The factor G defined by (5.17) is shown as a function of the strip thickness, where the strip thickness is expressed in terms of the skin thickness of the metal.

where

f_c = critical frequency in cycles;
σ = conductivity of metal in mhos per centimeter cube;
μ_r = relative permeability of the metal;
a = thickness of the strip in centimeters.

A quantitative examination of this relation will be made in the following chapter which relates to strip heating.

Chapter 6

STRIP HEATING

The heating of metal strip is often required for the purpose of hardening, tempering, or annealing the strip, to bake a finish thereon, or even to smooth out a tin plating.* The practical aspects of induction heating as applied to the heat treatment of metal strip will be considered in this chapter. In the preceding chapter, an expression (5.18) was derived for the critical frequency for efficient coupling to a thin sheet. Fig. 48 shows the critical frequency as obtained from this expression plotted against sheet thickness for a number of metals at various temperatures. These curves are similar to those for wire shown in Fig. 21. A comparison of equations (2.13) and (5.18) shows that the critical frequencies for a wire and a thin sheet are the same when the radius of the wire is equal to the thickness of the sheet.

Experiments in Heating Thin Sheet. Using the oscillator shown in Fig. 24 but operating at a frequency of 38 megacycles, a series of tests were conducted to determine the relative field intensities required to heat small sheets of steel and brass of various thicknesses to several selected temperatures. The power was applied for a period of time sufficiently long for the temperature to reach a steady-state condition. Under this condition, the power absorbed by the sheet was equal to the power lost by radiation and conduction. Since the thickness of the sheets was small compared to the other dimensions, the loss for a given temperature was essentially the same for all the thicknesses used. Consequently, the power absorbed was also the same. The relative field intensities were obtained by measuring the current through the coupling coil. The higher temperatures were measured by means of a Leeds and Northrup optical pyrometer, and the lower temperatures were measured by the use of Tempil Pellets.† Oxidation of the samples and subsequent change of thickness were prevented by subjecting the samples to an atmosphere of nitrogen. Fig. 49 gives the results of these tests.

---

* H. C. Humphrey, "Electronic Tin Fusion," *Proc. I.R.E.*, Vol. 32, No. 2, February 1944, pp. 61–66.

† Tempil Corporation, New York, N. Y.

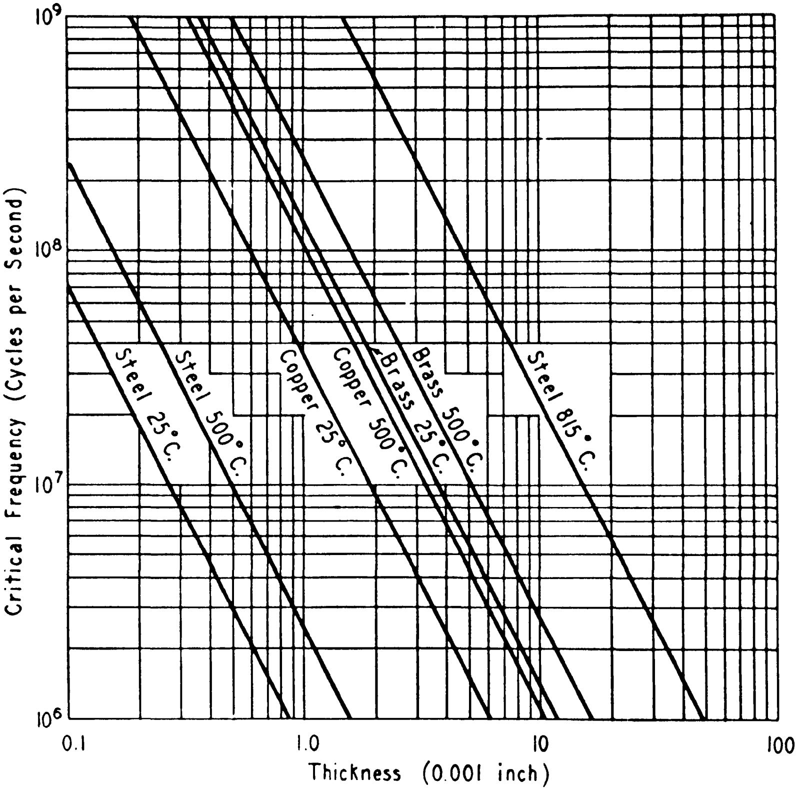

FIG. 48. Critical frequency as a function of strip thickness, for a number of strip materials.

The critical thickness is defined as the minimum thickness for efficient coupling at a given frequency. The expression for critical thickness may be obtained from (5.18).

$$\text{Critical thickness} = \sqrt{\frac{128.5 \times 10^6}{\sigma \mu_r f}} \text{ centimeters.} \qquad (6.01)$$

Calculated values for critical thickness are shown by the vertical arrows on Fig. 49. It should be noted that the experimental values of relative field intensity rise abruptly when the thickness is only slightly less than the calculated critical thickness.

Power Requirements for Strip Heating. To obtain the power required to continuously heat metal strip to a desired temperature, it is necessary to consider the power required to raise the temperature of the strip as well as that lost by radiation from the heated area.

The power required to raise the temperature can be calculated as follows:

$$P = 0.528W \cdot \rho \cdot \Delta u, \qquad (6.02)$$

where P = power in watts;
W = weight of strip to be heated, in pounds per hour;
ρ = specific heat of strip material, in calories per gram per degree Centigrade;
Δu = temperature rise, in degrees Centigrade.

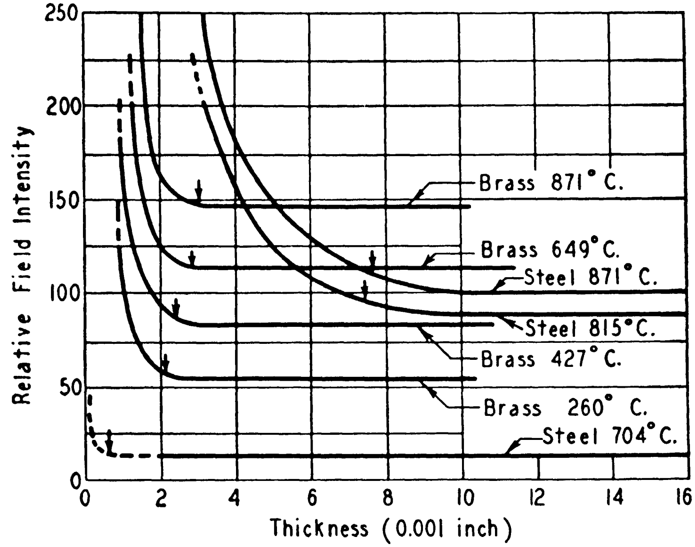

FIG. 49. Relative field intensity as a function of strip thickness. These data were measured at a frequency of 38 megacycles. The vertical arrow on each curve represents the critical thickness calculated from (6.01).

The radiation loss can be calculated by equation (3.01) using for the area the heated portion of the strip before it leaves the coupling coil. Fig. 50 shows the calculated (solid line) and observed (dots) radiation loss for an oxidized steel surface plotted against temperature.

Illustrative Example. It will be assumed that it is desired to harden and temper steel strip 1 inch wide and 0.010 inch thick at a rate of 50 pounds per hour.

To harden steel it is necessary to heat it to a temperature of about 815° C and then cool it quickly. Tempering is then accomplished by reheating it to a lower temperature of 225° C to 300° C depending on the temper desired. Fig. 51 shows a set-up for the continuous hardening and tempering of steel strip. Here the strip is guided through a coupling coil where it is heated to a temperature of about 815° C and then cooled quickly by passing it between water-cooled quench blocks. It then passes through another coil which heats it to about 275° C for tempering and it is again cooled by another set of quench blocks. The coupling coils and quench blocks are enclosed to permit the operation to be performed in a neutral atmosphere so that oxidation and scaling will not occur.

The critical frequency for the heating of steel to 815° C as obtained from equation (5.18) or Fig. 48 is 22 megacycles.

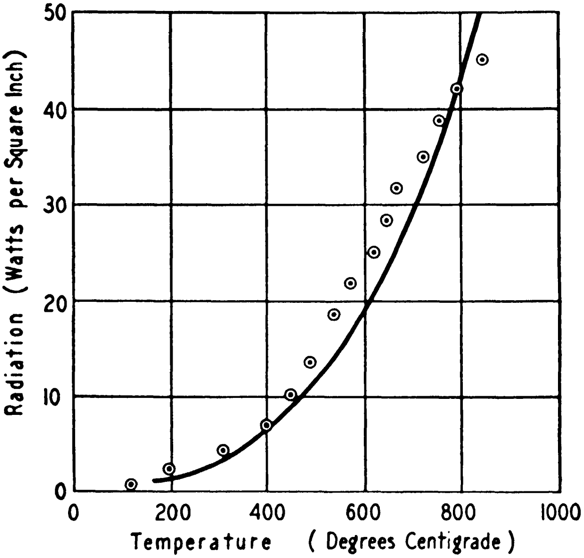

Fig. 50. Calculated and observed radiation loss from oxidized surface, as a function of temperature.

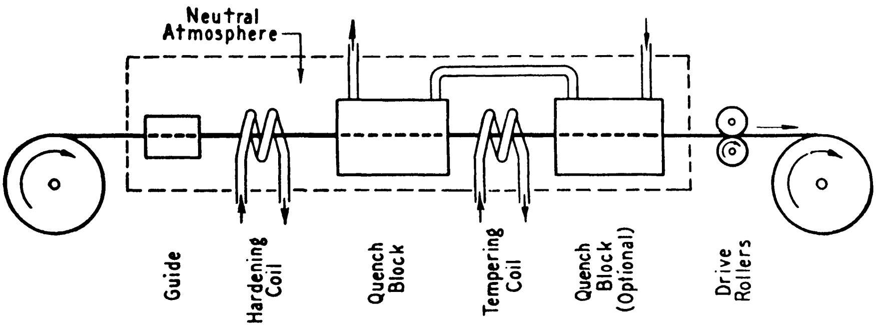

Fig. 51. Arrangement for the continuous hardening and tempering of steel strip by frequency heat.

The power required to raise the temperature of the strip to the hardening temperature is found from (6.02) to be

$$P = 0.528 \times 50 \times 0.16 \times (815 - 25) = 3350 \text{ watts.}$$

The power lost by radiation from both sides of the strip in the hardening coil, assuming that a length of strip of $\frac{1}{2}$ inch will be heated in the coil, is, from (3.01),

$$\text{Radiation loss} = 5.735 \times 10^{-12} \times 2.54^2\,(1088^4 - 298^4) = 46.3 \text{ watts.}$$

The power required to reheat the strip for tempering to 300° C is

$$P = 0.528 \times 50 \times 0.12 \times (300 - 25) = 872 \text{ watts.}$$

The radiation loss for this condition is small and can be neglected.

The values of specific heat used in the above computations were obtained from Fig. 139.

The total power required is the sum of the above values or 4268 watts. This is the power that must be delivered to the strip and does not take into account the losses in the coupling coil.

The curves of Fig. 49 well illustrate the advantage of operating somewhat above the critical frequency. If the frequency is slightly below the critical frequency and the strip to be heated varies slightly in thickness, it is easy to slide along the steep part of the curves on the left of Fig. 49. While thinner strip requires less energy to raise the temperature, the relative-efficiency curves are so steep that a net loss occurs with consequent under-heating of the thin parts of the strip.

To insure even current distribution over the entire surface of a strip, the inducing coil should stay well away from the edges of the strip. The distance from the edge of the strip to the portion of the coil which curves around the edge should be at least as great as the spacing of the center of the strip from the nearest part of the coil.

Chapter 7

CURRENT FLOW IN LAMINAR SHEETS

In a rather restricted number of applications, a study of current flow and power generation in laminar sheets may prove to be of interest. In Fig. 52, we find a layer of metal with a thickness, a, in intimate contact with another semi-infinite block of metal. The outer layer will be designated as Region 1, and the thick inner block, Region 2. Subscripts will be used to distinguish the physical constants of the two metals. That is,

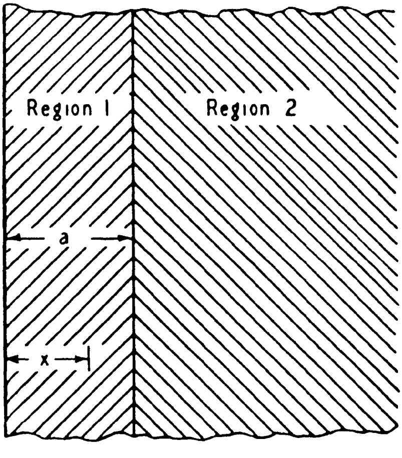

FIG. 52. Laminar metal sheets, where Region 1 is the surface layer of metal and Region 2 is the thick inner block.

μ_1 = the relative permeability of the metal in Region 1.
σ_1 = the conductivity of the metal in Region 1.
s_1 = the skin thickness of the metal in Region 1.
μ_2 = the relative permeability of the metal in Region 2.
σ_2 = the conductivity of the metal in Region 2.
s_2 = the skin thickness of the metal in Region 2.

The derivation of the pertinent equations follows the same line of attack as that used in preceding chapters. However, the algebraic manipulation is very tedious. Because of the limited interest in the problem, only the more useful results will be given. Teare and Webb* have treated a similar case in cylindrical coordinates and have applied their equations to the problem of copper-clad steel conductors.

---

* B. R. Teare, Jr. and Josephine R. Webb, "Skin Effect in Bimetallic Conductors," *A.I.E.E. Transactions*, Vol. 62, June 1943, pp. 297–302.

When P_t is the total power applied to 1 square centimeter of surface of the outer layer, the power density in Region 1 a distance x from the outer layer is

$$P_1(\text{watts per cubic centimeter}) = \frac{2}{s_1} P_t \left[\epsilon^{-\frac{2x}{s_1}} + \frac{\left(1 - \sqrt{\frac{\mu_1\sigma_2}{\mu_2\sigma_1}}\right)^2}{\left(1 + \sqrt{\frac{\mu_1\sigma_2}{\mu_2\sigma_1}}\right)^2} \cdot \epsilon^{-\frac{2(2a-x)}{s_1}} + \frac{2\left(1 - \sqrt{\frac{\mu_1\sigma_2}{\mu_2\sigma_1}}\right)}{\left(1 + \sqrt{\frac{\mu_1\sigma_2}{\mu_2\sigma_1}}\right)} \cdot \epsilon^{-\frac{2a}{s_1}} \cos\frac{2(a-x)}{s_1} \right] \div D, \quad (7.01)$$

where

$$D = 1 - \epsilon^{-\frac{2a}{s_1}} + \frac{\left(1 - \sqrt{\frac{\mu_1\sigma_2}{\mu_2\sigma_1}}\right)^2}{\left(1 + \sqrt{\frac{\mu_1\sigma_2}{\mu_2\sigma_1}}\right)^2} \left(\epsilon^{-\frac{2a}{s_1}} - \epsilon^{-\frac{4a}{s_1}}\right) + \frac{2\left(1 - \sqrt{\frac{\mu_1\sigma_2}{\mu_2\sigma_1}}\right)}{\left(1 + \sqrt{\frac{\mu_1\sigma_2}{\mu_2\sigma_1}}\right)} \cdot \epsilon^{-\frac{2a}{s_1}} \sin\frac{2a}{s_1} + \frac{4\sqrt{\frac{\mu_1\sigma_2}{\mu_2\sigma_1}}}{\left(1 + \sqrt{\frac{\mu_1\sigma_2}{\mu_2\sigma_1}}\right)^2} \cdot \epsilon^{-\frac{2a}{s_1}} \quad (7.02)$$

The power density in Region 2, where x is measured from the outer surface of Region 1, is

$$P_2(\text{watts per cubic centimeter}) = \frac{2}{s_1} P_t \left[\frac{4\sigma_2}{\sigma_1} \cdot \frac{\epsilon^{-\frac{2a}{s_1}} \cdot \epsilon^{-\frac{2(2x-a)}{s_2}}}{\left(1 + \sqrt{\frac{\mu_1\sigma_2}{\mu_2\sigma_1}}\right)^2} \right] \div D. \quad (7.03)$$

The resistance to current flow of a 1-centimeter square, is

$$R = \frac{1}{s_1\sigma_1} \cdot D \div \left[1 + \frac{\left(1 - \sqrt{\frac{\mu_1\sigma_2}{\mu_2\sigma_1}}\right)^2}{\left(1 + \sqrt{\frac{\mu_1\sigma_2}{\mu_2\sigma_1}}\right)^2} \cdot \epsilon^{-\frac{4a}{s_1}} - \frac{2\left(1 - \sqrt{\frac{\mu_1\sigma_2}{\mu_2\sigma_1}}\right)}{\left(1 + \sqrt{\frac{\mu_1\sigma_2}{\mu_2\sigma_1}}\right)} \cdot \epsilon^{-\frac{2a}{s_1}} \cos\frac{2a}{s_1} \right]. \quad (7.04)$$

When steel is heated to the neighborhood of 800° C, the permeability of the metal drops from a high value to unity. If the material is heated by induced currents, the region near the surface will reach the Curie point before material at greater depths. However, even when extremely short heating times are used, the heat flows quickly inward so that the temperature gradient for some distance into the metal is not great. Only a thin layer will be above the Curie point but adjacent regions will be heated almost to the Curie point.

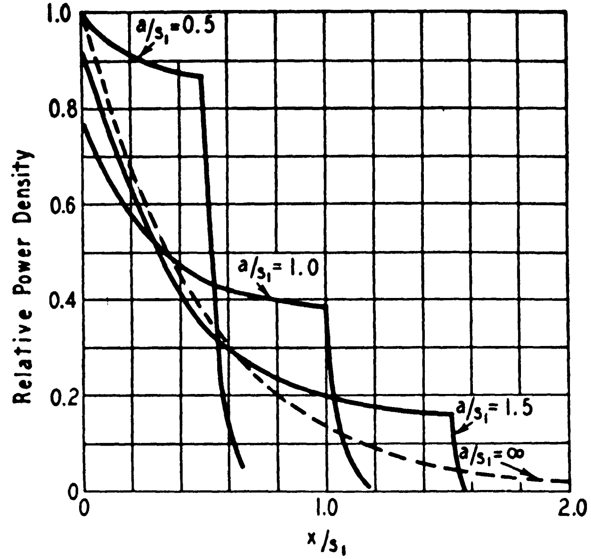

FIG. 53. Relative power densities through laminar materials. The relative permeability in Region 1 is unity, whereas the relative permeability in Region 2 is assumed to be 100.

Therefore, the electrical conductivity will not be changed greatly as we proceed into the metal.

Nevertheless, there may be an abrupt change in the relative permeability of the material. To study this case, we assume that the conductivity in Region 1 of Fig. 52 is the same as the conductivity of Region 2. However, we also assume that the permeability of Region 1 is unity while the permeability in Region 2 is 100. Then $\sqrt{\frac{\mu_1\sigma_2}{\mu_2\sigma_1}} = 0.1$. The power density for this case is shown in Fig. 53 as a function of the distance into the metal. These curves were obtained from the bracketed expressions shown in (7.01) and (7.03), each divided by the quantity D shown in (7.02). An abrupt drop in the power density may be noted as soon as the boundary between the two regions is passed. However, the departure from the exponential distribution is not great and it seems reasonable to use this distribution in the heat-flow analysis of later chapters.

Other authors*† have shown qualitative results based on the assumption that an abrupt change in conductivity occurs at the same point where the permeability changes. This causes a concentration of current at a point beneath the surface, with a consequent power-density maximum at the same point. The authors believe, however, the assumptions leading to the results of Fig. 53 represent the true state of affairs more accurately.

Equation (7.04) is useful in considering the problem of plating a poor conductor with a good conductor. For example, a steel plate may be plated with copper to decrease the resistance. Care should be exercised to insure that the copper plating is properly polished and buffed in order to make a continuous copper coating. We shall assume that in Region 1 (copper)

$$\sigma_1 = 5.8 \times 10^5 \text{ mhos for a centimeter cube,}$$
$$\mu_1 = \text{unity,}$$

and for Region 2 (steel)

$$\sigma_2 = 10^5 \text{ mhos for a centimeter cube,}$$
$$\mu_2 = 100.$$

Then $\sqrt{\dfrac{\mu_1\sigma_2}{\mu_2\sigma_1}} = 0.0415$. It may be noted that the quantity $\dfrac{1}{s_1\sigma_1}$ is the resistance if the copper were infinitely thick. Thus, the quantity D divided by the bracketed expression in (7.04) may be regarded as the ratio of the resistance of the laminar condition to the resistance of a thick copper sheet. This resistance ratio is tabulated below.

Thickness of Copper Coating (measured in terms of the skin thickness of copper)	Resistance Ratio
0	24.1
0.25	3.57
0.5	1.94
1.0	1.085
∞	1.0

We thus see that a copper coating on a steel conductor, where the copper coating is at least as thick as the skin thickness of copper, produces losses which exceed the losses in a solid copper conductor by only $8\frac{1}{2}$ per cent.

---

* G. Babat and M. Losinsky, " Heat Treatment of Steel by High Frequency Currents," *Journal of the Institution of Electrical Engineers*, Vol. 86, February 1940, p. 165.

† W. M. Roberds, " The Use of Radio Frequencies to Obtain High Power Concentrations for Industrial Heating Applications," *Proc. I.R.E.*, Vol. 33, No. 1, January 1945, pp. 10–11.

Chapter 8

CONDUCTORS CARRYING CURRENT PARALLEL TO FLAT METAL SHEETS

At times, it becomes necessary to couple to a cylinder of metal with a single-turn coil closely spaced to the work. Then the coil impedance is very low and a transformer must be used to obtain efficient operation. This is true in many soldering operations and in the practice of scanning for case-hardening of steel by self-quenching. Before considering the transformers which may be used in these operations, it seems desirable to examine the action of the single-turn coupling coil. If the cylinder to be heated is of large diameter, the case may be simplified by treating the problem as a straight conductor parallel to a flat sheet of metal of great thickness. In Fig. 54, we see a long conductor parallel to a conducting layer and *h* units above the layer. This filamentary conductor is carrying current into the

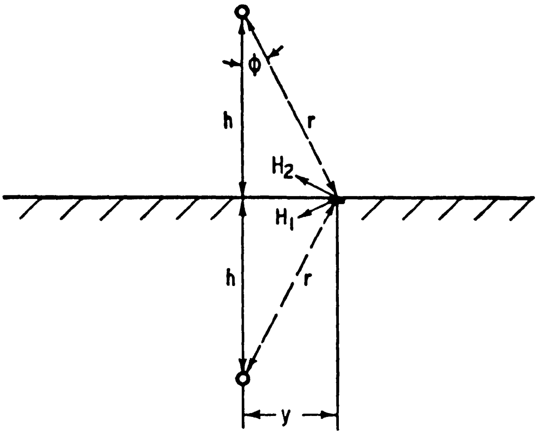

FIG. 54. Current-carrying conductor above and parallel to a conducting sheet.

paper. For the purpose of computing fields above the metal layer, we place another conductor or image h units below the surface of the layer. This image is effectively a conductor carrying current out of the paper. At a point y units along the conducting layer, as shown in Fig. 54, the current-carrying conductor above the metal sheet sets up a magnetic intensity vector $\boldsymbol{H}_1$ which is at right angles to the line r drawn from the conductor to the point in question. This magnetic intensity is

$$\boldsymbol{H}_1 = \frac{\boldsymbol{I}}{2\pi r}, \tag{8.01}$$

where

$$r = \sqrt{h^2 + y^2}.$$

The magnetic intensity due to the image is $\boldsymbol{H}_2$ and is equal to $\boldsymbol{H}_1$ in magnitude and phase but points in the direction shown in Fig. 54. The sum of these two vectors is parallel to the surface of the layer and has a magnitude which is

$$\boldsymbol{H} = 2\boldsymbol{H}_1 \cos \phi = 2\boldsymbol{H}_1 \cdot \frac{h}{r} \cdot \tag{8.02}$$

Now since the metal surface is a good conductor, the current in the metal sheet will be concentrated near the surface. Then the current density $\boldsymbol{J}$ in amperes per centimeter in the little patch shown in Fig. 54, where the patch is of unit width and x and h are in centimeters, is

$$\boldsymbol{J} = \boldsymbol{H} = \frac{\boldsymbol{I}}{\pi} \cdot \frac{h}{h^2 + y^2} = \frac{\boldsymbol{I}}{\pi h} \cdot \frac{1}{1 + \left(\frac{y}{h}\right)^2} \cdot \tag{8.03}$$

The equality of $\boldsymbol{J}$ and $\boldsymbol{H}$ is obtained directly from (4.29).

Fig. 55 shows the current distribution in the sheet for a number of values of h with the current $\boldsymbol{I}$ in the conductor equal to 1 ampere. We see that as the conductor is placed closer to the layer or sheet, the current density increases directly below the conductor, but drops off quickly in a lateral direction.

To sum up all the current in the sheet, we integrate (8.03) from $y = -\infty$ to $y = +\infty$. Then

$$\int_{y=-\infty}^{y=\infty} \boldsymbol{J} \cdot dy = \frac{2h\boldsymbol{I}}{\pi} \int_{y=0}^{y=\infty} \frac{dy}{h^2 + y^2} = \frac{2\boldsymbol{I}}{\pi} \tan^{-1}\left(\frac{y}{h}\right) \Bigg|_{y=0}^{y=\infty} = \boldsymbol{I}. \tag{8.04}$$

The total current flowing in the sheet is thus equal to the current assumed to be flowing in the single conductor.

Bennett* and Carson† have obtained complicated infinite integral expressions for the current density in the sheet. Numerical results given by these authors are in substantial agreement with the simplified treatment here presented.

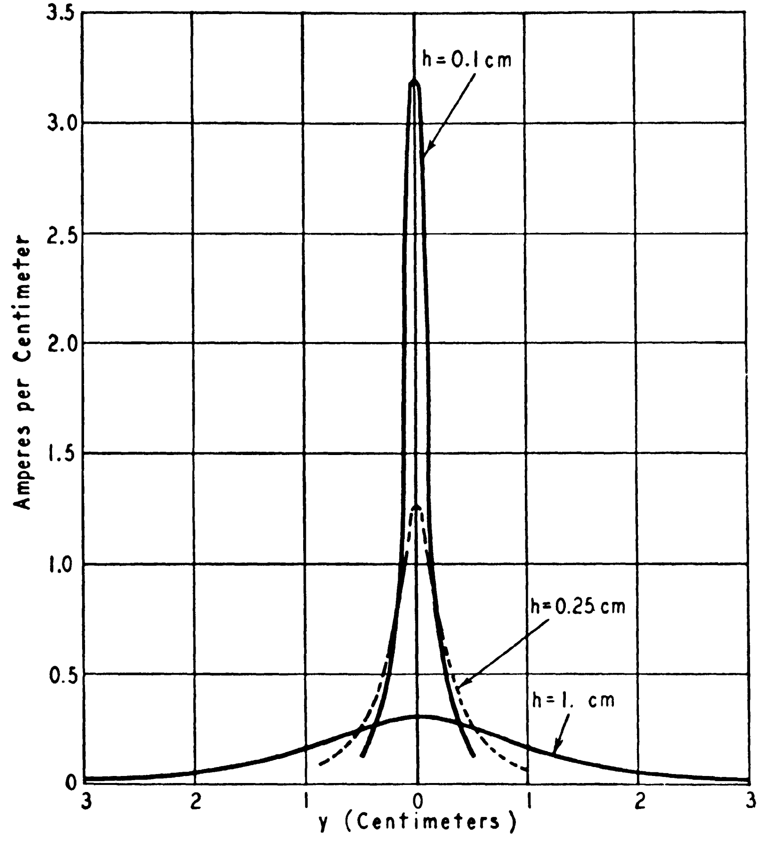

FIG. 55. Current distribution in the sheet for a filamentary conductor at various heights above the sheet. Current in the conductor is 1 ampere.

We shall now proceed with a consideration of the power losses in the sheet. The current density J flows out of the paper in a small patch of unit lateral width and of thickness s. This dimension, s, is the skin thickness defined by (1.46). The current flowing out of the patch shown in Fig. 56 is $J \cdot dy$.

---

* Edward Bennett, "The Proximity Effect; Its Application to the Concentration of Heating Currents in Predetermined Strips," *Transactions A.I.E.E.*, Vol. 51, September 1932, p. 625.

† John R. Carson, "Wave Propagation in Overhead Wires with Ground Return," *B.S.T.J.*, Vol. 5, October 1926, p. 542.

The resistance of the patch shown, with a length of 1 centimeter into the paper, is

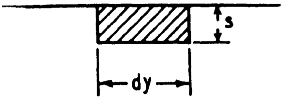

FIG. 56. Current-carrying patch on the surface of a conducting sheet.

$$dR = \frac{1}{\sigma s \cdot dy}. \tag{8.05}$$

The power lost (I^2R) in this small element is

$$(J \cdot dy)^2 dR = \frac{J^2 dy}{\sigma s} \text{ watts.} \tag{8.06}$$

If we now substitute (8.03) in (8.06) and integrate from $y = -\infty$ to $y = +\infty$, we have the power lost in the sheet in a slice taken at right angles to the conductor, where the thickness of the slice in the direction along the conductor is 1 centimeter. If P_m equals the power lost in a 1-centimeter slice of the metal sheet,

$$P_m = \frac{1}{\sigma s}\int_{y=-\infty}^{y=\infty} J^2 \cdot dy = \frac{2h^2I^2}{\pi^2\sigma s}\int_{y=0}^{y=\infty}\frac{dy}{(h^2+y^2)^2}. \tag{8.07}$$

But

$$\int_{y=0}^{y=\infty}\frac{dy}{(h^2+y^2)^2} = \frac{1}{2h^3}\tan^{-1}\left(\frac{y}{h}\right)\Bigg|_{y=0}^{y=\infty} = \frac{\pi}{4h^3}, \tag{8.08}$$

so that (8.07) becomes

$$P_m = \frac{I^2}{2\pi\sigma s h} = \frac{I^2}{h}\sqrt{\frac{\mu_r f \cdot 10^{-9}}{\sigma}}. \tag{8.09}$$

Since the cylindrical conductor generally has a conductivity and a relative permeability different from the metal sheet, we should distinguish between the quantities. Let

σ_m = conductivity of the metal sheet;
σ_c = conductivity of the current-carrying conductor placed parallel to the sheet;
μ_m = relative permeability of the metal sheet;
μ_c = relative permeability of the current-carrying conductor.

Then (8.09) should be

$$P_m = \frac{I^2}{h}\sqrt{\frac{\mu_m f \cdot 10^{-9}}{\sigma_m}}. \tag{8.10}$$

If the conductor of radius a is placed far enough from the sheet so that the presence of the sheet does not alter the current distribution on the conductor, the current on the conductor will flow in a thin layer s equal to the skin thickness, as shown in Fig. 57. Then, from Chapter 1, the power lost on 1 centimeter of conductor is

$$P_c = \frac{I^2}{2\pi a s_c \sigma_c} = \frac{I^2}{a}\sqrt{\frac{\mu_c f \cdot 10^{-9}}{\sigma_c}} \tag{8.11}$$

and the ratio of the power spent in the metal sheet to the power lost in the conductor is

$$\frac{P_m}{P_c} = \frac{a}{h}\sqrt{\frac{\mu_m \sigma_c}{\mu_c \sigma_m}}. \tag{8.12}$$

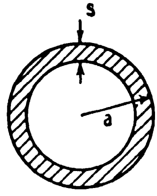

FIG. 57. Current distribution on a cylindrical conductor far removed from sheet.

Before interpreting (8.12), let us examine the effect of the altered current distribution on the sheet and on the conductor due to close spacing.

When the conductor has a finite radius a with the axis of the conductor a distance h above the metal sheet, the fields external to the conductor may be computed by replacing the cylindrical conductor by a filament carrying the current I at a new height h' where

$$h' = \sqrt{h^2 - a^2} = h\sqrt{1 - \left(\frac{a}{h}\right)^2}. \tag{8.13}$$

The effect on the current density in the metal sheet may be studied by substituting h' for h in (8.03). Then

$$J(\text{amperes per centimeter}) = \frac{I}{\pi h}\,\frac{\sqrt{1 - \left(\frac{a}{h}\right)^2}}{1 - \left(\frac{a}{h}\right)^2 + \left(\frac{y}{h}\right)^2}. \tag{8.14}$$

The current-density distribution computed from (8.14) is shown in Fig. 58 for a number of values of the radius, where the height of the conductor is equal to 1 centimeter. Increasing the radius of the cylinder has the same effect as bringing a thin filament closer to the metal sheet, that is, the current concentration directly under the conductor is increased, and the drop-off in a lateral direction is more rapid. Fig. 59 shows the distribution for a number of conductor heights, with the radius of the conductor fixed at 0.5 centimeter. Here again we see the increase in concentration when the conductor is brought closer to the metal sheet. In Fig. 60, we see the effect of holding the spacing between the metal sheet and the nearest point on the periphery of the conductor equal to 0.5 centimeter, while the radius and height are altered. It may be seen that a very fine conductor ($a/h \doteq 0$) gives the greatest concentration.

This crowding of the current density under the conductor is an exceedingly important effect in the practice of induction heating. The conductor may be bent in a variety of useful shapes to cause the heating current to flow in desired areas. A few of these applications will be treated in later chapters.

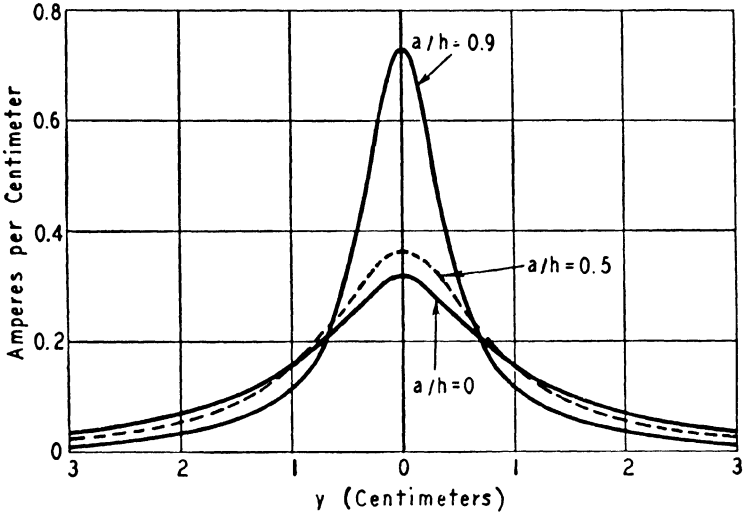

FIG. 58. Current distribution in the conducting sheet when the conductor has a finite radius and height h equals 1 centimeter. (Distance from sheet to center of conductor fixed.)

The power lost in the metal sheet may be obtained by substituting h' for h in (8.10) with the result that

$$P_m = \frac{I^2}{h}\sqrt{\frac{\mu_m f\cdot 10^{-9}}{\sigma_m}}\cdot\frac{1}{\sqrt{1-\left(\frac{a}{h}\right)^2}} \tag{8.15}$$

The current distribution around the surface of the cylindrical conductor may be obtained by using the construction of Fig. 61. By means of a tedious algebraic manipulation, it may be shown that the current density on the surface of the conductor, confined to a layer s_c centimeters in thickness, is

$$J\text{(amperes per radian)} = \frac{I}{2\pi}\frac{\sqrt{1-\left(\frac{a}{h}\right)^2}}{1-\frac{a}{h}\cos\theta}\cdot \tag{8.16}$$

By substituting 360° for 2π radians in (8.16), we may express the current density in amperes per degree. This has been done in constructing the

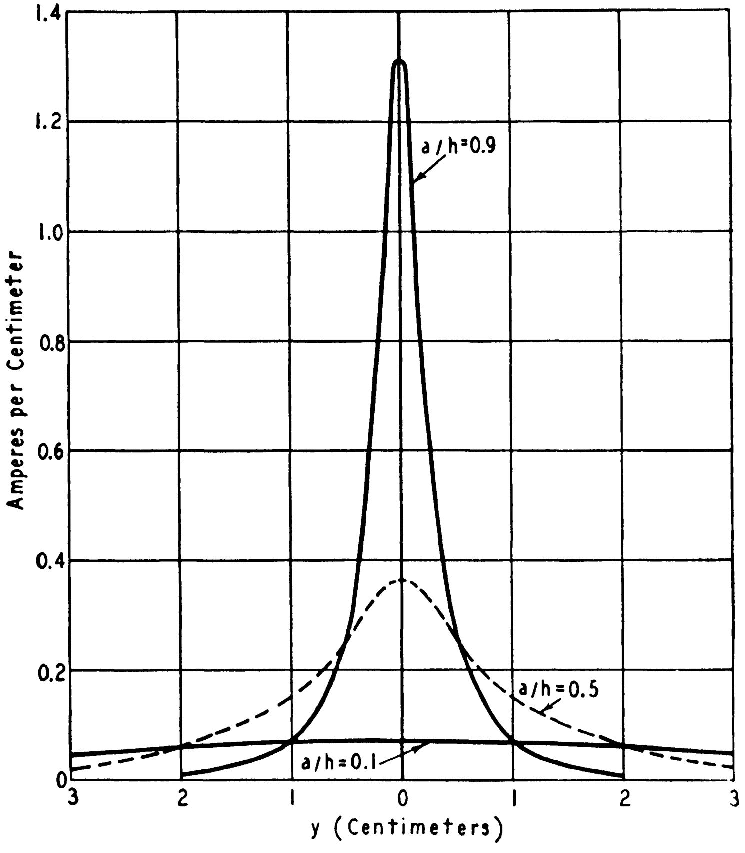

FIG. 59. Current distribution in the conducting sheet when the conductor radius is 0.5 centimeter and the distance from the sheet to the center of the conductor varies. (Radius fixed.)

curves of Fig. 62. The current-density distribution depends only upon the ratio of radius to height. When the conductor is brought very close to the

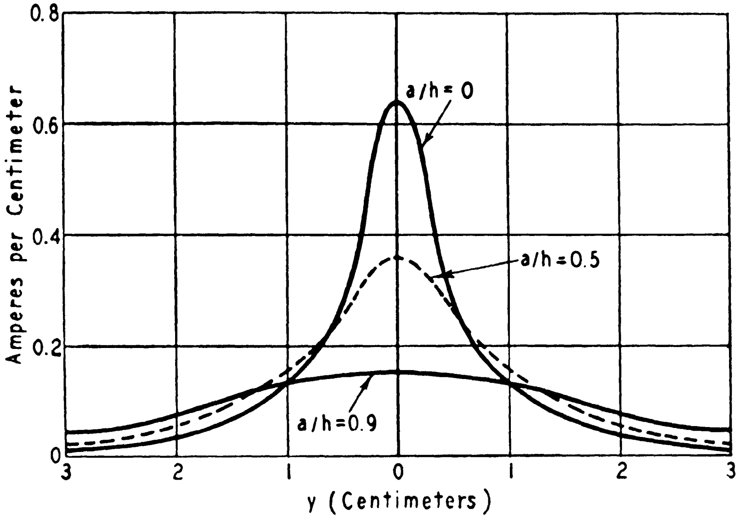

Fig. 60. Current distribution in the conducting sheet. (Spacing between conducting sheet and conductor fixed at 0.5 centimeter, while radius of conductor and distance from conducting sheet to center of conductor both change.)

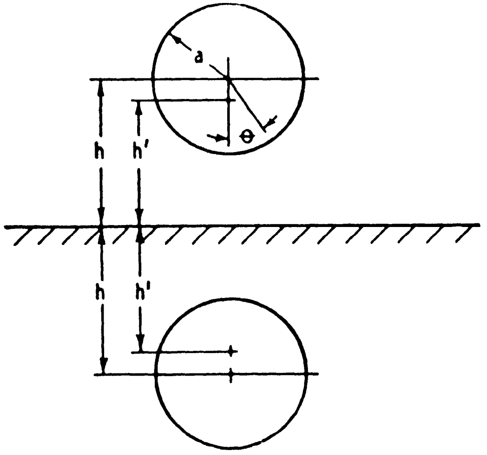

Fig. 61. Cross section of cylindrical conductor and image in the sheet.

metal sheet, the current on the conductor crowds around to the side closest to the sheet. The effect of crowding on both the conductor and on the sheet is displayed qualitatively in Fig. 63.

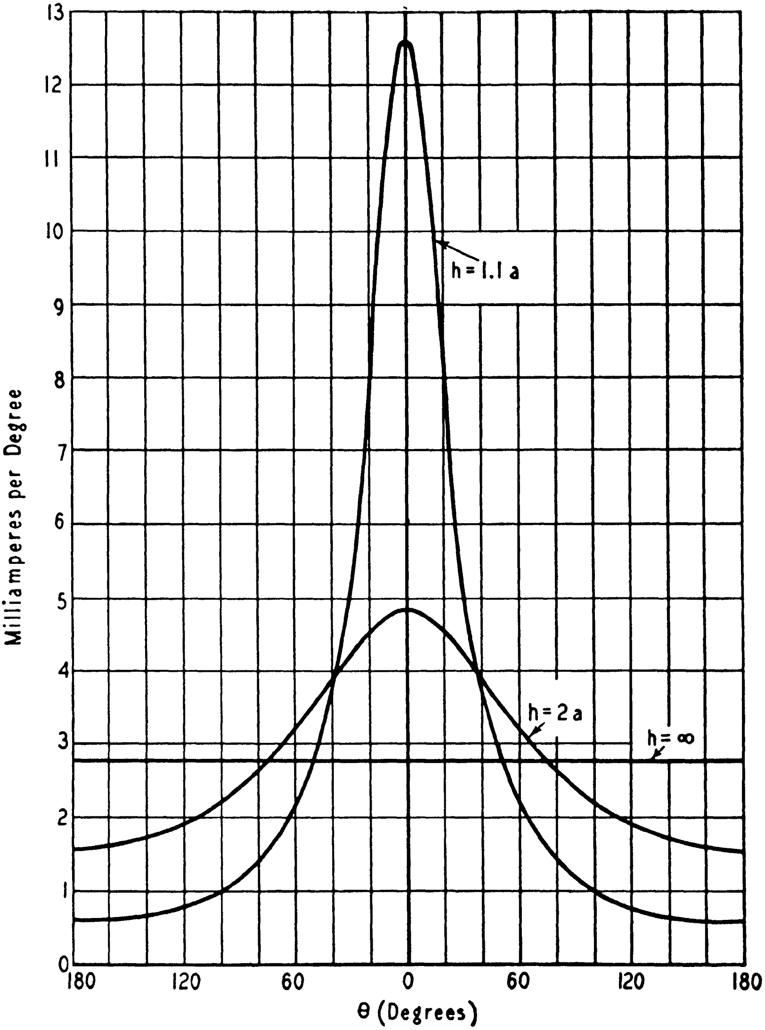

FIG. 62. Current distribution on the cylindrical conductor occasioned by the presence of the metal sheet.

The power loss in the conductor is found by integrating the I^2R loss around the circumference of the conductor. Then

$$P_c = 2\int_{\theta=0}^{\theta=\pi} \frac{(J\cdot d\theta)^2}{\sigma_c s_c a\cdot d\theta}$$

$$= \frac{I^2}{2\pi^2 a\sigma_c s_c}\left[1-\left(\frac{a}{h}\right)^2\right]\int_{\theta=0}^{\theta=\pi}\frac{d\theta}{\left(1-\frac{a}{h}\cos\theta\right)^2}. \tag{8.17}$$

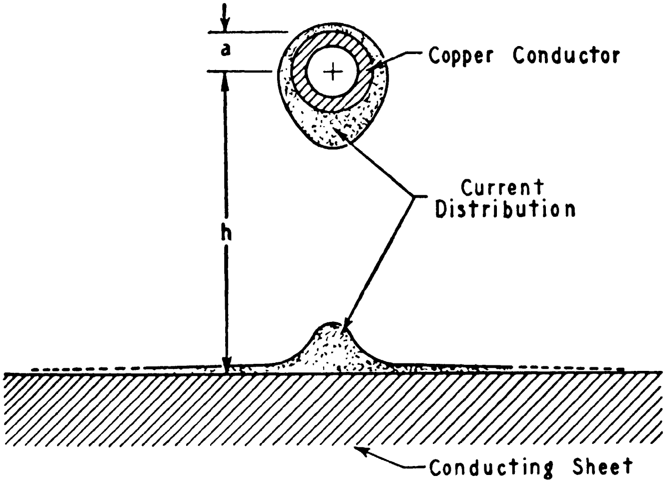

Fig. 63. The proximity of the conductor and the metal sheet causes crowding of current on both surfaces.

The integral itself is equal to

$$\frac{\pi}{\left[1-\left(\frac{a}{h}\right)^2\right]}\cdot\frac{1}{\sqrt{1-\left(\frac{a}{h}\right)^2}},$$

so that

$$P_c = \frac{I^2}{2\pi a s_c\sigma_c}\cdot\frac{1}{\sqrt{1-\left(\frac{a}{h}\right)^2}} = \frac{I^2}{a}\sqrt{\frac{\mu_c f\cdot 10^{-9}}{\sigma_c}}\cdot\frac{1}{\sqrt{1-\left(\frac{a}{h}\right)^2}}. \tag{8.18}$$

If we now divide (8.15) by (8.18), we obtain

$$\frac{P_m}{P_c} = \frac{a}{h}\sqrt{\frac{\mu_m\sigma_c}{\mu_c\sigma_m}}. \tag{8.19}$$

It is a somewhat surprising fact that this result is identical with the result shown in (8.12) which was deduced from simple assumptions which did not take into account the redistribution of current due to the finite conductor size.

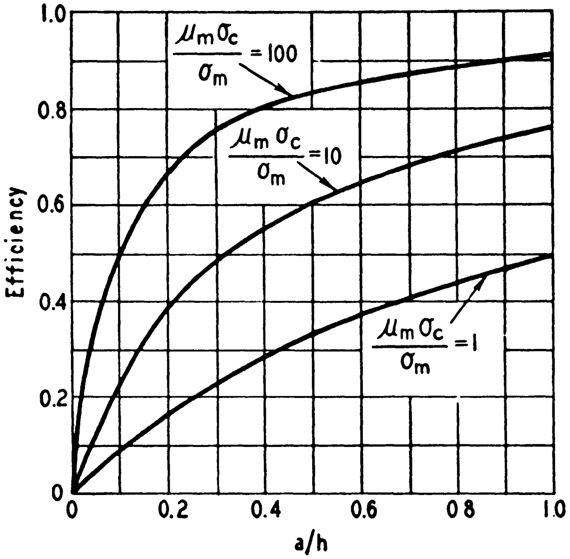

FIG. 64. Coupling efficiency of cylindrical conductor parallel to a metal sheet.

Since in inductive heating, the coupling coil is usually made of copper, the relative permeability μ_c may be set equal to unity for simplicity. The efficiency of the system is obtained as follows:

$$\text{Efficiency} = \frac{P_m}{P_m + P_c} = \frac{1}{1 + \dfrac{P_c}{P_m}} = \frac{1}{1 + \dfrac{h}{a}\sqrt{\dfrac{\sigma_m}{\mu_m \sigma_c}}}. \qquad (8.20)$$

Fig. 64 shows the variation of efficiency with the ratio a/h. The need for close conductor spacing is readily seen. Fig. 65 shows the efficiency curves replotted as a function of $\mu_m\sigma_c/\sigma_m$. The conductivity of the conductor is important in determining the coupling efficiency. Where a copper conductor is used to couple to iron, the coupling efficiency may become high. However, it is sometimes necessary to heat a copper article by induction. At the start of the heating cycle, the ratio σ_c/σ_m is unity ($\mu_m = 1$ for copper). From Fig. 65, we see that the best possible efficiency is 0.5 when the radius of the conductor is equal to the height above the sheet. However, for practical purposes a/h is less than unity, so that the coupling efficiency will be less than 50 per cent at the start of the heating cycle. Fortunately, the picture does not continue to be so gloomy. The coupling coil or conductor is usually hollow tubing through which cooling water flows, so that the conductivity of the conductor does not change as time passes. The load begins

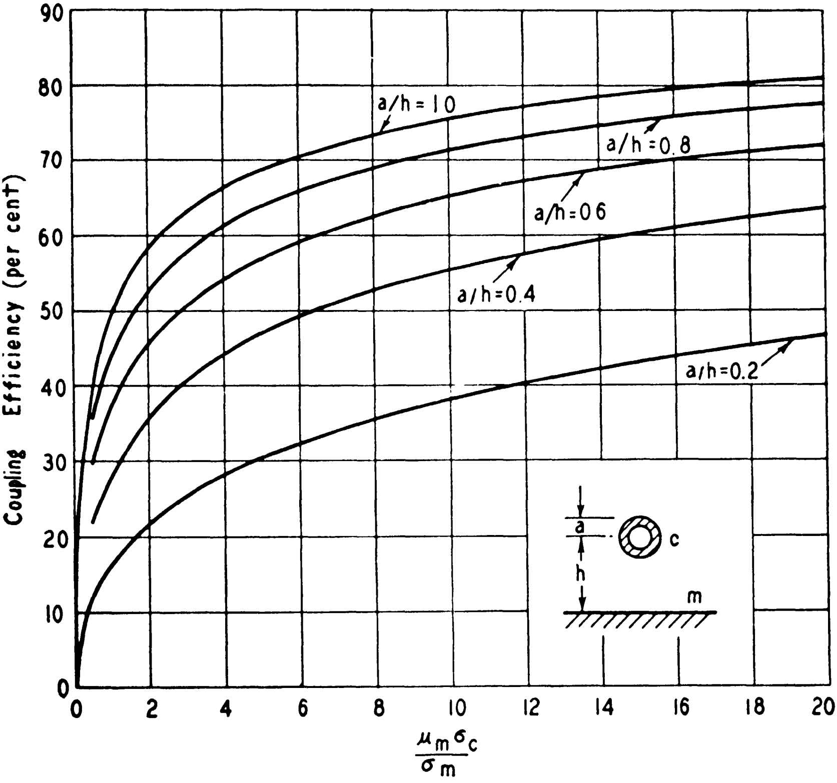

Fig. 65. Coupling efficiency as a function of conductivity and permeability.

to heat so that its conductivity decreases. This results in an improvement in efficiency so that the conductivity decreases still faster and soon the efficiency assumes reasonable proportions.

If the heating coil is wrapped around a cylindrical load which has a radius many times larger than the diameter of the conductor which makes up the coil and large compared to the spacing between the coil and the work, we may use these results obtained for a conductor parallel to a flat sheet. If the circumference of the load is C centimeters, the resistance at the terminals of a single turn coil (the resistance due to losses in the coil and in the metal load) may be obtained from (8.15) and (8.18). This resistance is

$$R = \frac{C}{a} \frac{\sqrt{\dfrac{f \cdot 10^{-9}}{\sigma_c}}}{\sqrt{1 - \left(\dfrac{a}{h}\right)^2}} \left(1 + \frac{a}{h}\sqrt{\frac{\mu_m \sigma_c}{\sigma_m}}\right). \tag{8.21}$$

We see that this resistance is proportional to the square root of the frequency. That is

$$R \propto f^{1/2}$$

For a constant input power, the current in the coil is

$$I = \sqrt{\frac{P}{R}},$$

so it may be seen that

$$I \propto \frac{1}{f^{1/4}}.$$

To obtain the reactance, we must first have available the expression for the characteristic impedance of the conductor over the flat sheet. This is

$$Z_c = 60 \log_\epsilon \left\{\frac{h}{a}\left[1 + \sqrt{1 - \left(\frac{a}{h}\right)^2}\right]\right\} \tag{8.22}$$

This characteristic impedance as a function of a/h is shown in Fig. 66.

The single-turn coil around the load is usually fed in push-pull. Then the mid-point of the coil is at ground potential. The reactance between one terminal of the coil and the work is then the characteristic impedance multiplied by the tangent of the electrical length of the semi-circumference. The total reactance is twice this value. Then

$$X = 2Z_c \tan\left(\frac{2\pi}{\lambda_0}\frac{C}{2}\right) \doteq \frac{2\pi C Z_c}{\lambda_0} = \frac{2\pi f Z_c C}{3 \cdot 10^{10}}. \tag{8.23}$$

This latter expression shows that the reactance is directly proportional to frequency. Since the resistance is usually small compared to the reactance, the voltage across the terminals of the coil is the product of current and reactance. We have seen that the current, for a constant power, varies inversely with the one-fourth root of the frequency, so

$$V \propto f^{3/4}.$$

In the course of the development, we have assumed that the frequency is high enough to insure skin effect on the conductor. Also the frequency, with respect to the radius of the load must be greater than the critical frequency established by (2.13). We may thus sum up our observations, remembering the assumptions that have been made:

1. The efficiency of power transfer is independent of frequency.
2. The reactance at the input terminals of the work coil varies directly with the frequency.
3. The resistance at the terminals of the work coil varies with the square root of the frequency.
4. The current in the work coil, for a constant power input, varies inversely as the one-fourth power of the frequency.
5. The voltage at the terminals of the work coil, for a constant power input, varies directly as the three-fourths power of the frequency.

We now have at hand the necessary formulas for computing the efficiency, resistance, reactance, current, and voltage. The magnitude of the values encountered when a single-turn coil is used will be shown by means of an example. The following constants will be used:

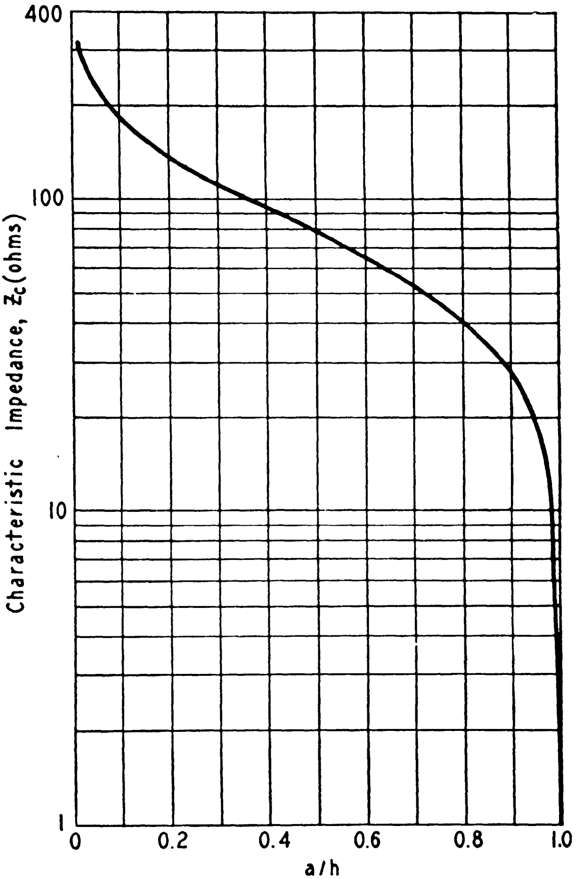

FIG. 66. Characteristic impedance of cylinder parallel to metal sheet.

C = 15.0 centimeters.
a = 0.24 centimeter.
h = 0.44 centimeter.
σ_c = conductivity of copper coil = 580,000 mhos for a centimeter cube.
σ_m = conductivity of hot steel = 6000 mhos for a centimeter cube.
μ_m = unity for steel above the Curie point.
f = 10^6 cycles per second.

From (8.20), we find that the efficiency is 84.2 per cent. Substituting the numerical values in (8.21) gives a resistance of 0.0195 ohm, with a current of 226.0 amperes for a power of 1000 watts.

Since a/h is 0.545, Fig. 66 gives 73 ohms for the characteristic impedance. Then (8.23) shows that the reactance is 0.23 ohms. This reactance multiplied by the current gives a voltage across the terminals of the coil of 52 volts.

Table 4 gives a summary of these numerical data for a few values of h. It may be seen that increasing h results in a slight increase in the current to be handled and a sharp increase in the voltage appearing at the terminals of the coil. Values of current and voltage for an operating power of 100,000 watts are also shown in this table. The current is far in excess of the values of tank-circuit current that may be obtained in a vacuum-tube oscillator so that it is virtually impossible to place this coil directly in the tank circuit. A suitable transformer will be described in the next chapter.

TABLE 4. SINGLE TURN COIL AROUND A STEEL BAR.

h (centimeters)	0.44	0.54	0.64
Efficiency (per cent)	84.2	81.4	78.5
R(ohms)	0.0195	0.0156	0.0131
Z_c(ohms	73	87	97
X(ohms)	0.23	0.273	0.304
I(amperes for 1000 watts)	226	253	276
V(volts for 1000 watts)	52	69	84
I(amperes for 100,000 watts)	2260	2530	2760
V(volts for 100,000 watts)	520	690	840

The treatment in this chapter has related to single conductors parallel to a flat metal sheet. However, (8.03) may be used to examine the current distribution obtained from multi-turn coils. When the charge to be heated has a large radius, the arrangement of Fig. 67 may be used to establish certain interesting facts. Here we have represented the condition of a coil which has two turns. The spacing between turns is d. Each turn carries I amperes. We may note that $y_1 = z - \frac{d}{2}$, whereas $y_2 = z + \frac{d}{2}$. Then the total current density in the sheet, a distance z from the center line, is found by applying (8.03) to each conductor and adding.

$$J = \frac{I}{\pi h}\left[\frac{1}{1 + \left(\frac{2z - d}{2h}\right)^2} + \frac{1}{1 + \left(\frac{2z + d}{2h}\right)^2}\right]. \tag{8.24}$$

The resulting current densities are shown in Fig. 68, for a number of turn spacings. It may be seen that when the turn spacing equals $1.4h$ the current-density curve flattens off on the top. As the spacing is increased, a dip appears in the center of the curve. When the spacing is greatly increased two entirely discrete curves occur, with each curve similar to those shown in Fig. 55.

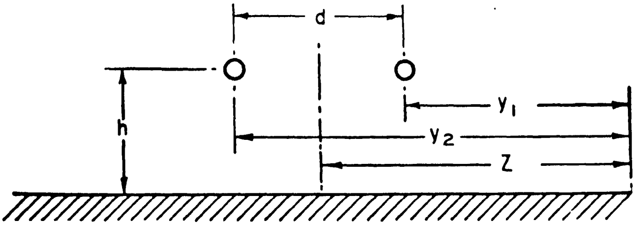

FIG. 67. Two conductors parallel to a metal sheet.

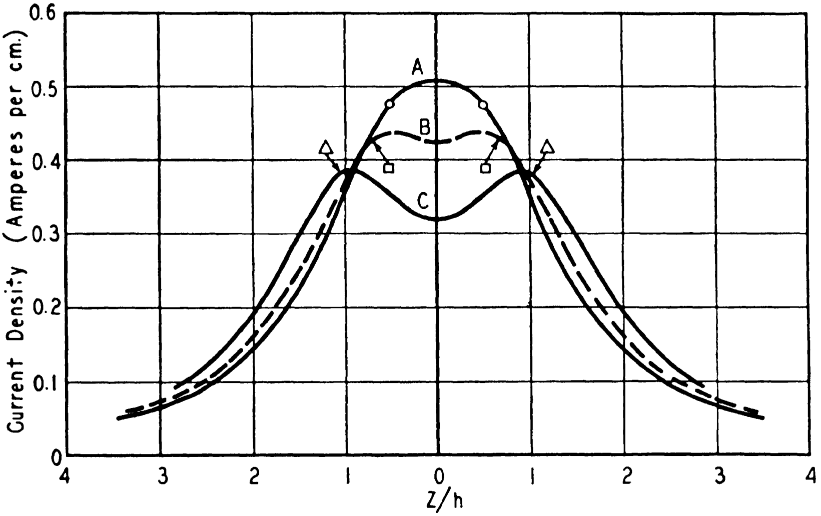

FIG. 68. Current density in a sheet under a two-turn coil.

Here, as well as in Figs. 69 and 70, the circles, squares, and triangles represent the lateral location of the conductors.

Curve A: $d = h$
Curve B: $d = 1.4h$
Curve C: $d = 2h$

In Fig. 68, the current I was chosen to be 1 ampere. The current-density scale is expressed in amperes per centimeter when the height h is 1 centimeter. When h is not 1 centimeter, Fig. 68 still applies when the ordinate scale is divided by the height in centimeters. For example, in Fig. 68, the peak of Curve A has a value of 0.51 ampere per centimeter. If h were chosen as

3 centimeters, this same peak would have a value of 0.17 ampere per centimeter.

Fig. 69 is similar to Fig. 68, except that three turns or conductors are used. The central turn now lies on the center line and z is measured from this center line as before. The spacing between adjacent turns is again designated as d. Here we see that no real flattening of the curve occurs.

When four conductors are used, the results are as shown in Fig. 70. While these curves show no pronounced flattening over the entire length of the coil, it should be observed that where the heating is continued for several seconds, heat will be transferred from one region to another with consequent uniformity of temperature. Only with extremely short heating periods will striation be important.

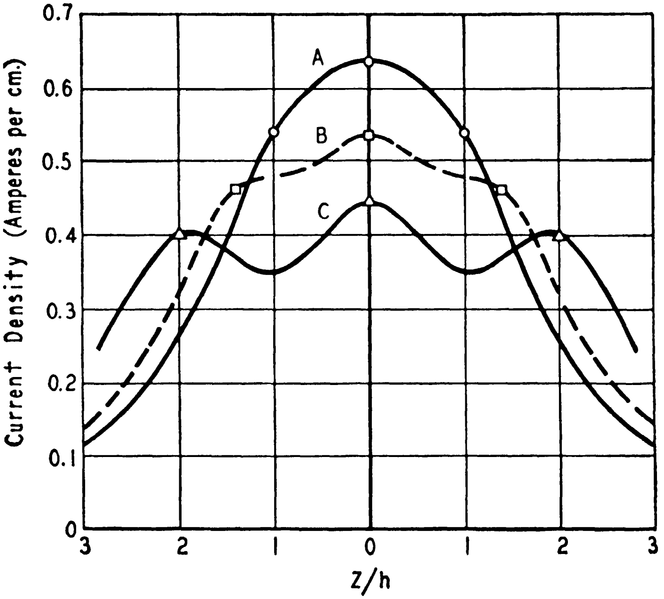

FIG. 69. Current density in a sheet under a three-turn coil.

Curve A: $d = h$
Curve B: $d = 1.4h$
Curve C: $d = 2h$

If the coil consists of many closely-spaced turns and thus has great length, the current density in the sheet under the central portion of the coil will be nearly uniform. However, the conditions near the end of the coil may be of interest. In Fig. 71, we measure z from the last turn of the coil. For negative values of z, we find ourselves outside of the coil. Curve A in Fig. 72 shows the current density for 1 ampere in the coil and with a spacing between

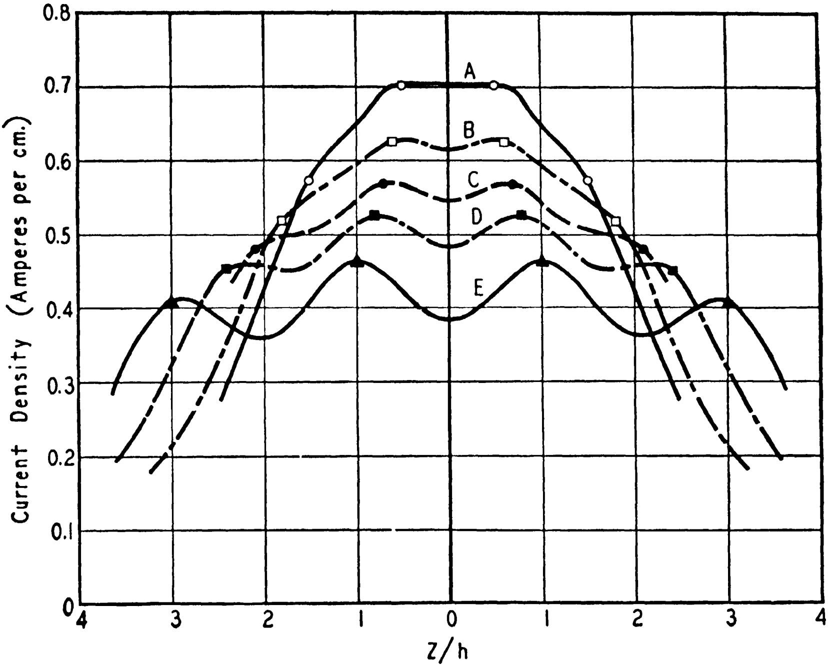

FIG. 70. Current density in a sheet under a four-turn coil.

Curve A: $d = h$
Curve B: $d = 1.2h$
Curve C: $d = 1.4h$
Curve D: $d = 1.6h$
Curve E: $d = 2h$

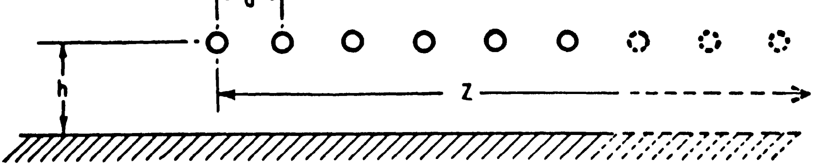

FIG. 71. Conditions near the end of a long coil.

turns equal to the height of the conductors above the sheet. In Curve B, where the spacing has been increased to twice the height, the current in the coil was taken as 2 amperes, so that the ampere-turns per centimeter of coil length remains the same. Curve A shows only a slight wiggle, while the greater spacing of Curve *B* produces pronounced oscillations. Curve *C* shows the current density when the coil turns are very close together so that the coil might be represented by a continuous current sheet. This current sheet itself has a current density of *I* amperes per centimeter, and for the purposes of calculation of Fig. 72 was taken as 1 ampere per centimeter.

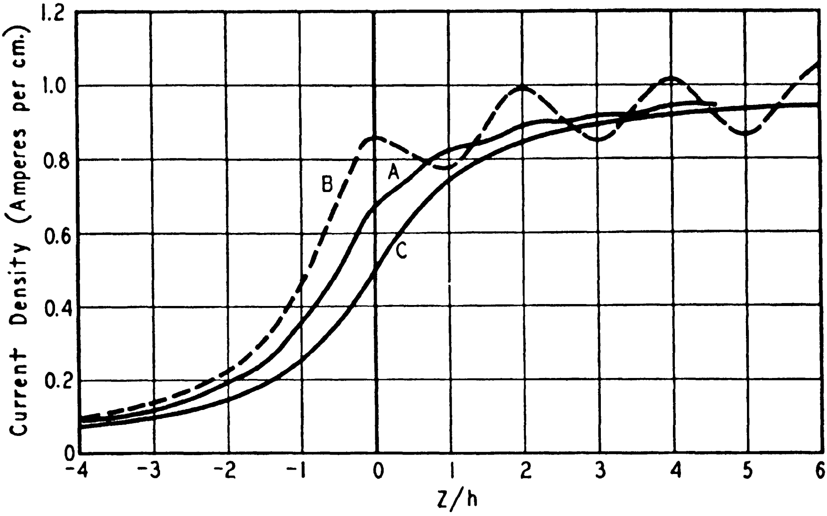

FIG. 72. Current density in the metal sheet near the end of a long solenoid.
Curve A: $d = h$
Curve B: $d = 2h$
Curve C: $d = 0$ (Continuous exciting current sheet).

By performing an integration of (8.03) over the current sheet which represents the coil, we find

$$J = I\left[\frac{1}{2} + \frac{1}{\pi}\tan^{-1}\left(\frac{z}{h}\right)\right]. \tag{8.25}$$

When z approaches infinity, $\tan^{-1}(z/h)$ becomes $\pi/2$ so (8.25) shows that the current density J in the sheet is equal to the current density I in the exciting current sheet.

For points outside of the coil, z takes on negative values so the last part of the bracket in (8.25) is negative. When z approaches negative infinity, (8.25) becomes zero.

In the treatment of multi-turn coils presented here, we have assumed that the conductors are filaments with a radius small compared to the other dimensions being considered. When the radius is considered to be finite the curves of current density shown in Figs. 68, 69, 70, and 72 may be considerably different in detail, but the general conclusions remain unchanged.

Chapter 9

THE EFFICIENCY OF INDUCTION-HEATING COILS

In the preceding chapter, the relations existing near a conductor parallel to a metal sheet or half-space were extrapolated to handle the problem of coupling to a cylinder of metal where the cylinder was of large radius. In Chapter 2, the analysis applied to heating a cylinder with a long solenoid, but there were no restrictions placed on the radius of the cylinder to be heated. The purpose of the past treatment was to establish certain quantitative relations as well as to show the physics of the problem of induction heating. The purpose of this chapter is to give a more qualitative picture of the problem of coupling to a metal load by an inductance coil, and to show the results of certain measurements made to apply the theory.

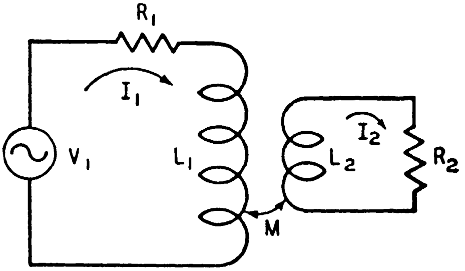

FIG. 73. Equivalent circuit for induction heating.

When the metallic object to be heated is placed in the field of a suitably-designed coil which is carrying an alternating current, currents are induced in the object, generating heat without contact. The action is similar to that of a transformer with the secondary short-circuited.

In the circuit of Fig. 73*, a coil of inductance L_1 and resistance R_1 is placed across the terminals of a generator which is developing a voltage V_1. The generator may be a rotating machine, a spark-gap oscillator, or a vacuum-tube oscillator. A piece of metal to be heated may be represented as the shorted secondary turn with a resistance R_2 and an inductance L_2. The circuit relations are

---

* This is the circuit treated briefly by C. B. Kirkpatrick, "Magnetic Induction Field of Air-Core Coils," *Wireless Engineer*, Vol. XX, No. 239, August, 1943, p. 378.

$$V_1 = (R_1 + j\omega L_1)I_1 + j\omega M I_2 \tag{9.01}$$

and

$$0 = j\omega M I_1 + (R_2 + j\omega L_2) I_2, \tag{9.02}$$

where ω equals $2\pi f$, f is the frequency in cycles, and M is the mutual inductance in henrys. Elimination between these two equations gives the impedance presented to the terminals of the generator.

$$\begin{aligned} V_1/I_1 &= R_1 + j\omega L_1 + \frac{(\omega M)^2}{R_2 + j\omega L_2} \\ &= R_1 + \frac{(\omega M)^2 R_2}{R_2^2 + (\omega L_2)^2} + j\omega\left[L_1 - \frac{(\omega M)^2 L_2}{R_2^2 + (\omega L_2)^2}\right]. \end{aligned} \tag{9.03}$$

Thus we see that the primary resistance is effectively increased by the presence of the loaded or shorted turn, while the apparent inductance of the work coil has decreased.

Let $Q = \omega L_2/R_2$. Then the increase in resistance due to the presence of the metal to be heated is

$$\Delta R_1 = \left(\frac{M}{L_2}\right)^2 R_2 \cdot \frac{Q^2}{Q^2 + 1} \tag{9.04}$$

and

$$\Delta L_1 = -\left(\frac{M}{L_2}\right)^2 L_2 \cdot \frac{Q^2}{Q^2 + 1}. \tag{9.05}$$

The efficiency of the heating circuit, that is, the ratio of the power transferred to the work to the total power supplied, is

$$\begin{aligned} \text{Efficiency} &= \frac{\Delta R_1}{R_1 + \Delta R_1} \\ &= \frac{\left(\frac{M}{L_2}\right)^2 R_2 \cdot \frac{Q^2}{Q^2 + 1}}{R_1 + \left(\frac{M}{L_2}\right)^2 R_2 \cdot \frac{Q^2}{Q^2 + 1}}. \end{aligned} \tag{9.06}$$

The Q of the secondary circuit is generally much larger than unity for most of the frequencies used for induction heating. The variation of the factor $\frac{Q^2}{Q^2+1}$ as a function of Q is shown in Fig. 74. The reader may note a certain similarity between Fig. 74 and the function F displayed in Fig. 20 (Chapter 2).

It may be seen that, as Q becomes large, the factor in question approaches unity. If we make this limiting assumption, equation (9.06) becomes

$$\text{Efficiency} = \frac{\left(\frac{M}{L_2}\right)^2 \frac{R_2}{R_1}}{1 + \left(\frac{M}{L_2}\right)^2 \frac{R_2}{R_1}}. \tag{9.07}$$

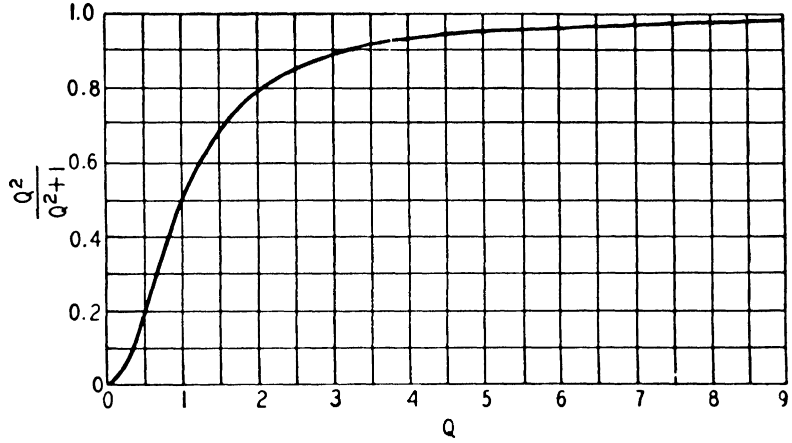

FIG. 74. Variation of factor in (9.06) with Q of induction-heating secondary circuit.

We have seen that at high frequencies, the current flowing in a conductor tends to concentrate near the surface, in a layer called the skin thickness. Since this layer varies inversely as the square root of frequency, it has been shown that the resistance varies directly as the square root of the frequency. The preceding statements are predicated on the assumption that the metal in question has a thickness at least a few times greater than the skin thickness.

Now, if the metal which is placed in the work coil has a thickness or diameter which satisfies these requirements, the resistance R_2 which appears in (9.07) will vary as the square root of the frequency. However, the same statement holds true for the resistance of the work coil, R_1. In this case, the ratio R_2/R_1 will be simply a constant which is independent of frequency, and the efficiency also becomes independent of frequency.

It should be remembered that we have assumed that Q is large, and that the skin thickness is small compared to thickness or diameter of the conductors in question. Also, it should be noted that this reasoning cannot be extrapolated into the extremely high frequencies where capacitance effects must be taken into account.

Since the efficiency is independent of frequency, it is interesting to examine other factors which may influence the choice of frequency. In a vacuum-tube oscillator, the power is limited by the characteristics of the particular vacuum tubes used in the oscillator. Then for a fixed power and large values of Q, the current in the primary is

$$I_1 = \sqrt{\frac{P}{R_1 + \Delta R_1}} = \sqrt{\frac{P}{R_1 + \left(\frac{M}{L_2}\right)^2 R_2}}$$

$$= \frac{1}{\sqrt{R_1}} \sqrt{\frac{P}{1 + \left(\frac{M}{L_2}\right)^2 \frac{R_2}{R_1}}}. \tag{9.08}$$

If R_2/R_1 is a constant ratio independent of frequency, the current in the primary for a constant power is inversely proportional to the square root of the primary resistance. But this resistance is directly proportional to the square root of the frequency, so that

$$I_1 \propto \frac{1}{f^{1/4}}. \tag{9.09}$$

Under the assumption we have been making, the inductance at the input terminals is independent of frequency. Also, the reactance at these terminals is generally large compared to the resistance, so the voltage at the terminals is

$$V_1 = \omega(L_1 + \Delta L_1)I_1. \tag{9.10}$$

Taking (9.09) into consideration, we see that

$$V_1 \propto f^{3/4}. \tag{9.11}$$

These results are in complete agreement with the five observations listed near the end of Chapter 8.

To test the foregoing conclusions, experimental data were assembled concerning a coil placed around a vacuum tube. The coil was a helix or solenoid, consisting of copper tubing which had a diameter of $\frac{5}{32}$ inch, wound to form 11 turns which were $2\frac{1}{2}$ inches in diameter. The length of the coil was $3\frac{1}{4}$ inches. The work or object to be heated was an RCA-6A6 vacuum tube.*

Measurements were first made of coil resistance and reactance with the vacuum tube removed. The coil was found to have an inductance of 2.76

---

* An RCA-6A6 tube was chosen as a convenient load for obtaining these data, but this heating operation was simply a laboratory experiment which had no connection with the manufacture of this type of tube.

microhenrys, which remained essentially constant over the range of frequencies at which measurements were made. The resistance R_1 varied with frequency as shown in Fig. 75. Then the vacuum tube was inserted in the coil and the measurements repeated. The inductance decreased only about 0.01 microhenry. The new resistance $R_1 + \Delta R_1$ is shown in Fig. 75.

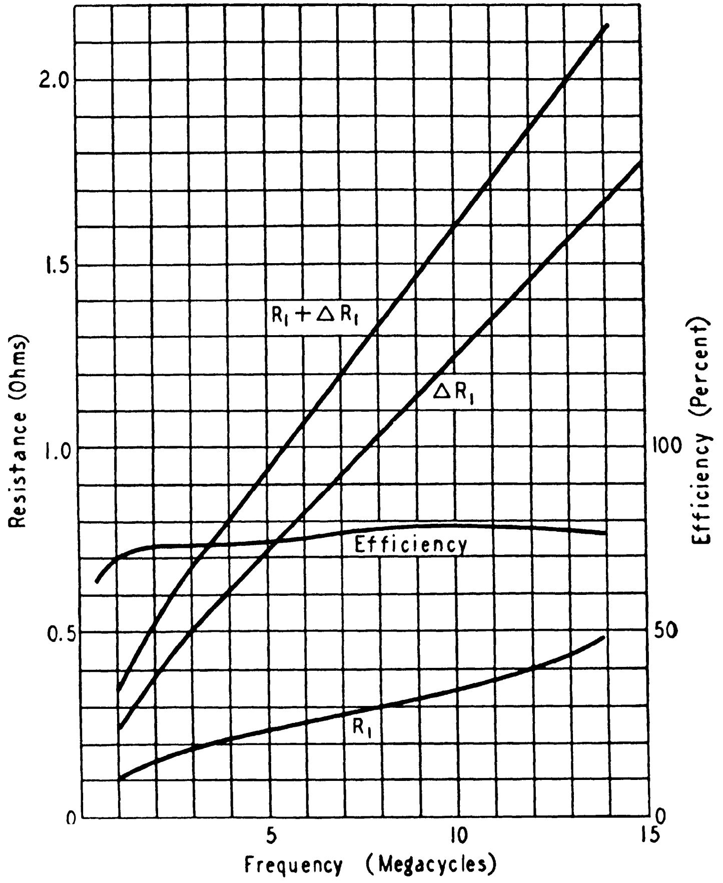

FIG. 75. Resistance and efficiency data for a work coil used in inductively heating an RCA-6A6 vacuum tube.

Efficiency of power transfer is also given in Fig. 75. This curve was computed directly from the measured values of resistance. We see that the efficiency lies between 72.0 and 78.5 per cent for all frequencies between 1 and 15 megacycles.

The current in the coil under load conditions and the voltage across the terminals of the coil are shown in Fig. 76 for the case where the available

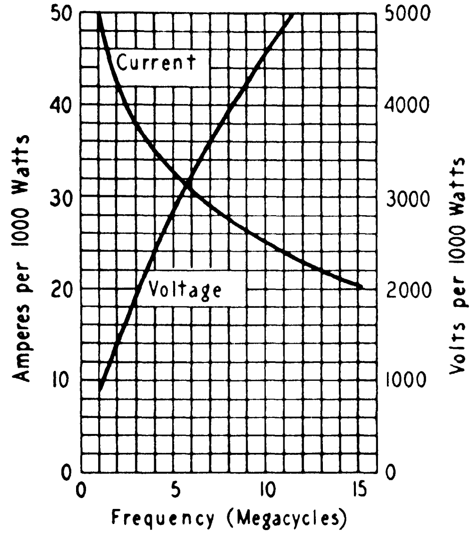

FIG. 76. Current and voltage values on the work coil used to heat the RCA-6A6 vacuum tube when the coil power is 1000 watts.

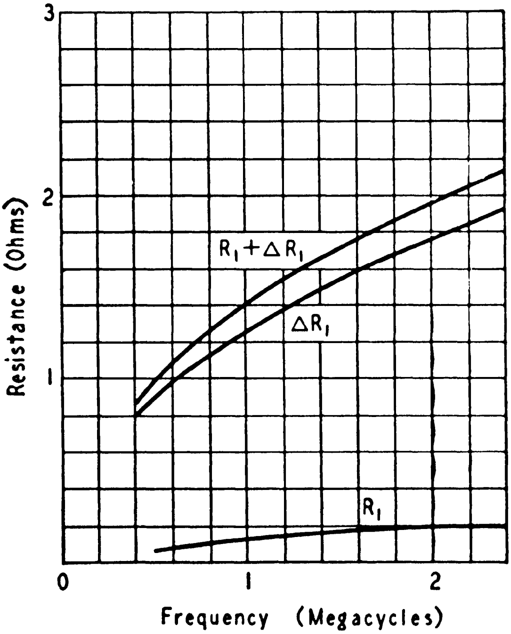

FIG. 77. Resistance values of multi-turn work coil closely coupled to steel load.

power is 1000 watts. The coil current is approximately 50 amperes at a frequency of 1 megacycle, and decreases to about 20 amperes when the frequency has increased to 15 megacycles. Since Fig. 75 shows that the efficiency is approximately the same at the two frequencies, the coil will not get any hotter with the increased current at the low frequency than it will at the higher frequency with less current. On the other hand, the voltage is less than 1000 volts at the low frequency while it rises to more than 5000 volts at 15 megacycles.

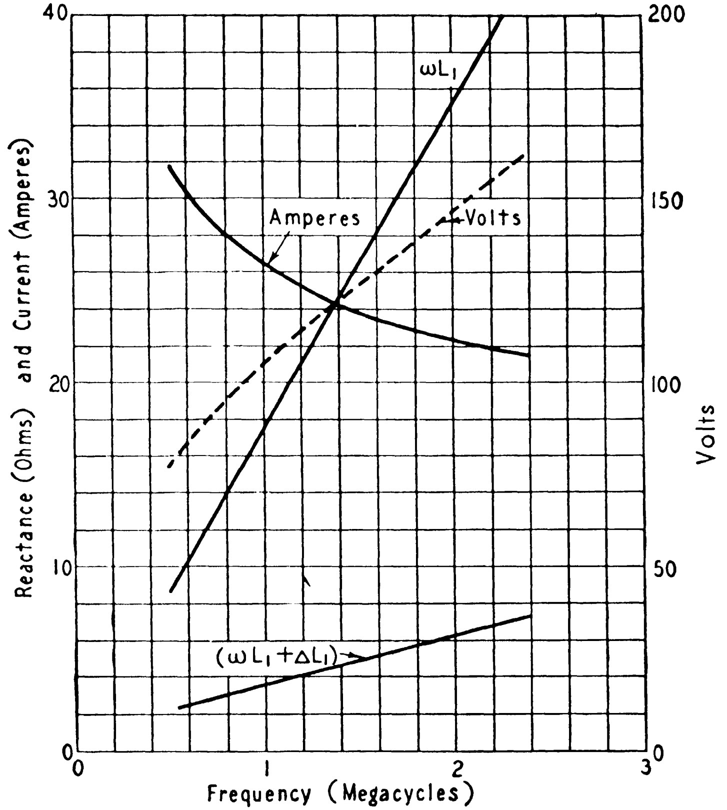

FIG. 78. Reactance, voltage, and current of multi-turn work coil closely coupled to steel load when the coil power is 1000 watts.

The high voltages shown here are due to loose coupling. Closer coupling to the work will make ΔL_1 have a greater numerical value, so that the total reactance will be decreased. This important effect of close coupling will be illustrated by means of another example. The work coil was very similar to the one used for coupling to the RCA-6A6 tube. Copper tubing which had a diameter of $\frac{5}{32}$ inch, was wound to form 11 turns. The total length of the coil was $3\frac{1}{4}$ inches, and the inside diameter of the coil was $1\frac{15}{16}$ inches. This coil was placed around a steel cylinder which had a diameter of $1\frac{7}{8}$ inches. Thus the spacing between the coil and the steel cylinder was $\frac{1}{32}$ inch.

The measured values of R_1 and $R_1 + \Delta R_1$ are shown in Fig. 77, together

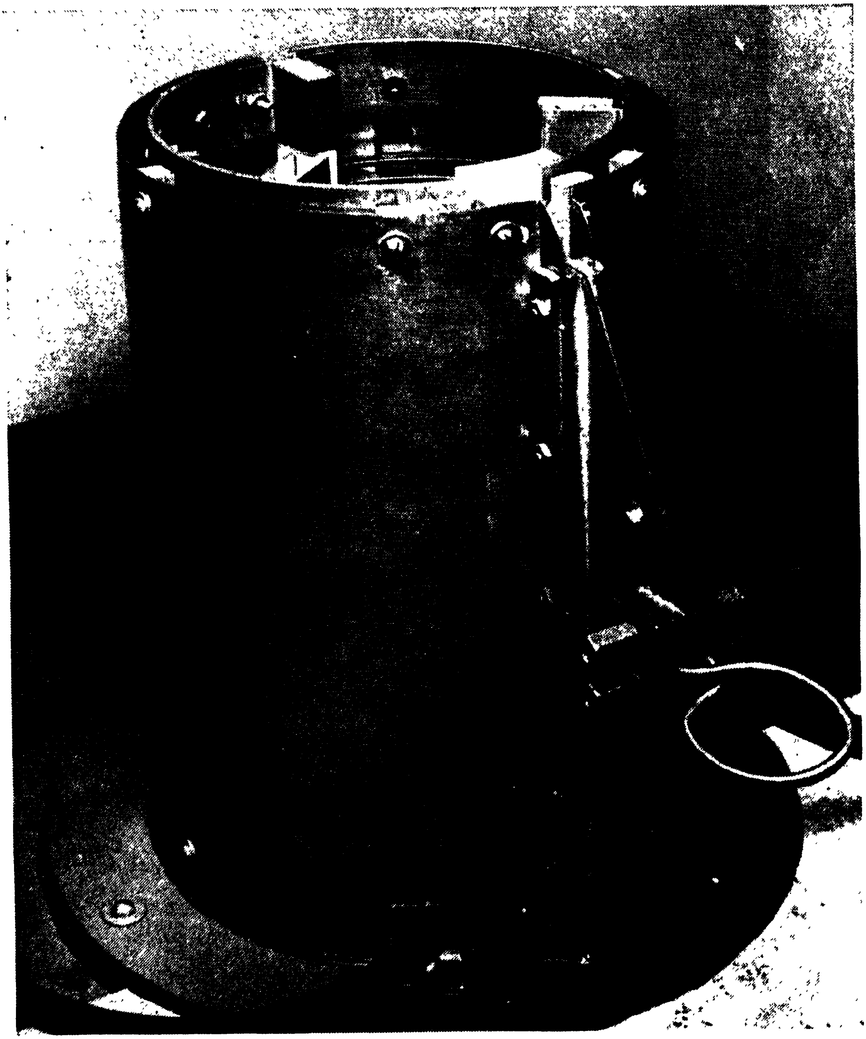

FIG. 79. A current transformer which is useful for inductive heating.

with the calculated values of ΔR_1. The efficiency calculated from equation

(9.06) is exactly 90 per cent over the range of frequencies at which measurements were made so there is no need to show the results in curve form.

The measured values of reactance with and without the steel cylinder are shown in Fig. 78. Because of the close coupling, the reactance drops a great deal when the cylinder is inserted. The effect of this is remarkable when the voltage across the coil is considered. Fig. 78 shows that this voltage lies between 80 and 160 volts when the operating frequency is between 0.5 and 2.4 megacycles, for a power of 1000 watts. The current in the coil for the same power is also shown as a function of frequency in Fig. 78.

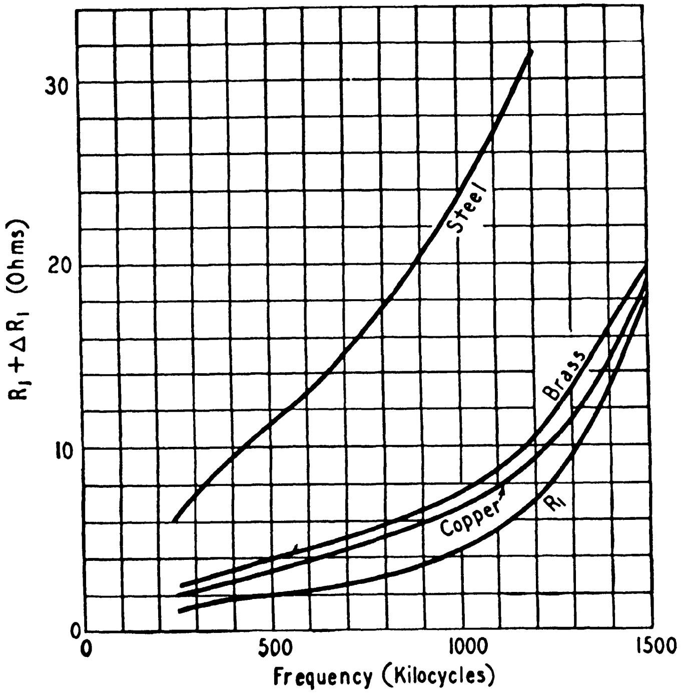

FIG. 80. Input resistance of transformer with copper, brass, and steel loads. The curve marked R_1 is the no-load resistance.

When single-turn coils of low resistance and reactance are used to couple closely to a load, transformers are necessary to properly match to the tank circuit. A transformer that has been extremely useful in working into low-impedance loads of the type being considered here is pictured in Fig. 79. This transformer consists of a multi-turn primary which is part of the tank circuit and a single-turn secondary which is really a sheet of copper wrapped around the primary with as close a spacing to the primary as is consistent with voltage requirements. Where the single-turn coil presents resistance values of the order of a few hundredths of an ohm and reactance values of a few tenths of an ohm, the resistance looking into the primary of the transformer may be several ohms, while the input reactance may be several hundred ohms.

Measurements of input resistance and reactance as well as efficiency were made on a transformer similar to the one shown in Fig. 79. The primary consisted of thirty-one turns. The secondary copper sheet fed into a single-turn coil which encircled a cylinder. Copper, brass, and steel cylinders were used. Fig. 80 shows the values of resistance for the three cylinders as well as the resistance measured when no cylinder was in the single-turn coil. The accompanying reactance values are shown in Fig. 81, whereas the efficiency curves are given in Fig. 82. The efficiency into a steel load is very good, while the efficiencies with copper and brass loads approach the maximum values that may be expected. The dropping off in efficiency at the higher frequencies is due to resonance effects in the transformer, brought about by distributed capacitance. The efficiency at the higher frequencies can be improved by the proper change in the design of the transformer. However, there is really very little need for this redesign because of the fact that in most

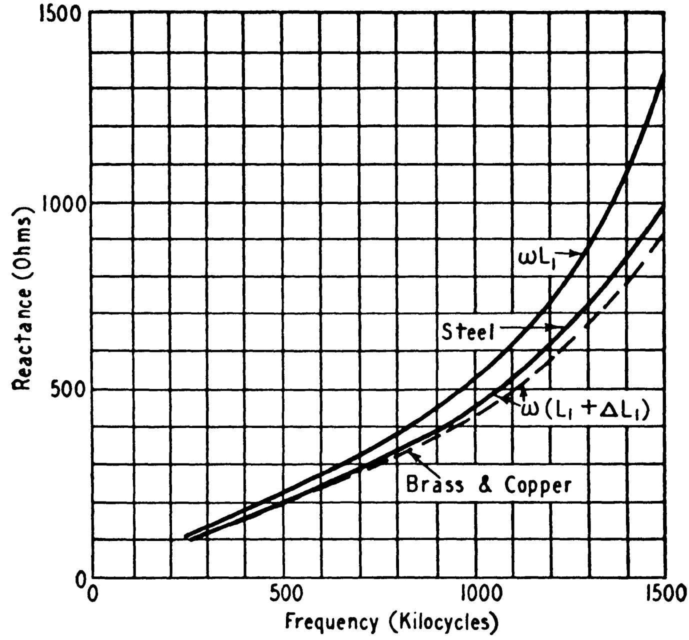

FIG. 81. Input reactance of transformer with copper, brass, and steel loads. The curve marked ωL_1 is the no-load reactance.

metal heating applications there is generally no point in using frequencies higher than a few hundred kilocycles.

In conclusion, it may be well to restate that while the simplifying assumptions made in the last two chapters show the efficiency of coupling to metal loads is independent of frequency, factors such as distributed capacitance come into play at the higher frequencies. At the lower frequencies, the skin thickness may be of the same order of magnitude as the dimensions of the object to be heated, with a consequent sharp reduction in efficiency. This latter effect is explained by the analysis of Chapter 2.

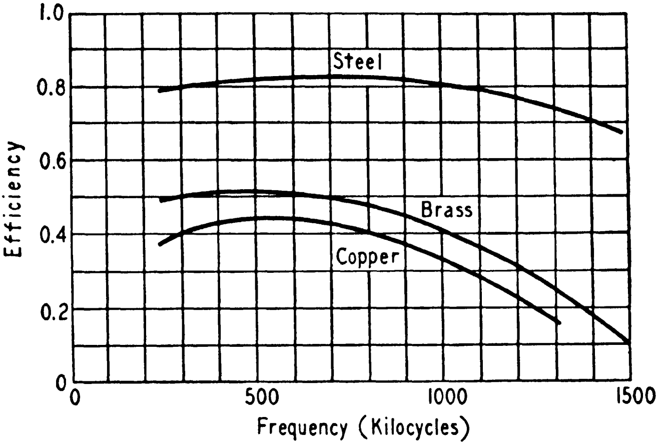

FIG. 82. Efficiency of coupling to copper, brass, and steel by means of a transformer.

Chapter 10

THE EFFECT OF TEMPERATURE ON THE ELECTRICAL PROPERTIES OF METALS

In previous chapters, references have been made to the " skin thickness " of metals, and specific values have been computed in a few cases. The results have depended upon an assumed value of conductivity of the metal being considered. The experiments to be described in this chapter were carried out in order to study the temperature dependence of the conductivity of a few ordinary metals and to establish a test procedure for a future study of metals whose properties are unknown.

A coil, consisting of 11 turns of copper tubing, was formed to have an inside diameter of $3\frac{1}{2}$ inches and a length of $3\frac{3}{4}$ inches. The copper tubing had an outside diameter of $\frac{3}{16}$ inch.

A copper cylinder with an outside diameter of $1\frac{7}{8}$ inches, an inside diameter of $1\frac{5}{8}$ inches, and a length of 6 inches was fitted with an internal heating coil consisting of nichrome strip wound on a ceramic tube. Ceramic cement was used to fill any space within the copper tube and the cement was then set by baking at high temperatures. In the experiments, the copper cylinder was heated by applying a 60-cycle voltage to the nichrome heater.

Similar tubes of brass, iron, and tool steel were prepared in the same way. Since the iron and tool-steel cylinders were heated to extremely high temperatures, rings of fire-brick were used to insulate the tubes. Without the insulation, the nichrome heaters were apt to burn out in the course of the experiment. Fig. 83 shows a cylinder arranged coaxially with the coil. The coil was mounted on the terminals of a Q-meter.*

Because of the much greater resistance encountered with a steel load, accurate measurements could not be obtained for steel with a Q-meter. Here it was necessary to transfer the coil and load to a radio-frequency impedance bridge.† The laboratory arrangement is shown in Fig. 84. The

---

* Type 160-A, Boonton Radio Corporation, Boonton, N. J.

† Type 516-C, General Radio Company, Cambridge, Mass.

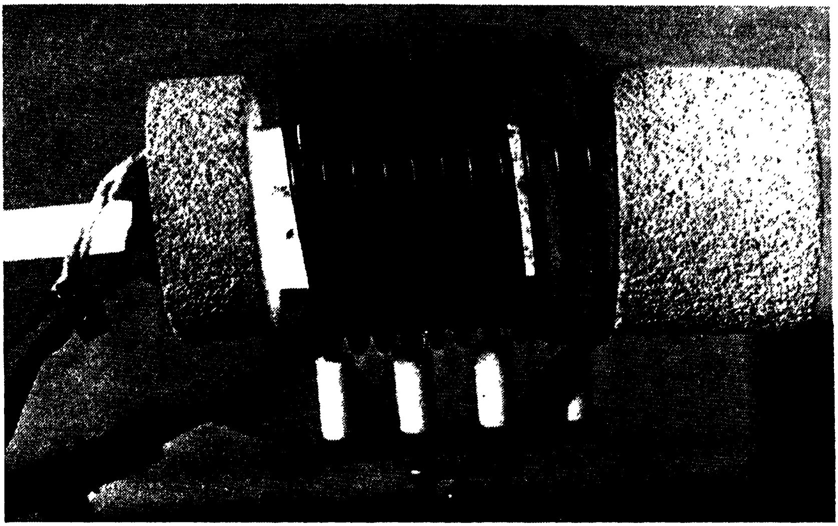

Fig. 83. The radio-frequency coil mounted coaxially with the heated cylinder. Here the fire-brick has been partially removed to show the heated cylinder.

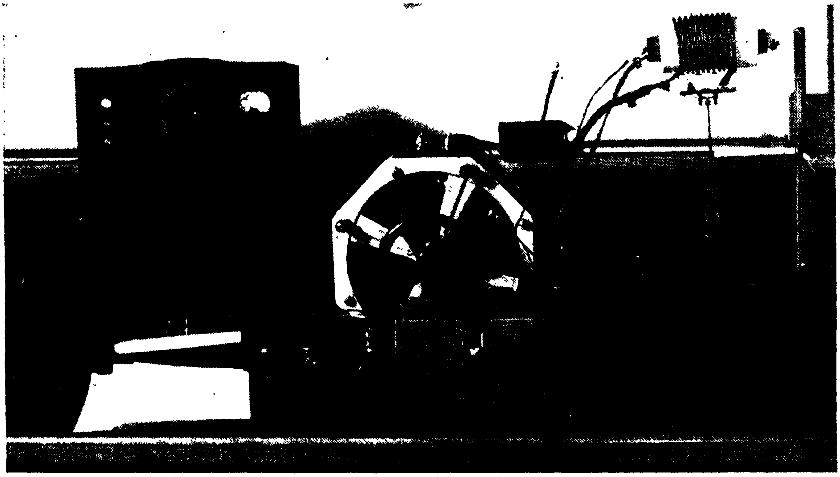

Fig. 84. The laboratory arrangement using a radio-frequency bridge.

coil leads were extended so that the heated load was well away from the bridge, thus avoiding any changes in the initial balance of the bridge due to heat conduction into the bridge. The radio receiver used as a null indicator for the bridge may be seen on the left, while the signal generator is on top of the receiver. The temperature of the heated cylinder was measured with a thermocouple welded to the cylinder.

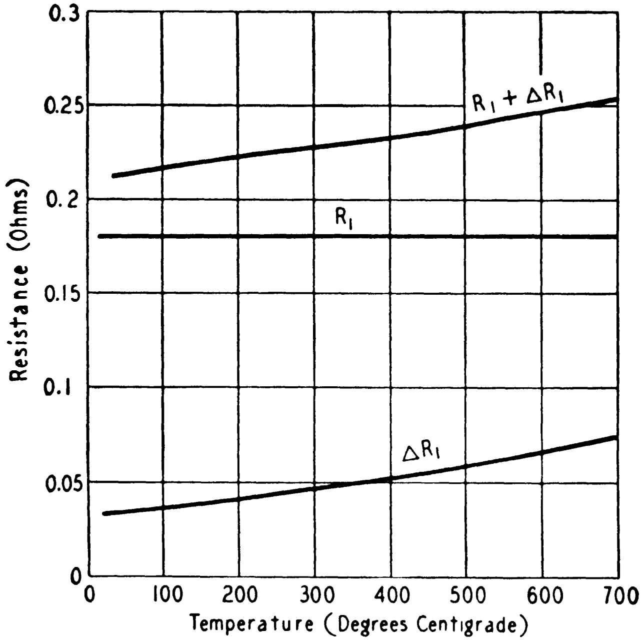

FIG. 85. Resistance measurements with a copper cylinder. R_1 is the resistance of the coil alone, $R_1 + \Delta R_1$ is the resistance measured at the coil terminals when the heated copper cylinder is inserted in the coil.

All the measurements described here were made at a frequency of 1 megacycle. First the copper cylinder was removed and the resistance of the coil was measured with the Q-meter. Using the notation of Chapter 9 this resistance is shown in Fig. 85 as R_1. Then the copper cylinder was inserted in the coil, and the power into the internal heater adjusted so that the cylinder was raised to a temperature where a measurement was desired. The copper coil was kept cool by running compressed air through it. The air was admitted at the low-potential end of the coil. The rather large spacing between the coil and cylinder was chosen so that the coil would not be heated appreciably by the cylinder. In addition, this large spacing insured the fact that the current distribution on the conductor of the coil would remain the same with the cylinder present or not.

A new series of measurements of the coil resistance with the cylinder present was made as a function of temperature. These values are shown in Fig. 85 as $R_1 + \Delta R_1$. The resistance added to the coil by the presence of the cylinder is obtained by subtracting the coil resistance from the total resistance. This result is shown as ΔR_1 in Fig. 85. Equation (9.04) shows that this incremental resistance is directly proportional to the resistance of the secondary circuit. Inspection of (8.15) reveals that for a specific configuration and frequency, the incremental resistance is proportional to the square root of the product of the permeability and resistivity of the material of which the cylinder is composed. That is,

$$\Delta R_1 = K\sqrt{\mu_m \rho_m}. \tag{10.01}$$

For the copper cylinder, the relative permeability, μ_m, is unity. From the results of many experimenters, we know that the resistivity of copper at 20° C is 1.724×10^{-6} ohm for a centimeter cube. Then, from (10.01),

$$K = \frac{(\Delta R_1)_{20^\circ}}{\sqrt{1.724 \times 10^{-6}}}\cdot \tag{10.02}$$

At a new temperature, T, the resistivity of the copper is

$$\rho_T \text{ (ohms for a centimeter cube)} = 1.724 \times 10^{-6}\left[\frac{(\Delta R_1)_T}{(\Delta R_1)_{20^\circ}}\right]^2\cdot \tag{10.03}$$

From Fig. 85, we see that ΔR_1 is 0.032 ohm at 20° C, and ΔR_1 is 0.074 ohm at 700° C. When these results are substituted in (10.03), we find that the resistivity at 700° C is 9.22×10^{-6} ohm for a centimeter cube. Equation (10.03) and Fig. 85 were thus used to construct the lower curve of Fig. 86, which shows the resistivity of copper as a function of temperature.

A brass cylinder equipped with heating coil was next used in the same exciting coil. A new curve of ΔR_1 for the brass cylinder as a function of temperature was then obtained. Since the brass cylinder had exactly the same dimensions as the original copper cylinder, the resistivity of brass was obtained from (10.03), where $(\Delta R_1)_{20^\circ}$ was taken as 0.032 ohm, the value obtained with the copper cylinder. The resultant resistivity of brass as a function of temperature is shown by the upper curve of Fig. 86.

With the method here described, one is able to determine the unknown resistivity of metal by preparing and measuring two cylinders, one of which is made of copper while the other is made of the metal to be tested.

In the case of metals which have a permeability greater than unity, we are unable to unscramble the resistivity from the product of resistivity and permeability. In this case, we must modify (10.03), obtaining

$$\mu\rho = 1.724 \times 10^{-6}\left[\frac{(\Delta R_1)_T}{(\Delta R_1)_{20^\circ}}\right]^2. \qquad (10.04)$$

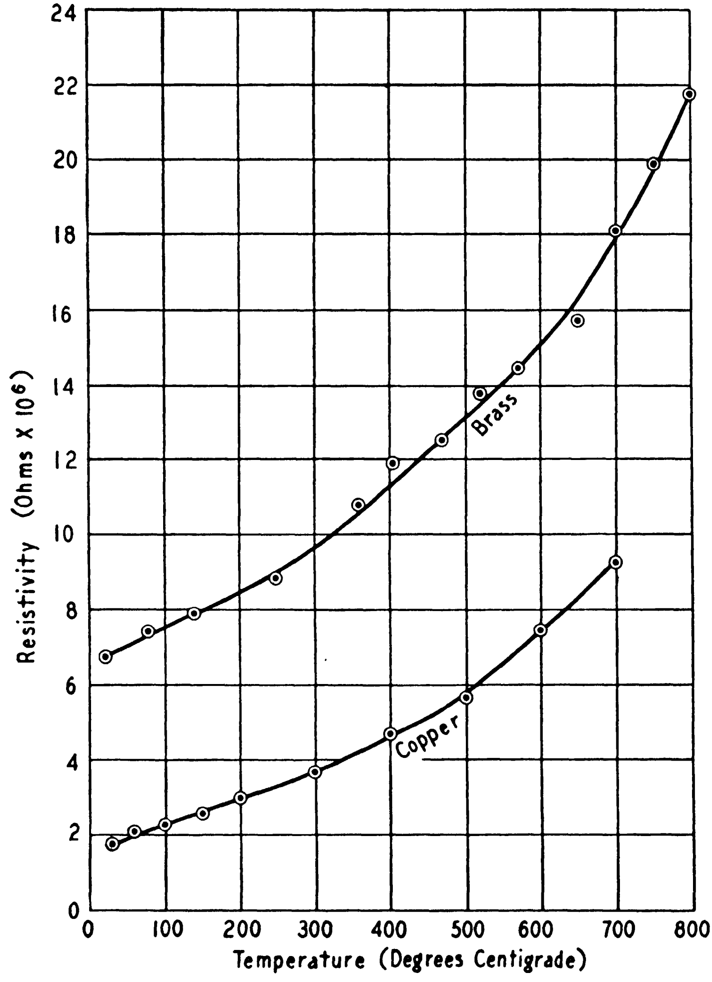

FIG. 86. Specific resistance of copper and brass as a function of temperature.

Fig. 87 shows values of ΔR_1 obtained with an iron cylinder and a tool-steel cylinder. Here we find remarkably great fluctuations. The resistivity of the ferrous materials increases with the temperature. With the low magnetizing currents used in these experiments, it is likely that the permeability also increases with increasing temperature. However, when the temperature goes above 740° C for the iron or 725° C for the tool steel (the Curie point), the permeability drops rapidly to values close to unity. The product of permeability and resistivity, calculated from (10.04), is shown in Fig. 88.*

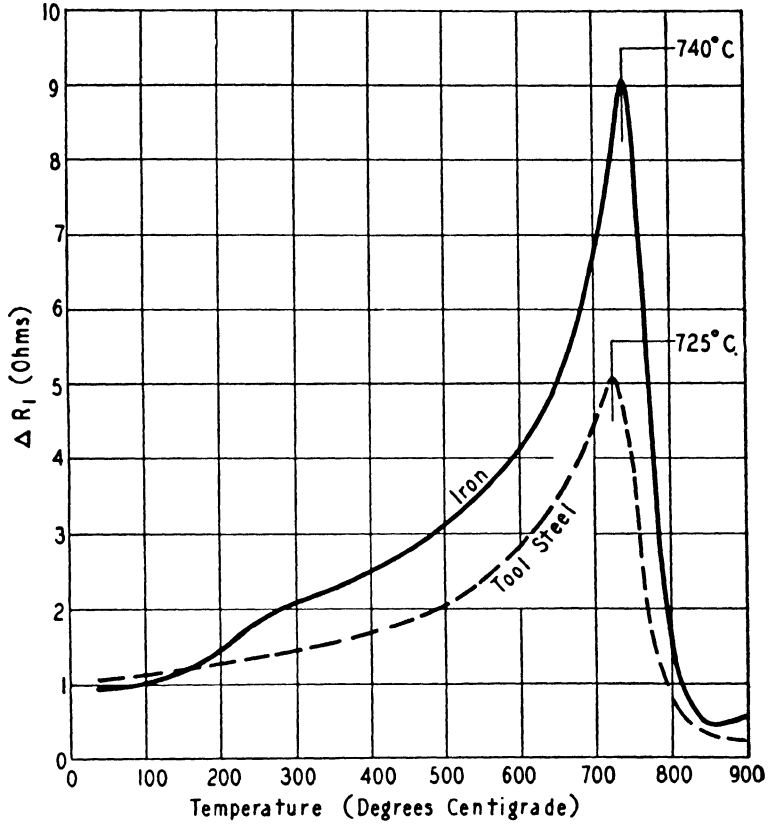

FIG. 87. The incremental resistance obtained with a tool-steel cylinder and an iron cylinder.

As stated above, the resistivity and permeability cannot be separated here so the data presented in Fig. 88 cannot be used to determine the skin thickness. However, it may be used to calculate the transfer resistance. The values of Fig. 88 may be substituted directly into (8.20) to obtain the efficiency relation. It is important to note that

$$\frac{\mu_m}{\sigma_m} = \mu_m \rho_m.$$

---

* Somewhat similar curves are presented and discussed by George I. Babat, "Some Peculiarities of Heating Steel by Induction," *Journal of Applied Physics*, Vol. 15, No. 12, December 1944, p. 835.

It should be pointed out that in a typical induction-heating application, the magnetic intensities are usually so high that the iron is working far past saturation, so that the effective permeability may be close to unity. Then the results shown in Fig. 88 may be far from the true state of affairs.

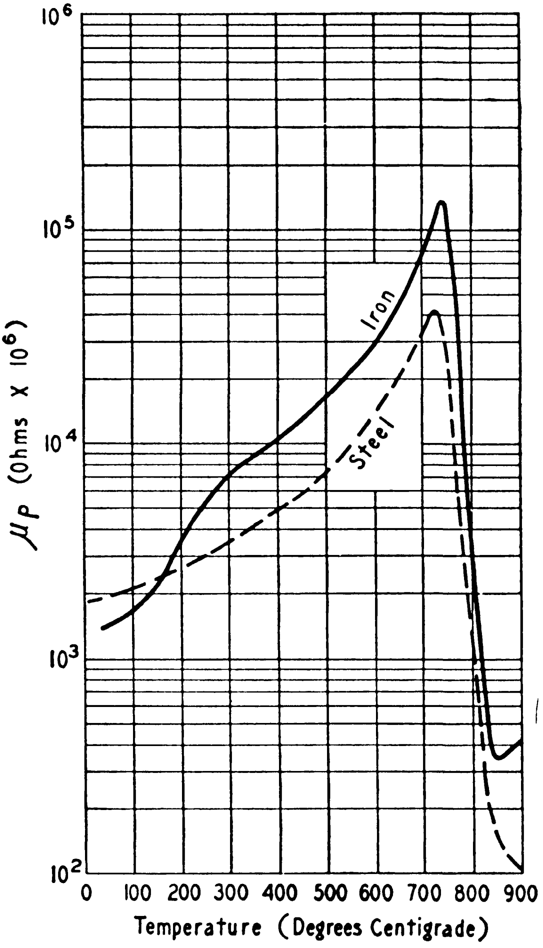

FIG. 88. The product of relative permeability and resistivity of iron and steel as a function of temperature.

The measurements which yielded the results plotted in Fig. 87 were all taken with increasing temperature, since these are the significant figures where induction heating is being applied. However, the experimental technique yields results which may be of interest to the metallurgist in the study of the properties of steel. The curve for tool steel in Fig. 87 shows an increase of the transfer resistance with increasing temperature, up to 725° C. This increase is primarily due to the increase of resistivity with temperature, although part of the increase in resistance may be attributed to an increase in the relative permeability of the steel. However, at 725° C, the electrons attached to the iron atoms are thrown out of their orbital relations so that they no longer act as concealed currents which set up the additional flux densities which are manifested by high permeabilities.* As a result, the permeability approaches unity at temperatures above 725° C, with an abrupt drop in the transfer resistance. With the electrons disrupted from their ordered orbital relationship by the elevated temperature, a reluctance to resume this ordered condition is displayed as the material is cooled. Fig. 89-I shows a repetition of the curve for tool steel shown in Fig. 87, with the addition of the resistance measured as the steel cylinder cooled. The temperature of the steel was raised to 890° C before cooling began. The low transfer resistance was observed until the temperature dropped to 630° C. As the temperature dropped further, there was a slight increase in the transfer resistance, indicating some recovery of magnetism. However, the material did not appear to return to its initial state until complete cooling took place.

In taking the data shown in Fig. 89-I, the fire-brick insulation was not used so the cooling was rapid. In order to more thoroughly explore the vagaries of the material structure at a more leisurely rate, the fire-brick insulation was added. The other curves shown in Fig. 89 were taken with this insulation in place so the cooling rate was not as rapid as in Fig. 89-I. It should also be observed that continued reheating of the same sample alters the structure so that identical results are not obtained on successive runs.

In Fig. 89-II, we see the results of measurements taken as the steel was heated to 700° C. Cooling was then started and the resistance curve practically retraced itself. After cooling to room temperature, the material was again heated, this time to 740° C, a temperature which brought us well past the peak of the curve and down to low values of resistance. When cooling started, the resistance stayed constant for a small temperature drop but soon started upward toward the original curve. This may be seen in Fig. 89-III. A comparison of Figs. 89-I and 89-III indicates that raising the temperature to 890° C rather thoroughly disrupts the orbital relations which are not then restored until the material reaches low temperatures again while heating to a point only a little above the Curie point causes a disruption which is readily overcome by slight cooling. When the temperature had dropped to 600° C as shown in Fig. 89-III, heating was again started and the temperature raised to 730° C as shown in Fig. 89-IV. Here only a slight drop in resist-

---

* Edward Bennett and Harold M. Crothers, *Introductory Electrodynamics for Engineers*, 1st ed., McGraw-Hill Book Company, Inc., New York, p. 575.

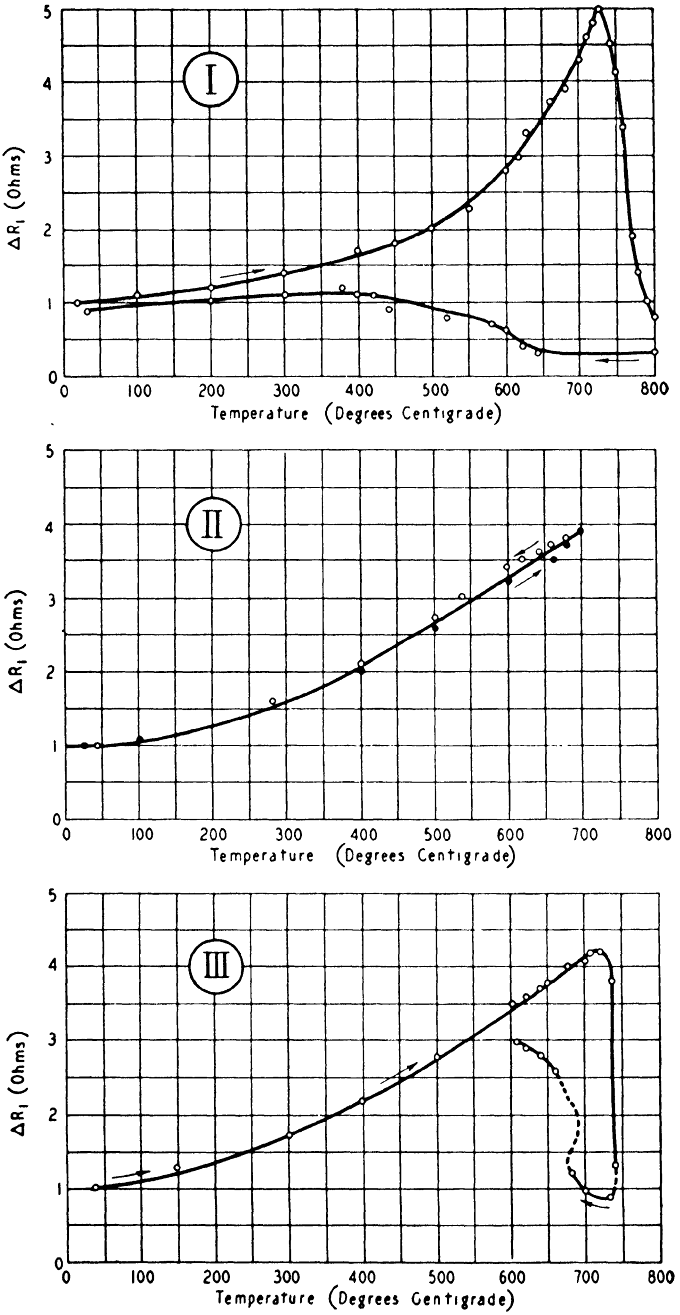

FIG. 89. The incremental resistance obtained with a steel

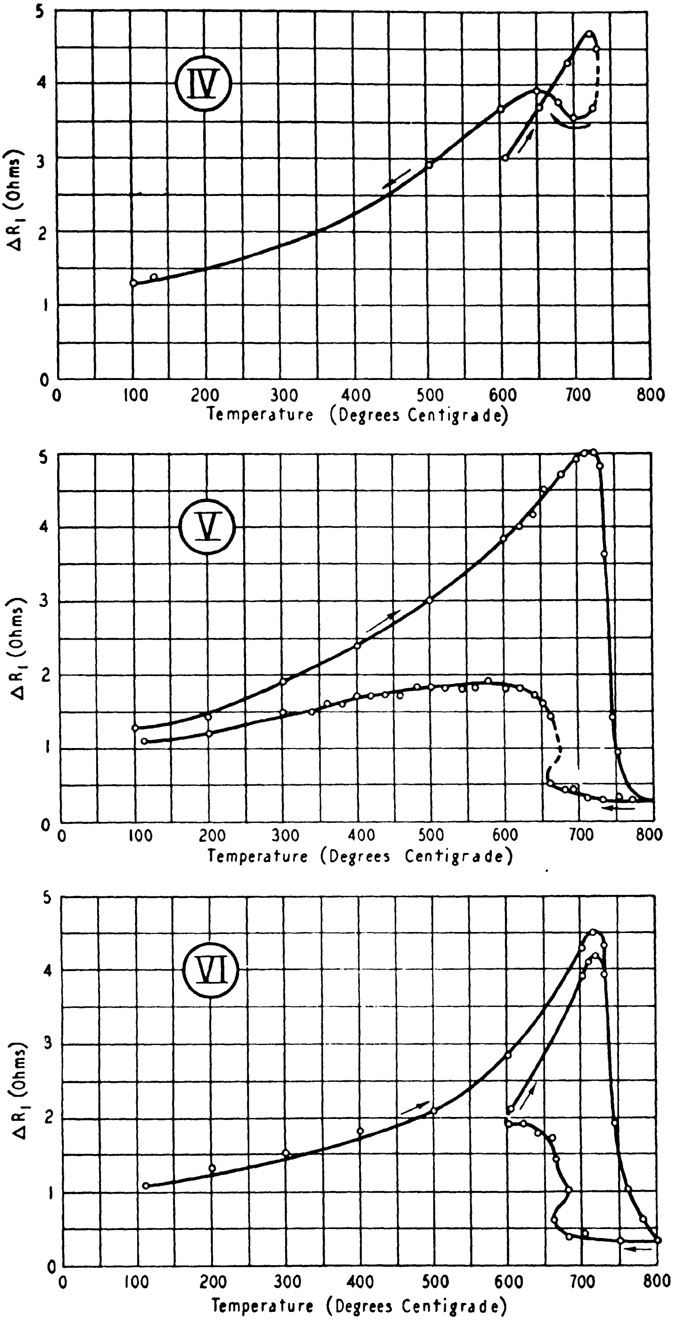

cylinder subjected to a variety of heating and cooling conditions.

ance was encountered since we had gone only slightly above the Curie point. The recovery with dropping temperature is quite apparent in Fig. 89-IV. Here the material was cooled to 100° C.

Heating was again started and a normal curve obtained with increasing temperature, as shown in Fig. 89-V. The steel was now heated to 800° C and then allowed to cool. We see a partial recovery taking place in the neighborhood of 660° C, but no full recovery until the material had been brought to

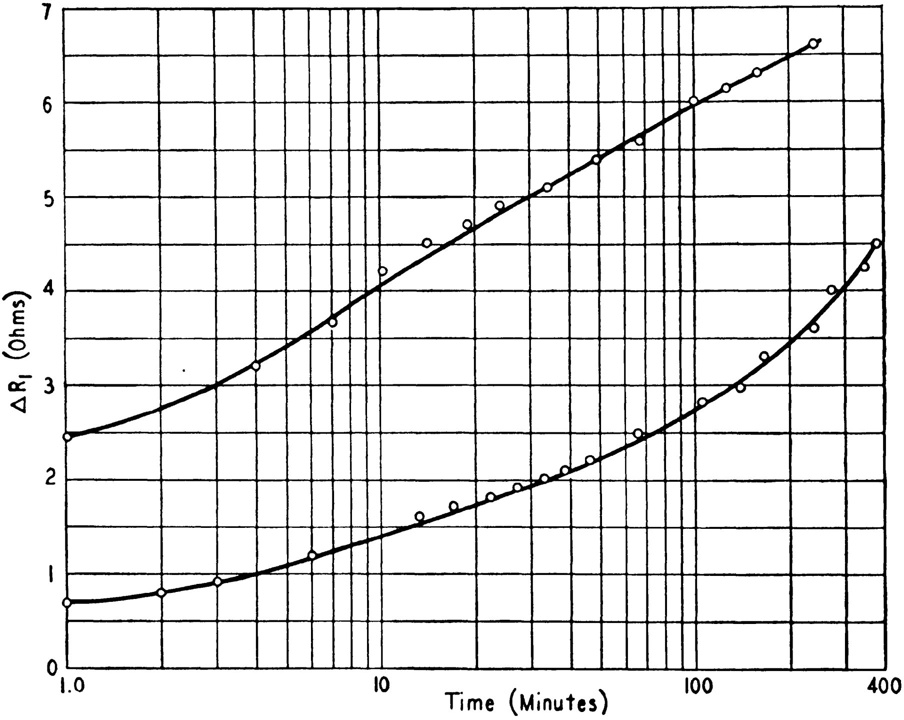

FIG. 90. Recovery curves of steel as a function of time. The steel was heated above the Curie point, cooled to 700° C and held at that temperature. The recovery rate is influenced by the time that the material is held above the Curie poont.

low temperatures. It may be observed that the results of Fig. 89-V lie intermediate to those shown in Figs. 89-I and 89-III.

In Fig. 89-VI, the steel was heated to 800° C. Then the steel was cooled to 600° C with substantially the same results as shown in Fig. 89-V. At this temperature, heating was again applied with a consequent increase of resistance. The resistance continued to increase until a temperature of 725° C was reached when a characteristic drop in resistance occurred.

In obtaining the data of Figs. 89-III and 89-V a point of " recalescence " or increase in temperature during the cooling period was noted, but in Fig. 89-VI an actual measurement of resistance and temperature was obtained as shown.

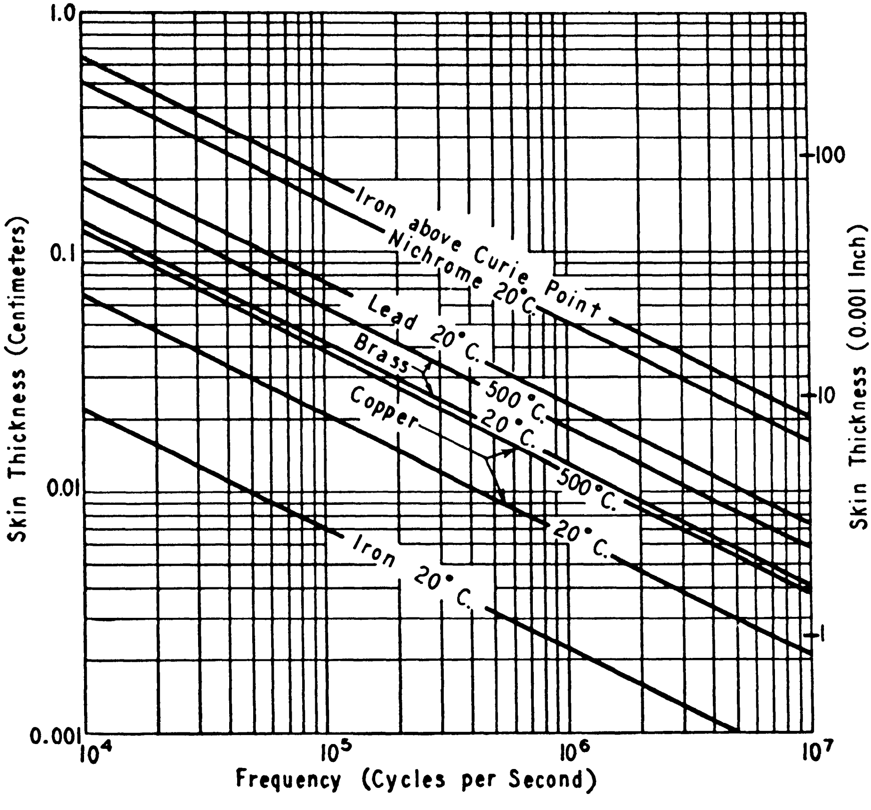

Fig. 91. The skin thickness of a number of metals as a function of frequency.

The degree of recovery as well as the range of temperatures at which recovery of magnetism occurs when cooling from above the Curie point depends upon the maximum temperature reached, the length of time held at this temperature, the cooling rate, and in fact upon the whole previous history of the sample. Sauveur* has published an excellent resumé of phenomena occurring at the thermal critical points which is in substantial agreement with the results which we have presented.

To illustrate the effect of the time factor in degree of recovery, the steel sample was heated from 20° C to a temperature well above the Curie point.

---

* Albert Sauveur, *The Metallography and Heat Treatment of Iron and Steel,* 3d ed., The University Press, Cambridge, Mass., pp. 129–142.

The steel was held at this elevated temperature for at least 15 minutes. Then it was cooled to 700° C. The sample was then held at this temperature for a long period of time, during which the transfer resistance was measured quite frequently. The lower curve of Fig. 90 shows the increase of transfer resistance as a function of time, with the curve approaching the value obtained at 700° C during the initial heating. Several days later, the sample was again heated from 20° C to a temperature above the Curie point. It was held at this temperature only a few minutes before cooling to 700° C. The transfer resistance obtained when the metal was held at 700° C is shown by the upper curve of Fig. 90.

The measurements presented in this chapter, as well as a great deal of information from other sources, were of assistance in preparing Fig. 91. Here the skin thickness as a function of frequency is presented for a number of metals. This figure will be referred to in later considerations.

Chapter 11

ANNEALING BRASS AND BRONZE BY RADIO-FREQUENCY HEATING

When brass or bronze is subjected to cold working such as rolling or drawing, severe distortion of the grain structure occurs. The effect of this is manifested by a sharp decrease in ductility and an increase in hardness to a point where metal failure will occur unless it is annealed. It is customary to anneal the metal for 1 hour in a furnace, usually maintained at 600° C, so that ductility, hardness and grain size will reach values permitting further cold working. After brass is annealed in this manner, it must be pickled in an acid bath to remove the heavy scale which was formed as a result of the long period at high temperature.

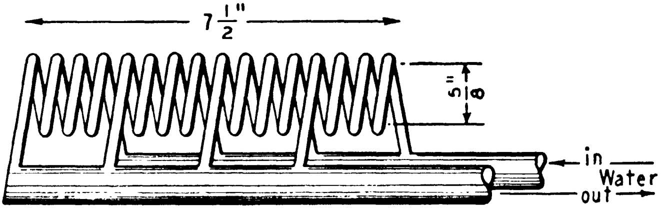

FIG. 92. The coil used for heating hard-drawn brass rod.

The annealing process is a time-temperature function of a rather complex nature. Quick annealing demands a high temperature. Rapid heating with radio-frequency power is possible for almost any desired temperature under conditions that can be carefully controlled and readily reproduced. A number of laboratory experiments were carried out to establish some of the important facts relating to annealing by means of radio-frequency power.

Annealing Cartridge-Brass Rod. A plentiful supply of hard-drawn cartridge-brass rod was obtained. These rods were $\frac{1}{2}$ inch in diameter and 7 inches long. A multiple coil was prepared. This coil, shown in Fig. 92, consisted of several inductances in parallel with a total length sufficient to heat the whole rod at once.

In annealing these rods, the power input to the oscillator remained essentially constant for each test ranging, on the average, from 2980 watts at the start to 3330 watts at the end of each run. The procedure was to turn on the oscillator for a sufficient time to allow the sample to reach a particular designated temperature. Then the oscillator was turned off and the sample allowed to cool slowly in air. The time that the oscillator was operating was recorded, as well as the temperature of the sample at the end of that time. In Figs. 93 to 98, inclusive, the complete results of this annealing process are summarized by showing Rockwell " F " readings taken along the rod, photomicrographs of grain size, and the physical properties of the rod. A tabulation of the data pertinent to Figs. 93 to 98 is presented in Table 5. These data are graphically correlated in Figs. 99 and 100. The material shown in Figs. 93 to 98 was furnished by R. S. Pratt, Metallurgist, Bridgeport Brass Company, Bridgeport, Connecticut. A set of annealing curves based on an anneal of cartridge-brass strip at various furnace temperatures for 1 hour are also shown in Figs. 99 and 100. These curves* are marked " P " to distinguish from the results marked " RF " which pertain to the annealing with radio-frequency power for short times.

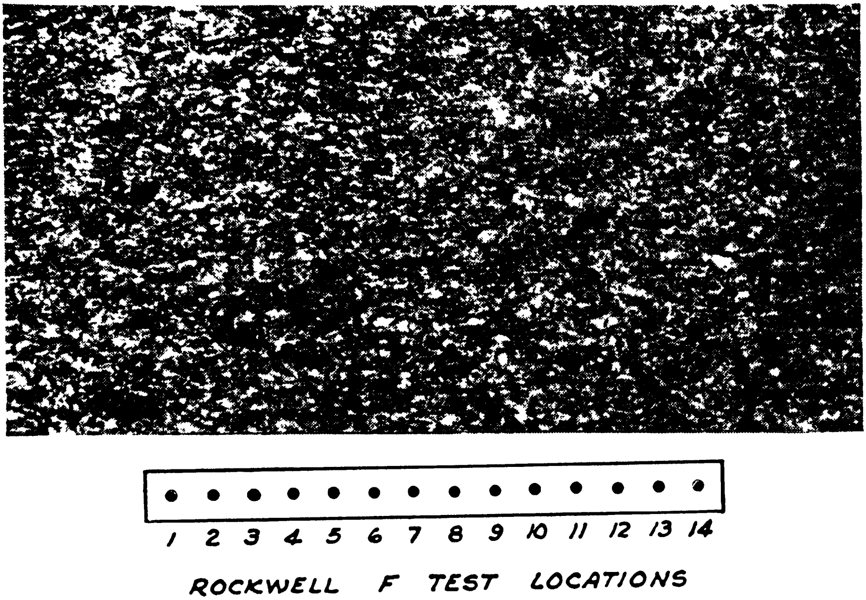

FIG. 93. Photomicrograph of unannealed brass rod. Magnification 115×. All tests made on 70–30 brass rod, ½ inch × 7 inch.

---

* R. S. Pratt, *Physical Properties of Brass Cartridge Cases*, presented at the Annual Meeting, American Society of Mechanical Engineers, New York City. Dec. 1–5, 1941.

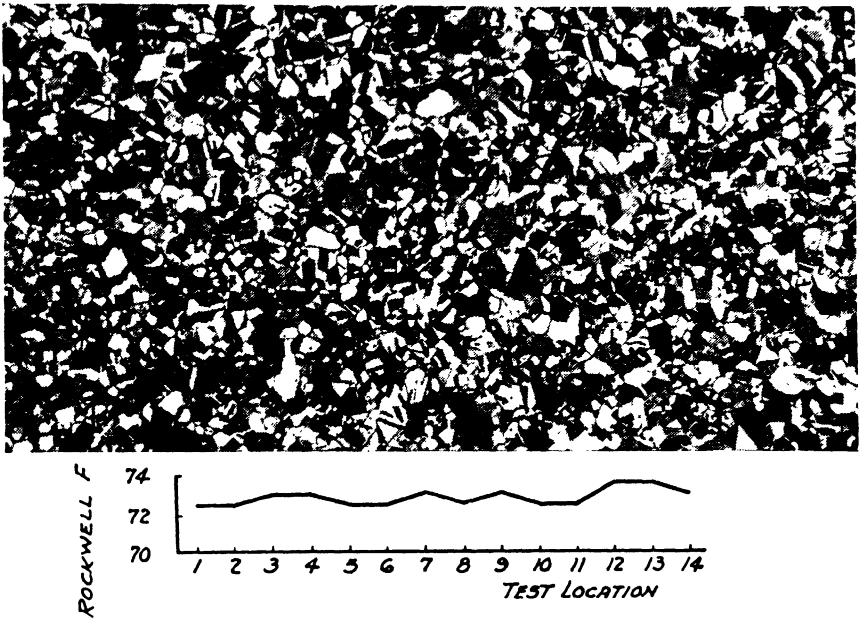

Fig. 94. Brass rod heated for 50 seconds to 600° C. Grain size 0.023 millimeter.

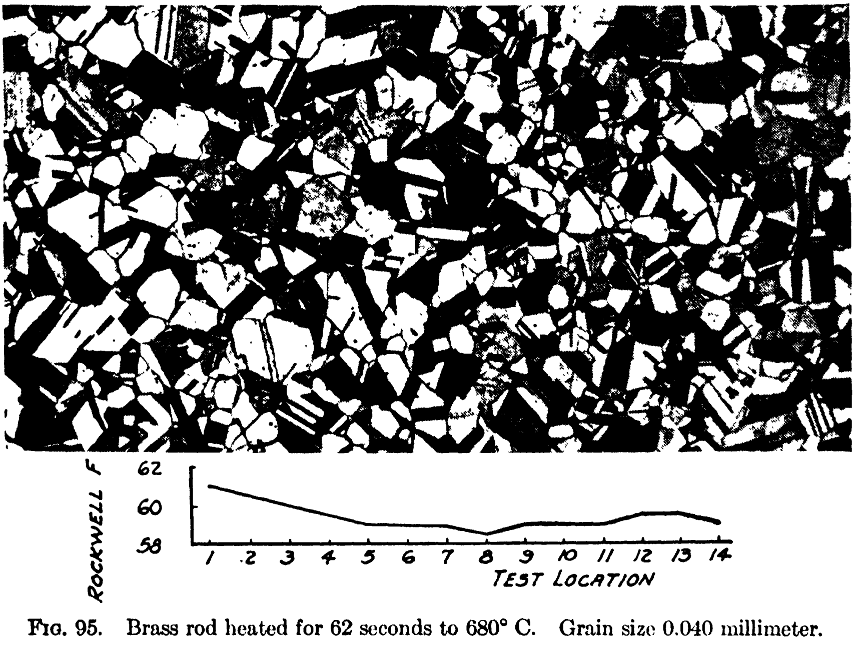

Fig. 95. Brass rod heated for 62 seconds to 680° C. Grain size 0.040 millimeter.

It is evident that grain size increases very rapidly as the final temperature of the rod is made higher but that tensile strength, Rockwell " F," per cent elongation and per cent reduction in area do not show any important changes in magnitude. The uniformity of the anneal is good and it definitely appears that any furnace-annealing condition can be duplicated by radio-frequency heating. On the basis of present annealing practice, a final temperature of 700° C to 750° C attained by radio-frequency heating in approximately 1 minute should produce acceptable results, such as are shown in Figs. 95 and 96.

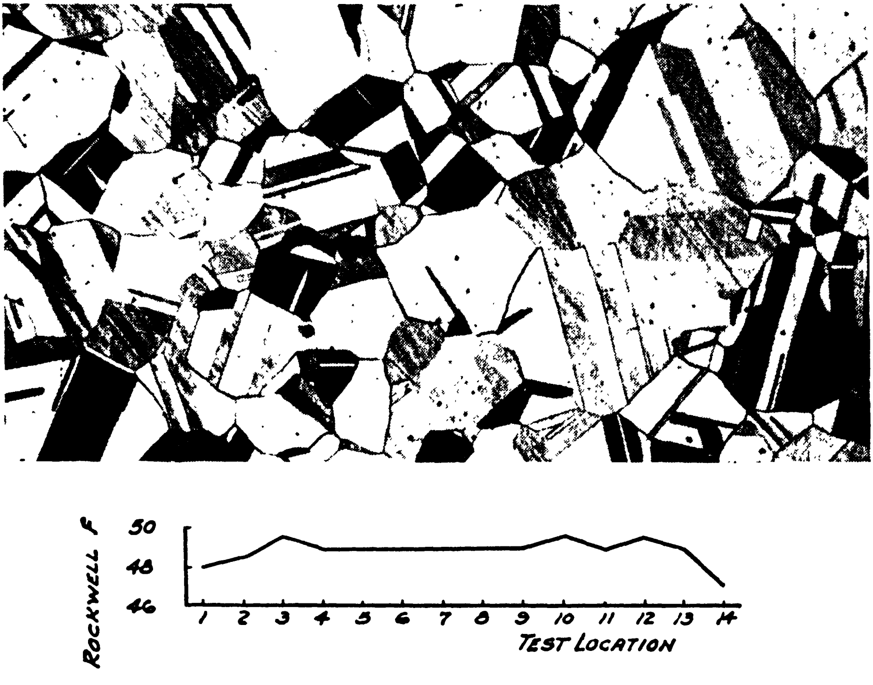

Fig. 96. Brass rod heated for 70 seconds to 760° C. Grain size 0.095 millimeter.

Annealing Cartridge Cups. In the light of the results obtained in annealing brass rod, it was felt desirable to apply radio-frequency heating to brass cartridge cases in order to anneal them. The samples selected for annealing experiments were 20-millimeter cups in the hard state after the third draw. The total weight of these cups is 117 grams. Of this weight about 49 grams are in the heavy base which need not be annealed, because in the subsequent drawing operation all work is done on the sides of the case.

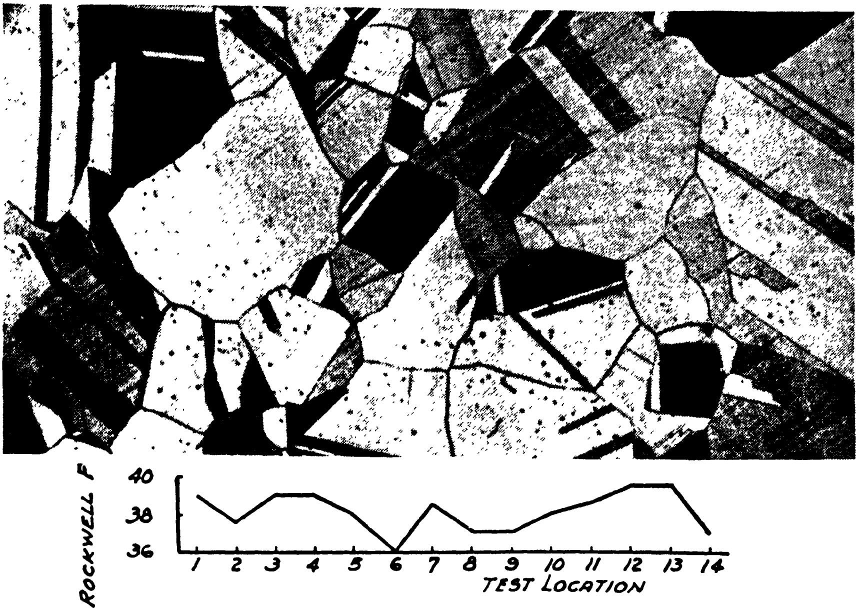

Fig. 97. Brass rod heated for 80 seconds to 800° C. Grain size 0.160 millimeter.

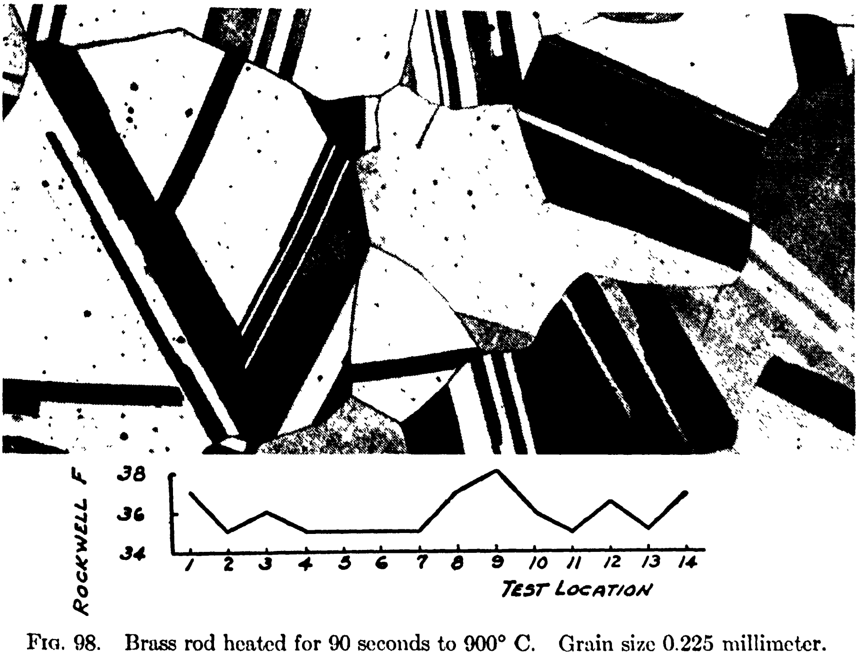

Fig. 98. Brass rod heated for 90 seconds to 900° C. Grain size 0.225 millimeter.

TABLE 5. DATA PERTAINING TO MICROPHOTOGRAPHS OF BRASS.

Photomicrograph shown in	Heating Time (seconds)	Final Temp. (° C)	Rockwell F	Grain Size (millimeters)	Tensile Strength (pounds per square inch)	Elongation (per cent)	Reduction Area (per cent)
Fig. 93	Unannealed	. . .	108	. . .	100,000	14	60.0
Fig. 94	50	600	72.5–73.5	0.023	52,000	51	77.6
Fig. 95	62	680	58.5–61.0	0.040	48,900	59	78.8
Fig. 96	70	760	48.0–49.5	0.095	46,400	63	79.6
Fig. 97	80	800	36.0–39.5	0.160	44,000	64	78.5
Fig. 98	90	900	35.0–38.0	0.225	43,000	64	77.4

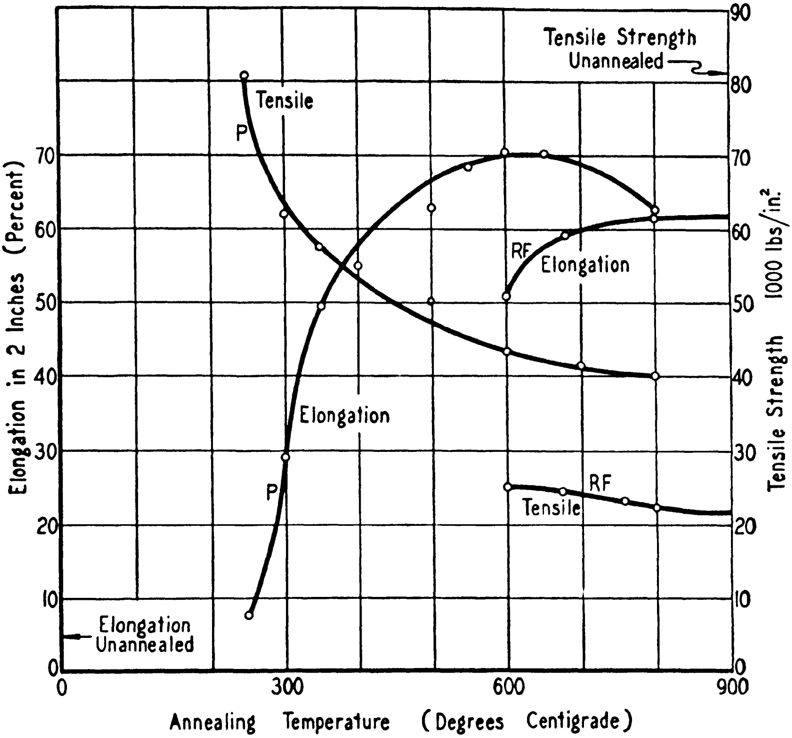

FIG. 99. Tensile strength and elongation of brass as a function of annealing temperature.

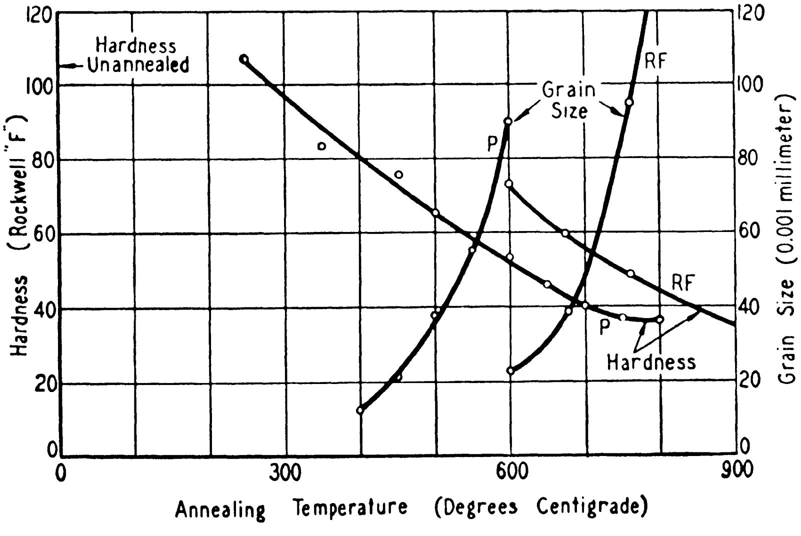

FIG. 100. Hardness and grain size of brass as a function of annealing temperature.

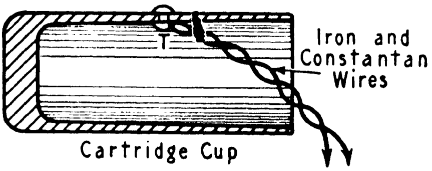

FIG. 101. Cartridge cup with thermocouple attached.

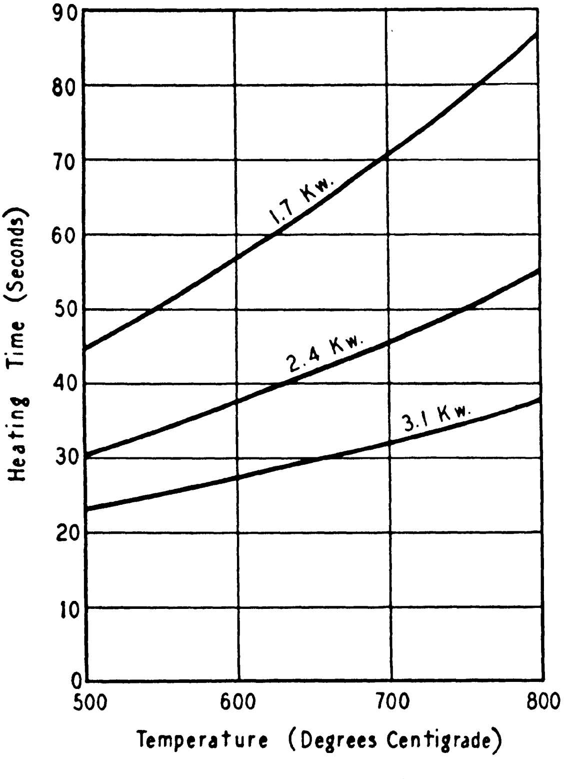

FIG. 102. Time-temperature calibration chart for annealing cartridge cups with a number of oscillator input powers.

Actual annealing of the samples was done according to two general plans, using a frequency of 850 kilocycles.

I. Heating to specific temperatures (650° C, 700° C, 750° C, and 800° C), with input power the independent variable and time to attain temperature the dependent variable.

II. Heating for a specific time (40 seconds), with input power the independent variable and final temperature the dependent variable.

To facilitate the determination of temperature a test cup was prepared as shown in Fig. 101, with a thermocouple riveted to the case at " T." The cup was then subjected to heating with various oscillator input powers, noting the time it took to reach several different temperatures. From a plot of these data as shown in Fig. 102 it was possible to select suitable parameters for actual test anneals.

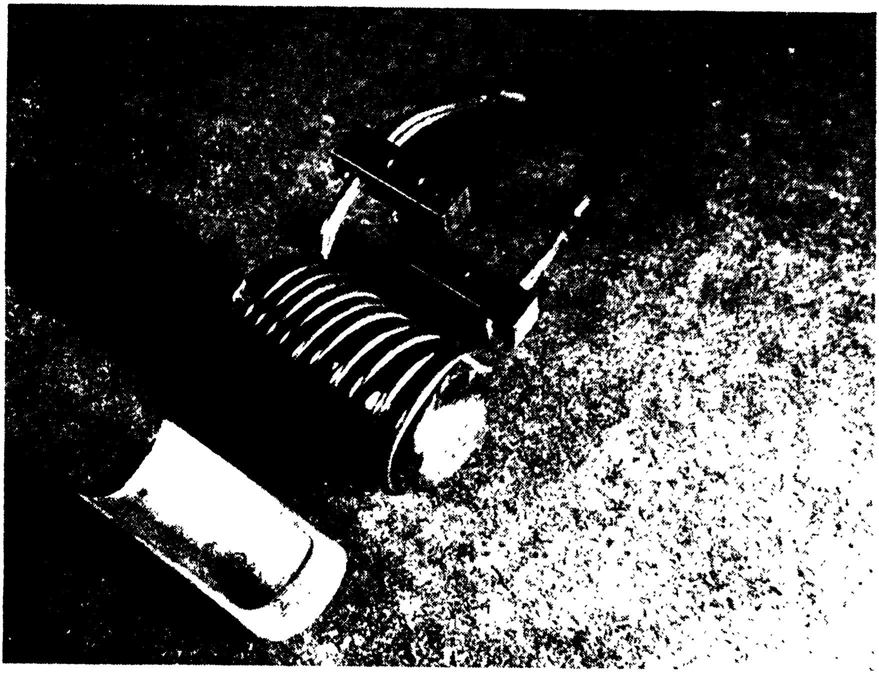

Fig. 103. The coupling coil used in heating the cartridge cups.

The coupling coil used for heating the cases is shown in Fig. 103. The coil was slightly conical in shape so that the thinner wall at the mouth of the cup would not be overheated. The same results could be obtained by spacing the turns more at the open end.

It was decided to anneal a number of cases in accordance with Plan I, choosing three suitable input powers from Fig. 102, for each temperature. Final tabulated results in Table 6 represent the average of the findings. Some of these results are shown graphically in Figs. 104 and 105.

A detailed study of the grain sizes at seven different locations, indicated by A, B, C, D, E, F, G in Fig. 106 was made of one group of cups, those heated to 650° C. Although actual heating times ranged from 30 seconds to

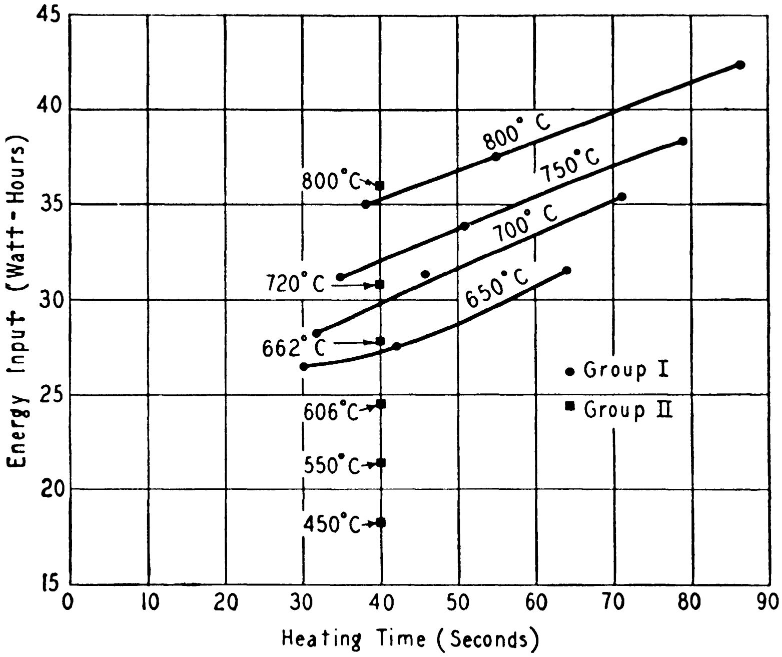

Fig. 104. Oscillator energy input versus heating time to attain the final temperatures shown.

TABLE 6. THE RESULTS OF ANNEALING BRASS CUPS.

Input Power (kilowatts)	Input Energy (watt-hours)	Temp. (°C)	Time (seconds)	Rockwell "F" (average)	Grain Size (millimeters)
3.22	35.0	800	38	47.0	0.115
2.45	37.5	800	55	45.7	0.135
1.77	42.2	800	86	43.0	0.145
3.20	31.1	750	35	54.0	0.090
2.40	33.9	750	51	52.0	0.095
1.75	38.4	750	79	48.0	0.095
3.16	28.1	700	32	61.0	0.045
2.40	31.4	700	46	60.0	0.040
1.75	34.4	700	71	55.3	0.052
3.16	26.4	650	30	65.3	0.036
2.37	27.5	650	42	64.3	0.036
1.72	31.4	650	64	63.7	0.038

64 seconds, Table 6 and Fig. 105 show that there was very little change in either grain size or Rockwell " F " values. Accordingly, the average of the three samples done at 650° C and marked " RF " was taken in plotting the bar graph of Fig. 106. The average of three samples done in a furnace at 600° C for 1 hour furnished the data for sketching the bars marked " P." An inspection of Fig. 106 will reveal:

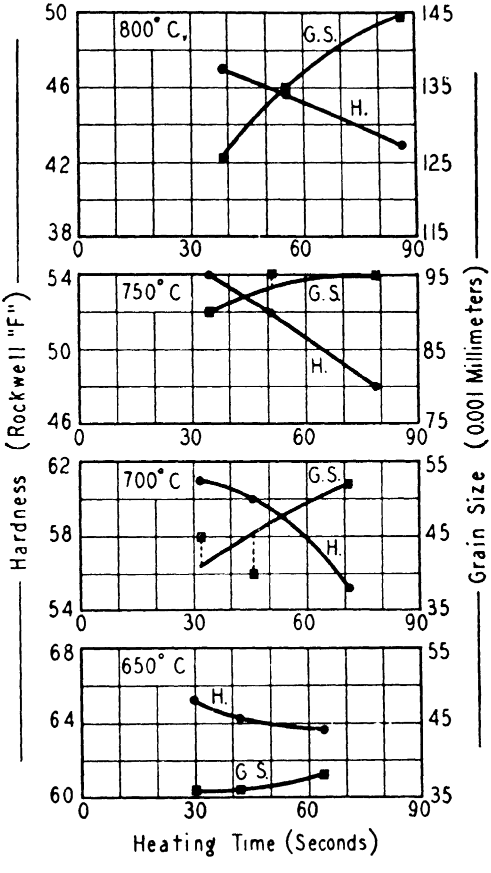

FIG. 105. Rockwell "F" and grain size for 20-millimeter cartridge cups heated to a number of final temperatures.

1. Uniformity of grain size along the walls (A, B, C). The smaller grain size of the " RF " samples is due to low annealing temperature. Had a detailed analysis been made of " RF " samples annealed at 700° C and 750° C, the grain size would have been identical to the " P " values.

2. Large grain sizes at E. Actually, grain size at this point is indeterminate since parts of the shoulder are worked and some parts are not. The larger value of " RF " sizes is probably accounted for by the previous history

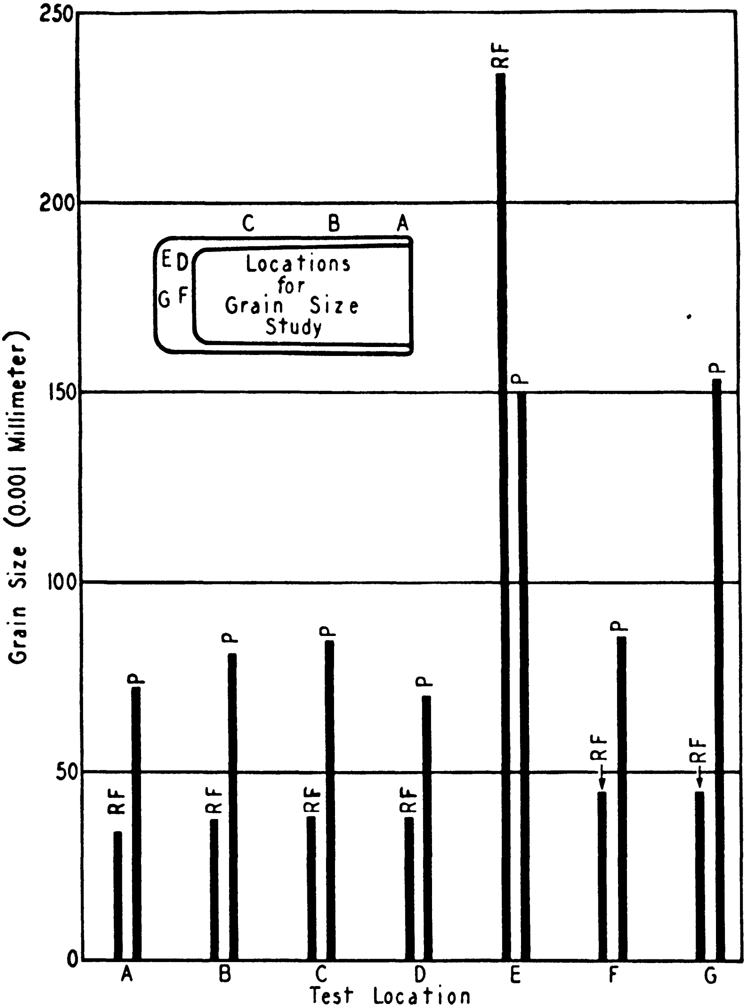

FIG. 106. Grain-size study of 20-millimeter cartridge cases taken at a number of locations on samples annealed by radio-frequency heat in 40 seconds at 650° C and on samples annealed in furnace for 1 hour at 600° C.

of the particular cups. In one case, the grain size was identical with " P "; in the other cases, much larger.

3. At D, F, and G the " RF " grain sizes are much smaller than the " P "

grain sizes. This illustrates one of the advantages that radio-frequency annealing has to offer. In drawing the cases there is practically no work done on the brass at these points, with the result that there is a continual growth of grain sizes. Radio-frequency annealing does not over-anneal these parts; an effect particularly noted at G.

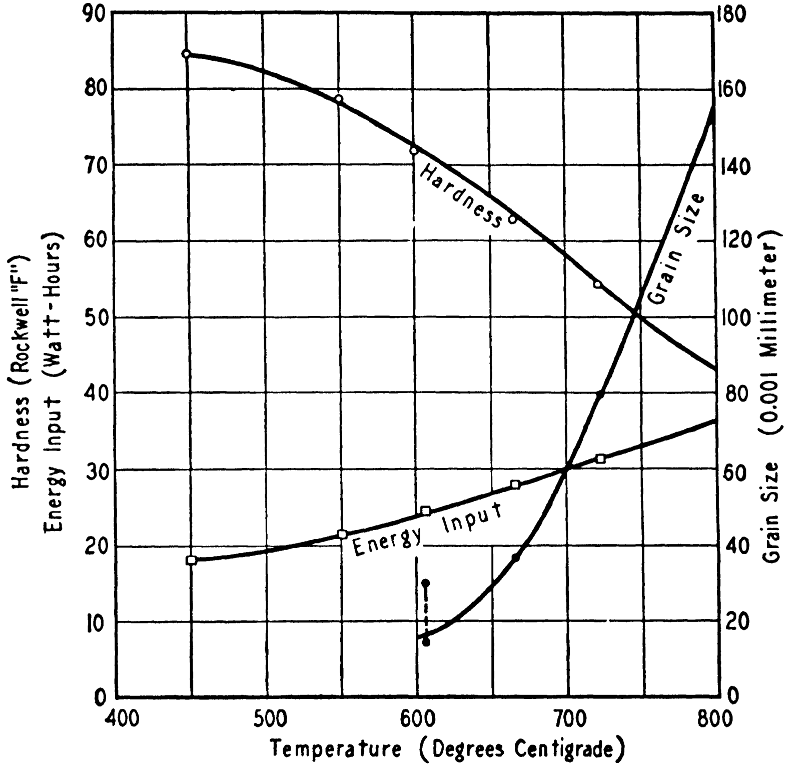

FIG. 107. Properties of 20-millimeter cartridge cups annealed by radio-frequency heat in 40 seconds at various temperatures.

In annealing a series of cases in accordance with Plan II, it was decided to fix the time of heating at 40 seconds and control power input to the oscillator by the simple expedient of choosing six suitable input voltages. The results of this procedure, set forth in Table 7, represent the average of two samples for each condition. For a graphical representation of these data, we may refer to Fig. 107.

There was one very evident advantage of radio-frequency annealing that became apparent in the course of this investigation. Due to the rapid heating, and consequently the short time during which the cartridge case was

TABLE 7. THE EFFECT OF POWER AND TEMPERATURE ON THE ANNEALING OF BRASS.

Input Power (kilowatts)	Input Energy (watt-hours)	Temp. (° C)	Rockwell " F " scale	Grain Size (millimeters)
1.64	18.2	450	84.5	Partial recrystallization
1.93	21.4	550	78.5	Recrystallization nearly complete
2.22	24.6	606	72.0	Complete, irregular 0.015–0.030
2.50	27.8	662	63.0	0.038
2.77	30.8	720	54.5	0.080
3.24	36.0	800	43.0	0.160

at high temperature, the formation of scale was very greatly reduced. Where furnace-annealed cases showed a heavy grey scale the radio-frequency annealed cases showed only a thin film of oxide through which the characteristic yellow of the brass readily showed. Translated into manufacturing procedure this means a saving in pickling time as well as a saving in material removed as oxide.

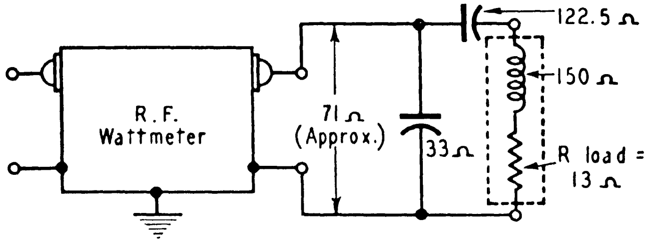

FIG. 108. Impedance-matching network used in conjunction with the radio-frequency wattmeter measurements.

Radio-Frequency Wattmeter Measurements. Power relationships for radio-frequency annealing of brass under the various conditions to be investigated may be most readily compared by measurement of input power to the oscillator. Such information is, however, of only secondary importance when the actual design of equipment for annealing is to be carried through. The completion of a radio-frequency wattmeter* made facilities

* George H. Brown, J. Epstein, and D. W. Peterson, " Direct-Reading Wattmeters For Use at Radio Frequencies," *Proc. I.R.E.*, Vol. 31, No. 8, August 1943, pp. 403–410.

available for more accurate measurements of the output of the oscillator. Since the wattmeter was designed and calibrated for best operation for a 70-ohm load, the matching network shown in Fig. 108 was necessary.

The results of two series of measurements made with the wattmeter are shown in Fig. 109. An average oscillator output of about 1330 watts raised the temperature of the cup to 705° C in 60 seconds. This represents an energy of 22.5 watt-hours delivered by the oscillator. When the oscillator output was reduced to an average of 735 watts, it took 190 seconds to raise the temperature of the brass to 700° C. This corresponds to an energy of 38.8 watt-hours delivered by the oscillator. Thus, 72.5 per cent more energy was necessary to attain the same temperature. Other values showing the advantage of short heating time to attain various temperatures were calculated from Fig. 109 and are shown in Fig. 110.

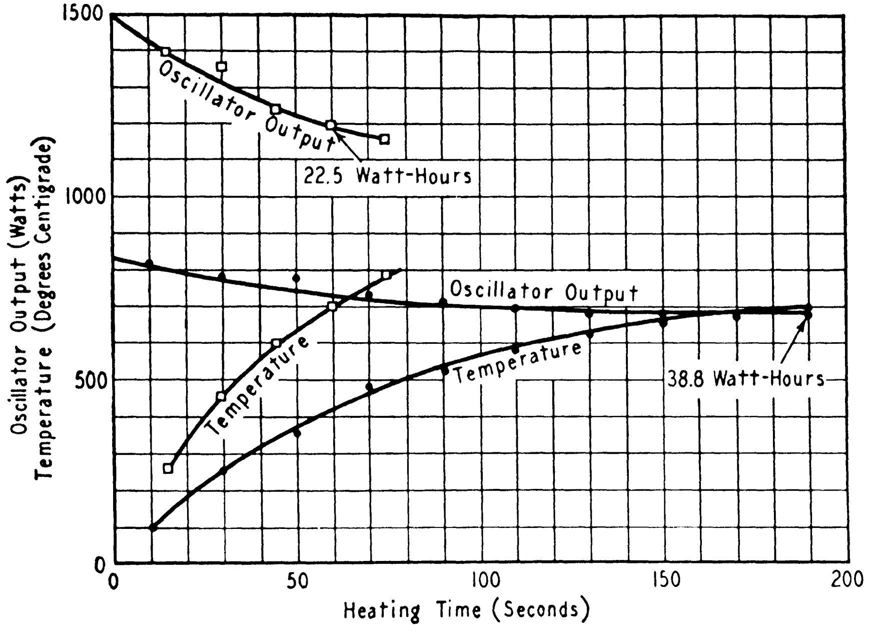

FIG. 109. Comparison of 60-second and 190-second heating cycles.

The above values of power represent that power delivered to the heating coil. Part of this power is used for copper losses in the coil, whereas the remainder is delivered to the brass load. The coil was constructed of cost per tubing with a radius of $\frac{1}{16}$ inch, and the spacing from the center of the copper tubing to the cartridge cup was approximately $\frac{1}{8}$ inch. The conductivity of copper was from 3.75 to 7.8 times that of the brass, depending on the temperature of the brass. If we assume an average value of 6.0, we may turn directly to Fig. 65 and find that the transfer efficiency of the coil is 54.5 per cent. With this figure at hand, the following tabulation is possible.

Plate Input to Oscillator (watts)	Power out of Oscillator (watts)	Power into Brass (watts)	Oscillator Efficiency (per cent)	Transfer Efficiency (per cent)	Over-all Efficiency (per cent)
2004.	1330.	725.	66.4	54.5	36.2
1105.	735.	400.	66.4	54.5	36.2

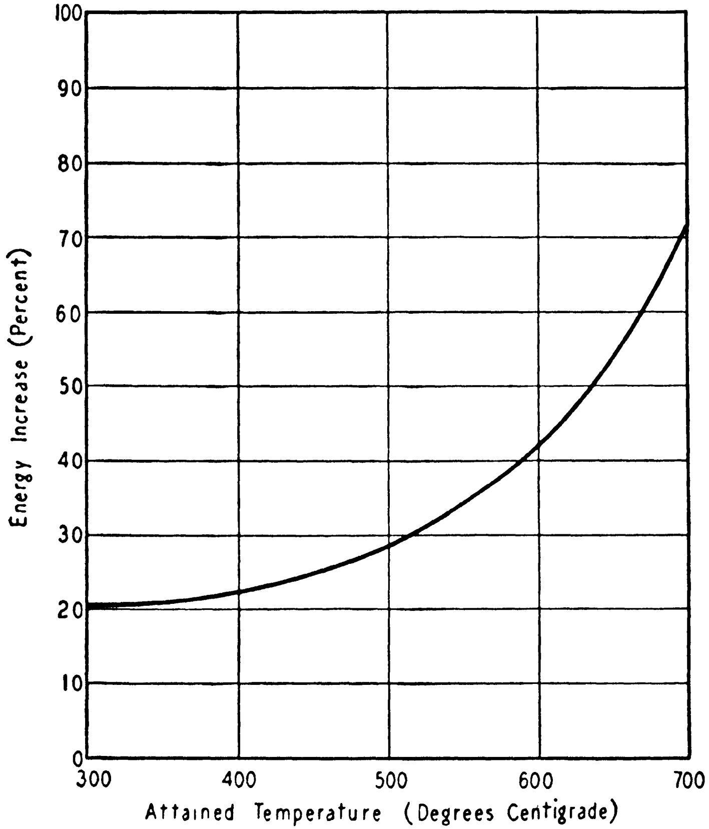

FIG. 110. Percentage increase in energy consumption necessary to attain a given temperature when the power output is reduced about 45 per cent.

Theoretical Consideration. It is evident from Fig. 109 that for a given power delivered to the brass an ultimate temperature is reached where the heat radiated from the brass cup is just equal to the power supplied. Thus we must use a power which is great enough to insure that this ultimate temperature is greater than the temperature necessary for annealing. A theoretical consideration serves to illustrate this point. For a given power,

$$P = KM\rho\frac{du}{dt} + CA(u^4 - u_0{}^4), \tag{11.01}$$

where P = power in watts;
K = a constant = 4.187 watt-seconds per gram-calorie;
M = mass of metal being heated, in grams;
ρ = specific heat of the metal, calories per gram per degree Centigrade;
C = radiation constant = 5.735×10^{-12} watts per square centimeter/degrees^4;
A = surface area of metal in square centimeters;
u = temperature in degrees Kelvin;
u_0 = starting temperature of metal and temperature of the ambient air in degrees Kelvin;
t = time in seconds.

Equation (11.01) is a linear differential equation which may be written as

$$\frac{du}{dt} = \frac{CA}{KM\rho}\left(\frac{P}{CA} + u_0{}^4 - u^4\right). \tag{11.02}$$

If we let $m^4 = \frac{P}{CA} + u_0{}^4$, and separate variables, (11.02) becomes

$$dt = \frac{KM\rho}{CA}\cdot\frac{du}{m^4 - u^4}. \tag{11.03}$$

Expanding in partial fractions,

$$dt = \frac{KM\rho}{CA}\cdot\frac{1}{2m^2}\left(\frac{du}{m^2 - u^2} + \frac{du}{m^2 + u^2}\right). \tag{11.04}$$

Integration of this equation yields

$$t = \frac{KM\rho}{CA}\cdot\frac{1}{2m^3}\left(\tan^{-1}\frac{u}{m} + \frac{1}{2}\log_e\frac{m + u}{m - u}\right)\Bigg|_{u_0}^{u} \tag{11.05}$$

or

$$t = \frac{KM\rho}{CA}\cdot\frac{1}{2m^3}\left[\tan^{-1}\frac{u}{m} + \tan^{-1}\frac{u_0}{m} + \frac{1}{2}\log_e\frac{(m + u)(m - u_0)}{(m - u)(m + u_0)}\right], \tag{11.06}$$

where u_0 is the initial temperature and u is the temperature reached in t seconds.

Illustrative Example. To illustrate the use of (11.06), we shall work the following problem. What heating time is necessary to raise a brass cartridge cup 6.0 centimeters long, 2.95 centimeters in diameter and weighing 117 grams to 700° C from 20° C when 500 watts are put into the brass? The average specific heat of the brass is 0.1. For use in (11.06):

$$KM\rho = 4.187 \times 117 \times 0.1 = 49.0;$$

$$A = 69.2 \text{ square centimeters, including both ends;}$$

$$CA = 396 \times 10^{-12} \text{ watts/degrees}^4;$$

$$u = 700^\circ \text{ C} = 973^\circ \text{ Kelvin;}$$

$$u_0 = 20^\circ \text{ C} = 293^\circ \text{ Kelvin;}$$

$$m = 1061.5;$$

When these values are inserted in (11.06), the time becomes

$$t = 51.64 \left(\tan^{-1} 0.92 - \tan^{-1} 0.277 + \frac{1}{2} \log_\epsilon \frac{23.6}{1.765} \right)$$

or

$$t = 91.6 \text{ seconds.}$$

Curves showing the relationship of time and temperature with 400 watts into the brass cartridge cup and with 725 watts into the cup have been calculated from (11.06) and are shown in Fig. 111. The indicated experimental points were taken from the data displayed in Fig. 109.

From an inspection of (11.06) we see that the time becomes infinite when u equals m. This relation establishes the ultimate temperature. Here the radiation losses are just equal to the power applied. This helps to establish a minimum power necessary to attain a specific temperature. If we assume that the minimum temperature for annealing brass is 700° C, we find from the relation,

$$m^4 = \frac{P}{CA} + u_0^4,$$

the minimum power into the metal is 5.13 watts per square centimeter of surface. Then for the particular cartridge cup which has an area of 69.2 square centimeters, we need at least 356 watts to reach 700° C.

Annealing Phosphor Bronze. The application of radio-frequency heating for annealing hard bronze rod was also investigated. A supply of $\frac{11}{16}$ inch bronze in the hard state was obtained. It was apparent that a continuous process of heating must be applied so means for scanning the rod were considered. The final arrangement consisted of passing the rod through a water-cooled coupling coil at a rate of 5 inches per minute with an oscillator input of 3800 watts at 850 kilocycles. The 6-turn coil was made of $\frac{1}{4}$-inch copper tubing and was $1\frac{1}{2}$ inches long with an inside diameter of $\frac{3}{4}$ inch. Mechanical tests of the radio-frequency annealed rod indicated that all important physical conditions were met. The rod was also successfully drawn from $\frac{11}{16}$ inch to $\frac{9}{16}$ inch. Photomicrographs of the bronze before and after the radio-frequency treatment are shown in Fig. 112.

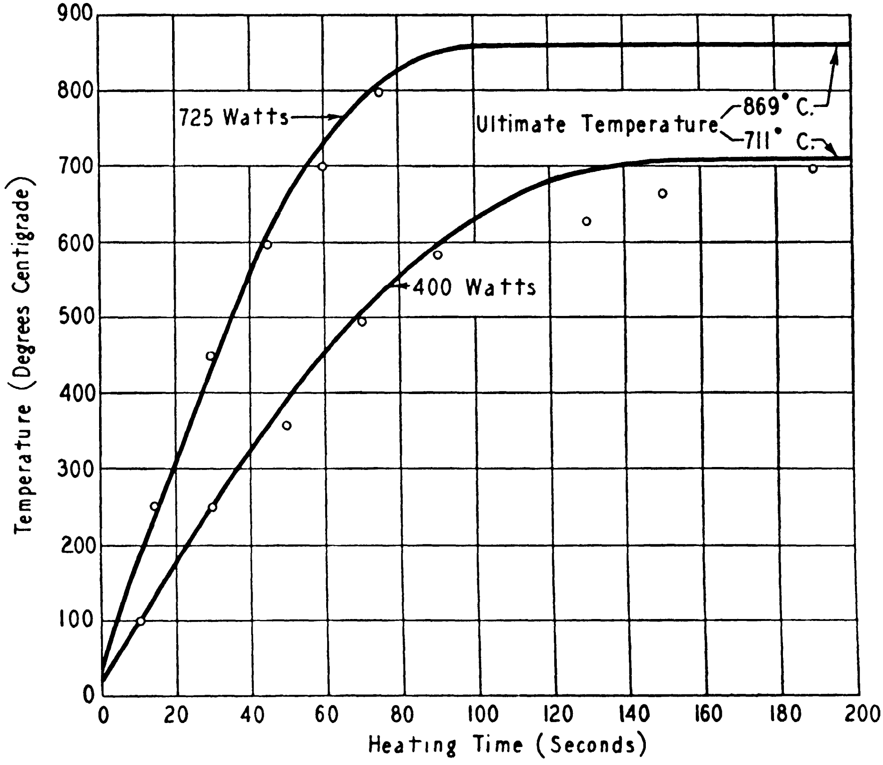

FIG. 111. Temperature as a function of heating time, calculated from (11.06). The lower curve assumes that the power into the cup is 400 watts, whereas the power for the upper curve is 725 watts. The experimental points were taken from the data displayed in Fig. 109.

The general problems associated with brass annealing as discussed in this chapter also apply to bronze. The slightly higher specific resistance of bronze makes it possible to couple somewhat more efficiently to it than to brass.

TABLE 8. TEST RESULTS ON BRONZE SAMPLES.

	Before Annealing	After Annealing
Tensile strength, pounds per square inch	77,600	48,000
Yield point, pounds per square inch	58,000	20,000
Per cent elongation, in 2 inches	36	85
Rockwell " B "	88.5	20
Per cent reduction in area		80

Conclusions. The results of our experiments with the radio-frequency annealing of brass and bronze may be summed up by the following conclusions.

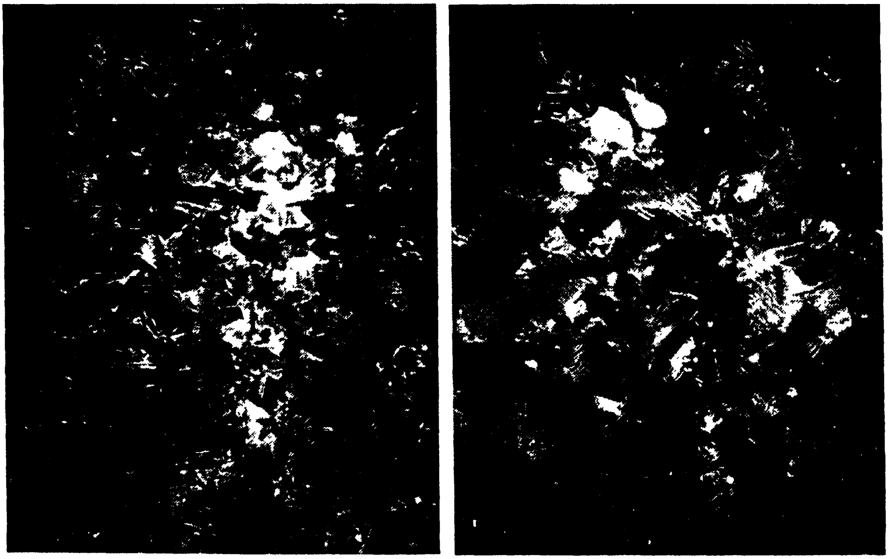
In the hard drawn state. After radio-frequency annealing.

FIG. 112. Photomicrographs of bronze magnification, 150×.

1. Brass and bronze may be effectively coupled to a radio-frequency oscillator so that the currents induced in the material are large enough to heat the material to a high temperature. A frequency of 850 kilocycles was used in this investigation, but the frequency may differ widely from this figure without materially altering the operation.

2. It is possible to couple enough power (7 kilowatts per pound) into a sample so that a suitable annealing temperature may easily be reached in 40 to 60 seconds. There is evidence that with higher power this time may be reduced, although melting of the surface is a limiting factor.

3. Comparative measurements made on grain size, tensile strength, reduction in area, elongation, and hardness of samples annealed by radio-frequency and by a conventional furnace show that exactly comparable results may be expected from the two methods. In general, where furnace annealing is usually done at 600° C, the necessary temperature for radio-frequency annealing is from 100° C to 150° C higher.

4. Radio-frequency annealing is readily accomplished on individual units or the method may be adapted to a continuous process such as would be necessary for rods and bars.

5. In this investigation, brass rods $\frac{1}{2}$ inch in diameter and 7 inches long were annealed as units in 60 to 90 seconds with an oscillator input of 2900 to 3200 watts.

6. Twenty-millimeter cartridge cases in the hard state after the third draw were individually annealed with an oscillator input of 2800 watts in 40 seconds. Lower input powers increased the time and lowered the efficiency since radiation losses increased.

7. Bronze rod $\frac{11}{16}$ inch in diameter was properly heated with radio-frequency power for annealing when it was scanned at a rate of 5 inches per minute with an oscillator input of 3800 watts.

8. The rapid heating possible when radio-frequency power is used greatly reduces the losses by radiation.

9. Outstanding reduction in scale formation is a corollary of the short heating cycle. The importance of this effect becomes apparent when the mass of material normally lost in the pickling process is considered.

Chapter 12

LABORATORY EXPERIMENTS WITH TYPICAL INDUCTION-HEATING PROBLEMS

In several previous chapters, we have examined the general theoretical aspects of induction heating. It is the purpose of the present chapter to describe a few laboratory arrangements which the authors have devised to solve a number of typical induction-heating problems. In each case, the work coil has been water-cooled and coupled to the oscillator by a current transformer of the type shown in Fig. 79.

Paint Baking. Certain of the newer finishes, particularly those of the synthetic urea or phenolic resin type are thermosetting in character and can be set or cured very rapidly if heated to a temperature of about 200° C. The heating of a paint film directly by radio-frequency power is impractical because of the poor efficiency of the coupling that can be realized. However, the baking of paint on metal objects may be expedited by induction heating of the metal object. Here the currents induced in the metal generate heat which is transferred to the paint. The paint is thus set or dried from the inside out, an obviously desirable condition. Fig. 113 shows an experimental arrangement for baking paint on metal radio tubes. After spraying with a synthetic urea resin paint, the tubes are conveyed through an elongated coupling coil. This coil has three conductors connected in parallel and arranged so that the spacing from the tubes may be adjusted to secure uniform heating. To further insure uniform heating, each tube rotates about its vertical axis as it progresses through the coil. This rotation is brought about by using a moving web belting on one track which guides the tubes, while the belting on the other track is fixed.

The tubes pass through the coil in 15 seconds and in that time are heated to a temperature of 200° C. This short baking period is sufficient to completely cure the finish. The appearance of the finished product is good, with no blistering. Acetone solubility tests indicate that the cure is complete. The arrangement shown is capable of handling 2400 vacuum tubes per hour with a radio-frequency power input of 2 kilowatts. In comparison, a conventional baking oven process requires 45 minutes and the oven occupies a space many times that of the radio-frequency generator and coupling device.

In addition, the heating of the bakelite base is now very slight so that crimping of the metal to the bakelite base may be done before painting.

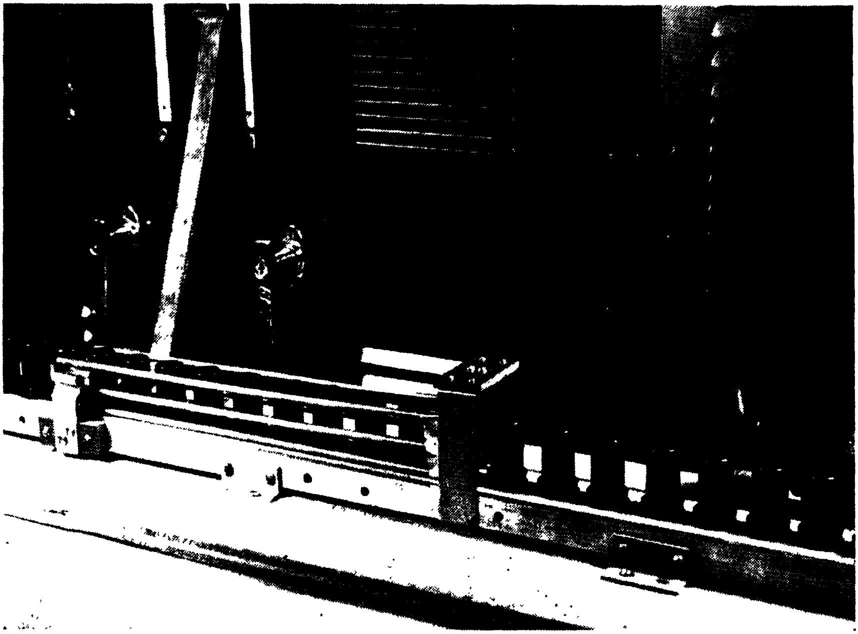

FIG. 113. Induction heating arrangement for baking paint on metal vacuum tubes.

The use of the current transformer with a Hartley oscillator circuit makes possible another important feature. The tubes need not be evenly spaced on the track. If only one tube were sent through the coil, only enough energy would be drawn from the oscillator to heat this single tube to exactly the proper temperature as it leaves the coil. If two or three more tubes are started at random through the coil, additional energy will be supplied so that each tube leaves the coil in just the proper condition.

Set-Screw Hardening. One of the characteristics of induction heating that often makes it advantageous to use is that the heating can be localized and accomplished so quickly that adjacent areas are not affected. An application of this nature is shown in Fig. 114. Here a steel set-screw with a screwdriver slot is hardened at the slotted end while the rest of the screw is left in the soft untreated condition. The set-screws are loaded onto a small rotating platform which carries them into a curved hairpin-shaped coupling coil. The coil is placed so that only the slotted end of the screw is heated. When the screw reaches the end of the coil, the temperature of the heated end has reached the value required for hardening, and the screw is dropped into a water bath for quenching. The heating period is about $1\frac{1}{2}$ seconds. This time is so short that the heat does not flow into the rest of the screw. As a result, the hardening is confined to the slotted end for a depth of about $\frac{3}{32}$ inch.

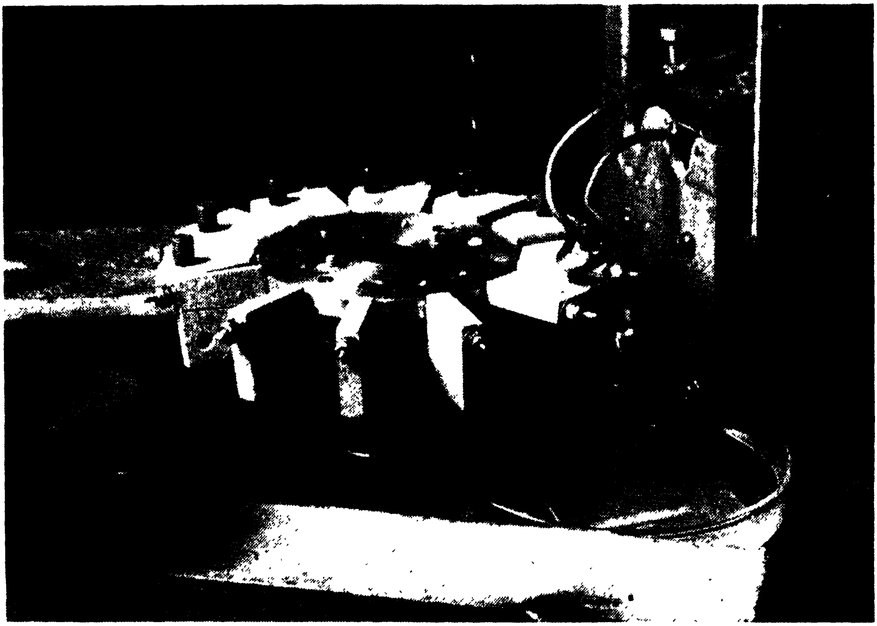

FIG. 114. Rotating fixture and heating coil used in hardening the tops of set-screws.

With 2 kilowatts of radio-frequency power, 2700 screws can be treated each hour.

Soldering and Brazing. Many difficult soldering and brazing operations, which by ordinary methods require the employment of highly skilled and experienced labor, can be performed faster and better through the use of induction heating even with inexperienced operators. Because induction heating can be accurately controlled and directed, great uniformity of results may be attained. Fig. 115 shows a cover assembly for a hermetically-sealed transformer case being soldered in one operation by induction heating. The insulated terminals are assembled on the cover with a ring of rosin-cored solder under each and placed in the curved coupling coil. Radio-frequency current is passed through the coil for about 13 seconds and the soldering operation is complete. The radio-frequency power required for this operation is about 500 watts.

A rather difficult silver-soldering problem was solved as shown in Fig. 116. An automatic grease cup assembly required the silver soldering of the body to a rather heavy base without overheating a neoprene cup-washer in the top of the body. A coupling coil was fashioned to heat the body and base at the joint to be soldered. The upper part of the body was placed in a water-cooled clamp to protect the cup-washer. A silver-solder ring was placed around the body at the joint and flux was applied to the surfaces to be joined. Radio-frequency power of 3500 watts applied for 15 seconds was required for the operation.

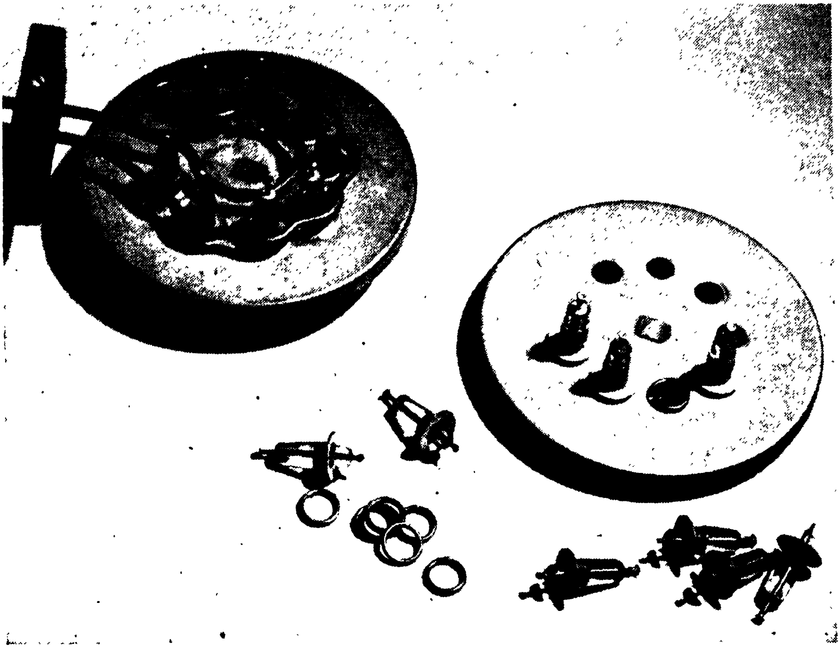

FIG. 115. Soldering by induced currents.

Often the parts to be soldered can be carried on a conveyor belt* through the coupling coil so that the soldering process can be carried on continuously. Brazing operations can be performed similarly except that higher temperatures are required. To prevent oxidation of the parts during the heating period, an atmosphere of forming gas or hydrogen may be employed to surround the work.

Welding. In the pressure-welding of iron and steel parts, the surfaces to be joined are placed in rather intimate contact, subjected to a pressure of about 5000 pounds per square inch, and heated to a temperature somewhat below the melting point. A good weld is obtained without the use of flux as the pressure forces any oxide from between the surfaces to be joined. The heating of the joint can best be accomplished by induction heating. An experimental set-up for welding $\frac{3}{4}$-inch steel chain is shown in Fig. 117. The links are made of two U-shaped pieces cut off square at the ends and butt-welded together. The water-cooled, single-turn coupling coil shown in Fig. 118 is split to permit removal when the weld is completed. Pressure is applied by means of a hydraulic jack. A radio-frequency power of about 6 kilowatts was applied for 35 seconds. The bulge at the weld is characteristic of pressure welding and usually is not objectionable. It may be removed

---

* J. P. Taylor, "High Speed Soldering with Radio-Frequency Power," *Electronics*, Vol. 17, No. 2, February 1944, p. 114.

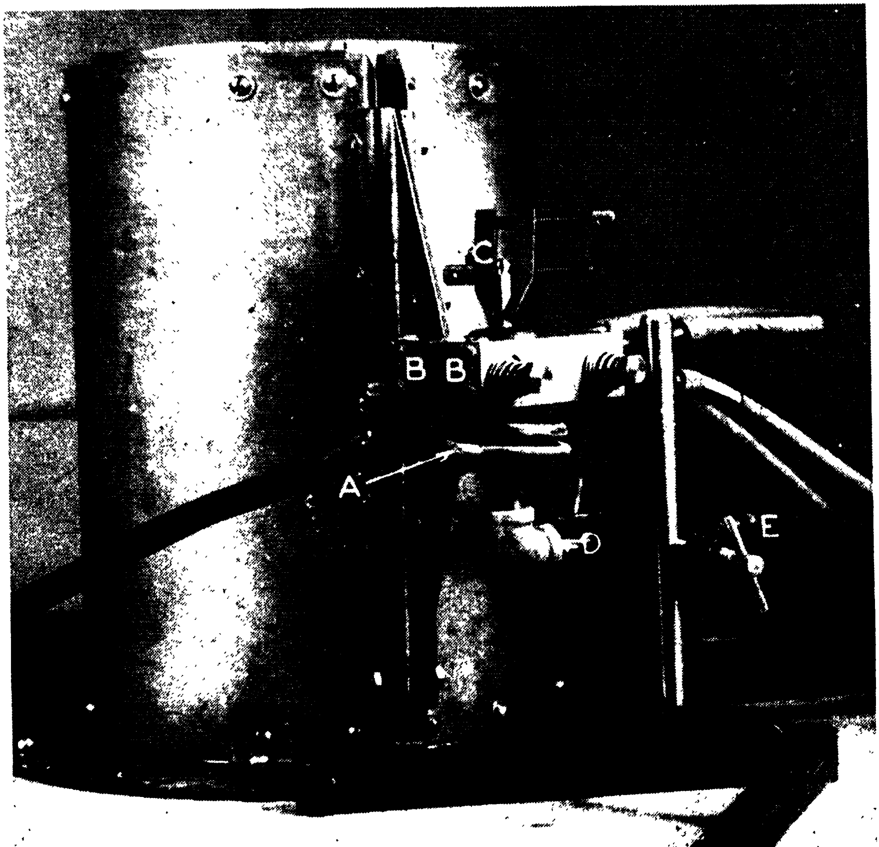

FIG. 116. In this silver-soldering operation, the inducing coil consisted of 2 turns of copper tubing. The protective clamp-block may be seen directly above the inducing coil.

by grinding. Tensile tests made on the welded links showed a breaking strength of 35,000–40,000 pounds, which is well above the required value of

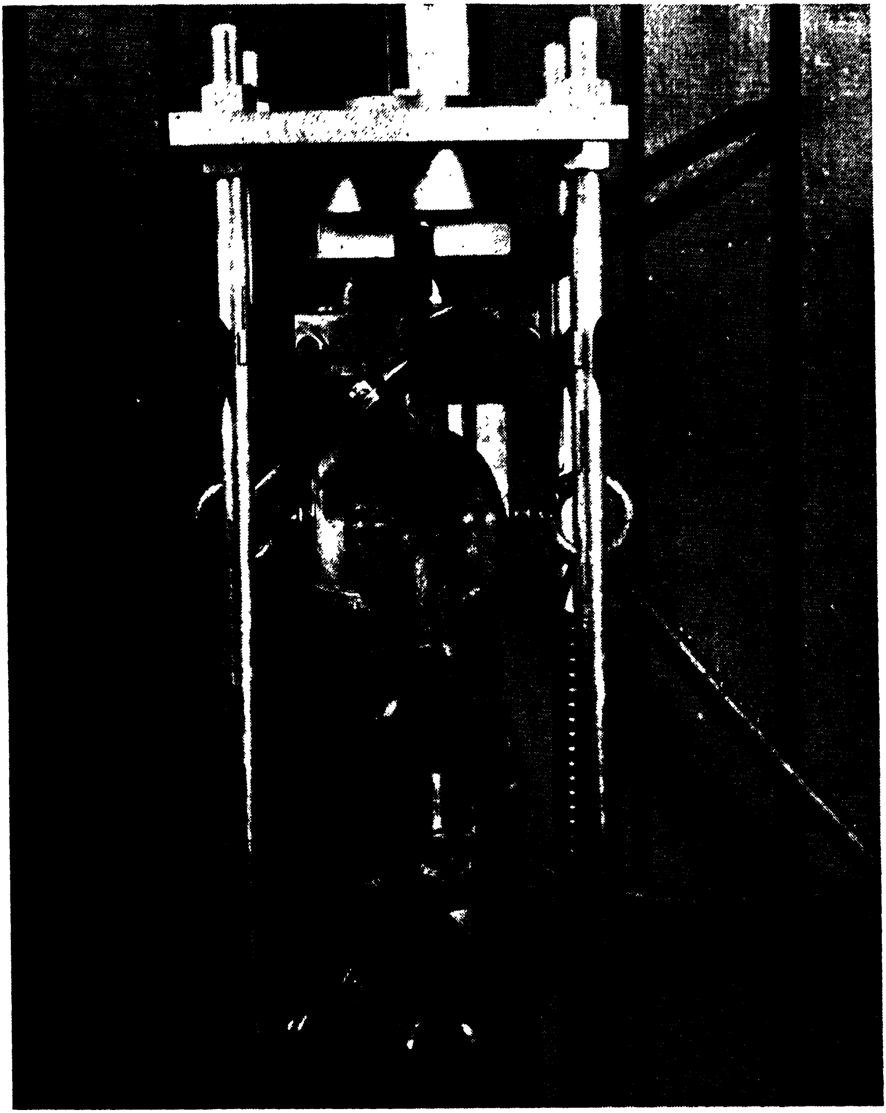

FIG. 117. Pressure welding steel chain links.

30,700 pounds. Failures occurred by elongation and rupture at points outside the weld.

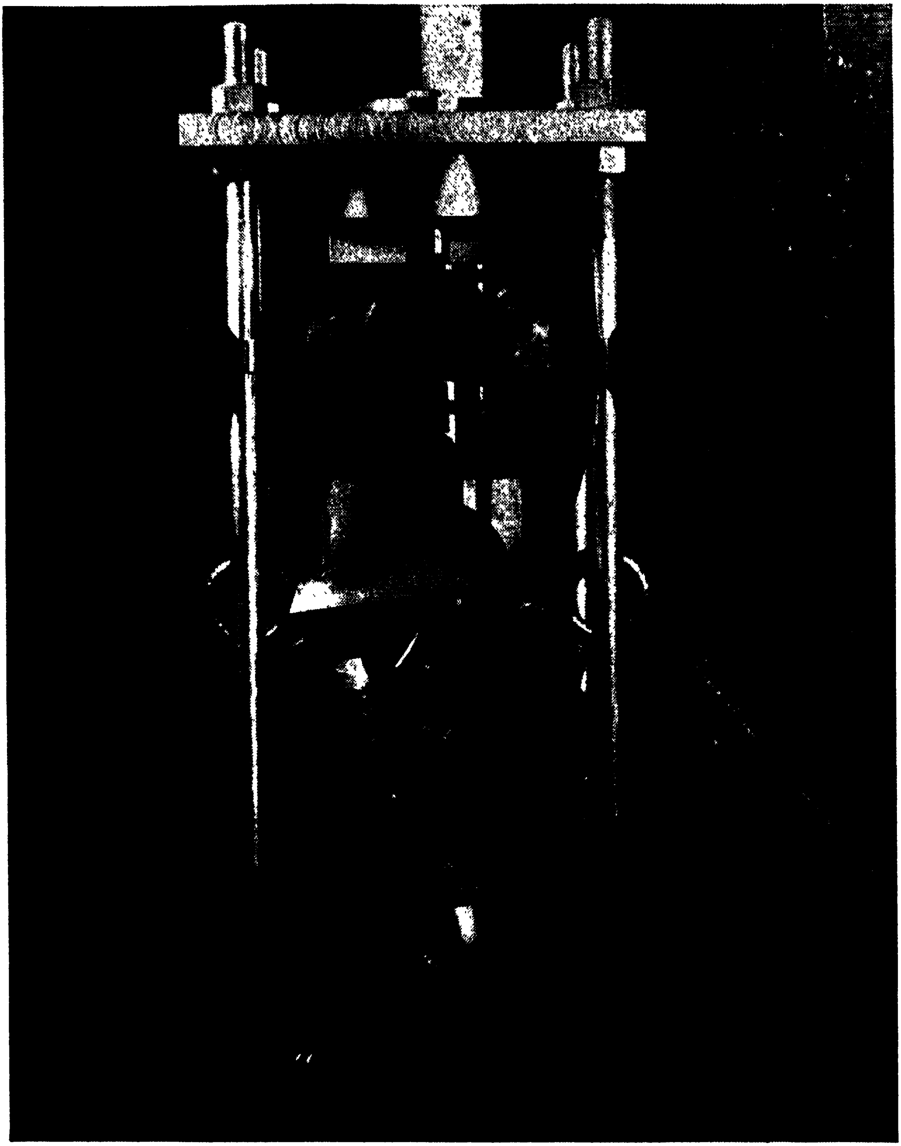

FIG. 118. Here the coupling coil has been disassembled to show the construction.

Chapter 13

THE DIFFERENTIAL EQUATION OF HEAT FLOW IN ONE DIMENSION

The most interesting and important features of radio-frequency heating are the ability to generate heat internally in a body of material if the material is a poor conductor of electricity, and to generate heat in a thin layer near the surface of a good conductor of electricity. The heat may be generated at a desired point, thus avoiding the need to conduct heat to the point through layers which may often be inherently poor thermal conductors. Once the heat is generated, however, thermal conduction takes place so that the temperature distribution through the mass may differ greatly from the law which describes the distribution of power generation.

In this chapter, we shall establish the differential equation of heat flow where the internal generation of heat is included. The problem is inherently complex.* By restricting the problem to flow in one direction or dimension, we simplify the notation and manipulation without great loss of generality.

Under this limiting condition — namely, that heat flows only in the x-direction — we shall now examine a small rectangular box within a body of material. This box, shown in Fig. 119, has a width of 1 centimeter, a height of 1 centimeter, and a length dx. Heat may be generated in each cubic centimeter by electrical or chemical means. Let $\mathcal{H}$ be the rate at which heat is generated measured in gram-calories per second per cubic centimeter. $\mathcal{H}$ is a function of both time and distance. Then the heat generated within the small box in a short time interval dt is

---

* Analytical studies of the flow of heat in solid bodies date back to 1812 when Fourier's memoir *Theorie du movement de la chaleur dans les corps solides* was presented to the French Academy. That the literature pertaining to heat flow is abundant is illustrated by calling attention to the references, seven hundred and eighty-nine in number, listed by William H. McAdams, *Heat Transmission*, 2d ed., McGraw-Hill Book Company, New York, 1942, pp. 419–448. It was the thought in preparing this chapter that it might be well to include the essential derivations so that the interested reader to whom the field is new could follow the reasoning without excursions to reference books which at times may not be readily available.

$$Q_0 = \mathcal{H} \cdot dx \cdot dt. \tag{13.01}$$

The temperature at point O is u degrees Centigrade. Then the increase in heat stored in the box during the time, dt, is

$$Q_1 = c\rho \cdot \frac{du}{dt} \cdot dt \cdot dx, \tag{13.02}$$

where c = density of the material in grams per cubic centimeter
ρ = specific heat of the material in calories per gram per degree Centigrade.

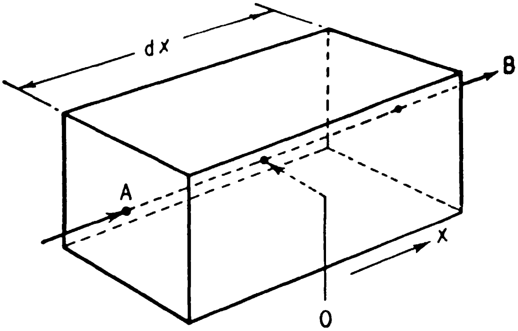

Fig. 119. Elementary box.

The temperature gradient at point O is $\left(\frac{du}{dx}\right)_O$. The gradient at point B on the right hand face of the box is

$$\left(\frac{du}{dx}\right)_B = \left(\frac{du}{dx}\right)_O + \left[\frac{d}{dx}\left(\frac{du}{dx}\right)\right]_O \cdot \frac{dx}{2}$$

and the gradient at point A on the left hand face of the box is

$$\left(\frac{du}{dx}\right)_A = \left(\frac{du}{dx}\right)_O - \left[\frac{d}{dx}\left(\frac{du}{dx}\right)\right]_O \cdot \frac{dx}{2}.$$

The heat flowing *out* through the face of the box at A in the time dt is

$$Q_2 = k\left(\frac{du}{dx}\right)_A \cdot dt, \tag{13.03}$$

where

k = thermal conductivity of the material, in calories/square centimeter/second per degree Centigrade/centimeter

The heat flowing out through the face at B is

$$Q_3 = -k\left(\frac{du}{dx}\right)_B \cdot dt. \tag{13.04}$$

From the conservation of energy,

$$Q_0 = Q_1 + Q_2 + Q_3. \tag{13.05}$$

Thus,

$$\mathcal{H} \cdot dx \cdot dt = c\rho\frac{du}{dt} \cdot dx \cdot dt - k\left[\frac{d}{dx}\left(\frac{du}{dx}\right)\right]_0 dx \cdot dt, \tag{13.06}$$

or*

$$\mathcal{H} = c\rho\frac{du}{dt} - k\frac{d^2u}{dx^2}\cdot \tag{13.07}$$

In order to handle the problem mathematically, it is necessary to assume that the specific heat and thermal conductivity are uniform throughout the material and do not change with temperature. This latter condition is not generally met in practice, but for purposes of analysis the picture is not altered seriously by making the assumption.

---

[*] Equation (13.07), which takes into account heat generated within the material, is given as equation (7–45), p. 232, Margenau and Murphy, *The Mathematics of Physics and Chemistry*, D. Van Nostrand Company, Inc., New York, 1943. However, further discussion of the solution of the equation by these authors is confined to the case where no time variation exists or to the case where no heat is generated within the material.

Chapter 14

SOLUTIONS OF THE HEAT-FLOW DIFFERENTIAL EQUATION

Before proceeding with the differential equation (13.07), it is well to restate that we are only considering heat flow in one dimension. As stated previously, $\mathcal{H}$ may be a function of time and distance. The solution of the differential equation will be effected by showing the direct analogy between the heat-flow problem and a particular transmission-line problem.

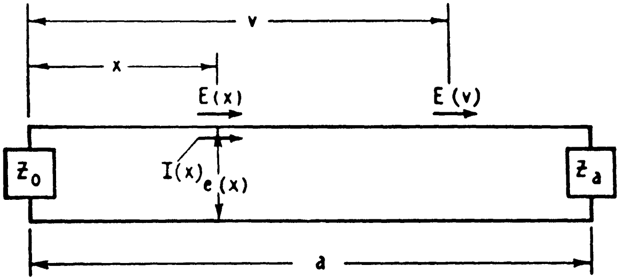

FIG. 120. The transmission line used as an analogue to the heat-flow problem. A distributed voltage is induced along the transmission line.

In Fig. 120, we have a transmission line of length, a. The uniformly distributed contants of the line are:

R = series resistance per unit length, ohms per centimeter;
L = series inductance per unit length, henrys per centimeter;
G = shunt conductance per unit length, mhos per centimeter;
C = shunt capacitance per unit length, farads per centimeter.

At one end, $x = 0$, the line is terminated in an impedance, Z_0, while at $x = a$, the line is terminated in an impedance Z_a. In series with the line, we have a voltage set up by an external force. This voltage may be brought about by an impinging electromagnetic field or by inserting a battery or generator in series with the line. This voltage intensity is $E(x)$ measured in volts per centimeter. We wish to find the current along the line at a point x units from the impedance Z_0 at any instant of time, under the condition that $E(x)$ is induced all along the line. $E(x)$ may be a function of both time and distance.

Let e = the voltage across the line x units from Z_0; and
i = the current in the line x units from Z_0.

Then

$$\frac{de}{dx} = -Ri - L\frac{di}{dt} + E(x) \tag{14.01}$$

and

$$\frac{di}{dx} = -Ge - C\frac{de}{dt}; \tag{14.02}$$

or making use of the Heaviside differential operator p,

$$\frac{de}{dx} = -(R + pL)i + E(x) \tag{14.03}$$

and

$$\frac{di}{dx} = -(G + pC)e. \tag{14.04}$$

From (14.04),

$$e = \frac{-1}{G + pC}\cdot\frac{di}{dx}\cdot \tag{14.05}$$

Differentiating (14.05) with respect to x, we obtain

$$\frac{de}{dx} = \frac{-1}{G + pC}\cdot\frac{d^2i}{dx^2}\cdot \tag{14.06}$$

Substituting (14.06) in (14.03), we find

$$E(x) = (R + pL)i - \frac{1}{G + pC}\cdot\frac{d^2i}{dx^2}\cdot \tag{14.07}$$

The solution for the current i at point x is*

$$\begin{aligned} i(x) = \Big\{ & [Z_c^2 + Z_aZ_0] \int_{v=x}^{v=a} E(v) \cosh \gamma(a + x - v)\, dv \\ & + [Z_c^2 - Z_aZ_0] \int_{v=0}^{v=a} E(v) \cosh \gamma(a - x - v)\, dv \\ & + [Z_c^2 + Z_aZ_0] \int_{v=0}^{v=x} E(v) \cosh \gamma(a - x + v)\, dv \\ & + [Z_cZ_a + Z_cZ_0] \int_{v=x}^{v=a} E(v) \sinh \gamma(a + x - v)\, dv \\ & + [Z_cZ_a - Z_cZ_0] \int_{v=0}^{v=a} E(v) \sinh \gamma(a - x - v)\, dv \\ & + [Z_cZ_a - Z_cZ_0] \int_{v=0}^{v=x} E(v) \sinh \gamma(a - x + v)\, dv \Big\} \\ & \div 2Z_c \sinh(\gamma a)\, [Z_c^2 - Z_0Z_a + (Z_0 + Z_a)Z_c \coth(\gamma a)], \end{aligned} \tag{14.08}$$

where

$$Z_c = \sqrt{\frac{R + pL}{G + pC}} \tag{14.09}$$

and

$$\gamma^2 = (R + pL)(G + pC). \tag{14.10}$$

We next propose that R, the resistance per unit length, and C, the shunt capacitance per unit length, be made zero. Then the transmission line has only the constants of series inductance L and shunt leakage G, as shown in Fig. 121. Under this condition, (14.07) becomes

$$E(x) = pLi - \frac{1}{G}\frac{d^2i}{dx^2} = L\frac{di}{dt} - \frac{1}{G}\frac{d^2i}{dx^2}, \tag{14.11}$$

and (14.05) is

$$e = -\frac{1}{G}\frac{di}{dx}. \tag{14.12}$$

When we compare (14.11) with (13.07), we see that if $i(x)$ is analogous to the temperature u, the following equalities must exist:

$$L = c\rho \tag{14.13}$$

$$\frac{1}{G} = k \tag{14.14}$$

---

* See Appendix A.

and

$$E(x) = \mathcal{H} \text{ gram-calories per second per cubic centimeter.} \tag{14.15}$$

From (14.12),

$$e = -\frac{1}{G}\frac{di}{dx} = -k\frac{du}{dx}, \tag{14.16}$$

so that the voltage on the line is analogous to the heat flow across a surface (proportional to temperature gradient).*

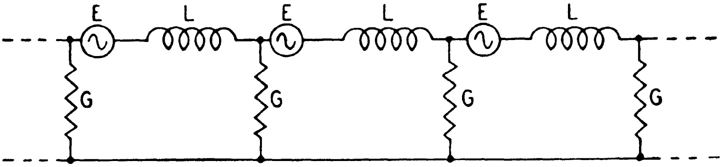

FIG. 121. To parallel the heat-flow problem, the transmission line is made up of series inductance and shunt leakage conductance.

Also,

$$Z_c = \sqrt{\frac{pL}{G}} = \sqrt{pc\rho k} \tag{14.17}$$

and

$$\gamma^2 = pLG = p\frac{c\rho}{k} = \frac{p}{\alpha^2}, \tag{14.18}$$

where $\alpha^2 = \dfrac{k}{c\rho}$ is called the " thermal diffusivity " of the material.

Representative values of the thermal constants of materials are presented in Table 9.

We shall now treat the specific problem of heat flow in a plate of thickness,

---

* In his book, *Heaviside's Operational Calculus,*" McGraw-Hill Book Company, New York, 1929, E. J. Berg points out in his Chapter XXVII the analogy between the heat-flow equations and the equations of a transmission line. He chooses to set temperature equal to voltage, and thus uses a transmission line which is made up of series resistance and shunt capacitance. This method is very useful for solving the ordinary heat-flow problems where hot plates are applied to a boundary, for then the constant temperature of the boundary is represented by a constant voltage at this point. In the case of internally-generated heat, it seems more reasonable to use current in relation to temperature, with a transmission line made up of series inductance and shunt leakage. In this way, one avoids the notion of constant current admitted to the line at a number of points in the line. It is evident that problems may be worked by either choice. After rather careful consideration, the authors decided on the temperature-current identity because of the nature of the problems to be considered.

TABLE 9. THERMAL CONSTANTS OF REPRESENTATIVE MATERIALS.

Material	Specific Heat, ρ $\left(\frac{\text{calories per gram}}{\text{degrees Centigrade}}\right)$	Density, c (grams per cubic centimeter)	Thermal Conductivity, k (calories/square centimeters/second per degree Centigrade/centimeter)	Thermal Diffusivity, α^2 (square centimeters per second)
Iron (average)	0.115	7.86	0.161	0.1785
Aluminum	0.186	2.56	0.48	1.01
Lead	0.03	11.34	0.084	0.247
Tin	0.054	7.3	0.15	0.385
Silver	0.055	10.4	1.10	1.96
Gold	0.032	19.3	0.70	1.125
Cadmium	0.055	8.54	0.22	0.465
Magnesium	0.249	1.74	0.37	0.86
Wood (average)	0.65	0.53	0.00036	0.00104

a, where the power is generated by induced currents. In Chapter 5, we saw that where the thickness of the plate was at least twice as great as the skin thickness of the metal for the particular frequency of excitation, the distribution described by (4.33) was an excellent approximation for the power density. However, for a finite thickness of the metal sheet, the quantity P_t in (4.33) is no longer exactly the total power delivered per square centimeter of surface. The total power, with the necessary correction term, is obtained in the following manner. The power density at a depth x is

$$P = \frac{2}{s} P_t' \epsilon^{-\frac{2x}{s}} \tag{14.19}$$

where we have primed the *apparent* total power. When (14.19) is integrated from $x = 0$ to $x = a$, the true total power is found to be

$$P_t = P_t' \left(1 - \epsilon^{-\frac{2a}{s}}\right) \tag{14.20}$$

or

$$P_t' = \frac{P_t}{1 - \epsilon^{-\frac{2a}{s}}}. \tag{14.21}$$

When (14.21) is substituted into (14.19),

$$P(\text{watts per cubic centimeter}) = \frac{\beta P_t \epsilon^{-\beta x}}{1 - \epsilon^{-\beta a}}, \tag{14.22}$$

where P denotes the power generated per cubic centimeter, P_t is the total power delivered to 1 square centimeter of surface and $\frac{2}{s}$ has been set equal to β for convenience.

In our analogy to a transmission line, the quantity $E(x)$ is set equal to the heat generated per cubic centimeter, expressed in gram-calories per second. Since a watt is a joule per second, and 4.187 joules equal 1 gram-calorie,

$$E(x) = \frac{\beta P_t \epsilon^{-\beta x}}{4.187\,(1 - \epsilon^{-\beta a})}. \tag{14.23}$$

The most powerful application of (14.08) to heat flow in metals is the study of the problem of case hardening of steels, where the power densities are extremely high and the hardening temperatures are reached in a few seconds and in some cases in a fraction of a second. Hence most of the applied power is used in raising the temperature of the surface metal and in overcoming the loss by heat conduction into the inner portions of the metal. The power lost by radiation from the surface is trivial in this case and may be neglected.

If it is to be assumed that no energy is lost by radiation at either surface of the metal, that is, at $x = 0$ and $x = a$, the temperature gradient at these two points must itself be zero. An examination of (14.16) then reveals that in our transmission line analogy, the voltage at each end of the line must be zero at all times. This is insured by placing a short-circuit at each end. Then in (14.08), we place $Z_a = Z_0 = 0$. Equation (14.08) then reduces to

$$\begin{aligned} i(x) = \Bigg[\int_{v=x}^{v=a} & E(v) \cosh \gamma(a + x - v)\, dv \\ & + \int_{v=0}^{v=a} E(v) \cosh \gamma(a - x - v)\, dv \\ & + \int_{v=0}^{v=x} E(v) \cosh \gamma(a - x + v)\, dv\Bigg] \\ & \div 2Z_c \sinh \gamma a \end{aligned} \tag{14.24}$$

When (14.23) is substituted in (14.24) and the indicated integration carried out, we obtain

$$i(x) = \frac{\beta P_t}{4.187\,(1 - \epsilon^{-\beta a})}\left\{\frac{-\gamma\epsilon^{-\beta x}}{Z_c(\beta^2 - \gamma^2)} + \frac{\beta}{Z_c(\beta^2 - \gamma^2)}\left[\frac{\cosh \gamma(a - x) - \epsilon^{-\beta a} \cosh \gamma x}{\sinh \gamma a}\right]\right\}. \tag{14.25}$$

A consideration of (14.17) and (14.18) reminds us that (14.25) is an operational equation which must still be integrated. In our transmission line, the little generators in series with the transmission line generate no voltage prior to the instant of time, $t = 0$. At the time, $t = 0$, each generator is turned on and develops the voltage shown in (14.23), corresponding to the position of the generator along the line. Thus (14.25) is essentially the total response at a point in the line to the many " unit functions " of voltage that have been applied to the line, where the unit functions are graded according to (14.23).

A Metal Sheet of Infinite Thickness. When the thickness of the material is infinite in extent, (14.25) yields a solution quite different in form from that obtained for a finite sheet. We now let a approach infinity in (14.25) and obtain

$$i(x) = \frac{\beta P_t}{4.187}\left[\frac{-\gamma\epsilon^{-\beta x}}{Z_c(\beta^2 - \gamma^2)} + \frac{\beta\epsilon^{-\gamma x}}{Z_c(\beta^2 - \gamma^2)}\right]. \tag{14.26}$$

When (14.17) and (14.18) are substituted, (14.26) becomes

$$i(x) = \frac{\beta P_t}{4.187}\left[\frac{-\sqrt{pLG}\cdot\epsilon^{-\beta x} + \beta\epsilon^{-\sqrt{pLG}\,x}}{\sqrt{\frac{pL}{G}}\,(\beta^2 - pLG)}\right]. \qquad (14.27)$$

At first glance, it may appear that $p = \frac{\beta^2}{LG}$ is a proper root of the denominator so that the Heaviside Expansion Theorem could be used. However, this same value makes the numerator zero and the Expansion Theorem leads us to untold difficulties. We must then turn to other methods of evaluating (14.26).

The first term in the bracket of (14.26) is

$$\frac{-\gamma\epsilon^{-\beta x}}{Z_c(\beta^2 - \gamma^2)} = \frac{-\sqrt{pLG}}{\sqrt{\frac{pL}{G}}}\cdot\frac{\epsilon^{-\beta x}}{(\beta^2 - pLG)}$$

$$= \frac{-G\epsilon^{-\beta x}}{\beta^2 - pLG} = -\frac{G}{\beta^2}\frac{\epsilon^{-\beta x}}{\left(1 - \frac{pLG}{\beta^2}\right)} \qquad (14.28)$$

When the denominator of (14.28) is divided out term by term, an infinite series is obtained.

$$-\frac{G}{\beta^2}\epsilon^{-\beta x}\left[1 + \frac{pLG}{\beta^2} + \left(\frac{pLG}{\beta^2}\right)^2 + \left(\frac{pLG}{\beta^2}\right)^3 + \cdots\right]. \qquad (14.29)$$

By rearranging (14.28) slightly before dividing, we also may express (14.28) as

$$\frac{G\epsilon^{-\beta x}}{\beta^2}\left[\frac{\beta^2}{pLG} + \left(\frac{\beta^2}{LG}\right)^2\frac{1}{p^2} + \left(\frac{\beta^2}{LG}\right)^3\frac{1}{p^3} + \cdots\right]. \qquad (14.30)$$

In (14.30), the operator appears in the form $\frac{1}{p^n}$. But when operating on a unit function,*

$$\frac{1}{p^n} = \frac{t^n}{\lfloor n}, \qquad (14.31)$$

where n is an integer.

---

* E. J. Berg, *Heaviside's Operational Calculus*," McGraw-Hill Book Company, Inc., 1929, p. 165, Example 17.

Then (14.30) becomes

$$\frac{G}{\beta^2}\epsilon^{-\beta x}\left[\frac{\beta^2 t}{LG} + \frac{1}{\underline{2|}}\left(\frac{\beta^2 t}{LG}\right)^2 + \frac{1}{\underline{3|}}\left(\frac{\beta^2 t}{LG}\right)^3 + \cdots\right]. \tag{14.32}$$

Close inspection of the infinite series of (14.32) reveals that it has the closed form

$$\frac{G}{\beta^2}\epsilon^{-\beta x}\left(\epsilon^{\frac{\beta^2 t}{LG}} - 1\right). \tag{14.33}$$

However, this solution does not tie in with the solution of the last term in (14.26) to yield a sensible solution to the heat-flow problem. In that event, we are happy to discard this solution which was obtained from (14.30) and return to (14.29), an alternative arrangement. Here the operator appears directly as p^n, which we choose to interpret as derivatives of unit function. For all values of time greater than $t = 0$ these derivatives are zero. Thus (14.29) and hence the first term in the bracket of (14.26) become very simply

$$-\frac{G}{\beta^2}\epsilon^{-\beta x}. \tag{14.34}$$

The reader may feel uncomfortable in the presence of the two solutions, (14.33) and (14.34), particularly when faced with the necessity of making a choice between them. In dealing with the more complicated operational problems, it is helpful to proceed with a certain degree of cheerful optimism. The work of Bush* may supply the necessary rigor to justify (14.34).

Turning now to the last term in (14.26), we may write

$$\begin{aligned}\frac{\beta\epsilon^{-\sqrt{pLG}\,x}}{\sqrt{\frac{pL}{G}}(\beta^2 - pLG)} &= \frac{G}{\beta}\cdot\frac{\epsilon^{-\sqrt{pLG}\,x}}{\sqrt{pLG}}\cdot\frac{1}{1 - \frac{pLG}{\beta^2}} \\ &= \frac{G}{\beta^2}\epsilon^{-\sqrt{pLG}\,x}\left[\left(\frac{LG}{\beta}\right)^{-1/2}\cdot p^{-1/2} + \left(\frac{LG}{\beta^2}\right)^{1/2}\cdot p^{1/2}\right. \\ &\qquad \left. + \left(\frac{LG}{\beta^2}\right)^{3/2}\cdot p^{3/2} + \cdots\right].\end{aligned} \tag{14.35}$$

Next, the exponential in (14.35) is expanded in an infinite series and multiplied term by term with the series already appearing in (14.35). We then make use of the following operational relations.*

---

* In the book *Operational Circuit Analysis,* John Wiley and Sons, Inc., 1929, pp. 274–280, Vannevar Bush has treated the identical operational form shown in (14.28), but in an entirely different fashion.

$$p^{1/2} = \frac{t^{-1/2}}{\sqrt{\pi}} \qquad p^{-1/2} = \frac{2t^{1/2}}{\sqrt{\pi}}$$

$$p^{3/2} = \frac{-t^{-3/2}}{2\sqrt{\pi}} \qquad p^{-3/2} = \frac{2 \cdot 2t^{3/2}}{1 \cdot 3\sqrt{\pi}}$$

$$p^{5/2} = \frac{1 \cdot 3t^{-5/2}}{2 \cdot 2\sqrt{\pi}} \qquad p^{-5/2} = \frac{2 \cdot 2 \cdot 2t^{5/2}}{1 \cdot 3 \cdot 5\sqrt{\pi}}$$

$$p^{7/2} = \frac{-\ 1 \cdot 3 \cdot 5t^{-7/2}}{2 \cdot 2 \cdot 2\sqrt{\pi}} \qquad p^{-7/2} = \frac{2 \cdot 2 \cdot 2 \cdot 2t^{7/2}}{1 \cdot 3 \cdot 5 \cdot 7\sqrt{\pi}}$$

When the terms are all collected, and (14.34) is added, the solution of (14.26) is

$$i(x) = \frac{P_t G}{4.187\beta} \cdot f(\theta, x), \tag{14.36}$$

where

$$\begin{aligned} f(\theta, x) = {} & -\beta x - \epsilon^{-\beta x} \\ & + \frac{2}{\sqrt{\pi}}\theta^{1/2} \\ & + \frac{1}{\sqrt{\pi}\,\theta^{1/2}}\left[1 + \frac{(\beta x)^2}{\underline{2|}}\right] \\ & - \frac{1}{2\sqrt{\pi}\,\theta^{3/2}}\left[1 + \frac{(\beta x)^2}{\underline{2|}} + \frac{(\beta x)^4}{\underline{4|}}\right] \\ & + \frac{1 \cdot 3}{2 \cdot 2\sqrt{\pi}\,\theta^{5/2}}\left[1 + \frac{(\beta x)^2}{\underline{2|}} + \frac{(\beta x)^4}{\underline{4|}} + \frac{(\beta x)^6}{\underline{6}}\right] \\ & - \frac{1 \cdot 3 \cdot 5}{2 \cdot 2 \cdot 2\sqrt{\pi}\,\theta^{7/2}}\left[1 + \frac{(\beta x)^2}{\underline{2|}} + \frac{(\beta x)^4}{\underline{4|}} + \frac{(\beta x)^6}{\underline{6|}} + \frac{(\beta x)^8}{\underline{8|}}\right] \\ & + \cdots \end{aligned} \tag{14.37}$$

and

$$\theta = \frac{\beta^2 t}{LG}. \tag{14.38}$$

---

* E. J. Berg, *loc. cit.*, p. 118.

It may be recalled that β is equal to $2/s$, where s is the skin thickness of the metal.

So far, we have kept our solution in terms of the transmission line constants. We are, of course, primarily interested in the heat-flow problem. Then the temperature (in degrees Centigrade) at any point in the metal is

$$u(x) = \frac{sP_t}{8.374k} \cdot f(\theta, x), \tag{14.39}$$

where

$$\theta = \frac{4t}{s^2 c\rho/k} = \frac{4\alpha^2 t}{s^2}. \tag{14.40}$$

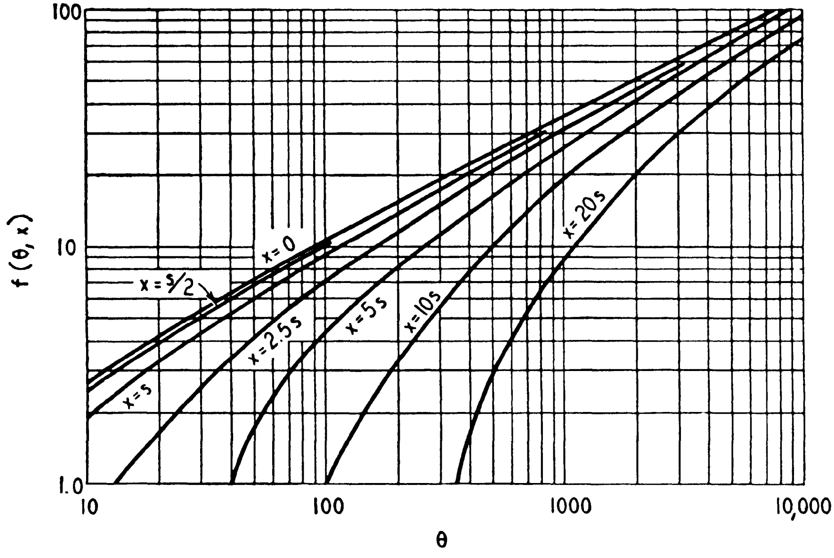

FIG. 122. The function $f(\theta, x)$ is shown as a function of θ. The quantity, x, is the distance into the metal to the point where temperature is measured. These curves apply for a metal plate of infinite thickness.

Since in our transmission line, we started the generators or unit functions at $t = 0$, there was no current flowing at that moment. This implies that all the metal concerned in the heat-flow problem was at 0° C at the start of the heating cycle. Actually, (14.39) may be viewed as the temperature *rise* from starting temperature rather than specific temperature starting from 0° C.

The function $f(\theta, x)$ given in (14.37) was used to compute the curves shown in Fig. 122. Here $f(\theta, x)$ is plotted as a function of θ, with the distance into the metal, x, as a parameter. While (14.37) is formidable in appearance, its asymptotic character simplifies the calculations. Fig. 123 shows the same curves in greater detail for small values of θ.

In Fig. 122, for large values of θ, we see that all the curves seem to be parallel to one another. This point may be better developed by considering the equation (14.37). For a distance x which is several times greater than the skin thickness, we may drop the term $\epsilon^{-\beta x}$ from (14.37). As time increases, θ becomes sufficiently large to permit (14.41) to be an approximation of (14.37). Then,

$$f(\theta, x) = \frac{2}{\sqrt{\pi}}\,\theta^{1/2} - \frac{2x}{s}\cdot \tag{14.41}$$

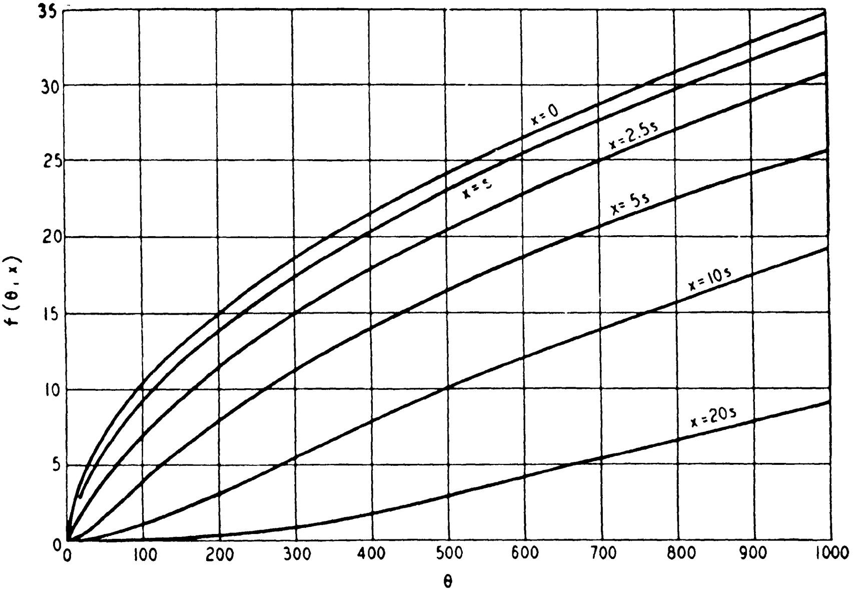

FIG. 123. Here the curves of Fig. 122 are shown on an expanded scale.

When (14.40) is substituted in (14.41) and the result inserted in (14.39), we find the temperature relation to be

$$u(x) = \frac{P_t}{8.374}\left[\frac{4t^{1/2}}{\sqrt{\pi k c \rho}} - \frac{2x}{k}\right]\cdot \tag{14.42}$$

Here we see that the frequency does not appear in the expression for temperature. However, the frequency is a factor in establishing our limiting statement that x is several times greater than the skin thickness.

To find the expression for the surface temperature for large values of θ, it is necessary to let $x = 0$ in (14.37). Then this expression is approximately

$$f(\theta, x)_{x=0} = \frac{2}{\sqrt{\pi}} \theta^{1/2} - 1. \tag{14.43}$$

This result substituted in (14.39) yields the surface temperature.

$$u(0) = \frac{P_t}{8.374} \left[\frac{4t^{1/2}}{\sqrt{\pi k c \rho}} - \frac{s}{k} \right]. \tag{14.44}$$

For large values of time, the last term in (14.44) may usually be dropped without materially affecting the result.

The curves of Figs. 122 and 123 are especially useful in studying the surface heating of ferromagnetic materials for the purpose of case hardening. Before proceeding with a detailed analysis of this application we shall establish the temperature relations in metal sheets of finite thickness.

Table 10 may prove helpful when specific calculations are made from Figs. 122 and 123.

A Metal Sheet of Finite Thickness. To establish the temperature relationship when the metal sheet has a finite thickness, we must return to the operational equation (14.25). Substituting (14.17) and (14.18) in (14.25), we find

$$i(x) = \frac{\beta P_t}{4.187\,(1 - \epsilon^{-\beta a})} \cdot \frac{1}{p} \cdot \frac{1}{Z(p)} \tag{14.45}$$

where the operational function $Z(p)$ is

$$Z(p) = \frac{(\beta^2 - pLG) \sinh (\sqrt{pLG}\, a)}{\left\{ \begin{aligned} &-Gp\epsilon^{-\beta x} \sinh (\sqrt{pLG}\, a) \\ &+ \beta \sqrt{\frac{Gp}{L}} \{\cosh [\sqrt{pLG}\, (a - x)] - \epsilon^{-\beta a} \cosh (\sqrt{pLG}\, x)\} \end{aligned} \right\}}. \tag{14.46}$$

The operational relation $\frac{1}{Z(p)}$ may then be solved by means of the Heaviside Expansion Theorem. Roots of (14.46) must be found. It should be emphasized that neither $p = 0$ nor $p = \frac{\beta^2}{LG}$ are roots of (14.46). We may proceed to evaluate $\frac{1}{Z(p)}$ and hence (14.45) in exactly the same manner as the method displayed in Appendix B. After a great amount of tedious manipulation, it is found that

$$i(x) = \frac{P_t G}{4.187\beta} f(\theta, x) \tag{14.47}$$

TABLE 10. SPECIFIC VALUES OF THE FUNCTION, $f(\theta, x)$.

	$f(\theta, x)$						
	$x = 0$	$x = 0.5s$	$x = s$	$x = 2.5s$	$x = 5s$	$x = 10s$	$x = 20s$
10	2.7409	2.4577	1.9436	0.6904	....	....	....
20	4.173	3.8662	3.829	1.6378	0.3437	....	....
30	5.283	4.9376	4.3077	2.5128	0.7872	....	....
50	7.0698	6.750	6.1011	4.0411	1.737	....	....
100	10.356	10.016	9.3332	7.0441	4.056	....	....
200	15.0798	14.6717	13.9845	11.5274	7.9883	3.3975	....
500	24.2752	23.9697	23.2407	20.5343	16.580	10.2147	3.175
700	....	....	....	....	....	....	5.538
900	....	....	....	....	....	....	7.938
1000	34.7179	34.3588	33.6185	30.9343	25.61	19.2288	9.1225
2000	49.5126	49.1509	48.4029	45.6638	41.14	33.0184	20.263
5000	79.008	78.6439	77.8889	75.1011	70.407	61.6041	46.32
10000	112.0	111.64	110.8819	108.069	103.288	94.1331	77.49

where

$$f(\theta, x) = \frac{\theta}{\beta a} + \frac{2\beta a}{\pi^2(1 - \epsilon^{-\beta a})} \sum_{n=1}^{n=\infty} \frac{\left[1 - \epsilon^{-\frac{n^2\pi^2\theta}{(\beta a)^2}}\right]\left[1 - (-1)^n \epsilon^{-\beta a}\right] \cos\left(\frac{n\pi x}{a}\right)}{n^2\left[1 + \left(\frac{n\pi}{\beta a}\right)^2\right]}. \tag{14.48}$$

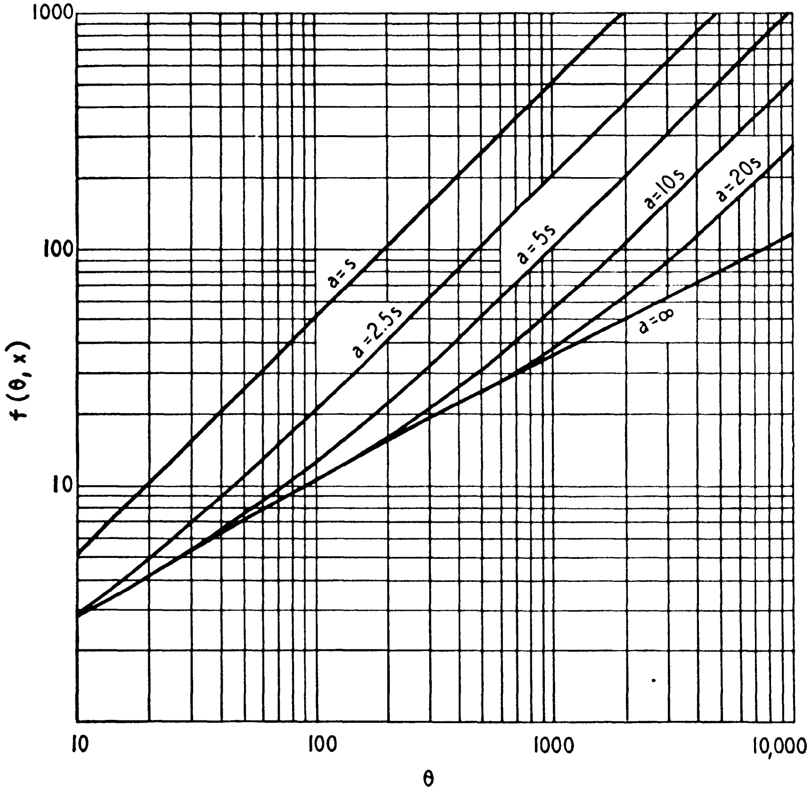

FIG. 124. The function $f(\theta, x)$ is shown as a function of θ, with $x = 0$ (temperature on the surface of the plate). These curves apply to a plate of thickness, a.

Here again, as in (14.38) and (14.40), θ is a function of time and the thermal constants, as well as the skin thickness.

$$\theta = \frac{\beta^2 t}{LG} = \frac{4kt}{s^2 c\rho} = \frac{4\alpha^2 t}{s^2} \tag{14.49}$$

In terms of the thermal constants of the materials, we may rewrite (14.47), so that the temperature is

$$u(x) = \frac{sP_t}{8.374k} \cdot f(\theta, x). \tag{14.50}$$

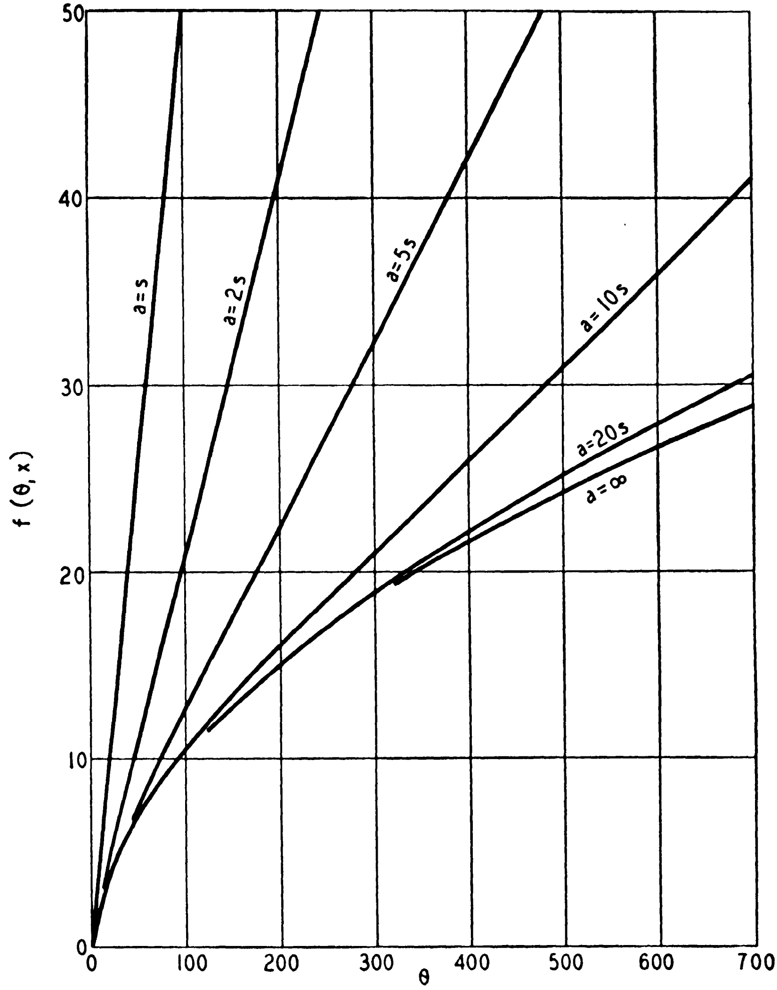

Fig. 125. The curves of Fig. 124 are shown here on an extended scale.

Equation (14.48) has been used to construct the curves of Fig. 124 which show the surface temperature ($x = 0$) as a function of θ for a number of thicknesses of the metal sheet. The curve $a = \infty$ is the top curve of Fig. 122, computed from (14.37). It should be remembered that $\beta = \frac{2}{s}$. Fig. 125 shows the curves of Fig. 124 in greater detail for small values of θ.

Fig. 126 shows the function $f(\theta, x)$ on the surface where the radio-frequency power is applied ($x = 0$) as well as the same function on the remote surface ($x = a$), when the thickness is 2.5 times the skin thickness. Here the sheet is rather thin so the temperature on the far side lags that on the near side by only a small amount. Similar curves for other thicknesses are shown in Figs. 127 and 128. In addition, the function $f(\theta, x)$ is shown when $x = a/2$. At this point (14.48) is greatly simplified. When $x = a/2$, the term $\cos\left(\frac{n\pi x}{a}\right)$ is zero for all values of n so at the exact center of the sheet,

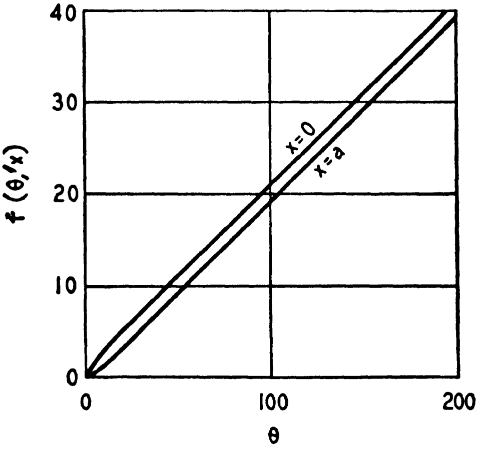

FIG. 126. The function $f(\theta, x)$ on the surface where power is applied ($x = 0$), and on the remote surface ($x = a$) when the thickness a is 2.5 times the skin thickness.

$$f(\theta, x) = \frac{\theta}{\beta a}, \tag{14.51}$$

and the temperature is

$$u(x)_{x=\frac{a}{2}} = \frac{P_t G\theta}{4.187\beta^2 a} = \frac{P_t t}{4.187La} = \frac{P_t t}{4.187c\rho a}. \tag{14.52}$$

Equation (14.52) shows the curious fact that the temperature at the exact center of the sheet increases with time exactly as it would if the power were generated uniformly throughout the thickness of the sheet.

In Figs. 126, 127, and 128, it is seen that the function $f(\theta, x)$ soon becomes a straight line. In the region where this is true, (14.48) may be expressed quite simply. On the surface, $x = 0$, this approximate relation is

$$f(\theta, x)_{x=0} = \frac{\theta}{\beta a} + A \cdot \beta a, \tag{14.53}$$

and on the surface, $x = a$, we may use the expression

$$f(\theta, x)_{x=a} = \frac{\theta}{\beta a} - B \cdot \beta a, \tag{14.54}$$

where A and B are shown in Fig. 129 as a function of a/s.

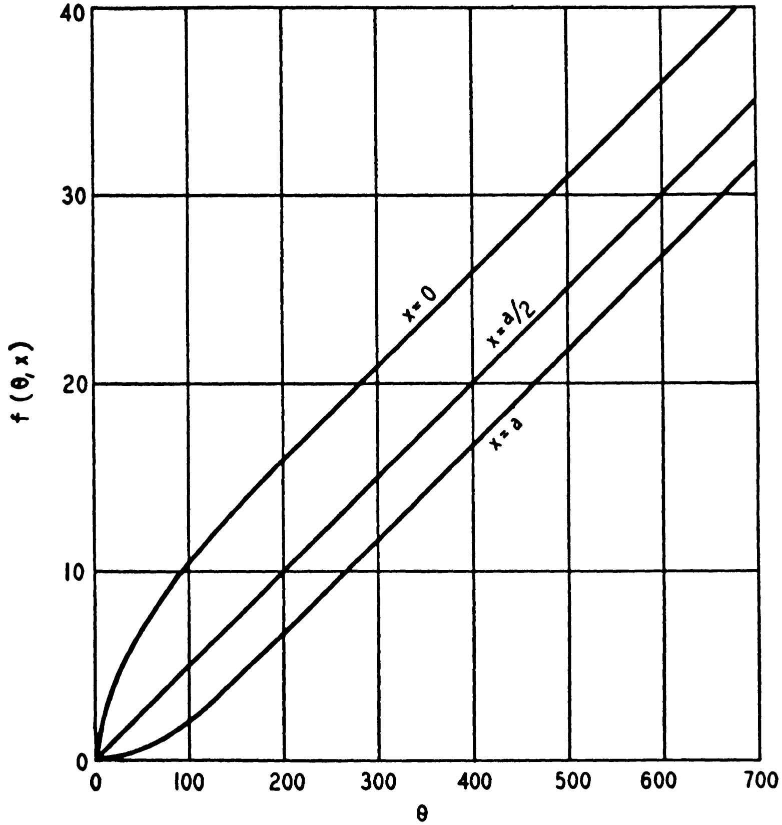

FIG. 127. The function $f(\theta, x)$ on the surface where power is applied ($x = 0$), at the exact center of the plate ($x = a/2$), and on the remote surface ($x = a$) when the thickness a is 10 times the skin thickness.

We may substitute the approximate expressions of (14.53) and (14.54) in (14.47) with interesting results. That is, when θ is large, the temperature on the surface, $x = 0$, is

$$u(\text{degrees Centigrade}) = \frac{P_t}{4.187}\left(\frac{t}{c\rho a} + \frac{Aa}{k}\right) \tag{14.55}$$

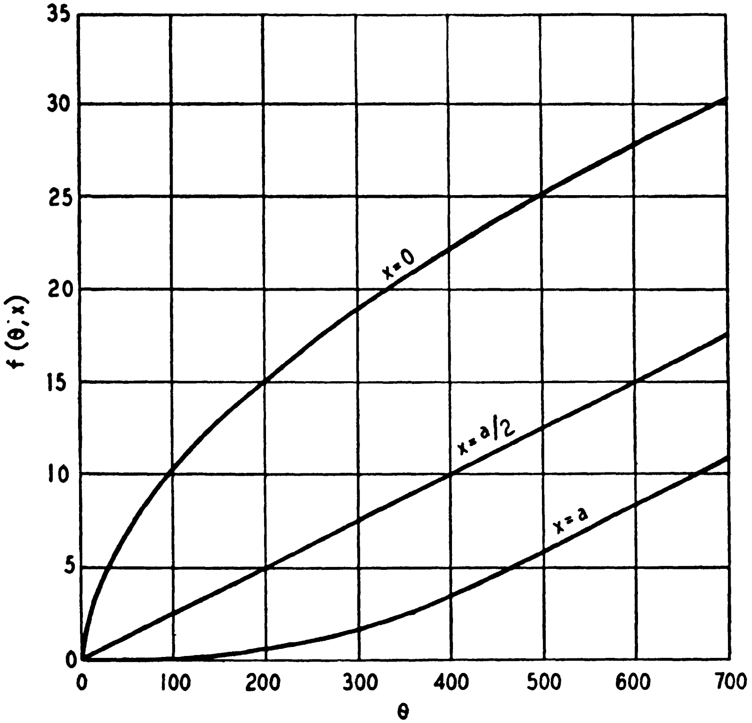

FIG. 128. The function $f(\theta, x)$ on the surface where power is applied ($x = 0$), at the exact center of the plate ($x = a/2$), and on the remote surface ($x = a$) when the thickness a is 20 times the skin thickness.

whereas the temperature on the surface, $x = a$, is

$$u(\text{degrees Centigrade}) = \frac{P_t}{4.187}\left(\frac{t}{c\rho a} - \frac{Ba}{k}\right). \tag{14.56}$$

It is of importance to note that (14.55) and (14.56), as well as (14.52), are functions of time which contain as parameters only the thermal constants of the metal and the power generated per square centimeter. The frequency of the induced currents is not contained in the equation.

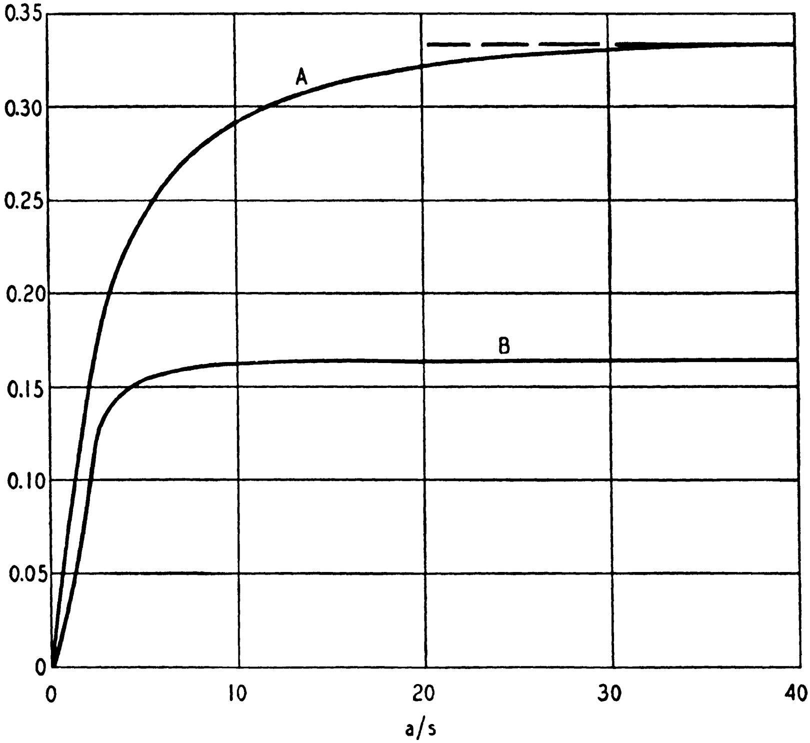

FIG. 129. The parameters A and B which are used in (14.53) and (14.54).

Equation (14.52) differs from (14.55) and (14.56) in the respect that the latter equations are approximations while (14.52) is exact for all values of time.

Chapter 15

ELEMENTARY APPLICATIONS OF THE HEAT-FLOW EQUATIONS

Sealing of Metal Tubes. The application of radio-frequency power serves as a ready means of sealing the bottom ends of metal tubes such as are used for containers of ointments and creams. Fig. 130 shows one such application where the coil which carries the exciting current serves as the pressure appliance for squeezing the tube to effect the closure. In this particular instance, the tube was made of lead, with a wall thickness of 0.0055 inch or 0.01395 centimeter. Since the two sides of the tubing are pressed tightly together, the effective thickness is 0.0279 centimeter. In establishing the critical frequency for the induction heating of thin strip in Chapter 5, we discovered that the thickness of the strip should be at least 2.25 times the skin thickness. Then for this application, the maximum skin thickness for good efficiency would be 0.0124 centimeter. An inspection of Fig. 91 shows that this skin thickness is obtained for lead at a frequency of 3.4 megacycles. In our experiments, the frequency was 30 megacycles with a skin thickness of 0.00417 centimeter, so we were far above the critical or necessary frequency. The higher frequency was used because of the availability of the equipment.

If power were applied from one side of the sheet only, we could use (14.52) directly to determine the temperature at the point of closure. Since the frequency is such that the thickness of the strip is about seven times the skin thickness of the metal, Fig. 46 shows that the distributions near each surface are practically independent of the conditions at the other surface. In this case, we may then use superposition of the temperature solutions. This is accomplished by doubling the value of (14.52). Then the temperature increment is

$$u(x)_{x=\frac{a}{2}} = \frac{2P_t t}{4.187 c\rho a}. \tag{15.01}$$

Here P_t is the power supplied to only one side of the tube, measured in watts per square centimeter. It was necessary to bring the material from

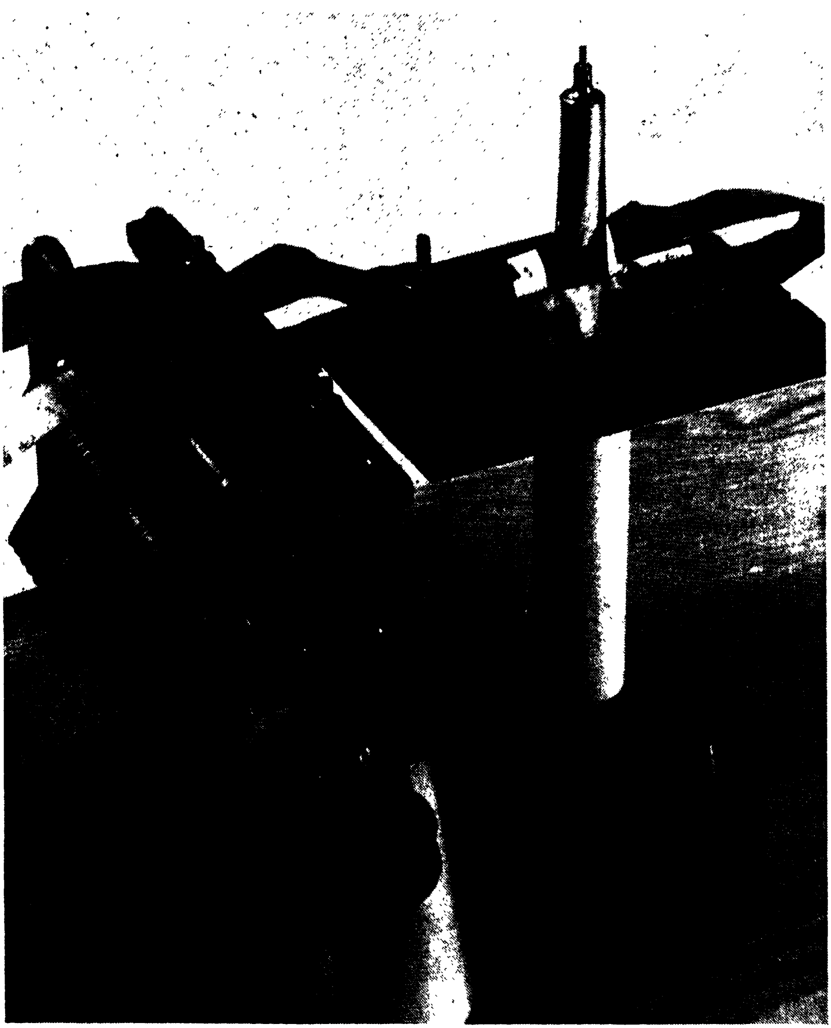

FIG. 130. An ointment tube in place in the clamp jaws which form the induction heating coil.

20° C to 350° C so the temperature increment to be used in (15.01) is 330° C. The other values to be substituted in (15.01) are:

t = heating time = 0.1 second;
a = 0.0279 centimeter;
ρ = specific heat from Table 9 = 0.03;
c = density = 11.34.

When (15.01) is solved for the power density, we find that 65.4 watts per square centimeter are required. This is the power supplied on one side of the tubing. To make a closure with a width of 0.2 centimeter, where the length of the closure around the tube is 3.4 centimeters, we need a total power delivered into the metal of 44.5 watts.

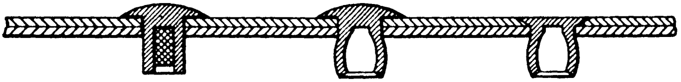

FIG. 131. Typical explosive rivets. On the left is a round-head rivet before detonation, and the characteristic form after detonation is shown in the center. A flat-head rivet after detonation may be seen at the right.

Detonation of Explosive Rivets with Radio-Frequency Power. One of the methods of " blind " riveting sometimes used in modern aircraft construction involves the use of explosive rivets.* These rivets carry an explosive charge in their hollow shank. The charge, when exploded by the application of heat, expands the rivet and fixes it in place. The explosive rivets commonly used at present are made of an aluminum alloy. For protection from corrosion, the rivets are given an anodized coating which has an extremely low thermal conductivity. Fig. 131 shows typical rivets, before and after detonation. The explosive charge is a special preparation which explodes properly when it is rapidly heated to about 140° C. The rate of heating is quite important, for if it is too slow the charge will melt and burn instead of exploding. A heating time of from one to six seconds is suitable, but a time of one to two seconds is desirable from the standpoint of high-speed production. The method most commonly used for detonating the rivets consists of heating them by conduction with an electrically-heated device similar to a soldering iron except for a solid silver tip shaped to fit the head of the rivet. To obtain a satisfactorily short firing time, it is necessary to maintain the tip at a temperature of about 550° C. Because of the poor thermal conductivity of the anodized coating, the temperature required at the tip of the heating tool to produce the required heat flow into the rivet is high enough to deteriorate the coating, often resulting in failures to pass corrosion tests.

To investigate the heat-conduction problem encountered with this type of detonation, the charge in a rivet which had the dimensions shown in Fig. 132 was removed. A thermocouple was inserted in the cavity, and the cavity packed with foil to insure intimate contact between the inner surface of the rivet and the thermocouple. A copper bar with its tip shaped to fit the round head of the rivet was heated to a temperature of 445° C. This bar was then placed firmly on the head of the rivet and internal temperature readings observed with the thermocouple. Fig. 133 shows the internal temperature as a function of time elapsed after positioning the heated bar. It may be seen that more than 2 seconds are required to attain firing temperature with the bar heated to 445° C. With a thicker anodized coating or a larger rivet, the firing time may become excessive.

---

* " Recent Applications of Physics," *Journal of Applied Physics*, Vol. 16, No. 1, January 1945, p. xviii.

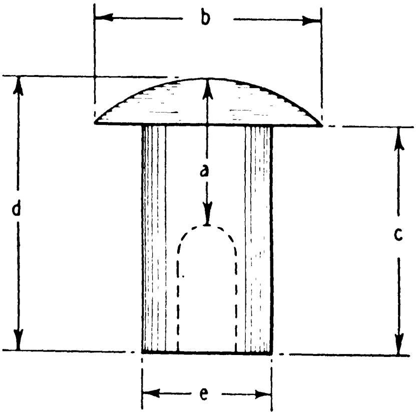

Fig. 132. Dimensions of a typical explosive rivet.

a = 0.495 centimeter
b = 0.762 centimeter
c = 0.762 centimeter
d = 0.915 centimeter
e = 0.44 centimeter

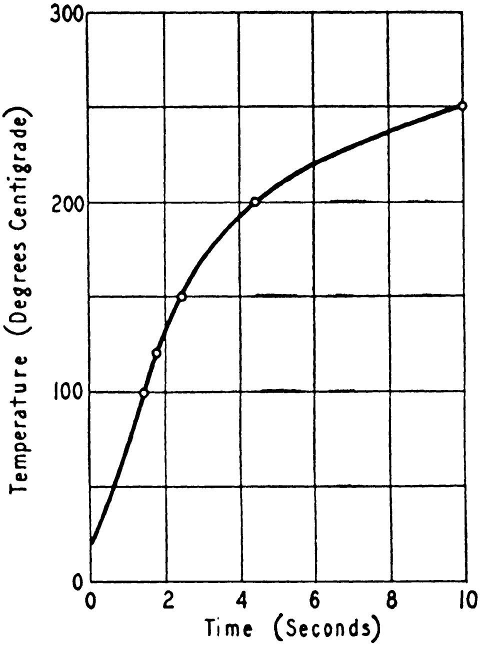

Fig. 133. Internal temperature of the rivet as a function of time, where the heating applicator has a temperature of 445° C.

The heating of the rivets by induction at radio-frequencies offers a means of overcoming the difficulties experienced with the heating irons, for the heat can be generated in the rivet head thus avoiding heat transfer through the insulating layer. An estimate of the power requirements may be made by a direct application of (14.56). We select the thermal constants of aluminum from Table 9. The thickness, a, in (14.56) corresponds to the dimension, a, in Fig. 132. At a frequency of 700 kilocycles, the skin thickness of aluminum

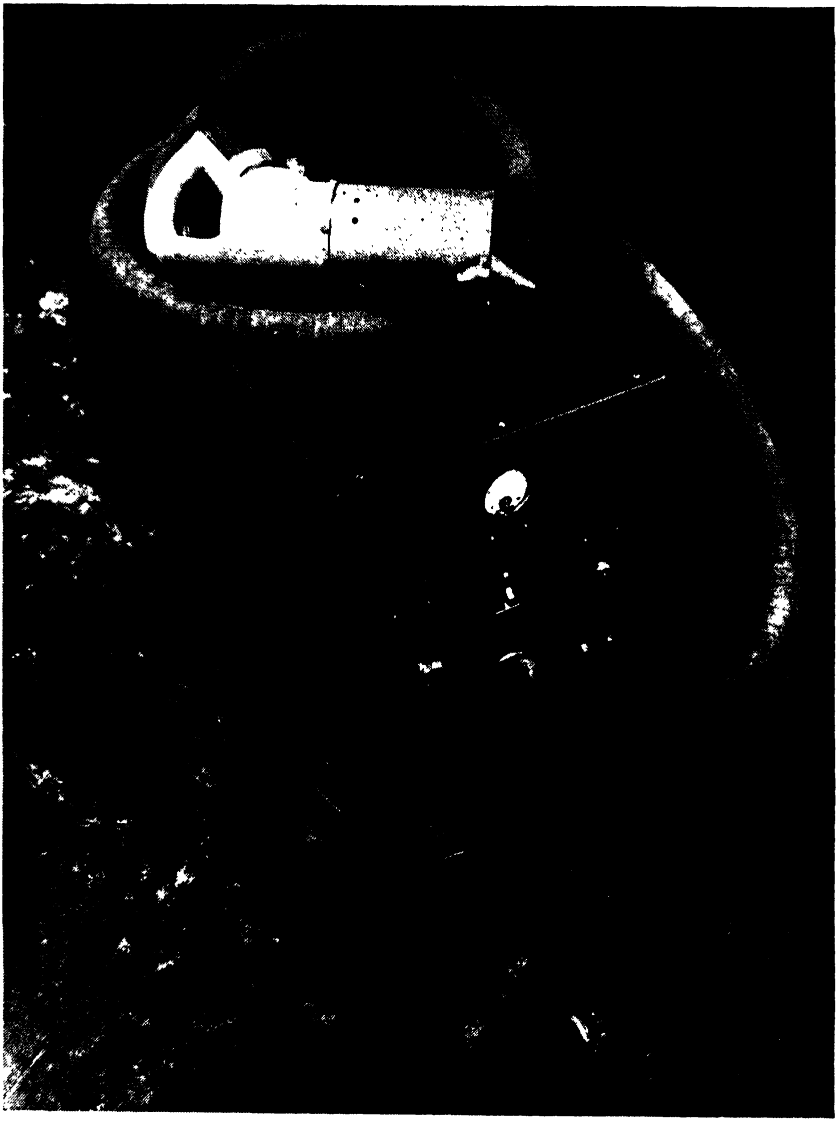

FIG. 134. A radio-frequency rivet detonator. The radio-frequency oscillator is in the box and the radio-frequency power is carried to the applicator by a flexible transmission line which runs through the large hose shown. This hose also carries the control wires from the trigger in the handle to the oscillator proper. Thus the oscillator is turned on at will by pressing the trigger.

is 0.01 centimeter, so a/s is 49.5, a value which may be used in Fig. 129 to yield 0.164 as the proper value of B to use in (14.56). Then (14.56) becomes

$$u(\text{degrees Centigrade}) = \frac{P_t}{4.187}(4.25t - 0.169). \tag{15.02}$$

Since we wish to raise the temperature from 20° C to 140° C, we set the temperature, u, in the above equation equal to 120° C. If the heating time is to be 1 second, the equation shows that the power required is 123 watts per square centimeter. The projected area of the head of the rivet is 0.457 square centimeter, so the power into the rivet is 56.2 watts. For a larger rivet, where the dimension a is 0.6 centimeter and the area is 0.635 square centimeter, the power required is 96 watts.

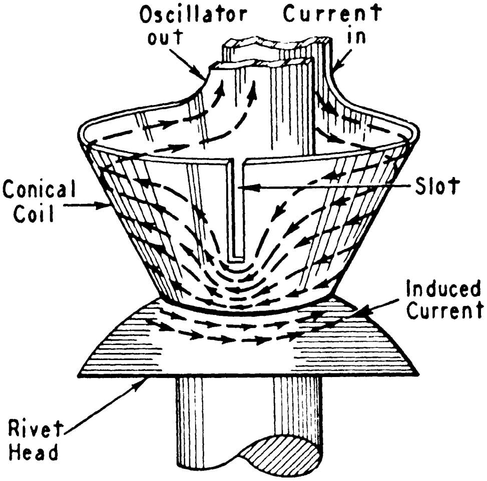

FIG. 135. The currents in the conical tip and the currents induced in the rivet are shown here.

Fig. 134 shows equipment developed for the radio-frequency detonation of explosive rivets. The gun consists of a primary winding of 52 turns surrounded by a single copper sheet which also serves as the outer shell of the gun. This transformer is of the same type as the one shown in Fig. 79. The copper-sheet secondary terminates in the conical nose which is essentially a small coil that may be pressed tightly to the head of the rivet. The currents in the conical tip and the currents induced in the head of the rivet flow somewhat as shown in Fig. 135. The shape of the tip was found to be suitable for the following reasons. The current concentration at the apex of the cone is high, resulting in fairly good coupling to a rivet placed adjacent to the cone. The heat, generated mostly at the apex where the current concentration is high, will be conducted rapidly to the entire cone where it can be removed by an air blast, thus preventing the temperature from becoming excessively high at any point. The applicator is strong enough mechanically so that adequate pressure may be applied to the rivet while it is being fired.

With the detonator described, the efficiency of the transformer system is about 35 per cent at 700 kilocycles. At a frequency of 350 kilocycles, the efficiency is 21 per cent on round-head rivets and 27 per cent on flat-head rivets.

With a power into the oscillator of approximately 500 watts and an operating frequency of 700 kilocycles, it is possible to fire short rivets in 1 second and the largest rivets encountered in 3 seconds.

Although the initial cost of the equipment is apt to be appreciably higher than the cost of heating irons, it is believed that this disadvantage is more than overcome by the following advantages.

1. All sizes of rivets may be fired in a time of 1 to 3 seconds.
2. The protective coating on the rivets is not damaged.
3. The time for putting the equipment into initial operation is about 30 seconds.
4. Power adjustments can be made instantly.
5. Round- and flat-head rivets can be fired indiscriminately with the same detonator tip.
6. To expedite production, it is possible to hold the rivets in place with adhesive tape and fire them through the tape. This procedure is not possible with the heating irons.
7. The tips should have a much longer life because of the much lower operating temperature.

Chapter 16

CASE-HARDENING OF STEEL

In previous chapters, we have shown that high-frequency currents tend to crowd toward the surface of metallic conductors. This crowding or skin-effect, with consequent generation of heat near the surface, has been widely used in the case-hardening of steels. The analysis of Chapter 14 demonstrated that the temperature distribution changes quickly from the initial distribution as heat flows inward to the cooler regions and that the choice of frequency is of minor importance. It is the purpose of this chapter to examine the heat-flow relations for specific examples and to demonstrate the importance of several variables. A rigorous analytical treatment is practically impossible because of the many variables. The thermal properties of the material change with temperature, and the experiments discussed in Chapter 10 show that resistance and permeability are subject to extreme changes over the range of temperatures to which the material is subjected. In addition, the sharp drop in permeability at the Curie point raises another formidable obstacle. Another factor to be reckoned with is the change of permeability with increasing magnetic intensities. As greater power densities are used, saturation is approached, where the magnetic flux density reaches an upper limit which is not exceeded no matter how high the exciting magnetic intensity becomes. However, the authors believe that an analysis based upon broad assumptions designed to simplify the mathematical manipulations is of value in establishing general relations.

Relative Permeability With High Magnetic Intensities. Since most induction heating of steels is accomplished by high power concentrations and hence high magnetic intensities, it is possible to make use of empirical formulas which have been found to be reliable in this region. A simple and useful relation is*

$$\mu_r = \frac{1}{a + bH} + 1, \tag{16.01}$$

---

* Edward Bennett and Harold M. Crothers, *Introductory Electrodynamics for Engineers*, 1st ed., McGraw-Hill Book Company, Inc., 1926, New York, p. 564.

where μ_r is the relative permeability of the material. The total permeability is this numeric multiplied by the permeability of free space, $\mu_0 = 4\pi \cdot 10^{-9}$. Bennett and Crothers call the quantity a the *coefficient of magnetic hardness* while b is the *saturation coefficient.* An inspection of (16.01) reveals the properties at the two extreme values of magnetic intensity. When the magnetic intensity H is very large, only the last term in the equation is of consequence. Thus the relative permeability is practically unity. On the other hand, when the magnetic intensity approaches zero, the relative permeability relation becomes

$$\mu_r \doteq \frac{1}{a} + 1. \tag{16.02}$$

Since a is a very small number, the relative permeability is very large for low magnetic intensities.

Although the magnetic properties of the many steels cover a wide range, it is possible to select values for a and b which are somewhat representative of the most interesting types. The values to be used in this treatment are

$$a = 10^{-3}$$

$$b = 7 \cdot 10^{-5}$$

Then (16.01) becomes*

$$\mu_r = \frac{1}{10^{-3} + 7 \cdot 10^{-5} H} + 1. \tag{16.03}$$

The solid curve in Fig. 136 shows the relative permeability of steel as calculated from the empirical relation of (16.03), for a range of magnetic intensities of interest in the practice of induction heating. This equation may be greatly simplified by neglecting the last term and by dropping the coefficient of magnetic hardness, a. Then (16.03) becomes

$$\mu_r = \frac{1}{bH} = \frac{14{,}300}{H}. \tag{16.04}$$

---

[*] In the treatment of current flow and heat generation carried through in this volume, we have dealt almost entirely with sinusoidally-varying electrical quantities of a single frequency. Therefore, currents and magnetic intensities have been expressed in r.m.s. values. This always enables us to calculate power by squaring the currents or magnetic intensities with an apparent disregard of $\sqrt{2}$ terms which are needed when instantaneous values are used. The variation of the relative permeability shown by (16.03) as the magnetic intensity changes most certainly gives rise to a complex magnetic flux density and probably to a non-sinusoidal current in the metal. A treatment which attempts to display these phenomena would be extremely complicated. Accordingly, we shall pretend that the relative permeability assumes an averaged value governed by the r.m.s. value of the magnetic intensity. Hence, in (16.03), the magnetic intensity H is the r.m.s. value.

This simplified relation for the relative permeability is shown by the broken curve of Fig. 136. It may be seen that no great loss of generality occurs when the simplified version is used.

Magnetic Intensity as a Function of Applied Power. In Chapter 4, where we considered current flow near the surface of metal sheets, the

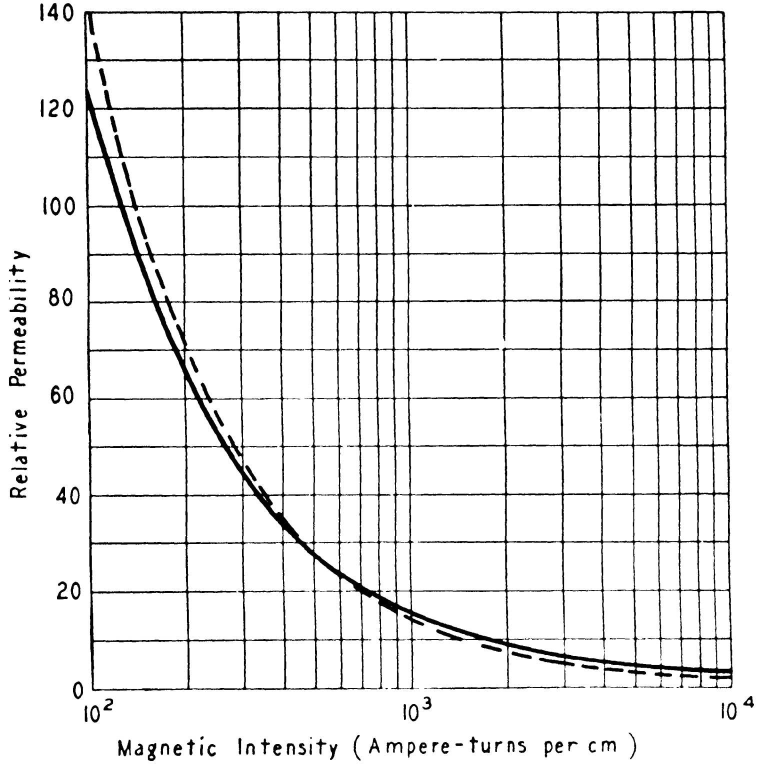

Fig. 136. The solid curve was calculated from the empirical relation shown in (16.03), whereas the broken curve corresponds to the simplified version expressed in (16.04).

permeability was assumed to be a fixed constant. Then the current density dropped off exponentially from the surface with the rate of decay determined by a parameter s which we called the skin thickness. The skin-thickness expression contained the relative permeability as a factor. Now we are confronted with a complex situation where the magnetic intensity is high at the surface of the metal with a consequent low permeability but as we go further into the metal, the magnetic intensity decreases with an attendant increase in relative permeability which causes a still faster decay of the magnetic intensity. This effect continues to cascade, leading us into greater and greater complications. We shall avoid embarrassing entanglements by simply assuming that the proper value of relative permeability to use in analysis is that determined by the magnetic intensity just inside the surface of the metal. Then we are able to lean heavily on the results of Chapter 4.

Now, (4.31) states that

$$(2H_1)^2 = s\sigma P_t \tag{16.05}$$

where $P_t =$ the power density supplied to the surface of the metal, watts per square centimeter;
$\sigma =$ conductivity of the metal, mhos for a centimeter cube;
$s =$ the skin thickness, centimeters;
$H_1 =$ the magnetic intensity impinging on the surface of the metal, ampere-turns per centimeter.

But from (4.20) and (4.21), we learned that the magnetic intensity just inside the metal was equal to twice the impinging value. Then (16.05) becomes

$$H^2 = s\sigma P_t, \tag{16.06}$$

where H is the magnetic intensity just inside the metal sheet. We next square both sides of (16.06) and substitute (1.46) for the skin thickness, in addition to inserting (16.04) for the relative permeability as it appears in the skin-thickness formula. Then

$$H^4 = \frac{\sigma b H P_t^2}{4\pi^2 \cdot 10^{-9} f}, \tag{16.07}$$

where f is the frequency in cycles per second.

Solving (16.07) for the magnetic intensity, we find

$$H = \left(\frac{\sigma b}{4\pi^2 \cdot 10^{-9} f}\right)^{1/3} \cdot P_t^{2/3}. \tag{16.08}$$

From this equation, we learn that the magnetic intensity just inside the metal varies directly as the two-thirds power of the applied power density and inversely as the one-third power of the frequency.

Fig. 137 shows the magnetic intensity as a function of power concentration for several frequencies. In computing the curves for this diagram, the following values for the parameters in (16.08) were used:

$\sigma =$ 6000 mhos for a centimeter cube;

$b = 7 \cdot 10^{-5}$, corresponding to equation (16.04).

An inspection of Figs. 136 and 137 reveals that, for the higher power concentrations, we are always operating in a region where the approximate expression for the relative permeability stated by (16.04) is valid.

The Skin Thickness of Steel. We now substitute (16.04) in (1.46) and obtain

$$s = \frac{1}{2\pi}\left(\frac{bH}{10^{-9}\sigma f}\right)^{1/2}. \tag{16.09}$$

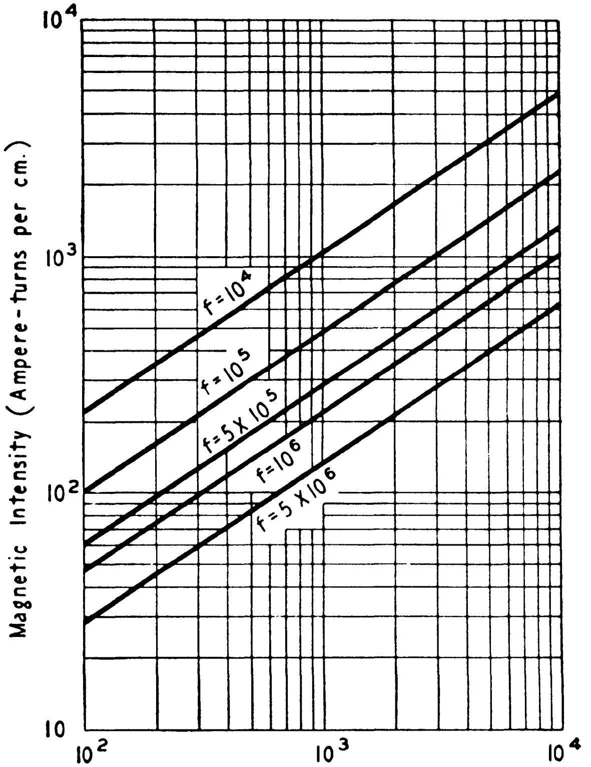

FIG. 137. Magnetic intensity at the surface of steel as a function of power density.

When (16.08) is inserted in (16.09), we find the skin-thickness expression to be

$$s = \left(\frac{P_t}{\sigma}\right)^{1/3} \cdot \left(\frac{b}{4\pi^2 \cdot 10^{-9} f}\right)^{2/3}. \tag{16.10}$$

We are thus confronted with the somewhat surprising fact that the skin thickness is a function of the power concentration, as well as the fact that the skin thickness varies inversely as the two-thirds power of the frequency instead of inversely as the one-half power, the relation for non-magnetic materials. Fig. 138 shows the skin thickness of steel as a function of power density, for a number of frequencies.

The Thermal Constants of Iron and Steel. Before proceeding with a consideration of heat flow in steel, we must decide on appropriate values of the thermal constants Both the specific heat and thermal conductivity change somewhat as the temperature varies. This is particularly true of the specific heat. Fig. 139 shows the variation of specific heat of iron as a function of temperature. The upper curve shows the incremental specific heat for small changes in temperature, whereas the smooth curve is the integrated average of the first curve.* The best that we can do is to select mean values of the thermal constants and assume that these quantities remain fixed throughout

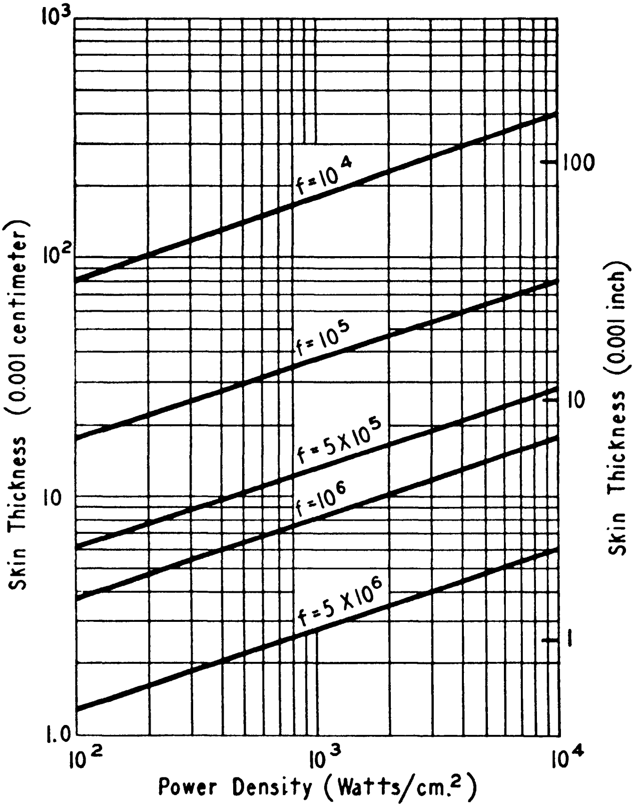

FIG. 138. The skin thickness of steel as a function of power density and frequency.

---

* *International Critical Tables*, McGraw-Hill Book Company, Inc., New York, Vol. V, p. 93.

the heating cycle. In the following numerical examples, we shall use the thermal constants for iron which are listed in Table 9, Chapter 14.

Temperature Distribution in Very Thick Plates as a Function of Frequency and Power Concentration. Our initial calculations will be directed to the problem of a very thick flat plate which is induction-heated from one side. A large cylindrical bar, with a radius so large that all the current flow and temperature changes take place relatively near the surface, might be considered to come within the scope of this examination.

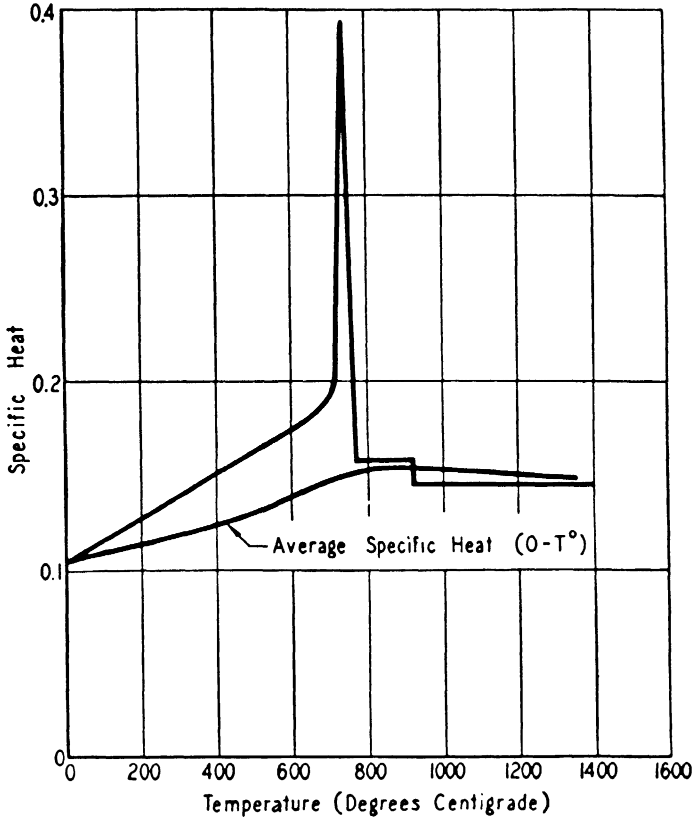

FIG. 139. Specific heat of iron as a function of temperature.

Fig. 140 was prepared by inserting the above-mentioned thermal constants in (14.39) and (14.40). The skin thickness was determined by reference to Fig. 138. Values of the function $f(\theta, x)$ in (14.39) were obtained from Fig. 122, using the curve corresponding to $x = 0$. Thus Fig. 140 shows the mode of variation of the surface temperature as a function of time for several frequencies, where the power density on the surface is 1000 watts per square centimeter. It may be seen that when the frequency is as low as 0.01 megacycle (10^4 cycles), the temperature does not rise quite as fast as it does for the higher frequencies. It should be noted that there is only a slight difference in results for the two frequencies, 0.1 megacycle and 5.0 megacycles.

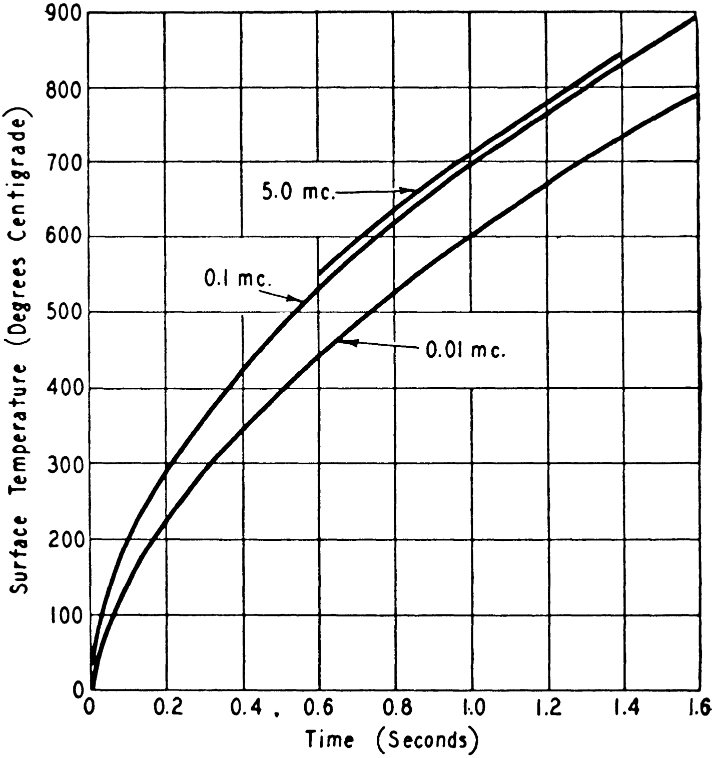

FIG. 140. Surface temperature of a thick steel plate as a function of time for a number of frequencies. The power density, P_t, is 1000 watts per square centimeter

When lower power concentrations are used, the heating time is prolonged and the heat flows into the metal still further. This heat flow away from the region where the heat is generated makes it still more difficult to find marked changes in the temperature relation for varying frequency. Fig. 141 shows the surface temperature when the power density is 500 watts per square centimeter. Here it is impossible to distinguish between the results at 1 and 5 megacycles.

A comparison of the rates of temperature rise for power concentration of 100 and 500 watts per square centimeter is made in Fig. 142. With a power

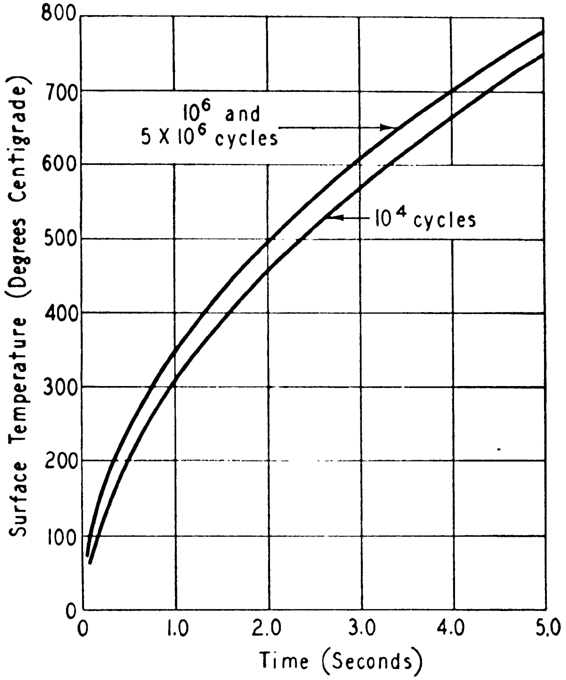

FIG. 141. Surface temperature of steel, when the power density is 500 watts per square centimeter.

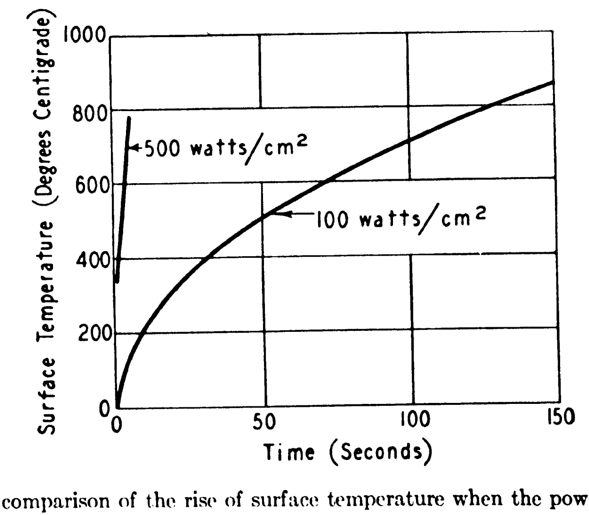

FIG. 142. A comparison of the rise of surface temperature when the power concentration is 100 and 500 watts per square centimeter.

concentration as low as 100 watts per square centimeter, it matters hardly at all whether the frequency is 10,000 cycles or 5,000,000 cycles.

Since the rate of temperature rise at the surface is so little affected by the choice of frequency, one might readily conclude that the temperature gradient throughout the metal is only slightly influenced by the frequency of the exciting source. To investigate this point, (14.39) and (14.40) were again utilized, with values of $f(\theta, x)$ obtained from the numerous curves of Fig. 122. The results of this calculation for one particular case are shown by Fig. 143.

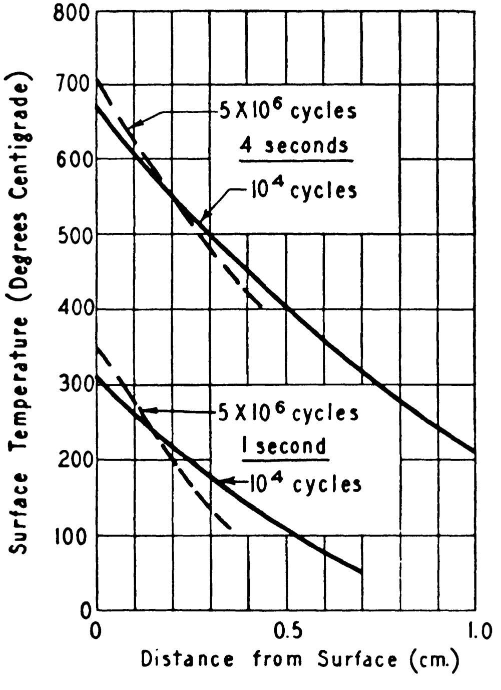

FIG. 143. Temperature distribution through the metal. The power density is 500 watts per square centimeter.

Here the power concentration is 500 watts per square centimeter. The two lower curves show the temperature distribution through the metal when 1 second has elapsed after turning on the power source. The solid curve is for a frequency of 10,000 cycles, while the broken curve corresponds to a frequency of 5,000,000 cycles. The upper two curves show the same conditions when 4 seconds have elapsed. Here the frequencies are in a ratio of 500: 1, with only an insignificant difference in temperature distribution.

Figs. 144a to 144d still further bring out the fact that frequency is not the controlling factor. It may be seen that as time passes the temperature gradient decreases. For all the frequencies used in the examples, the temperature distribution is essentially independent of frequency when the times considered are greater than 0.1 second. When the frequency is greater than 100,000 cycles, the temperature distributions are substantially independent of frequency for an elapsed time as short as 0.01 second.

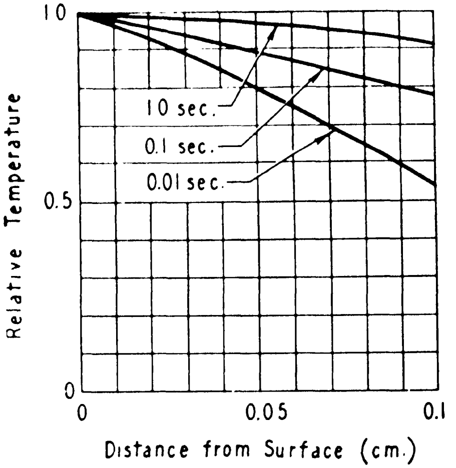

FIG. 144a. Relative temperature distribution. The frequency is 10,000 cycles.

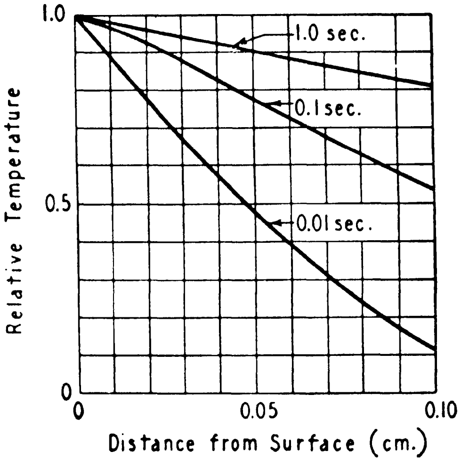

FIG. 144b. Relative temperature distribution. The frequency is 100,000 cycles.

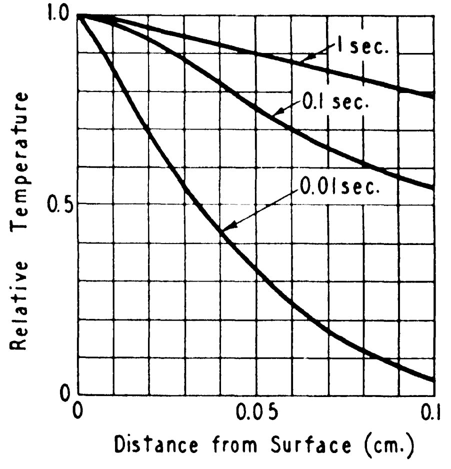

FIG. 144c. Relative temperature distribution. The frequency is 1,000,000 cycles.

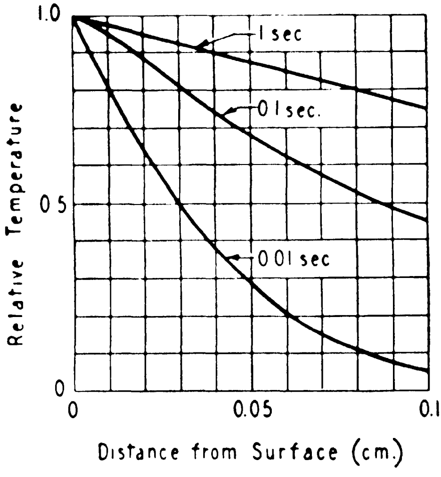

FIG. 144d. Relative temperature distribution. The frequency is 5,000,000 cycles.

We have already seen from Figs. 140, 141, and 142 how the heating rate is rapidly increased as the power concentration is raised. More readily comparable curves are displayed in Fig. 145, where a number of power concentrations were used. Here we see that it is possible to elevate the surface temperature to 800° C or more in a very small fraction of a second when powers of several thousand watts are applied to each square centimeter of surface. To bring about effective hardening of most steels the temperature must first be raised above 800° C. Then, quick cooling by quenching in a water or oil medium yields a hard product. If the surface were brought just to the proper temperature, only a thin layer would be hardened. It is thus necessary to raise the surface well above 800° C so that all points in a layer to be hardened are also brought above the critical temperature. Fig. 146 may serve as a reference to show the order of magnitude of the power concentration necessary to raise the surface to the neighborhood of the hardening

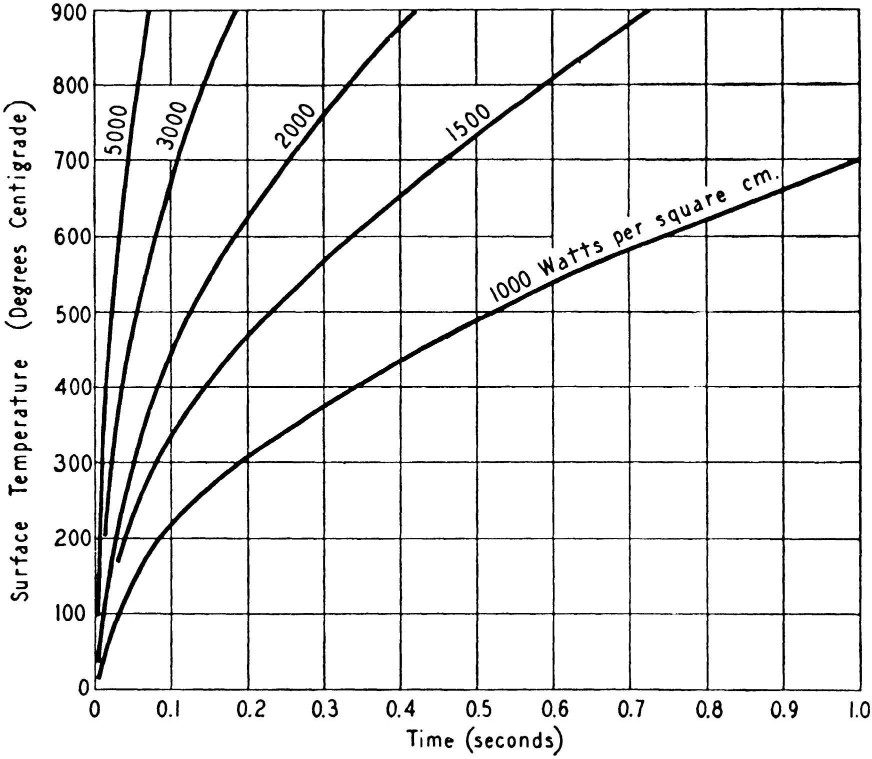

FIG. 145. Surface temperature as a function of time for a number of power concentrations. The frequency may be considered to be above 100,000 cycles.

temperature in a given time. It may be noted that the energy consumed (the product of power and time) is much less for the higher power concentrations.

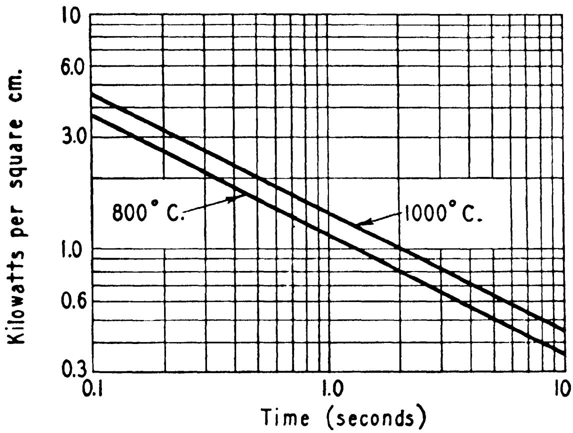

FIG. 146. Power concentration versus time of heating to obtain a surface temperature of 800° C and 1000° C. For 800° C, the power concentration, P_t (kilowatts per square centimeter) $= 1.13/t^{\frac{1}{2}}$. For 1000° C, $P_t = 1.425/t^{\frac{1}{2}}$ kilowatts per square centimeter.

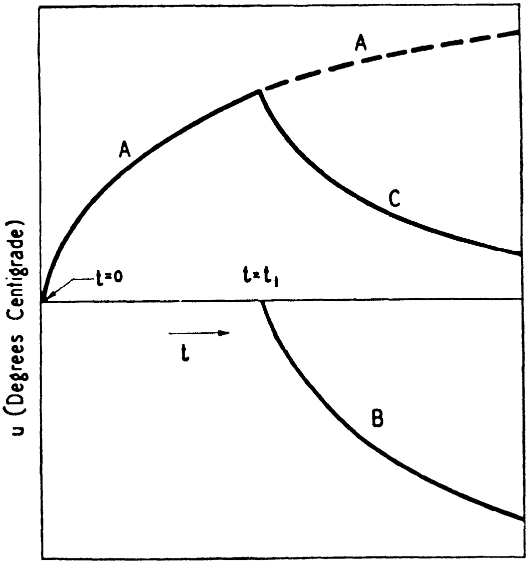

FIG. 147. Transient calculation by superposition method.

Surface Hardening of Steel by Self-Quenching. Another calculation of interest is that of the transient temperature state, where heat is generated within the metal from a time $t = 0$ to a time $t = t_1$. At this point, the heat generation is stopped and the temperature goes into a decline. We may treat this case mathematically by means of the superposition principle. The expression for temperature at some point in the metal as a function of time after the start of heat generation is given by curve A in Fig. 147. This heat continues to be generated for all time. However, at time $t = t_1$ and beyond, a negative generation of heat is imagined which just cancels the positive generation. The temperature resulting from this negative generation is given by curve B, Fig. 147. It should be noted that curve B is simply the negative of curve A, displaced to the right an amount equal to t_1. Then for time greater than t_1, the resultant temperature curve C is the algebraic sum of A and B. Once curve A has been calculated, it is a simple matter to construct curve C very quickly.

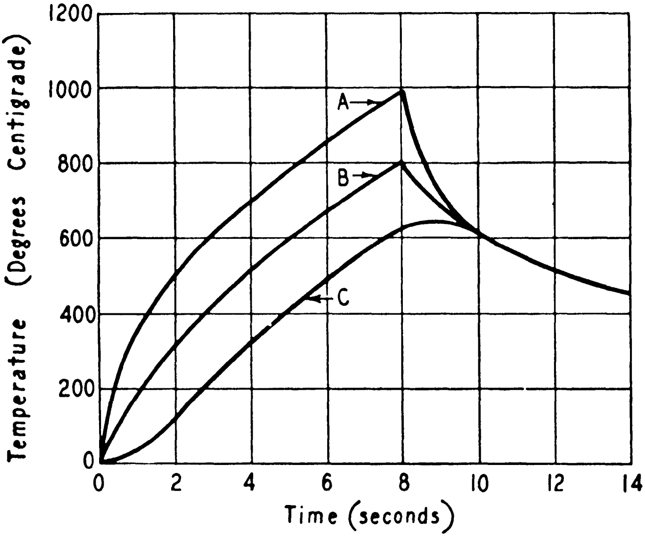

FIG. 148. Power concentration, P_t = 500 watts per square centimeter.

Curve A: $x = 0$
Curve B: x = 0.25 centimeter
Curve C: x = 0.5 centimeter

This procedure was followed in constructing the curves shown in Figs. 148 to 151, inclusive. For the curves of Fig. 148, a relatively low value of power concentration, 500 watts per square centimeter, was considered. We see that the surface reached a temperature of approximately 1000° C in 8 seconds. At this same instant, the metal 0.25 centimeter beneath the surface has just reached 800° C. When the application of power is stopped

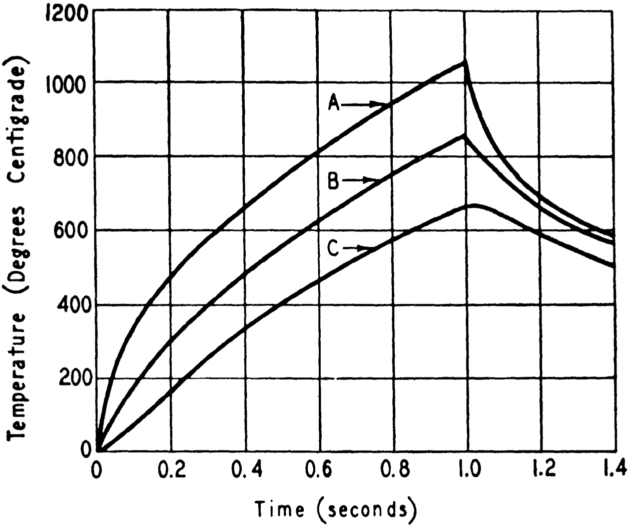

FIG. 149. P_t = 1500 watts per square centimeter.
Curve A: $x = 0$
Curve B: x = 0.0934 centimeter
Curve C: x = 0.1868 centimeter

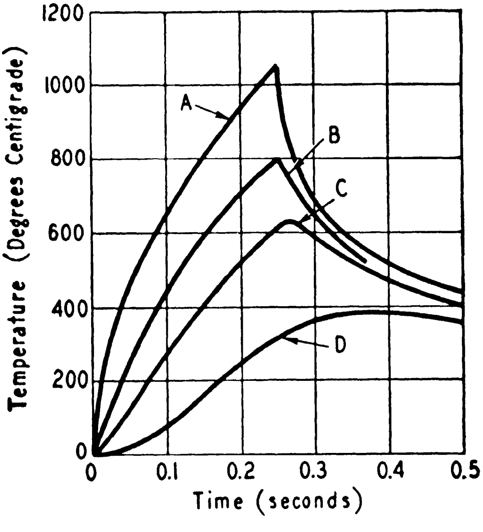

FIG. 150. P_t = 3000 watts per square centimeter.
Curve A: $x = 0$
Curve B: x = 0.0585 centimeter
Curve C: x = 0.117 centimeter
Curve D: x = 0.234 centimeter

at the end of 8 seconds, the surface temperature immediately starts to drop, since the cold interior quickly robs heat from the surface layers. Curve *C* shows that the relatively cooler metal 0.5 centimeter beneath the surface continues to rise in temperature for another second as heat is supplied from the surface layers. In the conventional practice of case hardening by means of radio-frequency heating, the power source of Fig. 148 would be turned off after 8 seconds and a water quench immediately applied. The curves of Fig. 148 do not take this water cooling into account. The drop in temperature shown in this figure is due entirely to the robbing of heat from the surface by the cool interior. If the temperature drop is fast enough, we may thus effect surface hardening without the liquid quenching. This procedure we call *self-quenching*. Since the minimum cooling speed required for full hardening of most steels is of the order of 55° C per second,* the power concentration used in Fig. 148 is definitely a borderline value. The higher

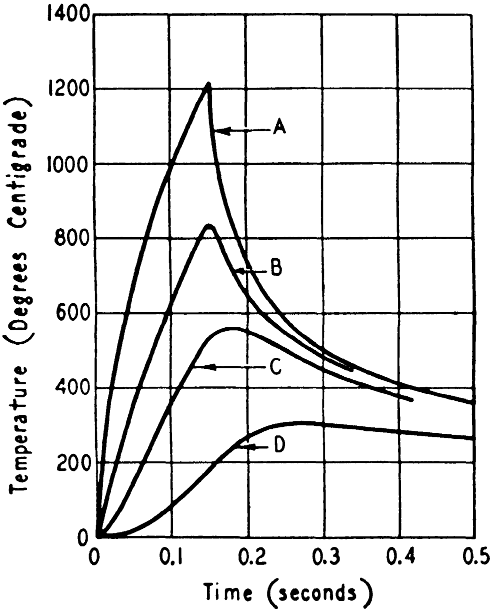

FIG. 151: P_t = 4500 watts per square centimeter
Curve A: $x = 0$
Curve B: x = 0.06715 centimeter
Curve C: x = 0.1343 centimeter
Curve D: x = 0.2686 centimeter

---

* A. L. Boegehold, " Use of Hardenability Tests for Selection and Specification of Automotive Steels," *SAE Journal* (*Transactions*), Vol. 49, No. 1, pp. 269–273.

power concentration used in Fig. 149 results in a surface temperature in excess of 1000° C in 1 second and a rapid cooling rate. Here self-quenching is entirely possible. With the extreme power concentration used in establishing the curves of Fig. 151, the heating and cooling is so rapid that it is doubtful whether water cooling would be of any importance.

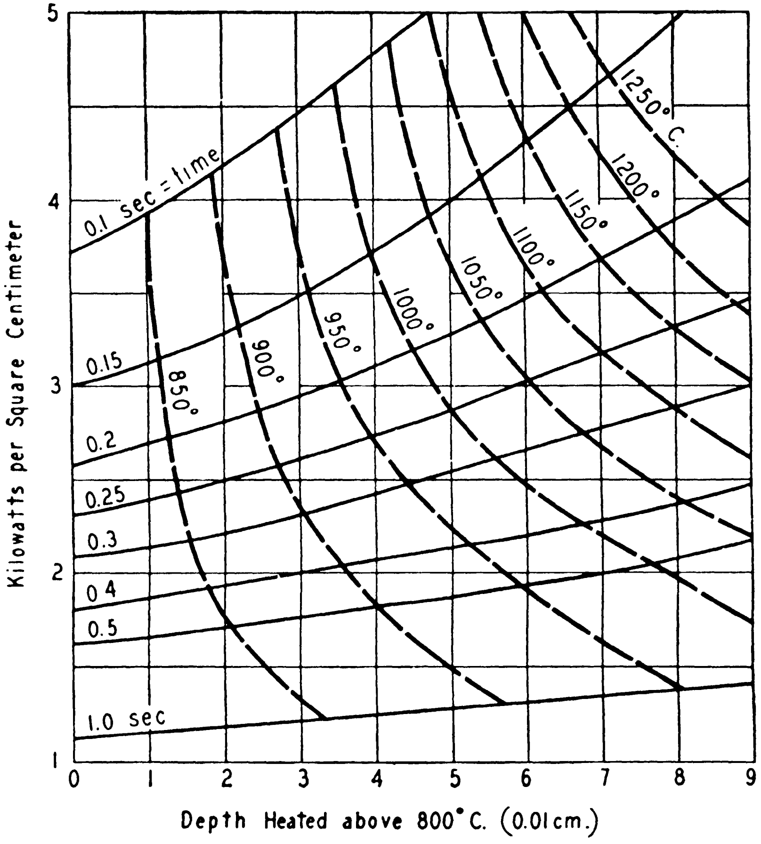

Fig. 152. Power concentrations necessary to heat all points in a given layer to a temperature above 800° C. The surface temperature and the time required are shown as parameters.

Reference to Curve *B*, Fig. 148, shows that when the surface temperature reaches 1000° C, a point 0.25 centimeter below the surface has just reached 800° C. Since we must cool from temperatures of at least 800° C to achieve hardness, we might expect a hardened layer 0.25 centimeter in thickness. When we turn to Fig. 150, we find that the point which just reaches 800° C (Curve *B*) lies 0.0585 centimeter beneath the surface. In this case, we have obtained a thinner layer heated above the critical temperature simply by increasing the power concentration.

By means of the curves shown in Figs. 148 to 151, as well as from many other similar curves not presented here, we have constructed Fig. 152. The ordinate of this diagram shows the power concentration necessary to raise the surface layer of the thickness shown by the abscissa to at least 800° C. The approximately horizontal lines have as a parameter the time required to raise this layer to the prescribed temperature, while the somewhat vertical lines indicate the surface temperature obtained when the innermost part of the layer has reached 800° C.

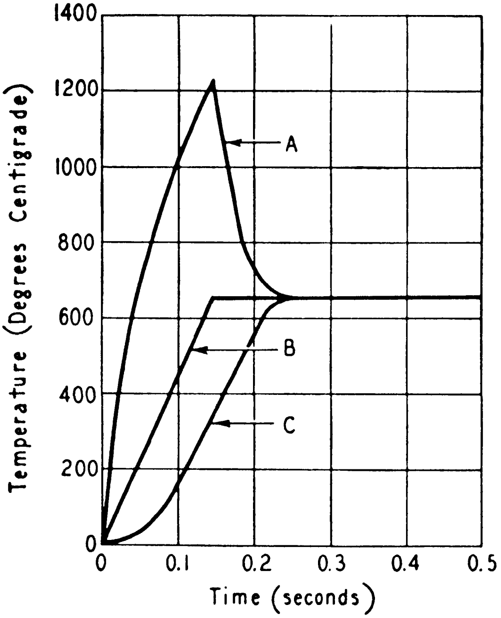

FIG. 153. Heating effect in a thin steel sheet. The power concentration is 4500 watts per square centimeter, and the frequency is 1 megacycle. The plate thickness is 0.2686 centimeter.

Curve A: Temperature of the surface nearest the exciting coil.
Curve B: Temperature at the center of the metal.
Curve C: Temperature at the far surface.

To illustrate the use of this chart, let us postulate that we wish to harden a layer having a thickness 0.04 centimeter. If we proceed vertically on the chart from this value and wish to achieve a surface temperature of 900° C, we learn that we must use a power concentration of 1.8 kilowatts per square centimeter and apply this power for 0.5 second. This consumes an energy of 0.9 kilowatt-seconds for each square centimeter of surface. However, if we wish to heat the surface to 1000° C and still harden a layer 0.04 centimeter in thickness, we learn that the required power is 3.7 kilowatts per square centimeter, applied for 0.155 second. The energy utilized is then 0.572 kilowatt-seconds per square centimeter of surface.

In utilizing the above data, it should be remembered that we have been considering very thick sections.

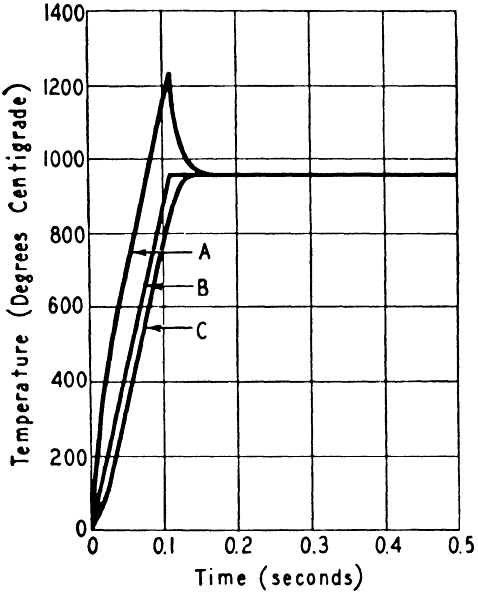

FIG. 154. The plate thickness is 0.1343 centimeter. All other conditions are the same as those applying to Fig. 153.

The Heating Effect in Thin Metallic Layers. Where the metal backing the heated layer is not sufficiently thick to absorb heat from the surface, it may become necessary to resort to liquid quenching after heating. Figs. 153 and 154 were constructed to illustrate this point. In both diagrams, a power concentration of 4500 watts per square centimeter was used. The frequency was taken as 1 megacycle. In Fig. 153, the metal was assumed to be 0.2686 centimeter in thickness, whereas Fig. 154 is based on a metal thickness of 0.1343 centimeter. The curves marked *A* show the temperature of the surface nearest to the inducing coil, while those marked *C* show the temperature of the far surface. Curves *B* in both diagrams indicate the temperature at the exact center of the metal sheet. Curves *A* and *C* were constructed from Figs. 127 and 128, using the procedure illustrated by Fig. 147.

While power is applied, the temperature rise at the center of the material is given by the simple but exact equation (14.52). The temperature rise at this point is thus a straight line with positive slope. When the construction of Fig. 147 is used, it is readily seen that the temperature at the center of the material remains constant when the power is removed. Then as the metal piece reaches a uniform equilibrium temperature, the two surfaces each come to the same temperature as the center.

For the thickness of metal considered in Fig. 153 (0.2686 centimeter), we see that there is a possibility of hardening one surface without hardening the other. However, it is likely that liquid quenching would be necessary. To achieve self-quenching, higher power and a shorter time would be needed. In the case of Fig. 154, the entire layer is heated above 800° C, so that liquid quenching would result in hardening throughout the piece.

Even though extremely high power concentrations may be available, it is not recommended that the self-quenching technique be attempted for layers which are less than $\frac{1}{2}$ centimeter thick.

Although the preceding analysis in this chapter has been restricted to flat surfaces, the general conclusions apply equally well to curved surfaces where the radius of curvature remains several times the skin thickness.

Self-Quenching By Scanning. In the foregoing treatment of hardening by self-quenching, we have assumed that the power is applied for a finite time and then stopped. The cold inner portion of the metal object then quickly cools the surface. Large amounts of power are required when large objects are to be treated. However, if the object to be hardened has a uniform cross section, it is possible to " scan " the surface; that is, the heating coil may be moved relative to the work. This procedure may be applied to long shafts, broaching tools, or to the inside surface of a cylinder wall. With sufficiently high power concentrations, it is possible to scan at a rate of a few inches per second.*

A Mathematical Formulation of the Scanning Problem. If the work is surrounded by a single-turn coil and if the radius of curvature of the work is large, we may regard a portion of the work as a flat surface and the work coil as a straight conductor parallel to the surface. This was the procedure carried out in Chapter 8.

The configuration to be considered is shown in Fig. 155. The conductor is at a height h' above the metal surface. This is the effective or virtual height given by (8.13) in terms of the actual height and the radius of the conductor. The virtual height will be used throughout this analysis. We are interested in the temperature conditions in a little patch of surface y units removed from the point directly under the conductor.

---

* H. C. Gillespie, " Operating Experience With High-Frequency Heating," *Electronic Industries*, Vol. 3, No. 2, February 1944, p. 82, Fig. 3.

Equation (8.03) gives the current density flowing in this little surface patch. When (8.03) is substituted in (8.06), we obtain the power expended in an element of surface, 1 square centimeter in area and y centimeters from the conductor. That is

$$P_e(\text{watts per square centimeter}) = \frac{J^2}{\sigma s} = \frac{I^2}{\sigma s \pi^2 (h')^2 \left[1 + \left(\frac{y}{h'}\right)^2\right]^2}. \tag{16.11}$$

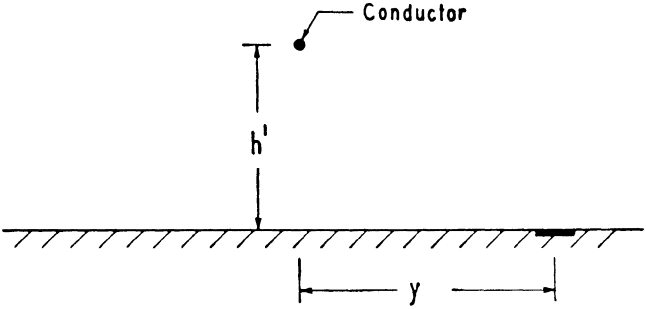

FIG. 155. A conductor parallel to a flat work piece.

But (8.09) gives the power lost in the sheet in a slice taken at right angles to the conductor, where the thickness of the slice in the direction along the conductor is 1 centimeter. The power is P_m. Then from (8.09),

$$I^2 = 2\pi\sigma s h'. \tag{16.12}$$

When (16.12) is placed in (16.11), we find

$$P_c = \frac{2P_m}{\pi h' \left[1 + \left(\frac{y}{h'}\right)^2\right]^2}. \tag{16.13}$$

Let us now assume that the conductor shown in Fig. 155 is moving to the the left at a constant velocity, v centimeters per second. Zero time will be counted when the conductor is directly over the patch in question. Hence for all positive values of time, the conductor will be to the left of the patch, while for negative values of time, the conductor will lie to the right of the patch. The dimension y is given by the relation

$$y = vt \tag{16.14}$$

so we see that (16.13) is now a function of time.

The solution may now be obtained by using the methods of superposition, or in the language of the mathematician, Duhamel's Theorem.

Let us assume for the moment that we know a function $u_0(t)$ which is the temperature response to the application of a step or unit function of power applied to 1 square centimeter of surface. That is, $u_0(t)$ is the expression for the temperature t seconds after 1 watt of power is applied to the patch in question. The power applied to a small element as a function of time may be regarded as being made up of a number of step functions of infinitesimal magnitude, all superimposed. Thus at a time t, the small step will be

$$\frac{dP_e}{dt} \cdot dt. \tag{16.15}$$

The temperature of the patch at a time t' resulting from this step function applied at a time t is then

$$u_0(t' - t) \cdot \frac{dP_e}{dt} \cdot dt \tag{16.16}$$

and the temperature at a time t' due to all the step functions occurring prior to this time is

$$u = \int_{t=-\infty}^{t=t'} u_0(t' - t) \frac{dP_e}{dt}\, dt. \tag{16.17}$$

Integrating (16.17) by parts, we obtain

$$u = u_0(t' - t)P_e \Big|_{t=-\infty}^{t=t'} - \int_{t=-\infty}^{t=t'} P_e \frac{d}{dt} \cdot u_0(t' - t)\, dt \tag{16.18}$$

We may obtain the response to a unit or step function by turning to (14.36) and (14.37). By retaining only the first three terms of (14.37) and setting the power per square centimeter at 1 watt, the function $u_0(t)$ is found to be

$$\begin{aligned} u_0(t) &= \frac{G}{4.187\beta}\left(\frac{2}{\sqrt{\pi}}\theta^{1/2} - \beta x - \epsilon^{-\beta x}\right) \\ &= \frac{2t^{1/2}}{4.187\sqrt{\pi k c \rho}} - \frac{1}{4.187k}\left(x + \frac{s}{2}\epsilon^{-\frac{2x}{s}}\right). \end{aligned} \tag{16.19}$$

The dimension x in (16.19) is the distance into the metal to the point where the temperature is to be reckoned. The use of (14.36) in obtaining the response to unit function infers that the action takes place rapidly, thus allowing us to disregard heat flow laterally in the metal, but with substantial heat flow away from the surface. This seems to be a reasonable assumption.

When we apply (16.13) and (16.19) in (16.18), we find that the temperature expression is

$$u(t') = \frac{-2P_m\left(x + \frac{s}{2}\epsilon^{-\frac{2x}{s}}\right)}{4.187\pi h'k\left[1 + \left(\frac{vt'}{h'}\right)^2\right]^2}$$

$$+ \frac{2P_m}{4.187\pi h'\sqrt{\pi k c\rho}} \int_{t=-\infty}^{t=t'} \frac{dt}{(t' - t)^{1/2}\left[1 + \left(\frac{vt}{h'}\right)^2\right]^2}. \qquad (16.20)$$

The details of the mathematical manipulation involved in the integration of the integral given above are displayed in Appendix C. Making use of these results we may write the temperature expression as

$$u(t') = \frac{0.294P_m}{\sqrt{\pi k c\rho}\cdot\sqrt{vh'}}\cdot g\left(\frac{vt'}{h'}\right) - \frac{2P_m\left(x + \frac{s}{2}\epsilon^{-\frac{2x}{s}}\right)}{4.187\pi h'k\left[1 + \left(\frac{vt'}{h'}\right)^2\right]^2}, \qquad (16.21)$$

where the function $g\left(\frac{vt'}{h'}\right)$ is

$$g\left(\frac{vt'}{h'}\right) = 0.287\left\{\left[3 + 2\left(\frac{vt'}{h'}\right)^2\right]\left[\sqrt{1 + \left(\frac{vt'}{h'}\right)^2} + \frac{vt'}{h'}\right]^{1/2}\right.$$

$$\left. + \frac{vt'}{h'}\left[\sqrt{1 + \left(\frac{vt'}{h'}\right)^2} - \frac{vt'}{h'}\right]^{1/2}\right\} \div \left[1 + \left(\frac{vt'}{h'}\right)^2\right]^{3/2}. \qquad (16.22)$$

This expression is shown in Fig. 156 as a function of the quantity vt'/h'. It is interesting to note that the maximum value is achieved when the distance y represented by vt' is one-half the virtual height h'. This effect will be noticeable in some of the numerical examples displayed below.

When the frequency is higher than a few hundred kilocycles, the term containing the skin thickness in (16.21) is not very important and may be dropped. Then the temperature at a depth x units below the surface of the metal is given by

$$u(t') = \frac{0.294P_m}{\sqrt{\pi k c\rho}\cdot\sqrt{vh'}}\cdot g\left(\frac{vt'}{h'}\right) - \frac{2P_m x}{4.187\pi h'k\left[1 + \left(\frac{vt'}{h'}\right)^2\right]^2}, \qquad (16.23)$$

while the temperature at the surface is given by the simple relation

$$u(t')_{x=0} = \frac{0.294P_m}{\sqrt{\pi k c \rho}\ \sqrt{vh'}} \cdot g\left(\frac{vt'}{h'}\right). \tag{16.24}$$

To apply these equations to specific problems, we may substitute the thermal constants for iron given in Table 9. Then (16.23) becomes

$$u(t') = \frac{0.437P_m}{\sqrt{vh'}} \cdot g\left(\frac{vt'}{h'}\right) - \frac{0.947P_m x}{h'\left[1 + \left(\frac{vt'}{h'}\right)^2\right]^2}, \tag{16.25}$$

while (16.24) reduces to

$$u(t')_{x=0} = \frac{0.437P_m}{\sqrt{vh'}} \cdot g\left(\frac{vt'}{h'}\right). \tag{16.26}$$

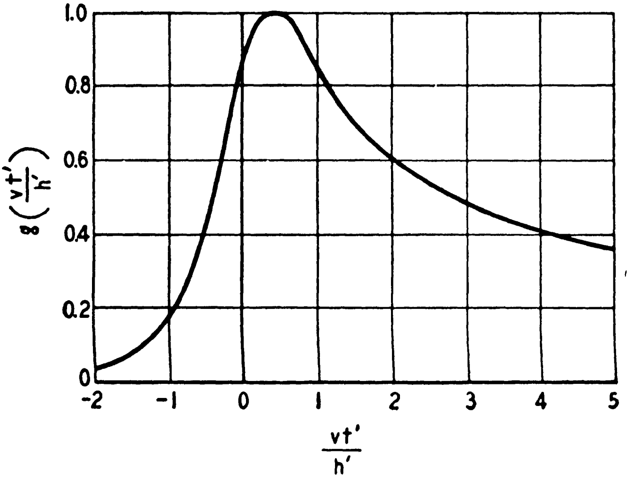

FIG. 156. The function $g(vt'/h')$ given by equation (16.22).

Surface Temperature as a Function of Scanning Speed and Power. It is quite apparent that the surface temperature will reach the highest temperature with slow scanning speed and high power. Quantitative relations may be displayed by means of a series of graphs, calculated from (16.26). Fig. 157 shows the surface temperature as a function of time for two scanning speeds where the power applied per unit length of conductor is the same for both speeds. That is, the power is 1000 watts per centimeter of length. If a cylindrical bar were being scanned, the total power required in the work would be obtained by multiplying P_m by the circumference of the work piece.

In preparing the curves of Fig. 158, the power P_m was increased to 2000 watts per centimeter and the scanning speed was stepped up to avoid melting of the surface. In each case, it is interesting to note that the maximum surface temperature occurs when the conductor has passed the point in question a distance which is exactly one-half the virtual height of the conductor. This displacement of the maximum-temperature point away from directly under the conductor is very evident in many scanning operations.

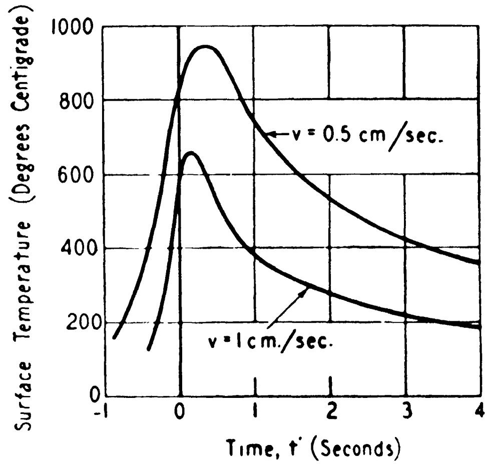

FIG. 157. Surface temperature as a function of time.
P_m = 1000 watts per centimeter
h = height of conductor = 0.5 centimeter
a = radius of conductor = 0.25 centimeter

When the power P_m is increased to 3000 watts per centimeter, the curves of Fig. 159 result. Here we see the extremely rapid decay of temperature which is so desirable in self-quenching operations.

In preparing Fig. 160, the scanning speed and power were adjusted to hold a constant maximum surface temperature. It is evident that high power with fast scanning gives faster quenching.

Surface Temperature As a Function of Conductor Height. Fig. 161 illustrates the need for crowding the conductor close to the work. Higher surface temperatures and quicker cooling are the results obtained from this procedure. Practical considerations such as mechanical tolerances and possibility of voltage breakdown between the coil and the work prevent this step being carried to the extreme.

A Nomograph for Determining Surface Temperature. A nomograph constructed from (16.26) is shown in Fig. 162. The dotted lines on this figure show the method of use A straight line is drawn from a desired point on the scale of virtual height to a point on the velocity scale. The point where this line crosses the vertical line A-A is marked. A straight line drawn from this point through a selected point on the power scale then intersects the surface temperature scale at the correct point. This surface temperature is, of course, the value of the maximum temperature achieved. With any three of the four variables known, the nomograph may be used to arrive at the value of the fourth variable.

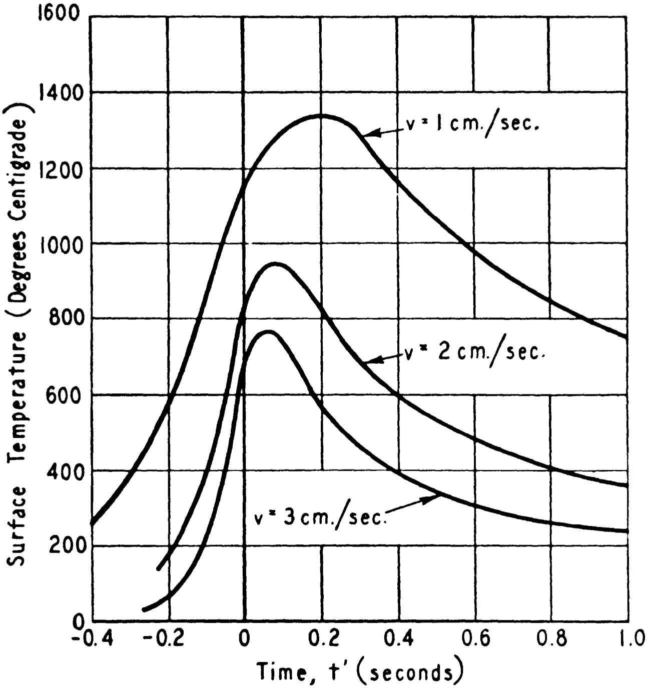

FIG. 158. Surface temperature as a function of time.

$P_m = 2000$ watts per centimeter
$h = 0.5$ centimeter
$a = 0.25$ centimeter

Control of Depth of Hardening. While the material presented above showed the factors affecting the temperature at the surface during scanning, a knowledge of the temperature distribution a short distance into the metal is important in studying a hardening problem where it is desired to control the depth of hardening. Equation (16.25) is especially useful for this purpose. Fig. 163 was constructed from this equation, and shows the rise and decay of the surface temperature as well as the temperature at two other points within the metal. We may note that a point which lies 0.08 centimeter from the surface of the metal reaches a temperature slightly below the temperature required for full hardening. Thus, with the set of conditions enumerated in the caption of Fig. 163, we might expect to harden a surface layer almost 0.08 centimeter in thickness. Also, we may note that the rate of cooling is high so that self-quenching might be expected.

A series of calculations similar to those presented in Fig. 163 were used to construct Figs. 164 and 165 Here, if we wish to heat a specified thickness of material to at least 800° C, we may find the conditions of power and scanning speed needed to bring about the desired result. In addition, the surface temperature may also be found. Fig. 164 applies where the virtual height of the conductor is 0.5 centimeter, while a virtual height of 0.25 centimeter was used in constructing Fig. 165.

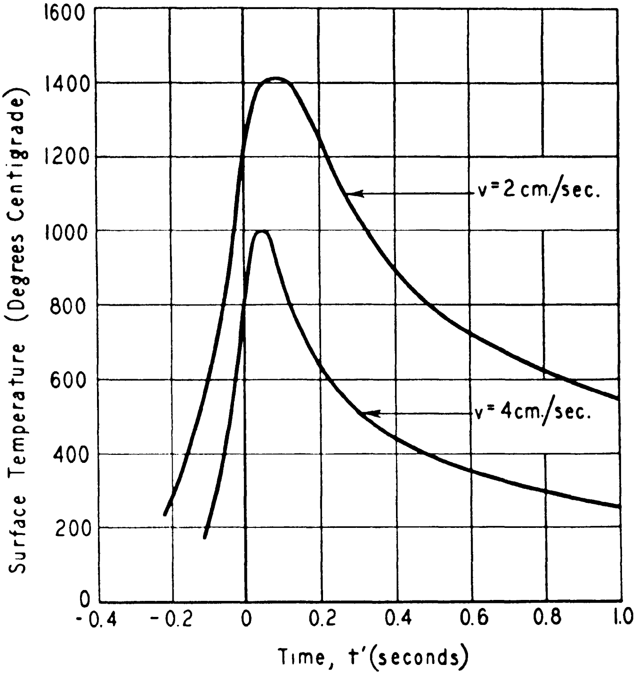

Fig. 159. Surface temperature as a function of time.
$P_m = 3000$ watts per centimeter
$h = 0.5$ centimeter
$a = 0.25$ centimeter

It should be remembered that the power requirements shown in these two figures do not include the power dissipated in the coupling coil. The power lost in the coupling coil may be estimated by the methods demonstrated in Chapter 8.

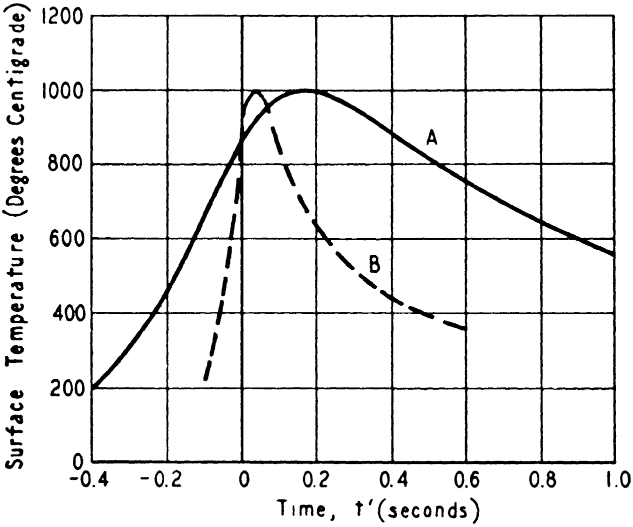

FIG. 160. Surface temperature as a function of time.
h = 0.5 centimeter, a = 0.25 centimeter
Curve A: P_m = 1500 watts per centimeter, v = 1.0 centimeter per second
Curve B: P_m = 3000 watts per centimeter, v = 4.0 centimeters per second

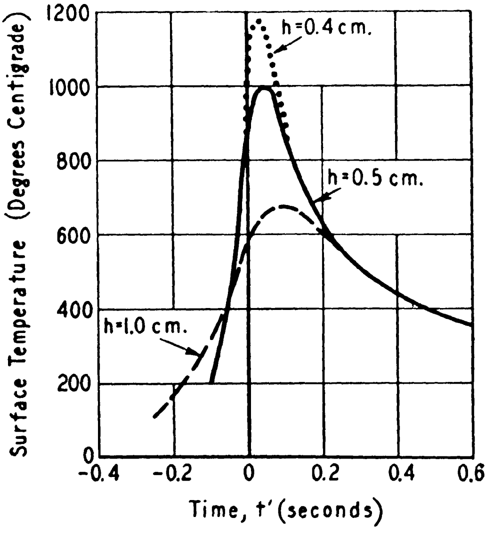

FIG. 161. Surface temperature for a number of conductor heights, where
a = 0.25 centimeter,
P_m = 3000 watts per centimeter, and
v = 4.0 centimeters per second.

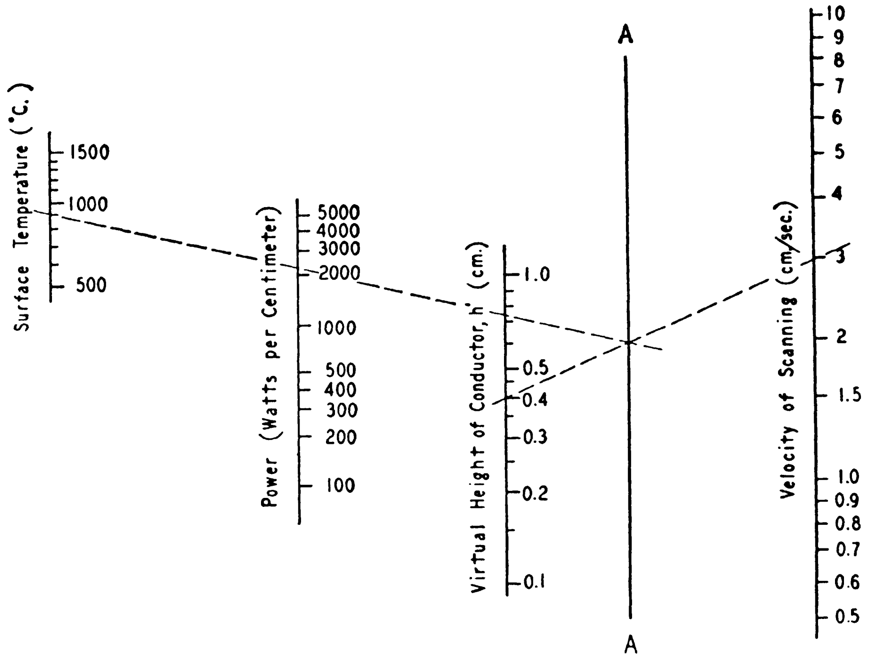
Surface Temperature (°C.)
1500
1000
500
Power (Watts per Centimeter)
5000
4000
3000
2000
1000
500
400
300
200
100
Virtual Height of Conductor, h' (cm.)
1.0
0.5
0.4
0.3
0.2
0.1
A
A
Velocity of Scanning (cm/sec.)
10
9
8
7
6
5
4
3
2
1.5
1.0
0.9
0.8
0.7
0.6
0.5

FIG. 162. A nomograph for determining maximum surface temperature when the scanning speed, virtual height of conductor, and velocity of scanning are known. The dotted lines illustrate the method of use.

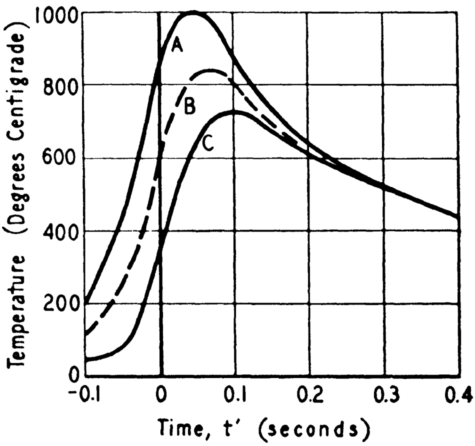

FIG. 163. Temperature variation at a number of points in the metal. The power per centimeter length is 3000 watts, while the scanning speed is 4.0 centimeters per second. The actual conductor height h is 0.5 centimeter, while the conductor radius is 0.25 centimeter.

Curve A: $x = 0$ Curve B: $x = 0.04$ centimeter Curve C: $x = 0.08$ centimeter

As an example of the use of these charts, let us suppose for the moment that we have been asked to harden the surface of the cylinder wall in an internal combustion engine to a depth of 0.05 centimeter. The cylinder has a circumference of 25 centimeters, and a length to be hardened of 20 centi-

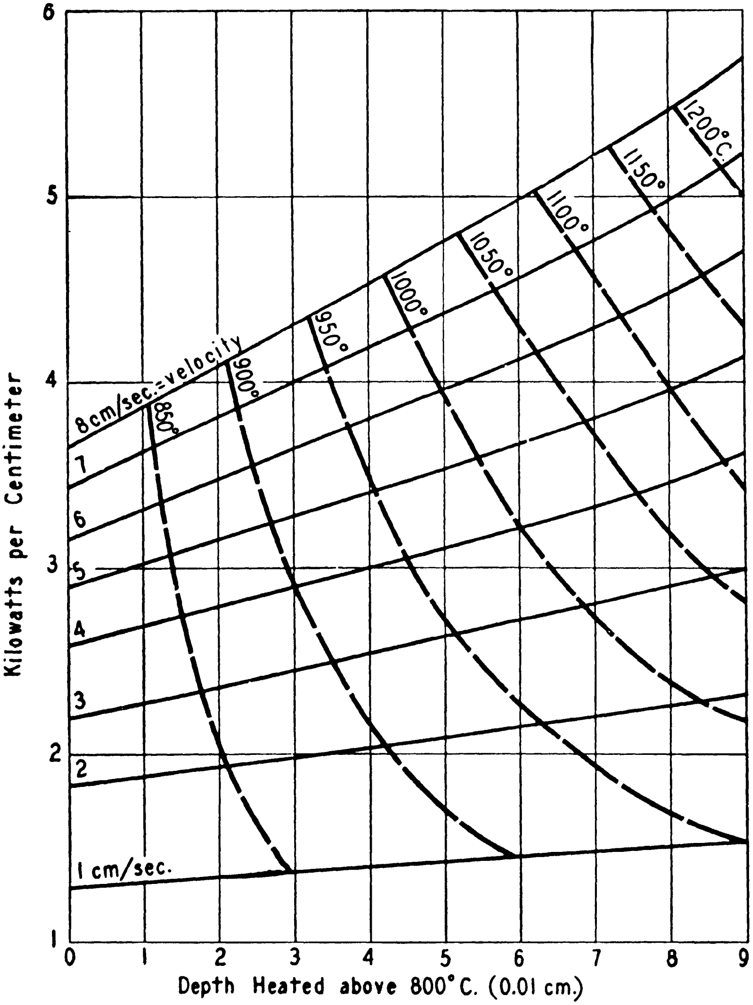

FIG. 164. Power concentrations (power per centimeter of length) necessary to heat all points in a given layer to a temperature above 800° C. The surface temperature and the scanning rate are shown as parameters. The *virtual* height of the scanning conductor is 0.5 centimeter.

meters. If we now choose a scanning speed of 5 centimeters per second, it is evident that 4 seconds will be required to completely scan the entire wall. On consulting Fig. 164, for the scanning speed specified and a depth of 0.05 centimeter to be heated above 800° C, we find that the power per centimeter of length along the inducing coil needs to be 3.54 kilowatts. Since the circumference is 25 centimeters, the total power into the steel is 88.5 kilowatts. The maximum surface temperature is 980° C.

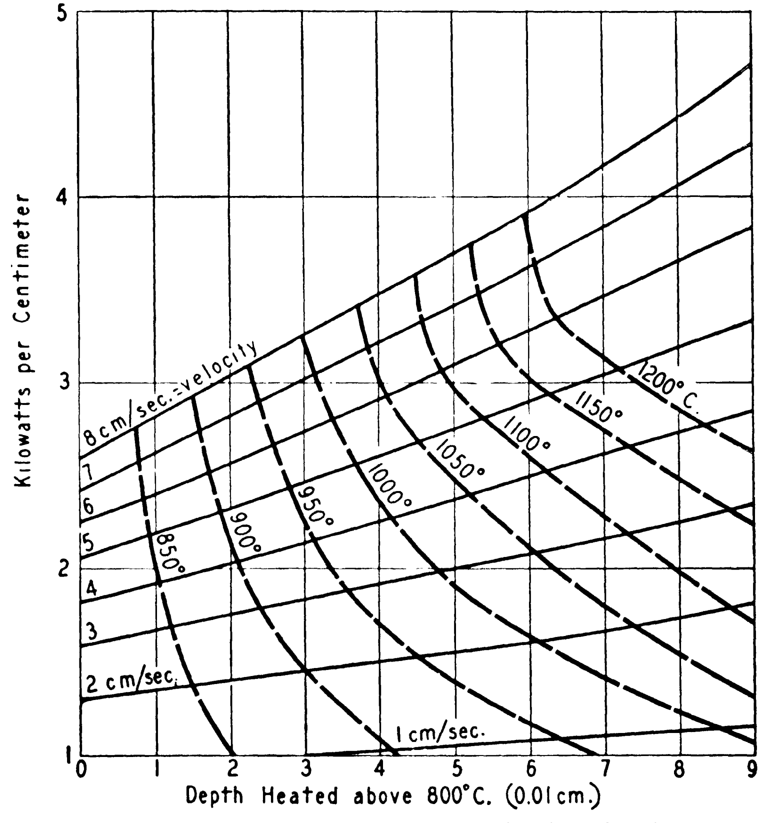

FIG. 165. Power concentrations necessary to heat all points in a given layer to a temperature above 800° C. The *virtual* height of the scanning conductor is 0.25 centimeter.

If we now drop the virtual height of the conductor to 0.25 centimeter, we find that the power per centimeter need only be 2.75 kilowatts, or a total power into the steel of 68.8 kilowatts. Over 20 per cent of the power is saved by using the closer coil spacing. In this case the surface temperature reaches 1075° C.

The Effect of Frequency on Scanning Efficiency. As stated previously, when the frequency is higher than a few hundred kilocycles, equation

(16.23) is a justifiable approximation. Here the temperature is entirely independent of frequency. At lower frequencies, this approximation is not valid and we must use equation (16.21). To find the temperature at the surface, we set $x = 0$ in (16.21) and obtain

$$u(t')_{x=0} = \frac{0.294P_m}{\sqrt{\pi k c \rho} \cdot \sqrt{vh'}} \cdot g\left(\frac{vt'}{h'}\right) - \frac{P_m s}{4.187\pi h' k\left[1 + \left(\frac{vt'}{h'}\right)^2\right]^2} \qquad (16.27)$$

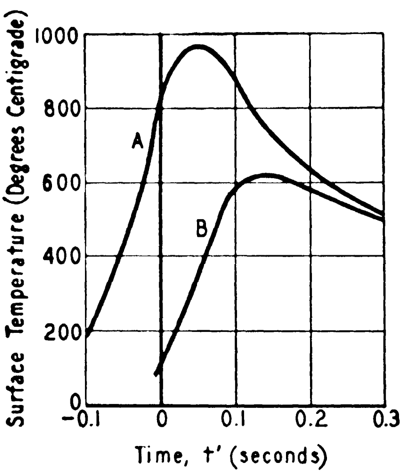

FIG. 166. A comparison of surface temperatures for two examples where the frequencies differ greatly. The conductor height, h, is 0.5 centimeter; the conductor radius, a, is 0.25 centimeter; and the velocity of scanning is 4.0 centimeters per second. The power concentration is 3000 watts per centimeter. Curve A: The frequency is 10^6 cycles per second. Curve B: The frequency is 10^4 cycles per second.

One is then confronted with the problem of assigning an appropriate power density to use in determining the skin thickness s from Fig. 138. For want of a better choice, we shall use as a power density that value occurring directly under the conductor. This is a maximum power density that a patch of surface is exposed to and it may be quickly determined by setting the dimension y equal to zero in (16.13).

Fig. 166 shows the surface temperature where the frequency is 1,000,000 cycles and again where the frequency is 10,000 cycles, with all other physical conditions unchanged. It is readily seen that the results with the low frequency are disappointing, since we must increase the power at least 50 per cent to reach the same surface temperature with the low frequency as we achieve with the higher.

Specific applications of radio-frequency power to the heating of metal objects are numerous. Many of these applications present interesting conditions in which the success of the method is limited only by the ingenuity of the engineer designing the coupling system. But the fundamental principles on which these applications must be based are those which have been carefully developed here. With a sound knowledge of the theoretical implications, the necessary " cut and try " experiments can be more objective and the evaluation of a practical solution has greater promise.

The literature [*], [†], [‡], [§], [||], [¶] is liberally sprinkled with descriptive details of actual " induction-heating " installations and reference to such descriptions is encouraged. It is often helpful to know how some analogous condition has been treated and then to adapt this procedure to the problem at hand. As time goes on these techniques may be improved and new applications may be discovered, but the fundamentals of heat-flow and the principles by which energy is coupled to the load are likely to remain unchanged. It is with this thought in mind that the authors have emphasized fundamentals and have refrained from an attempt to include numerous illustrative cases.

[*] Frank W. Curtis, *High-Frequency Induction Heating*, McGraw-Hill Book Company, Inc., New York.

[†] W. M. Roberds, " Coupling Methods for Induction Heating," *Electronic Industries*, Vol. 3, No. 4, April 1944, p. 80.

[‡] H. C. Humphrey, " Electronic Tin Fusion," *Proc. I. R. E.*, Vol. 32, No. 2, February 1944, p. 61.

[§] J. P. Taylor, " High-Speed Soldering with Radio-Frequency Power," *Electronics*, Vol. 17, No. 2, February 1944, p. 114.

[||] Edwin E. Spitzer, " Induction Heating in Radio Electron-Tube Manufacture," *Proc. I.R.E.*, Vol. 43, No. 3, March 1946, Section II, Waves and Electrons, pp. 110–115.

[¶] *Induction Heating*. Lectures presented by H. B. Osborne Jr., P. H. Brace, W. G. Johnson, J. W. Cable, and T. E. Eagan. American Society of Metals, Cleveland, Ohio, 1946.

Chapter 17

RADIO-FREQUENCY HEATING OF POOR ELECTRICAL CONDUCTORS

The Conduction of Current In Metals. In the previous chapters which treated the generation of heat by the flow of electric current in metals, we have characterized the heat-generating properties by assigning a value to the electrical conductivity. We have assumed that this specific conductivity was independent of frequency.

Metals, like all other matter, are made up of atoms characteristic to the particular substance. The atom in turn consists of the positively-charged nucleus and several negatively-charged electrons bound to the nucleus by forces of varying degree. An occasional electron frees itself from the nuclear forces so that in metals we find the structure to consist of the relatively-massive molecules formed by the combination of one or more atoms and a cloud of free electrons bouncing around at random with high velocities. Of course, the molecules also experience a random motion — that is, the motion associated with the heat-energy of the material. Because the free electrons are darting around in the spaces between the molecules, free electrons are continually being recaptured when they come under the influence of a molecule which lacks the normal complement of electrons. While this is taking place, other electrons are being freed so that the cloud of free electrons is kept at a fairly constant level.

Bennett and Crothers* indicate that in copper there may be as many as 1 free electron per atom and as few as 1 free electron per 3000 atoms, while Froehlich† indicates a value of 1 free electron per 2 atoms of copper. Estimates of this latitude indicate that the number of free electrons per cubic centimeter of copper lies between 3×10^{19} and 8×10^{22}.

When an electric field is impressed on a metal, the free electrons, negatively charged, are acted on by a force opposite in direction to the impressed field and the electrons thus are accelerated in this direction. Generally they do not go far but soon collide with a molecule. The energy of the moving electron is imparted to the molecule and thus contributes kinetic energy to the thermal motion of the molecule.

---

* Edward Bennett and Harold M. Crothers, *Introductory Electrodynamics For Engineers*, 1st ed., McGraw-Hill Book Company, Inc., New York, 1926, p. 203.

† Herbert Froehlich, *Elektronentheorie der Metalle*, Julius Springer, Berlin, pp. 189–190.

The directed motion of the free electrons in the direction opposite to the impressed field is superimposed upon the random motion of the electrons and represents a rather slow drift of the cloud of free electrons. This drift or motion represents what is usually called *conduction current.*

Dielectric Losses in Solids. Where the free electrons are great in number, as is the case in metals, the influence of the field in changing the orientation of atoms or molecules is trivial in comparison with the motion of the free electrons. In most solid materials which are not metallic, the free electrons are few in number. Then the action of the applied field on the massive particles becomes of importance. The applied fields cause displacement of electrons with respect to the nucleus of the atoms. In addition, there may be found a displacement of the atoms within the molecule.* This displacement, together with the rotation or orientation of the molecule, is most important in the range of frequencies which are useful for radio-frequency heating. As the molecules are rotated to line up with the electric field, an effective displacement of charge throughout the material takes place. Thus more capacity current flows than would be the case if the region were free space. The ratio of the capacity current through the material to the capacity current which would flow if the same field intensity were applied to free space is called the *dielectric constant.*

As the molecules rotate to come into alignment, they are acted on by forces of adjacent molecules and, of course, may collide with other moving molecules. These collisions impart kinetic energy to the thermal motion of the molecules, with accompanying temperature rise of the material. Thus we may speak loosely and say that the molecules are aligned by the impressed field and experience molecular friction during the alignment process. Since the energy necessary to overcome friction must be derived from the impressed field, an equivalent conduction current must flow into the material. That is, some of the current flowing into the material must be in phase with the voltage impressed on the material. Then the total current may be represented by (1.04), and we may begin to evaluate the results of the molecular action in engineering terms.

The power generated in a cube which is 1 centimeter on each side when a field intensity E volts per centimeter is impressed on the cube is

---

* For a very comprehensive treatment of the various factors involved in establishing the dielectric properties of materials, the reader is referred to an excellent series of papers on the subject: "The Dielectric Properties of Insulating Materials," E. J. Murphy and S. O. Morgan, *Bell System Technical Journal*, Vol. XVI, October 1937, pp. 493–512; Vol. XVII, October 1938, pp. 640–669; Vol. XVIII, July 1939, pp. 502–537.

$$P(\text{watts per cubic centimeter}) = E^2\sigma, \tag{17.01}$$

where σ is the conductivity of the centimeter cube. In the case of dielectrics, the conductivity may be a complicated function of frequency and is never a constant as in the case of metals.

When the conductivity, and hence the power factor (p.f.), is very small, equation (1.07) may be used to express the conductivity thus:

$$\sigma = 2\pi f p_0\epsilon \cdot (\text{p.f.}). \tag{17.02}$$

When (17.02) is substituted in (17.01), the power generated in a centimeter cube is

$$P = 2\pi f p_0\epsilon(\text{p.f.})E^2. \tag{17.03}$$

If the power factor and dielectric constant change slowly with frequency or if the product should chance to be a constant, it may be readily seen that the power generated for a constant value of electric intensity increases directly with frequency. Here lies the importance of the high frequencies for heating of poor conductors. This point will be further expanded in Chapters 19 and 20.

Equation (17.03) may be developed by another approach. When a capacitor is charged to a voltage, V, the potential energy stored in the capacitor is

$$\text{Stored energy (joules)} = \frac{CV^2}{2}. \tag{17.04}$$

We may postulate that if the capacitor contains a dielectric material the energy lost due to molecular rotation when the capacitor is charged to the voltage V and discharged is a constant fraction of the peak value of the stored energy represented by (17.04). We may call this constant fraction K.

Then the energy taken out during the course of a complete charge and discharge is

$$\frac{KCV^2}{2}.$$

In the case of a centimeter cube of material, the capacitance C is $p_0\epsilon$ where p_0 is the permittivity of free space and ϵ is the dielectric constant. In addition, we may assume that the applied voltage is varying sinusoidally with time, and the peak value of the voltage is $\sqrt{2} \cdot E$ where E is the r.m.s. value of the electric field intensity. Then the energy lost for a half cycle is

$$Kp_0\epsilon E^2$$

and the energy lost in a complete cycle is twice this value.

$$\text{Energy lost per cycle (joules)} = 2Kp_0\epsilon E^2. \qquad (17.05)$$

To obtain the energy lost per second, we multiply (17.05) by the frequency. This yields the power generated in a centimeter cube.

$$P(\text{watts}) = 2Kp_0\epsilon fE^2. \qquad (17.06)$$

A comparison of (17.06) with (17.01) shows that the effective conductivity is the coefficient of E^2 in (17.06), that is

$$\sigma = 2Kp_0\epsilon f. \qquad (17.07)$$

A more significant point is brought out by comparing (17.06) with (17.03). It is seen that

$$K = \pi \cdot (\text{p.f.}). \qquad (17.08)$$

Hence, if the postulate that the energy loss per cycle is constant holds true, we see that the power factor must also be a constant.

In some solid materials, the power factor is essentially independent of frequency. For many other solids, the power factor varies so slowly that it may be considered a constant for design purposes. It is in general difficult to properly design electrodes and coupling systems without knowing the values of the electrical constants of the materials to be heated. Much of the remainder of this chapter is devoted to describing in detail methods of measurement which the authors have found to be useful for the range of frequencies usually used in radio-frequency heating of dielectric materials.

Measurement of Dielectric Properties of Solids by Means of a *Q*-Meter. The type 160-A *Q*-meter, manufactured by the Boonton Radio Corporation, Boonton, New Jersey, affords a convenient and accurate means of determining the dielectric properties of materials for frequencies below 75 megacycles. A sandwich of the material to be measured is prepared and placed in the condenser shown in Fig. 167. The outer conducting sheet surrounds the dielectric material and is grounded, while the central plate forms the other plate of the condenser. The metal plates must be in good contact with the dielectric material. Since the outer sheet is grounded, a clamp may be placed on the specimen to insure adequate pressure.

The *Q*-meter contains a radio-frequency oscillator which produces a fixed voltage across a small resistor *r*, in Fig. 168. A vacuum-tube voltmeter indicates the voltage produced across the condenser *C*. The condenser *C* is tuned until the voltage registered by the vacuum-tube voltmeter is a maximum. The calibration of the instrument is such that the output meter registers the ratio of the voltage across the condenser to the voltage across the resistor *r*. This ratio is the *Q* of the entire circuit, and the output meter registers *Q* directly.

In Fig. 168, R_d represents the shunt resistance of the dielectric sample, while C_d is the capacitance of the sample.

A suitable coil is first placed on the proper terminals of the instrument, but the dielectric sample is not yet placed across the capacitor C. The capacitor C is adjusted to give a maximum reading on the output meter and the values of Q and C are recorded. Thus

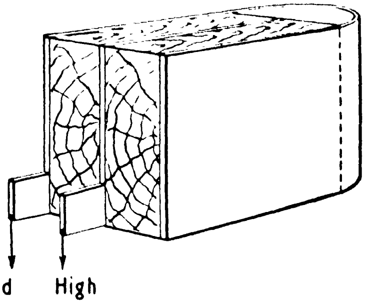

FIG. 167. Condenser for use with Q-meter in determining dielectric properties of solid materials.

Q_1 = value of Q measured without the dielectric sample.
C_1 = capacity used to tune the circuit under this condition, in micromicrofarads.

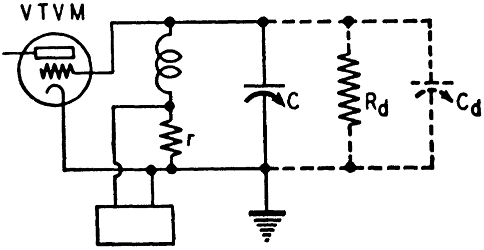

FIG. 168. Circuit of the Q-meter.

Next, the dielectric sample is placed on the terminals and new values of Q and C determined. Here

Q_2 = value of Q measured with dielectric sample in place.
C_2 = capacity used to tune the circuit when the dielectric sample is in place, in micromicrofarads.

These values are sufficient to yield the dielectric properties of the material. The capacity of the sandwich is

$$C_d = \frac{p_0 \epsilon A}{b} \text{ farads} = \frac{p_0 \epsilon A \cdot 10^{12}}{b} \text{ micromicrofarads,} \tag{17.09}$$

where

A = the total area of both sides of the central plate, in square centimeters;

b = the distance between the center plate and the ground plate, in centimeters;

p_0 = the permittivity of free space = 8.85×10^{-14};

ϵ = the dielectric constant of the material.

Since

$$C_d = C_1 - C_2, \tag{17.10}$$

the dielectric constant is

$$\epsilon = 11.3 \frac{b}{A} (C_1 - C_2). \tag{17.11}$$

If the conductivity σ of the dielectric material were known, the resistance R_d could be computed from

$$R_d = \frac{b}{\sigma A} \text{ ohms.} \tag{17.12}$$

The susceptance of the capacitor C_d is

$$\omega C_d = \frac{\omega p_0 \epsilon A}{b} \text{ mhos,} \tag{17.13}$$

where C_d is expressed in farads, and $\omega = 2\pi f$ (f = frequency in cycles per second).

Multiplying (17.12) by (17.13) yields

$$Q_x = \omega C_d R_d = \frac{\omega p_0 \epsilon}{\sigma}. \tag{17.14}$$

Equation (17.14) is the expression for the cotangent of the power-factor angle of the dielectric sample. The symbol Q_x has been introduced for convenience in writing the equations below.

Analysis of the circuits associated with the Q-meter shows that

$$Q_x = \frac{Q_1 Q_2}{Q_1 - Q_2} \cdot \frac{C_1 - C_2}{C_1}. \tag{17.15}$$

When (17.14) is substituted in (1.06), the power factor results:

$$\text{Power factor} = \frac{1}{\sqrt{Q_x^2 + 1}} \cdot \tag{17.16}$$

For values of Q_x greater than 10,

$$\text{Power factor} \doteq \frac{1}{Q_x} \cdot \tag{17.17}$$

An inspection of (17.15) and (17.16) shows that the power factor may be found without making use of the dimensions of the sample.

With Q_x and the dielectric constant at hand, the conductivity is obtained directly from (17.14).

$$\sigma(\text{mhos for a centimeter cube}) = \frac{\omega p_0 \epsilon}{Q_x} = \frac{55.6 \times 10^{-14} \epsilon\, f_{\text{cycles}}}{Q_x} \cdot \tag{17.18}$$

A sample of Douglas fir, with 7.5 per cent moisture, was prepared for measurement. A measurement was made at a frequency of 10 megacycles (10^7 cycles). The following quantities were measured:

C_1 = 97.5 micromicrofarads.
C_2 = 77.0 micromicrofarads.
Q_1 = 542.5.
Q_2 = 76.
A = 52 square centimeters.
b = 0.8 centimeter.

These numbers when substituted in (17.11) show that the dielectric constant ϵ is 3.56.

Next, substitution in (17.15) gives

$$Q_x = 18.6,$$

and in turn, making use of (17.17),

$$\text{Power factor} = 0.05375.$$

A simple substitution in (17.18) yields the specific conductivity.

$$\sigma = 1.063 \times 10^{-6} \text{ mhos for a centimeter cube}$$

$$= 1.063 \text{ micromhos for a centimeter cube.}$$

Fig. 169 shows measured values of dielectric constant, power factor, and conductivity for this same sample of Douglas fir as a function of frequency. The values below 100 megacycles were measured with the Q-meter, while those shown for frequencies above 100 megacycles were measured by methods which will be described later in this chapter. It may be seen that the power factor increases slightly with frequency, while the dielectric constant slowly falls. The result is that the product of dielectric constant and power factor remains fairly constant, and the conductivity increases almost as the first power of the frequency.

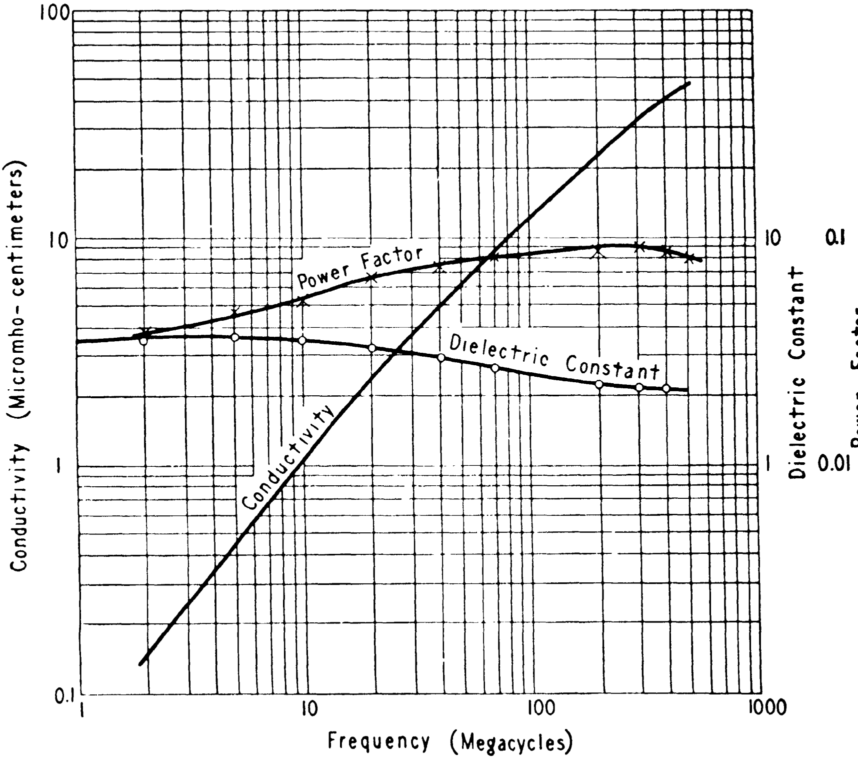

FIG. 169. Dielectric properties of Douglas fir. The moisture content is 7.5 per cent.

The Q-meter was used to measure the properties of four other materials. In each case, the dielectric constant remained essentially unchanged over the range of frequencies. The materials and the measured dielectric constants are listed.

Material	Dielectric Constant
1. White Vinylite (0.0625 inch thick)	3.7
2. Clear Vinylite (0.008 inch thick)	3.28
3. Mercerized Cloth	2.85
4. Natural Rubber	2.9

The power factors of these four materials are shown in Fig. 170. It may be noted that the power factor of the mercerized cloth and the natural rubber changes only slightly with frequency, while the power factor of Vinylite drops as the frequency increases. This drop is not great enough to overcome the effect of the frequency term in (17.02) so the conductivity still rises rapidly with frequency. The conductivity of the materials is shown in Fig. 171.

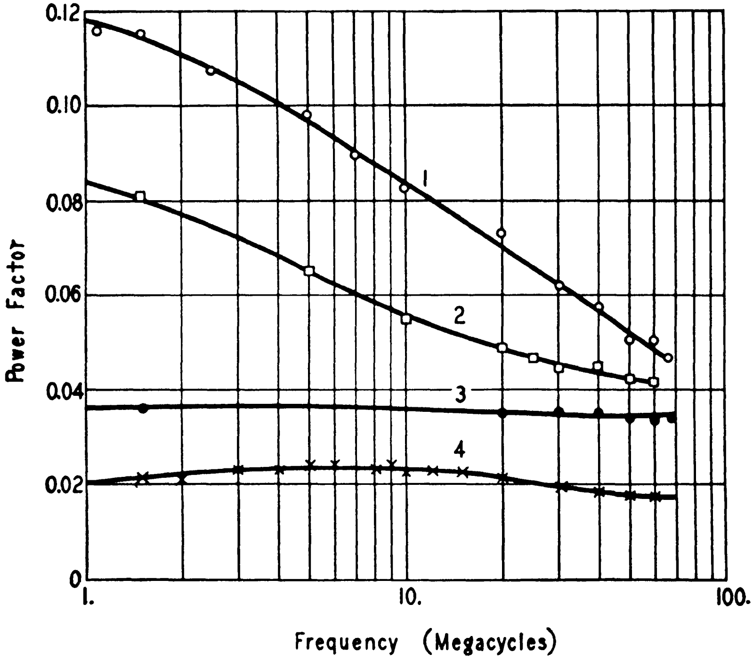

FIG. 170. Power factor of various materials.
1. White Vinylite
2. Clear Vinylite
3. Mercerized Cloth
4. Natural Rubber

Equation (17.01) may be used to find the field intensity in the material for a given power density. When the power generated in the material is 1 watt per cubic centimeter, the field intensity is

$$E(\text{volts per centimeter}) = \frac{1}{\sqrt{\sigma}} \tag{17.19}$$

where σ is expressed in mhos for a centimeter cube. The field intensity of the four materials under discussion is shown in Fig. 172 when the power

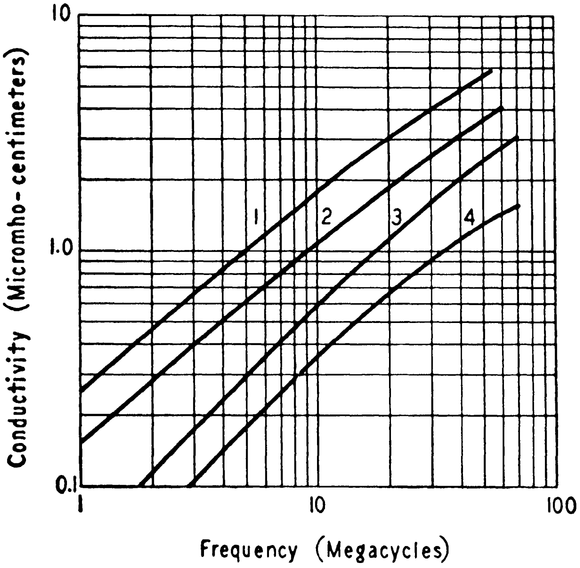

FIG. 171. Specific conductivity of the materials listed in Fig.170.

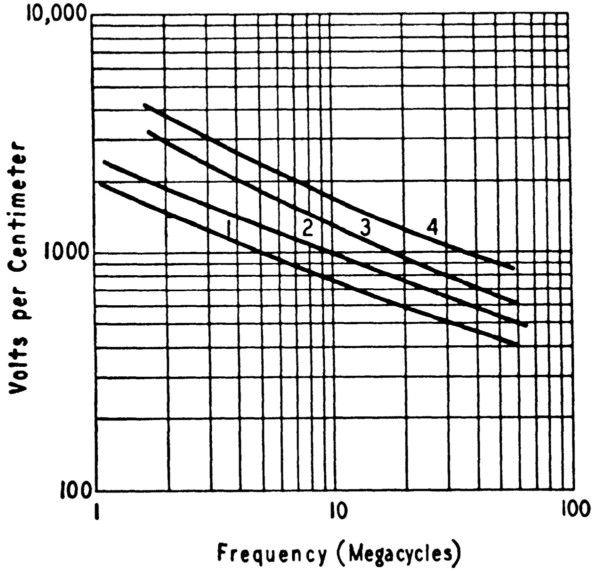

FIG. 172. Field intensity in materials, when the power concentration is 1 watt per cubic centimeter.

1. White Vinylite
2. Clear Vinylite
3. Mercerized Cloth
4. Natural Rubber

density is 1 watt per cubic centimeter. With a fixed power density, the electric intensity in the material drops rapidly as the frequency is increased. This effect indicates the desirability of high frequencies for dielectric heating, since high disruptive voltages may often be avoided by a shift to the high frequencies.

Measurement of Dielectric Properties of Liquids with a Q-Meter. The authors have found the Type 160-A Q-meter very useful in determining the dielectric properties of liquids. However, the technique of handling the material as well as the computations of the constants is quite different than the case of solid materials. A small cylindrical condenser is made up as shown in Fig. 173. This condenser is mounted on the terminals of the Q-meter and a suitable pipette is mounted above the condenser. The arrangement used by the authors is shown in Fig. 174. Three sets of readings are taken on the Q-meter. First, the condenser is removed from the terminals of the Q-meter and the Q of the coil and the tuning capacity are recorded. These values are called Q_1 and C_1, respectively. Then the empty condenser is placed on the terminals and a small amount of liquid is placed in the condenser. The amount need not be measured. Since the purpose is to eliminate edge effects in the next measurement, this first amount need only be enough to give a depth of liquid of about 1 centimeter. With this liquid in the container, the Q and tuning capacity are then measured. These values are called Q_2 and C_2. The third step is to inject a carefully measured amount of liquid until the Q is dropped considerably, taking care that the circuit is still tunable. With a volume V cubic centimeters injected, new values of Q and C are measured and called Q_3 and C_3.

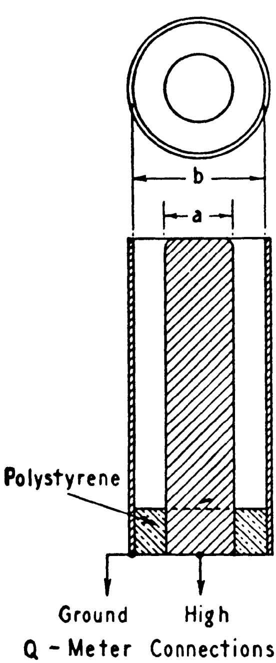

FIG. 173. Details of the cylindrical container used in measuring the properties of liquids and the Q-meter.

The diameter of the inside rod of the condenser is a centimeters, while the inside diameter of the outer conductor is b centimeters. Then the increase in height of the liquid when V cubic centimeters are injected is

$$h(\text{centimeters}) = \frac{4V}{\pi(b^2 - a^2)}. \tag{17.20}$$

The dielectric constant is then easily computed from the measurements.

$$\epsilon = \frac{(C_2 - C_3)(b^2 - a^2)\log_e \dfrac{b}{a}}{8p_0V} + 1, \tag{17.21}$$

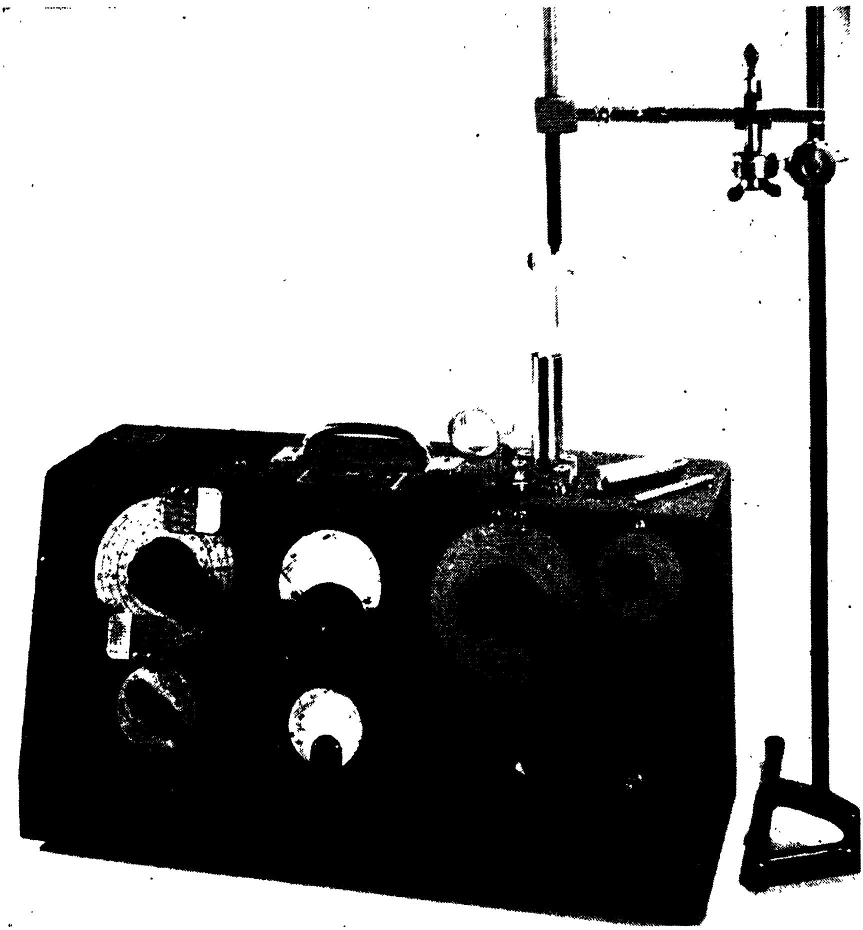

FIG. 174. A laboratory arrangement used to measure the properties of liquids.

where the capacities are expressed in farads and the logarithm is to the natural base. When the capacities are expressed in micromicrofarads, the formula is modified slightly.

$$\epsilon = \frac{1.414(C_2 - C_3)(b^2 - a^2)\log_e \frac{b}{a}}{V} + 1. \qquad (17.22)$$

The conductivity is given by the following equation:

$$\sigma(\text{mhos for a centimeter cube}) = \frac{0.786 f C_1 \cdot 10^{-12}}{V} \cdot \frac{(Q_2 - Q_3)}{Q_2 Q_3} (b^2 - a^2) \log_e \frac{b}{a}, \qquad (17.23)$$

where the frequency f is expressed in cycles and the capacity C_1 is measured in micromicrofarads. Then the power factor is found by means of either (1.06) or (1.07).

The method of measurement outlined above has been applied to many liquids. Fig. 175 shows typical values obtained with raw linseed oil. The dielectric constant is not displayed graphically since it was found to be essentially 2.7 over the entire range of frequencies The measurements shown in Fig. 175 for frequencies above 100 megacycles were made by the transmission-line method described below.

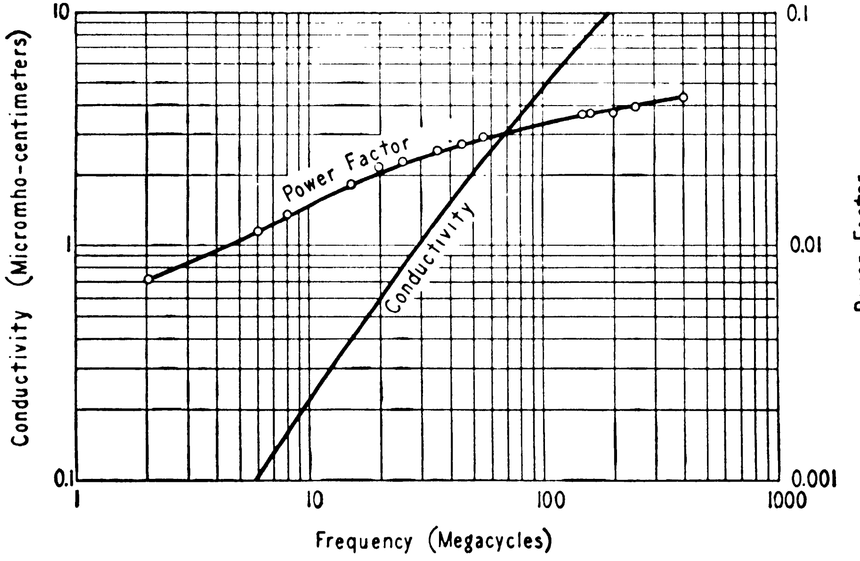

FIG. 175. Dielectric properties of raw linseed oil.

The Concentric Transmission-Line Method of Determining Dielectric Properties. When measurements of dielectric properties are needed at frequencies above 75 megacycles, it is necessary to turn to other techniques than those already described. The authors have found that a method centered about the determination of standing waves on transmission lines is very useful in the higher frequency range.

If a wave is sent along a transmission line which is short-circuited at the remote end, the reflected wave will interfere with the original wave and standing waves will be found along the line. In a concentric line these may be detected by a vacuum-tube voltmeter or a crystal detector probing into the line through a narrow slot in the outer conductor. Such a line is shown in Fig. 176, especially adapted for measuring the dielectric properties of fluids.

The signal at a desired radio-frequency, is fed into the line at the right side in Fig. 176, while the end at the left is short-circuited. There are no insulators supporting the inner conductor in the region where standing-wave measurement is to be made, as otherwise undesirable electrical discontinuities would be introduced. The inner conductor is supported by the short-circuiting plate on the left side and an insulator at the extreme right side of the line. It is important that the inner conductor be rigid enough to prevent sagging which may introduce spurious readings.

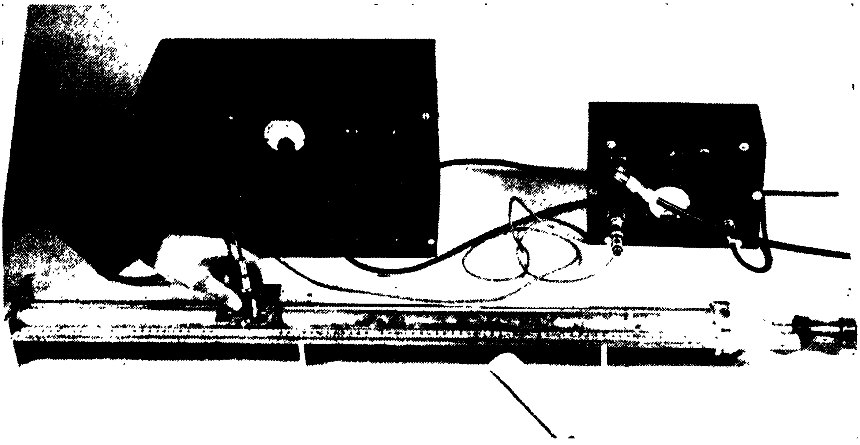

FIG. 176. Apparatus used in determining dielectric properties by the concentric transmission line method.

The probe on the line shown in Fig. 176 carries high-frequency signal to the receiver in the background. This receiver is of the superheterodyne type, with a crystal used for the first mixer stage. Several step-attenuators are used so that a wide range of received voltage may be measured. The oscillator which supplies signal to the line is not shown in Fig. 176.

The same transmission line may be used for the measurement of dielectric properties of solids. The sample of solid material may be prepared in the form of several short cylinders which are inserted in the line. Care should be exercised to insure a tight fit with both the inner and outer conductor In the foreground of Fig. 176 may be seen a piece of Douglas fir prepared for use in the transmission line. It may be noted that a groove has been provided for the probe. The measurements shown in Fig. 169 at frequencies above 100 megacycles were obtained by means of this transmission line filled with cylinders of Douglas fir. The high-frequency measurements on linseed oil shown in Fig. 175 were obtained with the same apparatus.

The experimental technique consists of moving the probe along the line from the short-circuited end toward the generator. The voltage at the short circuit is zero. As the probe is moved away from this point, the voltage rises rapidly to a maximum value which is recorded. As the probe is moved still further, the voltage passes through a minimum value. The minimum voltage as well as its position on the line are noted. Except in special cases which will be discussed later, the dielectric properties are then easily found from the ratio of the minimum voltage to the maximum voltage and the distance from the short-circuited end to the first minimum voltage point. Since the ratio of the voltages are used, it is not necessary that the probe and receiver have an absolute calibration. The only requirement is that the response of the receiver be linear with input voltage.

The behavior of a wave traveling along a transmission line may be described in terms of its complex propagation constant $\alpha + j\beta$, where α is the attenuation factor and β is the phase factor. The main wave traveling down the line toward the short circuit from the generator is

$$E_m = A\epsilon^{(\alpha+j\beta)x}, \tag{17.24}$$

where x is measured from the short circuit toward the generator. The reflected wave is

$$E_r = B\epsilon^{-(\alpha+j\beta)x}. \tag{17.25}$$

At the end of the line ($x = 0$) the total voltage must be zero. Thus, the factor B must be equal to A but with a negative sign. Then the total voltage at any point on the line is

$$E = E_m + E_r = A[\epsilon^{(\alpha+j\beta)x} - \epsilon^{-(\alpha+j\beta)x}]. \tag{17.26}$$

This equation may be rewritten thus:

$$E = A[(\epsilon^{\alpha x} - \epsilon^{-\alpha x}) \cos \beta x + j(\epsilon^{\alpha x} + \epsilon^{-\alpha x}) \sin \beta x], \tag{17.27}$$

and the absolute value is

$$E = A\sqrt{\epsilon^{2\alpha x} + \epsilon^{-2\alpha x} - 2 \cos 2\beta x}. \tag{17.28}$$

At any given frequency, α and β are constants, and therefore may be expressed as a constant ratio.

$$m = \frac{\alpha}{\beta} \tag{17.29}$$

When this substitution is made, (17.28) becomes

$$E = A\sqrt{\epsilon^{2m\beta x} + \epsilon^{-2m\beta x} - 2 \cos 2\beta x}. \tag{17.30}$$

The wave length λ_D in the dielectric medium may be defined as the distance that the main (or reflected) wave travels along the line while it undergoes a complete phase change of 2π radians. Hence,

$$\beta\lambda_D = 2\pi \tag{17.31}$$

and (17.30) becomes

$$E = A\sqrt{\epsilon^{4\pi mx/\lambda_D} + \epsilon^{-4\pi mx/\lambda_D} - 2\cos\left(\frac{4\pi x}{\lambda_D}\right)}. \tag{17.32}$$

Equation (17.32) is now in a form where we can begin to extract some important information. Fig. 177 shows the relative voltage distribution along the transmission line as a function of x/λ_D for a number of values of m. For $m = 0$, it may be seen that the voltage goes completely to zero at points which are exactly one-half wave apart. As m assumes finite values, the maximums rise slowly and the minimum values are no longer zero but increase uniformly along the line. In addition, it should be noted that the first minimum position shifts slightly to the left at the half-wave point.

For values of m less than 0.1, the first maximum occurs when x/λ_D is 0.25 and the first minimum occurs when x/λ_D is 0.5. We first let x/λ_D equal 0.25 in (17.32). Then

$$E(\text{first maximum}) = A\sqrt{\epsilon^{m\pi} + \epsilon^{-m\pi} + 2}. \tag{17.33}$$

By making use of the series expansion

$$\epsilon^{\pm\theta} = 1 \pm \theta + \frac{\theta^2}{2} \pm \frac{\theta^3}{2\cdot 3} + \frac{\theta^4}{2\cdot 3\cdot 4} \pm \cdots \tag{17.34}$$

and neglecting second order terms, (17.33) is seen to be

$$E(\text{first maximum}) \doteq 2A. \tag{17.35}$$

Next we set x/λ_D equal to 0.5 in (17.32). Then

$$E(\text{first minimum}) = \sqrt{\epsilon^{2m\pi} + \epsilon^{-2m\pi} - 2} \tag{17.36}$$

and when we use the first three terms of the series expansion for the exponential,

$$E(\text{first minimum}) = 2\pi mA. \tag{17.37}$$

Dividing (17.37) by (17.35) we find

$$m = \frac{\mathfrak{R}}{\pi}, \tag{17.38}$$

where $\mathfrak{R}$ is the ratio of the voltage at the first minimum point to the voltage at the first maximum point.

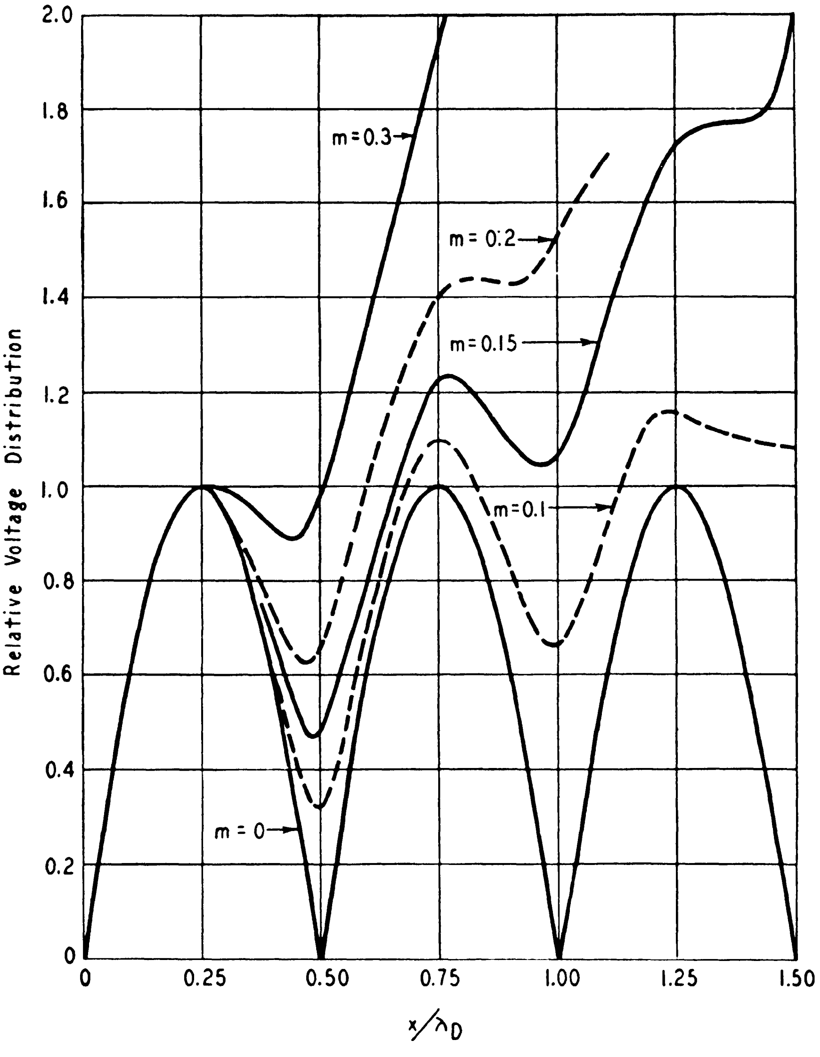

FIG. 177. Relative voltage distribution along the transmission line. The parameter m is the ratio of the attenuation factor to the phase factor.

The propagation constant for a uniform transmission line is*

$$\alpha + j\beta = \sqrt{(R + j\omega L)(G + j\omega C)}, \tag{17.39}$$

---

* E. A. Guillemin, *Communication Networks*, Vol. II, John Wiley & Sons, Inc., New York, p. 29, Equation (43a).

where

R = the series resistance per unit length of line;
L = the series inductance per unit length of line;
C = the shunt capacitance per unit length of line;
G = the shunt leakage conductance per unit length of line;
$\omega = 2\pi f$;
f = the frequency of the generator, in cycles per second.

In the case of our copper concentric measuring line, we may neglect the resistance R in comparison with the other factors. Then substituting (17.29) in (17.39),

$$\beta(m + j) = \sqrt{j\omega L(G + j\omega C)}. \tag{17.40}$$

Next, we square both sides of (17.40) and obtain

$$\beta^2(m^2 - 1 + j2m) = j\omega L(G + j\omega C) \tag{17.41}$$

or

$$G + j\omega C = \frac{2m\beta^2}{\omega L} + \frac{j\beta^2(1 - m^2)}{\omega L} \tag{17.42}$$

Equating the reals and then the imaginaries of (17.42), we find

$$G = \frac{2m\beta^2}{\omega L} \tag{17.43}$$

and

$$\omega C = \frac{\beta^2(1 - m^2)}{\omega L}\cdot \tag{17.44}$$

Dividing (17.43) by (17.44),

$$\frac{G}{\omega C} = \frac{2m}{1 - m^2}\cdot \tag{17.45}$$

We shall now define x_1 as the distance from the short-circuited end of the line to a point which is one-half wave length closer to the generator, where the wave length is defined by (17.31). The significance of this choice of nomenclature will soon be apparent. Then

$$\beta = \frac{\pi}{x_1} \tag{17.46}$$

and (17.44) yields

$$C = \frac{1 - m^2}{4f^2 L x_1{}^2}\cdot \tag{17.47}$$

The value C used above is the capacity per unit length of line, when the line is filled with the dielectric material. When the dielectric material is removed and only air remains between the conductors, the capacity per unit length is C_0. The inductance per unit length, L, is the same for both conditions. The ratio of these two values of capacitance is the dielectric constant of the medium. That is,

$$C/C_0 = \epsilon = \frac{1 - m^2}{4f^2LC_0x_1^2}. \tag{17.48}$$

But it may be recalled that in a simple transmission line which contains no dielectric medium,

$$c^2 = \frac{1}{LC_0} \tag{17.49}$$

where $c = 3 \times 10^{10}$ centimeters per second, the velocity of radio waves in free space. Then the wave length in free space is

$$\lambda_0 \text{ (centimeters)} = \frac{3 \times 10^{10}}{f}, \tag{17.50}$$

where the frequency f is expressed in cycles per second.

Using (17.49) and (17.50) in (17.48), we find

$$\epsilon = \frac{\lambda_0^2}{4x_1^2}(1 - m^2). \tag{17.51}$$

Since the leakage conductance G and the susceptance ωC are dimensionally alike, we may immediately write (17.45) in terms of the specific conductivity and the dielectric constant. Thus

$$\frac{\sigma}{\omega p_0 \epsilon} = \frac{2m}{1 - m^2}. \tag{17.52}$$

Hence, by substituting (17.52) directly in (1.06), we find

$$\text{Power factor} = \frac{2m}{1 + m^2}. \tag{17.53}$$

Again we turn to (17.52) to find the specific conductivity.

$$\sigma = \frac{2m\omega p_0 \epsilon}{1 - m^2}. \tag{17.54}$$

After substituting (17.51) and (17.50) in (17.54), and remembering that

$$\pi p_0 c = \frac{1}{120},$$

it may be seen that

$$\sigma \text{ (mhos for a centimeter cube)} = \frac{\lambda_0 m}{120x_1^2}. \tag{17.55}$$

It has thus been shown that the three important dielectric properties, dielectric constant, power factor, and conductivity are given by (17.51), (17.53), and (17.55), respectively, when the parameter m, the half-wave length in the dielectric medium x_1, and the wave length in free space λ_0 are known.

When the ratio of the first minimum of voltage to the first maximum $\mathcal{R}$ is found to be less than 0.3, (17.38) may be used immediately to find the parameter m. When the ratio $\mathcal{R}$ is greater than 0.3, the values of m may be found from the following table, which was constructed from Fig. 177.

TABLE 11. RELATION BETWEEN THE MEASURED RATIO $\mathcal{R}$ AND THE PARAMETER m.

$\mathcal{R}$	m	$\mathcal{R}$	m
0.30	0.0955	0.60	0.196
0.31416	0.10	0.65	0.213
0.35	0.1112	0.70	0.231
0.40	0.129	0.75	0.249
0.45	0.147	0.80	0.268
0.50	0.163	0.85	0.286
0.55	0.179	0.90	0.305

The distance x_1 has been defined as the half-wave length in the dielectric. When the ratio $\mathcal{R}$ is less than 0.3, the distance x_1 may be taken directly as the distance from the end of the line to the first minimum. For larger ratios, the measured distance is smaller than the correct half-wave length. Then it is necessary to refer to Table 12 to find the factor by which the measured distance to the first minimum of voltage must be multiplied to obtain the correct value of x_1 to be substituted in the above equations.

TABLE 12. CORRECTION FACTOR FOR FINDING THE HALF-WAVE LENGTH IN THE DIELECTRIC.

The Parameter m	The Factor which Multiplies the Measured Distance Between the End of the Line and the First Minimum-Voltage Point to Obtain the Value x_1
0.10	1.0040
0.125	1.0162
0.15	1.0225
0.175	1.0395
0.20	1.0526
0.225	1.0683
0.25	1.0869
0.275	1.1111
0.30	1.1312

As a specific example, we shall use the data obtained for Douglas fir, with the end results displayed in Fig. 169. At a frequency of 200 megacycles, the measured ratio $\mathcal{R}$ was found to be 0.135, with the first minimum of voltage occurring 50.2 centimeters from the end of the line. Here we may use (17.38) directly to find

$$m = \frac{0.135}{\pi} = 0.043.$$

A glance at Table 12 reveals that we need not correct the measured distance to the minimum voltage, so $x_1 = 50.2$ centimeters. At the operating frequency, $\lambda_0 = 150$ centimeters.

Then (17.51) yields the dielectric constant

$$\epsilon = 2.23.$$

Substitution of m directly in (17.53) shows the power factor to be 0.086 while (17.55) tells us that the conductivity is 21.4×10^{-6} mho for a centimeter cube.

When using the concentric transmission-line method to determine the dielectric properties of materials, great care must be exercised to provide adequate shielding of the receiver and the lead from the probe to the receiver. Otherwise, extraneous voltages may be induced in the receiver by the stray fields of the oscillator with large errors resulting.

The reader may be interested to note that (17.51), (17.53), and (17.55), which are used to calculate the dielectric properties, do not include dimensions of the transmission line. It is thus evident that any reasonable choice of diameters for the inner and outer conductors is possible.

Debye's Relation and the Equivalent Circuit of Polar Liquids. In order to account for the dielectric properties of certain liquids, Debye* has postulated the existence of *polar molecules*, that is, molecules in which the atoms are unsymmetrically located thus imparting a permanent electric moment to the molecule.

When no external electric field exists, the molecules may be oriented in random fashion. The application of an external electric field causes the polar molecules to rotate and orient themselves in the direction of the applied field. Thus an effective displacement of charge exists throughout the material, manifested by a large dielectric constant. It is assumed that the strong interaction between adjacent molecules exerts a frictional force proportional to the rotational velocity of the molecule.

At the low-frequency end of the spectrum, the rotational velocity is low, so little energy is converted to heat. However, the rotational orientation of the polar molecules is complete, thus producing a high dielectric constant.

---

* P. Debye, *Polar Molecules*, Chemical Catalogue Company, New York (1929), pp. 59–76.

On the other hand, when the frequency is very high, the molecules have only begun to orient themselves when it is time to move in the reverse direction. Then the contribution to the dielectric constant is small. At the same time, the rotational velocity is high resulting in large generation of heat.

Under the above assumptions, Debye* arrives at relations for the dielectric properties which he expresses as a complex dielectric constant. A certain amount of effort reveals that the Debye equation may be used to obtain the admittance of a centimeter cube of material in the following general form.

$$Y = \sigma + j\omega p_0\epsilon = a\frac{b^2f^2}{1+b^2f^2} + j\left\{cf + a\frac{bf}{1+b^2f^2}\right\}, \qquad (17.56)$$

where a, b, and c are constants of the material and f is the frequency.

Murphy and Morgan† point out that this equation may be represented by a circuit which consists of an air condenser in series with a fixed resistance, the whole combination shunted by another air condenser. Whitehead‡ recalls that A. Hess§ had also arrived at a circuit model which represented the action of dielectric materials.

To quote from Whitehead:

> "He conceived a simple model of a Maxwell dielectric consisting of two condensers in series, one having an infinite resistance and the other a definite value of conductivity. He investigated the behavior of this model under alternating potential difference and found that it accounted approximately for the results of experiment."

Either circuit model is sufficient to produce results in agreement with (17.56) but the authors have chosen to build around the model of Murphy and Morgan. This model is shown in Fig. 178. When free ions or electrons are present to a certain degree, a finite value of conductivity will exist at extremely low frequencies. Thus to fully represent the dielectric properties a resistance must be shunted across the circuit of Fig. 178 with the resulting network shown in Fig. 179. The admittance of this circuit may be shown to be

$$Y = \frac{1}{R_1} + \frac{1}{R_2}\cdot\frac{(\omega C_2R_2)^2}{[1+(\omega C_2R_2)^2]} + j\left\{\omega C_1 + \frac{1}{R_2}\cdot\frac{\omega C_2R_2}{[1+(\omega C_2R_2)^2]}\right\}. \qquad (17.57)$$

When the circuit is to represent the admittance of a centimeter cube of material, the specific conductivity is then

---

* P. Debye, *loc. cit.*, Equation (69), p. 97.

† E. J. Murphy and S. O. Morgan, "The Dielectric Properties of Insulating Materials," *Bell System Technical Journal*, Vol. XVIII, July 1939, pp. 515–516.

‡ J. B. Whitehead, *Lectures on Dielectric Theory and Insulation*, McGraw-Hill Book Company, Inc., New York, 1927, p. 83.

§ A. Hess, *Jour. Phys.*, 1: 145, 1893, and *Eclair. Elect.*, 205, 1895.

$$\sigma = \frac{1}{R_1} + \frac{1}{R_2} \cdot \frac{(\omega C_2 R_2)^2}{[1 + (\omega C_2 R_2)^2]}, \tag{17.58}$$

and the susceptance is

$$\omega p_0 \epsilon = \omega C_1 + \frac{1}{R_2} \cdot \frac{\omega C_2 R_2}{[1 + (\omega C_2 R_2)^2]}. \tag{17.59}$$

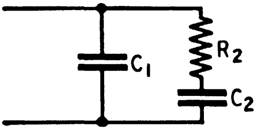

FIG. 178. The equivalent circuit proposed by Murphy and Morgan to represent the dielectric behavior of polar liquids.

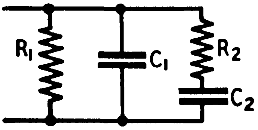

FIG. 179. A modified circuit which includes the effect of conduction by free ions or electrons.

We shall now demonstrate the method of evaluating the circuit constants by means of a specific example. A number of measurements were made on a sample of cyclohexanone.

Measurements of conductivity at a number of frequencies between 60 and 1000 cycles revealed that in this region the specific conductivity was constant at 0.59×10^{-6} mho for a centimeter cube. Examination of (17.58) reveals that the conductivity at low frequencies is $1/R_1$. Thus

$$\frac{1}{R_1} = 0.59 \times 10^{-6} \text{ mho}$$

or

$$R_1 = 1.695 \times 10^6 \text{ ohms.}$$

At extremely high frequencies, the dielectric constant becomes equal to the square of the index of refraction measured in the visible spectrum. For cyclohexanone, the index of refraction is 1.45 and the dielectric constant assumes a value of 2.1 for the extremely high frequencies.

For sufficiently high frequencies, the last term in (17.59) may be neglected. Then

$$\omega p_0 \epsilon = \omega C_1.$$

Hence

$$C_1 = p_0 \epsilon = 8.85 \times 10^{-14} \times 2.1 = 0.1858 \times 10^{-12} \text{ farad.}$$

When the frequency is low,

$$1 + (\omega C_2 R_2)^2 \doteq 1$$

and (17.59) becomes

$$\omega p_0 \epsilon = \omega C_1 + \omega C_2 = \omega(C_1 + C_2).$$

The dielectric constant was measured with the apparatus shown in Fig. 174, and for the low radio frequencies was found to be 15.4, a value which readily yields

$$C_1 + C_2 = p_0 \epsilon = 8.85 \times 10^{-14} \times 15.4 = 1.362 \times 10^{-12} \text{ farad}$$

and we then find

$$C_2 = 1.176 \times 10^{-12} \text{ farad.}$$

The conductivity of the liquid was then measured at a frequency of 30×10^6 cycles, that is, 30 megacycles. The conductivity had a value of 1.2×10^{-6} mho for a centimeter cube. We then turn to (17.58). At this frequency, the denominator of the last term may be placed equal to unity. Then

$$\sigma = \frac{1}{R_1} + (\omega C_2)^2 R_2.$$

Since we know all the quantities in this expression except R_2 we may easily solve for the latter quantity and find that

$$R_2 = 12.38 \text{ ohms.}$$

Now (17.58) and (17.59) may be used to calculate the dielectric properties of cyclohexanone since all the constants have been evaluated. The curves shown in Fig. 180 were calculated from these equations while the experimental points were obtained by means of the Q-meter. It may be seen that there is rather good agreement with the behavior predicted from the circuit model. Measurements of the dielectric properties were made up to 600 megacycles, using the concentric transmission-line method. The experimental data are shown in Fig. 181, together with the curves calculated from the circuit model.

We have thus constructed a model which has represented truly the state of the material from a frequency of 60 cycles to 600 megacycles, a range of 10,000,000: 1 in frequency. If we are then willing to extrapolate into the unknown, we may continue to calculate the values corresponding to higher frequencies. This procedure results in Fig. 182, where the highest frequency shown, 100,000 megacycles, corresponds to a wave length in free space of 3 millimeters. Here the dielectric constant has dropped almost to the value obtained from the square of the index of refraction. It is interesting to note the peak of power factor at a frequency of 30,000 megacycles, corresponding to a free-space wave length of 1 centimeter.

It is well to remember that the picture presented in Fig. 182 is entirely unsupported by experimental data at frequencies above 600 megacycles.

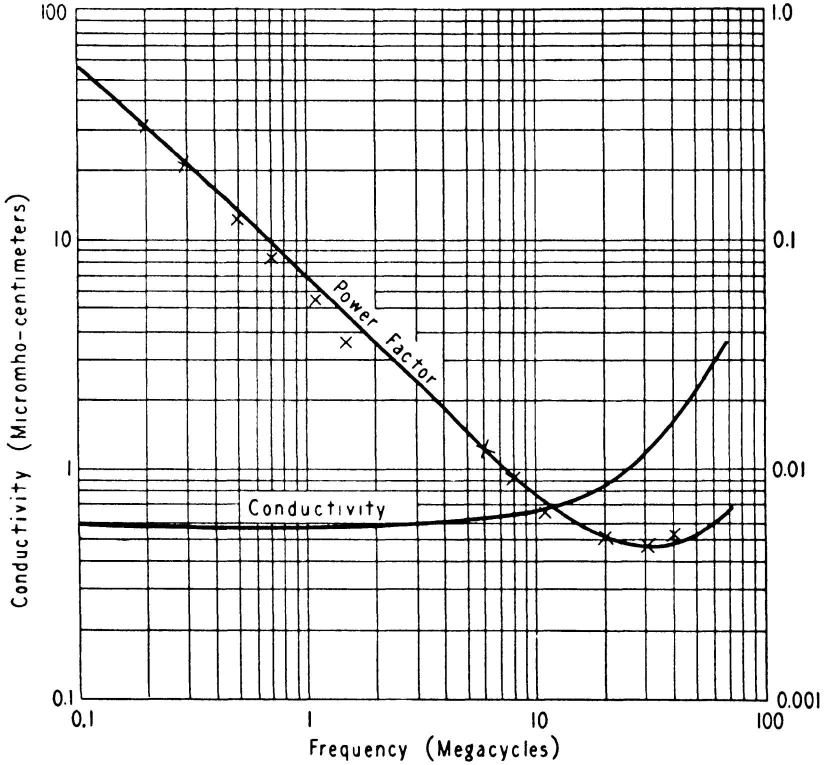

FIG. 180. Power factor and conductivity of cyclohexanone together with measured data The temperature is 20° C.

A similar equivalent circuit was constructed for glycerine. With a refractive index of 1.4729, we find the dielectric constant in the visible spectrum to be 2.17, while the low-frequency dielectric constant is 38.4. The appropriate circuit constants are then

$$R_1 = 3.09 \times 10^6 \text{ ohms};$$
$$R_2 = 188 \text{ ohms};$$
$$C_1 = 0.192 \times 10^{-12} \text{ farad};$$
$$C_2 = 3.208 \times 10^{-12} \text{ farad}.$$

The curves shown in Fig. 183 were calculated from the equivalent circuit

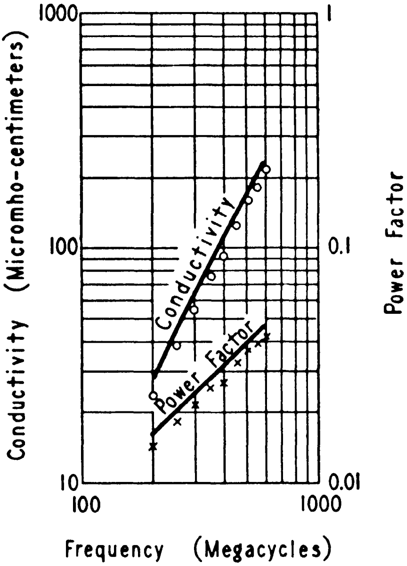

Fig. 181. Power factor and conductivity of cyclohexanone, calculated from the model circuit. The measured data was obtained by the concentric transmission line method.

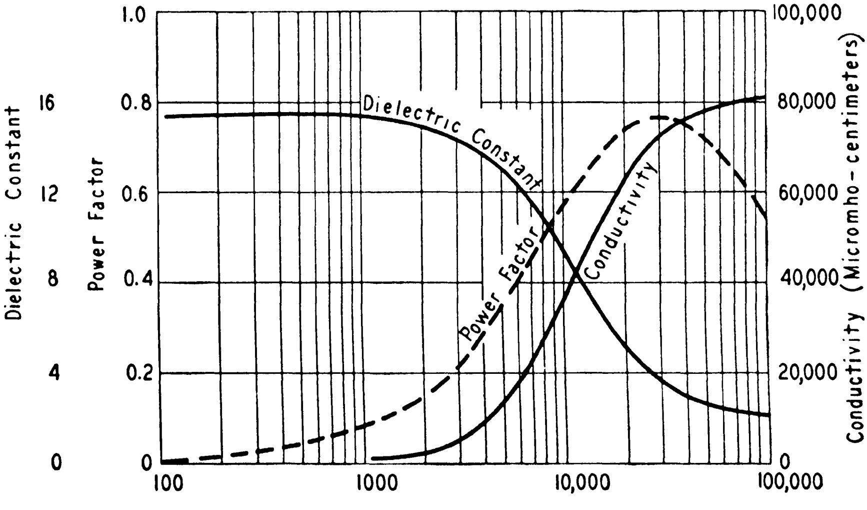

Fig. 182. Complete dielectric behavior of cyclohexanone, calculated from the model circuit

using the above values, while the experimental points were obtained with the Q-meter. When attempts were made to use the concentric transmission-line method to measure the dielectric properties at frequencies above 100 megacycles, it was found that the curves resembled the top curve of Fig. 177,

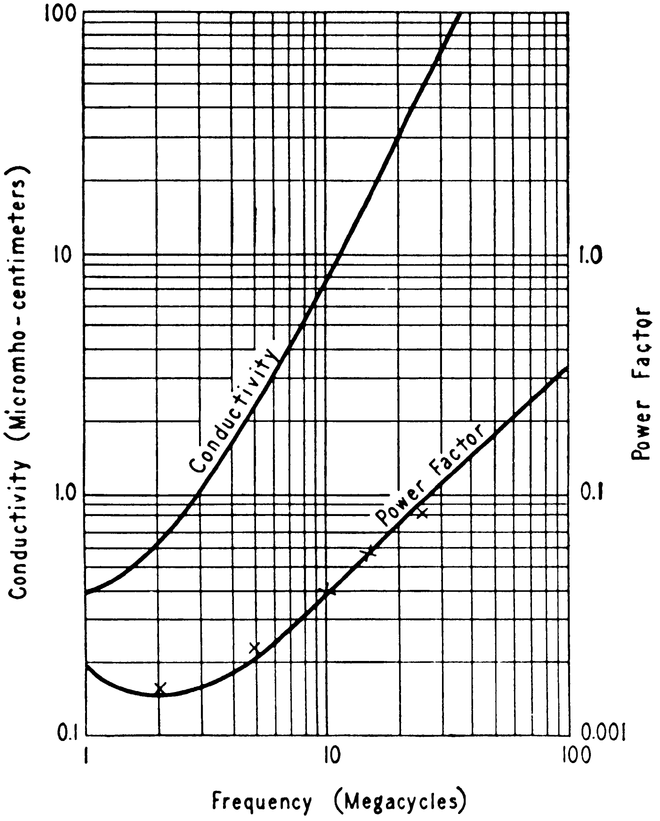

FIG. 183. Power factor and conductivity of glycerine, calculated from the model circuit, together with data obtained with the Q-meter. The temperature is 20° C.

so that no reasonable accuracy of measurement could be assured. However, to check the equivalent circuit, values computed from (17.58) and (17.59) were substituted in transmission-line equations to find the distribution of voltage along the line. This distribution was compared to the measured distribution by making the values coincident at a point 22 centimeters from the end of the line. The comparison is shown in Table 13.

Again, in Fig. 184, we have taken the liberty of extrapolating the circuit model far beyond the measured data. Here we see the dielectric constant dropping rapidly above 100 megacycles, with a peak of power factor occurring at 1000 megacycles. It may be noted that the conductivity flattens out at the high frequencies.

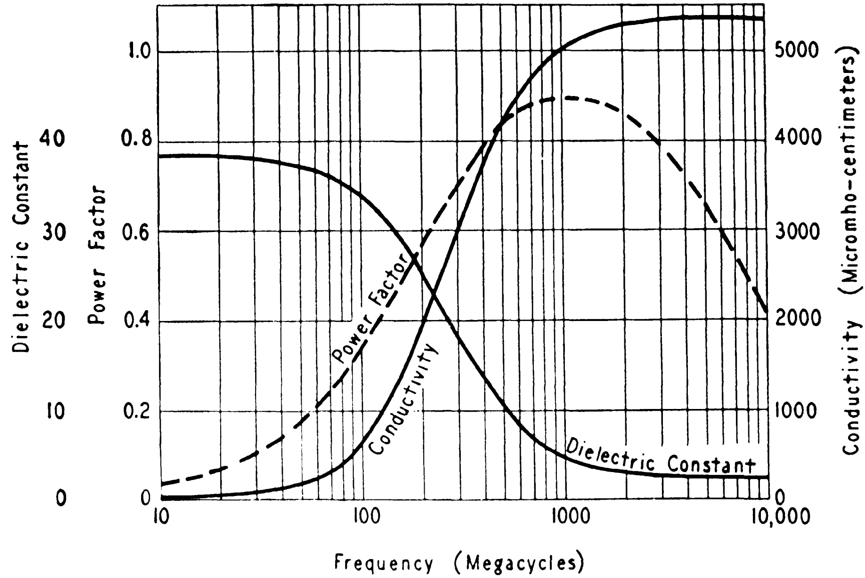

Fig. 184. Complete dielectric behavior of glycerine, calculated from the model circuit.

The behavior of many liquids may be found to depart materially from that of the simple network depicted in Fig. 179. In some cases, it may be possible to construct a more complicated network. However, this procedure is usually of academic interest and the measured data serves well the needs of the equipment designer.

TABLE 13. VOLTAGE DISTRIBUTION CALCULATED FROM THE EQUIVALENT CIRCUIT COMPARED WITH THE MEASURED DISTRIBUTION.

(Frequency is 150 megacycles)

Distance from the End of the Line (centimeters)	Relative Voltage	
	Measured	Calculated
5	0.59	0.615
7.5	0.73	0.785
10	0.76	0.827
12.5	0.70	0.76
15	0.63	0.652
17.5	0.67	0.65
20	0.84	0.82
22	1.0	1.0

Chapter 18

HEAT-FLOW PROBLEMS IN WOOD-GLUING PRESSES

Two Hot Plates. In Chapters 13 and 14 the general theory of heat conduction and heat distribution was developed for the case where heat is generated in the medium itself. The analysis which was there presented was applied directly to the heating effect of radio-frequency currents induced in metals. A later extension of this theory will include non-conductors which are heated by the passage of radio-frequency currents. Before this is done, however, a short investigation will be made of the way in which heat is conducted through a material placed in contact with massive heated plates. Under these conditions no heat is generated in the material itself but is conducted in from the outside so that (13.07) in Chapter 13 becomes

$$c\rho \frac{du}{dt} = k \frac{d^2u}{dx^2}, \tag{18.01}$$

since $\mathcal{H}$ is now zero. This equation is often written as

$$\frac{du}{dt} = \alpha^2 \frac{d^2u}{dx^2}, \tag{18.02}$$

where $\alpha^2 = k/c\rho$ is called the " thermal diffusivity." The temperature u at any point will depend upon the location of the point in the material being investigated and upon the time that has elapsed since the material was placed in contact with the heated plates. We may assume that u can be expressed as a product of two functions X and T, where X is a function of x alone and T is a function of t alone. Hence, applying the standard method of products to the solution of (18.02), we first write

$$u = X(x) \cdot T(t). \tag{18.03}$$

Appropriate differentiations of (18.03) are made and substituted in (18.02) to obtain the relationship

$$X \frac{dT}{dt} = \alpha^2 T \frac{d^2X}{dx^2}, \tag{18.04}$$

which is then rewritten in the form

$$\frac{1}{\alpha^2 T}\frac{dT}{dt} = \frac{1}{X}\frac{d^2X}{dx^2} \tag{18.05}$$

Since T is a function of t alone and X is a function of x alone, and since x and t are entirely independent variables, the relation of (18.05) may be satisfied only if each side of this equation is equal to a constant.

Then (18.05) appears as:

$$\frac{1}{\alpha^2 T}\frac{dT}{dt} = \frac{1}{X}\frac{d^2X}{dx} = -m^2, \tag{18.06}$$

where m is an unknown and arbitrary constant.

The two differential equations contained in (18.06) can be satisfied by the equation $T = C\epsilon^{-\alpha^2m^2t}$ and $X = A \cos mx + B \sin mx$, respectively. Using these two relationships (18.03) may now be written

$$u = \epsilon^{-\alpha^2m^2t}(M \cos mx + N \sin mx), \tag{18.07}$$

where m, M, and N must be determined by the boundary conditions. This equation is a solution of (18.02) and assumes practical value when applied, for example, to a study of the temperature distribution in wood as it is being glued in a hot-plate press.

In making an application of (18.07) let us consider several pieces of wood which are to be glued together and which have a total thickness designated by b. At a time $t = 0$ they are placed between the two metal plates of a press shown in Fig. 185. These plates are steam or electrically heated and have a thermal capacity large enough to keep the plate temperature essentially constant. In this press let

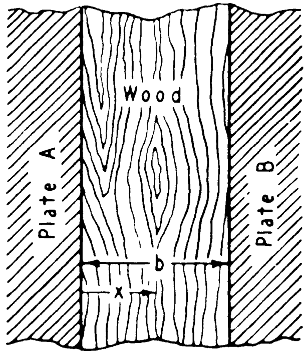

FIG. 185. Layer of wood between heated press plates.

β = temperature of plate A;
γ = temperature of plate B.

At the time that the wood is placed between the plates, the temperature distribution through the wood is $f(x)$, a known function. Therefore, the solution of (18.07) must satisfy the following boundary conditions:

$x = 0$, $u = \beta$ for all values of t;
$x = b$, $u = \gamma$ for all values of t;
$t = 0$, $u = f(x)$.

Then (18.07) becomes[*]

$$u = \beta + (\gamma - \beta)\left\{\frac{x}{b} + \frac{2}{\pi}\sum_{n=1}^{n=\infty}\left[\frac{(-1)^n}{n}\,\epsilon^{-n^2\pi^2\alpha^2(t/b^2)}\sin\left(\frac{n\pi x}{b}\right)\right]\right\}$$

$$+ \frac{2}{b}\sum_{n=1}^{n=\infty}\left\{\epsilon^{-n^2\pi^2\alpha^2(t/b^2)}\sin\left(\frac{n\pi x}{b}\right)\int_{\lambda=0}^{\lambda=b}[f(\lambda) - \beta]\sin\left(\frac{n\pi\lambda}{b}\right)d\lambda\right\}. \qquad (18.08)$$

The application of this equation will be developed for two cases. The first case will be for a press having two equal-temperature hot plates, and the second case will be for a press having only one heated plate; the other plate, which is the bed of the press, remaining at room temperature.

It is recognized that the first case represents the type of press most commonly used, but a study of the second case provides an interesting contrast and is included for this reason.

The most common hot-plate press has two equal-temperature plates, so that $\gamma = \beta$. Since the behavior of the temperature at various points throughout the wood depends on *differences* of temperatures rather than actual temperature, we shall assume for convenience that the wood is at constant temperature of 0° C throughout, at time $t = 0$. Then $f(x) = f(\lambda) =$ some constant $= 0$. Also we will set the plate temperature at 1° C, so $\gamma = \beta = 1$. Then (18.08) becomes

$$u = 1 - \frac{2}{b}\sum_{n=1}^{n=\infty}\left[\epsilon^{-n^2\pi^2\alpha^2(t/b^2)}\sin\left(\frac{n\pi x}{b}\right)\int_{\lambda=0}^{\lambda=b}\sin\left(\frac{n\pi\lambda}{b}\right)d\lambda\right]$$

$$= 1 - \frac{4}{\pi}\sum_{n=0}^{n=\infty}\frac{\epsilon^{-(2n+1)^2\pi^2\alpha^2(t/b^2)}}{(2n+1)}\sin\left[\frac{(2n+1)\pi x}{b}\right]$$

$$= 1 - \frac{4}{\pi}\left[\epsilon^{-\pi^2\alpha^2(t/b^2)}\sin(\pi x/b) + \frac{\epsilon^{-3^2\pi^2\alpha^2(t/b^2)}\sin(3\pi x/b)}{3}\right.$$

$$\left. + \frac{\epsilon^{-5^2\pi^2\alpha^2(t/b^2)}\sin(5\pi x/b)}{5} + \cdots\right]. \qquad (18.09)$$

Average values for the constants of wood are

ρ(specific heat)
= 0.65 calorie per gram per degree Centigrade.

c(density)
= 0.53 gram per cubic centimeter.

k(thermal conductivity)
= 0.00036 calorie per square centimeter per second when the temperature gradient is 1° C per centimeter.

α^2(thermal diffusivity) = $k/c\rho$
= 0.00104 square centimeter per second.

---

[*] W. E. Byerly, *Fourier's Series and Spherical, Cylindrical, and Ellipsoidal Harmonics*, Ginn and Company, New York, 1893, p. 108, Example 1.

When these values are inserted into (18.09) the equation reduces to

$$u = 1 - \frac{4}{\pi}\left[\epsilon^{-0.01025(t/b^2)} \sin(\pi x/b) + \frac{\epsilon^{-0.0923(t/b^2)} \sin(3\pi x/b)}{3} + \frac{\epsilon^{-0.2563(t/b^2)} \sin(5\pi x/b)}{5} + \cdots\right]. \qquad (18.10)$$

where

t = heating time, in seconds;
b = thickness of the wood, in centimeters;
x = distance into the wood, in centimeters;
u = relative temperature.*

Equation (18.10) is plotted in Fig. 186 and shows the temperature of the wood at several levels below the surface in terms of the ratio t/b^2.

In practical applications, however, it may be more convenient to measure the heating time in minutes and the thickness of the wood in inches. It is also usually most important to know the temperature at the center where $x = b/2$ so that a very useful form of (18.10) is given by

$$u = 1 - \frac{4}{\pi}\left[\epsilon^{-0.0956(t_m/b_i^2)} - \frac{\epsilon^{-0.861(t_m/b_i^2)}}{3} + \frac{\epsilon^{-2.395(t_m/b_i^2)}}{5} - \cdots\right], \qquad (18.11)$$

where now t_m = heating time, in minutes;
b_i = thickness of wood, in inches;
u = relative temperature.

The relationship expressed by (18.11) is plotted in Fig. 187. A tabulation of heating times required to attain various temperatures at the center of the

---

[*] Attention is directed to the fact that u may be considered here as a ratio expressing relative temperature. It may be regarded as a *fraction* of the temperature interval between the initial wood temperature and the plate temperature. Then

$$u = \frac{u_x - u_0}{u_p - u_0}$$

where: u_x = temperature of the wood at x, as a function of time;
u_0 = initial temperature of the wood;
u_p = temperature of the hot plates.

By considering u as a fraction it is apparent that all other temperatures may be expressed in either the Centigrade or Fahrenheit scale.

Since u_x, the temperature of the wood at the point x, is the information usually required, the expression above should be rearranged as

$$u_x = u(u_p - u_0) + u_0.$$

The value of u may be read off from graphs in Figs. 186, 187, and others where the ordinate is indicated in relative temperature.

wood, where $x = b/2$, is given in Table 14. Using values of t_m/b_i^2 from Fig. 187 the table has been prepared for three different thicknesses of wood. The slow conduction of heat through thick sections of wood is clearly evident

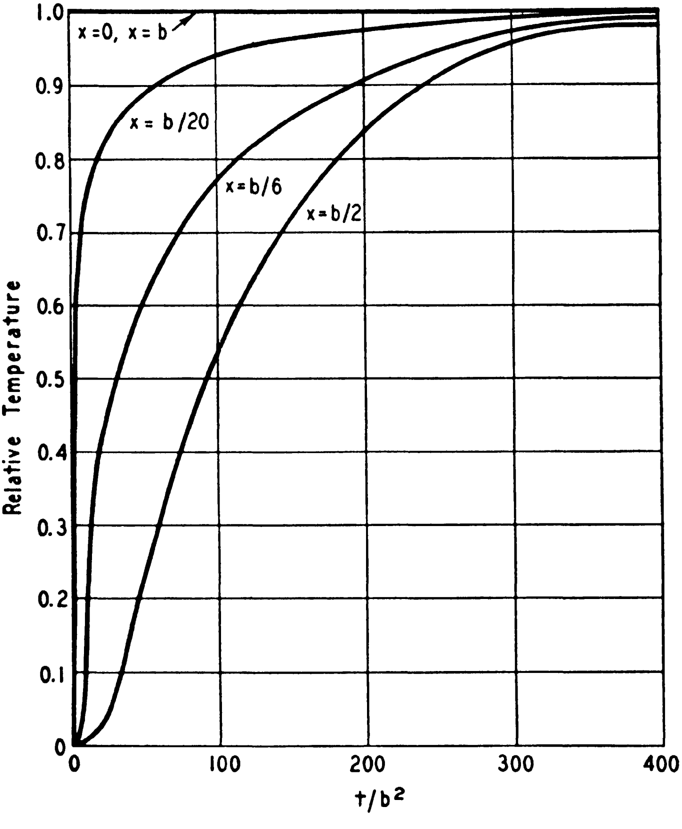

FIG. 186. Specific wood temperature as a function of time t in seconds and thickness b in centimeters, at various distances x from the surface when two equal-temperature hot plates are used.

when the heating time for a ½-inch section is compared with the heating time for a 5-inch section. It will be noted that heating time increases as the square of the thickness.

Fig. 188 represents (18.10) in a somewhat different manner and shows the temperature distribution across the wood, from plate to plate, at the end of three different time intervals. The ratios of the time intervals corresponding to curves numbered 1, 2 and 3 are 1: 2½: 5, respectively. Specific

TABLE 14. HEATING TIME OF WOOD IN A HOT-PLATE PRESS.
Initial Wood Temperature = 80° F
Plate Temperature = 280° F

Center Temperature / Thickness	100° F (u = 0.1)	180° F (u = 0.5)	240° F (u = 0.8)	276° F (u = 0.98)
b_i = 0.5 inch	0.9 min.	2.44 min.	4.75 min.	10 min.
b_i = 1.0 inch	3.6 min.	9.76 min.	19 min.	40 min.
b_i = 5.0 inches	90 min.	244 min.	475 min.	1000 min.

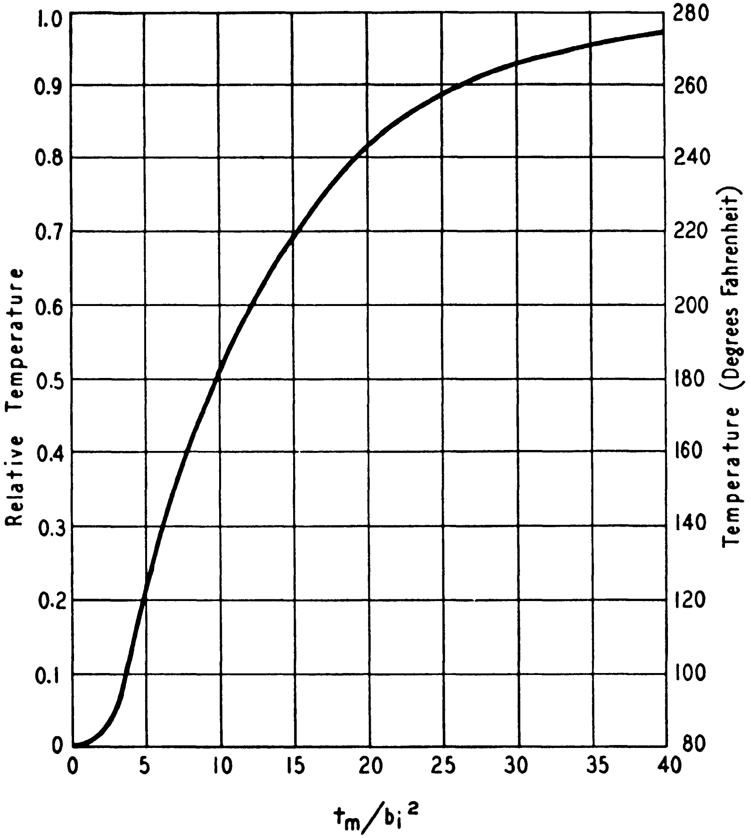

FIG. 187. Center-temperature of wood between plates maintained at 280° F in terms of time t_m in minutes and thickness b_i in inches.

values of time for three different thicknesses of wood are given in the table appearing below Fig. 188.

Although this temperature distribution is interesting, in a practical case we desire to attain some specified temperature at the center of the wood, such as 240° F, required for setting certain urea-resin glues. With this in mind Fig. 189 was constructed from Fig. 188 and shows the calculated plate temperatures necessary to raise the center of the wood, originally at 80° F,

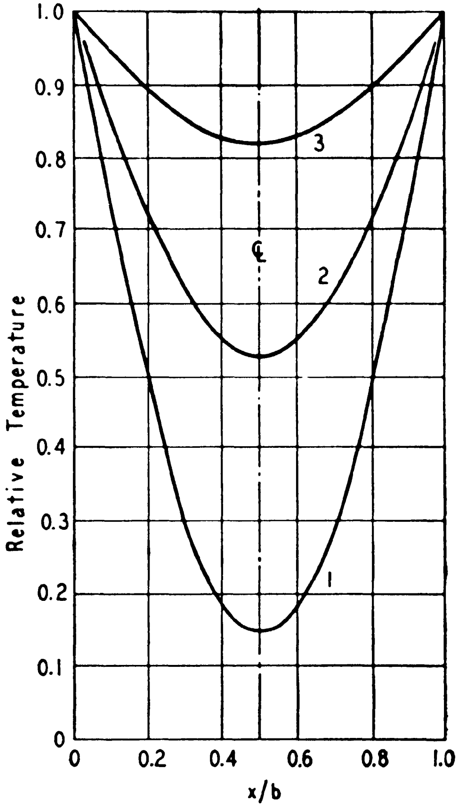

Fig. 188. Specific temperature distribution across a stack of wood between two equal-temperature hot plates.

Curve Number	Heating Time, Minutes		
	Thickness Being Heated		
	0.5 inch	1.0 inch	5.0 inches
1	1.0	4.0	100
2	2.5	10.0	250
3	5.0	20.0	500

to at least 240° F in three different time intervals and for three different thicknesses of wood as described in the table appearing below the graph.

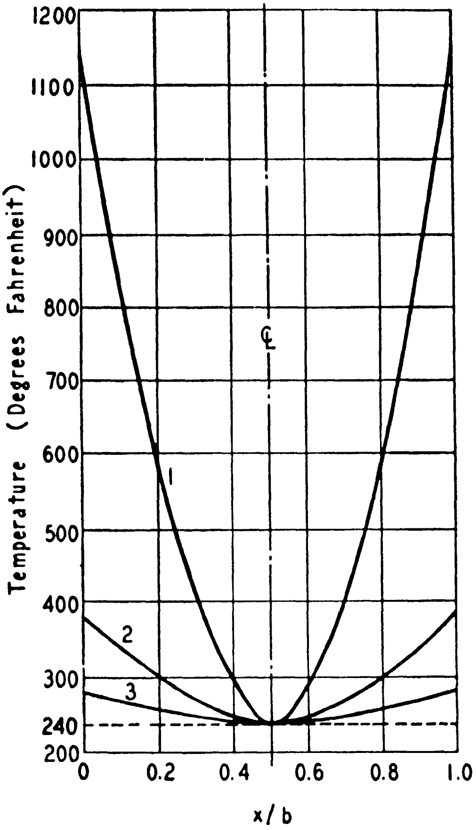

FIG. 189. Temperature distribution through the wood for a number of plate temperatures which will bring the center line to 240° F in the time interval chosen.

Curve Number	Heating Time, Minutes			Plate Temperature
	Thickness Being Heated			
	0.5 inch	1.0 inch	5.0 inches	
1	1.0	4.0	100	1145° F
2	2.5	10.0	250	375° F
3	5.0	20.0	500	289° F

Curve 1 is, of course, an absurd case since a plate temperature of 1145° F would set the wood on fire immediately. It is included, however, to illustrate the extreme temperature gradient that would be required to force heat rapidly through a poor conductor such as wood.

The curves of Fig. 188 present a clear picture of the temperature gradient across the wood in a press using heated plates. The surface of the wood is at the highest temperature while the central part is the coolest. In using modern thermo-setting glues it is imperative that all parts shall have reached a certain minimum temperature which is required to harden the glue. For a catalyzed urea-resin glue this is about 240° F. If it is known that the glue-line at the center of a stack of wood has attained the required temperature, then all other glue lines must have been sufficiently heated. Unless temperature gradients are very steep, as shown in the empirical case of curve 1, Fig. 189, there is little danger of overheating a glue line as long as the wood is not scorched. Practical experience has shown that plate temperatures in excess of 400° F will scorch the wood except for very short heating times. The high plate temperatures dry out the wood considerably and it is not uncommon practice to dip the finished article into water immediately upon its removal from the press in order to partially restore the moisture which has been driven out.

The effect of various plate temperatures on the gluing time can be observed by reference to Fig. 190 which has been developed from (18.11). The ordinate of this graph shows the temperature at the center of the wood in terms of t_m/b_i^2 where t_m is the heating time in minutes and b_i is the thickness in inches. This graph has been developed by using t_m/b_i^2 ratios from Fig. 187, but using several plate temperatures ranging from 240° F to 400° F.

The desired temperature level of 240° F at the glue line is indicated by a heavy dotted line. It should be noted in Fig. 190 that with a plate temperature of 240° F the wood will reach 240° F at the center only after an infinite time — which is what we would expect. But as the plate temperatures are made higher, the time required to obtain 240° F is greatly shortened. A tabulation under Fig. 190 presents some typical values.

The actual heat-energy supplied to the wood in the course of a gluing cycle can be calculated by considering a prism of wood 1 square centimeter in cross section and b centimeters long. This prism has an initial temperature of u_0 and is placed between plates maintained at a temperature of u_p. In the time interval between the application of the hot plates and any time t the heat energy supplied is

$$\text{Calories} = c\rho\,\Delta u \cdot \int_{x=0}^{x=b} u(x)\,dx, \tag{18.12}$$

where $\Delta u = u_p - u_0$, measured in degrees Centigrade. When (18.09) is substituted in (18.12) and multiplied by 4.187, the mechanical equivalent of heat, we have the energy per square centimeter of surface in joules (watt-seconds) as

Joules per square centimeter =

$$4.187c\rho b\,\Delta u\left\{1-\frac{8}{\pi^2}\left[\epsilon^{-\pi^2\alpha^2(t/b^2)}+\frac{\epsilon^{-3^2\pi^2\alpha^2(t/b^2)}}{3^2}+\frac{\epsilon^{-5^2\pi^2\alpha^2(t/b^2)}}{5^2}+\cdots\right]\right\}\cdot \quad (18.13)$$

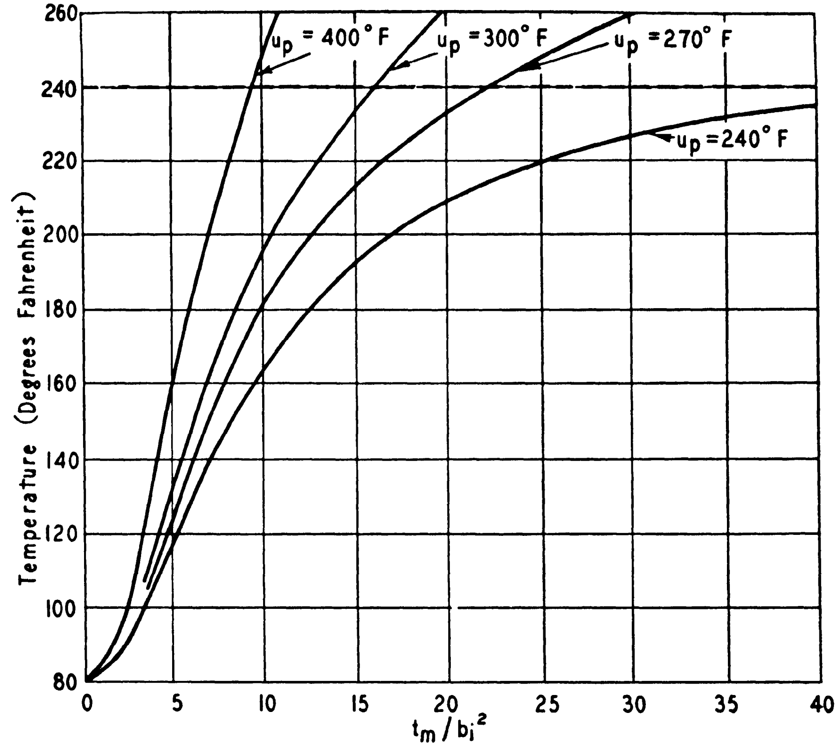

FIG. 190. Temperature at center of wood for a number of plate temperatures, u_p. Initial temperature of wood was 80° F.

Temperature of Press Plates	Heating Time, Minutes, to Attain 240° F at Center		
	Thickness Being Heated		
	0.5 inch	1.0 inch	5.0 inches
240° F	∞	∞	∞
270° F	5.6	22.4	560
300° F	4.0	16	400
400° F	2 75	9.5	2.75

When the average constants for wood, as previously used, are rewritten in English units we have

$c\rho$ = 3.15 calories per cubic inch per degree Fahrenheit,
α^2 = 0.0095 square inches per minute.

Using these values in (18.13) we have:

Watt-seconds per square inch =

$$13.2b_i\,\Delta u_F\left\{1-\frac{8}{\pi^2}\left[\epsilon^{-0.0954(t_m/b_i^2)}+\frac{\epsilon^{-0.859(t_m/b_i^2)}}{9}+\frac{\epsilon^{-2.38(t_m/b_i^2)}}{25}+\cdots\right]\right\} \quad (18.14)$$

where t_m = time, in minutes;
b_i = thickness, in inches;
Δu_F = temperature increment, in degrees Fahrenheit.

When plate temperatures and the ratio t_m/b_i^2 are chosen from Fig. 190 and inserted in (18.14) we can determine the energy absorbed by the wood. A tabulation in Table 15 gives the energy absorbed by the wood for several values of b_i. In each case the time was that required to raise the center of the wood to 240° F from 80° F.

TABLE 15. ENERGY ABSORBED BY WOOD PLACED IN A PRESS WITH TWO HOT PLATES.

Plate Temperature	Watt-Seconds Per Square Inch		
	b_i = 0.5 inch	b_i = 1.0 inch	b_i = 5.0 inches
240° F	1055	2110	10,550
270° F	1130	2260	11,300
300° F	1195	2390	11,950
400° F	1415	2830	14,150

One Hot Plate and One Cold Plate. Manifestly less efficient than a press which applies a hot platen to both sides of the wood being glued, this type of press finds some favor for certain operations. Generally, the bed of the press is unheated and remains at or near room temperature. By virtue of this, wood placed in contact with this plate will not be dried out or scorched, but will retain its original condition. This is important where sheets of plywood, for example, are to be joined together by gluing thin gusset strips along the junction of the sheets. To make up for the inefficiency of heating from one side only, the hot plate in contact with the gusset can be maintained at or near the scorching temperature of wood since heating time is short and the gusset strip is not exposed to view as later used.

To permit ready comparison of this type press with the one previously discussed the analysis will proceed along analogous lines. The following assumptions will be made:

a. Plate A in Fig. 185 represents the heated plate, maintained at 1° C throughout. Thus $\beta = 1$.

b. Plate B in Fig. 185 represents the unheated plate, remaining at 0° C. Thus $\gamma = 0$.

c. The wood is at 0° C when placed in the press. Thus $f(\lambda) = 0$.

d. Thermal diffusivity, α^2, will be taken as 0.0097 square inch per second or 0.00104 square centimeter per second from (18. 10).

Hence (18.08) becomes:

$$u = 1 - \frac{x_i}{b_i} - \frac{2}{\pi}\left[\epsilon^{-0.0956(t_m/b_i^2)} \sin\frac{\pi x_i}{b_i} + \frac{\epsilon^{-0.383(t_m/b_i^2)}}{2} \sin\frac{2\pi x_i}{b_i} + \frac{\epsilon^{-0.861(t_m/b_i^2)}}{3} \sin\frac{3\pi x_i}{b_i} + \frac{\epsilon^{-1.53(t_m/b_i^2)}}{4} \sin\frac{4\pi x_i}{b_i} + \cdots\right], \quad (18.15)$$

where: u = relative temperature;
b_i = thickness of wood, in inches;
x_i = distance into the wood, in inches;
t_m = heating time, in minutes.

This equation is plotted in Fig. 191 and shows the temperature at a number of different levels in the wood as a function of t_m/b_i^2. The left-hand ordinate expressed as " relative temperature " is useful in applying the curves to any temperature interval that may exist between the hot plate and the initial temperature of the wood; the right-hand ordinate applies to the case where the hot-plate temperature is 400° F and the initial temperature of the wood is 80° F, which is also the temperature at which the press-bed remains.

To present a picture of the temperature distribution across the wood (c.f. Fig. 188), Fig. 191 has been redrawn in the form presented in Fig. 192, in which distance is measured from the hot plate toward the cold plate. On the basis of an initial temperature of 80° F and a hot-plate temperature of 400° F, curve 1 represents, for example, the heat distribution in a stack of wood 1 inch thick at the end of 4 minutes, while curve 4 shows the distribution after an infinite time. The illustrative application of these curves to some other thicknesses and heating times is made in the table appearing under Fig. 192.

Inspection will show that for glue lines close to the hot plate, little difficulty is experienced in reaching the 240° F required to set catalyzed urea-resin glue. But at, or beyond, the center line the problem rapidly becomes hopeless. When Fig. 192 is contrasted with Fig. 188 and the table of Fig. 192 with Table 14, the tremendous advantage of having two hot plates, whenever possible, becomes clearly evident.

The actual energy necessary to accomplish a given temperature rise when only one hot plate is used cannot be reckoned from (18.12) because some heat is lost into the cold plate B. However, there is another method which is just as simple.

Consider again a prism of wood 1 square centimeter in cross section and b centimeters long. The temperature of the hot plate at one face of the prism is u_p and the temperature of the cold plate at the other face, as well as the initial temperature of the wood, is u_0. The temperature gradient along this prism in the direction $x = 0$ to $x = b$ is $-\frac{du}{dx}$. If the thermal conductivity is k, the time-rate of heat flow is $-k\frac{du}{dx}$ so that:

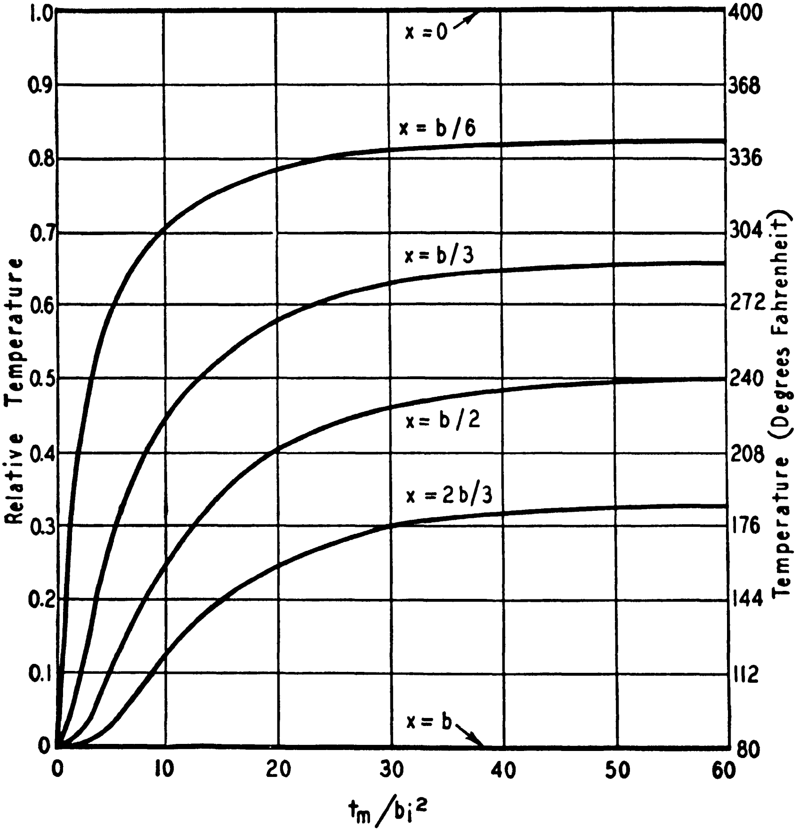

FIG. 191. Temperature as a function of time and thickness at various distances from the surface when wood is placed between one plate at 400° F and another at 80° F.

$$\text{Calories supplied} = \int_{t=0}^{t=t}\left[-k\frac{du}{dx}\right]dt \qquad (18.16)$$

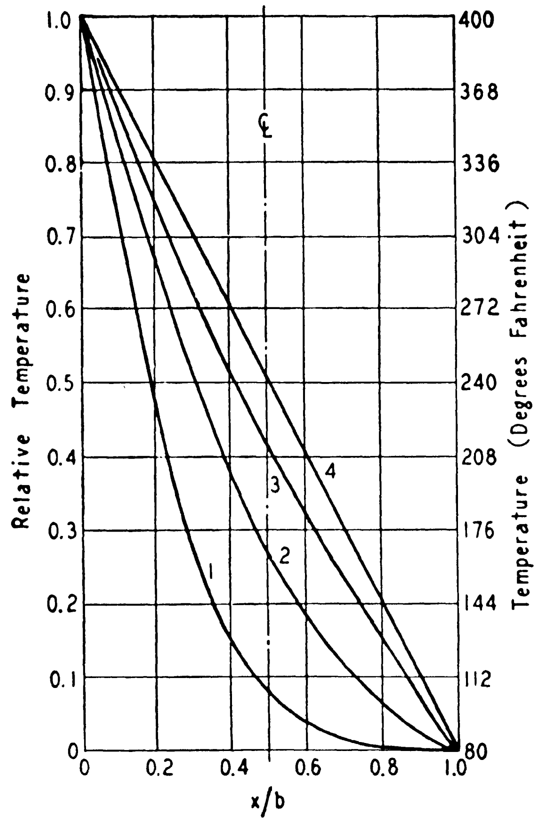

FIG. 192. Temperature distribution through the wood with one hot plate and one cold plate (400° F and 80° F, respectively).

Curve Number	Heating Time, Minutes		
	Thickness Being Heated		
	0.5 inch	1.0 inch	5.0 inches
1	1.0	4.0	100
2	2.5	10.0	250
3	5.0	20.0	500
4	∞	∞	∞

When (18.16) is converted to watt-seconds and the indicated operations performed we have:

Watt-seconds per square centimeter =

$$4.187(u_p - u_0)b\left\{\frac{kt}{b^2} + \frac{2c\rho}{\pi^2}\left[1 - \epsilon^{-\pi^2\alpha^2(t/b^2)} + \frac{1 - \epsilon^{-2^2\pi^2\alpha^2(t/b^2)}}{2^2} + \frac{1 - \epsilon^{-3^2\pi^2\alpha^2(t/b^2)}}{3^2} + \cdots\right]\right\}. \qquad (18.17)$$

Since $\frac{2}{\pi^2}\left[1 + \frac{1}{2^2} + \frac{1}{3^2} + \cdots\right] = \frac{2}{\pi^2}\cdot\frac{\pi^2}{6} = \frac{1}{3}$, (18.17) becomes:

Watt-seconds per square centimeter =

$$4.187(u_p - u_0)b\left\{\frac{kt}{b^2} + \frac{c\rho}{3} - \frac{2c\rho}{\pi^2}\left[\epsilon^{-0.01025(t/b^2)} + \frac{\epsilon^{-0.041(t/b^2)}}{2^2} + \frac{\epsilon^{-0.0923(t/b^2)}}{3^2} + \cdots\right]\right\}. \qquad (18.18)$$

Fig. 193 was constructed from (18.18). The solid curve shows the total energy (joules or watt-seconds) supplied by the hot plate from starting time. The broken curve A is the temperature at the center of the wood while curve B shows the temperature in the wood if the same energy were released uniformly with no loss.

Radio-Frequency Heating with Cold Plates. In the discussion just concluded a study was made of the heat distribution and temperature gradients existing in wood when heat flowed into it from the outside. When heat is generated internally by electrical or chemical means its distribution in the material depends on the rate of generation, boundary conditions, and the physical properties of the material.

In order to permit ready comparison between conclusions reached in this section and those reached previously, wood will again be used as the illustrative material. It is a material which is a relatively poor dielectric and is easily heated when placed in a strong alternating electric field.

The simplest way to insure that the material will be located in a strong uniform field is to place it between the plates of a condenser to which a suitable radio-frequency voltage is applied. The presence of this voltage across opposite surfaces of the wood will cause a current to flow through the wood and its temperature will rise as a result of dielectric losses. Generally, the most efficient use of the voltage across the condenser plates is made when the plates are in intimate contact with the material to be heated. Under these conditions, there will be a continual flow of heat out of the material into the metal electrodes — particularly if they are massive and remain at or near room temperature. This is the case in a wood-gluing press which has been arranged to heat wood by the passage of a radio-frequency current. The way in which the cooling effect of the plates modifies the temperature distribution at various points in the wood will now be analyzed, and the influence of this effect on practical operating practice will be studied.

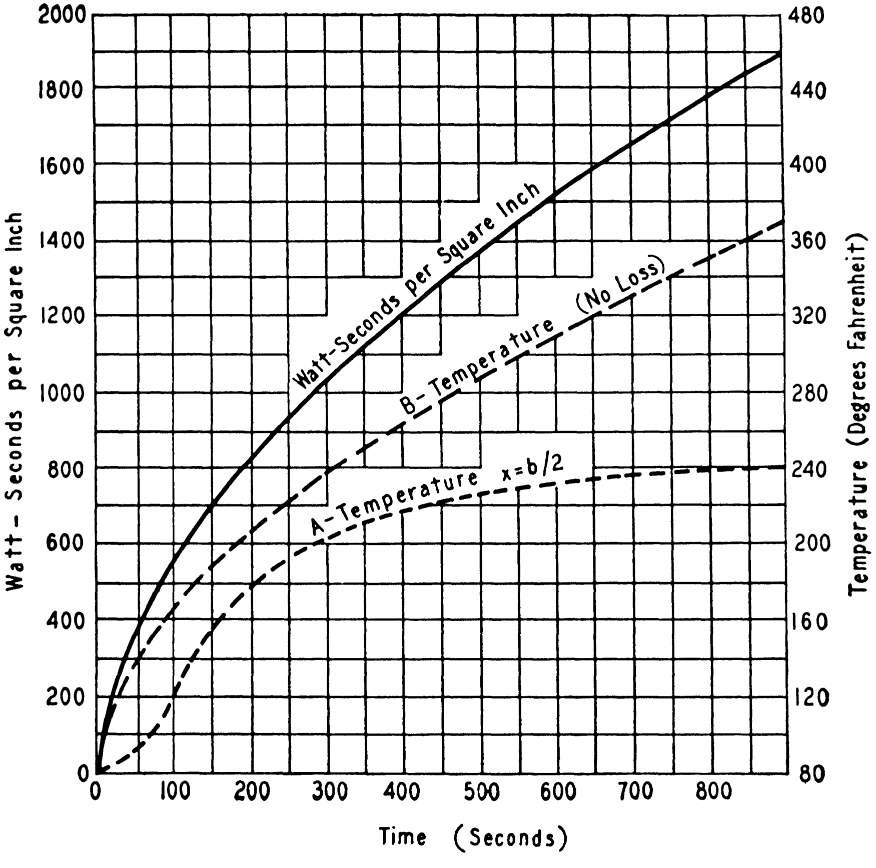

FIG. 193. Energy supplied and temperatures attained in terms of heating time for a ½-inch thick layer of wood between one plate at 400° F and another at 80° F. The solid curve shows the total energy supplied from starting time. Curve A shows actual temperature at center. Curve B shows the temperature of the wood if the same energy were released in the wood with no loss.

Before launching out on the development of the theory of heat conduction from internally-heated material into cooler electrodes, some assumptions will be made:

1. The electrodes are in intimate contact with the wood.

2. The electrodes remain at constant temperature. For convenience, this will be taken as 0° C.
3. Heat is generated uniformly throughout the material.
4. Heat flow is considered to take place in one dimension only.

As pointed out in Chapter 14, the heat-flow equations can be made analogous to equations describing the operation of a transmission line, and through their solution in this manner a concise picture of the temperature distribution in the material becomes a reality.

Since it has been assumed that the heat is generated uniformly throughout the wood, the relationship $\mathcal{H} = E(x)$ in (13.07) and (14.07) is a constant. Also, with the plates remaining at 0° C throughout the operating cycle, we can say, in the transmission-line analogy that $i_{x=0} = 0$ and $i_{x=b} = 0$ at all times. In the transmission line this is accomplished by open-circuiting the line at both ends, which makes $Z_b = Z_0 = \infty$. Under these conditions (14.08) becomes

$$i_x = u_x = \frac{E}{2Z_c \sinh(\gamma b)} \left[\int_{v=x}^{v=b} \cosh \gamma(b + x - v)\, dv \right.$$

$$\left. - \int_{v=0}^{v=b} \cosh \gamma(b - x - v)\, dv + \int_{v=0}^{v=x} \cosh \gamma(b - x + v)\, dv \right], \tag{18.19}$$

or

$$u_x = \frac{E}{\gamma Z_c} \left[\frac{\sinh(\gamma b) - \sinh(\gamma x) - \sinh \gamma(b - x)}{\sinh(\gamma b)} \right]. \tag{18.20}$$

Substituting (14.17) and (14.18) in (18.20),

$$u_x = \frac{E}{pL} \left\{ \frac{\sinh(\sqrt{pLG}\, b) - \sinh(\sqrt{pLG}\, x) - \sinh[\sqrt{pLG}\,(b - x)]}{\sinh(\sqrt{pLG}\, b)} \right\}. \tag{18.21}$$

The operational solution of (18.21) is*

$$u_x = \frac{4EGb^2}{\pi^3} \sum_{s=1}^{s=\infty} \frac{\sin[(2s - 1)(\pi x/b)]}{(2s - 1)^3} [1 - \epsilon^{-(2s-1)^2\pi^2 t/b^2 LG}] \tag{18.22}$$

Substituting (14.13) and (14.14) in (18.22),

$$u_x = \frac{4\mathcal{H}b^2}{\pi^3 k} \sum_{s=1}^{s=\infty} \frac{\sin[(2s - 1)(\pi x/b)]}{(2s - 1)^3} [1 - \epsilon^{-(2s-1)^2\pi^2\alpha^2 t/b^2 LG}]$$

$$= \frac{4\mathcal{H}b^2}{\pi^3 k} \left[(1 - \epsilon^{-\pi^2\alpha^2(t/b^2)}) \sin\left(\frac{\pi x}{b}\right) + \frac{1 - \epsilon^{-3^2\pi^2\alpha^2(t/b^2)}}{3^3} \sin\left(\frac{3\pi x}{b}\right) \right.$$

$$\left. + \frac{1 - \epsilon^{-5^2\pi^2\alpha^2(t/b^2)}}{5^3} \sin\left(\frac{5\pi x}{b}\right) + \cdots \right], \tag{18.23}$$

---

* See Appendix B, equation (B.20)

where

u_x = temperature increment, degrees Centigrade, at a distance x centimeters from one surface;

$\mathcal{H}$ = gram-calories per second per cubic centimeter;

b = thickness of the wood, in centimeters;

k = thermal conductivity (0.00036 calorie/square centimeter/second per degree Centigrade/centimeter;

α^2 = thermal diffusivity (0.00104 square centimeter per second);

t = heating time, in seconds.

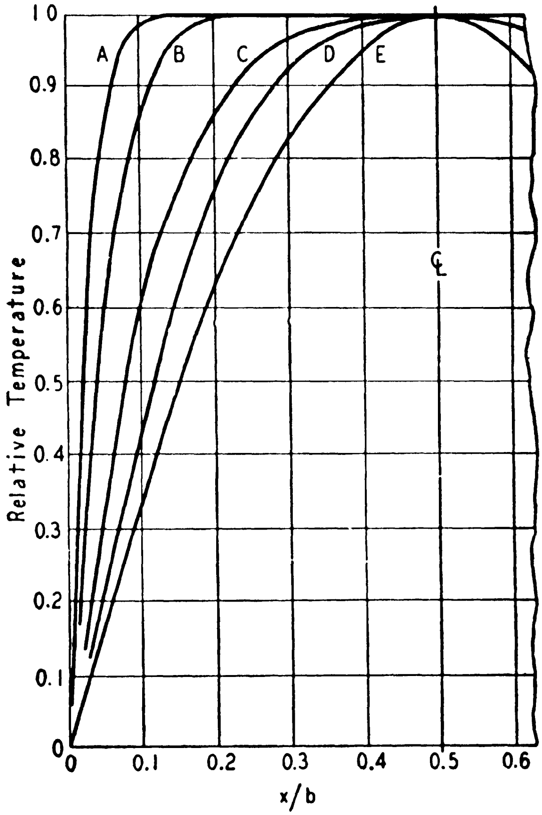

FIG. 194. Specific temperature-distribution curves through wood in contact with cold plates and heated by the passage of a radio-frequency current. The curves are drawn for various values of the parameter t/b^2 in (18.23) when time is in minutes (t_m) and thickness is in inches (b_i). Ratios of t_m/b_i^2 depicted above are: A, 0.11, B, 0.45, C, 2.0; D, 4.0; E, ∞.

In equations (18.09) and (18.15) which express the conditions in hot-plate presses, it was possible to consider u, the temperature of the wood, as the *fraction* of the temperature interval that existed between its initial temperature and the plate temperature — values that could definitely be determined. In (18.23) u_x has no upper limit that can easily be established depending, as it does, upon rate of heat generation, thickness and conductivity of wood, and time. Where all temperatures are given in degrees Centigrade, the actual temperature of the wood is easily found by adding u_x from (18.23) to the initial temperature of the wood, which is also the plate temperature. To determine the final temperature in Fahrenheit degrees, u_x from (18.23) must be multiplied by 1.8, the conversion factor from Centigrade to Fahrenheit, before adding the initial (plate) temperature.

The information contained in (18.23) yields a number of interesting facts concerning radio-frequency heating, a few of which we shall examine. In the following calculations the values for the constants in (18.23) are those for wood and are the same as were previously used in the hot-press calculations.

To provide a general set of curves which represent (18.23), Fig. 194 has been prepared in which detailed curves have been drawn for only one-half of the total thickness since the temperature distribution is symmetric about the center. For a specified heating time t and thickness of wood b, each curve indicates the relative temperatures which exist in the wood between one of its surfaces and its center for constant power input. The curves marked A, B, C, D, E in Fig. 194 represent various values of t/b^2, a ratio which relates the effect of heating time and the thickness of wood. Specific values that apply in this case are given directly below the figure.

It is readily seen (c.f. curves D and E) that an increase in heating time narrows the region in the central part of the wood which attains a desired temperature or which experiences a desired temperature increment. This is because the cold plates are continually taking heat out of the surface layers. When the heating time is long, because of low power concentration, there will be a considerable region contiguous to the plates which has reached only a small fraction of the temperature appearing at the center of the load. Herne* has cited an illustrative example in which a stack of 14 laminations is to be glued by radio-frequency heating in a press where the plates remain at room temperature. Using wood of slightly different physical constants ($\alpha^2 = 0.00161$) he gives the figures listed in Table 16.

* H. Herne, "Thermal Conduction With Radio Heating," *Wireless Engineer*, Vol. 21, No. 251, August 1944, pp. 377–382. This article contains an excellent development of the problem of thermal conduction when heat is internally generated, by using Duhamel's Theorem. The use of this theorem was considered in the preparation of this volume but was set aside in favor of the operational method outlined in Chapter 14. The main reason for doing this was that by the operational method it was possible to solve the problem of induction heating where heat generation is non-uniform as well as the problem of dielectric heating where the generation of heat is uniform throughout the material. Thus a broader base of operation can be established upon which the mathematical development of both dielectric and induction heating can proceed.

TABLE 16. THE TEMPERATURE OF A GLUE-LINE AT $x = b/14$ AS A PERCENTAGE OF THE TEMPERATURE AT THE CENTER FOR SEVERAL HEATING TIMES.

Heating time (seconds)	50	300	600	900
Temperature ratios (per cent)	99.92	89.60	77.93	69.96

For a broad region to attain a specified temperature, a short heating cycle is required so that heat loss into the electrodes is reduced. This means an increase in power with consequently higher voltages. As there is a practical limit to the voltages that can be tolerated, this condition frequently restricts the rate at which wood can be heated, without recourse to other plans. This inter-relationship is further discussed in Chapter 19 under voltage and power concentration.

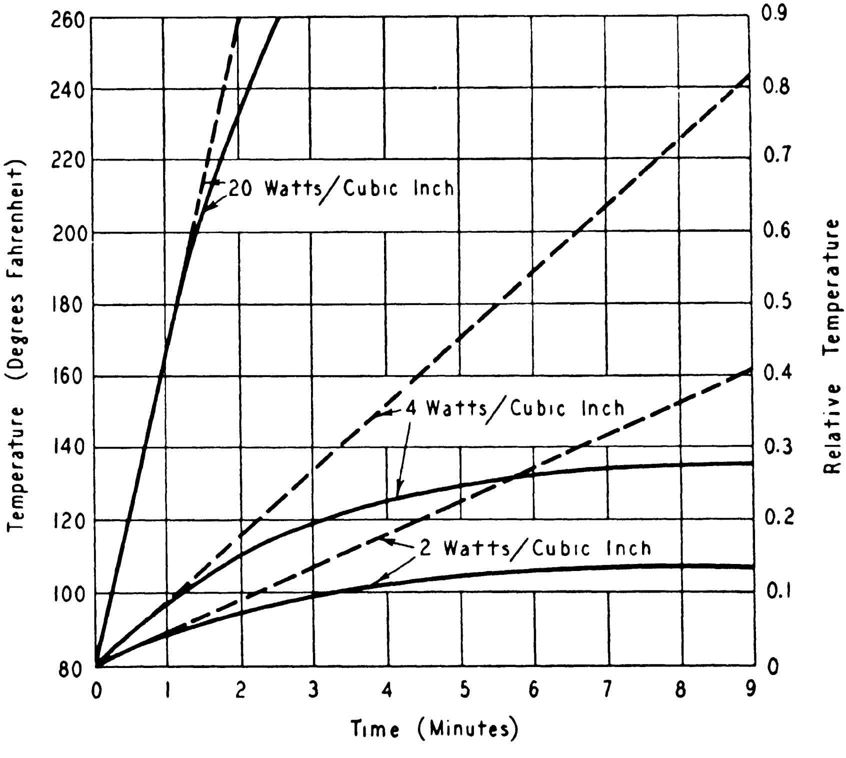

FIG. 195. Temperature rise at the center of wood, ½-inch in thickness, for various rates of energy generation. Dotted curves show temperature without plate loss and solid curves show actual temperature with plate loss.

As we are generally interested in temperatures at the center of the wood, (18.23) may be simplified somewhat by noting that at this location $x = b/2$. Hence, from (18.23)

$$u_{x=b/2} = \frac{4\mathcal{H}b^2}{\pi^3 k}\left[1 - \epsilon^{-\pi^2\alpha^2(t/b^2)} - \frac{1 - \epsilon^{-3^2\pi^2\alpha^2(t/b^2)}}{3^3} + \frac{1 - \epsilon^{-5^2\pi^2\alpha^2(t/b^2)}}{5^3} - \cdots\right]. \tag{18.24}$$

The value of u in (18.24) is, as before, the temperature increment in degrees Centigrade which occurs during the heating cycle.

It is often more desirable to consider the power concentration in watts per cubic centimeter rather than the generation of heat in gram-calories per second per cubic centimeter as was done in (18.24). Also, in practical applications, it is customary to use dimensions in inches, rather than centimeters, and time in minutes. When these changes in the units of (18.24) are made, the calculations completed and plotted, we have the solid curves of Fig. 195 to illustrate the effect of various power concentrations on the heating time of wood. They apply specifically to a section $\frac{1}{2}$ inch thick and show the temperature rise at the center of the wood. Idealized conditions in which there is no heat loss into the electrode plates are portrayed by the dashed lines. In making these calculations it has been assumed that initially the wood and the electrodes were at a uniform temperature of 80° F and that the electrodes remained at this temperature. Fig. 195 shows that for low power concentrations the wood does not approach the necessary glue-setting temperature of 240° F. At a high power concentration the desired temperature is not only reached in a short time, but also the plate-loss is very much less.

It is interesting to examine (18.24) as t approaches infinity in order to establish the limits of temperature for various thicknesses. Thus, at $x = b/2$ and $t \doteq \infty$

$$\begin{aligned} u &= \frac{4\mathcal{H}b^2}{\pi^3 k}\left(1 - \frac{1}{3^3} + \frac{1}{5^3} - \frac{1}{7^3} + \cdots\right) \\ &= \frac{4\mathcal{H}b^2}{\pi^3 k}\left(\frac{\pi^3}{32}\right) \\ &= \frac{\mathcal{H}b^2}{8k}. \end{aligned} \tag{18.25}$$

When (18.25) is rewritten so that power concentration W is given in terms of watts per cubic inch, the thickness b_i in inches, and the temperature rise is taken as 240° F − 80° F = 160° F, then we have

$$W(\text{watts per cubic inch}) = 2.72/b_i^2 \tag{18.26}$$

as the minimum power required to reach the glue-setting temperature of

240° F at the center. It will be noted that the power varies inversely as the square of the thickness. Now, if there were no loss of heat at the pressure plates, the temperature increment u in a time t seconds would be

$$u_{\text{no loss}} = \mathcal{H}t/cp \tag{18.27}$$

When (18.24) is divided by (18.27), we have the ratio of the temperature increment with plate losses to that with no plate losses at the center of the wood. For equal power densities this ratio is:

$$\frac{u_{\text{loss}}}{u_{\text{no loss}}} = \frac{4b^2}{\pi^3\alpha^2 t}\left[1 - \epsilon^{-\pi^2\alpha^2(t/b^2)} - \frac{1 - \epsilon^{-3^2\pi^2\alpha^2(t/b^2)}}{3^3} + \frac{1 - \epsilon^{-5^2\pi^2\alpha^2(t/b^2)}}{5^3} - \cdots\right], \tag{18.28}$$

recalling that $\alpha^2 = k/cp$. The relationship contained in (18.28) is of some interest and several illustrative values are given in Table 17.

TABLE 17. THE RATIO OF TEMPERATURE INCREMENTS AT THE CENTER, WITH AND WITHOUT PLATE LOSSES; THE RATIO OF POWER REQUIREMENTS TO ATTAIN A SPECIFIED CENTER TEMPERATURE WITH AND WITHOUT PLATE LOSSES, IN TERMS OF VARIOUS HEATING TIMES AND THICKNESSES. THESE CURVES APPLY TO WOOD HEATED BY RADIO FREQUENCY IN A PRESS WITH PLATES REMAINING AT ROOM TEMPERATURE.

$\frac{t_m}{b_i^2}$	Heating Time, in Minutes			$\frac{u_{\text{loss}}}{u_{\text{no loss}}}$	$\frac{W_{\text{loss}}}{W_{\text{no loss}}}$
	b_i = 0.5 inch	b_i = 1.0 inch	b_i = 5.0 inches		
0	0	0	0	1.00	1.00
2	0.5	2	50	0.98	1.01
4	1.0	4	100	0.95	1.06
6	1.5	6	150	0.90	1.10
8	2.0	8	200	0.85	1.19
10	2.5	10	250	0.78	1.23
20	5.0	20	500	0.55	1.82
30	7.5	30	750	0.38	2.60

However, a much more important relationship than this can be found from (18.24) and (18.27). Solve these two equations for $\mathcal{H}$ and designate the corresponding values as $\mathcal{H}_{\text{loss}}$ and $\mathcal{H}_{\text{no loss}}$, respectively. Then for identical temperature increments,

$$\frac{\mathcal{H}_{\text{loss}}}{\mathcal{H}_{\text{no loss}}} = \frac{W_{\text{loss}}}{W_{\text{no loss}}} = \frac{\pi^3\alpha^2 t}{4b^2} \div \left[1 - \epsilon^{-\pi^2\alpha^2(t/b^2)} - \frac{1 - \epsilon^{-3^2\pi^2\alpha^2(t/b^2)}}{3^3} + \frac{1 - \epsilon^{-5^2\pi^2\alpha^2(t/b^2)}}{5^3} - \cdots\right], \tag{18.29}$$

where W = power density.

This equation is plotted in Fig. 196 and shows the correction factor that must be applied when heat loss into the electrodes is accounted for. In conjunction with (18.27) the information in Fig. 196 is of particular value for estimating purposes in planning a gluing installation.

By way of example it was found* that 28 kilowatts applied to a press raised the temperature of a set of spruce boards to at least 260° F in 2 minutes. The boards were each 13 feet long, 6 inches wide, and $\frac{5}{16}$ inch thick. Three boards were stacked, making a total volume of 878 cubic inches, and $b_i = \frac{15}{16}$ inch. Assuming a starting temperature of 80°F, we need an increment of 180° F. We can easily find the power concentration required to effect a temperature increment of 180° F in 2 minutes without plate loss when (18.27) is rewritten into English units as follows:

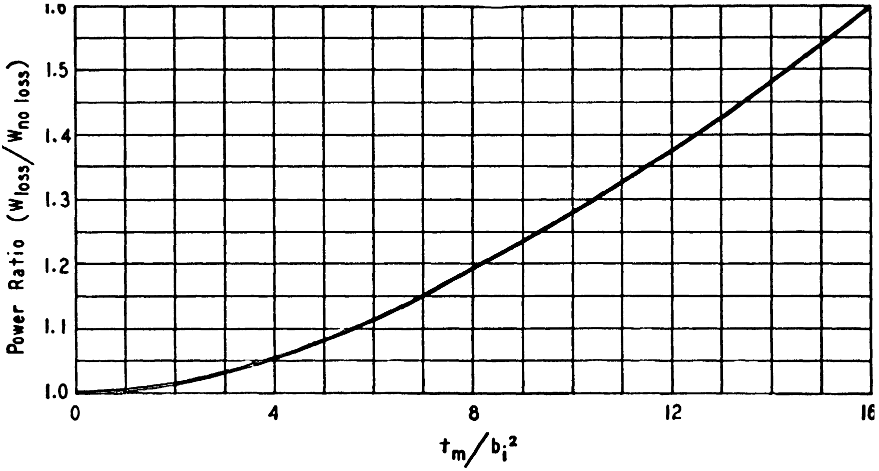

FIG. 196. The power ratio is the correction factor that must be applied to (18.27) to account for heat lost into the electrodes for various values of t_m/b_i^2.

$$W_i = \frac{0.218\Delta u_F}{} \tag{18.30}$$

where W_i = power concentration, in watts per cubic inch;
Δu_F = temperature increment, in degrees Fahrenheit;
t_m = time, in minutes.

Thus, in this example, (18.30) yields

$$W_i = \frac{0.218 \times 180}{2} = 19.6 \text{ watts per cubic inch.}$$

---

* R. A. Bierwirth and C. N. Hoyler, "Radio-Frequency Heating Applied to Wood Gluing," *Proc. I.R.E.*, Vol. 31, No. 10, October 1943, pp. 529–537.

To take into account the heat conducted into the plates, reference must now be made to Fig. 196. In the example cited, $b_i = \frac{15}{16}$ inch so that $t_m/b_i^2 = 2/(\frac{15}{16})^2 = 2.275$. Then, from Fig. 196 the power ratio is 1.025 and the power density required to produce a temperature increment of 160° F, including losses, is $1.025 \times 19.6 = 20.1$ watts per cubic inch. For the volume of 878 cubic inches which must be heated, the total power requirement is $20.1 \times 878 = 17{,}650$ watts. Comparing this figure with the 28,000 watts fed into the press and coupling system, the efficiency is about 63 per cent. This low efficiency is not astonishing, since an insulating wood plank 2 inches thick is in parallel with the sections being glued. This loss might be eliminated by using a low-loss insulator in place of the plank. A sketch of this installation is given in Fig. 217.

Another application was that of gluing plywood gusset joints, in which the total thickness was $b_i = \frac{1}{2}$ inch. The gusset strip had a width of $2\frac{1}{2}$ inches and a length of 13 feet. The total volume was then 195 cubic inches. For a gluing time of 1.1 minutes and a temperature rise of 160° F, a solution of (18.30) shows a power concentration of approximately 32 watts per cubic inch with no heat loss. Here $t_m/b_i^2 = 1.1/(\frac{1}{2})^2 = 4.4$ and then from Fig. 196 the correction factor for power is 1.07. This indicates that the total power requirement for this operation is $32 \times 195 \times 1.07 = 6680$ watts. Experimentally it was found that the total input to the press was 7500 watts.

Another application of interest is that of a blank 6 feet long, 20 inches wide, and 6 inches thick, representing a total volume of 8650 cubic inches. Suppose that we have a power into the press of 50,000 watts and a press efficiency of 75 per cent. Then the power density is 4.33 watts per cubic inch. From (18.30), this corresponds to 8.2 minutes for a temperature rise of 160° F with no heat loss. Turning to Fig. 196, and noting that $b_i = 6$ inches and $t_m = 8.2$ minutes and hence $t_m/b_i^2 = 8.2/6^2 = 0.228$, we find the correcting factor to be essentially unity, so we might expect the 50,000-watt oscillator to do the job in 8.2 minutes.

Table 18 summarizes the above results, and compares the radio-frequency method with the best heating time obtained by a hot-plate press using the plates at a scorching temperature of 400° F.

For the illustrative examples wood has been selected, since the earliest applications of radio-frequency heating were applied to wood-gluing problems. The equations are, however, entirely general, and calculations for any dielectric material can be made when the physical properties of the material are known.

One field in which radio-frequency heating has been extensively applied is that of preheating plastics before molding. The uniform softening of the material before placement into the mold has resulted in shorter time-cycles, lower pressures, reduced wear on the molds, and an improved product. The actual applications of radio-frequency heating to such problems have been carried out by application engineers in this field. Accordingly no ex-

TABLE 18. COMPARISON OF RADIO-FREQUENCY HEATING WITH HOT-PLATE HEATING. FOR RADIO-FREQUENCY HEATING THE PRESS PLATES REMAINED AT 80° F. FOR HOT-PLATE HEATING THE PLATES WERE MAINTAINED AT 400° F.

	Radio-Frequency Method			Hot-Plate Method		Comparison of Methods	
	Power into Wood (watts)	Gluing Time (minutes)	Energy (watt-minutes)	Gluing Time (minutes)	Energy (watt-minutes)	Hot-Plate to Radio-Frequency Ratios	
						Time Ratio	Energy Ratio
Gusset Joints $13' \times 2\frac{1}{2}'' \times \frac{1}{2}''$ $(b_i = \frac{1}{2}'')$	6,670	1.1	7,350	2.375	8,520	2.155	1.16
Spar $13' \times 6'' \times \frac{11}{16}''$ $(b_i = \frac{11}{16}'')$	17,900	2.0	35,800	8.32	40,700	4.16	1.138
Blank $6' \times 20'' \times 6''$ $(b_i = 6'')$	37,500	8.2	307,500	342.	409,000	41.7	1.33

tended discussion will be given here, for there is an extensive literature.[*][†][‡][§][‖]

Hot Plates and Radio-Frequency Heating. For many applications involving dielectric heating it is unnecessary to strive for an entirely uniform temperature gradient across the load. Indeed, the cooling effect of the electrodes on the outer surfaces frequently has a beneficial effect, as indicated earlier in this chapter and also in Chapter 20.

There are, however, situations in which a non-uniform distribution of temperature cannot be tolerated. In curing materials that are impregnated with phenolic resins, for example, it is important that all regions are uniformly heated. The common practice of using the pressure plates of the press as electrodes in radio-frequency heating applications places a relatively cold surface in contact with the material, and its outer layers will not be completely cured. One way to circumvent this situation is to maintain the plates at the required temperature by heating them with steam or electricity. Then the temperature distribution will be a combination of the hot-plate curves like those in Fig. 188 and the radio-frequency curves like those in Fig. 194.

---

[*] V. E. Meharg and A. P. Mazzucchelli, "Progress in Heatronic Molding," *Modern Plastics*, Vol. 21, No. 10, June 1944, pp. 108–113, 160.

[†] V. W. Sherman, " High Density Through High Frequency," *Modern Plastics*, Vol. 21, No. 7, pp. 108–109, 172.

[‡] J. P. Taylor, " R-F Heating Speeds Plastic Molding," *Electronics*, Vol. 16, No. 9, September 1943, pp. 102–107, 204–211.

[§] A. R. Tinnerholm, " High Frequency Preheating," *Modern Plastics*, Vol. 23, No. 8, April 1946, pp. 180–182.

[‖] " Methods of Testing," *Plastics Catalogue* 1944, Plastics Catalogue Corporation, 122 East 42d St., New York, p. 39.

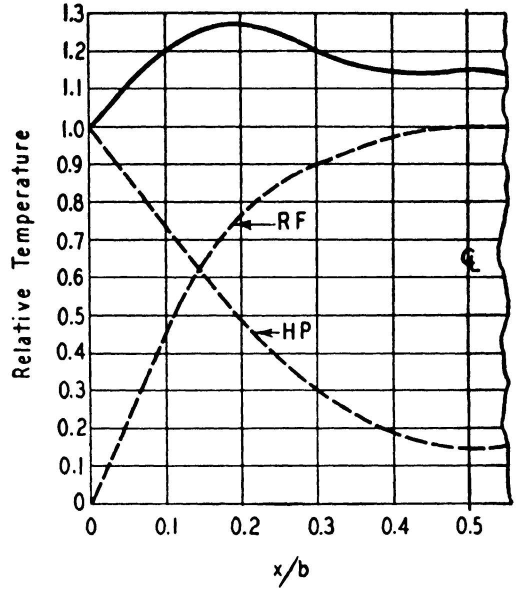

FIG. 197. The solid curve shows the temperature distribution for a combination of hot plate (HP) and radio-frequency (RF) heating when $t_m/b_i^2 = 4$.

For an illustrative case consider a 5-inch section of wood which is to be treated for a 100-minute period. Then $t_m/b_i^2 = 4$ and curve 1 in Fig. 188 shows the temperature distribution across the wood 100 minutes after it was placed in contact with hot plates at some specified temperature. This curve is redrawn in Fig. 197 and labelled HP.

To realize the same specified temperature at the center by dielectric heating in 100 minutes, using cold plates, requires a certain power concentration which may be computed from (18.30) and Fig. 196. The temperature distribution across the wood under these conditions is given by curve D in Fig. 194 — also reproduced in Fig. 197 and labelled RF. The solid curve shows the addition of these two dashed curves and reveals a temperature hump 25 per cent above plate temperature in a region one-fifth of the distance across the wood, while at the center the temperature is 15 per cent above plate temperature. Where a wide tolerance in temperature is permissible this condition is not serious, but in some cases excessive temperature levels induce exothermic reactions which may destroy the material being treated. Most phenolic resin compounds are susceptible to such a condition and the development of hot spots must be avoided.

A similar set of curves is shown in Fig. 198 for a value of $t_m/b_i^2 = 0.45$ which represents a heating time of 11.2 minutes for a 5-inch slab. The solid curve shows a temperature peak 22 per cent above plate temperature quite close to the surface but about 60 per cent of the central region is at or near the specified temperature. Unfortunately there are no combinations of fixed plate temperature and radio-frequency heating which will eliminate this hump completely.

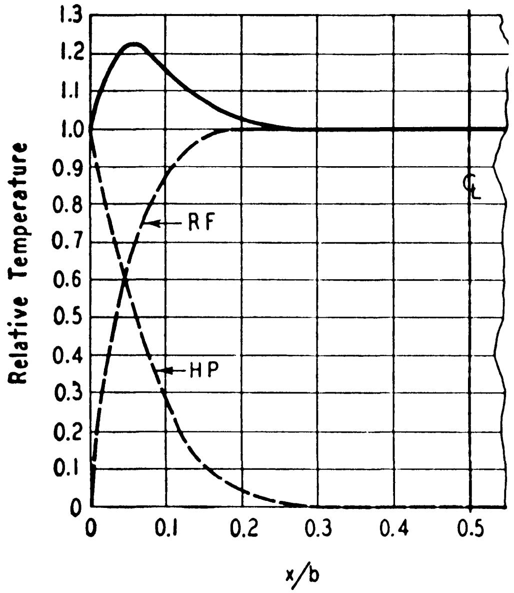

Fig. 198. The conditions of Fig. 197 repeated for $t_m/b_i^2 = 0.45$.

In passing it is of interest to compare the HP curve of Fig. 198 with the family of curves in Fig. 194. It will be seen in Fig. 198 that the temperature drops off very rapidly and that 60 per cent of the interior has not experienced any heating from the hot plates for a value of $t_m/b_i^2 = 0.45$. In any practical case, where hot-plate heating is to be used, such a short time of 11 minutes for a 5-inch slab would not be considered except for gluing thin veneers where only a shallow region adjacent to the surface was to be heated.

A more desirable means of attaining a uniform temperature distribution is to raise the temperature of the plates at the same rate at which the interior temperature is rising due to dielectric heating. Since there is no heat loss into the electrodes the entire mass must be at a uniform temperature. In many cases where such uniform heating is desirable, it is also desirable or necessary to cool the load in the press, under pressure. Hence cold water will be circulated through the plates and it will be necessary to reheat them for each new cycle. Thus, bringing them to temperature at a controlled rate is not a major problem or one that introduces extra operations.

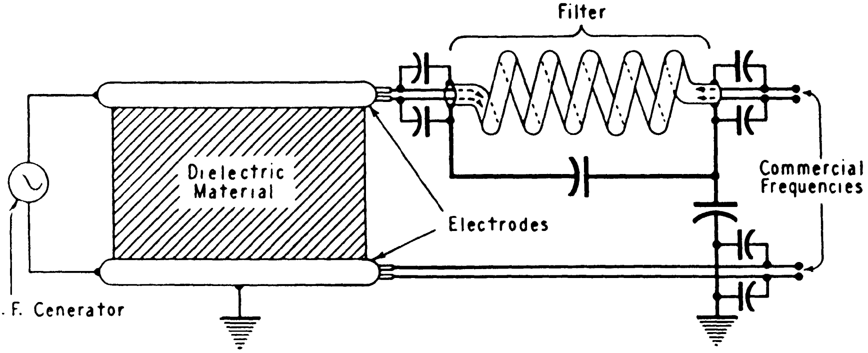

FIG. 199. A by-passed parallel-tuned filter isolates commercial-frequency lines from an electrode operated at high radio-frequency potential.

A method must be found of supplying heat energy to the plates which are also maintained at a radio-frequency potential. Many presses use steam-heated plates which may then be cooled by passing cold water through the steam coils. Supplying the steam and cold water to the high-potential radio-frequency plate through a length of rubber hose generally provides sufficient insulation.

In electrically-heated plates the 60-cycle supply line must be isolated from the radio-frequency voltage. This may be done in several ways. One way is suggested in Fig. 199 where the 60-cycle or other commercial frequency is led through a parallel-tuned filter to the electrode operating at high radio-frequency potential. The leads to the heating coils in the plate are passed through a length of copper tubing which is then formed into a coil and resonated by a capacitor to the nominal frequency of the radio-frequency generator. By-pass condensers between the wires and the coil and also to ground are shown for reducing the possibility of stray radio-frequency voltages.

Another method is similar in principle to this and is particularly useful at high frequencies. It makes use of a well-known property of concentric transmission lines by which a high impedance is developed across one end of a quarter-wave line when the other end is short-circuited. If the leads which are to carry the current to the heater in the high potential electrode are led through and by-passed to the inner conductor of a concentric line, those emanating from the short-circuited end will be at ground potential and can be connected to any suitable source of electrical power. The leads leaving the open end of the line are isolated from the ground by a high impedance and may then be operated at any radio-frequency potential. An illustrative sketch of such a quarter-wave filter is given in Fig. 200. It is obvious that such a method can be used for any single frequency that is high enough to permit the use of a reasonable length of line.

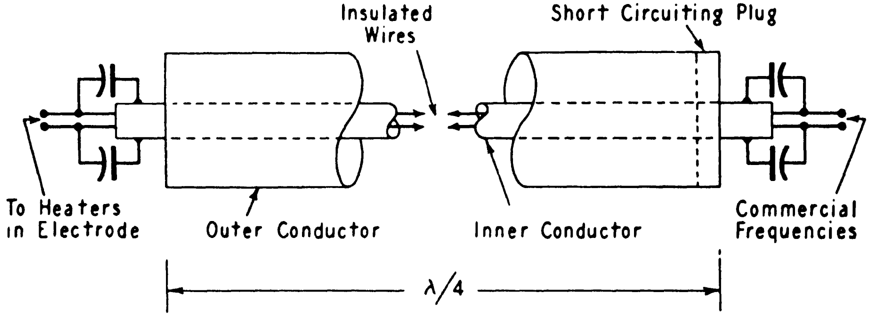

FIG. 200. A quarter-wave line acts as an isolating transformer.

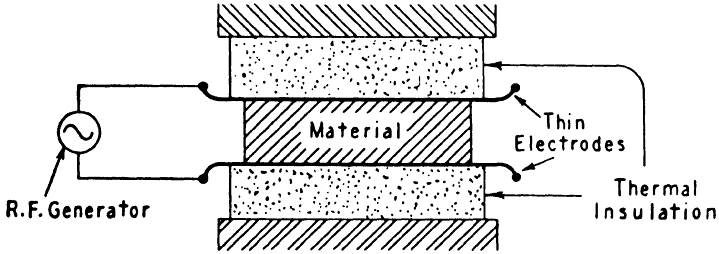

FIG. 201. Thermal insulation and electrodes of low thermal capacity permit an essentially-uniform temperature gradient across material being heated.

Under some conditions a somewhat simpler plan may be used. The pair of wires can be wound in the form of a choke-coil, and where the radio-frequency voltage is not high, sufficient isolation is possible by this method. In any event the " cold " end of the choke-coil should be by-passed to ground.

Where the " sandwich stack " of Fig. 212 in Chapter 19 is used, supplying the pressure plates with heat is no problem as they are at ground potential. A thin electrode at the center has low thermal capacity, and the amount of heat that is conducted out of the stack is negligible.

There is a modification of the " heated electrodes " method which does not require any source of external heat. In place of the massive pressure plates of the press, thin sheets of conducting material are used as electrodes and backed up by a suitable layer of thermal insulation. This layer should also be of high-quality electrical insulation to isolate the electrodes from the structure of the press. When the electrodes have a low thermal capacity as compared to the material being heated, the percentage heat-loss into the plates is negligible and a relatively uniform temperature gradient across the material results. The sketch of Fig. 201 shows one method of arranging such an installation

Chapter 19

SOME SPECIFIC PRESS PROBLEMS

In planning an installation where a dielectric material is to be heated by a radio-frequency current, one of the questions arising relates to the frequency to be used. Many times this is answered in terms of available equipment, but in a general case it should be possible to evaluate the choice of frequency in an intelligent manner.

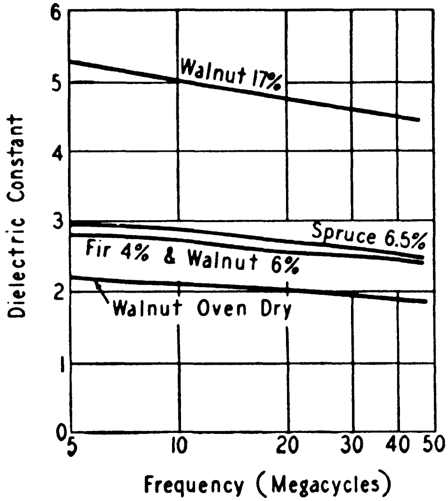

FIG. 202. Effect of frequency on dielectric constant of several species of wood at indicated moisture content.

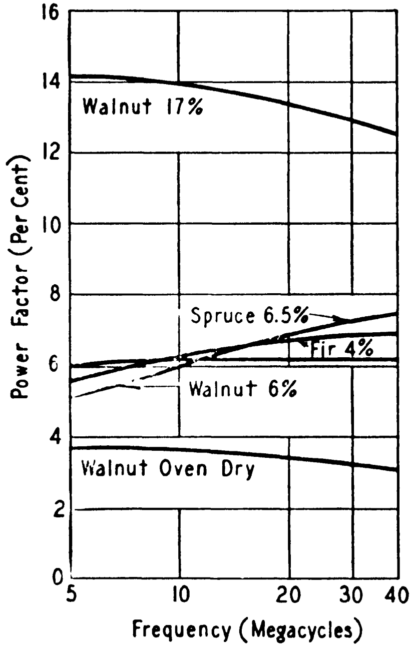

FIG. 203. Effect of frequency on power factor of several species of wood at indicated moisture content.

In Chapter 17 some indication of the importance of frequency was given in the discussion following (17.03). This equation shows the power generated in a centimeter cube, and for convenience is again presented here.

$$P = 2\pi f \cdot p_0\epsilon \cdot (\text{p.f.}) \cdot E^2. \tag{17.03}$$

It is apparent from (17.03) that, at a given frequency, the power absorbed by a dielectric is directly related to its dielectric constant and the power factor. For wood these values are not constant but change with frequency as shown in the curves of Figs. 202 and 203. To assemble the data represented by these curves, measurements were made on a number of samples of fir plywood, Sitka spruce, and walnut all of which were 4 inches long, $2\frac{1}{4}$ inches wide, and $\frac{1}{4}$ inch thick. These measurements were made on a Q-meter as described in Chapter 17. Attention must be drawn to the fact that the curves of

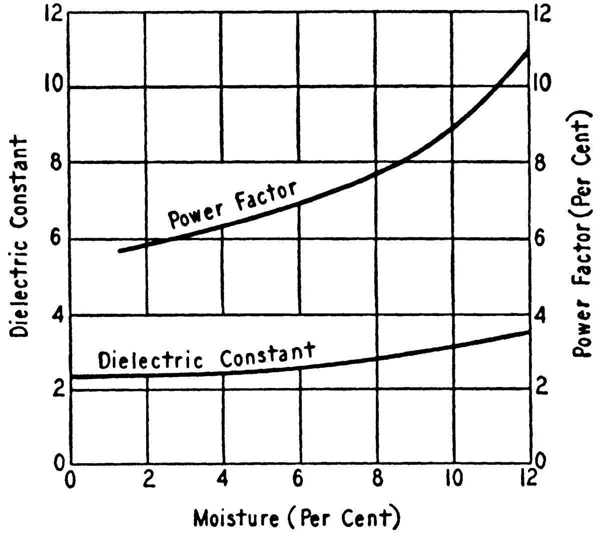

FIG. 204. Variation of power factor and dielectric constant with moisture content for spruce at 45 megacycles.

Figs. 202 and 203 represent an average of a number of measured values as considerable variation is evident between samples. Such evidence is found in the behavior of several samples, each with $6\frac{1}{2}$ per cent moisture content, that were taken at random from a stock of spruce. Their measured power factor varied from 7 to $8\frac{1}{2}$ per cent and the dielectric constant varied between 2.6 and 3.2.

There is also a considerable change in power factor and dielectric constant as moisture content increases. In Fig. 204, curves are drawn which show this interdependence in the case of spruce for measurements made at 45 megacycles.

In view of the wide variations in the electrical properties of these woods it may appear hopeless to find any equitable basis by which (17.03) may be adapted to simplified use. Nevertheless, for a first approximation, the curves of Figs. 202 and 203 show that for a moisture content of from 4 to 7 per cent the product of ϵ and power factor is found to be reasonably close to 0.177 by which (17.03) may be simplified to

$$P_i(\text{watts per cubic inch}) = 25 \times 10^{-8} E_i^2 \cdot f_{mc} \qquad (19.01)$$

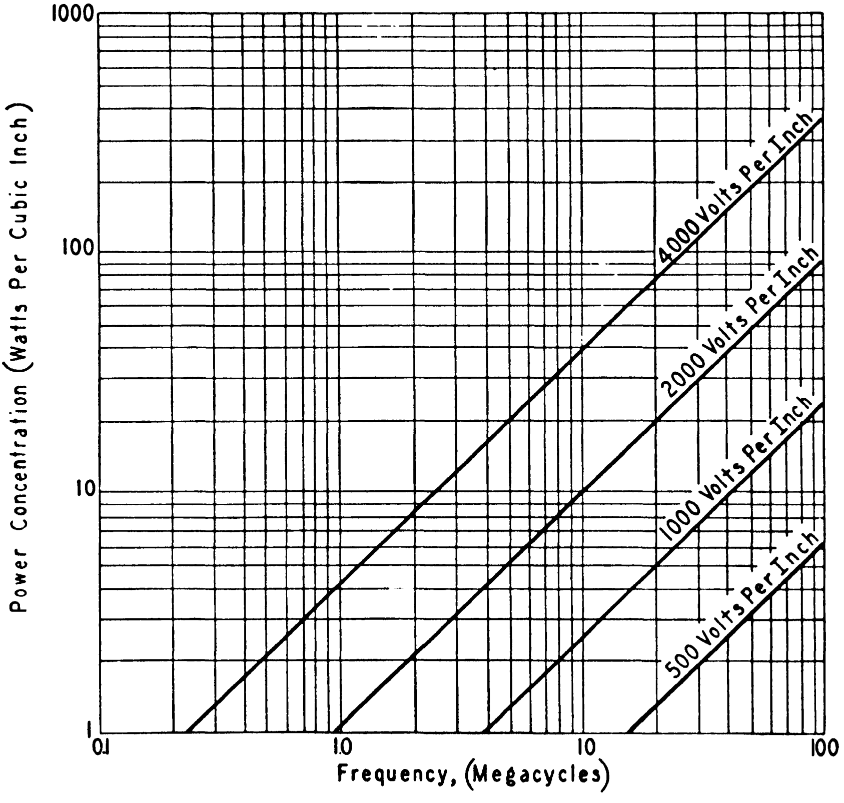

FIG. 205. Relationship of power concentration and frequency at various voltage gradients for spruce with 6½ per cent moisture content.

where:

E_i = volts per inch
f_{mc} = frequency in megacycles

In a specific application of dielectric heating, the permissible voltage across the electrodes is limited by such factors as their configuration, dielectric strength of the material, presence of moisture with possible generation of steam, or irregularities in the wood such as knots. Since the power concentration will usually be fixed by oscillator output and volume of material being heated, a helpful revision of (19.01) is its solution in terms of the electric field. Thus:

$$E_i(\text{volts per inch}) = 2000\sqrt{P_i/f_{mc}} \tag{19.02}$$

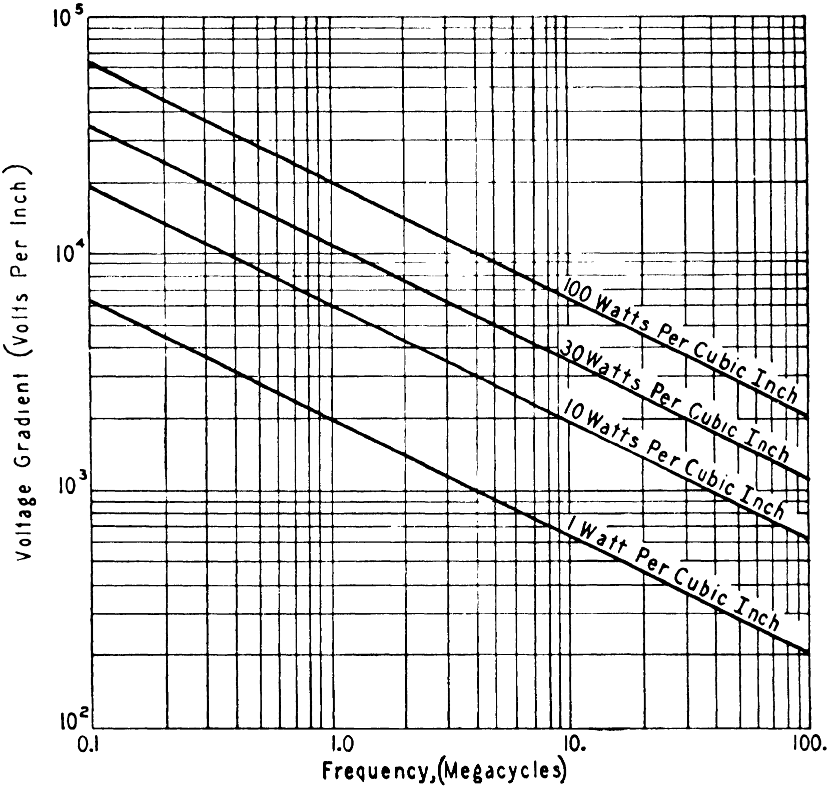

FIG. 206. Relationship of voltage gradient and frequency for various power concentrations in spruce with 6½ per cent moisture content.

The restrictions as to moisture content made above may be justified on the grounds that this range of 4 to 7 per cent is representative of values which are frequently encountered in the wood-gluing industry.

Allowing the approximations that have been made it can then be said that the voltage gradient across a condenser with wood between its plates is directly proportional to the square root of power concentration and inversely proportional to the square root of frequency. Curves showing the relationships expressed by (19.01) and (19.02) are given in Figs. 205 and 206, respectively. Although these curves relate specifically to Sitka spruce they may be used for similar woods having moisture contents normally encountered. In actual gluing operations the power concentration has varied from 5 to 75 watts per cubic inch and the voltage gradient from 1000 to 4000 volts per inch at various frequencies ranging from 1.5 to 45 megacycles. In the gluing of wood, the voltage gradient that may be safely used rarely exceeds 4000 volts per inch and may be as low as 1000 to 2000 volts per inch where considerable moisture is present either in the wood or in the glue.

The curves of Figs. 205 and 206 show clearly the great advantage of using the higher frequencies for heating dielectrics in order that large power concentrations may be used without excessive voltage gradients. Unfortunately, high power at high frequency becomes difficult to generate so that the actual choice of operating frequency may be a compromise. Practical experience has shown that frequencies in the 5-megacycle to 30-megacycle range can be economically generated so that their use for wood-gluing applications can be readily justified.

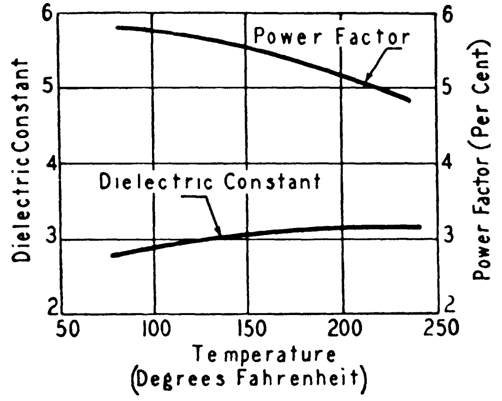

FIG. 207. Variation of dielectric constant and power factor of fir as temperature rises during a gluing cycle.

Another factor that affects the electrical properties of a wood is its temperature. In the course of a gluing cycle, the temperature at the glue line may reach 240° F for catalyzed urea-resin glues and somewhat higher for the phenol glues. The curves of Fig. 207 represent typical changes in the dielectric constant and the power factor as temperature is increased. Here, it will be noted, the product of dielectric constant and power factor does not remain constant, so that a change in the voltage gradient and power concentration will become apparent. The capacitance will also change with dielectric constant, so that the consequent detuning may have an undesirable influence on the oscillator. Means for reducing the effect of this condition will now be discussed.

In practice, it is generally found necessary to connect the press electrodes to the oscillator through a short transmission line which preferably should be of the concentric type in order to eliminate grounding difficulties. To reduce to a minimum the volt-amperes which the line must transmit, it is desirable to tune the press to parallel resonance by connecting an inductance of the proper value in shunt with the electrodes. However, Fig. 207 shows that the dielectric constant of wood varies with temperature so that the capacitance of the press will change during the gluing cycle thereby detuning the circuit and changing the oscillator loading. If the oscillator is self-excited, the frequency will shift to make partial compensation for the detuning, but unless the oscillator tank circuit is very closely coupled to the press the change in loading may be appreciable. In Fig. 208 curves are drawn which show the changes in resistance and reactance that occur in a parallel-tuned press when there in is a change its capacitance.

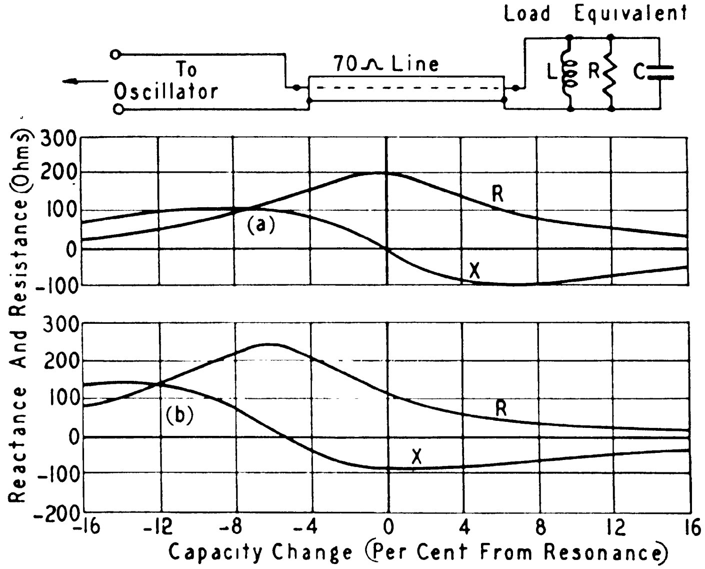

FIG. 208. Effect of capacitance change in the load on the resistance and reactance presented to the oscillator when coupled: (a) directly and (b) through a 70-ohm line, 18° long.

In the curve marked (a) the oscillator is directly coupled to the press, while in (b) a 70-ohm concentric line, 18 degrees long, connects the press to the oscillator. Under typical operating conditions a 10 per cent change in capacitance is frequently encountered during a heating cycle. From Fig. 208

it is seen that such a change in capacitance produces a large change in effective resistance. The use of a quarter-wave transmission line, coupled to the oscillator through a comparatively large reactance, has proved helpful in reducing the changes in loading brought about by the variations in press capacitance. In Fig. 209, curve (a) shows the resistance and reactance presented to the oscillator by a quarter-wave line when loaded at the other end by a parallel-tuned press. Now a 10 per cent change in capacitance results in only about a 10 per cent change in resistance, although the reactance change is larger. However, if the line were supplied with a constant current, as can be approximated by feeding it through a reactance having a value 5 to 10 times that presented by the line, the oscillator loading will be fairly constant. In Fig. 209, curve (b) shows the total reactance when a 400-ohm series reactor is connected into the circuit.

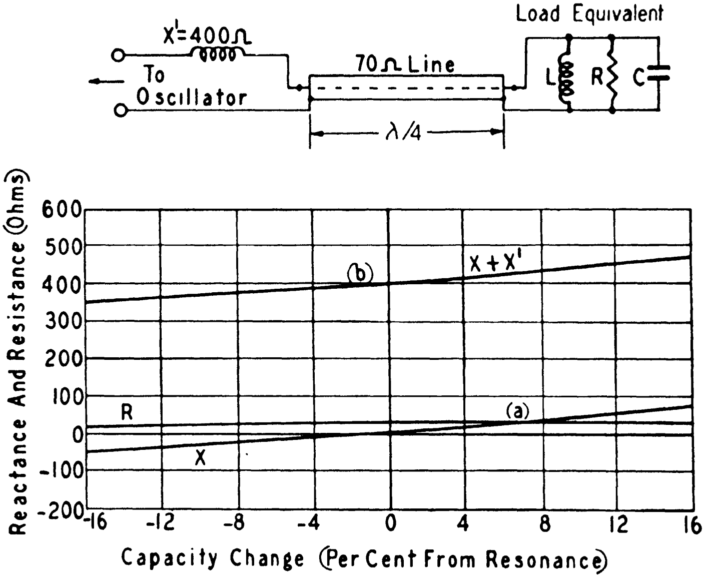

FIG. 209. Effect of capacitance change in the load on the resistance and reactance presented to the oscillator when coupled through a quarter-wave line. (a) Resistance and reactance without series reactor X'. (b) Reactance with 400-ohm series reactor X'. (Resistance remains the same as in (*a*).)

If a line of a quarter-wave length cannot be conveniently employed, it can be partly or entirely replaced by a T or π network. Any transmission line may be represented by an equivalent T network* as shown in Fig. 210 in which

---

* E. A. Guillemin, *Communication Networks*, John Wiley and Sons, Inc., New York, 1936, Vol. II, p. 178.

$$Z_1 = Z_c \tanh P/2 \qquad (19.03)$$

$$Z_2 = Z_c/\sinh P, \qquad (19.04)$$

where Z_c = characteristic impedance of the line;
P = propagation factor of the line in the form $\alpha + j\beta$;
α = attenuation factor, negligible for a short line;
β = phase shift, in degrees.

Thus for a short line (19.03) becomes

$$\begin{aligned} Z_1 &= Z_c \tanh j\beta/2 \\ &= Z_c \sinh j\beta/(1 + \cosh j\beta) \\ &= jZ_c \sin \beta/(1 + \cos \beta), \qquad (19.05) \end{aligned}$$

and (19.04) becomes

$$\begin{aligned} Z_2 &= Z_c/\sinh j\beta \\ &= -jZ_c/\sin \beta. \qquad (19.06) \end{aligned}$$

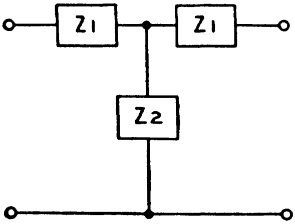

FIG. 210. Equivalent T-network for a transmission line.

In one laboratory application, the concentric line feeding the press was 18 degrees long for an operating frequency of 10 megacycles and had a characteristic impedance of 70 ohms. To "lengthen" this line to 90 degrees required the addition of a network which had a phase shift of 72 degrees. From (19.05) and (19.06)

$$\begin{aligned} Z_1 &= 70 \sin 72°/(1 + \cos 72°) \\ &= 50.8 \text{ ohms, equivalent to 0.8 microhenry at 10 megacycles.} \\ Z_2 &= -70/\sin 72° \\ &= -73.5 \text{ ohms, equivalent to 218 micromicrofarads at 10 megacycles.} \end{aligned}$$

In adapting a press for radio-frequency heating, the design of electrodes and their insulation will largely be dependent on the structure of the press. In general, however, there are two fundamental arrangements by which radio-frequency power may be applied to a press. The first one, shown in Fig. 211, requires an addition to the upper pressure plate of an insulated electrode which is operated at high radio-frequency potential and also becomes the actual upper pressure plate. This insulation must be of low-loss material, otherwise some of the applied energy will be absorbed by the insulator and the efficiency of this press will be reduced. This was the case in the illustrative example given in Chapter 18 where the efficiency of the press was reduced to 63 per cent.

Another arrangement is shown in Fig. 212 where the high-potential electrode is sandwiched between two identical loads and thus the insulation losses of Fig. 211 are eliminated. This method permits the ready adaptation of existing presses to radio-frequency heating since the entire press remains at ground potential.

The Elimination of Standing Waves on Large Presses. The gluing of spars and similar long structures requires the use of presses having a length of 20 feet or more. As mentioned above, to obtain a reasonably short gluing cycle and realize freedom from flashovers it is desirable to use a frequency in the order of 10 to 20 megacycles. However, when power at such a frequency is applied to long electrodes, the voltage distribution along the electrodes will be non-uniform because of standing waves unless proper precautions are taken. The long electrodes may be considered as an unterminated transmission line and the standing waves thereon will have a length dependent on the frequency and the dielectric constant of the material between the electrodes.

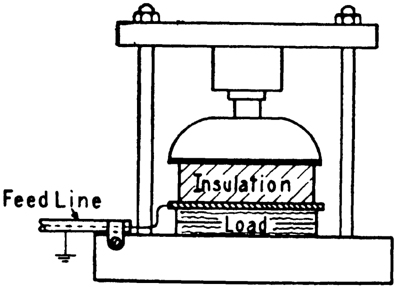

FIG. 211. Method of applying radio-frequency power to a wood-gluing press in which the high-voltage electrode is insulated from the press.

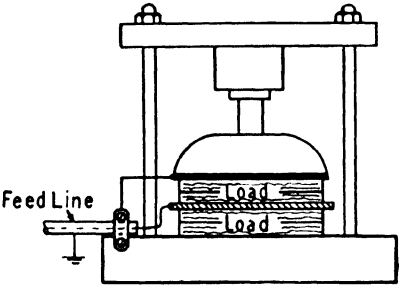

FIG. 212. Balanced loads permit application of radio-frequency power to a press without additional insulation.

In free space, the wavelength is given by the expression

$$\lambda_1(\text{meters}) = v_1/f, \tag{19.07}$$

where v_1 is the wave velocity in free space (3×10^8 meters per second) and f is the frequency in cycles per second. The ratio of the wave velocity v in any other medium to that in free space is

$$\frac{v}{v_1} = \sqrt{\frac{\mu_1 \epsilon_1}{\mu \epsilon}}, \tag{19.08}$$

where $\dfrac{\mu_1}{\mu} = \dfrac{\text{the permeability of free space}}{\text{the permeability of the medium}} = 1$, for wood;

ϵ_1 = the dielectric constant of free space = 1;

ϵ = the dielectric constant of the medium.

The wavelength, when the press is loaded with wood, can be obtained by combining (19.07) and (19.08) as

$$\lambda(\text{meters}) = 3 \times 10^8/(f\sqrt{\epsilon}). \qquad (19.09)$$

For the wavelength in feet and the frequency in megacycles this expression becomes

$$\lambda(\text{feet}) = 984/(f_{mc}\sqrt{\epsilon}). \qquad (19.10)$$

If voltage at a frequency of F megacycles is applied to the plates at one end

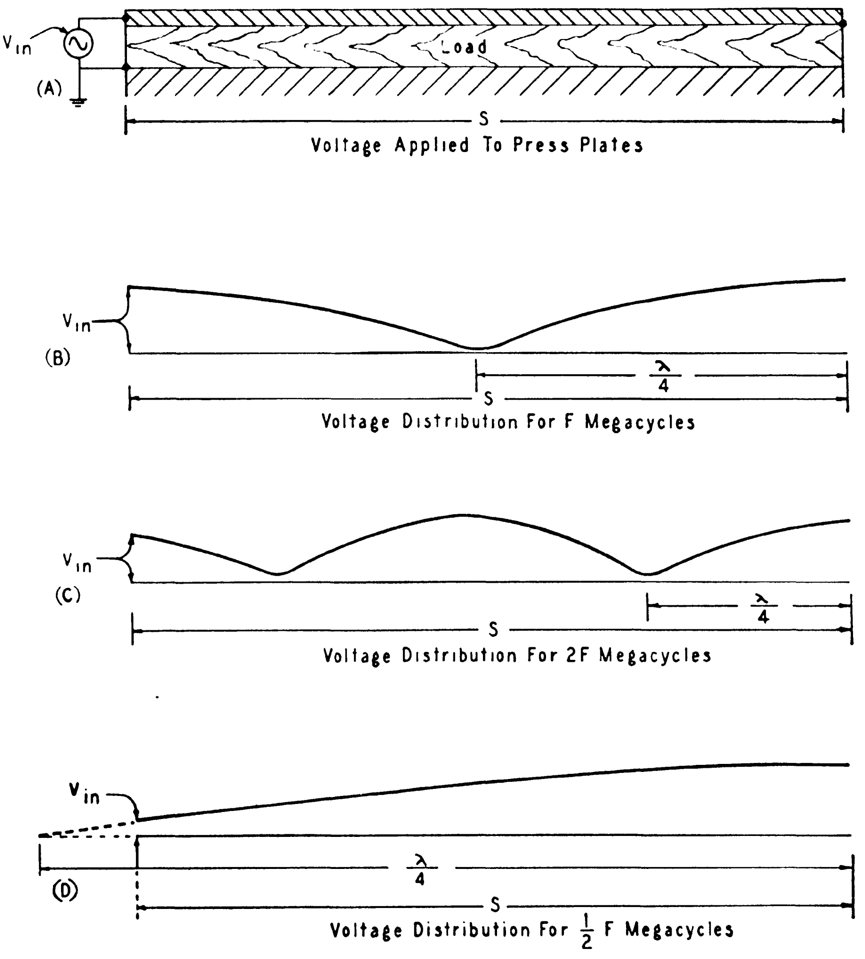

V_{in}
(A)
Load
S
Voltage Applied To Press Plates
V_{in}
(B)
$\frac{\lambda}{4}$
S
Voltage Distribution For F Megacycles
V_{in}
(C)
$\frac{\lambda}{4}$
S
Voltage Distribution For 2F Megacycles
V_{in}
(D)
$\frac{\lambda}{4}$
S
Voltage Distribution For $\frac{1}{2}$ F Megacycles

FIG. 213. Voltage distribution on long presses for several frequencies.

of a press *S* feet long, as shown in Fig. 213A, then the standing wave of voltage may be as shown in Fig. 213B. The standing waves will have maxima at the open end and at a half-wave length and multiples thereof from the open end. The voltage will approach zero at points a quarter-wave length from the maxima. Figs. 213C and 213D show the standing waves for double and half the frequency, respectively, of Fig. 213B. In order to get reasonably uniform voltage on the plates when they are fed in this manner, it is apparent that the frequency applied to the press must be such that a quarter-wave length is considerably greater than the length of the press. For this condition the ratio of the minimum to the maximum voltage appearing on the press plates is given by

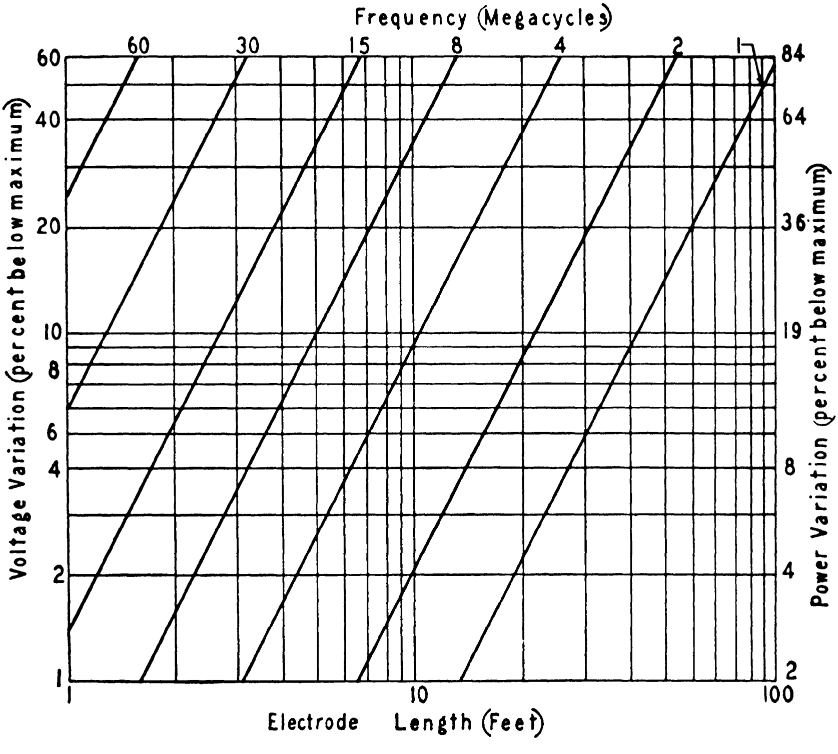

FIG. 214. Variation in power and voltage at several frequencies due to standing waves on long electrodes which are fed at one end.

$$E_{\min}/E_{\max} = \cos\,(360^\circ\, S/\lambda), \tag{19.11}$$

where *S* is the length of the press in feet. Eliminating λ from (19.10) and

(19.11) and solving for the frequency f_{mc} yields

$$f_{mc} = \frac{2.74}{S\sqrt{\epsilon}} \cos^{-1} \frac{E_{\min}}{E_{\max}}; \tag{19.12}$$

where $\cos^{-1} (E_{\min}/E_{\max})$ is expressed in degrees. Since it is desirable to keep the ratio of the minimum to the maximum voltage 0.9 or greater, long presses

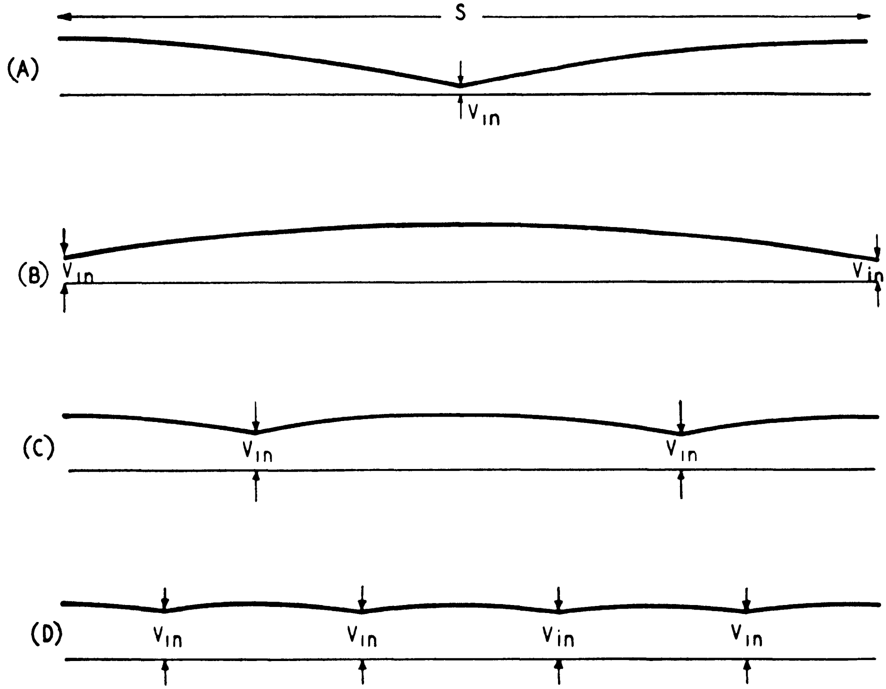

FIG. 215. Voltage distribution on press electrodes of length S when a voltage V is applied at various points.

would require such a low frequency for a desirable voltage distribution that the power concentration for a safe operating voltage as obtained from Fig. 206 would be insufficient for a reasonably-short gluing cycle.

A relationship between the length of a press and percentage variation in voltage or power due to standing waves is given by the graph of Fig. 214 for a number of different frequencies. If the voltage is applied to the plates at the center, each half of the press may be considered separately and the frequency for a given voltage variation is twice that permissible for the case where the voltage is applied at one end. This suggests a means whereby a more uniform voltage distribution may be realized. By feeding the press simultaneously at the centers of two or more equal divisions of the plates, a more uniform voltage distribution results, as shown in Fig. 215. As the number of divisions is increased, the frequency that may be used for a given voltage variation increases proportionately.

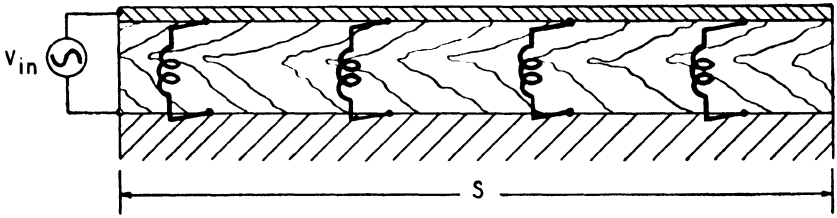

Tuning Inductances Connected Across Press Plates

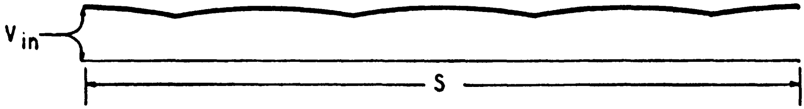

Voltage Distribution Along Press

FIG. 216. Voltage distribution on press electrodes of length S fed at one end and "multiple tuned" by inductors.

The application of identical voltages at various points along the press plates by this method presents a somewhat difficult problem involving the use of a properly-proportioned network of transmission lines. However, the improved distribution resulting from this use of multiple feed lines can be more readily obtained by multiple tuning; that is, by replacing each feed line with an inductor of the proper value to tune its division to parallel resonance, as illustrated in Fig. 216. The transmission line from the oscillator may be connected to the plates at the end or at any other convenient point. The spacing d of these tuning elements for any desired voltage ratio and frequency may be obtained from (19.12), noting that the value of S in that expression is equal to one-half of the spacing. Thus, in terms of d, (19.12) becomes

$$d \text{ (feet)} = \frac{5.48}{f_{mc}\sqrt{\epsilon}} \cos^{-1} \frac{E_{\min}}{E_{\max}}. \tag{19.13}$$

The quantity ϵ in the above expression is the average dielectric constant of the material between and around the plates. If the dielectric constant of the wood between the plates only is used, the value of spacing obtained will be somewhat conservative.

Since the tuning inductors placed in parallel across the electrodes must collectively tune the capacitance of the press to parallel resonance, the inductance of each tuning inductor is given by

$$L \text{ (microhenrys)} = (n \times 10^6)/(4\pi^2 f_{mc}{}^2 C), \qquad (19.14)$$

where n = the number of equally-spaced tuning elements;
f_{mc} = the frequency in megacycles;
C = the capacitance of the press plates in micromicrofarads.

At resonance the press will then present to the feed line a resistive load having a value of approximately

$$Z_r \text{ (ohms)} = 10^6/(2\pi f_{mc} C \cos\theta). \qquad (19.15)$$

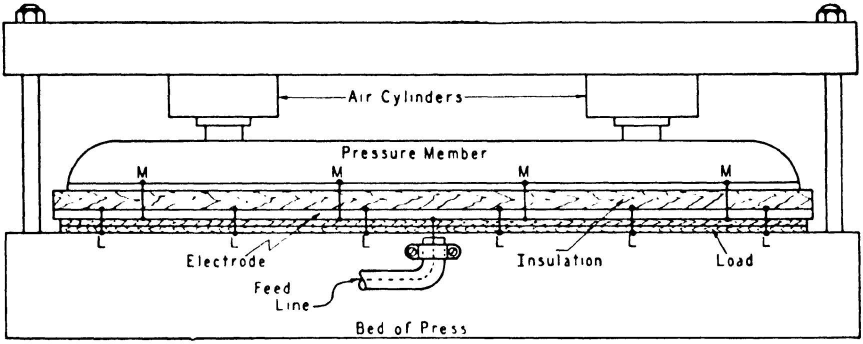

Fig. 217. Wood-gluing press adapted for radio-frequency heating at 45 megacycles as described in the text.

Two illustrative examples of the use of multiple tuning in the elimination of standing waves on press plates will be given. A conventional hot-plate gluing press with plates 13 feet long was adapted for the radio-frequency gluing of spruce spars. The spars were made up of three laminations each 13 feet long, 6 inches wide, and $\frac{5}{16}$ inch thick. As shown in Fig. 217, a thick piece of fir planking was used to insulate the upper electrode from the upper pressure member of the press, and the bed of the press was used as the lower, grounded electrode. An oscillator with an operating frequency of 45 megacycles was available. Without multiple tuning the standing waves which resulted from the application of power at this frequency to the center of the press are shown by the curve in Fig. 218 labelled "stubs disconnected." Measurement of this voltage distribution was made by taking vacuum-tube-voltmeter readings at 6-inch intervals along the press when low power was applied. The spacing of the tuning inductors used to correct this condition was calculated from (19.13) using the following constants:

f_{mc} = 45 megacycles
ϵ = 2.4 (dielectric constant for spruce, from Fig. 202);
$\cos\theta$ = 0.076 (power factor for spruce, from Fig. 203);
S = 13 feet (length of the press);
$E_{\min}/E_{\max}$ = 0.9 (chosen value of voltage ratio);

$$d = \frac{5.48}{45\sqrt{2.4}}\cos^{-1} 0.9 = 2.04 \text{ feet (tuning stub spacing).}$$

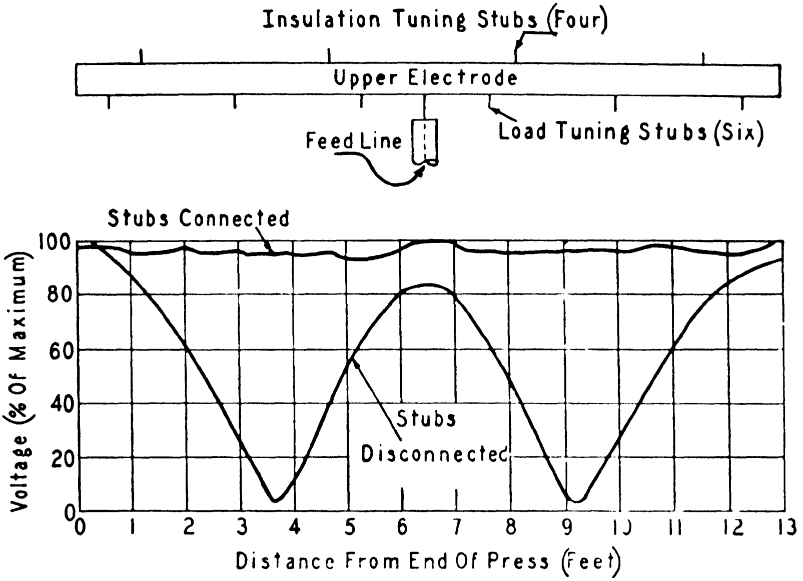

FIG. 218. Measured voltage distribution along the press electrodes of Fig. 217 at 45 megacycles.

Actually six tuning elements were used with a spacing of 2.17 feet. After measuring the capacitance of the press and finding it to be 700 micromicrofarads, the inductance value was obtained from (19.14) thus:

$$L = 6/(4\pi^2 \times 45^2 \times 700) = 0.107 \text{ microhenrys.}$$

Each inductor was made by bolting a 6-inch piece of $\frac{1}{2}$-inch copper tubing to the upper and lower electrodes of the press and joining the ends by a movable strap to facilitate final tuning. With low power applied to the press, adjustment of the strap was made for maximum deflection in a thermogalvanometer loosely coupled to the inductor by a coil across its terminals. When the press is tuned to resonance its impedance is given by (19.15) as

$$Z_r = 10^6/(6.28 \times 45 \times 700 \times 0.076) = 66 \text{ ohms (approximate).}$$

In Fig. 218 the curve labelled " stubs connected " shows the voltage distribution when the radio-frequency energy was supplied to the center of the press and the tuning elements were connected at the locations shown in the figure. It will be noted that four tuning inductors were also connected from the upper electrode to the upper pressure member of the press to tune the insulation.

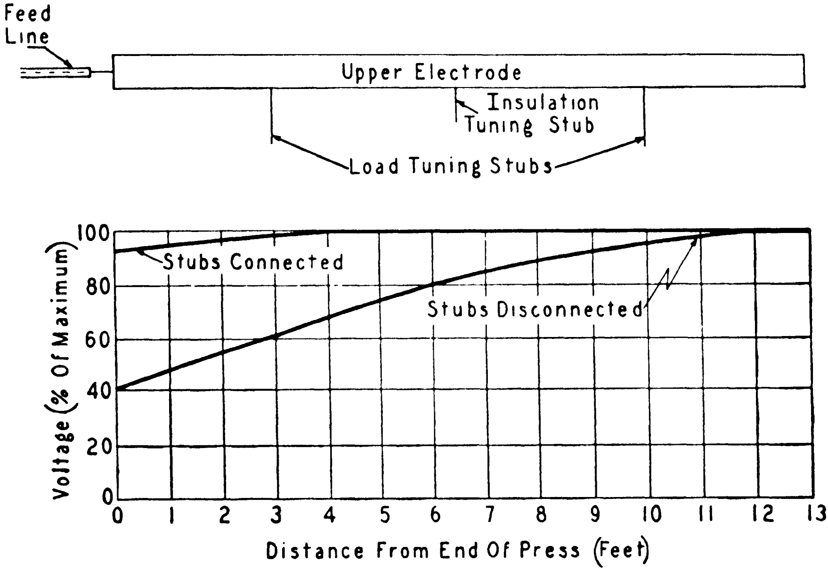

FIG. 219. Measured voltage distribution along electrodes when the press of Fig. 217 was adapted for radio-frequency heating at 10 megacycles. Note changed location of tuning stubs.

This same press was later modified for the gluing of gusset joints in large plywood sheets. Because the large sheets had to be fed through the press, the tuning-inductor arrangement of Fig. 218 was impracticable. The frequency was lowered to 10 megacycles so that only two tuning inductors would be required to give a sufficiently uniform voltage distribution. These inductors which had a value of about 0.6 microhenry were connected to the upper electrode at points 3 feet from the ends. As they were long enough to extend to the ends of the press where they were connected to the press bed, the passage of large sheets through the press was not obstructed. The voltage distribution on the press plates with and without the tuning inductors connected is shown in Fig. 219 for an application of radio-frequency energy to one end of the press. This gluing operation involved the heating of a glue line at the center of a volume of fir plywood $2\frac{1}{2}$ inches wide, $\frac{1}{2}$ inch thick, and 13 feet long to a temperature of 240° F and was accomplished in 1.1 minutes with a power input to the press of $7\frac{1}{2}$ kilowatts.

Chapter 20

A RADIO-FREQUENCY SEWING MACHINE

Bonding Thin Thermoplastic Sheets. The discussion in Chapter 18 may lead the reader to feel that for very thin sheets or plies the advantage of radio-frequency heating may be offset by the additional precautions needed to prevent loss of heat into the electrodes. There are some materials, however, to which this objection cannot be applied, and which respond particularly well to the use of radio-frequency heating for bonding them. These materials include many of the synthetic resins which are readily extruded, pressed or rolled into sheet form, a few thousandths of an inch thick. They are chemically inert; more or less impervious to water, moisture, or gas; light in weight; physically strong; and pleasing in appearance. The physical properties of several such materials are listed in Table 19.

These materials are all thermoplastic and soften readily when temperature is elevated. At approximately 150° C and with moderate pressure it is then generally possible to fuse or weld them together without any solvent, cement, or adhesive. They are, however, all comparatively good heat insulators and if an attempt is made to bond together two or more sheets of such material by applying hot plates or rollers, the outer layers must be heated to such a high temperature that they become gummy and sticky long before the inner contiguous surfaces have attained the temperature of plasticity. This state of affairs is graphically represented in Fig. 220 where hot plates A and B are shown in intimate contact with the outside surfaces of sheets (a) and (b) which are to be bonded along the surface (c). The plates must be maintained at a sufficiently high temperature *Plate* so that the interfacial temperature *Bond* will be high enough above room temperature *Room* to make the material plastic in the region to be bonded. A typical temperature distribution across the material under these conditions is shown by the dotted curve HP, which also indicates the relative plasticity of the material between its external faces.

It is apparent that the hot plates will produce excess softening of the outer surfaces, with consequent extrusion of the material when pressure is applied, as indicated by Fig. 221. The greatly-softened surface is weakened along the seam by extrusion and in its gummy condition sticks to the hot plates which must frequently be cleaned during production. In addition, the low thermal conductivity of most thermoplastic materials limits the speed at which sealing may be done.

When a radio-frequency field is applied across the seam, heat is generated uniformly by dielectric loss. When sufficient power is used, the temperature of plasticity may be attained in a very short time. Referring again to Fig. 220, consider A and B as the electrodes between which an electric field is established, while (a) and (b) represent, as before, the thermoplastic sheets to be bonded along line (c). The good heat conductivity of the metal electrodes keeps the outer layers of the material comparatively cool so that a typical temperature distribution across the material is that shown by the curve RF, which also represents the relative plasticity of the material between the plates under these conditions.

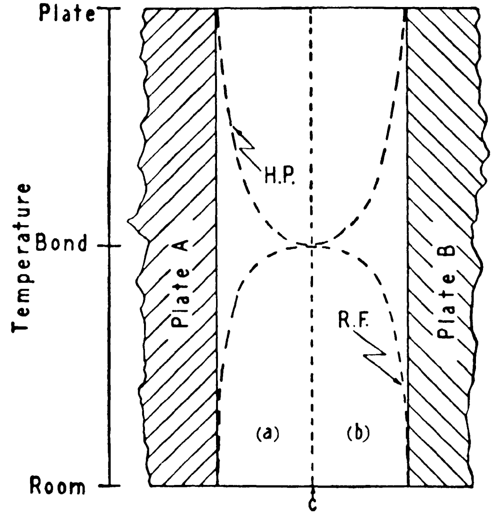

Fig. 220. Typical temperature distribution curves across thermoplastic material to be bonded. HP: Curve for hot-plate heating, RF: Curve for radio-frequency heating.

It is apparent that the highest temperature is in the central region, where the greatest softening should occur for the two layers to be properly fused. When the electrodes are made to exert a slight pressure during the application of the radio-frequency field, the softened interfacial surfaces will bond as shown in Fig. 222, with negligible deformation of the outer surfaces.

TABLE 19. PHYSICAL PROPERTIES OF TYPICAL THERMOPLASTIC MATERIALS.*

	Pliofilm	Vinylite	Koroseal	Saran
Manufactured by	Goodyear Tire & Rubber Company	Carbide & Carbon Chemicals Company	B. F. Goodrich Company	Dow Chemical Company
Chemical family	Rubber hydrochloride	Vinyl chloride resin	Vinyl chloride resin	Vinylidene chloride resin
Thermal conductivity (k) (cal./sec./sq. cm. per ° C./cm.)	3.0×10^{-4}	4.0×10^{-4}	4.0×10^{-4}	2.2×10^{-4}
Specific heat (c) (cal./gr.)	0.39 to 0.43	0.32 to 0.51	0.32 to 0.51	0.32
Density (ρ) (gr./c.c.)	1.64	1.2 to 1.6	1.2 to 1.6	1.65 to 1.75
Thermal diffusivity (α^2) (sq. cm./sec.)	4.56×10^{-4}	10.4×10^{-4} to 4.9×10^{-4}	10.4×10^{-4} to 4.9×10^{-4}	4.0×10^{-4}
Softening temperature (for fusing)	110° C	90° C to 150° C	90° C to 150° C	110° C to 140° C
Breakdown voltage	250 to 450 volts per mil	250 to 450 volts per mil	250 to 450 volts per mil	350 volts per mil.

---

[*] From "Plastics Properties Chart," Plastics Catalog, published by Plastics Catalog Corporation, 122 East 42d Street, New York.

The sealing process may be made continuous when the fixed electrodes of Fig. 220 are replaced by rotating electrodes between which the material to be bonded may pass in a manner similar to that of a sewing machine. Uniform feeding of the material is accomplished by gearing the electrodes together in such a way that their peripheral speeds are identical. Unless both wheels are driven there is considerable slippage between layers on long seams, with consequent improper registry or wrinkling.

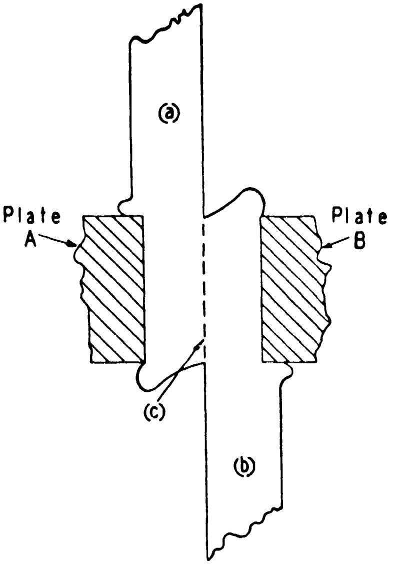

Fig. 221. Application of heated plates A and B cause extrusion due to excessive softening at the surface.

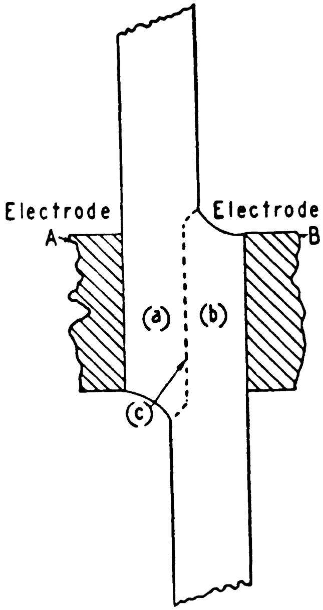

Fig. 222. Cool electrodes A and B prevent overheating of the surface. Contiguous surface (c) is softened most by radio-frequency heating.

The radio-frequency field may be readily established between the electrodes by coupling them to the output of a small oscillator through a suitable transmission line. Later in this chapter some attention will be given to practical ways of coupling the oscillator to such electrodes.

An outstanding advantage of this method of heating lies in its flexibility. Having once determined suitable operating parameters such as speed, power, and pressure, the controls can be instantly adjusted to reproduce any desired condition.

An experimental model of a complete operating unit was developed by the authors for bonding various types of thermoplastic sheeting. A photograph

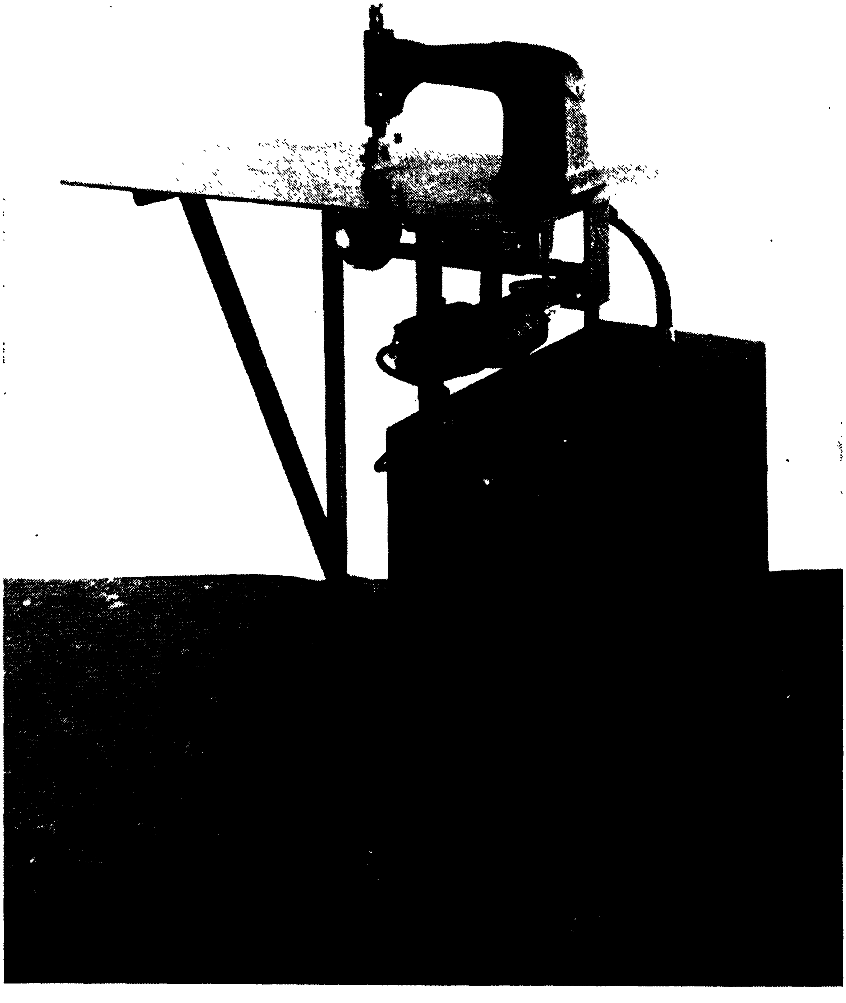

FIG. 223. Experimental model of radio-frequency sewing machine built by the authors.

of this machine is shown in Fig. 223. A framework supports the rotating electrodes and work table at convenient level, with the oscillator and its power supply housed in an integrally-associated metal cabinet. Power and tuning controls are mounted on the front panel of the metal cabinet. A variable-speed drive is geared to the rotating electrodes so that the small upper and larger lower electrodes have the same peripheral speeds.

The radio-frequency power is conducted from the oscillator to the elec-

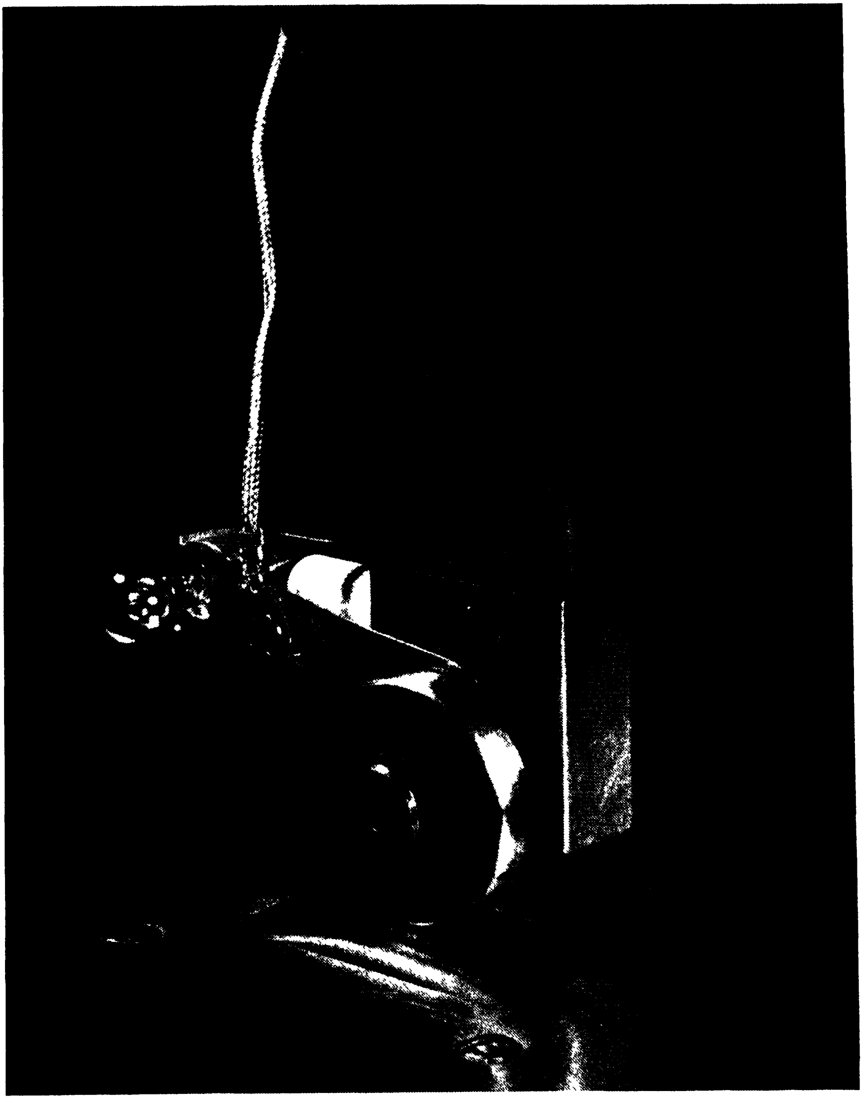

FIG. 224. Detail of rotating electrodes.

trodes by a concentric line which is carried through a modified sewing-machine head. In this model the small wheel which serves as the upper electrode operates at a radio-frequency potential above ground. It is insulated from the head of the machine by a high-grade insulating material and derives its voltage from the inner conductor of the transmission line through a brush.

Details of this arrangement are shown in Fig. 224. The outer conductor is solidly grounded to the head at a point near the small electrode-wheel. The current in the outer conductor flows back on the outside of the head to the large lower electrode-wheel. At 60 megacycles this inductive loop in series with the line is not a serious handicap and it is not difficult to develop sufficient voltage across the electrodes to bond material having a total thickness as great as $\frac{1}{8}$ inch.

The simplest way to supply this voltage to the electrodes is to make the transmission line essentially a quarter-wave in length. Then there will be a maximum current at the pickup loop and a maximum voltage at the end to which the electrodes are connected. The oscillator is tuned until its operating frequency is such that this condition is realized, as indicated by maximum brilliance of a small neon lamp mounted near the high-potential electrode. In the 60-megacycle region such a system is practical but at higher frequencies some of the advantages fade away. The line may become too short for convenience and with a longer line, an odd number of quarter-waves in length, the losses generally become excessive. More serious is the effect which the inductive loop of the head introduces. At higher frequencies this is considerable and it may be difficult to develop sufficient voltage across the electrodes. Also radio-frequency voltages may appear on some parts of the head, so that auxiliary means must be found for keeping the entire head at ground potential. This is readily done by a half-wave open-wire line short-circuited at the far end. One side of the line can be connected to the head on the side away from the operator and at the point where the outer conductor of the transmission line terminates. The other side of the line is grounded to the lower electrode by a brush. In many cases the work table is metallic and it can then serve as one of the conductors of the half-wave line. This plan has been used with good success when the sewing machine of Fig. 223 was adapted for operation from an auxiliary 200-megacycle 100-watt oscillator. In this case the load was tuned by stubs placed across the transmission line, rather than by tuning the oscillator until its frequency matched the load requirement.

The choice of a suitable frequency for operation is a matter of some importance. Early experimental tests were made at 15 megacycles and then at 45 megacycles where considerable improvement in operation was noted. The final choice of a 60-megacycle oscillator in the experimental machine of Fig. 223 was dictated largely by the simplicity of power generation at this frequency and the ease with which energy could be conducted to the electrodes by a quarter-wave line of convenient length. For some materials operation at this frequency is practical, but when reference is made to Fig. 228 it will be seen that the voltage across the material may exceed its breakdown resistance as speed of operation is increased. Other materials having relatively low loss, may require the application of an excessive voltage before sufficient heating occurs, unless subjected to the highest frequency possible. It should also be noted that those materials particularly designed to be good insulators cannot be bonded by this method. Polyethylene and unplasticized Vinylite are illustrative examples of this group.

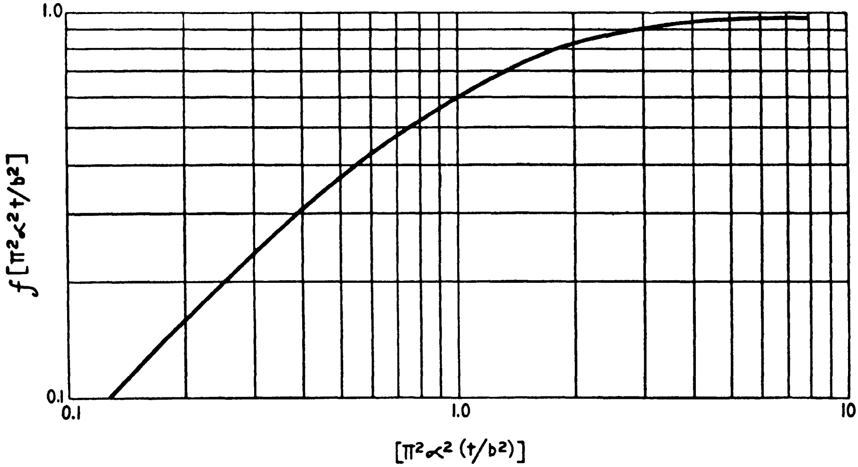

FIG. 225. Graphical relationship of equation (20.02) for numerical solution of heat-flow problems of the type described in the text.

The actual power required to make a bond, allowing for heat lost into the electrodes, is low and may be calculated from the general equation (18.24) for any material whose physical constants are known. As this equation is somewhat cumbersome to use in making computations a graphical short cut will be introduced.

Inspection of (18.24) reveals that it is of the form:

$$u_{x=b/2} = \frac{4\mathcal{H}b^2}{\pi^3 k} \cdot f[\pi^2\alpha^2(t/b^2)], \tag{20.01}$$

where

$$f[\pi^2\alpha^2(t/b^2)] = [1 - \epsilon^{-\pi^2\alpha^2(t/b^2)} - \frac{1 - \epsilon^{-3^2\pi^2\alpha^2(t/b^2)}}{3^3} + \cdots] \tag{20.02}$$

Thus a relationship exists between the numerical value of the right-hand side of (20.02) and the numerical value of the modulus $[\pi^2\alpha^2(t/b^2)]$. This is the relationship plotted in Fig. 225, and the method of using it is developed in the following paragraphs.

From (20.01) the power required per unit volume to produce a temperature increment u is found to be

$$\text{Watts per cubic centimeter} = \frac{4.187\pi^3 ku}{4b^2 \cdot f[\pi^2\alpha^2(t/b^2)]}. \tag{20.03}$$

When making a bond having a width of d centimeters, the actual volume heated at any instant can be considered as being a right circular cylindrical element d centimeters in diameter and b centimeters high. Its volume is then $\pi d^2 b/4$ cubic centimeters. Thus the total power, P_t, to heat this cylindrical element will be (20.03) multiplied by $\pi d^2 b/4$ or

$$P_t\ (\text{watts}) = \frac{4.187\pi^4 kud^2}{16b \cdot f[\pi^2\alpha^2(t/b^2)]} \tag{20.04}$$

where P_t = total power, in watts, to heat cylindrical element;
k = thermal conductivity (4×10^{-4});
u = temperature increment (130° C);
d = width of bond, in centimeters;
b = total thickness of material being sealed, in centimeters;
α^2 = thermal diffusivity, in square centimeters per second (6.7×10^{-4});
t = time of heating each cylindrical element = d/v seconds;
v = velocity of sealing, in centimeters per second.

In the tabulation just preceding, the numerical values in parentheses are typical values for Vinylite selected from Table 19. When these values are inserted in (20.04) with d set equal to 0.2 centimeter, we have

$$P_t = \frac{0.0528}{b \cdot f\left[\dfrac{13.2 \times 10^{-4}}{b^2 v}\right]}, \tag{20.05}$$

which expresses the power requirement for bonding Vinylite in terms of thickness and speed.

In practical use, it is usually customary to speak of velocity in feet per minute rather than centimeters per second as required in the foregoing equations. Hence,

$$v_{\text{ft./min.}} = \frac{v_{\text{cm./sec.}} \times 60}{12 \times 2.54} = 1.97 v_{\text{cm./sec.}} \tag{20.06}$$

It is of interest to note that as an approximation one may say the velocity in " feet per minute " is *twice* the velocity in " centimeters per second."

The power requirements for bonding two layers or three layers of 0.01-centimeter Vinylite are shown in Fig. 226 at speeds up to 20 feet per minute. These curves were calculated from (20.05) after the numerical value of

$f\left[\frac{13.2 \times 10^{-4}}{b^2 v}\right]$ had been determined from Fig. 225 for various speeds v, in centimeters per second, and the appropriate value of b, the total thickness in centimeters. The voltage V appearing across the material under the conditions defined in (20.04) and displayed in Fig. 226 can be found from the relationship

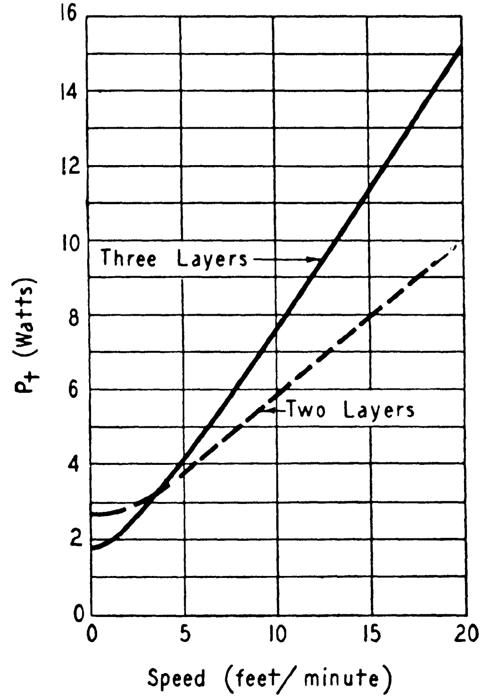

FIG. 226. Power requirements in terms of speed for bonding Vinylite sheets, nominally 4 mils (0.01 centimeter) thick.

$$P_t = V^2 G, \tag{20.07}$$

where V = total voltage appearing across material;
G = total conductivity in mhos
$= \frac{\sigma A}{b} = \frac{\sigma}{b} \cdot \frac{\pi d^2}{4}$;
A = area, in square centimeters;
σ = conductivity in mho-centimeters,
d = diameter of cylindrical element, in centimeters.

Then (20.07) becomes

$$P_t = \frac{V^2 \sigma \pi d^2}{4b}, \tag{20.08}$$

and

$$V = \sqrt{\frac{4bP_t}{\pi d^2 \sigma}}. \tag{20.09}$$

When it is recalled that the conductivity σ is proportional to frequency, dielectric constant, and power factor as expressed in (17.02), then it is seen that (20.09) is a more general form of (19.02) which was developed for wood-gluing.

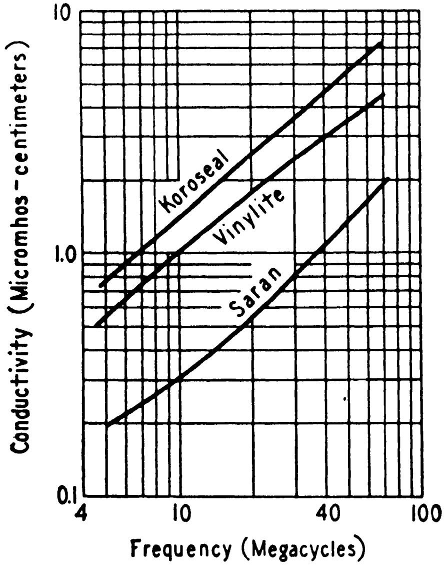

FIG. 227. Change of conductivity with frequency for three thermoplastic materials.

To permit a solution of (20.09) it is necessary to know the conductivity of the material under examination for the frequency at which bonding is to take place. Measurements on three common thermoplastics have been made at several frequencies ranging from 5 to 200 megacycles and the measured values of conductivity have been plotted against frequency in Fig. 227.

The voltages required to bond Vinylite in two layers and three layers at speeds up to 20 feet per minute have been calculated from (20.09) and Figs. 226 and 227 for three different frequencies. These calculations have been plotted in Fig. 228 and indicate how rapidly the voltage rises as speed is increased. Experience has shown that successful bonding cannot be done when voltage is near the breakdown value for the material. Data presented in Table 19 show that Vinylite should withstand 250 to 450 volts per mil, but actually it is far better not to exceed 100 to 125 volts per mil when bonding with the radio-frequency sewing machine. Thus, for two layers of 0.01-centimeter (nominally 4-mil) material the maximum voltage should not be over 1000 volts. For 60-megacycle operation this places the operating speed at 10 to 12 feet per minute, but at 200 megacyles speeds in excess of 20 feet per minute can be realized.

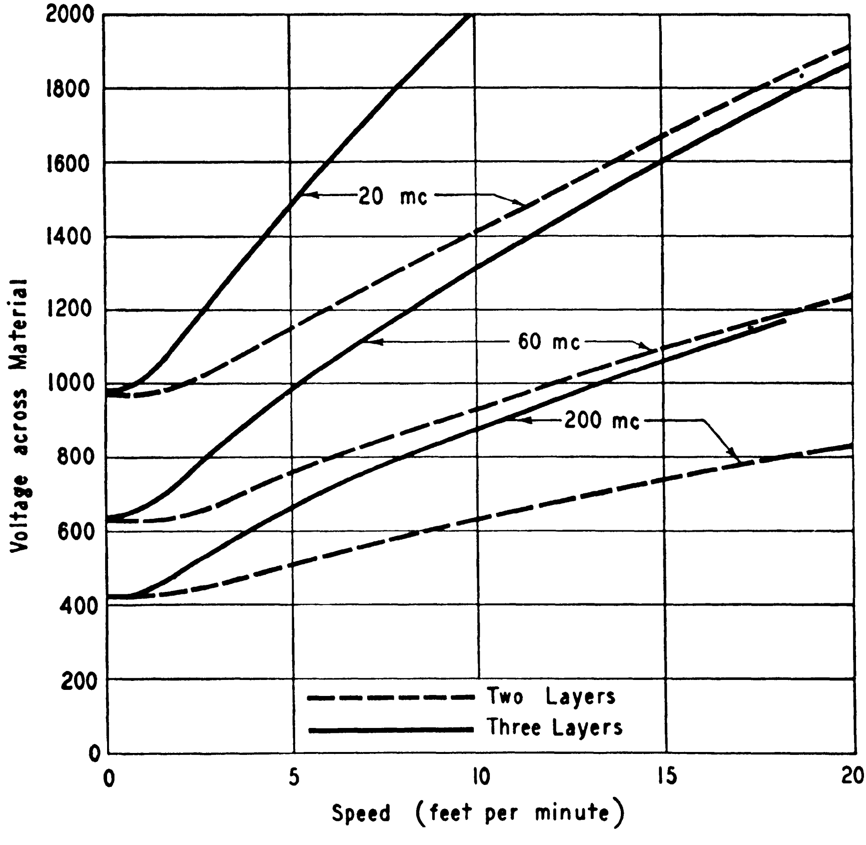

FIG. 228. The effect of speed on the voltage developed across two or three layers of 4-mil Vinylite when bonded at 20, 60, or 200 megacycles.

It is instructive to examine (20.05) from the standpoint of power requirements in terms of thickness. Curves expressing this relationship appear in Fig. 229 which show that as the thickness decreases more power is needed. This increase in power represents that necessary to replace the heat lost into the wheels. With an increase in power the voltage across the material must also rise and breakdown often occurs. This effect was noticed by the authors when attempting to bond 1-mil Koroseal, a material similar to Vinylite. It was not successfully done until a tape of similar material, 2 mils thick was fed between the two sheets of Koroseal. This additional thickness reduced the voltage gradient sufficiently to eliminate breakdown completely.

It is of interest to note in Fig. 229 that for each speed there is a thickness at which minimum power is required to affect a bond. As applied to Vinylite minimum power is required to bond a total thickness of 0.01 centimeter (0.004 inch) at 20 feet per minute; or 0.017 centimeter (0.007 inch) at 10 feet per minute; or 0.02 centimeter (0.008 inch) at 5 feet per minute.

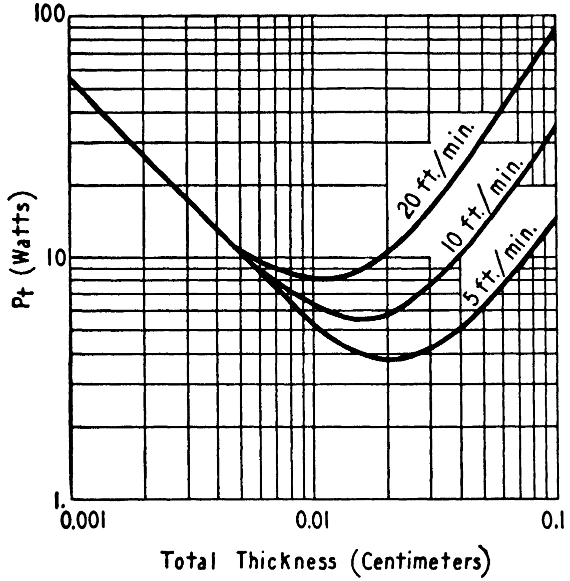

FIG. 229. Comparison of power requirements in terms of total thickness for several bonding speeds.

For repetitive work where numerous identical bonds are to be made, the rotating electrodes of the sewing machine can be replaced by suitably-shaped bar electrodes. A photograph of such a modification as applied to an early experimental model is shown in Fig. 230. The use of bar electrodes greatly increases the volume to be heated, but a longer time cycle may be used. The net result of this is a sharp reduction in the voltage that must be applied across the load.

Compare, for example, the conditions required to make a bond 6 inches long when rotating electrodes are used to those when bar electrodes are used.

At a bonding speed of 10 feet per minute for the rotating electrodes, 3 seconds would be required to make a seal 6 inches long. For two layers of Vinylite, each 0.01 centimeter thick, the power required from Fig. 226 would be 5.8 watts and at 60 megacycles the total voltage across the material from Fig. 227 would be 930 volts. If a bar 6 inches long were used the volume to be sealed would be 0.061 cubic centimeter which is about 100 times the volume being heated at any instant with rotating electrodes.

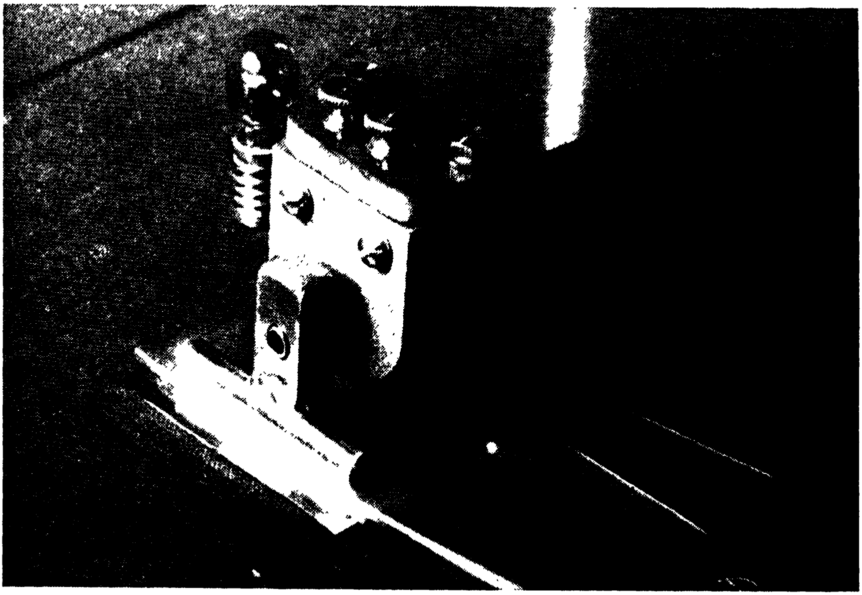

FIG. 230. Bar-sealing attachment applied to an early experimental model of the radio-frequency sewing machine.

Now assume that it is desired to make the 6-inch seam with bar electrodes in 0.3 second. Then from (20.03) and Fig. 225 we find that for a volume of 0.061 cubic centimeter the power requirement is

$$P_t = \frac{4.187\pi^3 ku}{4b^2 \cdot f[\pi^2\alpha^2(t/b^2)]} \times 0.061 = 255 \text{ watts}, \qquad (20.10)$$

which is applied over an area of 3.04 square centimeters. For this amount of power, the voltage appearing across the load can be found from (20.09) and Fig. 227 as

$$V = \sqrt{\frac{255 \times 0.02}{4.2 \times 10^{-6} \times 3.04}} = 633 \text{ volts}.$$

This is a value considerably below that necessary for rotating electrodes, and in the example cited, the bond is made in one-tenth the time. Devoting a longer time than 0.3 second to this operation has negligible effect on the power requirement, since the numerical value of $f[\pi^2\alpha^2(t/b)^2]$ (from Fig. 225) changes imperceptibly as time is increased, and hence (20.10) remains essentially constant for $t > 0.3$ second.

The bars may be as long or short as desired and, in general, result in considerable reduction of the voltage gradient required to make the seal. But against this advantage must be weighed the fact that only straight-line bonds or those having a fixed curvature can effectively be made with a device that uses bars as electrodes, while the sewing machine with rotating electrodes can make any seam, straight or curved.

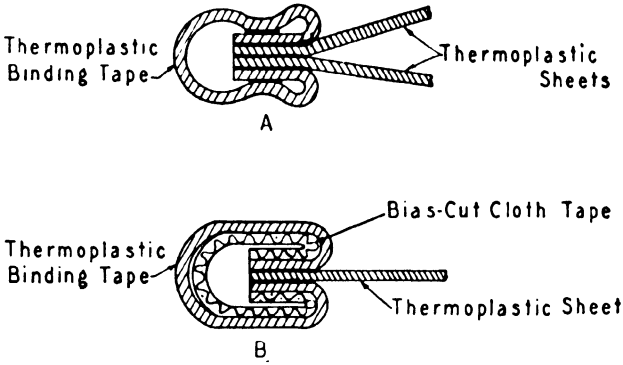

FIG. 231. Cross-section of bindings applied to thermoplastic sheeting. Conventional sewing machine attachments were used on the radio-frequency sewing machine.

Where straight closures are to be made continuously a pair of narrow endless metallic belts of suitable length may be substituted for the bar electrodes. Driven by pulleys similar to the rotating electrodes of the radio-frequency sewing machine, the belts provide a relatively long heating period so that the lower voltages of the bar-sealing method are realized.

Some of the attachments designed for conventional sewing machines may be effectively adapted to the radio-frequency model. One such device is a binding attachment which folds a plastic tape upon itself to bind a raw edge of thermoplastic material for enhancing appearance and increasing strength. The attachment is also helpful for reinforcing and finishing a seam made by joining two layers of material together, as suggested in Fig. 231A. Such a taped seam is particularly useful in the assembly of bags or containers which must hold liquids or gases under pressure.

A bias-cut cloth tape may be folded in simultaneously with plastic tape

FIG. 232. Early experimental model of the radio-frequency sewing machine equipped with a conventional binding attachment.

to obtain a color contrast, or to provide additional reinforcement of the edge. When a bias-cut cloth tape is used in conjunction with a thermoplastic tape, an unusual result can be achieved, as may be seen by reference to Fig. 231B. With the layers of cloth acting as a heat insulator, only the three inner layers of thermoplastic material will attain the temperature of plasticity and bond together. In effect, this is equivalent to bonding or " sewing " on the inside only.

An early experimental model of the radio-frequency sewing machine equipped with a binding attachment is shown in Fig. 232. Here the operator is binding the edges of a tobacco pouch by feeding Vinylite and cloth tapes simultaneously through the binding attachment.

Hemmers are used to fold over raw edges of material to produce a finished edge. In conventional sewing, a hem is usually secured by single stitching, although where wide hems are desired double or triple stitching may be used. A similar result may be realized with the radio-frequency sewing machine by using a suitably-grooved wheel as one of the electrodes.

When sewing cloth, operators assist the hemming attachment by starting the fold by hand, but for plastic sheeting such a method is not suitable since the material does not crease easily and is somewhat more slippery when in contact with itself than cloth. Experience indicated that thermoplastic sheeting needed a longer folding channel than those ordinarily provided in commercial hemming attachments. When such a folding channel is provided a uniform hem can readily be made. A cross-section of a wide hem, bonded with a double wheel, is shown in Fig. 233A.

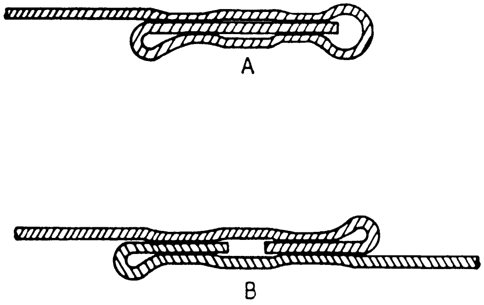

Fig. 233. Cross-section of bonds made on radio-frequency sewing machine equipped with a double or grooved electrode-wheel. A. Wide hem made with hemming attachment. B. Imitation strap seam made with folding attachment.

It is frequently desirable to join two sheets of material by a lapped or imitation strap seam, in which a double stitch is ordinarily utilized. Attachments for doing this are available and may be used on the radio-frequency sewing machine in making a seam as shown in Fig. 233B. It is apparent that a double wheel is desirable for this operation.

Several broad categories of use have been suggested for the radio-frequency sewing machine, involving applications where a water- or gas-tight seam is required.

Wearing Apparel. Raincoats and protective coverings fabricated from various thermoplastic sheet material are not necessarily completely moisture-proof when sewed together by conventional means. It is frequently necessary to cement seams both before and after stitching to make them completely impervious to moisture. Also, the perforation of needles through the material weakens it and permits high concentration of force around the needle holes. With radio-frequency bonding this is not the case so that, in addition to obtaining tight seams, the strength of the finished article is improved.

Packaging. Most thermoplastic sheet materials are particularly useful in packaging in that they are highly impervious to gases, are chemically inert and physically strong. The reliable seal that can be made when interfacial surfaces are heated is of utmost importance where foodstuffs are concerned. Radio-frequency bonding appears to be practically adapted for vacuum closures. It is probable that use of a " bar sealer " will be more important for this application than the use of rotating electrodes as the entire seal may often be made in one operation.

Inflatable Articles It has been found that the diffusion rate of gas is extremely low and that resistance to deterioration by ultraviolet rays is high for some kinds of vinyl-resin sheeting, which suggests the use of thermoplastic sheeting for the construction of balloons. Also, bladders to be enclosed in a covering of cloth or other material may be effectively fabricated with the aid of radio-frequency bonding.

Coated Materials. Cloth may be coated or impregnated with thermoplastic resins and, in such form, can be joined by the radio-frequency sewing machine. Cloth may also be woven from thermoplastic threads, or from coated strands, so that dielectric heating may serve to bond such fabrics. Ravelling which occurs at cut edges of some materials has been eliminated in a number of cases by applying a thermoplastic binding with the radio-frequency sewing machine

Chapter 21

ELECTRODES OF SPECIAL SHAPES

Occasionally the need arises for heating irregularly-shaped objects by a radio-frequency field. Insight into the behavior of the field under such conditions is helpful in arranging electrodes so that uniform heating is achieved. In general, we may assume that the voltage distribution on the electrodes will be essentially uniform at all points — either because the electrodes are small for the frequency used (c.f. Chap. 1) or because suitable inductive tuning stubs have been provided (c.f. Chap. 19). The electrodes establish an equipotential surface and can often be formed so that they develop a desired field in the material to be heated.

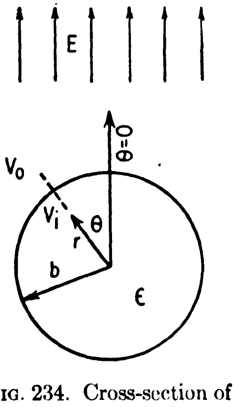

FIG. 234. Cross-section of uniform cylinder with dielectric constant ε at rest in an electric field.

As an illustration, a study will be made of the electrode requirements for uniformly heating a dielectric cylinder. An obvious way of doing this is to rotate or spin the cylinder on its axis in an electric field of suitable intensity. By rotation, all points will have experienced the same average field strength and uniform heating will result. However, it may not always be practical to use this method, and other means must be adopted to obtain uniform heating.

Consider a cylinder at rest as shown in Fig. 234 with its axis set perpendicular to an electric field. Before the cylinder was immersed in the field the intensity was E at all points. After immersion in this uniform field Smythe* shows the potential at points outside the cylinder to be:

$$V_o = E\left(r - \frac{\epsilon - 1}{\epsilon + 1}\cdot\frac{b^2}{r}\right)\cos\theta, \qquad (21.01)$$

---

* William R. Smythe, *Static and Dynamic Electricity*, McGraw-Hill Book Company, Inc., New York, 1939, pp. 65–67.

and the potential at points inside the cylinder to be:

$$V_i = \frac{2E}{\epsilon + 1} r \cos \theta, \tag{21.02}$$

where, with reference to a zero-potential origin,

V_o = potential outside the cylinder;
V_i = potential inside the cylinder;
E = intensity of the applied electric field;
r = distance from origin;
θ = angle of direction;
b = radius of cylinder;
ϵ = dielectric constant of the cylinder.

Inspection of (21.02) reveals that under the conditions described the field inside the dielectric is uniform,* which is the desired objective.

One way to provide a uniform external field is to use large parallel plates having a separation that is great with respect to the diameter of the cylinder. Generally, however, this is not practical because of the high voltages that must be used to provide adequate field strength. A better plan is to use electrodes conforming to an equipotential surface and place them as close as possible to the dielectric cylinder. Such electrodes will then produce a configuration of the electric field which provides the uniform field, and hence uniform heating, in the dielectric.

The equation of the required equipotential surface can be found by a manipulation of (21.01). Let r, the distance from the origin to the point under examination, be designated by r_0 when $\theta = 0$. Then (21.01) becomes:

$$\frac{V_o}{E} = r_0 - \frac{\epsilon - 1}{\epsilon + 1} \cdot \frac{b^2}{r_0}. \tag{21.03}$$

At any other value of θ, (21.01) becomes

$$\frac{V_o}{E} = \left(r - \frac{\epsilon - 1}{\epsilon + 1} \cdot \frac{b^2}{r}\right) \cos \theta. \tag{21.04}$$

By equating the right-hand sides of (21.03) and (21.04) we can write:

$$\cos \theta = \frac{r_0 - \dfrac{\epsilon - 1}{\epsilon + 1} \cdot \dfrac{b^2}{r_0}}{r - \dfrac{\epsilon - 1}{\epsilon + 1} \cdot \dfrac{b^2}{r}}. \tag{21.05}$$

---

* $r \cos \theta = x$

$$\therefore V_i = \frac{2E}{\epsilon + 1} x$$

and $\dfrac{dV_i}{dx} = \dfrac{2E}{\epsilon + 1}$, a constant.

Since $r_0 > b$ we can write

$$r_0 = kb, \tag{21.06}$$

where $k > 1$.

Insert (21.06) in (21.05) and solve for r, obtaining:

$$r = b\,\frac{k^2 - \dfrac{\epsilon - 1}{\epsilon + 1} + \sqrt{\left(k^2 - \dfrac{\epsilon - 1}{\epsilon + 1}\right)^2 + \left(\dfrac{\epsilon - 1}{\epsilon + 1}\right)(2k \cos\theta)^2}}{2k\cos\theta}, \tag{21.07}$$

where: r = distance from origin;
b = radius of dielectric cylinder;
$k = r_0/b$ = proportionality constant from (21.06);
θ = angle of direction.

In (21.07), we have an equation which will yield an equipotential surface, passing through the point $(r_0, 0)$. Thus (21.07) also describes the electrode shape required to establish a uniform field in a dielectric cylinder of any dielectric constant ϵ and for any desired air spacing as defined by k. Under these conditions the field in the air space will no longer be uniform although internal uniformity, as defined by (21.02), is maintained. Several such equipotential surfaces have been sketched for different spacings and for different dielectric constants.

Fig. 235 shows such surfaces for a cylinder with a dielectric constant of 5 and for spacings ranging from zero to half the radius of the cylinder. For a dielectric constant of this value, the modification of the electrodes from straight plates is not great, even at close spacing. Contrast this situation with that sketched in Fig. 236, which shows the equipotential surfaces for a cylinder with a dielectric constant of 81, at similar spacings. Now the plates must be formed to follow the contour of the cylinder rather closely when the air space is small, and as a consequence the field intensity in the air space is very high.

A comparison of the equipotential surfaces for several values of dielectric constant and with an air space equal to 10 per cent of the cylinder's radius ($k = 1.1$) is portrayed in Fig. 237. These curves emphasize the increased care required in electrode forming as the dielectric constant of the cylinder is increased.

It will be noticed that the electrode configuration is simplified as the spacing is increased or as the dielectric constant of the material approaches unity. Although we cannot control the dielectric constant of the material to be heated, the possibility of using a large air space to simplify electrode shapes may appear attractive. But let us examine the behavior of voltage requirements as the air space is increased.

From (21.01) we find that, with reference to the axis of the cylinder, the

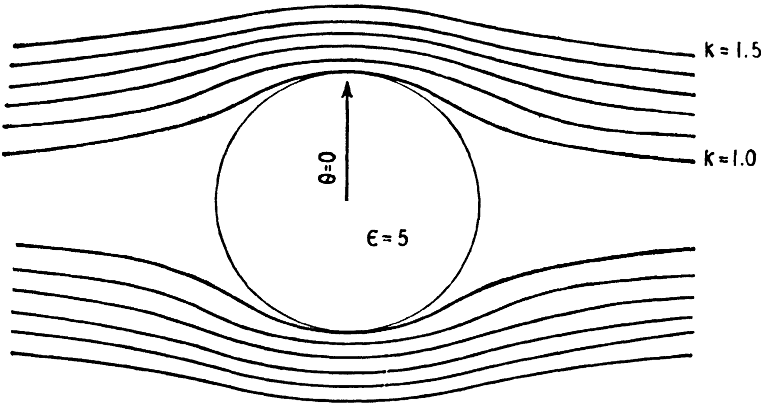

FIG. 235. Equipotential surfaces which will produce a uniform electric field in a cylinder with dielectric constant ε = 5.

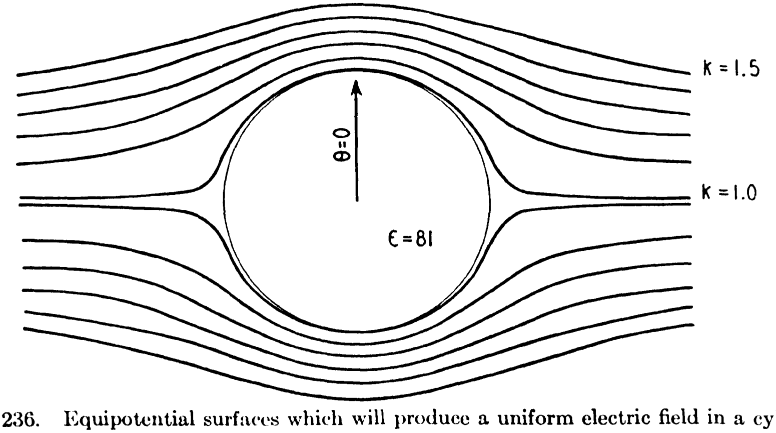

FIG. 236. Equipotential surfaces which will produce a uniform electric field in a cylinder with dielectric constant ε = 81.

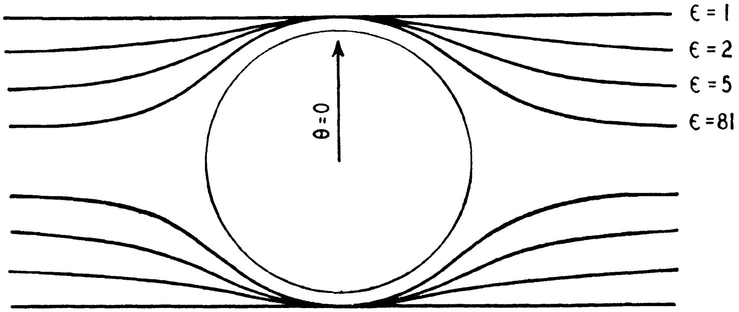

FIG. 237. Comparison of equipotential surfaces required to produce a uniform electric field in cylinders for several values of dielectric constant ε when is $k = 1.1$.

potential at $(r_0, 0)$ is:

$$V_o = E\left(r_0 - \frac{\epsilon - 1}{\epsilon + 1}\cdot\frac{b^2}{r_0}\right), \tag{21.08}$$

and hence the total voltage between the electrodes is double this value.

The potential appearing at the surface of the cylinder can be found from (21.02) to be

$$V_i = \frac{2Eb}{\epsilon + 1}. \tag{21.09}$$

The field E_i, in volts per centimeter, inside the dielectric cylinder is

$$E_i = \frac{2V_i}{2b} = \frac{V_i}{b}, \tag{21.10}$$

and thus,

$$E_i = \frac{2E}{\epsilon + 1}. \tag{21.11}$$

The power P absorbed per unit length is given by

$$\begin{aligned} P &= E_i^2 \sigma \pi b^2 \\ &= E_i^2 \frac{\sigma}{2\pi f p_0 \epsilon} \cdot 2\pi f p_0 \epsilon \cdot \pi b^2 \\ &= E_i^2 2\pi^2 f b^2 p_0 \epsilon (\text{p.f.}). \end{aligned} \tag{21.12}$$

Justification for setting $\frac{\sigma}{2\pi f p_0 \epsilon} = (\text{p.f.})$, the power factor, is found in (1.07), since in most dielectric materials the power factor is not very high.

Solving (21.12) for E_i, in volts per centimeter, we have

$$E_i = \frac{1}{b}\sqrt{\frac{P}{2\pi^2 f p_0 \epsilon (\text{p.f.})}} = \frac{1}{b}\sqrt{\frac{P}{\pi\sigma}}. \tag{21.13}$$

This is the field throughout the cylinder. The field just outside the cylinder at $r = b$ and $\theta = 0$, in the air space, will be ϵ times this value. Thus the desirability of eliminating any air space — particularly in materials of high dielectric constant — becomes quite apparent. Now, using (21.08), (21.11), and (21.13) we can write the total voltage between the electrodes as

$$\begin{aligned} 2V_o &= (\epsilon + 1)\left(\frac{r_0}{b} - \frac{\epsilon - 1}{\epsilon + 1}\cdot\frac{b}{r_0}\right)\sqrt{\frac{P}{2\pi^2 f p_0 \epsilon (\text{p.f.})}} \\ &= (\epsilon + 1)\left(\frac{r_0}{b} - \frac{\epsilon - 1}{\epsilon + 1}\cdot\frac{b}{r_0}\right)\sqrt{\frac{P}{\pi\sigma}}. \end{aligned} \tag{21.14}$$

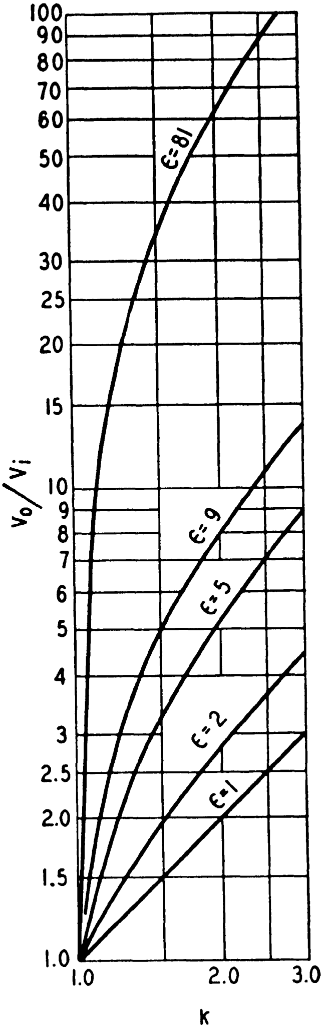

FIG. 238. The ratio of the voltage appearing across the electrodes to that appearing across a dielectric cylinder in terms of spacing and dielectric constant.

The total voltage appearing across the cylinder is

$$2V_i = 2E_ib = 2\sqrt{\frac{P}{2\pi^2 f p_0 \epsilon(\text{p.f.})}} = 2\sqrt{\frac{P}{\pi\sigma}}. \tag{21.15}$$

When these two voltages are compared by dividing (21.14) by (21.15) we get

$$\frac{V_0}{V_i} = \frac{(\epsilon + 1)\left(k^2 - \dfrac{\epsilon - 1}{\epsilon + 1}\right)}{2k}. \tag{21.16}$$

The ratio V_0/V_i is plotted against k for several values of dielectric constant in Fig. 238. For a given voltage across the load, this graph shows how rapidly the voltage on the plates rises as the air space is increased. The effect becomes more severe as dielectric constant becomes larger.

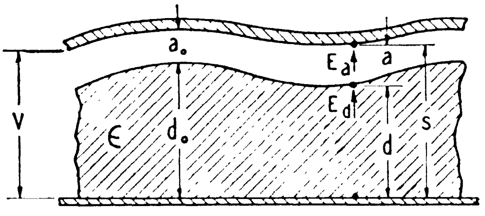

FIG. 239. Modification of electrode shape to provide uniform heating in dielectric materials having irregular shape.

This is not surprising when one recalls that a system composed of a dielectric with air spaces between the dielectric and the capacitor plates is equivalent to three capacitors in series: C_a, C_ϵ, C_b, where C_a and C_b are the capacitances of the air spaces, and C_ϵ the capacitance of the space occupied by a dielectric of constant ϵ. The total capacitance C of such a system is found from the simple expression:

$$\frac{1}{C} = \frac{1}{C_a} + \frac{1}{C_\epsilon} + \frac{1}{C_b}. \tag{21.17}$$

When the total air space is increased C_a and C_b decrease in value and a larger percentage of the total voltage appears across the air gap. Thus for practical purposes it is always desirable to keep the air gap to a minimum, if not eliminated entirely.

It should be stated, however, that there are occasions when this phenomenon can be put to good use. In irregularly-shaped objects the effective voltage across sections of varying thickness can be adjusted by suitable spacing of the electrodes, so that the heating of the dielectric may be essentially uniform.

The analytical solution of a general case in which lines of equipotential are to be found for any shape is impractical to develop. It is possible, however, to arrive at a simplified guide which can be of assistance in arranging electrodes for heating irregular objects. Consider the conditions illustrated in Fig. 239, in which a section of an irregularly-shaped dielectric is shown between formed plates. At any chosen point the intensity of the electric field in the air space can be designated by E_a and the field in the dielectric as E_d. In a material of dielectric constant ϵ, E_d bears the following relationship to E_a:

$$E_d = \frac{E_a}{\epsilon}. \tag{21.18}$$

At the region under observation the length of the dielectric path is d and the length of the air path is a. Thus the total voltage V across the plate is

$$\begin{aligned} V &= dE_d + aE_a \\ &= dE_d + a\epsilon E_d \\ &= E_d(d + a\epsilon) \end{aligned}$$

or

$$\frac{V}{E_d} = d + a\epsilon. \tag{21.19}$$

Since the applied voltage V will be constant and it is desired that E_d, the voltage gradient in the material, should also be constant, the values of a must be so chosen that the ratio V/E_d will remain constant over the entire region to be heated.

Let the greatest thickness of the dielectric be d_0 and let the air space at that location be designated by a_0. Then

$$\frac{V}{E_d} = d_0 + a_0\epsilon. \tag{21.20}$$

At any other point where the dielectric thickness is d and the air space is a, the conditions may be expressed as

$$\frac{V}{E_d} = d + a\epsilon. \tag{21.21}$$

Then, equating (21.20) and (21.21):

$$d_0 + a_0\epsilon = d + a\epsilon, \tag{21.22}$$

from which the required air space a at that point is found to be:

$$a = \frac{d_0 - d}{\epsilon} + a_0. \tag{21.23}$$

Then the total electrode spacing, s, at that location is given by

$$s = d + a = \frac{d_0 + d(\epsilon - 1)}{\epsilon} + a_0. \tag{21.24}$$

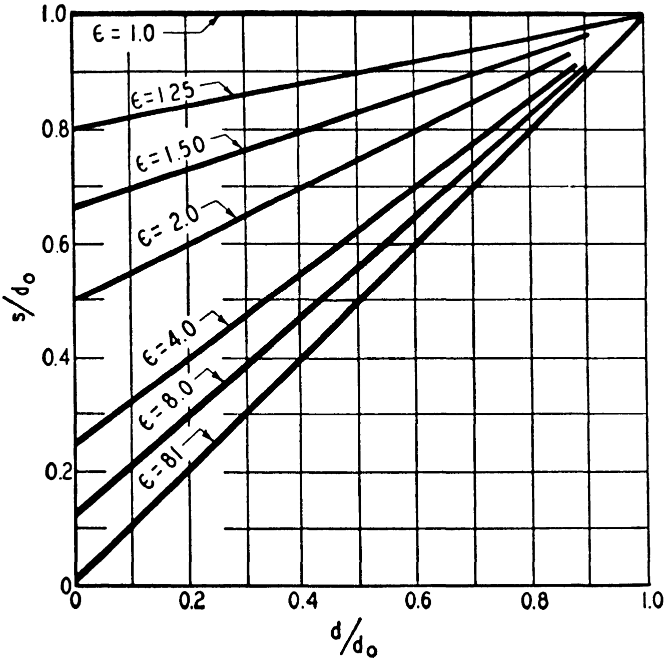

FIG. 240. The relationship expressed in (21.25) plotted for various values of dielectric constant.

Compared to the greatest thickness of dielectric d_0, the spacing s of the plate is

$$\frac{s}{d_0} = \frac{1 + \dfrac{d}{d_0}(\epsilon - 1)}{\epsilon} + \frac{a_0}{d_0}. \tag{21.25}$$

It will be noted that the term $\dfrac{a_0}{d_0}$ is a constant determined by the spacing chosen at the thickest section. For conditions where $a_0 = 0$, the relationship of (21.25) is plotted in Fig. 240 for several values of ϵ. Careful forming of the plates is not necessary because slight irregularities of heating are compensated for by lateral heat flow between various regions.

For heating or drying paper-thin sheet materials in an electric field, the use of parallel-plate electrodes is not satisfactory. Coupling efficiency is poor when an air space is used and as the spacing is reduced the capacitance increases to undesirable values. Often intimate contact of electrodes with the sheets cannot be tolerated, either because of heat loss into the electrodes or because of printing on the surface of the sheets.

The authors solved this problem by passing the sheets over a grid composed of metal bars, alternately connected together so that a high-frequency field could be established between adjacent bars. Now a radio-frequency current passing from one bar to another follows a relatively long path through the material with little or no air space encountered. This greatly improves the efficiency and permits operation under conditions of minimum voltage. If the paper or sheeting is moving, the grid-electrode structure can be made as long as desired so that power concentration and hence voltage requirements may be reduced to practical values.

Chapter 22

RADIO-FREQUENCY DEHYDRATION

Radio-Frequency Drying in a Reduced Atmosphere. Many drying processes are slow and wasteful of space because of the difficulty in supplying the heat of vaporization of the liquid. This is especially true in the drying of bulky materials which are poor conductors of heat. In ordinary oven drying the drying progresses from the outer surfaces inward and the energy required to evaporate the moisture on the inside must be conducted through the outer portion. Since radio-frequency heating provides a means of generating heat uniformly throughout a nonconducting mass, its use results in the rapid and uniform drying of many materials.

In the drying of materials labile to heat, the materials may be subjected to a reduced atmosphere. Then the problem of supplying the heat of vaporization is even more difficult. Here again radio-frequency heating may be used to advantage but precautions must be taken to prevent ionization which may occur because of the lowered breakdown strength of the atmosphere at reduced pressure.

Power Requirements For Drying. The energy required for the drying of a given material consists of the heat of vaporization of the liquid to be removed plus the heat required to raise the material to the temperature at which the vaporization occurs. Then

$$\text{Energy (B.t.u.)} = H_v W_1 + (K_1 W_1 + K_2 W_2)(\Delta F), \qquad (22.01)$$

where H_v = heat of vaporization of the liquid, in B.t.u. per pound;
W_1 = weight of the liquid removed, in pounds;
W_2 = weight of the dried material, in pounds;
K_1 = specific heat of the liquid, B.t.u. per pound per degree Fahrenheit;
K_2 = specific heat of the dried material, B.t.u. per pound per degree Fahrenheit;
ΔF = difference between the initial temperature and the temperature at which the liquid is vaporized, in degrees Fahrenheit.

The power required to accomplish the drying in T hours may be expressed as

$$P(\text{watts}) = \frac{H_v W_1 + (K_1 W_1 + K_2 W_2)(\Delta F)}{3.415T} \tag{22.02}$$

When the drying is performed in a vacuum so the temperature of the material does not change appreciably during the drying cycle, (22.02) may be simplified.

$$P(\text{watts}) = \frac{H_v W_1}{3.415T}. \tag{22.03}$$

Since the heat of vaporization of water is approximately 975 B.t.u. per pound, equation (22.03) becomes

$$P(\text{watts}) = \frac{285 W_1}{T} \tag{22.04}$$

when water is being evaporated. Thus we see that a power of 285 watts is required to boil off 1 pound of water per hour.

Rayon Drying. A problem in the manufacture of viscose rayon is the drying of the yarn as it comes from the washing process. The rayon yarn is commonly handled in the form of cakes* or self-supporting annular forms about 7 inches in diameter, 6 inches high, and 1½ inches thick. The cakes contain about twice their weight in water and when dry weigh about 1 pound. The popular method of removing the 2 pounds of water which each cake contains is to pass the cakes through large drying ovens in which they are subjected to circulating hot air. The temperature must not exceed 140° F or the yarn may be damaged. The drying time is about 100 hours. Consequently, the size of the ovens required to handle a production of several thousand pounds of rayon per hour is very great. Moreover, since the drying progresses from the outside of the cake inwardly, and since rayon shrinks when it dries, strains are often set up in the yarn which result in a non-uniform product.

By placing the cakes in a moderate vacuum of about 40 millimeters of mercury and subjecting them to a radio-frequency field, it was found to be possible to dry the cakes uniformly in less than an hour. Fig. 241 shows a laboratory arrangement used by the authors for drying rayon. The cake was placed between circular electrodes in an evacuated bell jar. Power was supplied from an oscillator operating at a frequency of 25 megacycles, with an available power output of 2 kilowatts. During most of the drying period, the temperature of the rayon yarn remained near 90° F, rising only at the finish to about 125° F.

---

* H. R. Mauersberger and E. W. K. Schwarz, *Rayon and Staple Fiber Handbook*, 3d ed., Rayon Handbook Co., New York, pp. 98 and 785.

Tests made in conjunction with the American Viscose Corporation showed that viscose rayon yarn dried in this manner was much more uniform than oven-dried yarn. In fact, when the yarn was woven into cloth a complete absence of shiny filaments was noted, while similar cakes dried in the more common oven process produced cloth with distinct streaks due to the nonuniformity of the threads.

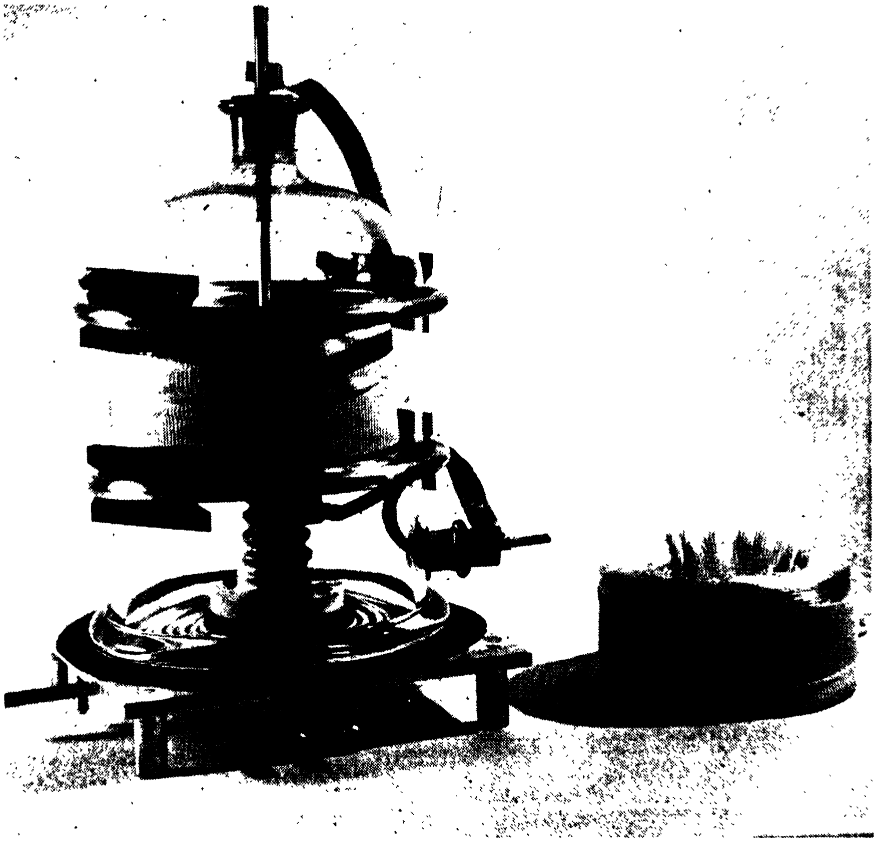

FIG. 241. Experimental arrangement for drying rayon cakes. Guard rings are external to the bell jar to prevent corona at the edges of the electrodes.

The impedance and power factor of rayon cakes vary considerably during the drying cycle so that the loading of the oscillator changes. At the beginning of the cycle, the losses are high and the oscillator is loaded quite heavily. At the end of the cycle, the losses are low so the oscillator is practically unloaded. In a commercial installation, it would, of course, be desirable to operate the oscillator at full power output at all times. An arrangement whereby such a condition may be approached makes use of a number of chambers with a switching system to connect them to the oscillator successively so that at all times there would be connected to the oscillator chambers containing cakes at various degrees of dryness In this way, the loading of the oscillator is held reasonably constant and the full capabilities of the oscillator may be realized.

The power requirements for drying rayon in the manner described above may be obtained from (22.04). For example, it may be assumed that 100 cakes are to be dried per hour. Since each cake contains about 2 pounds of water, the power needed will be 57,000 watts.

Penicillin Dehydration. The authors' previous work in dehydration of materials by means of radio-frequency power, particularly the drying of rayon cakes in a vacuum, pointed to the possibilities of contributing to the processing of pharmaceuticals which are sensitive to heat. The particular problem of drying penicillin for packaging seemed important for two reasons. First, penicillin in a water solution soon lost its bactericidal properties so it was necessary to thoroughly dry the product before storage or shipment. Secondly, penicillin solution was so sensitive to heat that it was necessary to keep the solution in a frozen condition before drying and even to dry in the frozen state. This freeze-drying process was expensive and took a long time.

Because there was no background of experience in the type of processing proposed by the authors, it was necessary to carry out extensive laboratory investigations. This was particularly true since we proposed to use vacuums of the order of 20 to 40 millimeters of mercury so that the material remained in a liquid state during the drying stages. Because many of the problems of drying by means of radio-frequency heating required solution by the development of new techniques, it seemed desirable to carry the investigation far beyond the normal research stage. The remainder of this chapter will be devoted to a description of a few of the pertinent laboratory tests and to a discussion of the equipment which was developed, capable of handling production quantities of penicillin and other pharmaceuticals.

In order to orient the reader, it seems desirable to say a few words concerning the methods of testing for bactericidal properties and the means of expressing these properties, since the purpose of our early experiments was to determine how our radio-frequency methods affected these properties.

Penicillin Activity or Potency. Pure crystals of penicillin salt are believed to be very stable and to have constant bacteria-destroying properties for a given weight. Pure crystals are difficult to obtain. However, in limited amounts, these crystals are useful in testing solutions of penicillin which contain impurities and are of unknown activity. The Oxford Unit* of activity was selected shortly after the discovery of penicillin so the unit is smaller than necessary for convenient use. Pure crystals of penicillin possess 1667 Oxford Units of activity per milligram.

---

* One Oxford Unit is that amount of penicillin which, when dissolved in 50 milliliters of meat extract broth, just inhibits completely the growth of the test strain of *Staphylococcus aureus*.

In testing a solution of unknown potency, various dilutions of the substance are placed on a bacteria culture. At other spots on the same plate, a penicillin solution of known activity is placed. After incubation for a fixed period of time, observations are made of the dimensions of the zones of inhibition.

Another test makes use of observations of turbidity of various dilutions of penicillin in cultures of bacteria. Again the observations are correlated with a known solution.

The accuracy or consistency of these bacteriological determinations is not very great. A number of measurements of potency taken on the same sample may show deviations as high as plus or minus 15 per cent from the average.

In our experiments, control samples were kept so that any deterioration of the solution with time could be sorted out from the effect of radio-frequency.

Initial Experiments with Radio-Frequency Heating. To dry by conventional freeze-drying methods,* it is necessary to maintain a vacuum of between 100 and 300 microns (0.1 to 0.3 millimeter of mercury). We were not interested in freeze-drying with radio-frequency power for a number of reasons. In the first place, if we were to contribute to the penicillin program by furnishing a faster and simpler system, the elimination of the expensive high-vacuum systems, complicated condensers, and elaborate refrigeration seemed to be the most important step. Secondly, for the same voltage or electric intensity, the residual atmosphere ionizes much more readily with a vacuum of 100 microns than it does at a vacuum of about 20 to 40 millimeters, which is the order of vacuum that we had in mind for our purpose. In addition to the fact that the air ionizes easier at 100 microns, the solution is frozen when under this vacuum. The electrical conductivity of frozen penicillin is so much lower than that of the liquid that much higher voltages must be used to generate the same power. This effect is very pronounced. When attempts were made to dry in the frozen state with radio-frequency power, it was necessary to reduce the radio-frequency voltages to such an extent that it became apparent that most of the heat of vaporization was being supplied by heat conduction from the warm air of the laboratory through the glass walls of the container.

In these tests, the sample was in a thin-walled glass bottle which was connected to a manifold. Here the entire bottle was exposed to the warm air of the laboratory. In practice, where thousands of these bottles are placed in large vacuum tanks, no circulation of warm air takes place. The drying time by this method may take from 8 to 20 hours.†

* Earl W. Flosdorf, Lewis W. Hull, and Stuart Mudd, "Drying by Sublimation," *The Journal of Immunology*, Vol. 50, No. 1, January 1945, pp. 21–54.

† Earl W. Flosdorf, Lewis W. Hull, and Stuart Mudd, *loc. cit.*, p. 38.

Samples of penicillin supplied by many producers of the material were then dried by subjecting the penicillin to vacuums varying from 3 to 40 millimeters of mercury and applying radio-frequency power from a small laboratory oscillator. The various samples contained from 3000 to 100,000 Oxford Units of penicillin. After drying, the samples as well as appropriate controls were assayed by the organizations who originally supplied the material. These initial tests have been repeated many times, always with the same result — no loss in potency.

A Radio-Frequency Bulk-Reducer for Penicillin. As a result of these initial successes, much interest was exhibited by a number of penicillin producers. It seemed extremely desirable to review the work and consider how best to fit radio-frequency power into the picture.

After the penicillin mold is grown and the penicillin harvested, the material goes through a number of complex chemical processes from which it finally emerges as a weak water solution of a sodium or calcium salt of penicillin, with varying amounts of impurities. At the time that we were interested in considering the situation, it was the practice to freeze or shell this solution on the walls of a number of large glass bottles which were then attached to a manifold of a vacuum system. The vacuum was maintained at about 100 microns. The only heat supplied was by conduction through the walls of the bottles. After many hours, the material was considered to be dry and was then scraped from the bottles and pulverized. A measurement of potency, in Oxford Units per milligram, was then made to determine the amount by weight that would be placed in the final container. Since it was necessary to maintain a high degree of sterility, this operation was done in an air-conditioned box containing an analytical balance, a tray of penicillin powder, a rack of bottles, and the necessary loading tools. The operator manipulated the apparatus by inserting his arms into a pair of rubber gloves that were anchored to two openings in the box and by peeping through a small glass window in the wall of the box. This process was slow and expensive, as well as tedious and inaccurate.

Most processors were considering a modification in which freeze-drying in the large bottles would be halted at a point where the activity of the residue would be between 10,000 and 100,000 units per cubic centimeter. The material would then be allowed to melt and the liquid would be assayed for potency. Depending on the activity attained, between 1 and 10 cubic centimeters of material could be accurately measured into each final container. Then a rack of containers would be frozen and inserted in a large vacuum chamber and the pressure reduced to about 100 microns, for the final drying. Because of this change of procedure, it was decided that a radio-frequency bulk-reducer was first in order of importance. The bulk-reducer could then be used to remove sufficient water to concentrate to a potency of 100,000 units per cubic centimeter, after which 1 cubic centimeter of the material would be

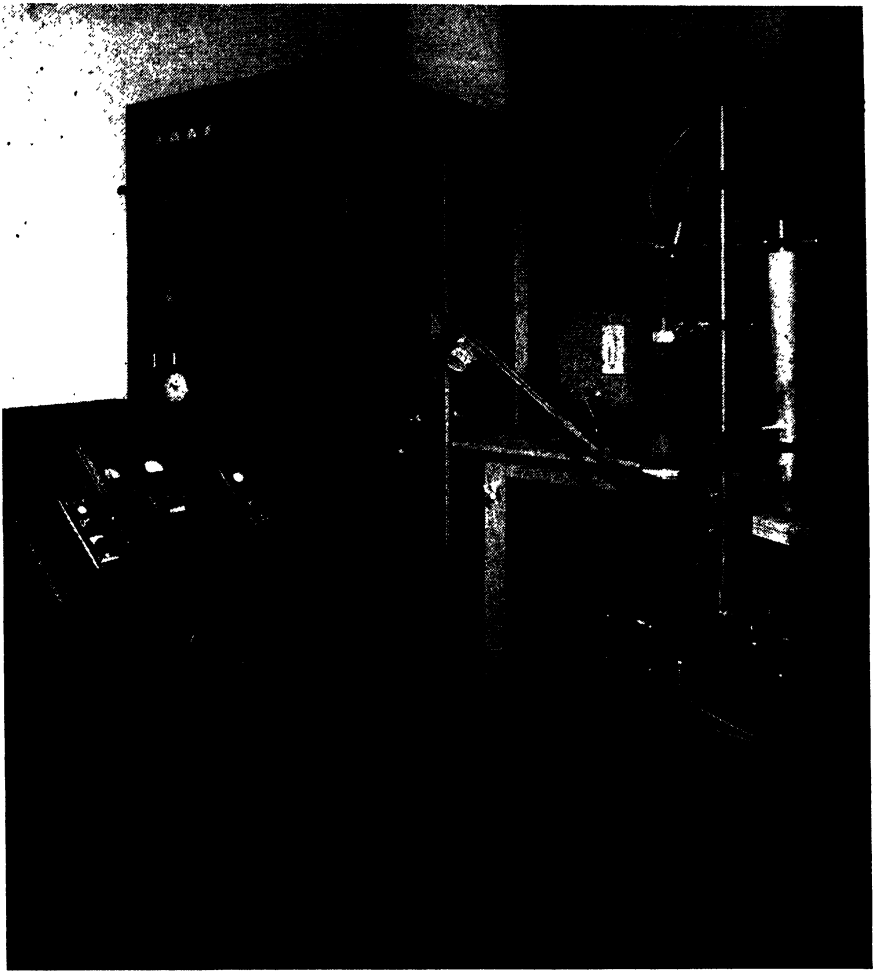

FIG. 242. First experimental bulk-reducer.

measured into each of the final containers and taken down to complete dryness by the freeze-drying high-vacuum chambers. The two-fold advantage of the radio-frequency bulk-reducer is that the expensive high-vacuum bulk-reducer and refrigeration system is eliminated and the output of the final freeze-drying cabinets is increased because only 1 cubic centimeter of water remains to be removed from each final container.

The first experiments in bulk reduction were conducted with a laboratory oscillator which could be readily changed to a number of frequencies. The frequencies investigated particularly corresponded to the frequencies of commercially available oscillators.

The experimental arrangement is shown in Fig. 242. The pencillin was contained in the large bottle at the table's edge. The tall chimney was necessary to prevent losses of material from splashing. The electrodes were simply thin sheets of metal taped to the outside surface of the bottle. The bottom of the bottle was made concave so the load presented to the oscillator would remain fairly constant throughout the concentration cycle. This enabled us to use wider electrodes and still preserve this constancy of load

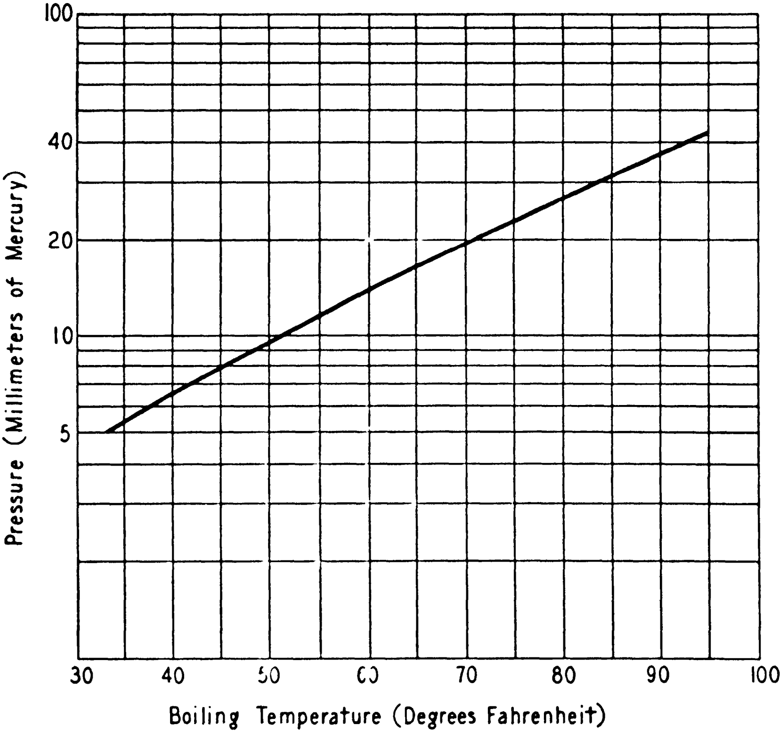

FIG. 243. Boiling temperature of aqueous solution of penicillin versus pressure.

With a flat bottom, the liquid was sometimes concentrated below the level of the electrodes so that there was danger of ionization in the air space and sometimes arcing from the electrodes.

Attempts were made to operate at a frequency of 10 megacycles, but we were not able to overcome sparking at the electrodes. Further experiment showed that at a frequency of 28 megacycles there was little danger of electrode trouble, provided the concave bottom was used.

A vacuum pump with a capacity of 6 cubic feet per minute was used throughout the experiments with the bulk-reducer and in the final model.

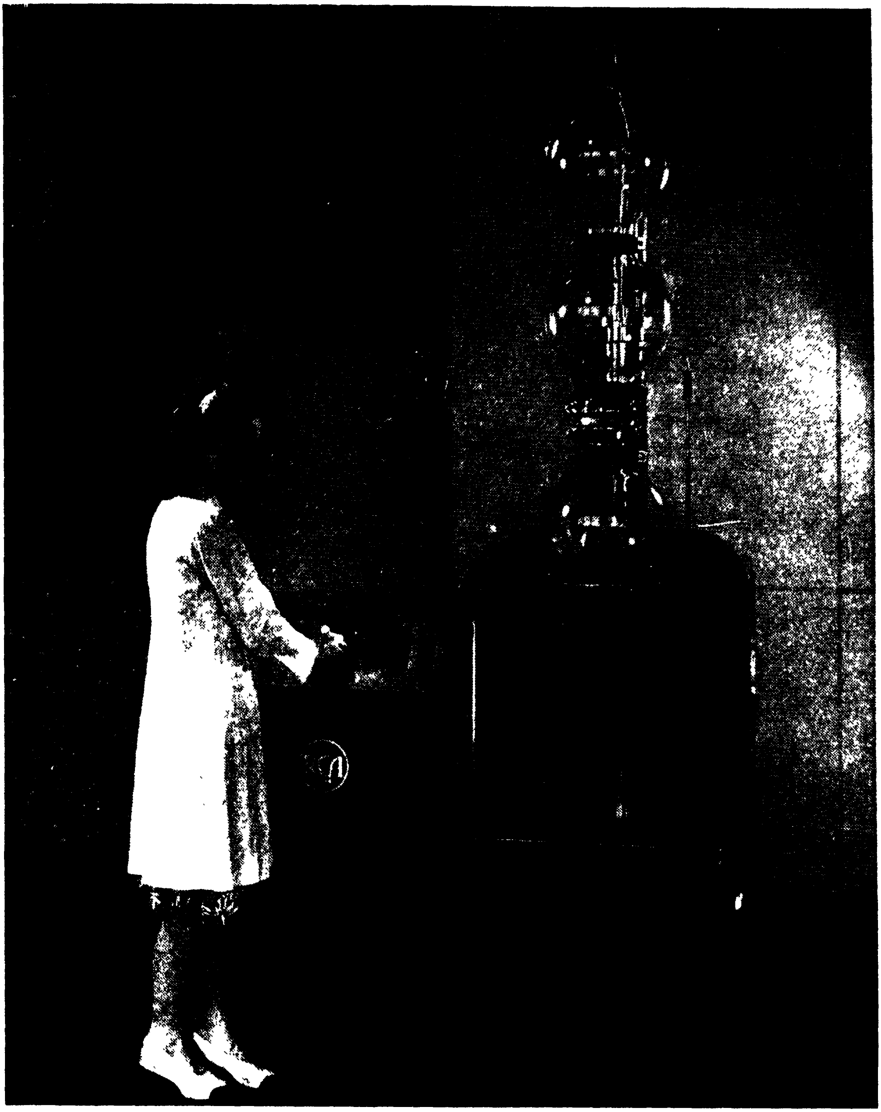

FIG. 244. A complete bulk-reducer capable of evaporating approximately 3 liters of water per hour.

Although the pump was designed to handle water vapor, a water-cooled condenser was used to secure more efficient operation of the pump.

A large number of experiments were carried out to learn the necessary technique for a practical system. Further tests were necessary to determine the safe range of temperatures and pressures, which could be used without harming the penicillin. The temperature at which water boils as a function of pressure is shown in Fig. 243. While much of our operation took place at a pressure between 10 and 20 millimeters of mercury, we have run the equipment at pressures up to 40 millimeters without loss in potency of the penicillin.

A pilot unit was next constructed which served as a prototype for the equipment shown in Fig. 244. The oscillator consisted of two RCA-833A vacuum tubes acting as a conventional oscillator at 28 megacycles, with a power output of 2 kilowatts. The three large glass bottles provide room for foaming of the liquid when the vacuum is applied. Penicillin solution is extremely foamy so that our efforts in suppressing the foam were extensive. A baffle plate was inserted in the middle bottle. Also, a coil made of silver-plated copper tubing was inserted between the bottom and the middle bottles. The arrangement is shown in Fig. 245. Warm water (125° F) was passed

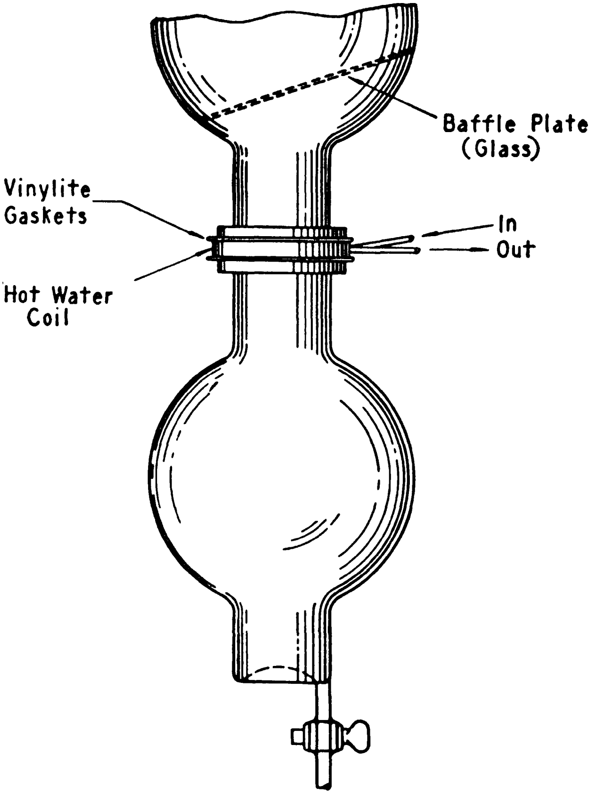

FIG. 245. Diagram of bottles with baffle plate and water coil in place.

through this coil. When the foam and bubbles rise and contact the warm coil, the part of the bubble in contact with the coil evaporates and the bubble collapses.

In using the bulk-reducer, the sequence of operations is as follows. The hot-water supply for the bubble-breaking coil and the cold-water supply for the condenser are turned on and the vacuum pump started. When a liter of material is ready for treatment, a flask containing the solution is placed beneath the bottom bottle and the pet cock is opened. The penicillin solution is thus sucked up into the bottle. The pet cock is then closed and the oscillator turned on. With full power supplied, 1000 cubic centimeters of liquid will be reduced to 100 cubic centimeters in 18 minutes.

After turning off the oscillator, the vacuum pump is stopped and the relief valve is opened. Then the pet cock below the bottom bottle is opened and the penicillin solution drained from the bottle. After this operation the pump is started and a new supply of penicillin is drawn into the bottle.

Drying in the Final Container. In the early experiments the drying was carried out in large test tubes or ampoules. The material spattered up on the walls of the container when the vacuum was applied and spattered some more when the radio-frequency power was turned on. This resulted in a messy appearance when finally dried. However, we were interested in the effect on the activity and for the moment were not concerned with appearance. When later attempts were made to dry in the final bottle, it became apparent that it was almost impossible to keep all the material in the bottle. Initial application of the vacuum usually resulted in loss of a certain amount of solution due to spattering. After the application of power, severe bumping sometimes entirely emptied the bottle. Numerous expedients were resorted to in an attempt to solve this problem. Rotating the bottle at high speed during the evacuating and drying period revealed that this was a way to eliminate these difficulties. The liquid and solids in the liquid are then formed in a thin layer on the walls of the bottle and held there by a force estimated to be at least 100 times that of gravity when the rotational speed is 3000 revolutions per minute. When vacuum is applied, no material is lost. Then as radio-frequency power is applied, the material dries in a thin film on the side of the bottle with a rather pleasing appearance. Dried samples may be seen in Fig. 246.

A single-unit drier consisting of a plastic cup driven at a speed of 3000 revolutions per minute and a set of electrodes is shown in Fig. 247. This unit was found to be very useful in the laboratory and several hundred samples of penicillin solution have been dried under various conditions with this equipment. With approximately 20 watts of power at 30 megacycles, it is possible to remove most of the moisture from 1 cubic centimeter of solution in 3 minutes.

Typical data taken during a drying cycle are shown in Fig. 248. It may be seen that most of the water is removed in the first 60 seconds. The rate of drying progressively decreases as time passes. Measurements of the Q-factor of the circuit taken during the drying cycle are also shown in Fig. 248. As the material dries out the Q becomes high so there is quite a change in loading of the oscillator during the drying period. At the end of 3 minutes, the moisture content is reduced to about 4 per cent. Application of radio-frequency power for longer periods will reduce the moisture content still further. However, by the time the moisture content has been reduced to 4 per cent, the material is very stable and will stand much higher temperatures than it does when in the liquid condition.

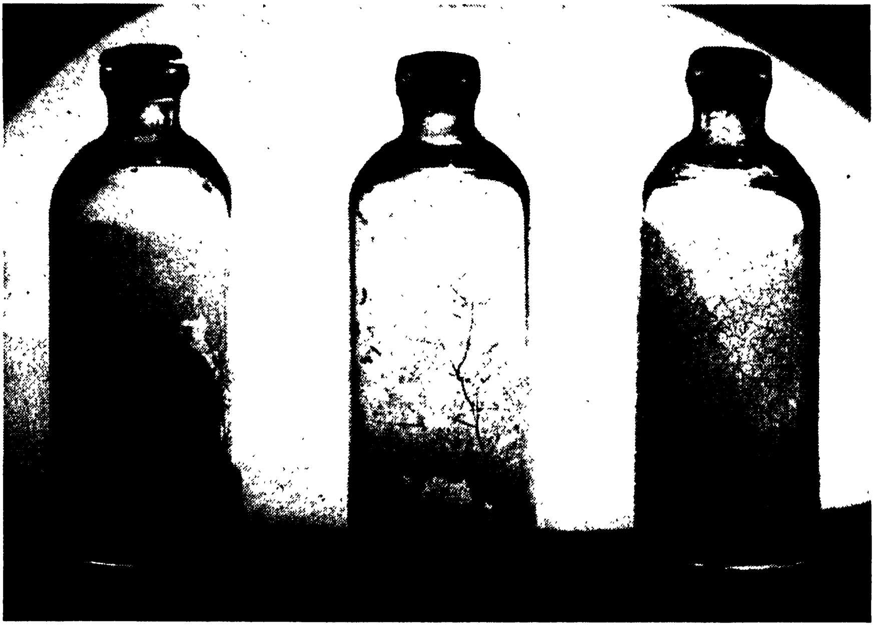

FIG. 246. Samples of penicillin dried by spinning in a radio-frequency field. Each bottle contains 100,000 units of penicillin, with varying amount of impurities.

This allows us to introduce another step which is important in the construction of final equipment since it permits the use of a minimum number of rotating cups. The bottles are transferred to metal plates which are heated by ordinary electric heaters. A bell jar is then placed over the heater plate and the system evacuated. Since the material is dried on the side of the bottle in a thin film, heat conduction through the glass bottle to remove the last traces of moisture is efficient.

Early in the investigation, a number of samples of penicillin solution were dried and tested for activity and moisture content. In each case the bottle was rotated for 3 minutes in a radio-frequency field, with a vacuum of 50 millimeters of mercury. Then the bottles were removed from the radio-frequency field and placed in a metal box which in turn was placed in a bell jar, with a vacuum of 8 millimeters of mercury. An electric heater, thermostatically controlled, heated the metal plate which supported the bell jar to a temperature of 65° C. At the end of the run, the bottles reached a temperature of 50° C to 55° C. The conditions of test as well as activity measurements are shown below.

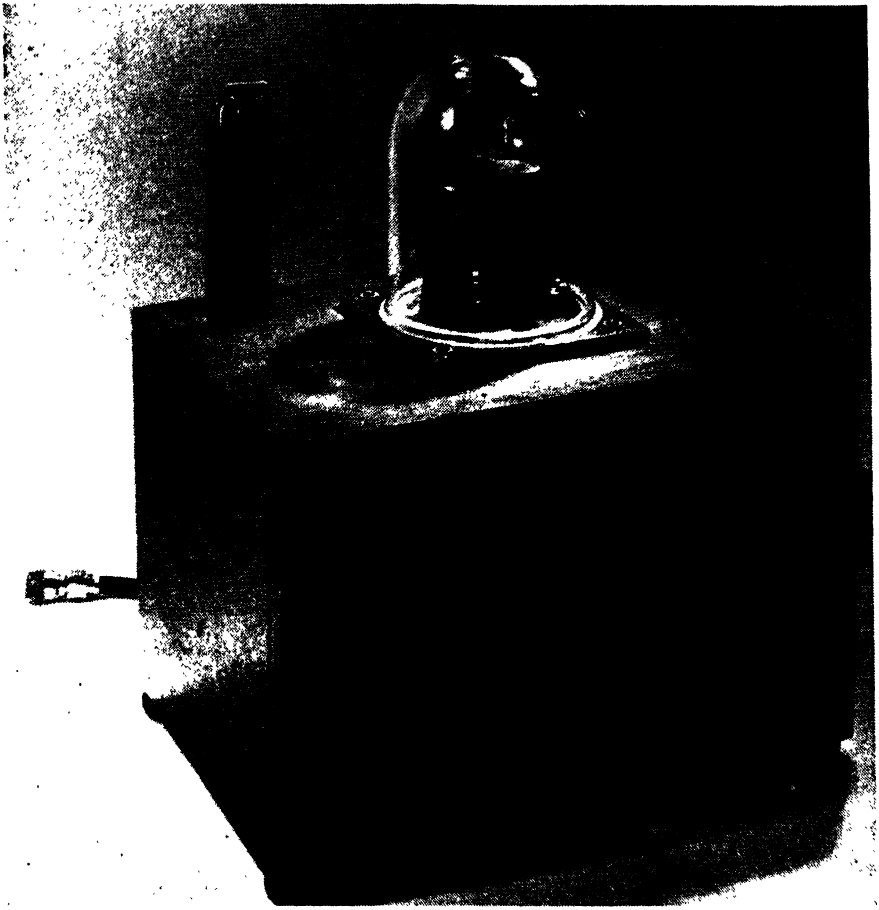

Fig. 247. A laboratory arrangement for drying one bottle at a time.

Sample	Time in Bell Jar	Activity (Oxford Units)	Number of Activity Tests
Control	...	95,954	8
Control	...	103,441	6
No. 204	2 hours	115,233	4
No. 205	2 hours	101,853	4
No. 206	2 hours	101,561	4
No. 212	1 hour	108,265	4
No. 214	1 hour	110,349	4

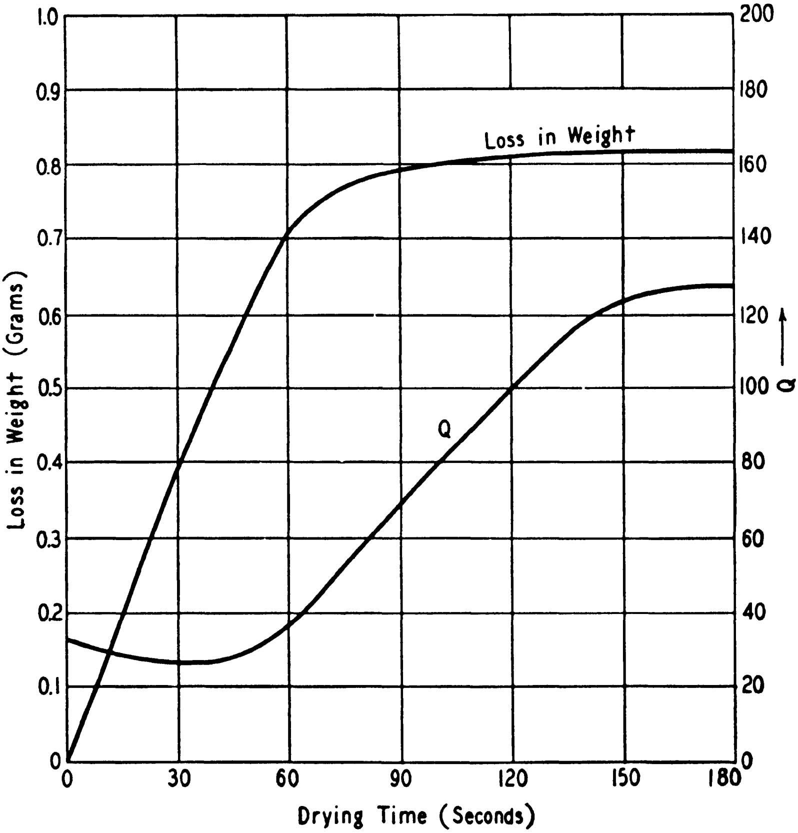

FIG. 248. Drying rate and Q of a single bottle as a function of time.

The moisture determinations were as follows.

Time in Bell Jar	Per Cent Moisture (Average of Three Samples)
2 hours	0.43
1 hour	0.60
Zero	4.13

With these and similar data at hand, the construction of a system which would handle large numbers of bottles was started. A unit of the system is shown in Fig. 249. A port-hole frame was adapted for use as a vacuum chamber. Thirty-four plastic cups are mounted on the peripheries of two circles. An electrode, insulated from ground, may be seen between the two rings of bottles. An inner metal ring and the wall of the port form the two ground electrodes. Radio-frequency power is fed in through a vacuum-tight insulating bushing. Each of the plastic cups is individually gear driven at a speed of 3000 revolutions per minute.

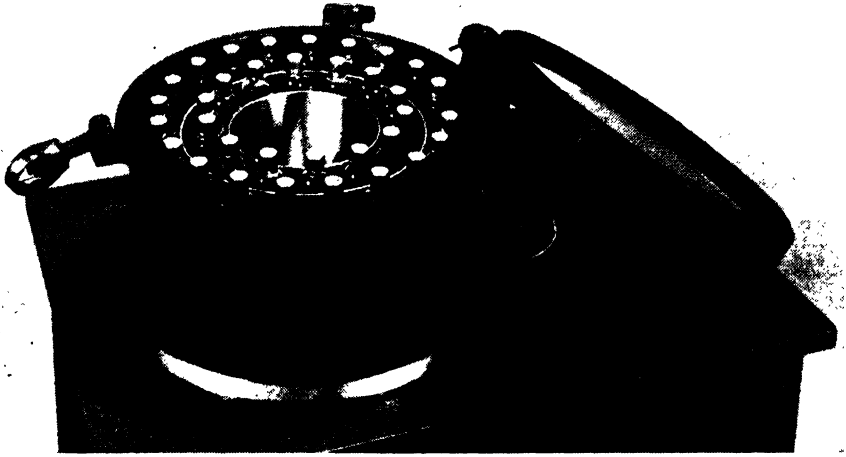

Fig. 249. An experimental drying chamber which holds 34 bottles.

Fig. 250 shows a circular table which supports six of these chambers. Each chamber is subjected to radio-frequency power for 5 minutes. A rotary switch is used so that 5 chambers are connected to the oscillator at one time. One chamber is in the wet stage, that is, it is in the first fifth of its drying cycle. Another chamber is in the second fifth of its drying cycle, and so on around the table. The fifth chamber is in the last stage of the drying cycle. At the end of 1 minute the chamber containing dry bottles is switched from the oscillator and a fresh chamber is connected in the group.* Thus the oscillator remains essentially fully loaded at all times. An examination of Fig. 248 reveals the reasoning behind this procedure. In addition, an automatic tuning circuit incorporated in the oscillator insures complete stability with respect to power output. Since one chamber of thirty-four bottles is unloaded every minute, over 2000 bottles are processed each hour.

---

* This cycling is based on a bottle fill of 1 cubic centimeter of liquid. Thus, it is first necessary to bulk-reduce to a potency of 100,000 Oxford Units per cubic centimeter.

The bottles are next loaded into aluminum trays and the trays are placed on the electrically-heated bases shown in Fig. 251. The metal domes are then closed and evacuated to about 5 millimeters of mercury. After $\frac{1}{2}$ hour in these auxiliary domes, the bottles are removed for capping.

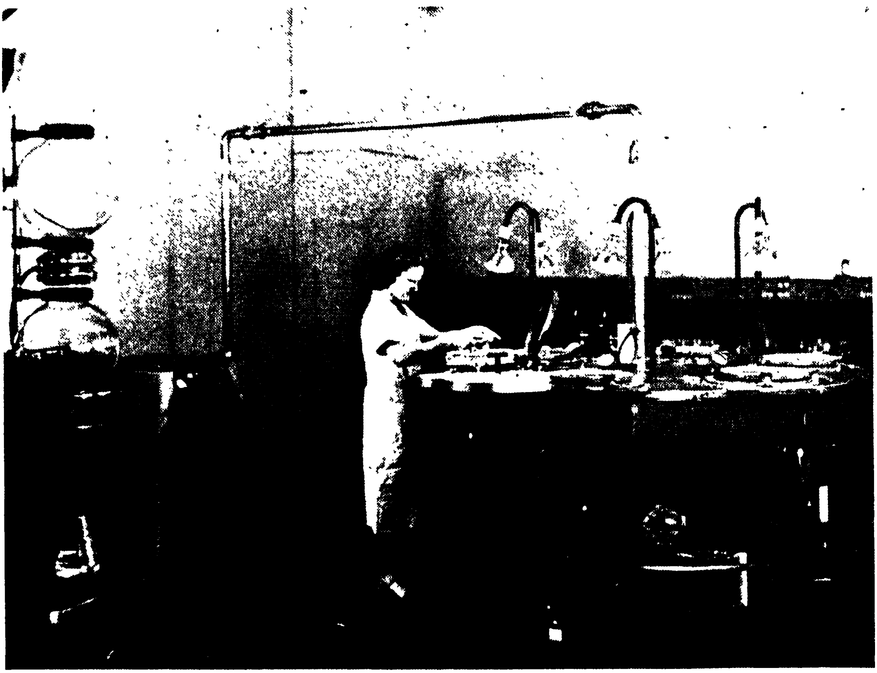

FIG. 250. A circular table with 6 drying chambers. This equipment dries 2000 bottles per hour. The infra-red lamps prevent condensation on the cold lids of the vacuum chambers.

The equipment shown in Fig. 250 is largely automatic. The operator's duties consist of operating the vacuum-applicator valves and vacuum-release valves on the side of the table, as well as opening the lids of the chambers, removing the processed bottles, and inserting new bottles to be dried. When the operator closes the lid to a chamber, a micro-switch is actuated and the bottles begin rotating. A green pilot light at each chamber indicates that the chamber may be opened. A red pilot light shows that radio-frequency power is being applied to the chamber. At the end of each minute, a timer turns off the oscillator, operates the rotary switch so that one chamber is dropped out and a fresh chamber connected, and then turns on the oscillator. If the operator has not yet processed this fresh chamber and thrown the vacuum-applicator valve to the final position, the oscillator will not turn on, and an amber pilot light will indicate the chamber that is delaying the proceedings. When the vacuum-applicator valve is finally thrown, the 1-minute cycles will then be resumed.

Electrical Conductivity of Penicillin. It has been suggested many times that we reconsider the situation and attempt to dry in the frozen state. Since we have shown that our method of drying produces a dry product with no loss in activity, there seems to be no point to the introduction of greater complications of higher vacuums and colder condensers. In addition, the high voltage required in the presence of the more perfect vacuum seems to be an obstacle which will not be solved easily. Early in this chapter, it was stated that the voltages necessary to develop power in the frozen material were markedly higher than for the liquid solution. This point may be illustrated by a specific example.

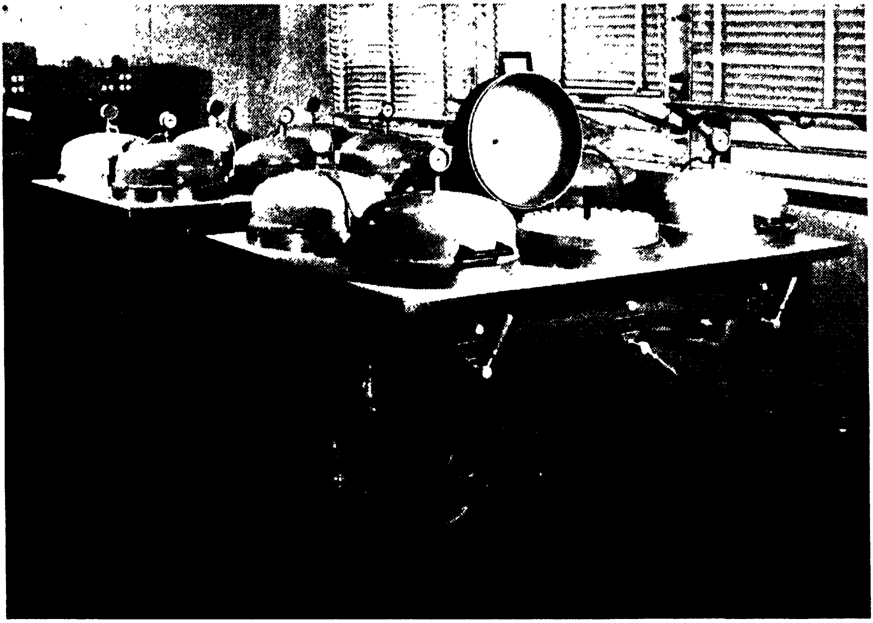

FIG. 251. The auxiliary drying chambers.

The power generated in a 1-centimeter cube of material is

$$P(\text{watts}) = E^2\sigma,$$

where σ = conductivity of the material, in mhos for a centimeter cube;
E = electric intensity in the cube, in volts per centimeter.

Then for 1 watt generated in the cube, the electric intensity is

$$E = \frac{1}{\sqrt{\sigma}}.$$

This electric intensity may be regarded as the voltage required between opposing faces of the cube.

Murphy and Morgan* show that the conductivity of ice increases as a function of frequency but flattens off completely when the frequency is greater than 10,000 cycles. For ice at $-0.8°$ C, they show a conductivity of 4.15×10^{-7} mho for a centimeter cube. When substituted into the above equation, it is seen that the voltage across the 1-centimeter cube for 1 watt is 1550 volts. However, this temperature is very close to the melting point of ice at atmospheric pressure. A few degrees drop in temperature reduces the conductivity appreciably. At $-45.8°$ C, a temperature where freeze-drying is usually carried out, the conductivity has dropped to 10^{-8} mho for a centimeter cube, with a resultant field intensity of 10,000 volts per centimeter.

Measurements on typical penicillin solution with a concentration of 100,000 Oxford Units per cubic centimeter in the liquid state (20° C) show that the conductivity is of the order of 0.1 mho for a centimeter cube. Thus, the field intensity necessary to generate 1 watt in a centimeter cube reaches the remarkably low value of 3.16 volts per centimeter.

In addition to these quantitative relations, the difficulties of coupling radio-frequency energy to ice may be realized by means of a simple experiment. A set of electrodes which will hold a penicillin bottle are mounted on the capacitor terminals of a conventional *Q*-meter. Then if a bottle containing several cubic centimeters of frozen penicillin solution and an empty bottle are successively plugged into the electrodes, it is impossible to detect a difference in the reading of the *Q*-meter.

Application of Radio-Frequency Heating to Other Pharmaceuticals. In the successful application of radio-frequency heating to the problem of drying penicillin, the process has been divided into three parts: first, bulk-reducing of the solution to achieve an activity of 100,000 units per cubic centimeter; second, drying 1 cubic centimeter of the concentrate in the final bottles until the moisture content is reduced to 4 per cent or lower; and third, completing the drying in auxiliary chambers. The equipment described is capable of producing 2000 dry bottles each hour, using inexpensive vacuum pumps and simple condensers. The whole system operates with a minimum of maintenance.

Because the techniques described in this chapter are so different from conventional methods of drying of pharmaceuticals and biologicals, it is difficult to predict what will happen to the many products which might be dried by these methods. For example, as the techniques of purifying penicillin solution were improved, it was noted that the radio-frequency dehydrating process described in this chapter produced a crystalline product while the material dried by high-vacuum application remained amorphous. When radio-frequency drying was applied to a butyl alcohol solution of penicillin the resulting crystalline structure was very easily achieved. The crystalline penicillin possessed a stability under high temperature storage not attained by the ordinary product. Until a broad experience has been built up, it is necessary to submit each product to experiment. The authors have dried a limited number of products with results which show great promise. These

---

* E. J. Murphy and S. O. Morgan, "The Dielectric Properties of Insulating Materials," *Bell System Technical Journal*, Vol. 18, No. 3, July 1939, p. 512.

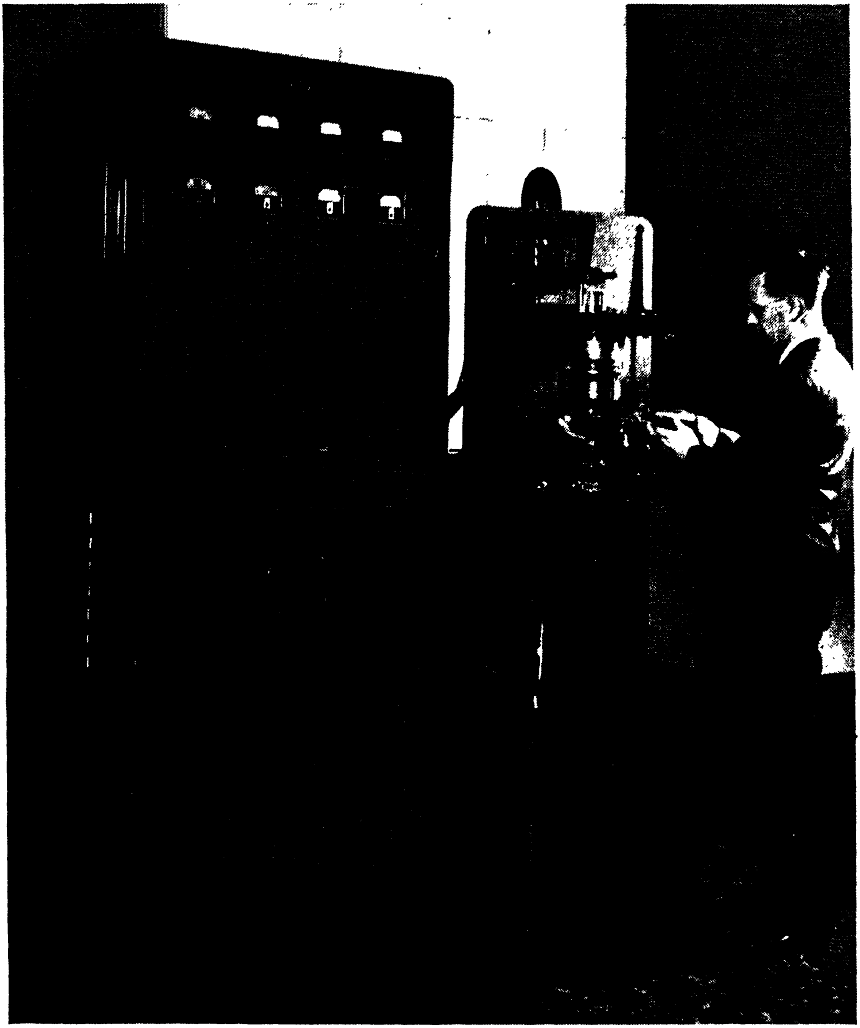

FIG. 252. A continuous bulk-reducer using a spinning cup.

include tetanus antitoxin, amino acids, injectable liver extract, and gas gangrene antitoxin.

The Spinning-Cup Principle Applied to a Continuous Bulk-Concentrator. Earlier in this chapter we related the way in which a baffle plate and a warm coil were used to reduce foaming. In some instances, the most violent foaming only filled the lower half of the bottom flask. Then it was not necessary to use the warm coil. In other cases, the penicillin showed a characteristic bumping which was not alleviated by the warm coil. When the bulk-reducer shown in Fig. 244 was used to concentrate certain serums and antitoxins, the foaming encountered was so violent that it was necessary to spasmodically increase the pressure. Since the spinning arrangement used in the final drier worked so well in entirely eliminating foaming, it seemed logical to apply this principle to the bulk-concentrator. However, merely increasing the size of the bottle and electrode system shown in Fig. 247 was not a complete solution. With the small bottles shown in Fig. 246, where the diameter was approximately 1 inch, it was possible to apply about 20 watts of power at 30 megacycles without danger of ionization, even with a vacuum of 20 millimeters of mercury. When the power was increased appreciably over this figure, breakdown of the space between the electrodes and the spinning cup was experienced. When the bottle size was increased to the

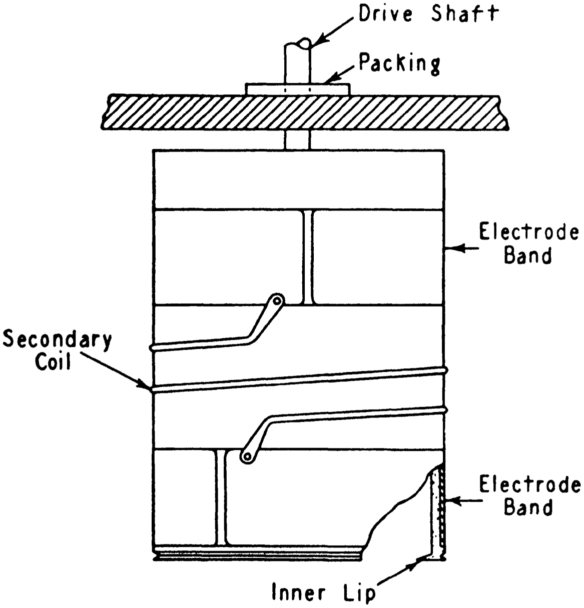

FIG. 253. Details of the plastic cup used in the bulk-concentrator.

point where it would accommodate 500 cubic centimeters of fluid while spinning, it was found that the voltage breakdown occurred with a power of the order of 200 watts. To be able to apply a power of 2000 watts would require a bottle so large as to present severe mechanical problems in the rotating systems.

Thus, to increase the power-handling capacity of the system, it was necessary to devise an arrangement where the rarified atmosphere would not be unduly stressed. Such an arrangement is shown in Fig. 252. Instead of a glass bottle, a polyethylene cup is used which is closed at the top and open at the bottom. The details of the cup may be seen in Fig. 253. The liquid is sucked from the outer container and squirted against the side of the cup, which is rotating at 900 revolutions per minute. The liquid is formed in a layer on the inner surface of the cup. The lip at the bottom of the cup retains the liquid until the layer is as thick as the lip. Excess liquid is thrown out of the cup, striking the bell jar and running down to the receiver at the bottom. Two metal electrodes are mounted on the cup, one electrode near the top and the other near the bottom. The electrodes are connected by 2 turns of $\frac{1}{8}$-inch diameter copper wire wound around the cup. The circuit is energized by a primary coil consisting of a single turn of $\frac{3}{8}$-inch copper tubing. The equivalent electrical circuit is shown in Fig. 254. The capacities represent the capacity between the metal electrodes and the liquid layer, with the polyethylene cup serving as the dielectric material. The resistance is that of the column of liquid. The inductance of the secondary coil mounted on the surface of the cup is adjusted to balance out the capacities at the operating frequency. With this arrangement, it is possible to introduce large amounts of power without unduly stressing the rare atmosphere. In addition, the batch operation of the original system has now become a continuous process.

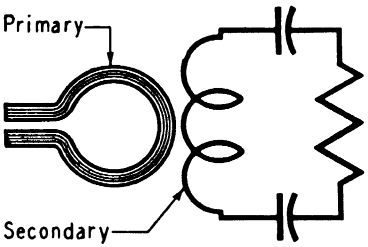

FIG. 254. The equivalent electrical circuit of the spinning cup system.

Chapter 23

PASTEURIZATION AND STERILIZATION

Radio-Frequency Treatment of Infested Products. The application of radio-frequency heating to dry food products such as cereals and flour which are infested with weevils and their eggs is a simple and straightforward process. Since the infesting objects usually contain more moisture than the bulk of material, selective heating often takes place and the mean temperature of the package need not reach excessive values. Experiments conducted by the authors with one-pound packages of cereal revealed that a mean temperature of 140° F was sufficient to completely inactivate weevils and the eggs. Since this technique is applicable to a variety of products and the ruggedness of the types of infestation varies, it is difficult to draw general conclusions as to the power and temperature requirements. It, seems best therefore, to subject the particular product to a series of experiments to establish the pertinent facts.

Pasteurization of Milk. (*a*) *Conventional Pasteurization of Milk.* In the normal method of pasteurizing, milk is heated to a temperature of 143° F and held at this temperature for 30 minutes. The milk is then cooled for storage or bottling. The bacteria content is usually reduced to about 1 per cent of the starting value. If times less than 30 minutes are used, the bacteria content is noticeably greater. When a longer time is used, a cooked flavor is usually present and the apparent cream volume is reduced. The most pathogenic bacteria are destroyed by this treatment. However, this pasteurizing temperature is nearly optimum for the growth of certain thermophilic bacteria, while many thermoduric bacteria such as *Bacillus subtilis* survive the treatment quite well.

Flash pasteurization methods in which the milk is heated to 161° F and held for 16 seconds have been the subject of experiment for some time. In some cases, the milk is spread in a thin film on heated plates and then quickly pumped over cooling plates. In another process, the milk is passed between two electrodes to which 60-cycle voltage is applied. Since the milk is a good conductor, current flows through the milk and generates heat. Difficulties with the electrodes appear to have kept this method from becoming popular. In flash pasteurization at 161° F, the time of 16 seconds appears to be the longest time at which the milk may be held at this temperature without altering the taste or cream volume.

Since heating by means of electric currents avoids heat-conduction problems and thus gives a means of achieving great heating rates, electric heating seems to be the logical method for exploring the effects to be encountered with temperatures far in excess of 161° F. The use of radio-frequency power appeared to make possible the heating of milk in continuous flow with the milk only in contact with glass. In order to learn the solution to certain fundamental problems connected with this procedure, the authors carried out a series of experiments which will be described here.*

(*b*) *Initial Experiments with Radio-Frequency Pasteurization.* In our first experiments, the milk was preheated to 140° F and was then run through a long glass tube, $\frac{1}{4}$ inch in diameter. The electrodes consisted of two pieces of copper foil wrapped around the glass tube. The radio-frequency current thus flowed as a capacity current from one electrode through the glass to the milk stream, as conduction current down the milk stream for a few inches, and then as capacity current from the milk stream to the second electrode. A thermocouple was inserted below the second electrode to indicate temperature. A measurement of the orifice size and milk flow showed that the heating time was about 0.067 second. The experiments proved that excellent pasteurization could be obtained, but it was not possible to obtain temperatures above 190° F. Above this temperature there was a great tendency to form steam pockets with uneven flow. This effect was believed to be due

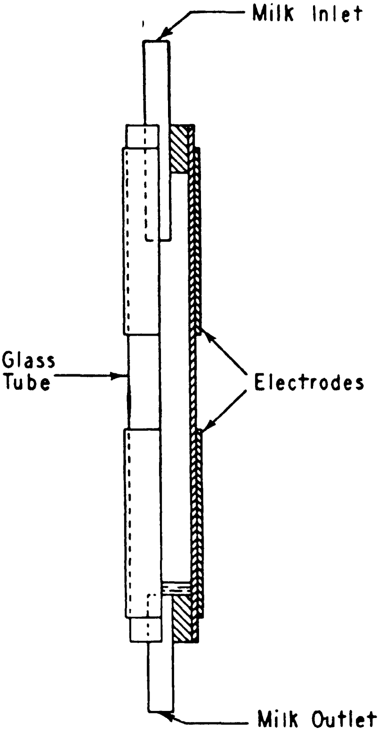

Fig. 255. Arrangement used to produce a freely-falling stream between electrodes.

---

* The general problems of pasteurization were discussed with Henry Jeffers, Jr., and J. S. Bryan of the Walker-Gordon Company and A. J. Powers of the Borden Company. As a result of this discussion, a systematic program was arranged. Mr. Bryan and Mr. Powers participated actively in this program and in particular carried out the many painstaking determinations of bacteria content, cream volume, and butter-fat content.

to non-uniform flow in the tube. The part of the milk stream adjacent to the glass wall was slowed down by friction and raised to a higher temperature than the center of the stream. To circumvent this effect, the arrangement shown in Fig. 255 was devised. Here the milk stream is freely falling while passing through the electrodes. With this arrangement, the milk could be heated to 205° F without steaming or breaking.

(*c*) *Experiments with Uniform Flow.* A series of experiments was made using the uniform-flow arrangement. The bacteriological tests were excellent. The preheating was accomplished by flowing the milk through tubing of pure tin, which in turn was submerged in a tank of warm water. The milk then flowed through the electrodes and was cooled by flowing over a set of fins through which ice water was pumped. Many samples of milk were tasted and the conclusion reached that all samples which had been heated to 190° F or higher had a definite cooked flavor. It is, of course, important that any pasteurizing process must not change the flavor of the milk. The heating time for these tests was again about 0.067 second, with a cooling time of 5 seconds. This cooling time was apparently too long.

The cooling time also influences the apparent cream volume. Roadhouse and Henderson* state that " to the consumer, usually, a large cream volume on bottled milk means a high milk-fat content; a small cream volume, a low milk-fat content. Dealers, in many instances, have promoted this idea in an attempt to secure new business. The cream volume of milk, however, indicates the fat content only when the normal creaming properties of the milk have not been influenced by processing or storage."

(*d*) *Experiments with Vacuum Cooling.* To cool quickly by injecting the milk stream into a vacuum chamber, the arrangement shown in Fig. 256 was used. A closer view of the milk spraying into the bottle is given by Fig. 257. Several cases of empty bottles were capped and sterilized. For each sample, a fresh bottle was put in place. It is estimated that the heating time was 0.067 second and the cooling time was 0.2 second. The milk was cooled to 135° F by means of the vacuum expansion. Then a small sample for bacteriological tests was taken from the bottle by means of a sterile pipette. The remainder of the milk was then poured over cooling fins to cool down to 40° F. Cream-volume samples were taken at this point.

Samples of milk which were tasted showed no traces of cooked flavor at any temperature used. Even the sample taken at 205° F could not be differentiated from the raw milk.

The pertinent data for a supply of milk called X are shown in Table 20, while the bacteriological results are shown graphically in Fig. 258. A number of facts may be gleaned from Table 20. It may be noted that the pasteurization obtained by radio-frequency heating to 205° F is extremely effective, with a bacteria concentration which is well below 1 per cent of the concentration remaining in normally-pasteurized milk. In addition to the absence of cooked flavor, the butter-fat content is unchanged.

---

* C. L. Roadhouse and J. L. Henderson, *The Market-Milk Industry*, McGraw-Hill Book Company, Inc., New York, 1941, p. 330.

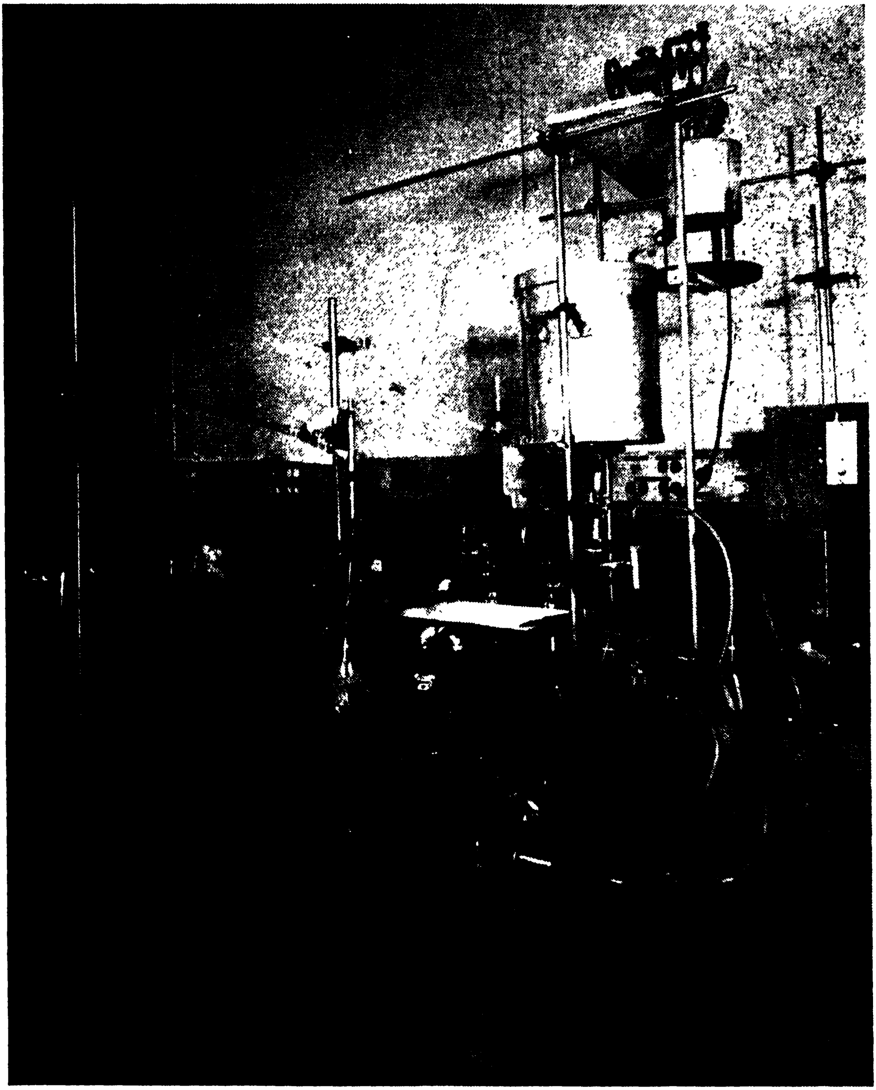

FIG. 256. Laboratory arrangement for pasteurizing of milk by means of radio-frequency power, with vacuum cooling.

FIG. 257. A view of the electrode arrangement and the vacuum-cooling arrangement used in the experiments.

The phosphatase test is satisfactorily negative when the temperatures used are in excess of 180° F. The phosphatase test is highly regarded by health authorities as a quick means of determining that milk has been heated.

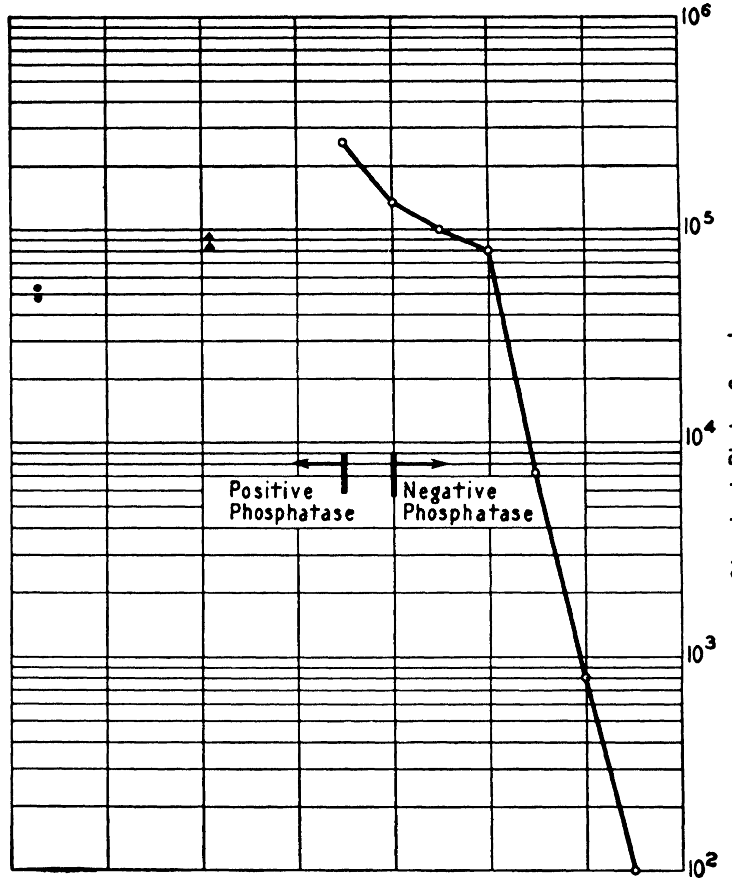

FIG. 258. Bacteriological results obtained with Milk Supply X. The solid dots at the left are the plate counts obtained on samples which were pasteurized in a water bath at 143° F for 30 minutes, while the triangles apply to samples heated to 161° F for 16 seconds in a water bath. Plate counts on two raw samples were 5,320,000 and 4,830,000 colonies per cubic centimeter.

The status of the enzymes changes at temperatures determined by the holding time. It is quite possible to have a high bacteria count with a negative phosphatase record. However, it is used as a test method to a large extent, so it is extremely desirable that any new technique yield a negative phosphatase test.

It may also be seen that the apparent cream volume is greatly reduced when the temperature exceeds 185° F. The authors have conducted numerous tests which involved many different degrees of vacuum in the cooling chamber as well as reheating the milk through a number of cycles. In all these tests, the remarkably low bacteria concentration has always been accompanied by extremely low apparent cream volume.

Table 21 shows the results of experiments on another supply of milk called Y. The results are in substantial agreement with those shown for Supply X. Again it is demonstrated that it is possible to effect bacteria kills far in excess of conventional methods, without a cooked flavor and with no loss of butter fat. The loss in apparent cream volume suggests that future applications of these techniques may be limited to homogenized milk or to milk which is to be packaged in cardboard containers. It is also quite possible to apply the same heating and cooling methods in the pasteurization of other fluids, such as fruit juices.

(*e*) *Loss of Water by Vacuum Cooling.* The temperature to which the milk is cooled by injecting into a vacuum chamber depends upon the degree of vacuum maintained in this chamber. The milk is cooled because some of the energy is used in vaporizing part of the water in the milk. This water vapor is pulled out of the chamber by the vacuum pump. Since it is not desirable to remove any water from the milk, it would be necessary in operation to condense this vapor in a vertical condenser so that the condensate would run back into the milk chamber. The percentage of water removed by evaporation may be calculated from the equation:

$$\text{Percentage of water lost by evaporation} = \frac{\Delta F}{9.7}, \qquad (23.01)$$

where ΔF is the difference in temperature between the hot milk entering the vacuum chamber and the boiling temperature established by the amount of vacuum, expressed in degrees Fahrenheit. Where the entering milk has a temperature of 205° F and the milk is cooled to 135° F, 7.2 per cent of the volume would be lost if it were not caught and returned by the condenser.

(*f*) *Power Requirements for Radio-Frequency Pasteurizing.* The energy requirements calculated from the specific heat of milk check rather well with our laboratory observations.

$$\text{Energy(watt-minutes per quart)} = 36.7\ \Delta F, \qquad (23.02)$$

where ΔF is the temperature increment obtained with radio-frequency power. If we preheat to 140° F and then use radio-frequency power to elevate the temperature to 205° F, the temperature increment due to the radio-frequency

TABLE 20. TEST RESULTS ON MILK SUPPLY X.

Temperature (degrees Fahrenheit)	Standard Plate Count	B. Coli	Phosphatase	Butter Fat (per cent)	Cream Volume (per cent)
205	100	0	−2	3.7	1.5
200	800	0	−2	3.7	1.5
195	7,200	0	−2	3.85	1.5
190	80,000	0	−2	3.7	1.5
185	100,000	0	−2	3.85	13.5
180	133,000	0	−2	3.7	16.5
175	256,000	0	5	3.7	17.5
170	T.N.T.C.*	0	5+	3.8	17.5
165	T.N.T.C.	0	5++	3.95	18.0
160	T.N.T.C.	0	5+++	3.7	18.0
Raw	5,320,000	+2	....	3.7	10.0
Raw	4,830,000	+2	....	....	....
143° F for 30 min.	48,300	+2	−2	....	....
143° F for 30 min.	52,600	0	−2	....	....
161° F for 16 sec.	90,800	+1	−2	....	....
161° F for 16 sec.	82,900	0	−2	....	....

* To numerous to count.

TABLE 21. TEST RESULTS ON MILK SUPPLY Y.

Temperature (Degrees Fahrenheit)	Standard Plate Count	B. Coli	Phosphatase	Butter Fat (per cent)	Cream Volume (per cent)
205	100	0	−2	3.45	1.0
200	300	0	−2	3.4	1.5
195	1,600	0	−2	3.5	1.5
190	5,100	0	−2	3.5	1.5
185	72,000	0	−2	3.4	11.0
180	138,000	0	−2	3.4	14.0
175	257,000	0	5	3.4	15.0
170	T.N.T.C.	0	5+	3.5	15.5
165	T.N.T.C.	+2	5++	3.5	16.0
160	T.N.T.C.	+2	5+++	3.4	16.0
Raw	7,910,000	+2	....	3.4	7.5
Raw	10,990,000	+2	....	....	....
143° F for 30 min.	64,600	0	−2	....	....
143° F for 30 min.	60,000	0	−2	....	....
161° F for 16 sec.	94,400	+2	−2	....	....
161° F for 16 sec.	102,800	+2	−2	....	....

supply is 65° F, and the radio-frequency energy required is 2380 watt-minutes per quart. Thus 1 kilowatt of radio-frequency power will pasteurize 25.2 quarts per hour.

(*g*) *Electric Heating with Contact Electrodes.* In the method of heating by means of radio-frequency currents described above, the milk is in contact only with glass. The metal electrodes are outside the glass so they need not be sterilized. As stated earlier in this chapter, another process attempted to heat the milk by electrical conduction through the milk with 60-cycle current. Since it seems evident that 60-cycle heating is much simpler in application than radio-frequency heating, the authors attempted to secure rapid heating to high temperatures by this means. An arrangement was made where the milk flowed through a tubular metal electrode and fell onto a lower plate electrode of the same material as the tube. The electrode materials consisted of the following: copper, tinned copper, steel, stainless steel, brass, and coin silver. The results, in general, were the same for all materials. With direct current, very pronounced darkening was noted at the electrodes, followed by gas formation at each electrode, where a green substance soon collected. With 60-cycle power, the darkening at the electrodes was very evident in a few seconds. The results with 800-cycle power were essentially the same as noted with 60-cycle power. An oscillator operating at 300,000 cycles was used with this same arrangement. A slight darkening of the electrodes resulted. When 30,000,000-cycle power was used with the metallic electrodes in contact with the milk, there was no evidence of corruption at the electrodes. However, if we must use frequencies as high as this, we may just as well use the capacity-coupling method, thus avoiding any possibility of metallic taste in the milk.

It is understood that some attempts have been made to use carbon electrodes. Because carbon is somewhat porous, some of the milk may be held in the electrodes for a short time. Even a few seconds at 200° F will give a cooked flavor to the milk.

Pasteurization of Beer. Bottled beer is usually pasteurized by flowing hot water over the surface of the bottles for an extended period of time. Here a typical heat-conduction problem exists as the liquid at the interior of the bottle rises slowly in temperature. In some instances, the hot water has a temperature of 155° F and the bottle is heated for 20 minutes. Since heating by means of radio-frequency power seemed an interesting possibility, the authors arranged a series of tests to help evaluate the merits of such a method.*

The experiments were carried out with 12-ounce bottles of beer, some simply unpasteurized, others " ruh " or unfiltered, and still others specially infected for the tests. Fig. 259 shows the electrode arrangment used in the laboratory. The oscillator operated on a frequency of 28 megacycles. In the early experiments, the bottles were heated to a desired temperature and then cooled by immersion in water at 55° F. It soon became apparent that the cork liner was shielded by the metal cap and any contamination in this region would not be subjected to the radio-frequency field. To reach this source of infection, the cold bath was eliminated and the hot bottles were inverted immediately upon removal from the electrodes so the hot liquid would

---

* The authors wish to express their appreciation to Mr. George E. Burghard, President of the George Ehret Brewery, who cooperated wholeheartedly in carrying out the experiments and in arranging for laboratory evaluations of the treated product.

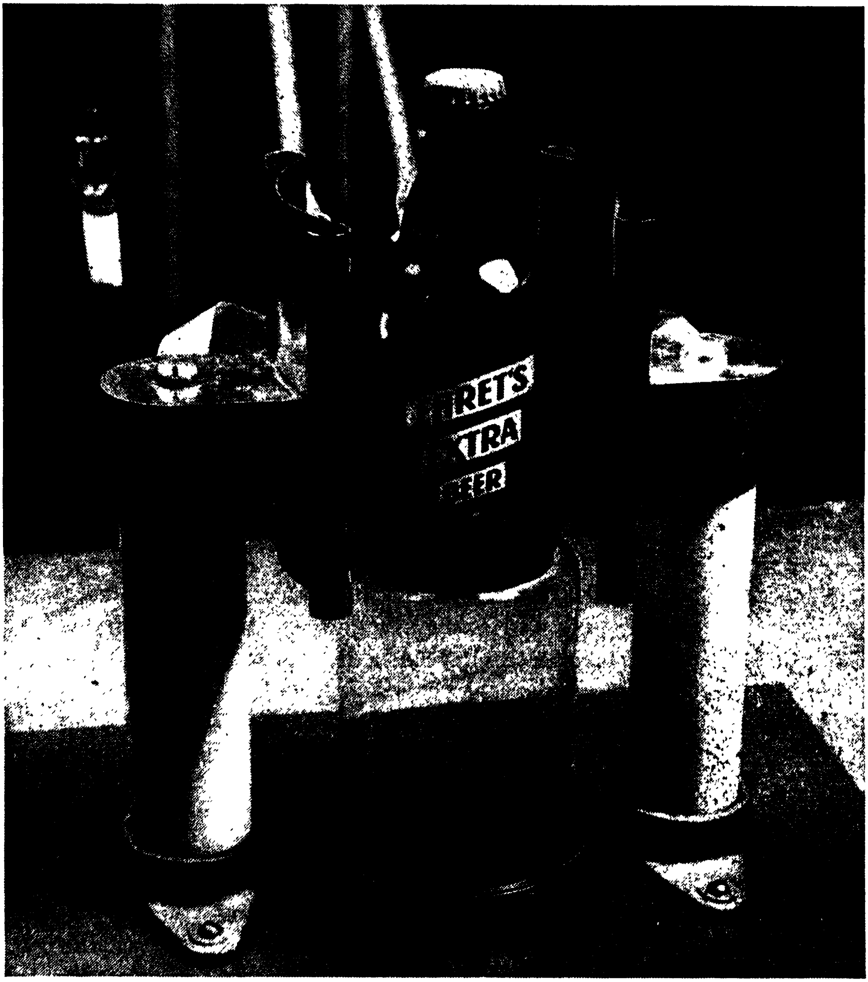

FIG 259. A laboratory arrangement used in beer-pasteurizing experiments.

effectively treat the neck of the bottle and the liner of the cap. The contents then cooled slowly, giving up their heat to the ambient air. The experiments effectively convinced the authors that complete pasteurization was possible by this method with temperatures of the order of 140° F, while yeast spores were effectively inactivated with a temperature as low as 125° F. Essentially similar conclusions were reached by Jones.*

Many storage tests were made, with the control samples showing yeast colonies and sediment, while the treated beer remained brilliant in appearance after 30 days of incubation at 68° F and 86° F. Typical laboratory data are displayed in Table 22.

TABLE 22. PLATE COUNTS OF UNFILTERED BEER.

Heat Treatment	Heating Time (seconds)	Plate Count (micro-organisms per cubic centimeter) Colonies developed on:	
		Beef Extract Agar Incubated at 98° F for 72 hours	Malt Wort Agar Incubated at 86° F for 72 Hours
Unpasteurized control	0	18 (chiefly cocci)	23,000 (yeast)
Heated to 125° F. Allowed to cool in inverted position	66	1 (cocci)	nil
Heated to 135° F. Allowed to cool in inverted position	73	nil	nil
Heated to 145° F. Immediately cooled in water bath at 80° F with the bottle on its side	82	2 (cocci)	nil
Heated to 160° F. Immediately cooled in water bath at 80° F with the bottle on its side	92	nil	nil

The radio-frequency power requirements may be estimated by (23.02). Since the beer is mostly water, its specific heat may be taken as unity. The glass bottle weighs approximately 10 ounces, with a specific heat of 0.2, so the water equivalent of the glass is about 2 ounces. Thus we might consider that we must heat 14 ounces of water or 0.435 quart. If we are to heat from 80° F to 140° F, ΔF in (23.02) is 60, and we see that the energy per quart is 2200 watt-minutes. Since the bottle of beer is the water equivalent of 0.435

---

* Lowell E. Jones, "Electronic Pasteurization," *The American Brewer*, September 1945, pp. 21–23.

quart, the energy per bottle is 956 watt-minutes. Thus a radio-frequency oscillator with a power output of 100,000 watts could pasteurize 105 bottles per minute or 6300 bottles per hour. However, if it were necessary to heat from 35° F to 140° F, the same oscillator would treat only 3590 bottles per hour. These calculations were verified by experiment during the course of the investigation.

The Effect of the Electric Field on Micro-Organisms. The literature is replete with references to the effect of the electric field on micro-organisms. The major difficulty encountered is that some of the reports are positive while others are negative. In any attempt to establish specific effects which might be attributed solely to the electric field, it is difficult to maintain the specimens at low temperature since most solutions which carry bacteria have a high conductivity and hence heat rapidly when the field is applied. Fleming* reports excellent destruction of bacteria in weak electrolytes, with very small powers. He finds the maximum effect at a frequency in the neighborhood of 60 megacycles, but also finds substantial effects at any frequency between 10 and 300 megacycles. The authors have attempted to repeat Fleming's experiments and have found no evidence of destruction of bacteria when such low power concentrations are used.

It seems appropriate to review a few typical experiments carried out during this investigation. In the previous discussion concerning the pasteurization of milk it was disclosed that great destruction of bacteria was accomplished by passing preheated milk through the electrode system shown in Fig. 255 and then cooling with the vacuum system shown in Fig. 257. It occurred to the authors that some of the destruction might be due to the action of the electric field *per se*. A specific experiment was carried out to check this point. Raw milk with a standard plate count of 45,000 per cubic centimeter was preheated to 140° F and then run through the radio-frequency pasteurizer where the temperature was elevated to 200° F. The bacteria count on samples of this treated milk was less than 1 per cent of the initial count. Next, raw milk at a temperature of 68° F was run through the radio-frequency pasteurizer with the same voltage on the electrodes as in the previous case. The temperature was elevated in this manner to 130° F. The plate count of samples of this milk showed 45,000 per cubic centimeter, exactly the same as the raw milk. Since the electric field in the milk was the same in both cases, it seemed fair to draw the conclusion that the destruction of bacteria was entirely due to temperature effects. In this experiment, it was estimated that a field of approximately 700 volts per centimeter existed in the milk for 0.067 second. The frequency of the oscillator was 27 megacycles.

Another experiment with low power concentrations was carried out, using the bulk-reducer shown in Fig. 244. Here milk was boiled in a vacuum with the energy supplied from a radio-frequency generator operating on a frequency of 27 megacycles. The use of the vacuum insured that the temperature was maintained at 80° F throughout the treatment. The power density was approximately 2 watts per cubic centimeter, with an accompanying field intensity of 20 volts per centimeter. Sterile water was fed into the chamber to keep the level constant at all times. Treatment for 10 minutes showed no destruction of bacteria, so the experiment was repeated with a total time of treatment of 1 hour. Again the results were negative.

---

* Hugh Fleming, "Effect of High-Frequency Fields on Micro-Organisms," *Electrical Engineering*, Vol. 63, No. 1, January 1944, pp. 18–21.

Many experiments at 185 megacycles and at 400 megacycles, with power densities of less than 10 watts per cubic centimeter for periods of time short enough to insure that the temperature rise was not great enough to kill bacteria always yielded negative results.

Nyrop* relates the results of certain experiments where he subjected the solutions to high electric field intensities for short times with great destruction of bacteria. He used field intensities of the order of 200 volts per centimeter or greater. A modulated oscillator reduced the average power while periodically subjecting the solutions to high field intensities.

Recently, Wendell C. Morrison† and one of the authors have carried out experiments with solutions subjected to field intensities of 700 to 1000 volts per centimeter, with indications of strong destructive effects. Since milk has a conductivity of approximately 0.005 mho for a centimeter cube, equation (17.01) shows that a field intensity of 1000 volts per centimeter in undiluted milk would generate a power of 5000 watts per cubic centimeter. Then 1200 calories would be generated each second in each cubic centimeter and the milk would boil in less than $\frac{1}{10}$ second after power was applied. Hence in these experiments, the milk was diluted in a ratio of 100: 1 with distilled water. Then the power density is substantially 50 watts per cubic centimeter with a field intensity of 1000 volts per centimeter. The dilute samples were placed in the containers shown in Fig. 260 and the voltage applied across the containers by connections to the metal end caps. Care was taken to see that the tubes were completely filled and that no air pockets existed. The procedure of treatment was to turn on the source of power for 0.2 second. The power was then turned off for 30 seconds and then applied for another period of 0.2 second. This procedure was repeated until the sample had been subjected to 25 pulses. Approximately 60 calories per cubic centimeter were delivered during the time of treatment, but the short time on with the long cooling period between pulses kept the solution below 50° C at all times. This treatment at a frequency of 30 megacycles brought about great destruction of bacteria, with sterility indications in some cases. Similar results have been obtained at a frequency of 190 kilocycles so it may be concluded that the effect of frequency is not critical.

---

* Johan E. Nyrop, "A Specific Effect of High-Frequency Electric Currents on Biological Objects," *Nature*, Vol. 157, No. 3976, January 12, 1946, p. 51.

† Research Engineer, RCA Laboratories, Princeton, N. J.

It should be mentioned that arrangements similar to those shown in Fig. 260 are necessary when applying high field intensities to aqueous solutions. If an air gap is allowed to exist in series with the water, it is not possible to achieve 1000 volts per centimeter in the water. The electric field in the air space is equal to the electric field in the water multiplied by the dielectric constant of water. Hence with 1000 volts per centimeter in the water, the field intensity in the air would exceed 80,000 volts per centimeter, a value far in excess of the dielectric strength of air. Thus it is not possible to place the sample in a dish between plates with an air gap and hope to achieve these high intensities.

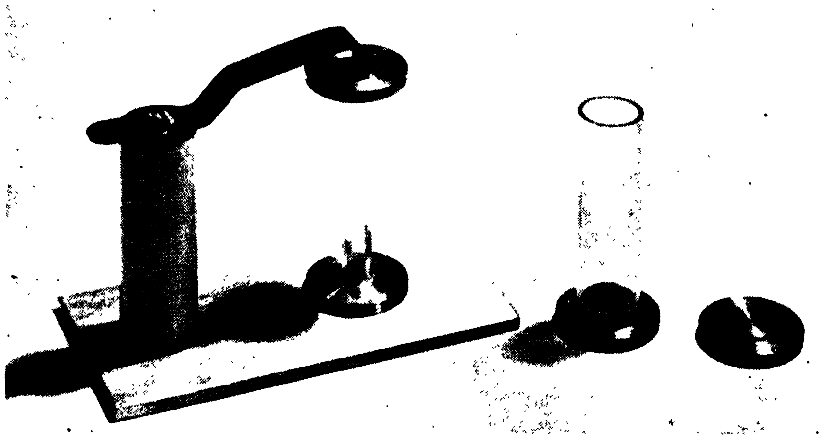

FIG. 260. Glass containers and metal end caps used to apply high electric fields to bacteria-bearing solutions.

On the basis of the present meager knowledge, the authors wish to draw only the following conclusions. Specific effects due to the electric field without heating are possible with high field intensities. Since the fields must be extremely great, heating results. Unless the solutions have low conductivity, temperature effects will destroy micro-organisms before sufficient time has elapsed for the electric field to bring about destruction. Extended research is necessary in this field.

Chapter 24

THE TREATMENT OF FOOD BY RADIO-FREQUENCY POWER

In the preceding chapters, the authors have examined the basic principles which apply to radio-frequency heating techniques. A number of experiments have been described which illustrate these principles, but no attempt has been made to enumerate the many special applications of radio-frequency heating that have become important to industry. For example, radio-frequency generators have been widely used and are accepted as a useful tool by producers of plastic articles. The radio-engineering techniques described in Chapters 18 and 19 apply to the heating of plastic objects as well as to wood. However, cooking by " electronic heat " has a popular appeal which has been fostered by extravagant tales which attribute almost magical powers to this new tool. Many experiments and lengthy cogitations have forced the authors to more conservative conclusions. When meat is cooked by the application of radio-frequency power, the result is a boiled product which differs in flavor, appearance, and texture from what is generally regarded as a culinary delicacy. Bread and biscuits may be baked in a few minutes, but unless the dough and electrodes are placed in a hot oven while the radio-frequency power is applied, the surface tends to remain unpalatable. Satisfactory biscuits have been produced in a few minutes where the oven temperature has been of the order of 500° F. However, the amount of equipment necessary to produce these results has been impressive.

Engineers of the Edison General Electric Appliance Company* have reached the conclusion that extensive use of radio-frequency heating in home cookery is unlikely because of high initial cost, limited scope, and low efficiency. The authors agree completely with these views.

However, in commercial establishments, where the equipment may be used continually and where a specific result is achieved, the above objections may not be valid. Dr. William H. Cathcart† has disclosed the successful application of radio-frequency power in bakeries for the purpose of destroying mold spores in freshly-baked wrapped bread. Freshly-baked bread may readily pick up air-borne spores before the bread is wrapped. After the bread is wrapped, the loaf may be quickly heated to 140° F, a temperature sufficient to destroy the spores without damage to the bread.

---

* *Electrical Manufacturing*, Vol. 37, No. 5, May 1946, pp. 232–234.

† *The Journal of Commerce* (New York), March 20, 1946, p. 17.

Roasting of coffee by radio-frequency power has been repeatedly proposed. The authors conducted numerous experiments to see if any benefits resulted from this treatment. In order to secure uniformity of heating, the coffee beans were placed in a glass cylinder which was slowly rotated. This rotation served to tumble the beans about during the heating process thus subjecting each bean to the proper treatment. These experiments showed that it was possible to cut the roasting time at least in half. However, the power requirements are high, with 1 kilowatt of radio-frequency power necessary to roast 12 pounds of coffee per hour. If any superiority in flavor results, the difference is so slight that it may be easily vitiated by slight deviations in the blending of the coffee mix.

Rapid thawing of frozen vegetables and meats is quite possible by means of radio-frequency power. Again, the large power requirements preclude the ready acceptance of this technique in the home, but for commercial establishments quite attractive possibilities are apparent. Care must be exercised in the thawing procedure for the application of too much power may result in excessive heating of the outer portions while the interior remains frozen. This is due to the fact that the conductivity of the frozen material changes rapidly with temperature. Hence, if non-uniform heating is present at the start, it will be further accentuated as some parts are warmed. These parts will then accept still more power at the expense of the colder portions.

The radio-frequency energy requirements may be estimated by the following equation:

$$\text{Energy (watt-seconds per pound)} = 950u_1 + 151{,}500 + 1900u_2, \qquad (24.01)$$

where:

u_1 = initial temperature of frozen material, numerical value in degrees Centigrade.
u_2 = final temperature of the material, numerical value in degrees Centigrade.

Also, in (24.01):

1st term = energy to bring frozen material to 0° C.
2nd term = energy to melt frozen material. (The assumption is that the material is largely composed of water.)
3rd term = energy to bring material to final temperature.

For example, if the frozen material has an initial temperature of −20° C,

u_1 is then +20 in (24.01). If it is desired to thaw this material and raise it to a final temperature of 60° C, (24.01) shows that 284,500 watt-seconds are required. If 1000 watts of radio-frequency power are available, the time required is 284.5 seconds or approximately 4.75 minutes.

It is of interest to examine the electrical characteristics of the load presented by a block of frozen material when placed between a pair of electrodes. To obtain typical data, a box of frozen spinach was placed between a pair of metal plates. The electrodes were separated from the spinach by an air space on either side of the box. This air space was maintained at $\frac{1}{4}$ inch.

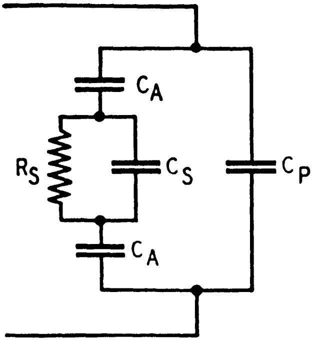

FIG. 261. Equivalent circuit of frozen spinach between spaced electrodes.

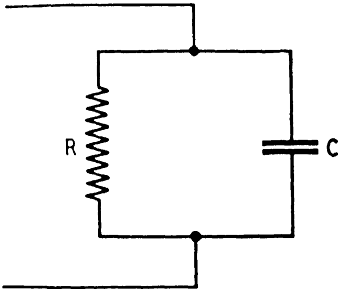

FIG. 262. Simplified circuit of frozen spinach with spaced electrodes. The shunt resistance, R, varies with frequency.

The box containing 14 ounces of spinach was 5 inches long, 4 inches wide, and $1\frac{5}{8}$ inches thick. The plates were each 6 inches square. The equivalent electrical circuit might be represented by Fig. 261, where C_A is the capacity from one plate to the surface of the spinach, C_S is the capacity through the spinach, and C_P is the stray capacity between the plates through the space around the spinach. The loss resistance of the spinach is represented as R_S. At any one frequency, the complex circuit may be specified in terms of the simple circuit of Fig. 262. The values of R and C as shown in this circuit were measured with a Q-meter, as described in Chapter 17. From these values, and the frequency, the power factor was determined. The voltage between the plates for a power dissipation of 1 watt is simply the square root of the resistance R, since the power is the square of the voltage divided by the resistance. The results with the spinach held at −32° C are shown in Table 23.

It may be seen from this table that the voltage across the plates is very high. In addition, it may be noted that the resistance and hence the voltage is substantially constant for all frequencies above 10 megacycles. However, it should not be concluded that high frequencies are not beneficial or useful in thawing since the results in Table 24 show a positive trend in favor of high frequencies.

TABLE 23. ELECTRICAL PROPERTIES OF BOX OF FROZEN SPINACH VERSUS FREQUENCY, WHEN THE TEMPERATURE IS —32°C

Frequency (megacycles)	Shunt Resistance (ohms)	Volts for 1 Watt	Volts for 1000 Watts	Power Factor (per cent)
1.5	71,500	267	8,450	11.4
10.	23,500	153	4,850	5.2
20.	20,000	141	4,470	3.1
30.	18,520	136	4,310	2.2
40.	17,850	134	4,220	1.7
50.	17,250	131	4,150	1.4
200.	16,150	127	4,010	0.38

TABLE 24. ELECTRICAL PROPERTIES OF BOX OF FROZEN SPINACH VERSUS FREQUENCY, WHEN THE TEMPERATURE IS −7° C.

Frequency (megacycles)	Shunt Resistance (ohms)	Volts for 1 Watt	Volts for 1000 Watts	Power Factor (per cent)
1.5	232,000	482	15,220	2.6
10.	16,660	129	4,080	5.5
20.	6,250	79	2,500	7.3
30.	3,570	59	1,888	8.5
40.	2,380	49	1,542	9.6
50.	1,695	41	1,302	10.7
200.	250	16	500	17.9

A similar set of data taken at a fixed frequency of 40 megacycles for a number of temperatures is shown in Table 25. Here it may be seen that, as the frozen material warms, the power factor increases and the material accepts more power for a given voltage. This list emphasizes the primary difficulty encountered in radio-frequency thawing of frozen materials. If one part is warmer than the rest of the body, this part accepts more power. Then the temperature rises in this zone with an increase in power factor and a still more pronounced increase in power concentration. If power is applied too rapidly, this portion may melt and even get quite warm while other portions remain frozen.

When the box of spinach is completely thawed and held at +20° C, the dielectric constant of the spinach becomes high so most of the applied voltage appears across the air gap and the field in the spinach is low. To heat this package to higher temperatures, it is desirable to use high frequencies so that

TABLE 25. ELECTRICAL PROPERTIES OF BOX OF FROZEN SPINACH VERSUS TEMPERATURE, WHEN THE FREQUENCY IS 40 MEGACYCLES.

Temperature (degrees Centigrade)	Shunt resistance (ohms)	Volts for 1 Watt	Volts for 1000 Watts	Power Factor (per cent)
−35	22,900	151	4,780	1.4
−20	6,860	83	2,620	4.4
−15	4,180	65	2,040	6.8
−10	2,710	52	1,645	9.8
− 8	2,455	49	1,568	10.0
− 6	2,455	49	1,568	10.0
− 5	2,585	51	1,602	9.2
− 3	3,350	58	1,830	6.9
− 2	4,520	67	2,120	5.0

the total applied voltage is low. The constancy of the power factor of the circuit is remarkable. The results appear in Table 26.

TABLE 26. ELECTRICAL PROPERTIES OF BOX OF SPINACH VERSUS FREQUENCY, WHEN THE TEMPERATURE IS +20° C.

Frequency (megacycles)	Shunt Resistance (ohms)	Volts for 1 Watt	Volts for 1000 Watts	Power Factor (per cent)
1.5	192,500	438	13,850	3.19
10.	29,400	171	5,420	3.14
20.	14,920	122	3,860	3.1
30.	9,900	99	3,140	3.1
40.	7,570	87	2,740	3.05
50.	5,950	77	2,440	3.12
200.	1,430	38	1,195	3.22

The data of Table 26 point the way to another application of radio-frequency power in the frozen food field, namely the blanching of vegetables before freezing in order to inactivate the enzymes. The usual procedure to secure blanching is to apply hot water or steam for a short time. Then the product is immersed in cooling water. Upon removal from this bath, the vegetables are packaged and frozen. This method leaches out large amounts of the vitamins present in the vegetables. The possibility of packaging the vegetables and then heating by means of radio-frequency power to deactivate the enzymes immediately suggests itself. Moyer and Stotz* have demonstrated that almost complete retention of vitamins is thus possible.

The energy requirements to elevate the temperature may be readily estimated from the following equation.

---

* James C. Moyer and Elmer Stotz, " The Electronic Blanching of Vegetables," *Science*, Vol. 102, No. 2638, July 20, 1945, pp. 68–69.

$$\text{Energy (watt-seconds per pound)} = 1900 \cdot \Delta u, \tag{24.02}$$

where Δu is the desired temperature rise in degrees Centigrade. To avoid loss of heat to the surrounding air with consequent cooling of the surface of the package, it is desirable to mount the electrodes in a warm oven.*

While heating in the package is very attractive, difficulties arise when rapid cooling is attempted. Unless rapid cooling is possible, the flavor may be impaired and it may prove necessary to heat the vegetables in bulk, possibly on a moving canvas belt, with rapid cooling brought about by a blast of refrigerated air.

A study of Table 26 indicates that frequencies between 100 and 200 megacycles are quite necessary in blanching vegetables, since it is only at these higher frequencies that the voltages are low enough to avoid arcing difficulties.

Another application of some interest in the food field is the heating of pork roll. Pork roll is a smoked meat product made of seasoned ground pork with some fat content and packaged in bags 4 inches in diameter, 16 inches long. Each pork roll weighs 6 pounds. To insure that trichina organisms are killed, all parts of the meat must have attained a temperature of 137° F. At present, the product is heated in the smoke-house immediately after it is smoked and kept there for 8 hours at a room temperature of approximately 190° F. The long time cycle ties up the smoke-house, and the high ambient temperature causes the juices to run out and stain the bag. By this process the center of the pork roll never attains a temperature in excess of 120° F so the salt content must be higher than desirable to insure an uncontaminated product. For meat that has not been heated to 137° F, the salt content must be not less than 3.5 per cent by weight.

It appeared profitable to study means for applying radio-frequency heating to the problem so that rapid and uniform heating to the desired temperature could be realized, and thus permit the use of somewhat less salt with consequent improvement in flavor.

At first thought, it might seem that the use of an electric field was an easy and obvious solution. The cylindrical shape of the pork roll pointed to the use of shaped electrodes as described in Chapter 21. A sample of the pork roll was measured and the conductivity was found to be 0.265 mho for a centimeter cube. This good conductor produced the same results described in Chapter 21 for material with an extremely high dielectric constant — namely, that the voltage in the air space would greatly exceed the voltage across the cylinder. To check this point, a set of electrodes which would give a uniform field in the meat was designed, following the principles delineated in Chapter 21. The contoured electrodes were $\frac{1}{4}$ inch away from the roll at the closest point. Then it was found that, with a frequency of 20 megacycles, the voltage between electrodes was between 8,000 and 10,000 volts while the voltage across the roll was less than 100 volts. Thus the heating by capacity coupling was seen to be utterly impractical.

---

* James C. Moyer, "Electronics in the Service of Food Technology," *Farm Research*, Vol. XI, No. 4, October 1945.

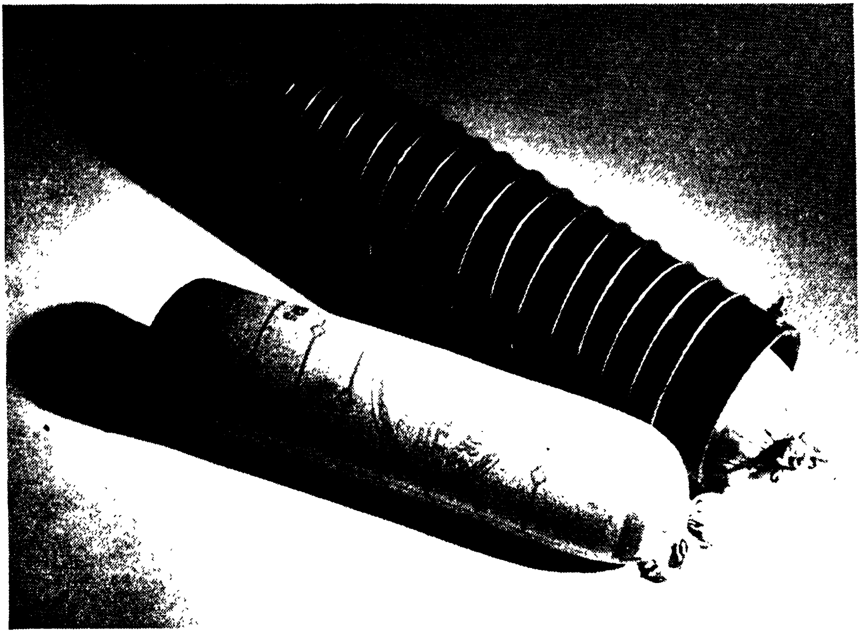

FIG. 263. The pork roll in an induction-heating coil.

With a good conducting material, induction heating seemed to be applicable. Using equation (2.13) with the conductivity stated above, we find that the critical frequency necessary to secure excellent coupling to the load is 19 megacycles. However, the induced currents would then be crowded to the surface and only the outer portions of the roll would be heated. If a much lower frequency was used, the coupling efficiency would be poor but the generation of power would be more uniform. It was therefore necessary to effect a compromise in the choice of frequency. The pork roll was placed in the coil as shown in Fig. 263 and measurements on a Q-meter were then made to determine the efficiency of coupling between the coil and the pork roll. The coupling efficiency as a function of frequency is tabulated in Table 27.

TABLE 27. COUPLING EFFICIENCY IN THE INDUCTION HEATING OF PORK ROLL.

Frequency (megacycles)	Coupling Efficiency (per cent)	
	Cold Pork Roll	Hot Pork Roll
0.7	19	33
1.0	34	49
1.5	50	66
2.0	60	75
3.0	73	85
4.0	80	90
5.0	84	92

A number of experiments with various heating rates and times revealed that the best plan was a 60-minute heating cycle at a frequency of 1.5 megacycles. At the end of the heating cycle the temperature distribution was not uniform but in a 20-minute period following the shut-down of power, the temperature distribution in the pork roll became quite uniform with all points having reached 137° F sometime during the cycle. Temperature distributions taken during the heating cycle are shown in Table 28.

TABLE 28. TEMPERATURE DISTRIBUTION IN INDUCTION-HEATED PORK ROLL.

Time (minutes)	Temperature (degrees Fahrenheit)			
	Surface	One-third in	Two-thirds in	Center
0 (start)	68	68	68	68
37	135	125	100	90
60 (power off)	165	160	143	122
80	137	140	142	143

An outgrowth of the heating experiments on the pork roll was the application of radio-frequency heating to a $\frac{1}{4}$-inch thick slice of pork roll in a bun. As shown above, the pork roll is a good conductor so heating is best accomplished by induction. On the other hand, the bun is a rather good insulator so there the heating may be brought about by passage of capacity currents. Then in order to simultaneously heat the meat by induced currents and the bun by capacity currents, a coil similar to that shown in Fig. 264 was used. The radio-frequency currents circulating in the coil induced currents in the meat and heated it, while the relatively high voltage across the coil and the capacity between the upper and lower windings of the coil caused capacity currents to flow through the bun which was consequently heated. An oscillator power output of about 300 watts with a frequency of 30 megacycles heated the sandwich in 10 seconds.

While radio-frequency power has been widely used in industry for welding, case-hardening, and soldering of metals and for the heating of wood and many plastic materials, extensive application in the food field awaits further research and development. It has been the purpose of this volume to establish basic engineering principles which may be helpful in the use of radio-frequency heating as an industrial tool. A knowledge of these principles must naturally be accompanied by a wide practical experience.

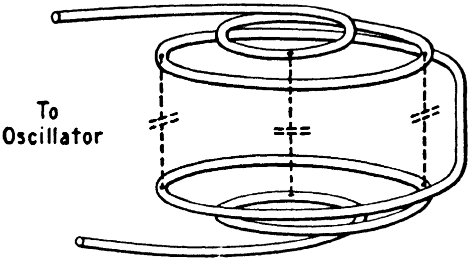

FIG. 264. Schematic diagram of the coil used to heat a sandwich.

The simple believeth every word, but the
prudent man looketh well to his going.

Proverbs XIV:15

Appendix A

A MEANS OF FINDING THE COMPLETE SOLUTION TO THE DIFFERENTIAL EQUATION (14.07)

The complete solution of the differential equation (14.07), as given by (14.08), looks rather formidable but usually degenerates to rather simple forms when applied to a specific problem.*

To proceed with the solution, we rewrite (14.07) thus,

$$\frac{d^2i}{dx^2} - \gamma^2 i = -(G + pC)\,E(x), \tag{A.01}$$

where

$$\gamma^2 = (R + pL)(G + pC). \tag{A.02}$$

Following the teachings of Fry,† a general solution of (A.01) is

$$i = \epsilon^{\gamma x}F_1(x) - \epsilon^{-\gamma x}F_2(x) + A\epsilon^{\gamma x} + B\epsilon^{-\gamma x}, \tag{A.03}$$

where A and B are arbitrary constants and $F_1(x)$ and $F_2(x)$ are indefinite integrals defined below.

$$F_1(x) = -\frac{(G + pC)}{2\gamma}\int \epsilon^{-\gamma x}E(x)\,dx. \tag{A.04}$$

$$F_2(x) = -\frac{(G + pC)}{2\gamma}\int \epsilon^{\gamma x}E(x)\,dx. \tag{A.05}$$

The arbitrary constants may then be evaluated in terms of the terminal conditions. At $x = 0$, the voltage on the line is

$$e_{x=0} = -Z_0\, i_{x=0}. \tag{A.06}$$

---

* George H. Brown, " A Consideration of the Radio-Frequency Voltages Encountered by the Insulating Material of Broadcast Tower Antennas," *Proc. I.R.E.*, Vol. 27, No. 9, September 1939, pp. 573–575.

† Thornton C. Fry, *Elementary Differential Equations*, D. Van Nostrand Company, Inc., New York, 1929, p. 188, Equation (195).

Combining (A.06) with (14.04), we have

$$\left(\frac{di}{dx}\right)_{x=0} = +(G + pC)Z_0\, i_{x=0}. \tag{A.07}$$

Similarly,

$$\left(\frac{di}{dx}\right)_{x=a} = -(G + pC)Z_a\, i_{x=a}. \tag{A.08}$$

Then (A.07) and (A.08) give us two independent equations from which to determine A and B. These equations are

$$\begin{aligned}&[\gamma - Z_0(G + pC)]A - [\gamma + Z_0(G + pC)]B \\ &\qquad = -[\gamma - Z_0(G + pC)]F_1(0) - [\gamma + Z_0(G + pC)]F_2(0)\end{aligned} \tag{A.09}$$

and

$$\begin{aligned}&[\gamma + Z_a(G + pC)]A\epsilon^{\gamma a} - [\gamma - Z_a(G + pC)]B\epsilon^{-\gamma a} \\ &\qquad = -[\gamma + Z_a(G + pC)]F_1(a)\epsilon^{\gamma a} - [\gamma - Z_a(G + pC)]F_2(a)\epsilon^{-\gamma a}.\end{aligned} \tag{A.10}$$

When these last two equations are solved for A and B and the results substituted in (A.03), we have the complete solution of the current equation. In making this substitution, it is convenient to note that

$$F_2(a) - F_2(0) = -\frac{(G + pC)}{2\gamma}\int_{v=0}^{v=a} E(v)\epsilon^{\gamma v}\,dv \tag{A.11}$$

and

$$F_2(x) - F_2(0) = -\frac{(G + pC)}{2\gamma}\int_{v=0}^{v=x} E(v)\epsilon^{\gamma v}\,dv. \tag{A.12}$$

Similar relations in $F_1(x)$ hold. Furthermore,

$$\begin{aligned}&F_2(a) - F_2(0) + F_1(a) - F_1(0) \\ &\qquad = -\frac{(G + pC)}{\gamma}\int_{v=0}^{v=a} E(v)\cosh(\gamma v)\,dv.\end{aligned} \tag{A.13}$$

After considerable tedious manipulation of these unwieldy expressions, (A.03) becomes the solution shown by equation (14.08).

Appendix B

THE OPERATIONAL SOLUTION OF EQUATION (18.21)

The operational equation (18.21) is

$$u = \frac{E}{pL}\left[\frac{\sinh(\sqrt{pLG}\,b) - \sinh(\sqrt{pLG}\,x) - \sinh(\sqrt{pLG}[b-x])}{\sinh(\sqrt{pLG}\,b)}\right]$$

$$= \frac{E}{pL}\left[1 - \frac{\sinh(\sqrt{pLG}\,x)}{\sinh(\sqrt{pLG}\,b)} - \frac{\sinh(\sqrt{pLG}\,[b-x])}{\sinh(\sqrt{pLG}\,b)}\right]. \qquad \text{(B.01)}$$

We shall first solve the operational relation $-\dfrac{\sinh(\sqrt{pLG}\,x)}{\sinh(\sqrt{pLG}\,b)}$ by means of the Heaviside Expansion Theorem. Let

$$y = -\frac{\sinh(\sqrt{pLG}\,x)}{\sinh(\sqrt{pLG}\,b)} = \frac{-1}{\left[\dfrac{\sinh(\sqrt{pLG}\,b)}{\sinh(\sqrt{pLG}\,x)}\right]} = \frac{Y(p)}{Z(p)}, \qquad \text{(B.02)}$$

where $Y(p)$ is a function of the operator p, and $Z(p)$ is a function of the same operator.

From (B.02),

$$Y(p) = -1 \qquad \text{(B.03)}$$

and

$$Z(p) = \frac{\sinh(\sqrt{pLG}\,b)}{\sinh(\sqrt{pLG}\,x)}. \qquad \text{(B.04)}$$

The Expansion Theorem gives as a solution of (B.02),

$$y = \left[\frac{Y(p)}{Z(p)}\right]_{p=0} + \left[\frac{Y(p)\epsilon^{pt}}{p\dfrac{dZ}{dp}}\right]_{p=p_1} + \left[\frac{Y(p)\epsilon^{pt}}{p\dfrac{dZ}{dp}}\right]_{p=p_2} + \cdots, \qquad \text{(B.05)}$$

where p_1, p_2, etc., are roots of $Z(p)$, that is, the values of p at which $Z(p)$ vanishes.

Before proceeding with (B.05), we define an arbitrary number m as follows:

$$-m^2 = pLG \tag{B.06}$$

or

$$\sqrt{pLG} = jm. \tag{B.07}$$

Then (B.04) becomes

$$Z(p) = \frac{\sin(mb)}{\sin(mx)}. \tag{B.08}$$

Roots of (B.08) are*

$$m = \frac{s\pi}{b},$$

where $s = 1, 2, 3$, etc., and from (B.06)

$$p_1 = \frac{-1}{LG}\left(\frac{\pi}{b}\right)^2$$

$$p_2 = \frac{-1}{LG}\left(\frac{2\pi}{b}\right)^2$$

and

$$p_s = \frac{-1}{LG}\left(\frac{s\pi}{b}\right)^2$$

where $s = 1, 2, 3$, etc.

Now,

$$\frac{dZ}{dp} = \frac{dZ}{dm}\cdot\frac{dm}{dp}. \tag{B.09}$$

From (B.06),

$$-2m \cdot dm = LG \cdot dp$$

---

[*] W. O. Pennell, "A Generalization of Heaviside's Expansion Theorem," *Bell System Technical Journal*, Vol. 8, No. 3, July 1929, pp. 489–490, evaluates an equation of the same form as (B.02) by a somewhat different approach. Pennell points out that m has both positive and negative roots and that a summation just twice what it should be results when both roots of m are used. Since both the positive and negative values of m, when squared, yield the same value of p, we need not consider the use of both roots of m. We are only interested in finding the total number of roots of (B.08) in terms of p.

or

$$\frac{dm}{dp} = \frac{-LG}{2m}. \tag{B.10}$$

From (B.08),

$$\frac{dZ}{dm} = \frac{b \sin mx \cos mb - x \sin mb \cos mx}{\sin^2 mx}. \tag{B.11}$$

Substituting (B.10) and (B.11) in (B.09), we obtain

$$\frac{dZ}{dp} = -\frac{LG}{2m}\left(\frac{b \sin mx \cos mb - x \sin mb \cos mx}{\sin^2 mx}\right). \tag{B.12}$$

From (B.06) and (B.12),

$$p\frac{dZ}{dp} = \frac{m}{2}\left(\frac{b \sin mx \cos mb - x \sin mb \cos mx}{\sin^2 mx}\right) \tag{B.13}$$

and

$$\left(p\frac{dZ}{dp}\right)_{p=p_s} = \frac{m_s b(-1)^s}{2 \sin (m_s x)} = \frac{s\pi(-1)^s}{2 \sin (s\pi x/b)}. \tag{B.14}$$

Also,

$$\left[\frac{Y(p)}{Z(p)}\right]_{p=0} = -\frac{x}{b}, \tag{B.15}$$

so that (B.02) becomes

$$y = -\frac{x}{b} - \sum_{s=1}^{s=\infty} \frac{2(-1)^s}{s\pi} \sin\left(\frac{s\pi x}{b}\right)\epsilon^{-\left(\frac{s\pi}{b}\right)^2 \frac{t}{LG}}. \tag{B.16}$$

The third term in (B.01) is handled in exactly the same way and becomes

$$\begin{aligned} z &= -\frac{b-x}{b} - \sum_{s=1}^{s=\infty} \frac{2(-1)^s}{s\pi} \sin\left[\frac{s\pi}{b}(b-x)\right]\epsilon^{-\left(\frac{s\pi}{b}\right)^2 \frac{t}{LG}} \\ &= -1 + \frac{x}{b} + \sum_{s=1}^{s=\infty} \frac{2(-1)^s}{s\pi} \cos(s\pi) \sin\left(\frac{s\pi x}{b}\right)\epsilon^{-\left(\frac{s\pi}{b}\right) \frac{t}{LG}}. \end{aligned} \tag{B.17}$$

Substituting (B.16) and (B.17) in (B.01),

$$u(x) = \frac{4E}{\pi L}\cdot\frac{1}{p}\left[\sum_{s=1}^{s=\infty} \frac{\sin\left[(2s-1)\frac{\pi x}{b}\right]}{(2s-1)}\epsilon^{-(2s-1)^2\left(\frac{\pi}{b}\right)^2 \frac{t}{LG}}\right]. \tag{B.18}$$

But operationally

$$\frac{1}{p} = \int_{t=0}^{t=t} dt$$

so

$$u(x) = \frac{4E}{\pi L}\left[-\left(\frac{b}{\pi}\right)^2 LG\right]\sum_{s=1}^{s=8}\frac{\sin\left[(2s-1)\dfrac{\pi x}{b}\right]}{(2s-1)^3}\,\epsilon^{-(2s-1)^2\left(\frac{\pi}{b}\right)^2\frac{t}{LG}}\Bigg|_{t=0}^{t=t} \qquad \text{(B.19)}$$

or

$$u(x) = \frac{4EGb^2}{\pi^3}\sum_{s=1}^{s=\infty}\frac{\sin\left[(2s-1)\dfrac{\pi x}{b}\right]}{(2s-1)^3}\left[1-\epsilon^{-(2s-1)^2\left(\frac{\pi}{b}\right)^2\frac{t}{LG}}\right], \qquad \text{(B.20)}$$

which is (18.22), a solution of (18.21).

Appendix C

THE SOLUTION OF THE INTEGRAL APPEARING IN THE SCANNING EQUATION

The integral appearing as part of the scanning equation (16.20) seems harmless in character. However, a certain amount of devious manipulation is necessary to secure the result shown by (16.22). Since the details of the derivation are not necessary for an understanding of the remainder of Chapter 16 and are of interest only to a serious student of the subject, it seems proper to relegate the proof of equation (16.22) to an appendix.

Let us designate the integral as

$$\mathcal{J} = \int_{t=-\infty}^{t=t'} \frac{dt}{(t'-t)^{1/2}\left[1+\left(\frac{vt}{h'}\right)^2\right]^2}. \tag{C.01}$$

We next change the variable in (C.01) by means of the relation

$$b = \sqrt{\frac{v}{h'}}\,(t'-t)^{1/2} \tag{C.02}$$

or

$$b^2 = \frac{v}{h'}\,(t'-t). \tag{C.03}$$

Then

$$2b \cdot db = -\frac{v}{h'} \cdot dt \tag{C.04}$$

and

$$\frac{dt}{(t'-t)^{1/2}} = -2\sqrt{\frac{h'}{v}} \cdot db. \tag{C.05}$$

With the substitution of these latter relations, together with the proper modification of the limits, (C.01) becomes

$$\mathcal{J} = 2\sqrt{\frac{h'}{v}}\int_{b=0}^{b=\infty} \frac{db}{\left[1 + \left(\frac{vt'}{h'} - b^2\right)^2\right]^2}. \tag{C.06}$$

By now introducing the operator $j = \sqrt{-1}$ and noting that

$$\left[1 - j\left(\frac{vt'}{h'} - b^2\right)\right]\left[1 + j\left(\frac{vt'}{h'} - b^2\right)\right] = \left[1 + \left(\frac{vt'}{h'} - b^2\right)^2\right], \tag{C.07}$$

equation (C.06) becomes

$$\mathcal{J} = 2\sqrt{\frac{h'}{v}}\int_{b=0}^{b=\infty} \frac{db}{\left[1 - j\left(\frac{vt'}{h'} - b^2\right)\right]^2\left[1 + j\left(\frac{vt'}{h'} - b^2\right)\right]^2} \tag{C.08}$$

or

$$\mathcal{J} = \frac{1}{2}\sqrt{\frac{h'}{v}}\int_{b=0}^{b=\infty} \left(\frac{1}{1 - j\frac{vt'}{h'} + jb^2} + \frac{1}{1 + j\frac{vt'}{h'} - jb^2}\right)^2 db. \tag{C.09}$$

Carrying out the squaring operation indicated in (C.09) yields

$$\mathcal{J} = \frac{1}{2}\sqrt{\frac{h'}{v}}\int_{b=0}^{b=\infty} \frac{db}{\left(1 - j\frac{vt'}{h'} + jb^2\right)^2} + \frac{1}{2}\sqrt{\frac{h'}{v}}\int_{b=0}^{b=\infty} \frac{db}{\left(1 + j\frac{vt'}{h'} - jb^2\right)^2}$$
$$+ \frac{1}{2}\sqrt{\frac{h'}{v}}\int_{b=0}^{b=\infty} \frac{2\,db}{\left(1 - j\frac{vt'}{h'} + jb^2\right)\left(1 + j\frac{vt'}{h'} - jb^2\right)}. \tag{C.10}$$

For convenience, we may write

$$\mathcal{J} = \mathcal{J}_1 + \mathcal{J}_2 + \mathcal{J}_3, \tag{C.11}$$

where

$$\mathcal{J}_1 = \frac{1}{2}\sqrt{\frac{h'}{v}}\int_{b=0}^{b=\infty} \frac{db}{\left(1 - j\frac{vt'}{h'} + jb^2\right)^2}. \tag{C.12}$$

Equation (C.12) may be partially integrated and reduces to*

$$\mathcal{J}_1 = \frac{1}{2}\sqrt{\frac{h'}{v}}\left[\frac{b}{2\left(1 - j\frac{vt'}{h'}\right)\left(1 - j\frac{vt'}{h'} + jb^2\right)}\Bigg|_{b=0}^{b=\infty} + \frac{1}{2\left(1 - j\frac{vt'}{h'}\right)}\int_{b=0}^{b=\infty}\frac{db}{1 - j\frac{vt'}{h'} + jb^2}\right]$$

$$= \frac{1}{2}\sqrt{\frac{h'}{v}}\left[\frac{1}{2\left(1 - j\frac{vt'}{h'}\right)}\int_{b=0}^{b=\infty}\frac{db}{1 - j\frac{vt'}{h'} + jb^2}\right]. \tag{C.13}$$

Similarly

$$\mathcal{J}_2 = \frac{1}{2}\sqrt{\frac{h'}{v}}\int_{b=0}^{b=\infty}\frac{db}{\left(1 + j\frac{vt'}{h'} - jb^2\right)^2}$$

$$= \frac{1}{2}\sqrt{\frac{h'}{v}}\left[\frac{1}{2\left(1 + j\frac{vt'}{h'}\right)}\int_{b=0}^{b=\infty}\frac{db}{1 + j\frac{vt'}{h'} - jb^2}\right] \tag{C.14}$$

and

$$\mathcal{J}_3 = \frac{1}{2}\sqrt{\frac{h'}{v}}\int_{b=0}^{b=\infty}\frac{2db}{\left(1 - j\frac{vt'}{h'} + jb^2\right)\left(1 + j\frac{vt'}{h'} - jb^2\right)}$$

$$= \frac{1}{2}\sqrt{\frac{h'}{v}}\left(\int_{b=0}^{b=\infty}\frac{db}{1 - j\frac{vt'}{h'} + jb^2} + \int_{b=0}^{b=\infty}\frac{db}{1 + j\frac{vt'}{h'} - jb^2}\right). \tag{C.15}$$

Substituting (C.13), (C.14), and (C.15) in (C.11) yields

$$\mathcal{J} = \frac{1}{2}\sqrt{\frac{h'}{v}}\left\{\left[1 + \frac{1}{2\left(1 - j\frac{vt'}{h'}\right)}\right]\int_{b=0}^{b=\infty}\frac{db}{1 - j\frac{vt'}{h'} + jb^2}\right.$$

$$\left. + \left[1 + \frac{1}{2\left(1 + j\frac{vt'}{h'}\right)}\right]\int_{b=0}^{b=\infty}\frac{db}{1 + j\frac{vt'}{h'} - jb^2}\right\}. \tag{C.16}$$

---

* B. O. Peirce, *A Short Table of Intergrals*, Ginn and Company, New York, 2d revised ed.; p. 8, Example 51.

Now*

$$\int_{b=0}^{b=\infty} \frac{db}{1 - j\frac{vt'}{h'} + jb^2} = \frac{1}{\sqrt{j\left(1 - j\frac{vt'}{h'}\right)}} \tan^{-1}\left(b\sqrt{\frac{j}{1 - j\frac{vt'}{h'}}}\right)\Bigg|_{=0}^{b=\infty}$$

$$= \frac{\pi}{2} \cdot \frac{1}{\sqrt{j\left(1 - j\frac{vt'}{h'}\right)}} \tag{C.17}$$

and

$$\int_{b=0}^{b=\infty} \frac{db}{1 + j\frac{vt'}{h'} - jb^2} = \frac{\pi}{2} \cdot \frac{1}{\sqrt{-j\left(1 + j\frac{vt'}{h'}\right)}} \cdot \tag{C.18}$$

Substituting (C.17) and (C.18) in (C.16), we obtain

$$\mathcal{G} = \frac{\pi}{8}\sqrt{\frac{h'}{v}}\left[\left(3 - j2\frac{vt'}{h'}\right)\left(1 + j\frac{vt'}{h'}\right)\sqrt{\frac{vt'}{h'} - j}\right.$$
$$\left. + \left(3 + j2\frac{vt'}{h'}\right)\left(1 - j\frac{vt'}{h'}\right)\sqrt{\frac{vt'}{h'} + j}\right]$$
$$\div \left[1 + \left(\frac{vt'}{h'}\right)^2\right]^{3/2} \cdot \tag{C.19}$$

We may express the radical

$$\sqrt{\frac{vt'}{h'} - j} = \sqrt{\left[1 + \left(\frac{vt'}{h'}\right)^2\right]^{1/2} (\cos\theta - j\sin\theta)}$$

$$= \left[1 + \left(\frac{vt'}{h'}\right)^2\right]^{1/4} \left[\cos\frac{\theta}{2} - j\sin\frac{\theta}{2}\right] \tag{C.20}$$

where

$$\cos\theta = \frac{vt'}{h'} \Big/ \sqrt{1 + \left(\frac{vt'}{h'}\right)^2} \tag{C.21}$$

and

$$\sin\theta = 1 \Big/ \sqrt{1 + \left(\frac{vt'}{h'}\right)^2} \cdot \tag{C.22}$$

---

* B. O. Peirce, *A Short Table of Integrals*, Ginn and Company, New York, 2d revised ed.; p. 8, Example 49.

Hence

$$\cos\frac{\theta}{2} = \sqrt{\frac{1}{2}\left[1 + \frac{vt'/h'}{\sqrt{1+\left(\frac{vt'}{h'}\right)^2}}\right]} \tag{C.23}$$

and

$$\sin\frac{\theta}{2} = \sqrt{\frac{1}{2}\left[1 - \frac{vt'/h'}{\sqrt{1+\left(\frac{vt'}{h'}\right)^2}}\right]}\cdot \tag{C.24}$$

When (C.23) and (C.24) are inserted in (C.20), it is seen that

$$\sqrt{\frac{vt'}{h'} - j} = \left[1+\left(\frac{vt'}{h'}\right)^2\right]^{1/4}\left\{\sqrt{\frac{1}{2}\left[1 + \frac{vt'/h'}{\sqrt{1+\left(\frac{vt'}{h'}\right)^2}}\right]}\right.$$
$$\left. - j\cdot\sqrt{\frac{1}{2}\left[1 - \frac{vt'/h'}{\sqrt{1+\left(\frac{vt'}{h'}\right)^2}}\right]}\right\}\cdot \tag{C.25}$$

Similarly

$$\sqrt{\frac{vt'}{h'} + j} = \left[1+\left(\frac{vt'}{h'}\right)^2\right]^{1/4}\left\{\sqrt{\frac{1}{2}\left[1 + \frac{vt'/h'}{\sqrt{1+\left(\frac{vt'}{h'}\right)^2}}\right]}\right.$$
$$\left. + j\cdot\sqrt{\frac{1}{2}\left[1 - \frac{vt'/h'}{\sqrt{1+\left(\frac{vt'}{h'}\right)^2}}\right]}\right\} \tag{C.26}$$

Substituting (C.25) and (C.26) in (C.19) and performing the indicated multiplication, we find

$$\mathcal{S} = \frac{\pi}{8}\sqrt{\frac{2h'}{v}}\left\{\left[3+2\left(\frac{vt'}{h'}\right)^2\right]\left[\sqrt{1+\left(\frac{vt'}{h'}\right)^2}+\frac{vt'}{h'}\right]^{1/2}\right.$$
$$\left. + \frac{vt'}{h'}\left[\sqrt{1+\left(\frac{vt'}{h'}\right)^2}-\frac{vt'}{h'}\right]^{1/2}\right\} \div \left[1+\left(\frac{vt'}{h'}\right)^2\right]^{3/2}\cdot \tag{C.27}$$

The expression which multiplies $\frac{\pi}{8}\sqrt{\frac{2h'}{v}}$ in (C.27) has a maximum value when $vt'/h' = 0.5$ and the maximum value is 3.48 so if we note that the reciprocal of the maximum value is 0.287, we may define the function $g(vt'/h')$ thus

$$g\left(\frac{vt'}{h'}\right) = 0.287 \left\{ \left[3 + 2\left(\frac{vt'}{h'}\right)^2\right] \left[\sqrt{1 + \left(\frac{vt'}{h'}\right)^2} + \frac{vt'}{h'}\right]^{1/2} + \frac{vt'}{h'}\left[\sqrt{1 + \left(\frac{vt'}{h'}\right)^2} - \frac{vt'}{h'}\right]^{1/2} \right\} \div \left[1 + \left(\frac{vt'}{h'}\right)^2\right]^{3/2} \qquad \text{(C.28)}$$

It should be noted that (C.28) is identical with (16.22). When (C.27) is rewritten to utilize the expression (C.28),

$$\mathcal{G} = \frac{3.48\pi}{8}\sqrt{\frac{2h'}{v}} \cdot g\left(\frac{vt'}{h'}\right). \qquad \text{(C.29)}$$

The expression given by (C.29) may be substituted directly for the integral appearing in (16.20). A simple multiplication of the numerical coefficients results immediately in the first term of (16.21).

INDEX

Activity of penicillin, 320
Admittance of a cube, 1, 2
  of a dielectric cylinder, 12
Air, thermal conductivity of, 36
Analogy, transmission line — heat flow, 148, 149, 156
Annealing, conclusions, 134, 135
Approximate admittance of a dielectric cylinder, 11, 12
Approximations for ber and bei functions, 50
Attenuation factor, 222
Axial current flow, 1–26

Babat, G., 71, 107
Bacillus subtilis, 328
Baffle plate in bulk reducer, 316
Balanced loads, 272
Bar electrodes, 292, 293
  sealer, 297
  -sealing attachment, 293
Beer pasteurization, 337
Bennett, Edward, 74, 109, 173, 174, 206
Berg, E. J., 149, 153, 155
Ber and bei functions, 18
  approximations for, 50
Bessel, differential equation, 5
  functions, 5, 49
Bias-cut tape, 295
Bierwirth, R. A., 256
Binding, attachment, 294, 295, 296
  thermoplastic, 297
Blanching of vegetables, 347
Boegehold, A. L., 188
Boiling temperature of aqueous penicillin solution, 314
Boonton Radio Corporation, 209
Brace, P. H., 205
Brass annealing, advantages of radio-frequency method, 127
  cartridge and rod, 115
  comparison of furnace and radio-frequency, 125, 126
  coupling coil for, 123
  efficiency, 130
Brass annealing, illustrative example, 132
  plans, 122, 123
  theoretical power requirements, 130
Brazing, 138
Bread, treatment of, 343, 344
Breakdown voltage of plastics, 282
Brown, George H., 128, 353
Bryan, J. S., 329
Bubble-breaking coil, 316, 317
Bulk reducer, 315, 316
  continuous, 325–327
  for penicillin, 312, 313
Burghard, George E., 337
Bush, Vannevar, 154
Butter-fat content, 331, 336, 337
Butyl alcohol solutions of penicillin, 325
Byerly, W. E., 236

Cable, J. W., 205
Cakes, rayon, 308
Carson, John R., 74
Case hardening, 151
  of steel, 173–205
Cathcart, William H., 343
Coated materials, 297
Coefficient of magnetic hardness, 174
  saturation, 174
Coffee roasting, 344
Coil for annealing brass, 115
Concentric transmission-line method of determining dielectric properties, 218
Conducting cylinder, 27
Conduction, current, 207
  loss, 36
  of current in metals, 206
Conductivity, 212
  of ice, 324
  of penicillin, 323
  of plastic materials, 290
Conductor of small diameter, 33, 34
  steel, copper-plated, 71
Contact electrodes, 337
Continuous bulk reducer, 325, 327
Continuous sealing process, 283

Coupling, by induction, summary, 85
  coil, for conductivity measurements, 102
  coil, single turn, 72
  to a metal load, 91
Critical frequency, as a function of wire size, 34
  for induction heating of cylinders, 32
  for steel, 66
  for thin strip, 62
Critical thickness, 64
Crothers, Harold M., 109, 173, 174, 206
Crystalline penicillin, 324, 325
Crystals of penicillin, 310
Curie point, 33
Current, crowding on conductor, 79, 81
  crowding on sheet, 79, 81
  density, 45, 51
  density distribution, 79
    due to coupling coil, 73
    in sheet under 2-turn coil, 87
    in sheet under 3-turn coil, 88
    in sheet under 4-turn coil, 88
    in sheet under end of long coil, 89, 90
  density, relative, 53
  distribution in thin strip, 59
  flow in thick metal sheets, 45–53
  in primary, 94
  transformer, 98, 99
    input reactance, 100
    input resistance, 100
Curtis, Frank W., 205
Cycles per second, 7
Cyclohexanone, 228, 230, 231
Cylinder, large, conducting, 49, 50
Cylindrical conductors, axial current flow in, 1–26

Debye, P., 226, 227
Deformation of outer surfaces, 281
Dehydration, radio-frequency, 307–327
Depth of hardening, control of, 198–200
Dielectric constant, 207, 216, 228, 229, 303, 305
  of fir, 268
  of wood, 264, 265
Dielectric cylinder, 298
  electric intensity in, 8, 9, 10
Dielectric losses in solids, 207
Dielectric properties of liquids, 216
Double electrode-wheel, 296
Douglas fir, 213, 219
Drying, in the final container, 317
  power requirements for, 307, 308
Duhamel's Theorem, 193
Dwight, H. B., 18, 49

Eagan, T. E., 205
Efficiency, effect of coil spacing, 82, 83
  effect of temperature on coupling, 83
  of metal load coupled inductively, 92, 93
  of rivet detonator, 172
Electrical conductivity of penicillin, 323
Electrical properties of metals, effect of temperature, 102–112
Electric heating of milk, 337
Electric intensity, 45–48
  in a conducting cylinder, 19
  in a dielectric cylinder, 8–10
  in metal, 56
  in thin strip, 60
Electrodes of special shapes, 298–306
Electrode spacing, 305
Electromagnetic wave, 47, 48
Electronic heat, 343
Electrons, free, 206, 227
Elimination of standing waves on large presses, 272–279
Endless metallic belts, 294
Energy per cycle, 209
Enzymes, inactivation of, 347
Epstein, J., 128
Equipotential surface, 298–302
Equivalent circuit, of liquid dielectric, 228
  of polar liquids, 226
  of spinach, 345
Extrusion due to excessive softening, 283

Field relations, surface of conductor, 54
Filter isolating high potential plate, choke coil, 262
  parallel tuned, 261
  quarter-wave line, 262
Fleming, Hugh, 340
Flosdorf, Earl W., 311
Food, treatment of, 343–351
Forming gas, 43
Fourier, 143
Free electrons, 206, 227
Freely-falling milk stream, 329
Free space wave length, 272
Freeze drying, 311
Frequency, 7
  critical, thin strip, 62, 63
Froelich, Herbert, 206
Fry, Thornton C., 353

Gillespie, H. C., 192
Gluing with radio-frequency heating, gusset joints in plywood, 257
  spruce boards, 256
  thick blank, 257

Glycerine, 230, 232, 233
Good conductor, 17
Grid electrodes, 306
Guillemin, E. A., 222, 270

Hardening of a layer, 189
  of steel, 33
Hardness, magnetic, 174
Heat energy absorbed by wood from one hot plate, 248
  from two hot plates, 242–244
Heat-flow analogy, operational solution, 153–155
Heat flow, differential equation, 145
  in plastic sheets, 287
  solution for plate of finite thickness, 149, 151, 152, 158, 160
  solution for plate of infinite thickness, 152, 153
Heating, effect in a thin steel sheet, 190, 191
  radio-frequency, and hot plates, 258–260
Heat treatment of knitting needles, 40, 42
  of surgical needles, 43, 44
Heaviside Expansion Theorem, 355
Henderson, J. L., 330
Hess, A., 227
Herne, H., 252
High conductivity, cylinder of, 19
High power factor, 14–16
Hot-plate heating, 281
Hoyler, C. N., 256
Hull, Lewis W., 311
Humphrey, H. C., 63, 205

Ice, conductivity of, 324
Impedance of a cylinder, 6
  of conducting cylinder, 20
  of dielectric cylinder, 9–11
  of metal load coupled to generator, 92
Index of refraction, 228, 229
Induced currents in cylindrical conductors, 27–32
Induction heating of small conductors, 33, 34
  of thin strip, 59
Infested products, 328
Inflatable articles, 297
Insulation of press, 272
  thermal, for presses heated by radio-frequency currents, 263
Insulator, perfect, 7
Integrated current, 52
Intensity, electric, in metal, 56
  in thin strip, 60
Intensity, magnetic, due to coupling coil, 73
  in metal, 56

Ions, free, 227
Iron, thermal constants of, 178
  specific heat of, 178, 179
Irregularly-shaped objects, 304

Jahnke and Emde, 5, 6, 18
Jeffers, Henry, Jr., 329
Johnson, W. G., 205
Jones, Lowell E., 339

Kelvin, 18
Kilocycle, 7
Kirkpatrick, C. B., 91
Knitting needles, heat treatment of, 40, 42
Koroseal, 282, 290, 292

Labile materials, 307
Laminar sheets, 68
Layer hardening, 202, 203
Line, transmission, 146
  solution for current, 147, 148
Linseed oil, 218
Losinsky, M., 71
Loss angle of a capacitor, 3
Loss of water by vacuum cooling, 334
Low power factor, 12

Magnetic field intensity, 27
Magnetic hardness, coefficient of, 174
Magnetic intensity, 46–48, 176
  as a function of applied power, 175–177
  in metal, 56
Margenau, Henry, 145
Mauersberger, H. R., 308
Mazzucchelli, A. P., 258
McAdams, William H., 143
Megacycle, 7
Meharg, V. E., 258
Mercerized cloth, electrical properties of, 213–215
Metal sheets of great thickness, 45–53
Micro-organisms, effect of electric field on, 340
Milk pasteurization, 328
Modification of electrode shape, 303
Mold spores, 344
Molecular friction, 207
Morgan, S. O., 207, 227, 324
Morrison, Wendell C., 341
Moyer, James C., 347, 348
Mudd, Stuart, 311
Multiple-tuned presses, 276
Murphy, E. J., 207, 227, 324
Murphy, George M., 145

Needles, heat treatment of, 40, 42–44
Nomograph for surface temperature, 197, 198, 201
Nyrop, Johan E., 341

Oil quenching, 184
Operational relations, 155
Osborne, H. B., Jr., 205
Oxford Units of penicillin, 310
Oxidized steel, radiation and conduction losses for, 37

Packaging, 297
Paint baking, 136
Parallel-tuned press, 269, 270
Pasteurization, and sterilization, 328–342
  of beer, 337
  of milk, 328
  radio-frequency, 329
Peirce, B. O., 361, 362
Penicillin bulk reducer of, 312, 313
  dehydration of, 310
  electrical conductivity of, 323
Pennell, W. O., 356
Perfect insulator, 7
Permeability, relative, in laminar sheets, 70
Permittivity of free space, 2
Peterson, D. W., 128
Phase factor, 222
Pharmaceutical products, 324, 325
Phenol glues, 268
Phosphatase test, 333
Phosphor bronze annealing, 132
Pierce, George W., 48
Pi-network, 270, 271
Plane electromagnetic wave, 47, 48
Plastics, preheating of, 257
Pliofilm, 282
Polar liquids, 226
  molecules, 226, 227
Poor electrical conductors, 206–233
Pork roll, 348–351
  induction heating of, 349, 350
Power, concentration, 185
    in wood, 266
  density, 52, 176
    in a copper cylinder, 25
    in laminar sheets, 69
    in metal, 57
    in thin metallic strips, 58
    relative, 53
  distribution, in a dielectric material, 13
  factor, 2, 3, 208, 209, 212, 224, 302
    high, 14–16
    of fir, 268
Power, factor, of wood, 264, 265
    very low, 12
  in a conducting cylinder, 29
  loss, in conductor, 81
  losses in sheet, 74
  loss in thin strip, 69
  minimum to attain required temperature, 254
  ratio between losses in sheet and coupling coil, 76
  ratio; loss to no-loss for radio-frequency heating and cold plates, 255
  requirements, for beer pasteurization, 339
    for drying, 307, 308
    for radio-frequency pasteurizing, 334
  to make a bond, 287–289, 292
Powers, A. J., 329
Pratt, R. S., 117
Press, electrodes, 269
  parallel-tuned, 269, 270
  problems, some specific, 264–279
  with one hot plate and one cold plate, temperature at any point, 245
  with two hot plates, differential equation for, 235
    temperature at any point, 236, 237
  wood gluing, assumptions for radio-frequency heating, 249, 250
    radio-frequency heating and cold plates, 248
    temperature at any point with radio-frequency heating, 250
    with one hot and one cold plate, 241
    with two hot plates, 234

Q-meter, 209, 216, 217, 229
  circuit of, 210
  connections, 210, 216
Q of penicillin, 320
Quarter-wave line and parallel-tuned press, 270
Quenching, water or oil, 184

Radiation loss, 35
Radio-frequency sewing machine, 280–297
Rayon, 308
  cakes, 308
  drying, 308
Reactance, per unit length, 20–23
  single-turn coupling coil, 84
Recalescence, 113
Reduced atmosphere drying, 307
Relative efficiency, 35

Relative field intensity as a function of wire diameter, 39, 41
  as a function of heating time, 40, 41
Relative permeability, 173, 176
  approximate expression for, 174, 175
Resistance, coupling, 84
  in laminar sheets, 69
  per unit length, 20–23
Resistivity, brass, 105
  copper, 105
  steel, 107
  tool steel, 109
Rivet detonation, radio-frequency, 172
  detonator efficiency, 172
Rivets, explosive, detonation of, 168
  power required for detonation, 171
  temperature rise, 171
Roadhouse, C. L., 330
Roasting of coffee, 344
Roberds, W. M., 71, 205
Rotating electrodes, 283–285
Rubber, electrical properties of, 213–215
Ruh beer, 337

Sandwich, pork roll, 350, 351
Saran, 282, 290
Saturation coefficient, 174
Savidge, H. G., 18
Sauveur, Albert, 113
Scanning,
  efficiency, effect of frequency on, 203, 204
  equation, 195, 359–364
  function, 196
  problem, a mathematical formulation of, 192
  self-quenching by, 192
  speed, 196, 197
Schwarz, E. W. K., 308
Sealing metal tubes, 166
Selective heating, 328
Self quenching, 185–191
  by scanning, 192
Setscrew hardening, 137
Sewing machine, radio-frequency, 280–297
Sheet, experimental heating of, 63
Sheets, laminar, defined, 68
Sherman, V. W., 258
Single-unit drier, 317, 319
Skin thickness, 17, 26, 52, 53
  of steel, 177, 178
Small diameter, conductors of, 33–44
Smythe, William R., 298
Softening temperature for fusing, 282
Soldering, 138
Solenoid, 27
Specific, conductivity, 224
  heat, of iron, 178, 179
Spinach, 345–347
Spinning cup, 326, 327
  principle of, 326
Spitzer, Edwin E., 205
Standard plate count, 333, 335, 336
Standing waves, elimination of, 272–279
Staphylococcus aureus, 310
Steel, case hardening of, 173–205
Step function, 194
Stored energy, 208
Stotz, Elmer, 347, 348
Strap seam, 296
Strip heating, power requirements, 64, 65
  illustrative example, 65
Superposition method, 185
  principle, 186
Surface hardening, 185
Surface temperature, 180, 184
  a nomograph for, 197, 198, 201
  as a function of conductor height, 197
  as a function of scanning speed, 196, 197
  rise of, 181
Surgical needles, heat treatment of, 43, 44

Taylor, J. P., 139, 205, 258
Teare, B. R., 68
Temperature,
  at any point in finite plate, 161
  at center of finite plate, 162
  at surface of finite sheet, 163, 165
  center of wood load, 254
  distribution, 182, 187, 188
    in plastic sheets, 281
    in very thick plates, 179
    in wood heated by radio-frequency, 252
    relative, 183
  expression for any point, 157
  expression for surface, 158
  increment, 255
  rise in explosive rivets, 171
  sealing metal tubes, 166
Tempil pellets, 63
Thawing of vegetables and meats, 344
Thermal, conductivity of air, 36
  conductivity of plastics, 282
  constants of iron and steel, 178
  diffusivity, 149
Thermoplastic, binding, 297
  binding tape, 294
  sheets, 280
Thick sheet, 47
Thin metallic layers, heating effect in, 191
Tinnerholm, A. R., 258

T-network, 270, 271
Tool steel, resistivity, 109
Total integrated current, 52
Transformer, current, 98, 99
Transient heat flow, 185
Tuning inductors, 277, 279

Uniform, external field, 299
  flow of milk, 330
  internal field, 299
Unit function, 194
Upper limit on frequency, 14
Urea-resin glues, 268

Vacuum cooling, of milk, 330–332
  loss of water by, 334
Vector current density, 53
Velocity of radio waves, 7
Vinyl chloride resin, 282
Vinylite, 282, 288–292, 296
  electrical properties of, 213–215
Virtual height of conductor, 76, 195
Viscose rayon, 308
Voltage, across electrodes, 303
  developed on plastic sheeting, effect of speed on, 291
  distribution on long presses, 273, 275
  distribution on multiple-tuned presses, 276, 278, 279
  gradient in wood, 266, 267
  variation on long electrodes, 274

Water quenching, 184
Wattmeters, radio-frequency, 128
Wave, electromagnetic, 47, 48
  incident on metal surface, 55
  length, 7, 272
  reflected by metal surface, 55
Webb, Josephine R., 68
Weevils, 328
Welding, 139
Whitehead, J. B., 227

DATE OF ISSUE

This book must be returned within 3/7/14 days of its issue. A fine of ONE ANNA per day will be charged if the book is overdue.